

https://dspace.org/

Phase transitions and structural motifs of inorganic-organic lead halide hybrids

Lemmerer, Andreas

2008-08-15T12:23:37Z
http://hdl.handle.net/10539/5390

Downloaded from a DSpace repository. https://dspace.org/

PHASE TRANSITIONS AND STRUCTURAL MOTIFS OF INORGANIC-ORGANIC LEAD HALIDE HYBRIDS

Andreas Lemmerer

A thesis submitted to the Faculty of Science, University of the Witwatersrand, Johannesburg, in fulfilment of the requirements for the degree of Doctor of Philosophy

Johannesburg, 2007

Declaration

I declare that this thesis is my own, unaided work. It is being submitted for the Degree of Doctor of Philosophy in the University of the Witwatersrand, Johannesburg. It has not been submitted before for any degree or examination in any other University.

_____

(Signature of Candidate)

_____day of_____2007

"*But to what extent can we really know the universe around us? ...Let us approach a much more modest question: not whether we can know the universe or the Milky Way Galaxy or a star or a world. Can we know, ultimately and in detail, a grain of salt? Consider one microgram of table salt, a speck just barely large enough for someone with keen eyesight to make out without a microscope. In that grain of salt there are about* 10^{16} *sodium and chlorine atoms. This is a 1 followed by 16 zeroes, 10 million billion atoms. If we wish to know a grain of salt, we must know at least the three-dimensional positions of each of these atoms. (In fact, there is much more to be known-for example, the nature of the forces between the atoms-but we are making only a modest calculation.) Now, is the number more or less than the number of things which the brain can know?*

How much can the brain know? There are perhaps 10^{11} *neurons in the brain, the circuit elements and switches that are responsible in their electrical and chemical activity for the functioning of our minds. A typical brain neuron has perhaps a thousand little wires, called dendrites, which connect it with its fellows. If, as seems likely, every bit of information in the brain corresponds to one of these connections, the total number of things knowable by the brain is no more than* 10^{14}*, one hundred trillion. But this number is only one percent of the number of atoms in our speck of salt.*

So, in this sense this universe is intractable, astonishingly immune to any human attempt at full knowledge. We cannot on this level understand a grain of salt, much less the universe.

But let us look a little more deeply at our microgram of salt. Salt happens to be a crystal in which, except for defects in the structure of the crystal lattice, the position of every sodium and chlorine atom is predetermined. If we could shrink ourselves into this crystalline world, we would see rank upon rank of atoms in an ordered array, a regularly alternating structure - sodium, chlorine, sodium, chlorine, specifying the sheet of atoms we are standing on and all the sheets above us and below us. An absolutely pure crystal of salt could have all the positions of every atom specified by something like 10 bits of information. This would not strain the information-carrying capacity of the brain.

If the universe had natural laws that governed its behaviour to the same degree of regularity that determines a crystal of salt, then, of course, the universe would be knowable."

From "Broca's Brain" by Carl Sagan.

"*Ever since I began working on X-rays, I have repeatedly sought to obtain diffraction with these rays; several times, using narrow slits, I observed phenomena which looked very much like diffraction. But in each case a change of experimental conditions, undertaken for testing the correctness of the explanation, failed to confirm it, and in many cases I was able to directly show that the phenomena had arisen in an entirely different way than by diffraction. I have not succeeded to register a single experiment from which I could gain the conviction of the existence of diffraction of X-rays with a certainty which satisfies me.*"

From W. C. Röntgen's Third Communication, March 1897.

Abstract

Layered inorganic-organic hybrid compounds have been widely studied as new potential sources of semiconductors and other optical devices. They simulate natural quantum well materials, where the inorganic part acts as semiconductors, separated by an organic part. This class of hybrid materials has no covalent bonds between the inorganic and organic parts; instead, weak hydrogen bonds and van der Waals forces bind and stabilise the overall structure.

The inorganic part is made up of layers of corner-sharing metal halide octahedra, MX_6, where the metal must be in a divalent state and the halides are Cl, Br or I. The 2-D layers extend infinitely in two directions and are separated themselves by layers of primary ammonium cations, with only one ammonium group at one end of the chain, $[(R\text{-}NH_3)_2MX_4]$, or two ammonium groups at either of the chain, $[(H_3N\text{-}R\text{-}NH_3)MX_4]$. Due to its similarity to the cubic perovskite structure, this inorganic motif is referred to as "layered perovskite-type". Depending on the choice of the organic ammonium cation, the materials can display phase transitions and / or have optical and electronic properties.

Various investigations of inorganic-organic hybrids have concentrated on the phase transitions of the hybrids of general formula $[(C_nH_{2n+1}NH_3)_2MX_4]$ and $[(NH_3C_nH_{2n}NH_3)MX_4]$ (n = 1-18; X = Cl, Br, I; M = Cu^{2+}, Mn^{2+}, Cd^{2+}) to elucidate their mechanism. There are two types of displasive transitions, a minor one were small conformational changes within the alkylammonium chain occurs, and a major one, when the entire alkylammonium chain becomes disordered along its long axis. The interlayer spacing between the inorganic layers increases with temperature and during the major phase transition. The methods used to identify the temperatures and the enthalpies of the phase transitions are Differential Scanning Calorimetry (DSC); and Single Crystal X-ray Diffraction (SC-XRD) as well as Powder X-Ray Diffraction (P-XRD) to follow the structural changes. In contrast, only a few reports on investigations of the lead iodide hybrids, $[(C_nH_{2n+1}NH_3)_2PbI_4]$ were found in the literature, with only two single crystal structures previously reported. Due to the difficulty in growing good quality crystals, the previous studies on the lead iodide hybrids have been only researched using DSC and P-XRD. The phase transition behaviour has been found to show the same trends as the previous hybrids. The primary aim of this study was to follow the same phase transitions via SC-XRD, ideally single-crystal to

single-crystal, and to determine the detailed structural changes with the hopes of elucidating their detailed phase transition mechanism.

A secondary aim was to synthesize as many inorganic-organic hybrids as possible using a variety of primary ammonium cations to find different inorganic motifs apart from the layered perovskite-type. Other inorganic motifs can have purely corner-, edge or face-sharing octahedra or combinations thereof to give 2-D net-type networks or 1-D extended chains. The effect that the identity of the ammonium cation has on the type of inorganic motif and the effect on the detailed structural geometry within the inorganic motif are investigated. Examples of structural geometries within the layered perovskite-type inorganic motif that can differ from compound to compound are the relative positions of the inorganic and organic moieties; the N---H….X hydrogen bonding geometry between the halides and the ammonium group; and the relative positions of successive inorganic layers.

Acknowledgements

My supervisor, Dave, for showing me a picture of a packing diagram that I did not understand at all when I was in honours. It was the first packing diagram I have ever seen. Also, he helped shape my life philosophy by sharing his views with me.

Manuel Fernandes for being my idol and mentor and teaching me everything I know about crystallography and helping me to solve those difficult structures.

Demetrius Levendis for being a patient consultant, who never charged for his services when I went to his office next door to me.

Bernard for not playing his annoying Kenyan music whenever I was around and being the most mature PhD student ever, raising a family already.

Gert Kruger at the University of Johannesburg for the use of his Mettler Toledo Calorimeter and Melanie Rademyer at the University of KwaZulu-Natal for helpful encouragement.

Susan Travis for casting her expert eye on various drafts of this manuscript.

The Beacon™ company for their delicious Sparkles™ and all the chocolate manufacturing companies, especially Milka™ and Cadbury™. The Toshiba™ computer company for manufacturing the laptop I wrote my thesis on.

And my family.

And lastly, to Bruker™ AXS in South Africa for their incomparable technical support in maintaining our beloved SMART and APEX II diffractometers.



Presentations and Posters

1) Oral Presentation: "Structural motifs of lead halide inorganic-organic hybrids", South African Chemical Institute, Young Scientist, Pretoria, 2005.

2) Oral Presentation: "Phase transitions and structural motifs of inorganic-organic lead halide hybrids", Departmental Seminar at the School of Chemistry, Johannesburg, 2007.

3) Poster Presentation: "Synthesis and Characterization of Organic-Inorganic Hybrid Perovskites", Indaba IV Conference, Skukuza, Kruger National Park, 2003.

4) Poster Presentation: "Synthesis and Characterization of Organic-Inorganic Hybrid Materials", European Crystallographic Meeting 21, International Conference Centre, Durban, 2003.

5) Poster Presentation: "Temperature Dependant Phase Transitions of Organic-Inorganic Hybrid Perovskites", International School of Crystallography's 35th Course: Diversity Amidst Similarity: A multidisciplinary Approach to Polymorphs, Solvates and Phase Relationships, Erice, Sicily, 2004.

6) Poster Presentation: "Temperature Dependant Phase Transitions of Organic-Inorganic Hybrid Perovskites", South African Chemical Institute, Pretoria, 2004 (Won RSC Poster Prize).

7) Poster Presentation: "Structural Transitions of the Layered K_2NiF_4 Type System $(C_nH_{2n+1}NH_3)_2PbI_4$; n = 12, 16, 18", Carman Symposium, Pretoria, 2005 (Won IUPAC Poster Prize).

8) Poster Presentation: "Structural Transitions of the Layered K_2NiF_4 Type System $(C_nH_{2n+1}NH_3)_2PbI_4$; n = 12, 16, 18", European Crystallographic Meeting 23, Leuven, Belgium, 2006 (Won IUCr Poster Prize).

9) Poster Presentation: "Structural Transitions of the Layered K_2NiF_4 Type System $(C_nH_{2n+1}NH_3)_2PbI_4$; n = 12, 16, 18", Indaba V conference, Berg-en-Dal, Kruger National Park, 2006.

Preface

The entire thesis has two styles of writing. The chapters of the introduction (Chapter 1), literature survey (Chapter 2) and experimental methods (Chapter 3) are detailed and exhaustive and written in a uniform style. The results chapters (Chapters 4-6) consist partly of published work in crystallographic specific journals such as those of the *International Union of Crystallography* and the *Royal Society of Chemistry*, and work that will be submitted or is currently under review. All the results chapters are subsequently written up in styles required for the different journals. The advantage is that a large amount of work, 76 new compounds and their single crystal structures, can be discussed concisely and the most important and relevant features described. Crystal structure determination has become a routine exercise as detector technology and computing speed has improved. Each structure is viewed more as a data point whereas previously, a whole thesis consisted of only a few single crystal structures. The figures in the literature survey are all in grey-scale, indicating that they are results published from previous work. The figures in the results chapters are all in colour, differentiating them explicitly as new work, except those in journals that do not usually publish in colour, specifically *Acta Crystallographica C*. The Cambridge Structural Database (CSD) (Version 5.27, August 2006 release; Allen, 2002) contains an inventory of all reported single crystal structures and is used throughout the literature survey. The reference codes for those structures as they appear in the CSD are given throughout.

Reprints of published work are supplied in the attached Compact Disc as pdf files. Crystallographic Informations Files (CIF) and CIF Tables of all structures are also supplied on the disc under the relevant chapters. Finally, the complete electronic version of the thesis can also be found on the disc.

Table of Contents

Page

Abstract **iv**

Acknowledgements **vi**

Posters and Presentations **vii**

Preface **viii**

Table of Contents **ix**

List of Figures **xii**

List of Tables **xx**

List of Schemes **xxi**

Abbreviations **xxii**

Section A: Background and Literature Survey

Chapter 1: Introduction

1.1 Overview 1
1.2 Basic cubic perovskite motif 2
1.3 Two-dimensional layered perovskite-type motif 3
1.4 Lower dimensional motifs on inorganic-organic hybrids 8
1.5 Zero-dimensional motifs 11
1.6 Hydrogen bonding in inorganic-organic layered perovskite-type hybrids 11
1.7 Hydrogen bonding in non layered perovskite-type inorganic-organic hybrids 14
1.8 Aims 14

Chapter 2: Literature Survey

2.1 First synthesis and structure determination 15
2.2 Inorganic-organic layered perovskite-type hybrids $[(C_nH_{2n+1}NH_3)_2MX_4]$ with simple alkylammonium chains 21
2.2.1 Phase transitions in inorganic-organic layered perovskite-type hybrids $[(C_nH_{2n+1}NH_3)_2MX_4]$ with $n \leq 3$ and M = Mn and Cd 23
2.2.2 Phase transitions in inorganic-organic layered perovskite-type hybrids $[(C_nH_{2n+1}NH_3)_2MX_4]$ with $n \geq 4$ 28
2.2.3 The lead halide inorganic-organic hybrids $[(C_nH_{2n+1}NH_3)_2PbX_4]$ with the layered perovskite-type motif 37
2.2.4 Phase transitions in inorganic-organic layered perovskite-type hybrids $[(C_nH_{2n+1}NH_3)_2PbX_4]$ 38

2.2.4.1 Alkylammonium chains with n = 1 38
2.2.4.2 Alkylammonium chains with n ≥ 4 38
2.3 Aromatic R groups and their photoelectric behaviour 42
2.4 Inorganic-organic layered perovskite-type hybrids [$(H_3N(CH_2)_nNH_3)MX_4$] with simple alkyldiammonium chains 51
2.4.1 Lead(II) halide inorganic-organic layered perovskite-type hybrids [$(H_3N(CH_2)_nNH_3)PbX_4$] and [$(H_3N\text{-}R\text{-}NH_3)PbX_4$] 52
2.4.2 Other divalent metals reported to form inorganic-organic layered perovskite-type hybrids [$(H_3N(CH_2)_nNH_3)MX_4$] with diammonium alkyl chains 58
2.4.3 Structural phase transitions of inorganic-organic layered perovskite-type hybrids [$(H_3N(CH_2)_nNH_3)MCl_4$] (M = Cd and Mn) with diammonium alkyl chains 61
2.5 Inorganic-organic layered perovskite-type hybrids [$(H_3N\text{-}R\text{-}NH_3)MX_4$] containing aromatic diammonium cations 63
2.6 Inorganic-organic layered perovskite-type hybrids with triammonium cations 64
2.7 Other metals and more complex ammonium cations contained in inorganic-organic layered perovskite-type hybrids 66
2.8 Multilayer inorganic-organic layered perovskite-type hybrids 75
2.9 Photopolymerization 77
2.10 Two-dimensional inorganic motifs 80
2.10.1 Two-dimensional motifs - NET 80
2.10.2 Two-dimensional motifs - based on corner-sharing layers 83
2.10.3 Two-dimensional motifs - based on face-sharing 84
2.11 One-dimensional inorganic motifs 86
2.11.1 Purely corner-sharing, edge-sharing and face-sharing 86
2.11.1.1 Motifs based on t*rans* corner-sharing 86
2.11.1.2 Motifs based on c*is* corner-sharing 88
2.11.1.3 Motifs based on face-sharing 91
2.11.1.4 Motifs based on edge-sharing 94
2.11.2 Motifs based upon combinations of edge- and face-sharing 97
2.11.3 One-dimensional "Ribbon" type motifs 97
2.12: Zero-dimensional inorganic motifs 102
2.13: Summary and Conclusion 107

Chapter 3: Experimental

3.1 Synthesis 109
3.1.1 Slow cooling 109
3.1.2 Slow evaporation 112
3.1.3 List of compounds prepared with corresponding chapter reference in this thesis 112
3.2 X-ray diffraction 119
3.2.1 Instruments used 119
3.2.2 Face-indexed absorption corrections 120
3.3 Thermal analysis 122
3.4 Elemental analysis 122
3.5 Hot Stage Microscopy

Section B: Results and Discussion

Chapter 4: Structural Motifs of Inorganic-Organic Hybrids

4.1 Introduction 125
4.2 Synthesis and crystal structures of inorganic-organic hybrids incorporating an aromatic amine with a chiral functional group 126
4.3 Inorganic-organic hybrids incorporating a chiral cyclic ammonium cation 139
4.4 Inorganic-organic hybrid materials incorporating primary cyclic ammonium cations: The lead iodide series 153
4.5 Inorganic-organic hybrid materials combining primary cyclic ammonium cations with bromoplumbate and chloroplumbate anions 164
4.6 Effect of heteroatoms in the layered perovskite-type system $[(XC_nH_{2n}NH_3)_2PbI_4]$, n = 2, 3, 4, 5, 6; X = OH, Br and I; and $[(H_3NC_2H_4S_2C_2H_4NH_3)PbI_4]$. 185
4.7 Inorganic-organic hybrids incorporating diammonium cations 204

Chapter 5: Phase Transitions of Inorganic-Organic Layered Perovskite-type Hybrids

5.1 Introduction 220
5.2 Synthesis, characterization and phase transitions in the inorganic-organic layered hybrids $[(C_nH_{2n+1}NH_3)_2PbI_4]$, n = 4, 5 and 6 221
5.3 Synthesis, characterisation and phase transitions of the inorganic-organic layered hybrids $[(C_nH_{2n+1}NH_3)_2PbI_4]$, n = 7, 8, 9 and 10 247
5.4 Structural transitions of the inorganic-organic layered perovskite-type hybrids $[(C_nH_{2n+1}NH_3)_2PbI_4]$; n = 12, 14, 16, 18 277

Chapter 6: Miscellaneous Structures and Motifs

6.1 Introduction 293
6.2 Bis[(S)-*β*-phenethylammonium] tribromoplumbate(II) 295
6.3 Bis(pentane-1,5-diammonium) decaiodotriplumbate(II) 299
6.4 *p*-phenylenediammonium tetraiodozincate(II) dihydrate 303
6.5 1-Naphthylammonium triiodoplumbate(II) 307
6.6 *catena*-Poly[tetrakis(3-phenylpropylammonium) [iodoplumbate(II)-tri-μ-iodo-plumbate(II)-tri-μ-iodo-plumbate(II)-di-μ-iodo]] 311
6.7 Bis(propane-1,2-diammonium) hexaiodoplumbate(II) trihydrate 315
6.8 Octakis(3-propylammonium) octadecaiodopentaplumbate(II): a new layered structure based on layered perovskites 319
6.9 *catena*-Poly[bis(*tert*-butylammonium) [plumbate(II)-tri-μ-iodo] iodide dihydrate] 323
6.10 Poly[bis[2-(1-cyclohexenyl)ethylammonium] di-μ-iodo-diodoplumbate(II)] 328
6.11 Two packing motifs based upon chains of edge-sharing PbI_6 octahedra 332

Chapter 7: Conclusion

7.1 Concluding remarks 339
7.2 Future work 340

Chapter 8 References 343

Appendix 357

List of Figures **Page**

1.1: Ball and stick model of the basic AMX_3 perovskite showing the unit cell structure and the polyhedral representation of how the structure extends in three dimensions. 3

1.2: The unit cell of the inorganic compound K_2NiF_4, that is the archetype for the 2-D layered perovskites that have staggered layers (left), and $RbAlF_4$, that is the archetype of the eclipsed inorganic layers (right). 5

1.3: Schematic Representation of single-layer perovskites with (a) monoammonium ($R\text{-}NH_3^+$) or (b) diammonium ($^+H_3N\text{-}R\text{-}NH_3^+$) organic cations. 5

1.4: The area generated by the four terminal halides, viewed perpendicular to the 2-D layers. (a) shows the biggest possible scenario of a square, when there is no tilting of the octahedra. (b) shows the actual scenario, when both Ψ and θ tilts are observed. 7

1.5: Schematic Representation of the two commonly encountered tilts in the layered perovskites. (a) (0Ψ0) tilt, leading to a corrugation of the sheets in one direction; (b) (00θ) tilt, leading to a rotation of adjacent octahedra relative to each other. 7

1.6: A space-filled representation of the packing arrangement of a typical inorganic-organic layered perovskite-type hybrid with atoms drawn with their van der Waals radii. The terminal iodides are shown as red coloured spheres. 8

1.7: An illustration of the n = 3 $[Pb_3I_{10}]_n^{4n-}$ 2-D net. 9

1.8: Example of a corner-sharing chain and the classification of the halides within the octahedra. 10

1.9: Example of an edge-sharing chain and the classification of the halides within the octahedra. 10

1.10: Example of a face-sharing chain and the classification of the halides within the octahedra. 11

1.11: Two hydrogen bonding configurations typically observed in the $[(R\text{-}NH_3)_2MX_4]$ and $[(H_3N\text{-}R\text{-}NH_3)\ MX_4]$ type structures: (a) the bridging halogen configuration, and (b) the terminal halogen configuration. 12

1.12: Two types of terminal halogen configuration: (a) equilateral configuration, where the three halides involved in hydrogen bonding are at the vertices of an equilateral shaped triangle (dashed blue lines) and (b) right-angled configuration, where the halides are at the vertices of a right-angled triangle. The obtuse 13

angled position is shown in (a) and the acute angled position in (b) relative to the parallelogram (green lines).

1.13: The correlation between the hydrogen bonding interactions and the tilting of the PbI_6 octahedra in the layered perovskite-type hybrid $[(C_3H_5NH_3)_2PbI_4]$. 14

2.1: The tilted and non-interdigitated decylammonium chains in $C_{10}MnCl$ (left). The non-tilted and interdigitated nonylammonium chains in C_9PbI (right). 22

2.2: The effect of the identity of the metal on the θ tilt of the octahedra is seen in the compounds C_4GeI (left) and C_4SnI (right). The (OOθ) tilt is 13.73° in the layered perovskite-type hybrid with Ge and 20.39(5)° with Sn. 23

2.3: The hydrogen bonding interactions of the layered hybrid with methylammonium and cadmium(II) chloride in phase **II**. 25

2.4: Phase **II** of C_2CdCl and its terminal halogen configuration. The ethylammonium cation is ordered in this phase. Phase **I** has the same ethylammonium cation disordered over two positions. The SC-XRD structure of phase **III** has not been determined. Figure adapted from Peyrard and Perret, 1979. 25

2.5: The two SC-XRD structures of phases **III** and **I** of C_3CdCl. 27

2.6: Schematic representation of DSC results of the homologous C_nCdCl4 series for n = 6 - 18. Inset: Transition enthalpies for n = 7-12. Asterisk represent the chain melting transition and filled circles the minor transition. Figure taken directly from Schenk and Chapuis, 1988. 33

2.7 The herringbone arrangement of the tilted decylammonium chains in $C_{10}CdCl$ in the monoclinic phase **III** (left) and the two independent chains in this phase (right). Taken from Kind et al, 1979. 36

2.8: Electron density contours from the orthorhombic phase **I** of $C_{10}CdCl$. Taken from Kind et al, 1979. 36

2.9: A schematic of the various phases of C_6PbCl and their unit cell parameters as determined by P-XRD. Adapted from Kammoun et al, 1996a. 39

2.10: DSC curve of C_9PbCl. Taken from Kammoun et al, 1997. 40

2.11: A schematic of the two possible packing arrangements, parallel (left) or herringbone (right), of the alkylammonium chains in C_nPbI (n = 12, 16, 18). All the bonds in the chains are in an all-*trans* conformation. Taken from Venkataraman et al, 2002. 41

2.12: A schematic of the phase transition of C_nPbI (n = 12, 16, 18). Taken from Venkataraman et al, 2002. 42

2.13: The hydrogen bonding interactions of the layered hybrid with anilinium and the two long and four short Cu-Cl bonds of the copper(II) chloride octahedra. 44

2.14: The packing arrangement of a complete unit cell of [(*p*-Ph-$C_6H_4NH_3)_2CuCl_4$]. 44

2.15: Hydrogen bonds in [$(C_6H_5CH_2NH_3)_2PbI_4$]. 46

2.16: The bridging halogen configuration of [$(C_6H_5(CH_2)_2NH_3)_2CuCl_4$]. 47

2.17: The simplest repeating unit of the perovskite sheets in [$(C_6H_5(CH_2)_2NH_3)_2PbCl_4$]. The four phenethylammonium cations adopt a J-shaped conformation. 48

2.18: A schematic of the organic-inorganic heterostructure electroluminescent device with approximate thickness of the layers and the structure of the organic component, OXD7, used. Figure adapted from Era et al (1994). 50

2.19: A schematic of the three-layered heterocontact organic-inorganic light emitting diode with a chiral layered-perovskite. Figure adapted from Gebauer and Schmidt (1999). 50

2.20: Optical absorption spectra of (a) [$(RNH_3)_2PbBr_xI_{4-x}$] and (b) [$(RNH_3)_2PbCl_xBr_{4-x}$] films measured at room temperature. Taken from Kitazawa (1997). 51

2.21: The packing diagram of a single unit cell of [$(H_3N(CH_2)_3NH_3)PbCl_4$] shown side-on (left) and from the top (right). The inorganic layer shown as light grey octahedra is staggered relative to the inorganic layers shown as dark grey octahedra. 52

2.22: Half of the unit cell of [$(H_3NCH_3CH(CH_3)(CH_2)_3NH_3)PbCl_4$] showing a magnified view of the arrangement of the cations between the layers. The methyl group has a repulsive effect on the cations in the crystallographic *c* direction. 53

2.23: The structure of phase **II** of [$(H_3N(CH_2)_4NH_3)PbCl_4$] showing a magnified view of the left-hand conformation of the cation between the layers. 54

2.24: The structure of [$(H_3N(CH_2)_6NH_3)PbI_4$]. The cation is centrosymmetric and the two halves are related by the symmetry operator (1-x, 1-y, 1-z), shown as atoms marked with dashes ('). 55

2.25: The molecule 5,5'''-bis-(aminoethyl)-2,2':5',5'',2'''-quaterthiophene, AEQT. 56

2.26: The unit cell of [(AEQT)$PbCl_4$]. The ethylammonium groups and the bridging bromides are disordered over two positions. 57

2.27: The molecule BAESBT. 57

2.28: The molecule AETH. 58

2.29: The hydrogen bonding configurations of $[(H_3N(CH_2)_4NH_3)HgCl_4]$ (left) and $[(H_3N(CH_2)_3NH_3)HgCl_4]$ (right). 59

2.30: The packing diagrams of phase **II** (left) and phase **I** (right) of $[(H_3N(CH_2)_4NH_3)MnCl_4]$. The two equivalent positions of the atoms are shown as light grey and dark grey spheres in phase **I**. 63

2.31: The packing diagrams of $[(H_3N\text{-}C_6H_4\text{-}NH_3)CdCl_4]$ (left) and $[(H_3N\text{-}C_6H_4\text{-}C_6H_4\text{-}NH_3)CuCl_4]$ (right). The C-H...π interactions are shown as dashed black lines. 64

2.32: Half of the unit cell of $[((H_3NCH_2CH_2)_2NH_2)CuCl_4]\cdot Cl$. Figure is taken from Ferguson and Zaslow (1971). 65

2.33: Half of the unit cell of $[((H_3NCH_2CH_2)_2NH_2)MnCl_4]\cdot Cl$. The hydrogen bonds to the interlayer chloride are shown as dashed black lines. 66

2.34: The packing diagram of $[(4\text{-}F\text{-}C_6H_4C_2H_4NH_3)_2SnI_4]$. The aromatic rings are parallel to each other. 68

2.35: The carbozole chromophore, n = 3-8, 12. 69

2.36: The packing diagram of $[(Cu(O_2C\text{-}(CH_2)_3\text{-}NH_3)_2PbBr_4]$. The $PbBr_6$ octahedra are shown as dark grey octahedra and the CuO_4Br square-planar pyramids are light grey. 71

2.37: The packing diagram of $[(HO_2C(CH_2)_3NH_3)_2PbI_4]$. The R groups have a carboxylic functional group that interacts strongly with adjacent R groups via O-H...O (d(O...H) = 1.8 Å) hydrogen bonds to strengthen the overall structure. 73

2.38: The packing diagram of $[(C_6H_8N_4)PbI_4]$. There are only four hydrogen bonds between the individual cations and the inorganic layers. 74

2.39: The packing diagram of $[((CH_3)_3N(CH_2)_2NH_3)SnI_4]$. 75

2.40: The packing diagram of the bilayer hybrid $[(CH_3NH_3)(H_3CC_6H_5(CH_2)NH_3)_2Pb_2I_7]$ (Papavassiliou et al, 2000; CSD ref. code: MEMYAE). 76

2.41: The packing diagram of the trilayer hybrid $[(CH_3NH_3)_2(C_4H_9NH_3)_2Pb_3I_{10}]$. The CH_3NH_3 cations are not shown as their positions were not accurately determined in the crystal structure (Mitzi et al, 1994; CSD ref. code: PIVCUS). 76

2.42: The basic idea of solid-state polymerization within layered type structures. Taken from Takeoka et al, 2001. 2 78

2.43: The geometries of the closest propargylammonium cations in the hybrid structure that undergoes possible photopolymerization. The octahedra consist of $CdCl_6$. 79

2.44: The 2-D net of $[(Me_2HN\text{-}C_2H_4\text{-}NHMe_3)Sn_3I_8]$. The cations are omitted for clarity. 81

2.45: 2-D net of $[(Pr_3N\text{-}C_2H_4\text{-}NPr_3)Pb(dmf)_6Pb_5I_{14}] \cdot DMF$. The cations and $[Pb(dmf)_6]$ anions are omitted for clarity. 82

2.46: The 2-D net of $[(Me_3N\text{-}C_3H_6\text{-}NMe_3)_3Pb_3I_9]$. The cations are omitted for clarity. 83

2.47: The $[SnI_4]^{2-}$ 2-D layers. The cations are omitted for clarity. 84

2.48: The twin 2-D layers of face-sharing $PbCl_8$ square antiprisms, separated by a monolayer of *p*-phenylenediammonium. The hydrogen bonds are shown as dashed black lines. 85

2.49: The mono 2-D layers of face-sharing $[PbCl_8]$, separated by bilayers of $H_3N\text{-}C_2H_4\text{-}NH_3$. The two different orientations of the cations are labelled I and II. 86

2.50: The quasi 0-D chains of $[(CH_3SC(=NH_2)NH_2)_3SnI_5]$. The activity of the stereochemical lone pair is in the direction of the chains. 87

2.51: The 1-D chain of corner-sharing octahedra is shown in light grey as cut-outs of the layered perovskite structure. The PbI_2 deficient sites repeat themselves every third row along the *b*-axis and are shown in dark grey. 88

2.52: The 1-D chains of $[(H_3N(CH_2)_6NH_3)BiX_5]$. 90

2.53: The 1-D chains of $[(Na_3(OCMe_2)_{12})Pb_4I_{11}(OCMe_2)]^{3-}$, which has face-sharing involving three I atoms or alternately, two I atoms and one O atom from an acetone solvent molecule. 92

2.54: The twin 1-D chain of face-sharing PbI_6 octahedra. 93

2.55: The 1-D chain of $[(Me_3N(CH_2)_6NMe_3)PbI_3]_2$. The face-shared octahedra are alternatively *cis* and *trans* related. 94

2.56: The 1-D chain of the hybrid $[(Pr_4N)PbI_3]$. 95

2.57: The 1-D chain of the hybrid $[(4\text{-}(CH_3)C_5H_3NH)CdBr_3]$, which has a single hydrogen bond between the anionic chain and the organic cation. 96

2.58: The 1-D chain of the hybrid $[((CH_3)_3NH)HgCl_3]$. 96

2.59: A single layer cutout of the CdI_2-Structure type. The octahedra in light grey show the twin anionic chains seen in lead iodide inorganic-organic hybrids. 98

2.60: The packing diagram of $[(C_{10}H_7CH_2NH_3)PbI_3]$ is shown on the left together with the hydrogen bonds in dashed lines. On the right is an illustration of the anionic twin chains of edge-sharing PbI_6 octahedra (Papavassiliou et al, 1999b; CSD ref. code: COTVUC). 98

2.61: The anionic polymeric chains of $[(Ph_4P)Sb_3I_{10}]$ (a) and $[((Me_2N)_3C_3)Sb_3I_{10}]$ (b) shown schematically (light grey octahedra) as cut-outs of the layer structure of CdI_2 (dark grey octahedra). 99

2.62: The cut-out of the K_2NiF_4 type inorganic motif that gives rise to the 1-D inorganic ribbons, shown as light grey octahedra. Every fourth row is missing, shown as dark grey octahedra. 100

2.63: Two inorganic ribbons, connected by hydrogen bond interactions between the terminal bromides and the oxygen molecules between them. 101

2.64: Twin anionic chains of face- and edge-sharing lead(II) iodide. 101

2.65: Twin anionic chains of edge- and corner-sharing Sn(II) bromide. 102

2.67: Twin anionic chains of lead(II) iodide, that has the three types of sharing in one structure. 102

2.68: Alternating organic and inorganic layers bridged by hydrogen bonds in $[(H_3N\text{-}C_6H_4\text{-}C_6H_4\text{-}NH_3)_2PbCl_6]$. 103

2.69: Incomplete part of the unit cell of $[(Cl\text{-}C_2H_4\text{-}NH_3)_6PbCl_6]\cdot 2Cl$, showing only a single ribbon of the hydrogen bonded interactions between the alternating $PbCl_6$ octahedra and the cations. 104

2.70: Two views of a filled unit cell of $[(CH_3NH_3)_4PbI_6]\cdot 2H_2O$. The cif file did not contain any hydrogen atom coordinates so the interactions are shown as dashed lines between the various acceptor and donor atoms. 105

2.71: The anions and cations of $[(Ph_4P)_2Pb_2I_6]$ (left), $[(Pr_4N)_2PbI_4]$ (middle) and $[(Bu_3N\text{-}(CH_2)_3\text{-}NBu_3)PbI_4]$ (right) that contain tetra-coordinated lead atoms. 106

2.72: The cluster anion $[Pb_{18}I_{44}]^{8-}$. 106

3.1: The basic experimental setup used to grow crystals of the inorganic-organic hybrids. 110

3.2: The pictures show the important stages of the slow cooling technique. An orange precipitate of the layered perovskite-type hybrid $[(C_8H_{17}NH_3)_2PbI_4]$ at room temperature slowly dissolves as the temperature of the solution increases to 100°C and then becomes a clear solution after a few hours. As the cooling takes place, orange plate-like crystals grow first at the surface of the solution 111

and then at the bottom.

3.3: The CCD instruments used. (a) SMART 1K with Kryoflex. (b) The Bruker APEX II with an Oxford Cryostream. (c) Close-up picture of the APEX II showing the centering video camera, CCD detector plate, collimator and heating tube. 120

3.4: Typical crystal shape of hybrid with the layered perovskite-type motif. 122

3.5: Locally modified Koffler Hot Stage. 123

7.1: The hexylammonium cations and the arrangement of the inorganic layers in the two phases of $[(C_6H_{13}NH_3)_2SnI_4]$. 341

List of Tables **Page**

1.1: Mean distances (Å) in N–H---A^- hydrogen bonds to halide ions with <(DHA) > 140°. 12

2.1: The composition of various CuCl inorganic-organic hybrids with simple alkylammonium chains. 16

2.2: Summary of $[(C_nH_{2n+1}NH_3)_2MX_4]$ and $[(NH_3C_nH_{2n}NH_3)MX_4]$ (n = 1-10) inorganic-organic layered perovskite-type hybrids in the literature. Numbers in superscript refer to the references listed at the end of the table. 18

2.3: Summary of $[(C_nH_{2n+1}NH_3)_2MX_4]$ and $[(NH_3C_nH_{2n}NH_3)MX_4]$ (n = 11-18) layered perovskite-type hybrids in the literature. Numbers in superscript refer to the references listed at the end of the table. 29

2.4: Summary of interlayer spacing, *c*, from X-ray spectra of powders for C_nMCl (1). 31

2.5: Summary of phase transition temperatures, enthalpies and entropies from DSC heating and cooling scans for C_nHgCl (1). 32

2.6: Summary of unit cell parameters of C_nCdCl inorganic-organic layered perovskite-type hybrids in their various phases, n = 8 - 16. 34

2.7: Unit cell constants of the layered perovskite-type hybrids C_nPbX at room temperature. 37

2.8: Unit cell constants and other structural data of the various phases of the hybrids $[CH_3NH_3PbX_3]$ that have a 3-D cubic perovskite motif (1). 38

2.9: The most common aromatic R groups that form inorganic-organic layered perovskite-type hybrids. 43

2.10: Structures of compounds that appear in the CSD. 60

2.11: $[(x\text{-}F\text{-}C_6H_4C_2H_4NH_3)_2SnI_4]$, x = 2, 3, 4. 68

2.12: $[(2\text{-}X\text{-}C_6H_4C_2H_4NH_3)_2SnI_4]$ (X = Cl and Br) (1). 68

2.13: Other bilayer inorganic-organic layered perovskite-type hybrids with their reported single-crystal structures if reported. 77

7.1: Summary of the inorganic motifs of the 76 inorganic-organic hybrids that were made in this thesis. 340

List of Schemes **Page**

2.1: The inter-relationship between the four phases of C_1CdCl and C_1MnCl as a function of temperature. 24

2.2: The phase sequence of C_3CdCl and their unit cell parameters (Å). 26

2.3: The phase sequence of C_3MnCl and their unit cell parameters (Å) with CSD reference codes. The greek numbering for the phases is taken from the literature. 27

Abbreviations

a_p	Cubic perovskite lattice parameter
CCDC	Cambridge Crystallographic Data Centre
CSD	Cambridge Structural Database
2-D	two-dimensional
1-D	one-dimensional
0-D	zero-dimensional
dmf	dimethylformamide
DSC	Differential Scanning Calorimetry
IR	Infrared
NMR	Nuclear Magnetic Resonance
NQR	Nuclear Quadropole Resonance
P-XRD	Powder X-Ray Diffraction
SC-XRD	Single Crystal X-Ray Diffraction

Chapter 1 Introduction

1.1 Overview

Inorganic-organic hybrid structures are able to combine excellent features from both types of constituents. Inorganic compounds have different band gaps and hence their electrical properties can vary from insulators to semiconductors right the way through to superconductors. Furthermore, they supply the hybrid structure with thermal stability and hardness as well as magnetic and dielectric properties. Organic materials can offer highly efficient luminescence and can show conducting properties. Their biggest advantage however is a structural diversity that enables us to produce a range of different compounds to suit our needs. This property can best be described as essential to crystal engineering.

As is sometimes the case, nature has long been aware of these materials and has incorporated the hybrid character into mollusc shells, and mammalian teeth and bone. The inorganic layer in sea shells consists of $CaCO_3$ crystals and alternates with proteinaceous organic matter. The strength comes from the contrasting properties of the two: the hard and brittle inorganic part and the softer, more plastic-like organic part. The inorganic phase in teeth consists of calcium phosphate, $Ca_{10}(PO_4)_6(H_2O)$, and the organic constituent of various protein matter. The resulting hybrid gives teeth their protective outer enamel shell with excellent wear resistant properties. Bone has the same inorganic compound but in this case alternates with fibres of the protein collagen. The softness of the organic constituent gives bone its flexibility; otherwise if it where only made up of the calcium phosphate it would shatter much more easily. In all three cases, the resultant strength is a case of the whole being greater than the sum of its parts, mainly due to the strength of the bonds that hold the framework together.

The inorganic part of inorganic-organic hybrids consists of metal halide octahedra, which can be corner-sharing to form a 3-D network based on the distorted cubic perovskite structure $[ABX_3]$ or they can form 2-D layers based on the $[A_2BX_4]$ or $[ABX_4]$ type families. Lower dimensional systems consist of simple 1-D chains of octahedra extending in one direction or completely isolated octahedra (0-D).

The bonding properties are another point of interest. The organic part makes use of covalent bonds whereas ionic attractions keep the inorganic framework of the hybrid intact. Between the inorganic and organic parts there exist ionic interactions between the $R\text{-}NH_3^+$ and I^- moieties, hydrogen bonding and other van der Waals interactions. The ultimate strength of the hybrid is a combination of all the various types of bonding present.

1.2 Basic cubic perovskite motif

The basic perovskite structure [AMX_3] consists of corner-sharing octahedral MX_6, where M is a divalent metal and X a halide. The cation A sits in the voids of this 3-D network (Figure 1.1) and hence has a limited radius. The formula that determines this maximum radius was derived by Goldschmidt (1926) and assumes that we have a perfect cubic perovskite structure and that all the spheres are in contact. If R_A, R_M and R_X are the ionic radii for the spheres, then the geometric limit imposed on R_A is

$$R_A + R_x = t\sqrt{2}\,(R_M + R_x)$$

where t is the tolerance factor and lies between 0.78 and 1.05 for compounds in the perovskite family (Randall et al, 1990).

For the inorganic-organic hybrids using the metal Pb^{2+} and the halide I^-, with R_{Pb} = 1.19 Å and R_I = 2.20 Å respectively (Shannon, 1976), a large cavity for A is created. If t = 1.0, then R_A = 2.6 Å and hence A can only consist of at maximum one C-C or C-N bond. This restriction is only fulfilled by the methylammonium cation and compounds with the general formula [$CH_3NH_3MX_3$], where M is Sn or Pb and X is Cl, Br and I have been synthesized (Poglitsch and Weber, 1987). The unit cell lattice constant varies from a_p = 5.657 (2) Å for [$CH_3NH_3PbCl_3$] to a_p = 6.3285 (4) Å for [$CH_3NH_3PbI_3$] and for the tin analogue, a_p goes from 5.89 Å to 6.24 Å (Mitzi, 1999a).

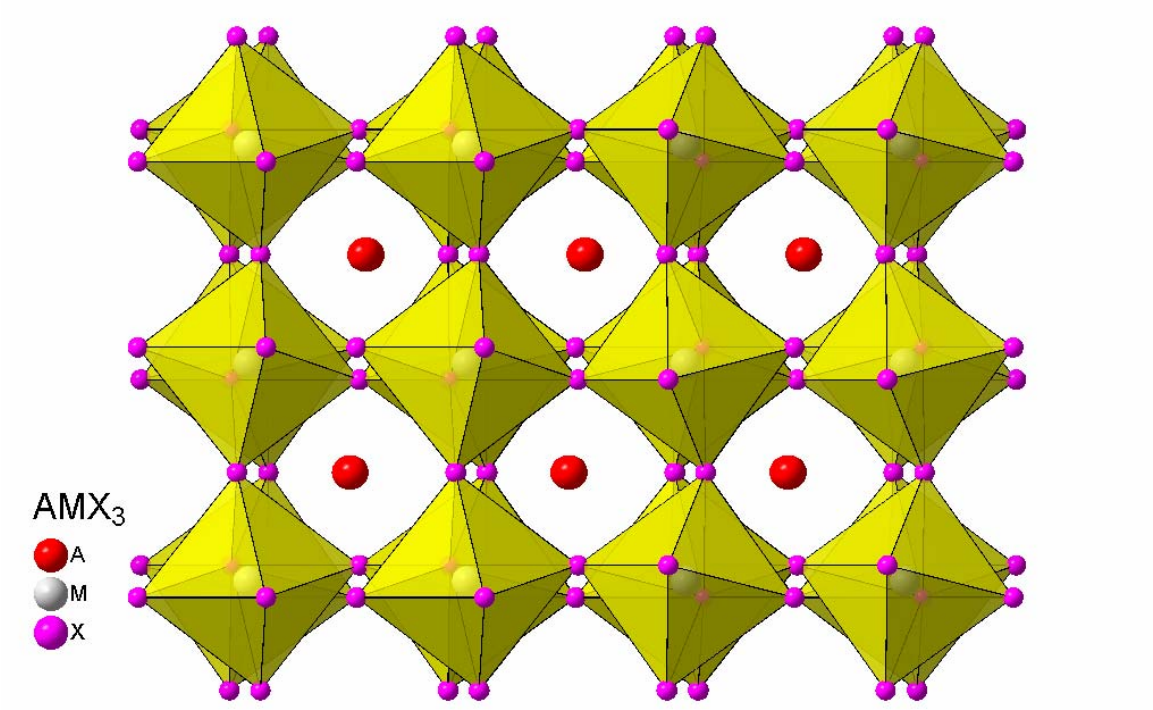


Figure 1.1: Ball and stick model of the basic AMX_3 perovskite showing the unit cell structure and the polyhedral representation of how the structure extends in three dimensions.

1.3 Two-dimensional layered perovskite-type motif

For larger organic molecules, where the A cation is replaced by an ammonium cation with two or more C-C or C-N bonds, the stable configuration requires layered octahedra that are based on the $[A_2BX_4]$ or $[ABX_4]$ structure type. The former structure type has staggered layers of corner-sharing BX_6 octahedra, as in $[K_2NiF_4]$ or $[K_2MgF_4]$ (Hatch et al, 1989), and the latter structure type has eclipsed layers of BX_6 octahedra, e.g. $[RbAlF_4]$ and $[TlAlF_4]$ (Hatch and Stokes, 1987) (Figure 1.2). In the inorganic-organic hybrids described in this thesis, the A cation gets replaced by the organic ammonium cation and sits in the interstitial sites between the layers. The organic cation can form bilayers between these inorganic layers if it has only one ammonium group or a monolayer for two ammonium groups on the same cation (Figure 1.3). The inorganic layer consists of $[MX_4]^{2-}$ corner-sharing metal halide octahedra. The four halides that are involved in the corner-sharing to adjacent octahedra are called 'bridging halides' and the two remaining halides that are above and below the inorganic layer are called 'terminal halides' as they undergo no sharing. To keep these larger cations effectively in place, there must exist hydrogen bonding

between one end of the organic molecule and the halide on the metal. This 'head' of the molecule is the primary ammonium $-NH_3^+$, and the rest of the molecule R is the tail. If the organic tail is very long, for example in the longer straight-chain alkylammonium chains, a large degree of interdigitation is possible for the spacious PbI_6 framework. The chloride and bromide transition metal analogues exhibit less interdigitation. If the organic cation has an $-NH_3^+$ group on both terminal ends of the molecule, both ammonium groups hydrogen bond to the inorganic layers that sandwich it. Furthermore, looking down the *c*-axis of the unit cell, the organic molecules have two different relative packing arrangements, similar to the inorganic layers. They can eclipse the next layer or be staggered. This depends on the size of the halide: the smaller chlorine and bromine enable staggered whereas the larger iodine atom can allow eclipsed. Also the monoammonium cation usually has a staggered and the diammonium cation an eclipsed conformation. The general formula then becomes $[(R\text{-}NH_3)_2MX_4]$ or $[(NH_3\text{-}R\text{-}NH_3)MX_4]$, where R can be aliphatic or aromatic. The two unit cell parameters that are parallel to the inorganic layers are of a length that is comparable to the cubic perovskite lattice parameter a_p. There are two different factors observed, the more common one being $\sqrt{2} \times a_P$ and the lesser one $2 \times a_p$. Inorganic-organic hybrids are classified as having either the $2a_p \times 2a_p$ or $\sqrt{2}a_p \times \sqrt{2}a_p$ superstructure (Mitzi, 1999a). The 2-D corner-sharing layers can also be viewed as "single layers of <100> orientated perovskite sheets separated by bilayers of organic ammonium cations" (Mitzi, 1999a). Hence, when discussing inorganic-organic hybrids that have either staggered or eclipsed 2-D layers, they will be referred to as having the layered perovskite-type motif. Inorganic-organic hybrids that have this motif have the potential of forming natural quantum well structures[1] when combined with Pb^{2+} and I^- (Papavassilliou et al, 1994; Hong et al, 1992a; Tanaka et al, 2005).

[1] Quantum well structures, also known as multiple quantum well structures (Atkins et al, 2006), are materials that combine different bandgaps within a structure, that alternate in a regular fashion. Here, the lead iodide forms a 2-D semiconductor layer, which alternates with the dielectric RNH_3 layer (Era et al, 1997)

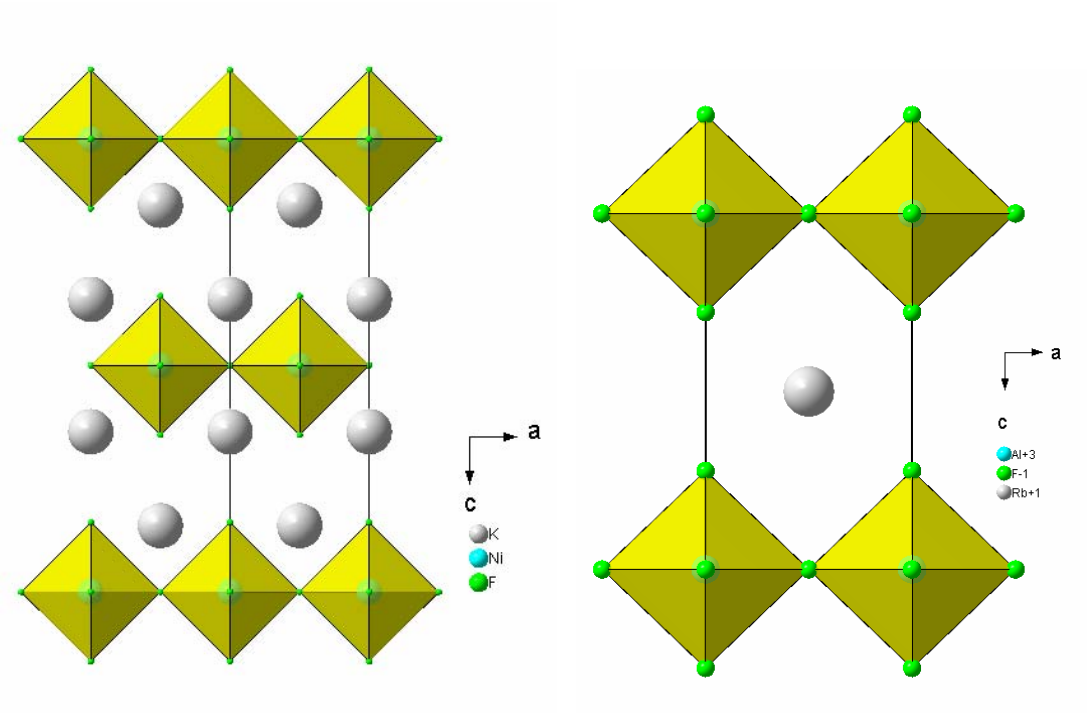


Figure 1.2: The unit cell of the inorganic compound K_2NiF_4, that is the archetype for the 2-D layered perovskites that have staggered layers (left), and $RbAlF_4$, that is the archetype of the eclipsed inorganic layers (right).

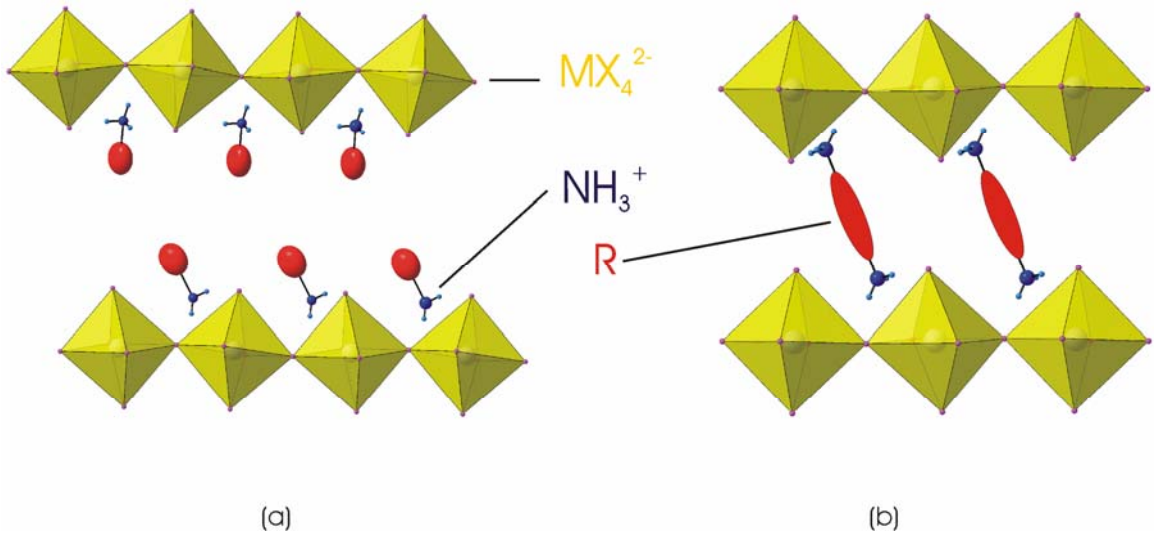


Figure 1.3: Schematic Representation of single-layer perovskites with (a) monoammonium (R-NH_3^+) or (b) diammonium (^+H_3N-R-NH_3^+) organic cations.

As in the 3-D cubic perovskite case, we can determine numerically the size of the organic cation we can fit in between the inorganic layers. The boundary is defined not by volume but by the cross sectional area of the quadrilateral formed by the four axial or terminal halides of the K_2NiF_4

or $RbAlF_4$ structure, labelled as the quadrilateral ABCD in Figure 1.4a. If this quadrilateral is shaped like a square in the case of the K_2NiF_4 or $RbAlF_4$ structures, then the side of the square is simply twice the length of the largest possible bond length between the lead and the halide. If we consider the bond to be ionic in character, then, using the values for ionic radii of Pb^{2+} (1.19 Å), I^- (2.20 Å), Br^- (1.96 Å) and Cl^- (1.81 Å) (Shannon, 1976), we get an area of 46 $Å^2$ for lead iodide. The analogous areas for $PbCl_2$ and $PbBr_2$ are 40 $Å^2$ and 36 $Å^2$ respectively.

In general however, this area described by the quadrilateral is much greater than required by the organic cation and the adjacent octahedra undergo various tilts to reduce the area and pack more efficiently. For the layered perovskite-type hybrids, two out of three possible tilts are encountered (Hatch et al, 1989); a tilt perpendicular to the inorganic sheets (θ tilt), so that adjacent corner-shared octahedra are rotated relative to each other. A geometric consequence is that the bond angle Pb-I(bridging)-Pb deviates from 180° (Figure 1.5b). If the layers are normal to the *c*-axis, then the notation would be (00θ), a tilt around the *c*-axis. The second kind of tilt is away from the perpendicular to the layers (Ψ tilt) so that the layers are corrugated in one direction. If the corrugation is along the *a*-axis as in Figure 1.5a, then the Ψ tilt is around the *b*-axis, abbreviated (0Ψ0). The net effect of a combination of these two tilts is to create a quadrilateral with a smaller area (Figure 1.4b). These distortions from the ideal square K_2NiF_4 or $RbAlF_4$ arrangement results in the closest possible packing arrangement (Figure 1.6). The tilting of the octahedra also facilitates the hydrogen bonding interactions between the ammonium group and the terminal halides. The area of the quadrilateral ABCD shown in Figure 1.4b is half of the product of the two diagonals AC and BD, measured in Angstroms (See appendix for derivation of formula).

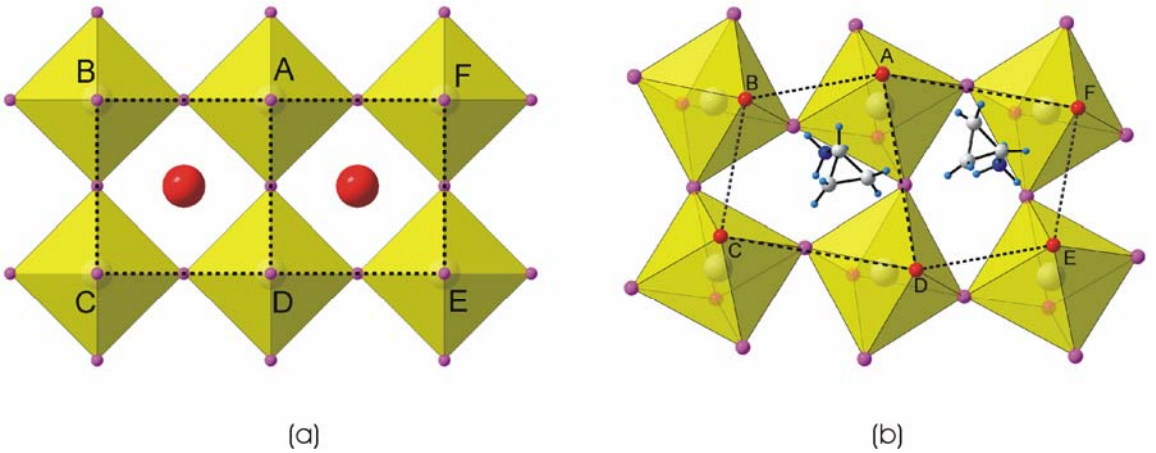


Figure 1.4: The area generated by the four terminal halides, viewed perpendicular to the 2-D layers. (a) shows the biggest possible scenario of a square, when there is no tilting of the octahedra. (b) shows the actual scenario, when both Ψ and θ tilts are observed.

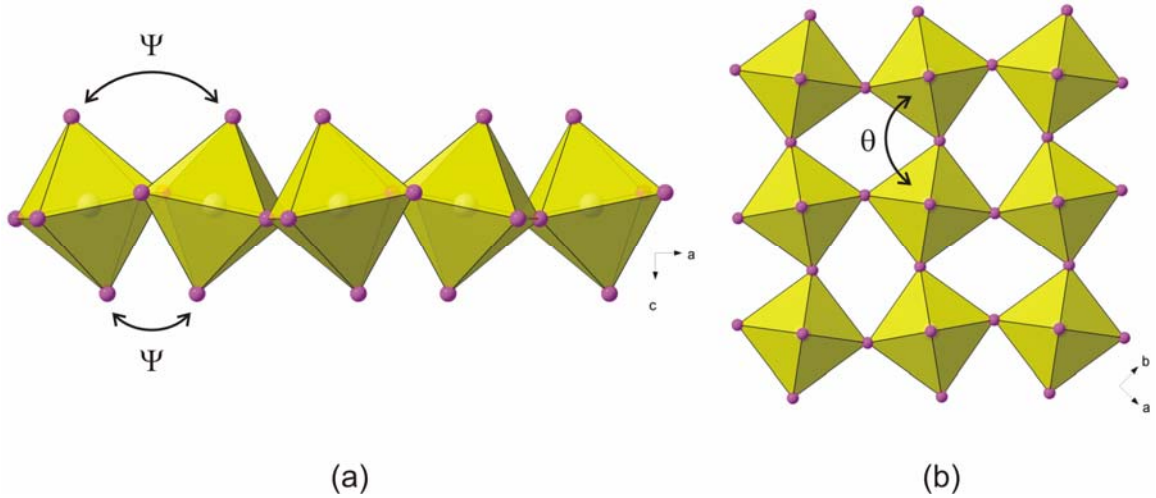


Figure 1.5: Schematic representation of the two commonly encountered tilts in the layered perovskites. (a) (0Ψ0) tilt, leading to a corrugation of the sheets in one direction; (b) (00θ) tilt, leading to a rotation of adjacent octahedra relative to each other.

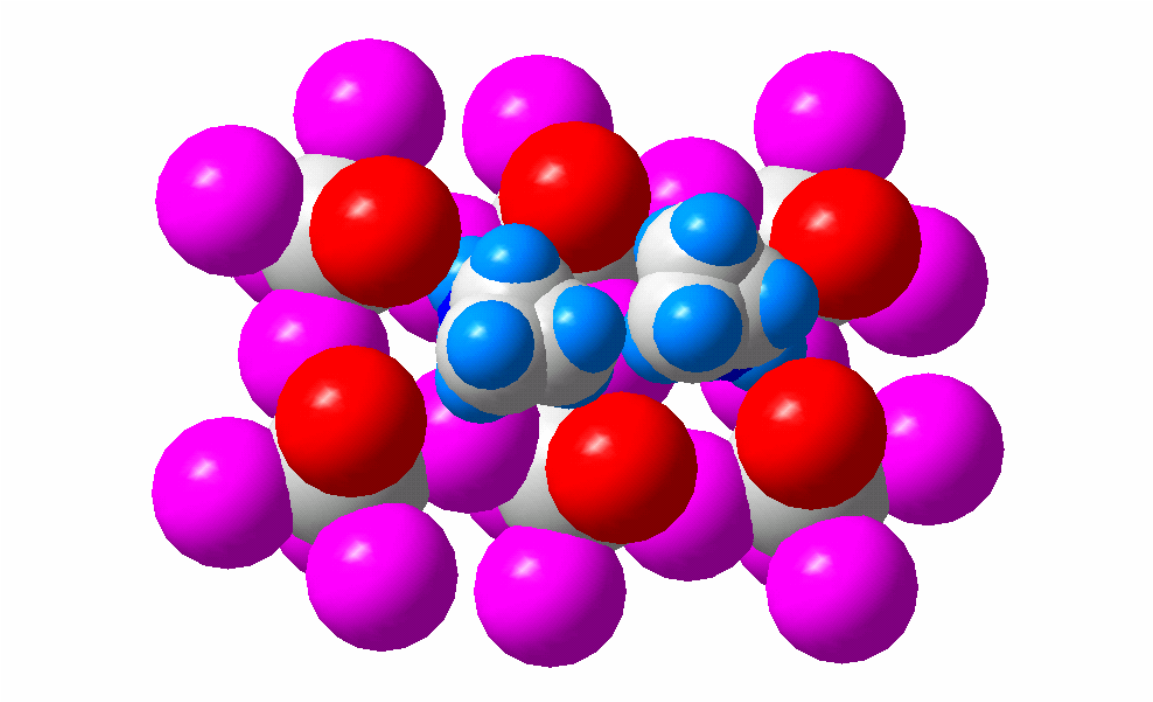


Figure 1.6: A space-filled representation of the packing arrangement of a typical inorganic-organic layered perovskite-type hybrid with atoms drawn with their van der Waals radii. The terminal iodides are shown as red coloured spheres.

1.4 Lower dimensional motifs of inorganic-organic hybrids

The most common structure type encountered in the family of inorganic-organic hybrids is the 2-D layers of corner-sharing octahedra as discussed above. However, it is possible to get motifs that comprise the sharing of two or three halides, otherwise known as edge- and face-sharing motifs. Combinations of any of the three types of sharing give a multitude of different motifs. One of the possible structural motifs also forms 2-D layers, where chains of two or three face-sharing octahedra are connected via corner-sharing on both ends (Figure 1.7). This situation can be summarized by the formula $[M_nX_{3n+1}]^{(n+1)-}$.

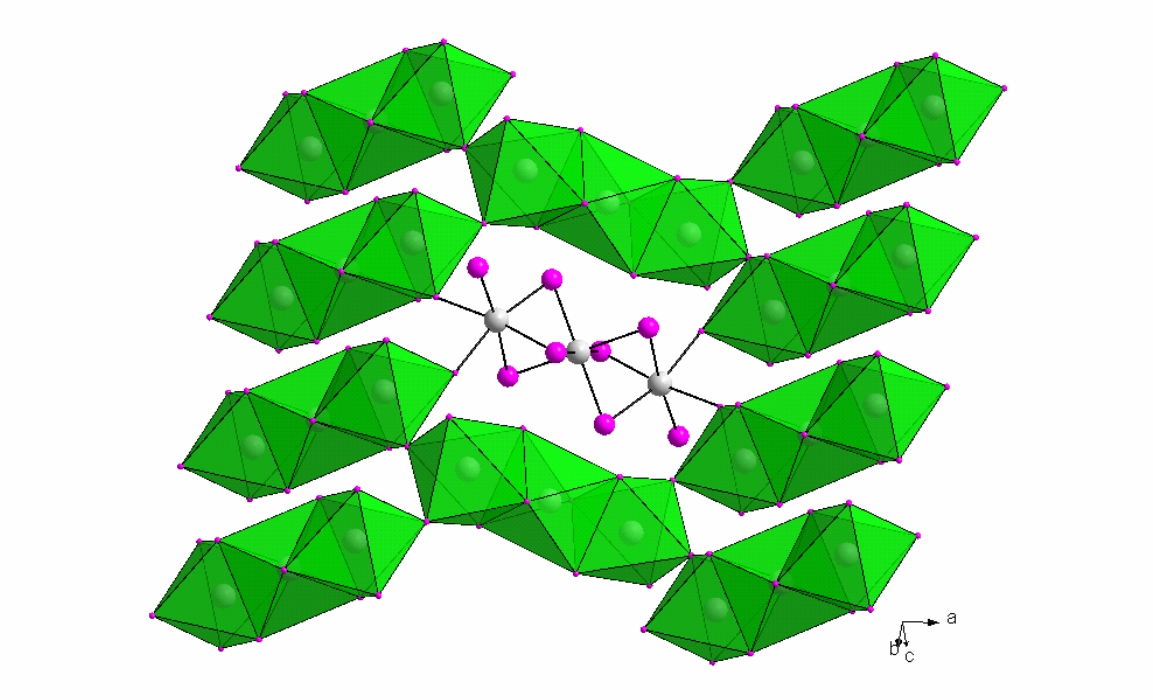


Figure 1.7: An illustration of the n = 3 $[Pb_3I_{10}]_n^{4n-}$ 2-D net.

If the space required by the R group is greater than the area provided by the 2-D type lead(II) iodide framework, then a different structural arrangement of the inorganic component is preferred, e.g. 1-D chains of inorganic metal halides. In this case, long chains of corner-sharing, edge-sharing or face-sharing MX_6 octahedra create channels within which the organic ammonium cations sit. The relative position of the halides within the octahedra is classified differently to that of the layered perovskite-type hybrids. For the corner-sharing chains, the two halides that bridge to two adjacent octahedra and the two halides that are *trans* to them are labelled the "equatorial halides". The last two halides extend out of the plane of the corner-sharing chain and are thus labelled as "axial halides" (Figure 1.8). In the edge-sharing chains, the four halides that bridge to adjacent octahedra all lie in a plane and are thus labelled as "equatorial halides". The "axial halides" are labelled in the same way as in the corner-sharing chains (Figure 1.9). In the face-sharing chains, the "equatorial halides" and the "axial halides" are labelled in the same way as in the edge-sharing chain case except that the axial halides also bridge to adjacent octahedra (Figure 1.10).

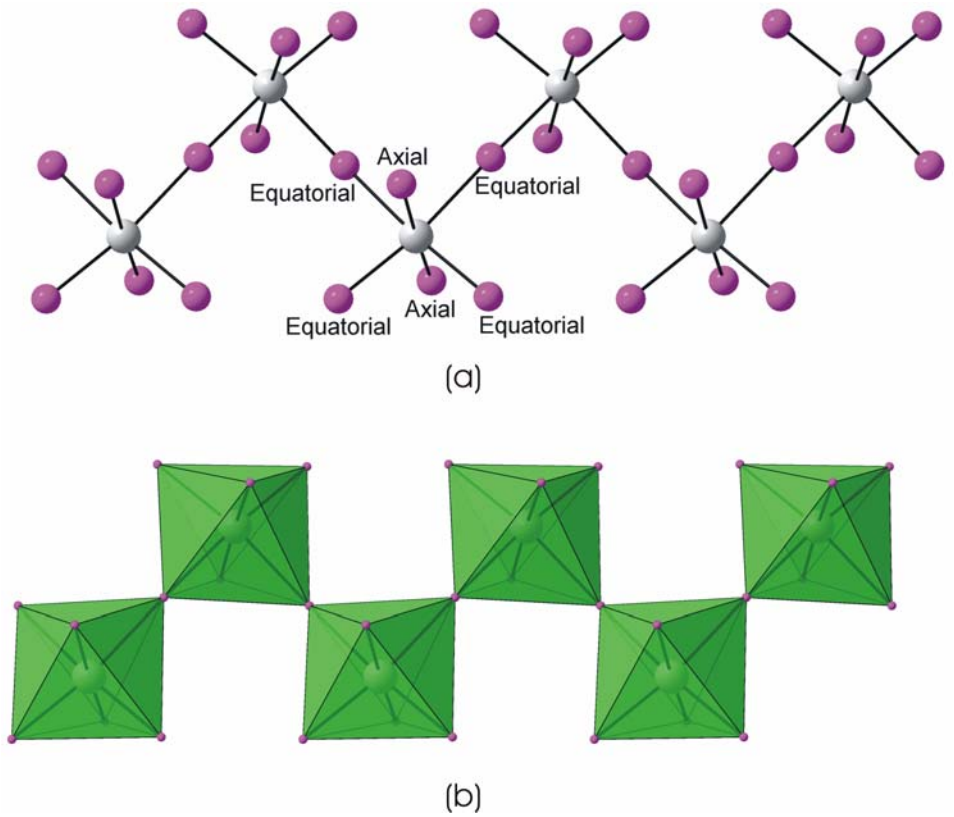


Figure 1.8: Example of a corner-sharing chain and the labelling of the halides within the octahedra.

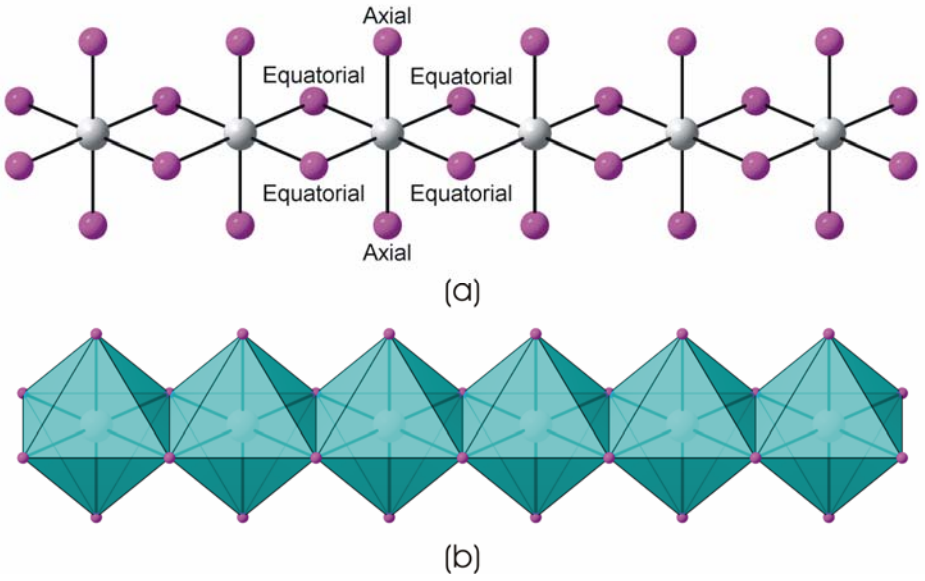


Figure 1.9: Example of an edge-sharing chain and the labelling of the halides within the octahedra.

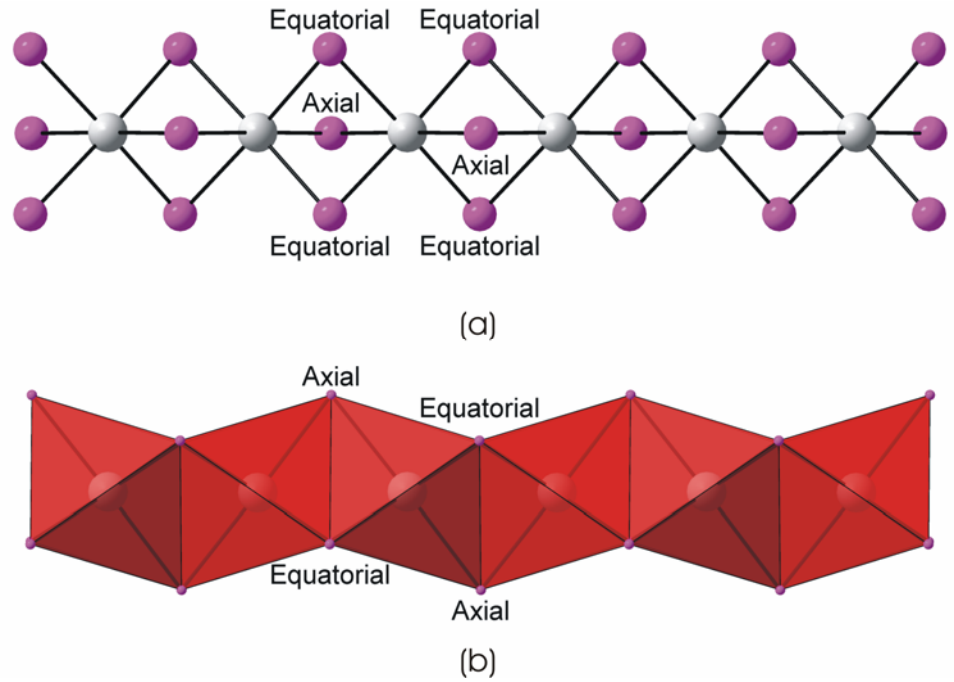


Figure 1.10 Example of a face-sharing chain and the labelling of the halides within the octahedra.

1.5 Zero-dimensional motifs

It is also possible to get 0-D structures where the octahedra and the organic cation are isolated from another. An example is $[(CH_3NH_3)_4PbI_6 \cdot 2H_2O]$, which has the anions PbI_6^{4-} and cations $(CH_3NH_3)^+$ isolated from one another and from water (Mitzi, 1999).

1.6 Hydrogen bonding in inorganic-organic layered perovskite-type hybrids

Another important determinant of the arrangement of the inorganic layers apart from the choice of the organic molecule, is the hydrogen bonding scheme between the primary ammonium head and the halides. There are four terminal and four bridging halides available to bond to the three hydrogens on the ammonium cation. However, the size of the ammonium group prevents the hydrogens from penetrating deeply into the "box" formed by the eight halides and hence only three halides are close enough to form hydrogen bonds. There are two possible scenarios: Two hydrogens can bond to the terminal halides and the third to the bridging halide (terminal halogen configuration) or the reverse case with two bridging and one terminal hydrogen (bridging halogen

configuration) (Figure 1.11). This classification of hydrogen bonding is taken from Mitzi (1999a). The length of the N---X interaction is greater than 2.2 Å and hence is classified as a weak hydogen bond (Jeffrey, 1997) with bond angles greater than 90°. Table 1.1 below gives the average distances for the three possible halides that are used, Cl, Br and I. The values where obtained from a study of the Cambridge Structural Database (CSD, June 1997 update with 167 797 entries; Allan and Kennard, 1993) done by Steiner (1998) of hydrogen bonds in organometallic crystal structures. The author excluded strongly bent geometries.

Table 1.1: Mean distances (Å) in N–H---A^- hydrogen bonds to halide ions with <(DHA) > 140°.

N–H donor	Cl^-	Br^-	I^-
D(H…A^-)	2.247(5)	2.49(2)	2.72(2)
D(N…A^-)	3.207(4)	3.44(1)	3.68(2)

From (Steiner, 1998).

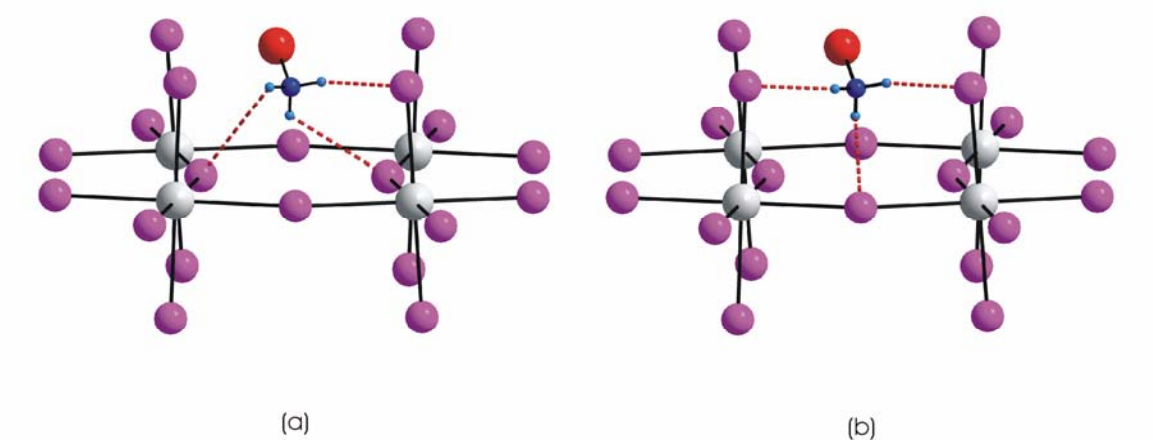


Figure 1.11: Two hydrogen bonding configurations typically observed in the $[(R\text{-}NH_3)_2MX_4]$ and $[(H_3N\text{-}R\text{-}NH_3)\ MX_4]$ type structures: (a) the bridging halogen configuration, and (b) the terminal halogen configuration.

However, there are two ways that the hydrogens can adopt either the terminal or bridging halogen configuration: The three halides to which the hydrogens bond can be at the vertices of either an equilateral triangle (equilateral configuration) or a right-angle triangle (right-angled configuration). Figure 1.12 shows the equilateral and right-angled configuration as observed in the terminal halogen configuration.

It is also important to be able to specify the position of the ammonium group relative to the inorganic layer. Due to the rotation of the MX_6 octahedra relative to each other, the area enclosed by four bridging halides is shaped like a parallelogram. In projection, the ammonium group is contained within this parallelogram defined by the four bridging halides, shown in green in Figure 1.12. By projection onto this parallelogram the ammonium group is found in proximity to either an acute or an obtuse angle of the parallelogram. There is a correlation between the position of the ammonium group and the type of hydrogen bonding configuration: If the ammonium group is in the acute angled position, the ammonium group has the right-angled configuration and if the ammonium group is in the obtuse angled position, the ammonium group has the equilateral configuration.

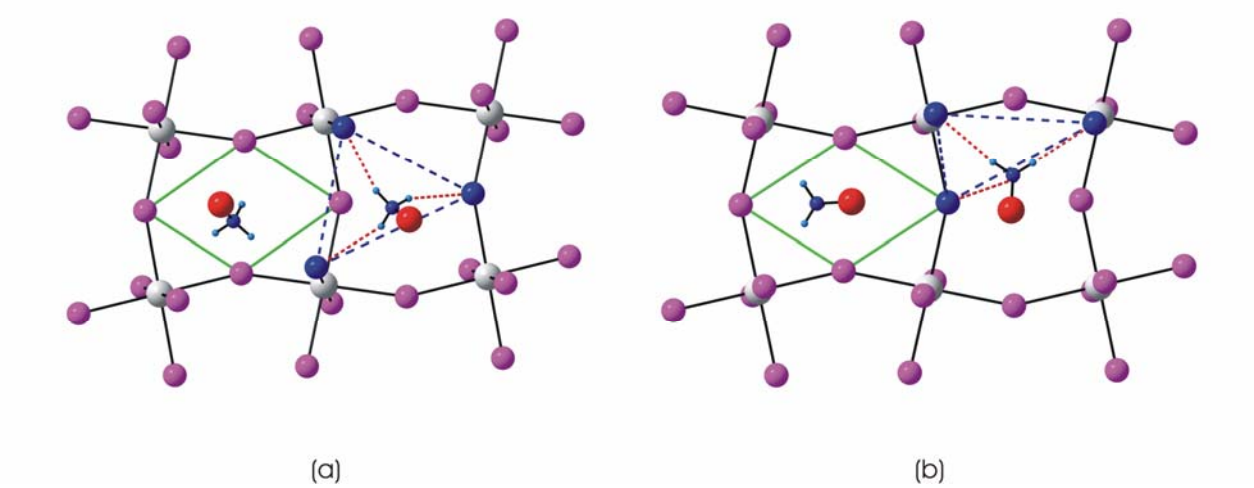


Figure 1.12: Two types of terminal halogen configuration: (a) equilateral configuration, where the three halides involved in hydrogen bonding are at the vertices of an equilateral shaped triangle (dashed blue lines) and (b) right-angled configuration, where the halides are at the vertices of a right-angled triangle. The obtuse angled position is shown in (a) and the acute angled position in (b) relative to the parallelogram (green lines).

From the picture in Figure 1.13, it is clear that the hydrogen bonding is associated with the corrugation of the MX_6 octahedra along a given direction. The bridging halides deviate from the plane and the terminal halides tip the octahedra towards the ammonium group.

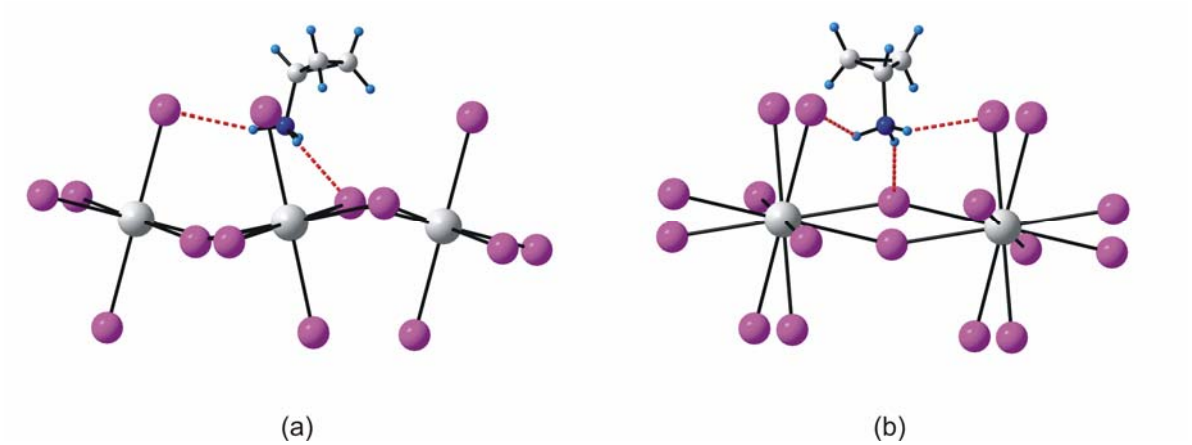


Figure 1.13: The correlation between the hydrogen bonding interactions and the tilting of the PbI_6 octahedra in the layered perovskite-type hybrid $[(C_3H_5NH_3)_2PbI_4]$.

1.7 Hydrogen bonding in non layered inorganic-organic hybrids

The classification of hydrogen bonds in inorganic-organic hybrids that do not have the layered perovskite-type motif is performed in a similar manner. If the acceptor halide atoms are predominantly in the axial position of the octahedra, then this geometry is referred to as "axial halogen configuration" and vice versa, if there are more hydrogen bonds to halides in equatorial than in axial positions, "equatorial halogen configuration". Bifurcated and trifurcated hydrogen bonds exist in these compounds.

1.8 Aims

The aims of this study was to use the structural diversity offered by organic ammonium compounds and observe how the supramolecular structure of the resulting inorganic-organic hybrid gets influenced. For simplicity, the inorganic framework was chosen to consist of the metal lead and the halides chlorine, bromine and iodine only. When the organic ammonium cation consisted of simple alkylammonium or alkyldiammonium compounds, ($C_nH_{2n+1}NH_3$) and ($H_3NC_nH_{2n}NH_3$), then the halide used was restricted to I, and when the R group consisted of aromatic and other hydrocarbons, (R-NH_3), then all three halides were used.

Chapter 2 Literature Survey

2.1 First synthesis and structure determination

The first reported synthesis of compounds with the general formula $[(R\text{-}NH_3)_2MX_4]$ was by Remy and Laves (1933). They prepared a series of compounds containing copper chloride and short alkyl chains with amino groups. The compounds made are listed in Table 2.1, which is adapted from their paper.

Table 2.1: The composition of various $CuCl_x$ inorganic-organic hybrids with simple alkylammonium chains.

Ratio of the two components in aqueous solution				
$CuCl_2$:AmCl =	1:1	1:2	1:3	1:6
Am = CH_3NH_3, $CH_3CH_2NH_3$ $CH_3CH_2CH_2NH_3$ $CH_3CH_2CH_2CH_2NH_3$	$[(Am)_2CuCl_4]$			
Am = $(CH_3)_2NH_2$	$[(Am)CuCl_3]$	$[(Am)_2CuCl_4]$		$[(Am)_3CuCl_5]$
Am = $(CH_3)_3NH$	$[(Am)CuCl_3]\cdot H_20$ or $[(Am)CuCl_3]$			$[(Am)_3CuCl_5]$
Am = $(CH_3)_4N$	$[(Am)_2CuCl_4]$			

The molecular formula of the resulting crystals reported in the paper was determined; electrolytically for copper, gravimetrically for chlorine and via titration for the ammonium component. More compounds were made by the authors from a non-aqueous solution containing alcohol or acetone which were not reported previously but confirmed to be $[((CH_3)_3NH)_3Cu_2Cl_7]$, $[((CH_3)_3NH)_2CuCl_4]$, $[((CH_3)_3CHNH)CuCl_3]$ and $[((CH_3)_3CHNH)_2CuCl_4]$. The results of the combination of the mono-ammonium compounds with copper(II) chloride are significant as they all have the molecular formula $[(Am)_2CuCl_4]$, regardless of the ratio of the reactants, and are possibly all layered perovskite-type hybrids.

The unit cell constants of the layered perovskite-type hybrid $[(CH_3NH_3)_2CuCl_4]$ were determined in 1933 by Greenwood (1933). They are a = 18.55 Å, b = 7.30 Å and c = 7.54 Å. The results were confirmed by Willett (1964) from Weissenberg and precession camera photographs. From the systematic absences, the two possible space groups were either *Cmca* or *C2ca* (*Aba2*). The

values for the *b*-axis and *c*-axis are characteristic of copper(II) chloride layered perovskites and the value for the *a*-axis suggests two complete inorganic layers per unit cell. The lattice constants for $[(C_2H_5NH_3)CuCl_4]$ were reported by Willett in the same paper to be a = 21.18(2) Å, b = 7.47(1) Å and c = 7.35(1) Å with the space group *Pbca*, which is commonly encountered in lead(II) iodide layered perovskites. The increase in the interlayer spacing is due to the extra carbon atom in the alkyl chains. The first reported fractional coordinates and structure solution was done for the compound $[(NH_4)_2CuCl_4]$ (Willett, 1964). The lattice constants were a = 15.46(2) Å, b = 7.20(1) Å and c = 7.20(1) Å. The space group was *Cmca* and 187 reflections were recorded, 173 of which were unique. The structure of the compound was presumed to be similar to K_2CuF_4, which contains infinite sheets of corner-sharing CuF_6 octahedra. There are three unique Cu-Cl bond lengths of 2.300(5) Å, 2.332(4) Å and 2.793(5) Å. The individual octahedra are not rotated relative to each other as the Cu-Cl-Cu bridging angle is 180.0(2)°. The distances between the chlorine and nitrogen atoms are in the range 3.34 Å to 3.61 Å, which could be indicative of hydrogen bonded interactions between the eight chlorine atoms that form the "box" within which the ammonium group sits.

From a detailed literature survey it is clear that the simplest and most studied inorganic-organic hybrids with the layered perovskite-type motif are the straight chain alkylammoniums with general formula $[(C_nH_{2n+1}NH_3)_2MX_4]$ and $[(NH_3C_nH_{2n}NH_3)MX_4]$ (n = 1-18; X = Cl, Br, I; M = Cu^{2+}, Mn^{2+}, Cd^{2+}, Sn^{2+}, Pb^{2+}, Hg^{2+} and Cr^{2+} (see Table 2.2 and Table 2.3)

Table 2.2: Summary of $[(C_nH_{2n+1}NH_3)_2MX_4]$ and $[(NH_3C_nH_{2n}NH_3)MX_4]$ (n = 1-10) inorganic-organic layered perovskite-type hybrids in the literature. Numbers in superscript refer to the references listed at the end of the table.

	Cu^{2+}	**Mn^{2+}**	**Cd^{2+}**	**Sn^{2+}**	**Pb^{2+}**	**Hg^{2+}**	**Cr^{2+}**
CH_3NH_3	Cl[9, 31, 49, 86, 109, 116, 118, 123, 125, 126, 127, 141] Br[109, 125, 126]	Cl[16, 35, 37, 71, 72, 73, 76, 85, 92, 114, 117, 120, 128, 135, 136]	Cl[34, 37, 39, 69, 70, 71, 88, 89, 90, 113, 127]	I[54]	Cl[62] Br[40, 55, 62] I[62, 61, 55]		Cl[83, 132, 133]
$NH_3CH_2NH_3$							
$C_2H_5NH_3$	Cl[2,49, 109, 116, 118, 121, 123, 125, 126] Br[109, 125, 126, 140]	Cl[16, 18, 19, 27, 41, 71, 72, 114, 119] Br[137, 142]	Cl[36, 69, 70, 71, 91, 107]	Cl[26]	Cl[5]	Cl[108]	Cl[132, 133]
$NH_3C_2H_4NH_3$	Cl[24, 68, 77] Br[24]	Cl[65, 130]	Cl[69, 70, 71]				
$C_3H_7NH_3$	Cl[4, 14, 48, 49, 75, 109, 125, 126] Br[109, 125, 126, 140]	Cl[3, 15, 16, 19, 20, 21, 23, 28, 60, 72, 87, 93, 114, 134] Br[134, 142]	Cl[12, 17, 69, 70, 87] Br[53]		Cl[6]		Cl[131]
$NH_3C_3H_6NH_3$	Cl[1, 50, 74, 77] Br[24, 78, 140]	Cl[67, 122, 130, 138]	Cl[25, 69, 70, 71] Br[53]		Cl[7]	Cl[63]	
$C_4H_9NH_3$	Cl[42, 57, 77, 109, 118, 125, 126] Br[109, 125, 126]	Cl[13, 72, 60]		Cl[26] I[10]	I[10, 40] Br[44]		
$NH_3C_4H_8NH_3$	Cl[22] Br[22, 78]	Cl[66, 124, 138]	Cl[69, 70, 71, 130]		Cl[33] Br[45]	Cl[64]	
$C_5H_{11}NH_3$	Cl[109, 125, 126] Br[109, 125, 126]	Cl[32, 72, 60]					Cl[131]
$NH_3C_5H_{10}NH_3$	Cl[22, 77] Br[22]	C1[138]	Cl[69, 70, 71, 130]				

	Cu^{2+}	Mn^{2+}	Cd^{2+}	Sn^{2+}	Pb^{2+}	Hg^{2+}	Cr^{2+}
$C_6H_{13}NH_3$	Cl[109, 126] Br[109, 125]	Cl[82]		Cl[26]	Cl[29, 30, 52] Br[45] I[99-105]		
$NH_3C_6H_{12}NH_3$	Cl[118]				Cl[8] Br[8, 45] I[8, 43]		
$C_7H_{15}NH_3$		Cl[32, 84, 60]	Cl[84]				
$NH_3C_7H_{14}NH_3$							
$C_8H_{17}NH_3$		Cl[60]	Cl[56, 80]	Cl[26]	Cl[52] Br[58] I[41]	Cl[115]	Cl[133]
$NH_3C_8H_{16}NH_3$					Br[45, 58]		
$C_9H_{19}NH_3$	Cl[47]	Cl[32, 41, 60, 110]	Cl[29]		Cl[29, 46] I[11]	Cl[115]	
$NH_3C_9H_{18}NH_3$							
$C_{10}H_{21}NH_3$	Cl[79, 109, 125, 126, 139]	Cl[59, 72, 89, 106, 111, 139]	Cl[51, 81, 139]	Cl[26]	Cl[52] Br[45] I[94-98]	Cl[112]	
$NH_3C_{10}H_{20}NH_3$							Cl[133]

Key to references in Table 2.2

1) Phelps et al, 1976.
2) Steadman and Willett, 1970.
3) Peterson and Willett, 1972.
4) Barendregt and Schenk, 1970.
5) Geselle and Fuess, 1997.
6) Meresse and Daoud, 1989.
7) Corradi et al, 1999.
8) Mousdis et al, 1999.
9) Pabst et al, 1987.
10) Mitzi, 1996.
11) Nagapetyan et al, 1988.
12) Doudin and Chapuis, 1988.
13) Depmeier and Chapuis, 1979.
14) Doudin and Chapuis, 1990.
15) Depmeier, 1981.
16) Depmeier et al, 1977.
17) Chapuis, 1978.
18) Depmeier, 1977.
19) Brunskill and Depmeier, 1982.
20) Steurer and Depmeier, 1989.
21) Harris et al, 1994.
22) Garland et al, 1990.
23) Depmeier and Mason, 1983.
24) Halversen and Willett, 1988.
25) Willett, 1977.
26) Yin and Yo, 1998.
27) Depmeier and Heger, 1978.
28) Depmeier and Mason, 1978.
29) Kammoun and Daoud, 1997.
30) Kammoun et al, 1996a.
31) Pabst et al, 1996.
32) Flandrois et al, 1995.
33) Courseille et al, 1994.
34) Chapuis et al, 1976.
35) Heger et al, 1976.
36) Chapuis, 1977.
37) Couzi et al, 1977.
38) Peyrard and Perret, 1979.
39) Kind, 1977.
40) Matsuishi et al, 2004.
41) Wortham et al, 2002.
42) Xiao et al, 2005.
43) Goto et al, 2003.
44) Kato et al, 2003.
45) Matsui et al, 2002.
46) Kammoun et al, 1996b.
47) Ning, 1995.
48) Jahn et al, 1994.
49) Jahn et al, 1989.
50) Phelps et al, 1976.
51) Kind et al, 1979.
52) Lee et al, 2000.
53) Ishihara et al, 1996.
54) Mitzi et al, 1995.
55) Tanaka et al, 2003.
56) Chanh et al, 1983.
57) Yamazaki, 1977.
58) Kitazawa et al, 2006.
59) Guillaiume et al, 1989.
60) Depmeier, 1979.
61) Hirasawa et al, 1994.
62) Poglitsch and Weber, 1987.
63) Spengler et al, 1998.
64) Amami et al, 2002.
65) Tichý et al, 1978.
66) Tichý et al, 1980.
67) Crowley, et al, 1982.
68) Birrell and Zaslow, 1972.
69) Levstik et al, 1976.
70) Blinc et al, 1977.
71) Tello et al, 1977.
72) Arend et al, 1973.
73) Knorr et al, 1974.
74) Soos et al, 1977.
75) Kempen et al, 1977.
76) Kind and Roos, 1976.
77) Snively et al, 1981.
78) Snively et al, 1982.
79) Koželj et al, 1981.
80) Ricard et al, 1985.
81) Ricard et al, 1984.
82) Van Oort and White, 1985.
83) Rahman et al, 1982.
84) White et al, 1983.
85) White et al, 1982.
86) White and Staveley, 1982.
87) White et al, 1981.
88) Blinc et al, 1978.
89) Seliger et al, 1976.
90) Chapuis et al, 1975.
91) Peyrard and Perret, 1979.
92) Heger et al, 1975.
93) Depmeier and Mason, 1982.
94) Xu et al 1991a.
95) Xu et al, 1991a.
96) Xu et al, 1991c.
97) Ishihara et al, 1989.
98) Hirasawa et al, 1993.
99) Kataoka et al, 1993a.
100) Kondo et al, 1998a.
101) Shibuya et al, 2002.
102) Tanaka et al, 2002.
103) Kondo et al, 1998b.
104) Kataoka et al, 1993b.
105) Tanaka et al, 2005.
106) Ciajolo et al, 1976.
107) Moral and Rodriuez, 1997.
108) Salah et al, 1983a.
109) Colpa, 1972.
110) Vacatello and Corradini, 1974.
111) Vacatello and Corradini, 1973.
112) Busico et al, 1979.
113) Seliger et al, 1976.
114) Bocanegra et al, 1975.
115) Busico et al, 1979.
116) Willett et al, 1967.
117) Lehner et al, 1975.
118) Whealy et al, 1959.
119) Depmeier, 1976.
120) Foster and Gill, 1968.
121) Mostafa et al, 1977.
122) Baberschke et al, 1977.
123) Heygster and Kleeman, 1977.
124) Hagen et al, 1977.
125) Bloembergen, 1977.
126) Bloembergen, 1976.
127) Stoelinga and Wyder, 1976.
128) Brinkmann et al, 1976.
129) Arend et al, 1976a.
130) Arend et al, 1976b.
131) Stead and Day, 1982.
132) Bellitto and Day, 1978.
133) Bellitto and Day, 1976.
134) Groenendijk et al, 1979.
135) Heger et al, 1973.
136) van Amstel and de Jongh, 1972.
137) Riedel and Willett, 1975.
138) Guillaume et al, 1989.
139) Wang et al, 1999.
140) Willett and Extine, 1973a.
141) Drumheller et al, 1972.
142) Willett and Extine, 1973b.

2.2 Inorganic-organic layered perovskite-type hybrids $[(C_nH_{2n+1}NH_3)_2MX_4]$ with simple alkylammonium chains

The $[(C_nH_{2n+1}NH_3)_2MX_4]$ materials, abbreviated C_nMX, often exhibit a range of temperature-dependant structural transitions that can be associated with changes in the ordering and hydrogen bonding of the organic cations. Further, the conformation of the inorganic layers can change between eclipsed and staggered at the phase transitions and the degree of distortion of the octahedral geometry decrease with increasing temperature. The structural phase transitions observed can be displasive phase transitions, associated with conformational changes within the ammonium chains or order-disorder transitions of the alkyl ammonium chains along their longitudinal axis. The latter ultimately leads to a "quasi-melting" of the hydrocarbon part (Chanh et al, 1989) in the highest temperature phases. The order-disorder transition is the only one observed when $n \leq 2$ and both types of transition have been reported in chain lengths when $n \geq 3$. The chain-melting transition is the major transition, usually the last one observed and with the highest enthalpy. Strikingly the crystal system of the structure often changes from monoclinic at the low temperature to orthorhombic at room temperature and finally tetragonal at the high temperature (Mitzi, 1999a). The sequence generally holds for most alkyl chain lengths. The nature of the phase transitions also depend on the packing arrangement of the alkyl chains. They can be either interdigitated or non-interdigitated and can be tilted at various angles and directions relative to the inorganic layers. The packing of the chains is often metal dependant, as in $C_{10}CdCl$, where the non-interdigitated chains on opposite sides of the $[CdCl_4]^{2-}$ layers are tilted at +40° and -40° relative to the normal of the inorganic layers in the compounds lowest temperature phase (Kind et al, 1979). This type of packing is not seen in the analogues compounds $C_{10}MnCl$ (Ciajolo et al, 1976) (Cambridge Structural Database (CSD) ref. code: DECAM) and $C_{10}CuCl$ (Koželj et al, 1981), where the chains are all parallel in one direction, tilted at approximately +40° relative to the inorganic layers. Interdigitated chains are present in the compounds that offer the largest separation between the metal atoms in the corner-sharing octahedra and have long chain lengths, as in C_9PbI (Nagapetyan et al, 1988) (CSD ref. code: KECKOS), which has a separation of 8.708(1) Å and 9.034(1) Å (See Figure 2.1). In $C_{10}MnCl$ for example, the separation is only 7.213(8) Å and 7.337(2) Å (Ciajolo et al, 1976).

There are three different systems of nomenclature used in the literature to designate the various phases. Some authors designate the phase stable at highest temperature with either Roman Numeral I or the greek letter α, the next lowest temperature phase II or β, and so on. This method works well when there are many phase transitions, as in C_3MnCl, which has six phases identified (Depmeier et al, 1977). In this survey, roman numerals will be used throughout.

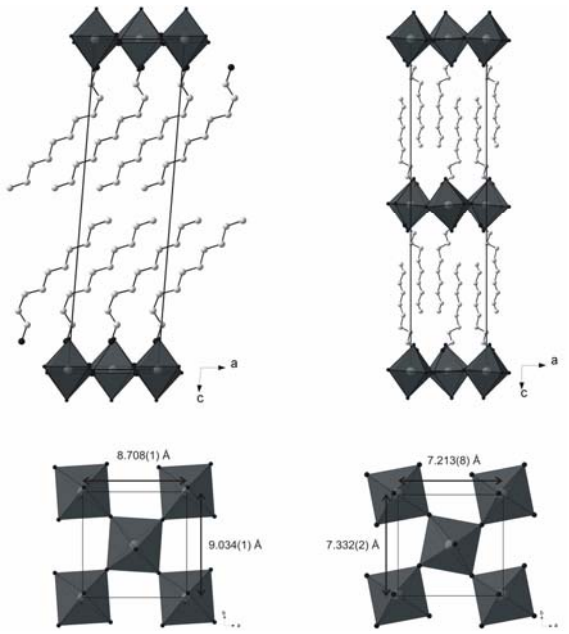


Figure 2.1: The tilted and non-interdigitated decylammonium chains in $C_{10}MnCl$ (left). The non-tilted and interdigitated nonylammonium chains in C_9PbI (right).

The rotation of the octahedra within the plane of the inorganic layers, the θ tilt, and the distortion of the octahedral geometry (bond lengths and bond angles) are both heavily dependant on the identity of the metal. The transition metals, that form the layered perovskite motif are divalent, the group 14 cations Ge, Sn and Pb and have a stereochemically active lone pair where the strength of the stereoactivity increases from Ge to Pb (Mitzi, 1996). In the layered perovskites C_4MI (M = Ge, Sn and Pb), the geometry of the GeI_6 octahedra (Ge-I: 2.837(2) Å to 3.217(2) Å; I-Ge-I: 174.46(7) to 175.38(9)°) is more distorted compared to PbI_6 (Pb-I: 3.175(2) Å to 3.200(2) Å; I-Pb-I: 180°) and SnI_6 (Sn-I: 3.133(1) Å to 3.160(2) Å; I-Sn-I: 180°) (Mitzi, 1996). The trend in the bridging angle between adjacent octahedra, which defines the θ tilt, is a decrease in the angle from 166.27(8)° (I-Ge-I) to 159.61(5)° (I-Sn-I) to smallest 155.19(6)° (I-Pb-I).

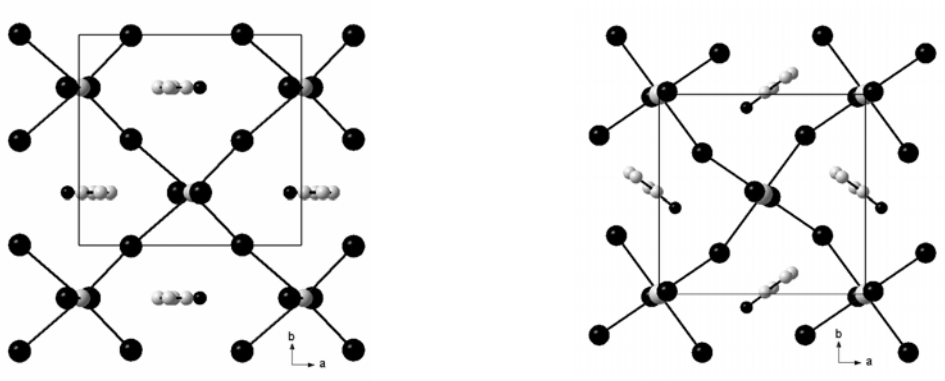


Figure 2.2: The effect of the identity of the metal on the θ tilt of the octahedra is seen in the compounds C_4GeI (left) and C_4SnI (right). The (OOθ) tilt is 13.73° in the layered perovskite-type hybrid with Ge and 20.39(5)° with Sn.

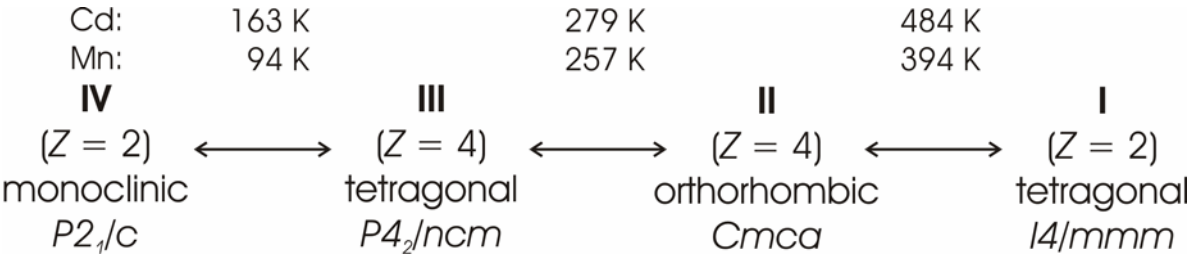
Another structural feature that is dependant on the chain length is the type of hydrogen bonding configuration. For n = 1, both the terminal halogen configuration and bridging halogen configuration are possible. However, for $n \geq 2$, the bridging halogen configuration is sterically unfavourable as it would bring the second carbon atom too close to a terminal halide and hence the terminal halogen configuration is the only configuration observed for longer alkyl chains.

2.2.1 Phase transitions in inorganic-organic layered perovskite-type hybrids $[(C_nH_{2n+1}NH_3)_2MX_4]$ with $n \leq 3$ and M = Mn and Cd

The complete sequence of phase transitions for $[(CH_3NH_3)_2CdCl_4]$, C_1CdCl, has been elucidated by many techniques and is summarized in Scheme 2.1 below. The compound has three phase transitions and the phases are labelled **I** through **IV** with decreasing temperature. The phase sequence is unusual as it goes through a tetragonal phase, **III**, before terminating at the lowest temperature monoclinic phase, **IV**. Only the single crystal data for the orthorhombic phase (**II**) (CSD ref. code: MATCCD) and tetragonal phase (**III**) (CSD ref. code: MATCCD01) are reported in the CSD. The details of the structural phase transitions between the four different phases were summarized by Couzi et al (1977) and are detailed below. In the highest temperature tetragonal phase **I**, the ammonium group has a bridging halogen configuration. The methylammonium cations are tilted randomly in four different directions, with a 1 in 4 probability of being in any particular direction. The methylammonium cations are disordered over the four potential wells. A disorder-order phase transition occurs at 484 K from phase **I** to

phase **II**, where the methylammonium cation is locked or "frozen" in one potential well, which is then favoured. There is no change in the hydrogen bonding configuration during this second order phase transition from **I** to **II**. The transition to phase **III** is first-order and such that there is now a 1 in 2 probability of the methylammonium cation being oriented in any one direction. SC-XRD results show a superposition of two orientations of the $CH_3NH_3^+$ cations. The X-Ray results give no indication of the type of hydrogen bonding configuration due to the five hydrogen positions in the structure. However, by performing ^{14}N NMR and Raman investigations (Blinc et al, 1978), the authors conclude that no changes in the hydrogen bonding configuration occur. Finally, the third phase transition to the monoclinic phase **IV** is first order and the cations are "frozen" into the terminal hydrogen bridging configuration.

The manganese analogue, C_1MnCl, exhibits the same sequence and has been studied via neutron diffraction (Heger et al, 1975), optical birefringence (Knorr et al, 1974), ^{35}Cl Nuclear Quadropole resonance (Kind and Roos, 1976) and P-XRD (Depmeier et al, 1977).



Scheme 2.1 The inter-relationship between the four phases of C_1CdCl and C_1MnCl as a function of temperature.

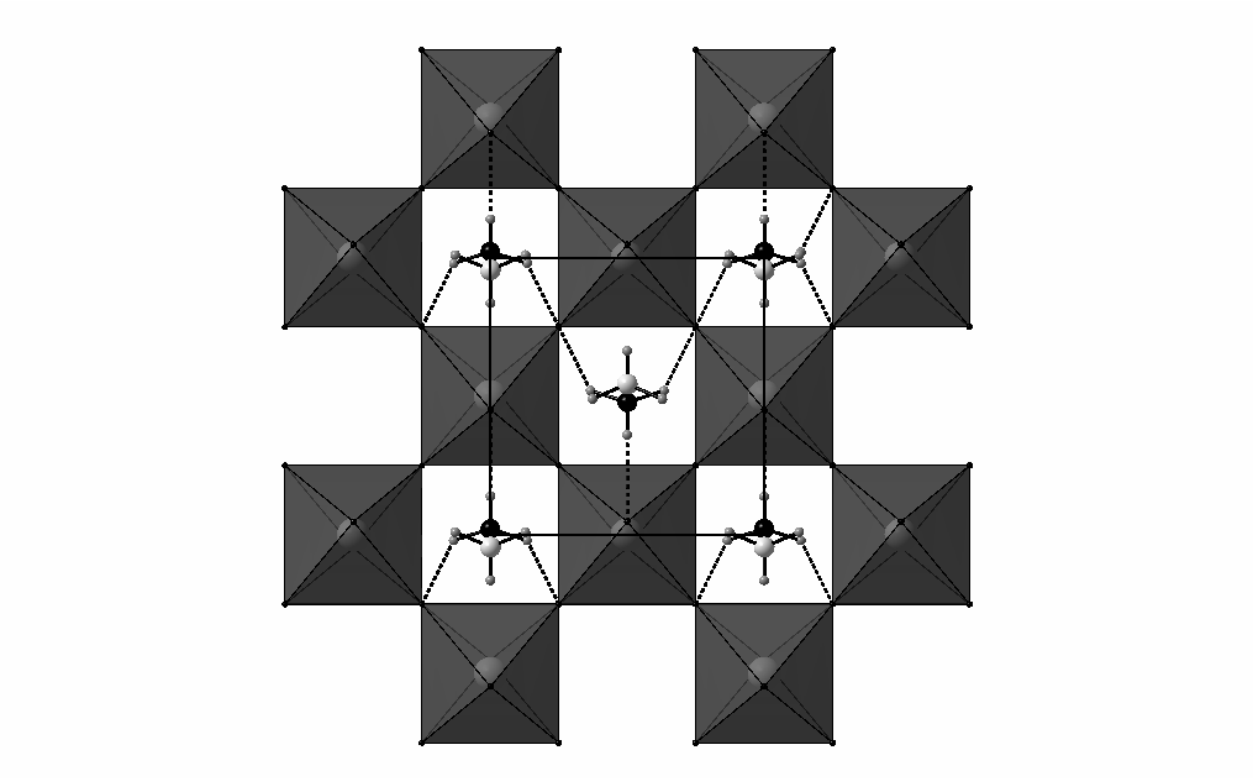


Figure 2.3: The hydrogen bonding interactions of the inorganic-organic layered perovskite-type hybrid with methylammonium and cadmium(II) chloride in phase **II**.

The ethylammonium layered perovskite, $[(CH_3CH_2NH_3)_2CdCl_4]$, C_2CdCl, displays only two phase transitions, at 114.2(9) K and 216.2(5) K, and decomposes at 450 K. Only the second phase transition has been studied by SC-XRD and corresponds to a first order transition from an orthorhombic phase, **II**, with space-group *Pcab*, to an orthorhombic phase, **I**, with space-group *Bmab* (Chapuis, 1977). C_2CdCl has no higher temperature phase with tetragonal symmetry. The structures of both phases **I** and **II** are reported in the CSD (EAMCDC01 and EAMCDC respectively), i.e. the structure of phase **III** has still to be determined. In phase **II**, the $CH_3CH_2NH_3^+$ cation is ordered (Figure 2.4). In the highest temperature phase **I**, the carbon atoms of the $CH_3CH_2NH_3^+$ cation become disordered over two positions, along the mirror plane inherent in the space group *Bmab*. The unsplit nitrogen atom has a large anisotropic displacement parameter perpendicular to the mirrorplane, about 0.28 Å (Chapuis, 1977). The two individual molecules influence the position of the terminal chlorides in the octahedra through their hydrogen bonding interactions. The anisotropic displacement parameters of the terminal chlorides are significantly elongated along the crystallographic *a*-axis (Figure 2.4). The Ψ and θ tilt of the

$CdCl_6$ octahedra increase by 1° and decrease by 5.5° respectively when changing from phase **II** to phase **I**. Phase **I** has a more regular, almost checkerboard-like pattern of $CdCl_6$ octahedra.

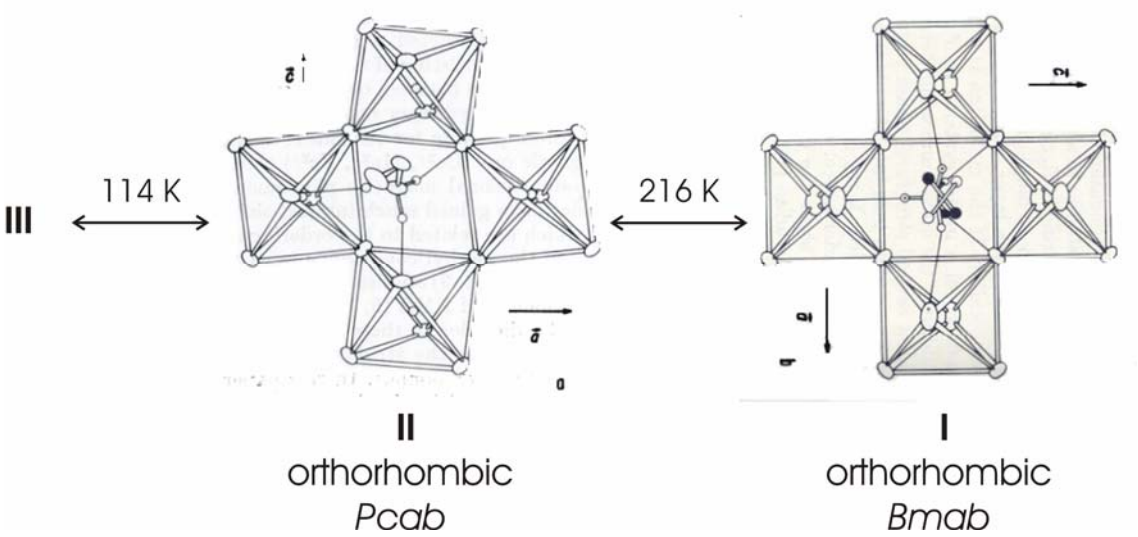


Figure 2.4: Phase **II** of C_2CdCl and its terminal halogen configuration. The ethylammonium cation is ordered in this phase. Phase **I** has the same ethylammonium cation disordered over two positions. The SC-XRD structure of phase **III** has not been determined. Figure adapted from Peyrard and Perret, 1979.

C_3CdCl has two phase transitions, summarized in Scheme 2.2 below. Phase **II** that exists between 180 K and 158 K is unique, as it is an intermediate modulated phase (Doudin and Chapuis, 1988). This intermediate phase is also observed in C_3MnCl (Depmeier and Mason, 1982). The orthorhombic phase **I** of C_3CdCl (Chapuis, 1978) (CSD ref. code: PRACDC) has two carbon atoms disordered across a mirrorplane along the *a*-axis (Figure 2.5). The incommensurate phase **II** shows large displacement amplitudes of the Cd and Cl atoms along the *c*-axis (Doudin and Chapuis, 1988) (CSD ref. code: PRACDC02). The final phase transition is a disorder-order transition at 158 K, where the propylammonium cation is now "locked" into one of the previous two equivalent positions. However, the middle carbon atom remains disordered in phase **III** (Chapuis, 1978) (CSD ref. code: PRACDC01).

III	158 K	**II**	180 K	**I**
(*Z* = 4)	⟷	(*Z* = 2)	⟷	(*Z* = 2)
orthorhombic		orthorhombic		orthorhombic
Pbca		*Abma*		*Abma*
a = 7.568(5)		*a* = 7.585(5)		*a* = 7.607(3)
b = 7.359(1)		*b* = 7.359(1)		*b* = 7.370(3)
c = 25.515(8)		*c* = 25.053(6)		*c* = 25.184(6)
PRACDC01		PRACDC02		PRACDC

Scheme 2.2: The phase sequence of C_3CdCl and their unit cell parameters (Å).

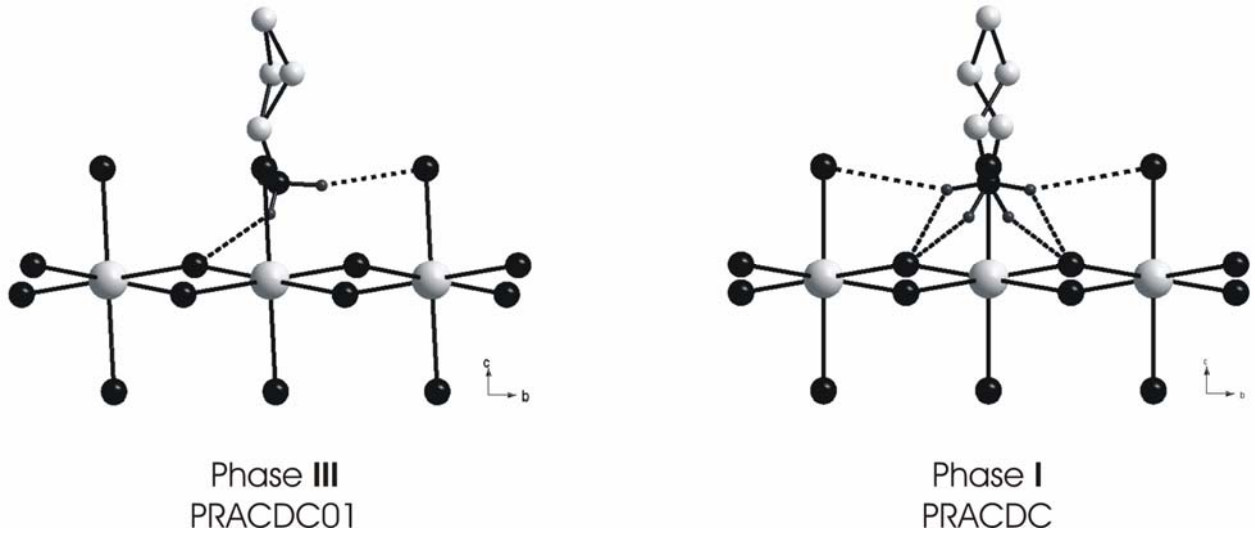


Figure 2.5: The two SC-XRD structures of phases **III** and **I** of C_3CdCl.

The phase behaviour of the layered perovskite C_3MnCl is unique in that it has the most phase transitions identified to date, three more than it's Cd analogue (Scheme 2.3 below), and a number of these are unusual, e.g. the phase transition from **IV** to **V** leads to a superstructure with a three-fold increase of the *b*-axis, **V** to **VI** is incommensurate to commensurate (Depmeier and Mason, 1983; Harris at al, 1994), **IV** to **III** goes from a commensurate to an incommensurate phase and **III** to **II** is incommensurate to commensurate (Depmeier and Mason, 1978).

VI	110 K	**V**	165 K	**IV**	344 K	**III**	396 K	**II**	446 K	**I**
(*Z* = 2)	⟷	(*Z* = 4)	⟷	(*Z* = 4)	⟷	(*Z* = 4)	⟷	(*Z* = 4)	⟷	(*Z* = 2)
ζ		ε		δ		γ		β		α
monoclinic		orthorhombic		orthorhombic		orthorhombic		orthorhombic		tetragonal
P2₁/b		*Pbna*		*Abma*		*Abma*		*Abma*		*I4/mmm*
a = 7.437(8)		*a* = 7.443		*a* = 7.458(9)		*a* = 7.39(1)		*a* = 7.40(1)		*a* = 10.465
b = 7.082(5)		*b* = 21.426		*b* = 7.169(9)		*b* = 7.25(1)		*b* = 7.34(1))		*b* = 10.465
c = 13.096(8)		*c* = 25.422		*c* = 25.61(5)		*c* = 26.72(5)		*c* = 27.45(10)		*c* = 27.500
PAMMNC13		PAMMNC17		PAMMNC01		PAMMNC26		PAMMNC04		PAMMNC11

Scheme 2.3: The phase sequence of C_3MnCl and their unit cell parameters (Å) with CSD reference codes. The greek numbering for the phases is taken from the literature.

2.2.2 Phase transitions in inorganic-organic layered perovskite-type hybrids $[(C_nH_{2n+1}NH_3)_2MX_4]$ with $n \geq 4$

The phase transitions of the compounds with longer alkyl chains, were $n \geq 10$, are of interest as they can act as models for the phase behaviour of lipid bilayers (Needham et al, 1984). Very little single-crystal work has been done on the structures of the various phases. The changes in unit cell parameters have, in general, only been inferred from P-XRD.

Table 2.3: Summary of $[(C_nH_{2n+1}NH_3)_2MX_4]$ and $[(NH_3C_nH_{2n}NH_3)MX_4]$ (n = 11-18) layered perovskite-type hybrids in the literature. Numbers in superscript refer to the references listed at the end of the table.

	Cu^{2+}	**Mn^{2+}**	**Cd^{2+}**	**Fe^{2+}**	**Pb^{2+}**	**Co^{2+}**	**Hg^{2+}**	**Cr^{2+}**
$C_{11}H_{23}NH_3$	Br^{15}	Cl^{19} Br^{15}					Cl^{20}	
$NH_3C_{11}H_{22}NH_3$								
$C_{12}H_{25}NH_3$	$Cl^{3,12,21,24}$ Br^{15}	$Cl^{3,18,21,24}$ Br^{15}	$Cl^{3,11,14,24}$	Cl^{21}	$I^{2,4,5}$		$Cl^{20,21}$	Cl^{23}
$NH_3C_{12}H_{24}NH_3$								
$C_{13}H_{27}NH_3$	Br^{15}	$Cl^{19,22}$ Br^{15}					Cl^{20}	
$NH_3C_{13}H_{26}NH_3$								
$C_{14}H_{29}NH_3$	$Cl^{3,24}$ Br^{15}	$Cl^{3,6,18,22,24}$ Br^{15}	$Cl^{3,16,24}$				Cl^{20}	
$NH_3C_{14}H_{28}NH_3$								
$C_{15}H_{31}NH_3$	Br^{15}	Cl^{19} Br^{15}					Cl^{20}	
$NH_3C_{15}H_{30}NH_3$								
$C_{16}H_{33}NH_3$	$Cl^{21,24}$ Br^{15}	$Cl^{18,21,24}$ Br^{15}	$Cl^{9,14,24}$	Cl^{21}	$I^{2,4,5}$	$Cl^{7,8}$	$Cl^{20,21}$	
$NH_3C_{16}H_{32}NH_3$								
$C_{17}H_{35}NH_3$		Cl^{19}						

	Cu^{2+}	**Mn^{2+}**	**Cd^{2+}**	**Fe^{2+}**	**Pb^{2+}**	**Co^{2+}**	**Hg^{2+}**	**Cr^{2+}**
$NH_3C_{17}H_{34}NH_3$								
$C_{18}H_{37}NH_3$	Cl^{24}	$Cl^{1,10,24}$	$Cl^{17,24}$		$I^{2,4,5}$			
$NH_3C_{18}H_{36}NH_3$								

Key to references in Table 2.3

1) Lee and Lee, 2003.
2) Venkataraman et al, 2002a.
3) Needham and Willett, 1984.
4) Barman et al, 2003.
5) Venkataraman et al, 2002b.
6) Almirante et al, 1986.
7) Ning et al, 1992a.
8) Ning et al, 1992b.
9) Chanh et al, 1989.
10) Lee at al, 2003.
11) Chanh et al, 1985.
12) Kang et al, 1993.
13) Chanh et al, 1983.
14) Ricard et al, 1985.
15) Vacatello et al, 1981.
16) Schenk and Chapuis, 1988.
17) White, 1984.
18) Vacatello and Corradini, 1973.
19) Vacatello and Corradini, 1974.
20) Busico et al, 1979.
21) Landi et al, 1977.
21) Landi et al, 1977.
22) Carfagna et al, 1977.
23) Stead and Day, 1982.
24) Wang et al, 1999.

DSC, IR and P-XRD studies on the series of compounds $[(C_nH_{2n+1}NH_3)_2MX_4]$ (M = Mn, Hg, Fe and Cu, X = Cl and Br, n = 9 - 17) has been done by Vacatello and co-workers (See Table 2.2 and Table 2.3 for details). The focus of their work was to determine the mechanism of the phase transitions and the conformations of the chains by measuring the changes in the interlayer spacing between the low- and high-temperature phases. Table 2.4 summarizes the changes in the interlayer spacing for two chain lengths and different metals. In general, they concluded that the low temperature phase has an ordered arrangement which changes to a disordered arrangement at the high temperature phase. The integrity of the inorganic layers remain practically unchanged during the solid-state phase transitions from the ordered to disordered phases (Landi et al, 1977). The disorder is mainly due to the "thermal liberation of movements around C-C bonds" (Vacatello and Corradini, 1973). Their systematic studies also show that the transition temperatures increase as the chain length increases and that the phase transitions are often reversible, with some thermal hysteresis observed (Table 2.5). The room temperature structure of

the layered perovskite $C_{10}MnCl$ is the only reported structure in the CSD that includes fractional coordinates (Ciajolo et al, 1976) (CSD ref. code: DECAM).

Table 2.4: Summary of interlayer spacing, *c*, from X-ray spectra of powders for C_nMCl (1).

n	M	*c*, Å, at 25°C	*c*, Å, at 120°C
12	Mn	30.28(5)	33.4(1)
	Cu	29.09(5)	32.0(1)
	Fe	30.23(6)	34.2(3)
	Hg	27.00(6)	29.7(2)
16	Mn	36.71(5)	41.8(1)
	Cu	36.12(5)	40.4(1)
	Fe	37.20(6)	43.3(3)
	Hg	32.96(6)	36.9(2)

(1) Taken from Landi et al, 1977.

Table 2.5: Summary of phase transition temperatures, enthalpies and entropies from DSC heating and cooling scans for C_nHgCl (1).

	Heating			Cooling		
n	*T*, K	ΔS, J K^{-1} mol^{-1}	ΔH, kJ mol^{-1}	*T*, K	ΔH, kJ mol^{-1}	ΔS, J K^{-1} mol^{-1}
8	297	0.6	2.0	289	0.6	2.1
	314	6.6	21.0	305	6.8	22.3
9	292	5.9	20.2	282	5.1	18.1
	303	6.1	20.1	296	5.4	18.2
10	318	18.3	57.5	311	19.0	61.1
11	323	19.9	61.6	317	19.4	61.2
	336	0.7	2.1	331	0.7	2.1
	476	24.6	51.7	472	17.9	37.9
12	332	27.9	84.0	326	29.3	89.9
	475	24.7	52.0	472	26.1	55.3
13	340	34.6	101.8	334	32.4	97.0
	473	26.5	60.3	470	24.5	52.1

(1) Taken from Busico et al, 1979.

The phase transitions of the C_nCdCl series have been extensively investigated via DSC for n = 6 - 18. Figure 2.6 summarizes some of the DSC results. Schenk and Chapuis (1988) found that for $n \geq 13$, there are four phase transitions, for $7 \leq n \leq 12$, two phase transitions, and there are several phase transitions for $n \leq 6$.

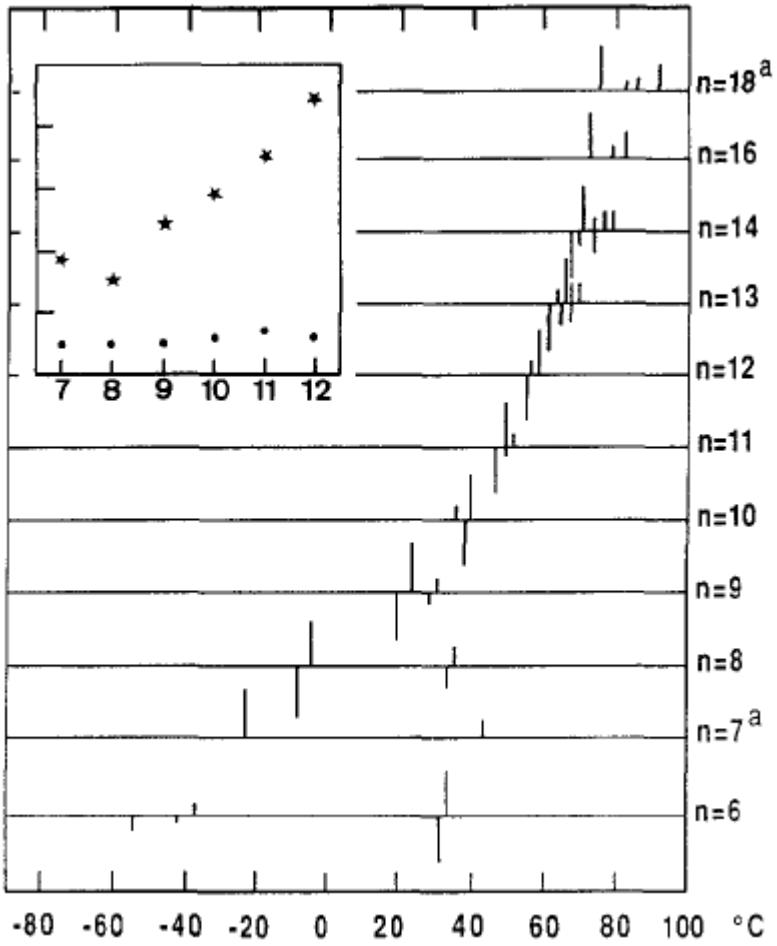


Figure 2.6: Schematic representation of DSC results of the homologous C_nCdCl4 series for n = 6 - 18. Inset: Transition enthalpies for n = 7-12. Asterisks represent the chain melting transition and filled circles the minor transition. Figure taken directly from Schenk and Chapuis, 1988.

The phase transitions of $C_{10}CdCl$, $C_{12}CdCl$, $C_{14}CdCl$, $C_{16}CdCl$ and $C_{18}CdCl$ in particular have been followed via X-ray powder diffraction to determine the unit cell parameters of their various phases (Table 2.6).

Table 2.6: Summary of unit cell parameters of C_nCdCl inorganic-organic layered perovskite-type hybrids in their various phases, n = 8 - 16.

	I	**II**	**III**	**IV**	**V**	Ref.
C_8CdCl	Orthorhombic T = 353 K *a* = 7.49(1) Å *b* = 7.58(1) Å *c* = 47.88(9) Å *Z* = 4 *Amaa*	Undetermined	Monoclinic T = 243 K *a* = 7.41(2) Å *b* = 7.53(2) Å *c* = 45.34(20) Å β = 96.55(28)° *Z* = 4 $P2_1/n$	N/A	N/A	1
$C_{10}CdCl$	Orthorhombic T = 318 K *a* = 7.460(2) Å *b* = 7.546(2) Å *c* = 54.64(2) Å *Z* = 4 *Amaa*	Orthorhombic T = 308 K *a* = 7.40(2) Å *b* = 7.54(2) Å *c* = 51.62(6) Å *Z* = 4 *Pmnn*	Monoclinic T = 294 K *a* = 7.354(1) Å *b* = 7.545(1) Å *c* = 51.620(3) Å β = 91.74(1)° *Z* = 4 $P2_1/n$	N/A	N/A	2 and 3
$C_{12}CdCl$	Tetragonal T = 360 K *a* = 5.310(1) Å *b* = 5.310(1) Å *c* = 64.31(4) Å *Z* = 2	Orthorhombic T = 334 K *a* = 7.470(7) Å *b* = 7.553(7) Å *c* = 63.50(4) Å *Z* = 4 *Amaa*	Monoclinic T = 293 K *a* = 7.463(1) Å *b* = 7.523(1) Å *c* = 59.152(8) Å β = 96.54(2)° *Z* = 4 $P2_1/n$	N/A	N/A	4
$C_{14}CdCl$	Orthorhombic T = N/A *a* = 7.46(1) *b* = 7.54(1) *c* = 35.77(6) *Z* = 2	Undetermined	Monoclinic T = N/A *a* = 7.32(3) *b* = 7.45(2) *c* = 33.60(7) β = 92.2(2) *Z* = 2	Undetermined	Triclinic T = 298 K *a* = 7.329(2) *b* = 7.482(1) *c* = 33.188(5) α = 98.19(1), β = 92.2(2), γ = 90.04(2) *Z* = 2 $P\bar{1}$	5
$C_{16}CdCl$	Tetragonal T = 360 K *a* = 5.298(2) Å *b* = 5.298(2) Å *c* = 80.03(7) Å *Z* = 2	Orthorhombic T = 354 K *a* = 7.383(18) Å *b* = 7.641(15) Å *c* = 76.45(11) Å *Z* = 4	Orthorhombic T = 348 K *a* = 7.437(10) Å *b* = 7.590(10) Å *c* = 75.24(8) Å *Z* = 4	Monoclinic T = 293 K *a* = 7.384(5) Å *b* = 7.546(11) Å *c* = 73.58(3) Å β = 96.27(6)° *Z* = 4 $P2_1/n$	N/A	6

Key to references in Table 2.6

1) Chanh et al, 1983.
2) Kind et al, 1979.
3) Ricard et al, 1984.
4) Chanh et al, 1985.
5) Schenk and Chapuis, 1988.
6) Chanh et al, 1989.

The most accurate structural data on the phase transitions of the long chain layered perovskite-type hybrids is found for $C_{10}CdCl$ (Kind et al, 1979) and can be used as a model for other long chain alkylammonium layered perovskite-type hybrids. The compound has two closely spaced first-order phase transitions, a minor one at 308 K and a major one at 312 K. In the monoclinic phase **III** (CSD ref. code DECACD), the decylammonium chains are ordered and are tilted at

+40° and -40° relative to the inorganic layer, which gives an overall herringbone-type arrangement of the chains (Figure 2.7). The asymmetric unit contains two unique decylammonium chains; chain A which has a gauche bond between the first and second carbon atom, beginning after the nitrogen atom in the chain, and chain B, which has the gauche bond between the second and third carbon atom. The remainder of the bonds within the chains have an all-*trans* conformation. In the intermediate orthorhombic phase **II**, both chains continuously switch between two equivalent positions along their long molecular axis, separated by 90° from each other. They still retain their tilting in this phase as the interlayer spacing between the layers has remained the same. This phase transition from phase **III** to phase **II** at 308 K is similar to the order-disorder transition seen previously in the short chain alkylammonium hybrids. The second phase transition at 312 K to the orthorhombic phase **I** (CSD ref. code: DECACD01) shows the "melting" transition, seen generally only in the longer chain alkylammonium hybrids and is generally the transition in the DSC scans with the greatest enthalpy, referred to as the "major" transition. This phase transition is called the "melting" transition as the bonds within the chains now have conformational freedom, akin to repeated diffusion of their gauche bonds through the whole chain. The decylammonium chains are disordered over two equivalent positions in phase **I**, related by a mirrorplane in the space group *Amaa*. The disordered chains are now tilted almost perpendicular to the inorganic layers, increasing the interlayer spacing by 1.5 Å. The electron density map in Figure 2.8 shows the positions of the carbon and nitrogen atoms in the chains. In summary, the major transition in $C_{10}CdCl$ is the chain melting transition, where the interlayer spacing increases significantly due to changes in the tilt angle of the chains; and the minor transition, where no change in the interlayer spacing is observed, a positional disorder of either the entire chain along its axis occurs or a torsional disorder of parts of the chain is observed (Needham et al, 1984).

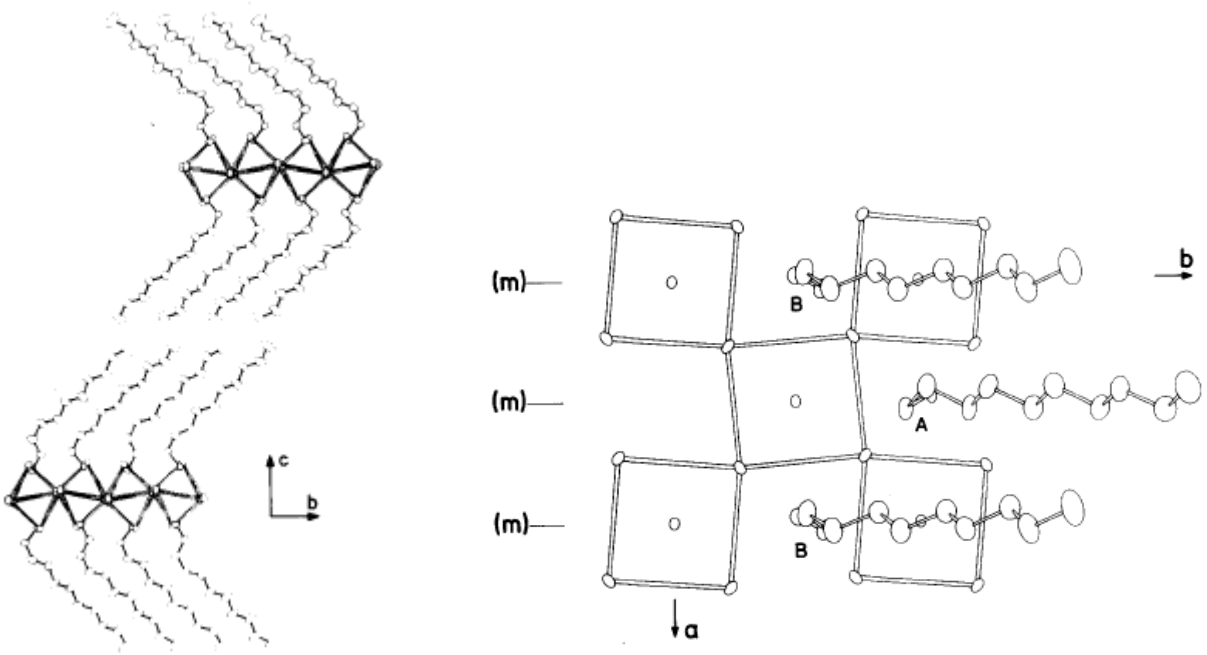


Figure 2.7 The herringbone arrangement of the tilted decylammonium chains in $C_{10}CdCl$ in the monoclinic phase **III** (left) and the two independent chains in this phase (right). Taken from Kind et al, 1979.

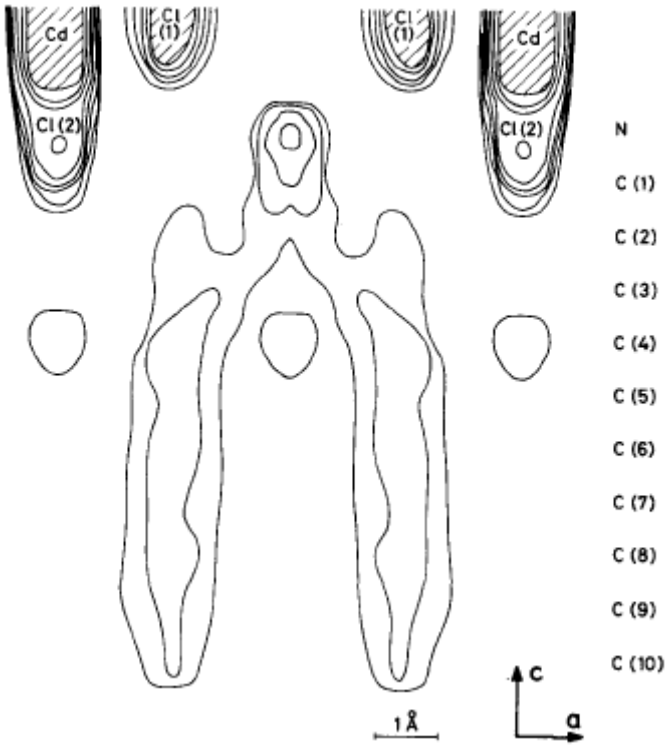


Figure 2.8 Electron density contours from the orthorhombic phase **I** of $C_{10}CdCl$. Taken from Kind et al, 1979.

2.2.3 The lead halide inorganic-organic hybrids $[(C_nH_{2n+1}NH_3)_2PbX_4]$ with the layered perovskite-type motif

The inorganic-organic hybrids C_nPbX that have the layered perovskite-type motif are the most recently studied of the inorganic-organic layered perovskite-type hybrids, as opposed to the Cd and Mn hybrids, which were the main focus for physicists and materials scientists initially. Very few single-crystal structures have been determined for the C_nPbX hybrids (See Table 2.7).

Table 2.7: Unit cell constants of the layered perovskite-type hybrids C_nPbX at room temperature.

X	n	*a* / Å	*b* / Å	*c* / Å	CSD	Reference
Cl	3	7.815(1)	25.034(3)	7.954(1)	JADLUV	Meresse and Daoud, 1989.
	6	7.78(6)	7.93(3)	38.1(4)	N/A	Lee et al, 2000.
	8	7.82(9)	7.96(3)	43.5(5)	N/A	Lee et al, 2000.
	10	7.86(2)	7.98(9)	49.0(9)	N/A	Lee et al, 2000.
I	4	8.863(2)	8.682(1)	27.570(2)	TECFAI	Mitzi, 1996.
	9	9.034(1)	8.708(1)	39.785(3)	KECKOS	Nagapetyan et al, 1988.
	10	8.968	8.667	42.51	N/A	Ishihara et al, 1990.
	12	8.882	8.529	49.02	N/A	Ishihara et al, 1990.

Interest in the C_nPbI compounds is due to their excitons[2], which are significantly enhanced as compared to $CH_3NH_3PbI_3$ and PbI_2. The exciton binding energy varies from 170 meV to 330 meV, while it is only 45 meV in $CH_3NH_3PbI_3$ and 30 meV in PbI_2 (Ishihara et al, 1990; Muljarov et al, 1995). The hybrids C_6PbI and $C_{10}PbI$ have been the most studied (Table 2.2) by measuring their electro-absorption, reflection, luminescence, magneto-absorption, magneto-reflection, absorption and emission spectra (See ref 99-105 in Table 2.2).

[2] An exciton is a "fundamental quantum of electronic excitation in condensed matter, consisting of a negatively charged electron and a positively charged hole bound to each other by electrostatic interaction. Typically, an exciton is created when a photon is absorbed in a solid; the exciton then moves through the crystal; and finally the electron and hole recombine, resulting in the emission of another photon, often at a wavelength different from the original photon." (McGraw-Hill, 2005)

2.2.4 Phase transitions in inorganic-organic layered perovskite-type hybrids $[(C_nH_{2n+1}NH_3)_2PbX_4]$

2.2.4.1 Alkylammonium chains with n = 1

The C_1PbI hybrids display a similar sequence of phase transitions as the Mn, Cu and Cd hybrids with methylammonium, being orthorhombic in the lowest temperature phase, tetragonal in the intermediate phase and finally cubic at the highest temperature (Table 2.8). Due to the larger ionic radii of the Pb^{2+} and I^- ions, the motif of the C_1PI hybrids is based on the cubic perovskite motif, described in Section 1.2 previously.

Table 2.8: Unit cell constants and other structural data of the various phases of the hybrids $[CH_3NH_3PbX_3]$ that have a 3-D cubic perovskite motif (1).

X	*T* / K	Crystal System (Phase)	Space group	*a* / Å	*b* / Å	*c* / Å	*Z*
Cl	>178.8	Cubic (I)	*Pm3m*	5.675	5.675	5.675	1
	172.9-178.8	Tetragonal (II)	*P4/mmm*	5.656	5.656	5.630	1
	<172.9	Orthorhombic (III)	$P222_1$	5.673	5.628	11.182	2
Br	>236.9	Cubic (I)	*Pm3m*	5.901(1)	5.901(1)	5.901(1)	1
	155.1-236.9	Tetragonal (II)	*I4/mcm*	8.322(2)	8.322(2)	11.832(7)	4
	149.5-155.1	Tetragonal (III)	*P4/mmm*	5.894(2)	5.894(2)	5.861(2)	1
	<144.5	Orthorhombic (IV)	$Pna2_1$	7.979(1)	8.580(2)	11.849(2)	4
I	>327.4	Cubic (I)	*Pm3m*	6.3285(4)	6.3285(4)	6.3285(4)	1
	162.2-327.4	Tetragonal (II)	*I4/mcm*	8.855(6)	8.855(6)	12.659(8)	4
	<162.2	Orthorhombic (III)	$Pna2_1$	8.861(2)	8.851(2)	12.620(3)	4

(1) Adapted from Mitzi, 1999a; Poglitsch and Weber, 1987.

2.2.4.2 Alkylammonium chains with n ≥ 4

The phase transitions in the C_nPbI inorganic-organic layered perovskite-type hybrids are characterized by thermochromic behaviour. The lowest temperature phase is yellow coloured and the highest orange. The temperature at which this colour change occurs is dependant on the chain length. For n = 4, 8, 9, 10 and 12, this critical temperature is 250, 235, 240, 275 and 310 K

respectively (Ishihara et al, 1990). The authors associate the phase transitions with "rearrangements of the alkylammonium chains". Furthermore, C_6PbI shows no phase transitions or colour change below room temperature. $C_{10}PbI$ has the most complex phase behaviour, with no less than three phase transitions and four distinct phases (Xu et al, 1991c).

Two very comprehensive studies on the phase transitions of C_6PbCl and C_9PbCl can be used as models for the phase transitions of other Pb hybrids. C_6PbCl has three phase transitions, all first-order and C_9PbCl, two phase transitions. The phase stable at the lowest temperature, phase **IV** in C_6PbCl and phase **III** in C_9PbCl, is completely ordered and has a gauche bond near the ammonium head group and the rest of the bonds within the chains are in an all-*trans* configuration. The first transition, with has the smallest enthalpy, involves the appearance of gauche bonds at the opposite end of the chains, near the methyl group. The last transition to phase **I** is the same as in the other layered perovskite-type hybrids, a complete chain melting and rotational disordering and the interlayer spacing increases, indicative of changes in the tilt angle of the alkylammonium chains (Figure 2.9). The DSC curves show a small thermal hysterises, especially in C_9PbCl. Smaller, second order transitions are also observed in the DSC curves of C_6PbCl and C_9PbCl (Figure 2.10).

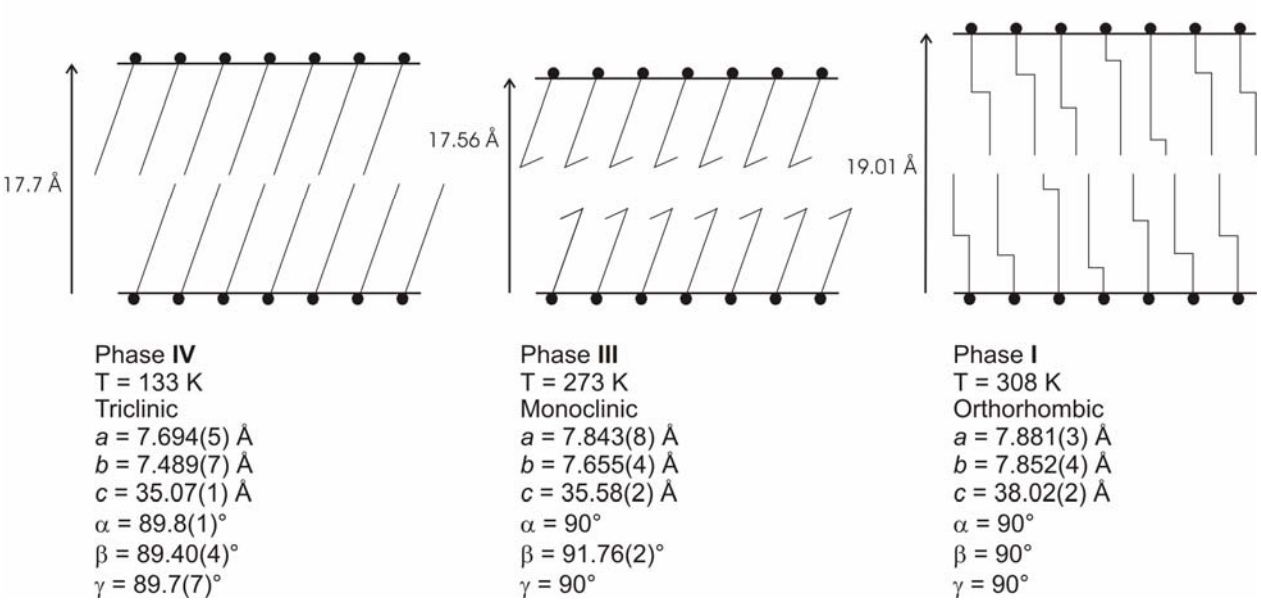


Figure 2.9: A schematic of the various phases of C_6PbCl and their unit cell parameters as determined by X-ray powder diffraction. Adapted from Kammoun et al, 1996a.

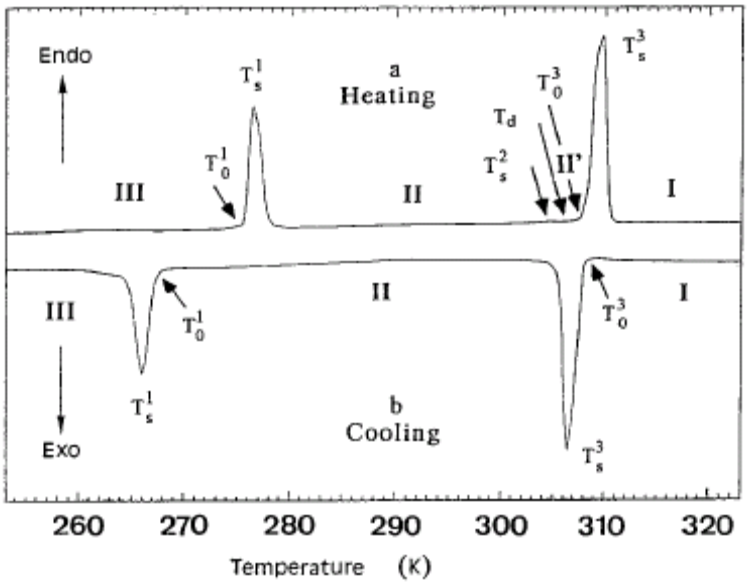


Figure 2.10: DSC curve of C_9PbCl. Taken from Kammoun et al, 1997.

The only long chains, n ≥ 12, alkylammonium inorganic-organic hybrids in the lead(II) iodide layered perovskite-type compounds that have been studied in detail are $C_{12}PbI$, $C_{16}PbI$ and $C_{18}PbI$. The packing of the alkylammonium chains was determined by ^{13}C NMR, IR and Raman spectroscopy and found to be in an all-*trans* configuration at room temperature. The tilt of the long chains in the three compounds relative to the inorganic layer was estimated at 55° from the infrared spectra (Venkataraman et al, 2002a; Venkataraman et al, 2002b). The direction of the tilt can either be the same for all chains to give a parallel arrangement, or alternate, to give a herringbone arrangement (Figure 2.11). The authors found no evidence of interdigitation in their study and classify interdigitated and non-interdigitated alkylammonium hybrids as separate polymorphic groups (Venkataraman et al, 2002a).

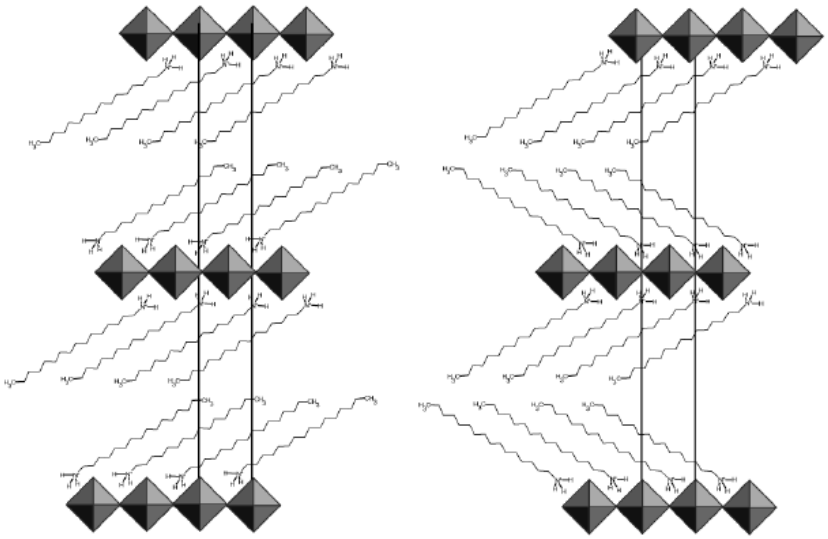


Figure 2.11: A schematic of the two possible packing arrangements, parallel (left) or herringbone (right), of the alkylammonium chains in C_nPbI (n = 12, 16, 18). All the bonds in the chains are in an all-*trans* conformation. Taken from Venkataraman et al, 2002.

The phase transitions for these three compounds all occur above room temperature (Barman et al, 2003). The authors have assigned the first, minor transition to the premelting transition and the second, major transition to the melting transition. On heating the samples, the two transitions appear as endothermic peaks and upon cooling immediately, only a single exothermic peak of the major transition appears. If the samples are heated immediately again, the premelting endotherm is not seen but returns after leaving the samples standing for a few days. The model according to Barman (2003) of the phase changes is as follows: the chains are in an all-*trans*, static conformation at room temperature and after the premelting transition, there is an increase in gauche conformers in the chains causing the interlayer spacing to decrease slightly at the premelting transition. In this phase, the NH_3^+ group becomes rotationally disordered within the cavity of the four terminal iodides. At the melting transition, there is an abrupt increase in the interlayer spacing attributed to a loss of the uniformity of the tilt angle across all the individual chains. There is also a marked increase in the conformational disorder in the chains. The packing of the chains before and after the melting transition is shown schematically in Figure 2.12.

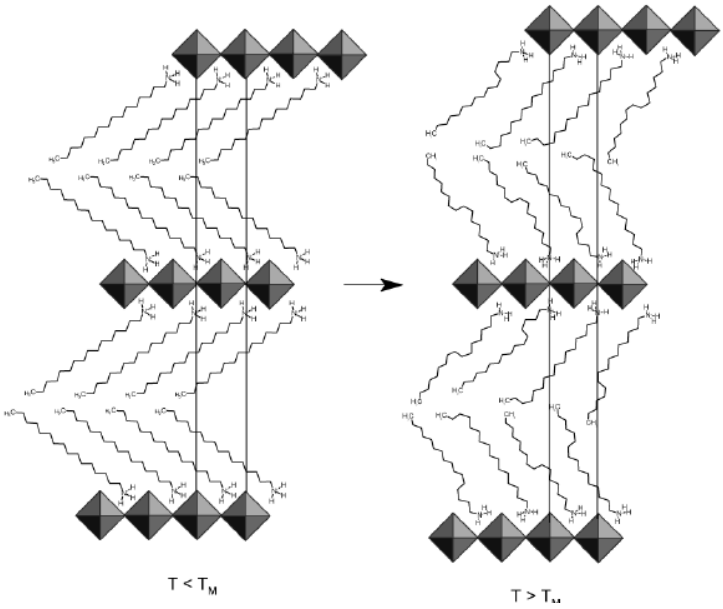


Figure 2.12: A schematic of the phase transition of C_nPbI (n = 12, 16, 18). Taken from Venkataraman et al, 2002.

2.3 Aromatic R groups and their photoelectric behaviour

Apart from the simple alkyl chains, another common choice encountered in the literature for the R group is an aromatic ring, separated from the ammonium group by short alkyl chain spacers. These have the general formula $[(C_6H_5(CH_2)_nNH_3)_2MX_4]$, n = 0-3, and the most common examples are summarized in Table 2.9 below. The most studied inorganic-organic layered perovskite-type hybrid is without doubt $[(C_6H_5(CH_2)_2NH_3)_2MX_4]$ as it is the material that has shown the most application potential. Various articles that summarize the application potential of inorganic-organic layered perovskites include *Organic-Inorganic Electronics* (Mitzi et al, 2001a), *Solution-processed inorganic semiconductors* (Mitzi, 2004), *Organic-Inorganic Hybrid Materials as Semiconducting Channels in Thin-Film Field-Effect Transistors* (Kagan et al, 1999), *Electronic properties of three- and low-dimensional semiconducting materials with Sn halide and Pb halide* (Koutselas et al, 1996), *Optical properties of PbI-based perovskite structures* (Ishihara, 1994) and *Some New Organic-Inorganic Hybrid Semiconductors Based on Metal Halide Units: Structural, Optical and Related Properties* (Papavassiliou et al, 1999a)

Table 2.9: The most common aromatic R groups that form inorganic-organic layered perovskite-type hybrids. Numbers in superscript refer to the references listed at the end of the table.

	Pb^{2+}	Sn^{2+}	Cu^{2+}	Cr^{2+}	Cd^{2+}
$C_6H_5NH_3$			Cl^{1}		
$C_6H_5(CH_2)NH_3$	I^{2} $Cl^{4, 32}$		$Cl^{19, 26}$ $Br^{18, 22}$	$Br^{5, 29}$	
$C_6H_5(CH_2)_2NH_3$	$Cl^{3, 6, 32}$ $Br^{6, 3, 7, 28}$ $I^{8, 7, 9, 10, 11, 12, 13, 17, 3, 23, 25, 27, 28, 30, 31}$	$I^{14, 15}$	$Cl^{16, 19, 26, 33}$ $Br^{16, 18}$		Cl^{20}
$C_6H_5(CH_2)_3NH_3$			$Cl^{19, 26}$ Br^{18}		
$C_6H_5(CH_2)_4NH_3$			Cl^{19}		
$\pm$-$C_6H_5CH_2(CH_3)NH_3$	Cl^{21} Br^{21} I^{24}				

Key to references in Table 2.9

1) Larsen, 1974.
2) Papavassiliou et al, 1999b.
3) Ueda et al, 1998.
4) Braun and Frey, 1999a.
5) Halepoto et al, 1989.
6) Mitzi, 1999b.
7) Mitzi et al, 1999a.
8) Era et al, 1994.
9) Hong et al, 1992a.
10) Cheng et al, 2003.
11) Kitazawa, 1998.
12) Shimizu et al, 2005.
13) Shimizu and Fujisawa, 2004.
14) Papavassiliou et al, 1994.
15) Kagan et al, 1999.
16) Willett, 1990.
17) Calabrese et al, 1991.
18) Zhou et al, 1992a.
19) Dupas et al, 1976.
20) Groh et al, 1997.
21) Gebauer and Schmidt, 1999.
22) Zhou at al, 1992b.
23) Hong et al, 1992b.
24) Billing, 2002.
25) Era et al, 1997.
26) Dupas el al, 1977.
27) Era et al, 1995.
28) Cheng et al, 2005.
29) Bellitto et al, 1986.
30) Fujita et al, 1998.
31) Fujita et al, 2000.
32) Braun et al, 1999a.
33) Kang and Jeon, 1995.

The simplest aromatic amine, aniline, is also the least studied, with only one inorganic-organic layered perovskite-type hybrid structure in the CSD (Ver. 5.27, including May 2006 update). The hybrid is $[(C_6H_5NH_3)_2CuCl_4]$ (Larsen, 1974) (CSD ref. code: ANILCP) and has the typical 4+2 coordination around the Cu atom and eclipsed inorganic layers. Four Cu-Cl bond lengths are short, 2.3007(5) Å and 2.2804(6) Å, and the other two are long, 2.9178(5) Å (Figure 2.13). If a phenyl group is bonded to the anilinium backbone in the *para* position, the inorganic layers become staggered. The two aromatic rings in $[(p\text{-Ph-}C_6H_4NH_3)_2CuCl_4]$ (Bourne and Mangombo,

2004) (CSD ref. code: HAJTAO) are twisted by 23.07(9)° relative to each other (Figure 2.14). The effect of smaller functional groups *para* to the ammonium group on the crystal structure has been systematically investigated using chloro (CSD ref. code: PAYDUO), nitro (CSD ref. code: PAYFAW) and cyano groups (PAYDOI) (Sekine et al, 1996a) together with copper(II) chloride (Sekine et al, 1996b). Other inorganic-organic layered perovskite-type hybrids with nitro groups are [(*p*-O_2N-$C_6H_4NH_3$)$CdCl_4$] (Azumi et al, 1995) (CSD ref. code: ZIKFOO) (Azumi et al, 1996) and [(*p*-O_2N-$C_6H_4NH_3$)$CuBr_4$] (Sekine et al, 1996c) (CSD ref. code: VACSAT); and with chloro groups are [(*p*-Cl-$C_6H_4NH_3$)$_2PbI_4$] (Liu et al, 2004) (CSD ref. code: FIXMOP).

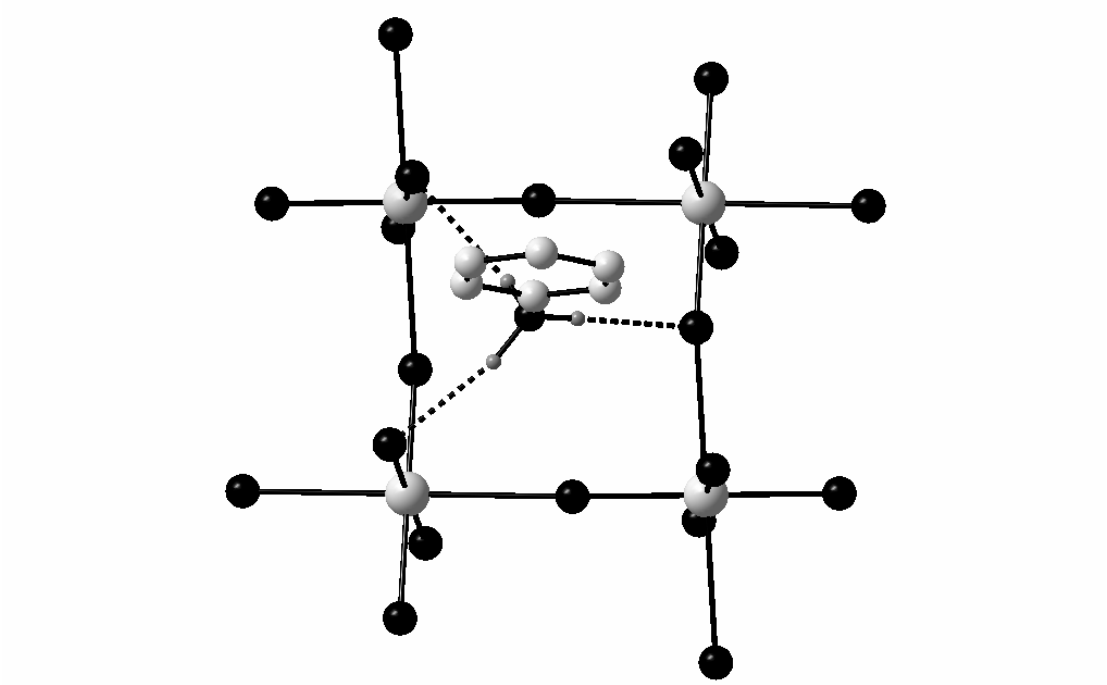


Figure 2.13: The hydrogen bonding interactions of the layered perovskite-type hybrid with anilinium and the two long and four short Cu-Cl bonds of the copper(II) chloride octahedra.

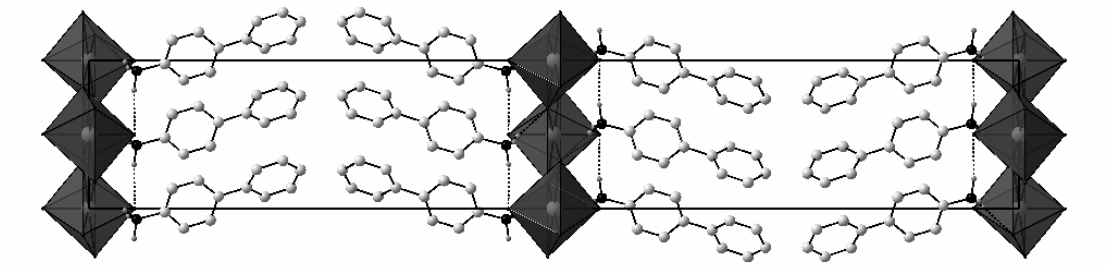


Figure 2.14: The packing arrangement of a complete unit cell of [(*p*-Ph-$C_6H_4NH_3$)$_2CuCl_4$].

The methylene spacer in benzylammonium causes the ammonium head group to adopt the right-angled hydrogen bonding configuration, as in $[(C_6H_5CH_2NH_3)_2PbI_4]$ (Papavassiliou et al, 1999b) (CSD ref. code: COTVIQ) (Figure 2.15), $[(C_6H_5CH_2NH_3)_2PbCl_4]$ (Braun and Frey, 1999a) (CSD ref. code: HORFAV) and $[(C_6H_5CH_2NH_3)_2CrBr_4]$ (Dost et al, 1989) (CSD ref. code: VAVNOV). In the anilinium compounds, the ammonium group has the equilateral hydrogen bonding configuration. The only reported structures with substituents on the benzylammonium backbone are with a methyl group, as in $[(p\text{-}CH_3\text{-}C_6H_4CH_2NH_3)_2PbX_4]$ (X = Cl, Br and I) (Papavassiliou et al, 2000; Makino et al, 2005) (CSD ref. codes: MEMYIM, MEMXUX and MEMYEI respectively); and a flouro group, $[(p\text{-}F\text{-}C_6H_4NH_3)_2PbI_4]$ (Kikuchi et al, 2003). The optical absorption spectra contain peaks at 397 nm and 515 nm respectively for the bromide and iodide inorganic-organic layered perovskite-type hybrids.

Inorganic-organic layered perovskite-type hybrids with large fused aromatic rings are also able to crystallize out as the perovskite-type layer structure providing it contains a methylene spacer, that prevents a steric interaction with the bulky R group and the terminal halides. Two such structures are known for lead(II) chloride with either 2-napthylmethylammonium (CSD ref. code: HORFEZ) (Braun and Frey, 1999b) and 2-anthrylmethylammonium (CSD ref. code: GOLJOG) (Braun and Frey, 1999c). Fullerene ammonium derivatives, such as *N*-methyl-2-(4-aminophenyl)-fulleropyroolidene, form a layered perovskite-type inorganic-organic hybrid with lead(II) iodide (Kikuchi et al, 2005). In this compound, the fullerene molecule is bonded to benzylammonium, which acts as the spacer between the bulky fullerene molecule and the terminal iodide halides.

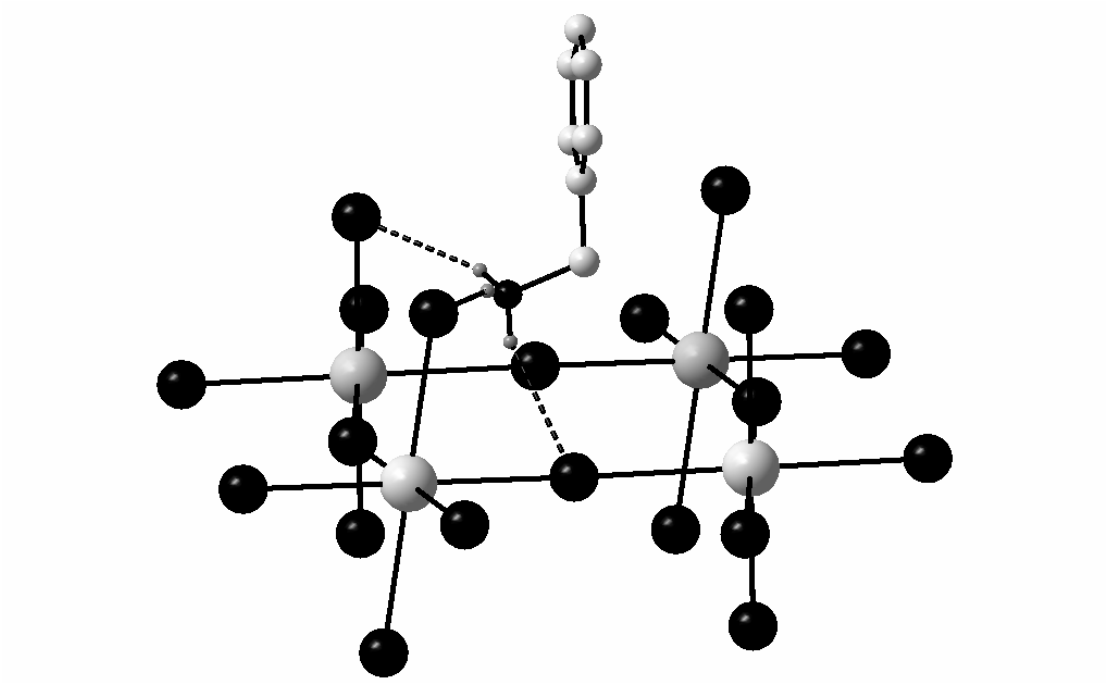


Figure 2.15: Hydrogen bonds in $[(C_6H_5CH_2NH_3)_2PbI_4]$.

The first mention of inorganic-organic layered perovskite-type hybrids in the literature with the phenylethylammonium cation is that of the ferromagnetic compound $[(C_6H_5(CH_2)_2NH_3)_2CuCl_4]$ in 1976 (Dupas et al, 1976). The reason its magnetic properties were investigated was to compare them to the magnetic properties of the alkyl ammonium series $[(C_nH_{2n+1}NH_3)_2CuCl_4]$ (Dupas et al, 1976). The authors surmised that the packing of the inorganic layers and the phenethylammonium cations is closely related to the structures of $[(NH_4)_2CuCl_4]$ and $[(CH_3NH_3)_2CuCl_4]$ after determining approximate values of the unit cell axis for $[(C_6H_5(CH_2)_2NH_3)_2CuCl_4]$ from X-ray powder data. The first complete single crystal study was performed by Willett (1990) on both the chloride and bromide inorganic-organic hybrids $[(C_6H_5(CH_2)_2NH_3)_2CuCl_4]$ (CSD ref. code: KEJCEH) and $[(C_6H_5(CH_2)_2NH_3)_2CuBr_4]$ (CSD ref. code: KEJCIL). Both hybrid compounds have staggered inorganic layers. The ethylammonium substituents on the benzene rings have an approximate all-*trans* conformation (Torsion angles: 173.5(5)° and 171.5(1)° respectively for X = Cl and Br) and have the bridging halogen configuration (Figure 2.16).

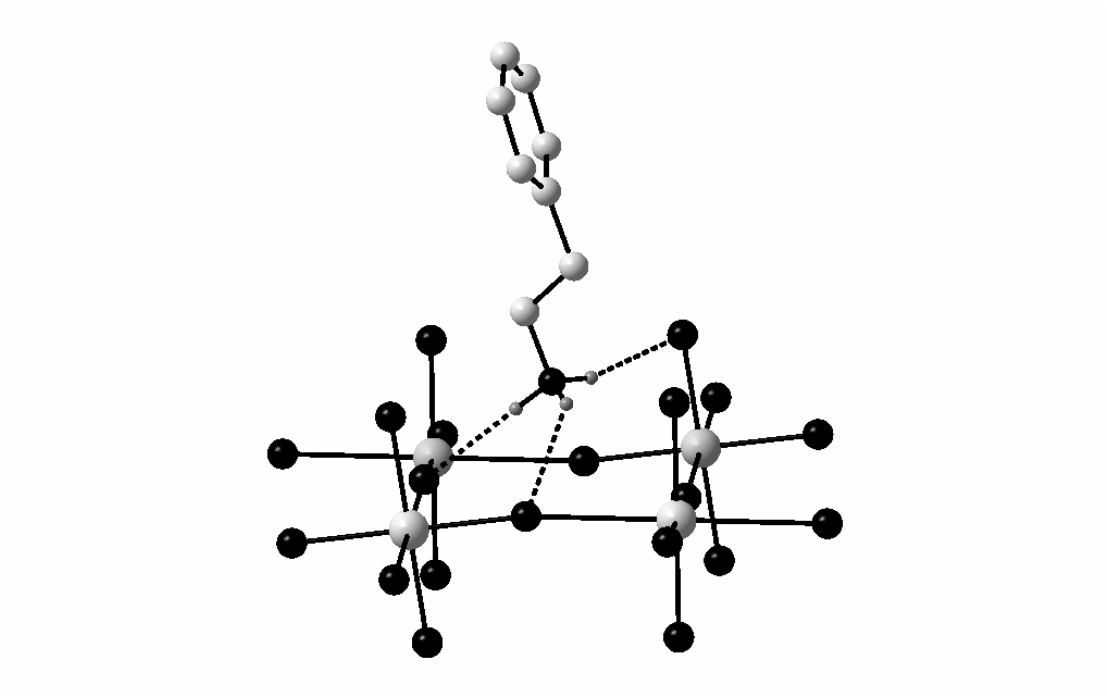


Figure 2.16: The bridging halogen configuration of $[(C_6H_5(CH_2)_2NH_3)_2CuCl_4]$.

The crystal structure and conformation of the phenethylammonium cation changes entirely when the metal cation is lead. The inorganic-organic layered perovskite-type hybrid $[(C_6H_5(CH_2)_2NH_3)_2PbCl_4]$ (CSD ref. code: MAPBIO) has the rare $2a_p$ x $2a_p$ superstructure, where a_p is the cubic lattice parameter of the ideal cubic perovskite $[(CH_3NH_3)PbCl_3]$ (Mitzi, 1999a). The unit cell axes are a = 11.1463(3) Å, b = 11.2181(3) Å and c = 17.6966(5) Å and the space group is triclinic $P\bar{1}$. In this structure, the lattice parameters a and b are parallel to the plane of the inorganic layers and are twice the cubic lattice parameter a_p = 5.657(2) Å (Mitzi, 1999a). The related crystal structure of the copper(II) chloride inorganic-organic layered perovskite-type hybrid has the smaller ratio to the cubic lattice parameter, namely $\sqrt{2}a_p$ x $\sqrt{2}a_p$. The author rationalizes these differences by the degree of distortion of the MCl_6 octahedra. If the octahedra were not tilted or rotated relative to each other, the unit cell dimensions within the corner-sharing layers would be simply a_p x a_p. The deviations from this ideal scenario accounts for the two possible superstructures of the two compounds. The $PbCl_6$ octahedra within the layers are more distorted than the $CuCl_6$ octahedra and the unit cell is larger in the directions parallel to the layers. The basic building block of the corner-sharing layers consists of four corner-sharing squares, as shown in Figure 2.17 below. The asymmetric unit is also correspondingly bigger and contains two lead and eight chloride atoms. Each square has a partner phenethylammonium

cation so that there are four unique cations in the asymmetric unit, labelled N1 to N4. The ethylammonium groups are not in the all-*trans* conformation seen in $[(C_6H_5(CH_2)_2NH_3)_2CuCl_4]$ and have torsion angles of -67.0(7)° (N1-C1-C2-C3-C4), -67.9(7)° (N2-C9-C10-C11-C12), 58.9(7)° (N3-C17-C18-C19) and -60.6(7)° (N4-C25-C26-C27). The resulting shape of the ethylammonium groups is "J-shaped" (Mitzi, 1999b) and is further stabilized by hydrogen bonding with the terminal halogen configuration and having the right-angled configuration. A preliminary single-crystal structure of the bromide inorganic-organic layered perovskite-type hybrid by the same author revealed an almost identical unit cell. However, not all reflections were indexed, suggesting a possible supercell and that the chloride and bromide structures are not isostructural.

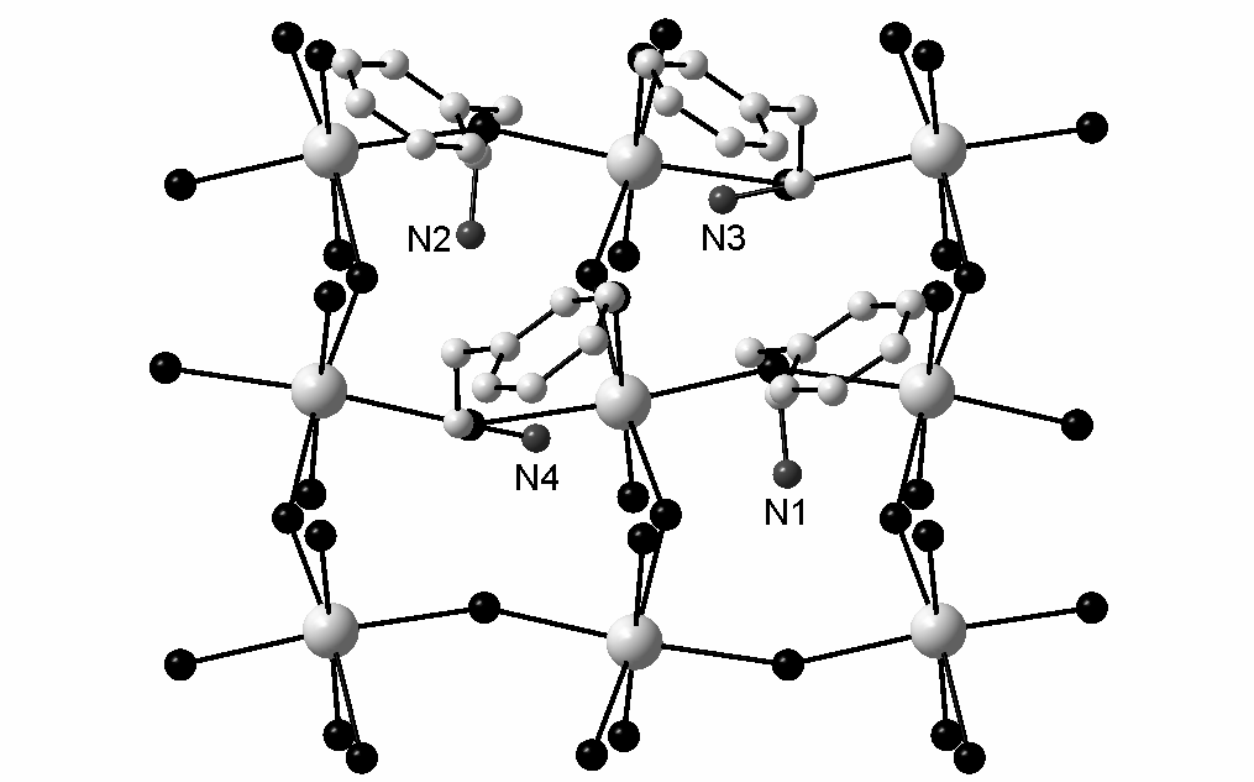


Figure 2.17: The simplest repeating unit of the perovskite sheets in $[(C_6H_5(CH_2)_2NH_3)_2PbCl_4]$. The four phenethylammonium cations adopt a J-shaped conformation.

The crystal structure of the iodide inorganic-organic layered perovskite-type hybrid, $[(C_6H_5(CH_2)_2NH_3)_2PbI_4]$ (CSD ref. code: JIMDEO), has the a_p x a_p structure (Calabrese et al, 1991). The space group is *C2/m* and the bridging iodides as well as the phenethylammonium

cations are disordered across the mirrorplanes in the unit cell and hence not much structural detail of the tilting and rotation of the PbI_6 octahedra and the conformation of the ethylammonium groups can be elucidated. The structure of $[(C_6H_5(CH_2)_2NH_3)_2SnI_4]$ (CSD ref. code: POFKOK) is isostructural to the lead(II) iodide inorganic-organic layered perovskite-type hybrid and shows the same disorder and/or superstructure defects (Papavassiliou et al, 1994). The structure of the phenethylammonium cations within the three inorganic-organic layered perovskite-type hybrids $[(C_6H_5(CH_2)_2NH_3)_2PbX_4]$ (X = Cl, Br and I) has also been investigated by ^{13}C cross polarization/magic angle sample spinning NMR technique (Ueda et al, 1998).

The properties of the phenethylammonium inorganic-organic layered perovskite-type hybrids have excited both physicists and materials scientists. For example, $[(C_6H_5(CH_2)_2NH_3)_2PbI_4]$ shows strong photoluminescence (Hong et al, 1992), electroluminescence (Hong et al, 1992a. 201), a very strong exciton absorption at 2.4 eV and a large exciton binding energy of 0.220 eV. For comparison, the position of the exciton for the tin(II) iodide derivative is at 2.0 eV and the exciton binding energy is 0.190 eV (Papavassiliou et al, 1994). To make use of the optical property of the lead(II) iodide inorganic-organic layered perovskite-type hybrid, Era et al (1994) combined the compound with an electron transporting oxadiazole derivative (OXD7) to construct an "organic-inorganic heterostructure electroluminescent device (EL)". A schematic of the device is shown in Figure 2.18. The hybrid $[(C_6H_5(CH_2)_2NH_3)_2PbI_4]$ (PAPI) is used as the emitter and OXD7 as the electron transport layer. The two layers were then sandwiched between an indium-tin-oxide anode and a MgAg cathode. The intensity reached a maximum of 10 000 cd m^{-2} at liquid nitrogen temperatures. To achieve this, a current density of 2 A cm^{-2} and a voltage of 24 V had to be applied. The colour of the emission was an intense green and peaked at 520 nm, a spectrum that corresponds well to the photoluminescent spectra obtained from a thin film of purely PAPI (Era et al, 1994) laid down. Other layered perovskite-type hybrids which have been studied with identical devices are $[(C_6H_9(CH_2)_2NH_3)_2PbI_4]$ and $[(C_6H_5(CH_2)_4NH_3)_2PbI_4]$ (Hattori et al, 1996). The maximum electroluminesence reached for these two cases were 4800 cd m^{-2} (50 mA cm^{-2}, 24 V) and 180 cd m^{-2} (25 mA cm^{-2}, 30 V) respectively. Two similar devices were constructed using a structural isomer of the phenethylammonium molecule, chiral $(C_6H_5CH(CH_3)NH_3)$ (See Figure 2.19) (Gebauer and Schmidt, 1999). The electron transport layer is the n-semiconductor called 'Starburst', the hybrids $[(C_6H_5CH(CH_3)NH_3)_2PbCl_4]$ (diode 1) or

$[(C_6H_5CH(CH_3)NH_3)_2PbBr_4]$ (diode 2) as the p-semiconductor and as a contact between the two semiconductors, a poly(N-vinylcarbazole)-layer doped with Coumarin6. Both diodes started showing green emissions at 7 V.

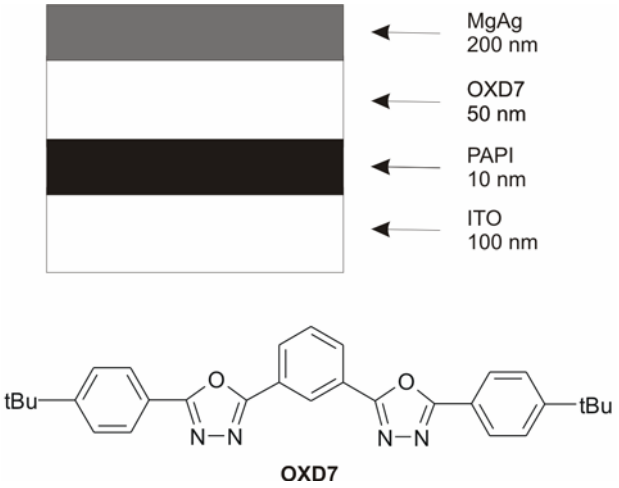


Figure 2.18: A schematic of the inorganic-organic heterostructure electroluminescent device with approximate thickness of the layers and the structure of the organic component, OXD7, used. Figure adapted from Era et al (1994).

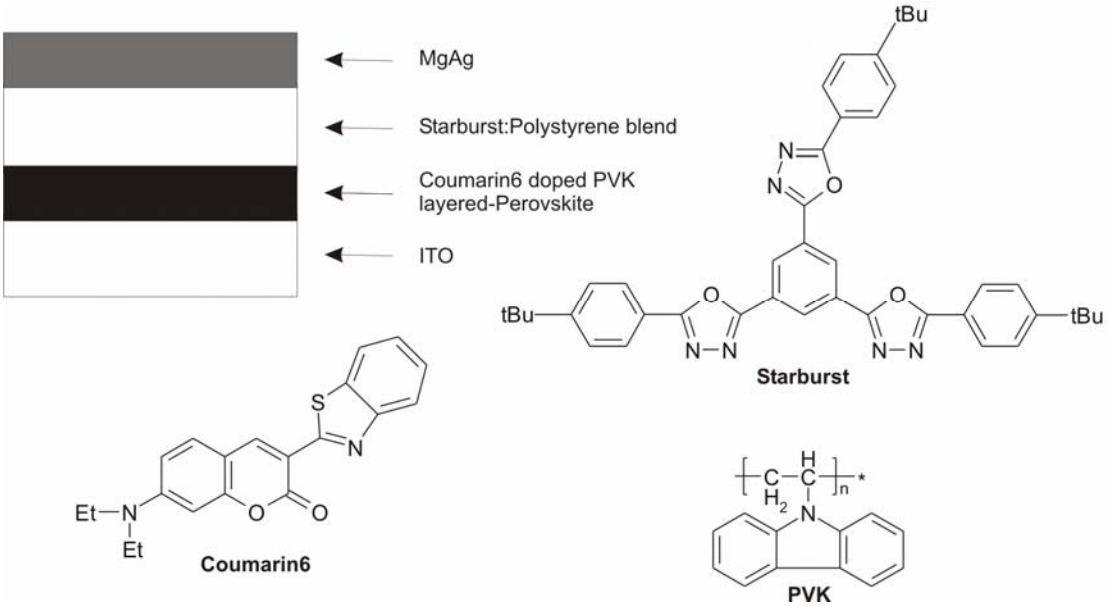


Figure 2.19: A schematic of the three-layered heterocontact inorganic-organic light emitting diode with a chiral layered-perovskite. Figure adapted from Gebauer and Schmidt (1999).

A novel way to tune the position of the exciton absorption and photoluminescence bands is by systematically replacing the halide in the lead(II) halide inorganic-organic layered perovskite-

type hybrids. Kitazawa (1997) prepared thin films of the hybrids $[(C_6H_5(CH_2)_2NH_3)_2PbBr_xI_{4-x}]$ and $[(C_6H_5(CH_2)_2NH_3)_2PbCl_xBr_{4-x}]$ and found that it was possible to smoothly shift the bands towards green-blue-violet regions as a function of x, as shown in Figure 2.20 below, taken directly from the article.

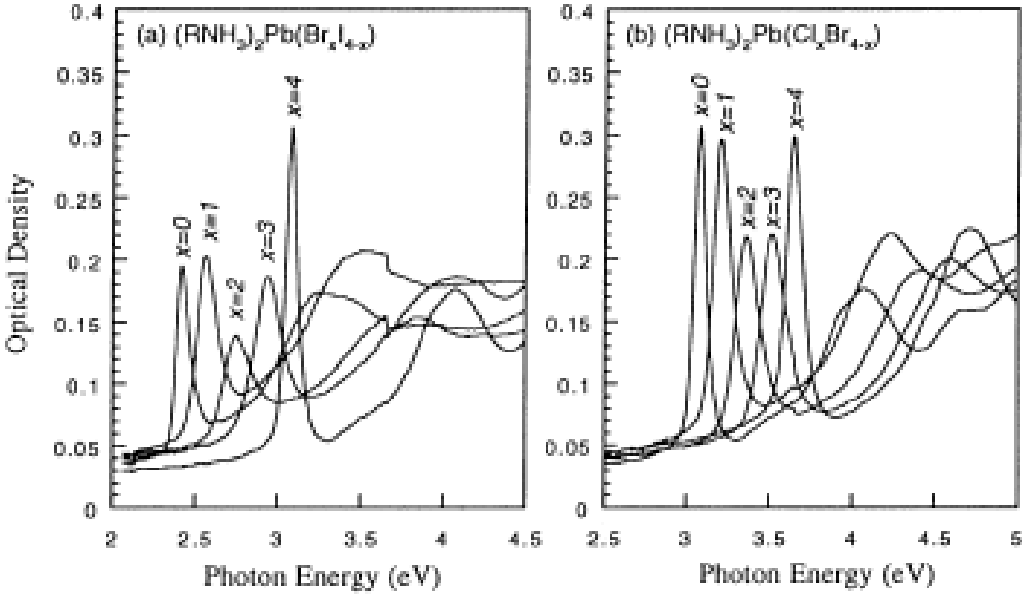


Figure 2.20: Optical absorption spectra of (a) $[(RNH_3)_2PbBr_xI_{4-x}]$ and (b) $[(RNH_3)_2PbCl_xBr_{4-x}]$ films measured at room temperature. Taken from Kitazawa (1997).

To improve the stability of the $[(C_6H_5(CH_2)_2NH_3)_2PbI_4]$ thin films against moisture, thermal annealing and photo-irradiation, Kitazawa (1998) prepared nanocrystalline films of the hybrid doped with poly(methyl methacrylate). The exciton binding energy increased to 0.300 eV from undoped films (cf. 0.200 eV for undoped) and the degradation could be suppressed. A similar study was performed on films of $[(C_6H_5(CH_2)_2NH_3)_2PbBr_xI_{4-x}]$ (Kitazawa et al, 2004).

2.4 Inorganic-organic layered perovskite-type hybrids $[(H_3N(CH_2)_nNH_3)MX_4]$ with simple alkyldiammonium chains

Compared to the simple straight chain aliphatic mono-amines, fewer inorganic-organic layered perovskite-type hybrids with diamines have been synthesized and characterized. The length of the simple straight alkyl chain studied is generally quite short with a maximum chain length of ten

carbon atoms. Structural phase transitions behave in a similar fashion to the mono-ammonium cations.

2.4.1 Lead(II) halide inorganic-organic layered perovskite-type hybrids $[(H_3N(CH_2)_nNH_3)PbX_4]$ and $[(H_3N\text{-}R\text{-}NH_3)PbX_4]$

The compound $[(H_3N(CH_2)_3NH_3)PbCl_4]$ (Corradi et al, 1999) (CSD ref. code: CAKBUL) has two unique inorganic layers in the unit cell (Figure 2.21). Adjacent layers are slightly offset relative to each other. The 1,3-diammoniumpropane cations are twisted along one end of the chain by 105.2(7)° to compensate for the shift of the layers. In the same study, two related inorganic-organic layered perovskite-type hybrids with the cation $H_3NCH_3CH(CH_3)(CH_2)_3NH_3$ where prepared with lead(II) chloride (CSD ref. code: CAJXUG) and lead(II) bromide (CSD ref. code: CAJZAO). These two compounds are isostructural and have the same staggered conformation of adjacent layers as the previous structure. The displacement of the layers is due to the steric effect of the methyl group on the 2-position of the pentane chains (Corradi et al, 1999) (Figure 2.22). The methyl groups have a repulsive effect on neighbouring cations and this is mirrored in the layer shift. The bond lengths between the lead and the halide atoms increases as expected with the increasing halide radius.

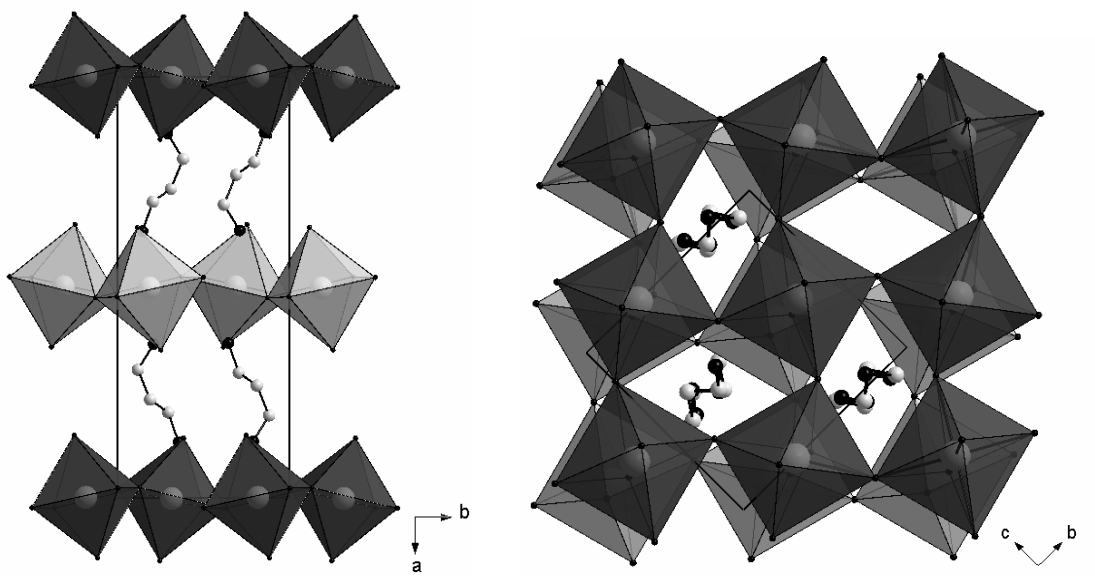


Figure 2.21: The packing diagram of a single unit cell of $[(H_3N(CH_2)_3NH_3)PbCl_4]$ shown side-on (left) and from the top (right). The inorganic layer shown as light grey octahedra is offset relative to the inorganic layers shown as dark grey octahedra.

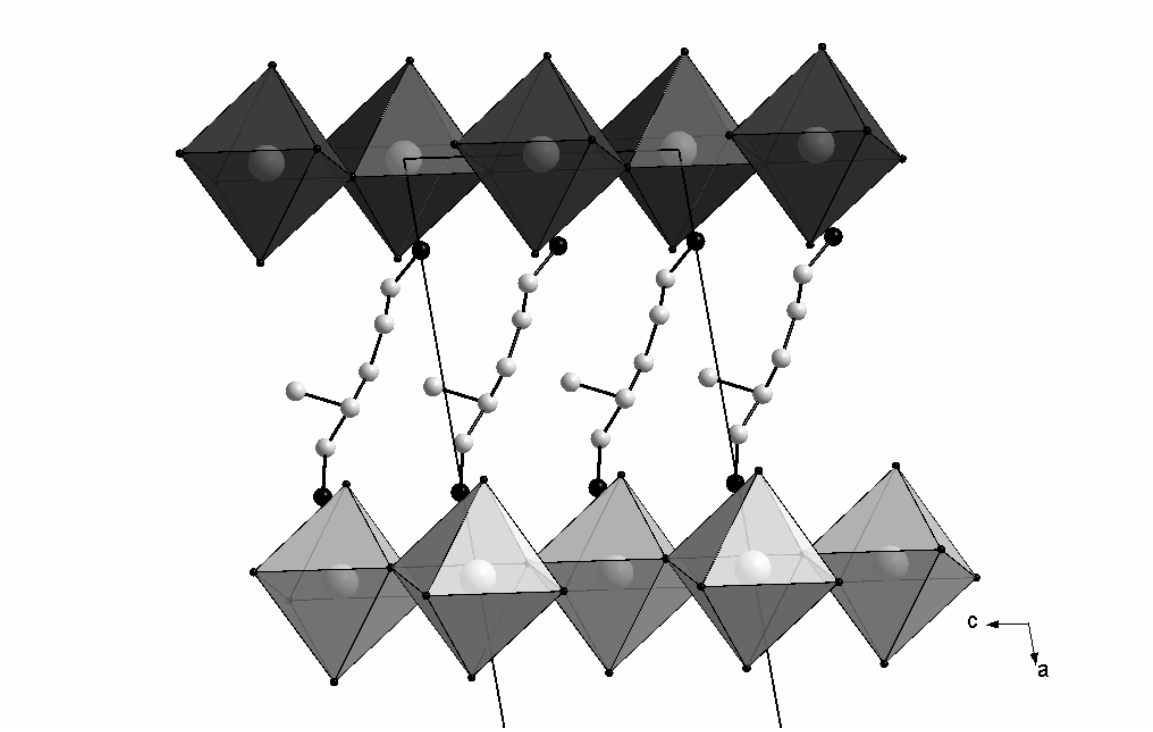


Figure 2.22: Half of the unit cell of $[(H_3NCH_3CH(CH_3)(CH_2)_3NH_3)PbCl_4]$ showing a magnified view of the arrangement of the cations between the layers. The methyl group has a repulsive effect on the cations in the crystallographic *c* direction.

One layered perovskite-type lead hybrid with a diammonium cation has been reported to display reversible phase transitions, studied via DSC, SC-XRD and P-XRD (Courseille et al, 1994), is $[(H_3N(CH_2)_4NH_3)PbCl_4]$ (CSD ref. code: YOVXAI). It has a monoclinic room temperature phase **II** and a monoclinic high temperature phase **I**. The transition temperature of the endothermic peak is T = 323.8 K when heating, and when cooling exhibits strong thermal hysteresis so that the exothermic peak is at T = 296.9 K. The monoclinic phase **II** has the unit-cell dimensions a = 7.944(2) Å, b = 7.772(5) Å, c = 19.761(8) Å and β = 94.84(3)°, space group is $P2_1/c$ and Z = 4. The structure contains two layers per unit cell that are staggered relative to each other. The 1,4-diammoniumbutane cation is non-centrosymmetric and has a "left-hand" conformation, as defined by the authors, at one extremity, as shown in Figure 2.23. The atoms N1, C1, C2, C3 and C4 form a quasi-perfect all-*trans* configuration (Courseille et al, 1994) and N2 is clearly bent out of the plane of those atoms. The room temperature structure was determined from SC-XRD data. The structure of the high temperature phase **I** had its initial unit-cell dimensions determined from precession photographs and refined from 34 peaks from P-XRD data determined at 353 K. The unit-cell dimensions are a = 7.963(5) Å, b = 7.735(6) Å, c = 11.011(1) Å and β = 102.22(9)°. The

space group is $P2_1/a$ and Z = 2. The authors surmise that the cation untwists to give a centrosymmetric and stretched conformation where all the atoms are in a planar arrangement and *trans* to each other. The increase in molecular length consequently results in an increase in the interlayer spacing of the layers. Phase **II** has a spacing of 19.761(8)/2 = 9.881(8) Å and phase **I** a spacing of 11.011(1) Å. Not mentioned in the study is the possibility of the layers shifting relative to each other. The unit-cell axis halves in the direction perpendicular to the layers when transforming from phase **II** to phase **I**; this could be indicative of a change from a staggered to an eclipsed arrangement of the layers.

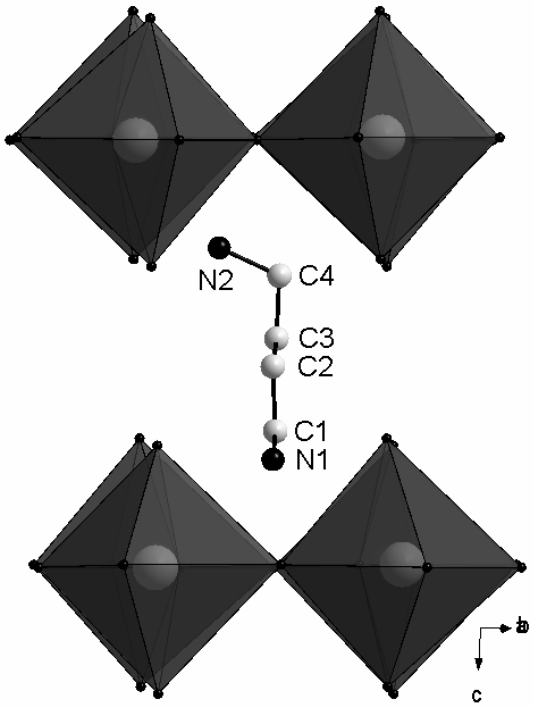


Figure 2.23: The structure phase **II** of $[(H_3N(CH_2)_4NH_3)PbCl_4]$ showing a magnified view of the left-hand conformation of the cation between the layers.

Eclipsed layered perovskite-type layers are seen in the series of compounds $[(H_3N(CH_2)_6NH_3)[PbX_4]$ (X = Cl, Br and I) (Mousdis et al, 1999) (CSD ref. codes: WOGJEH, WOGJIL and WOGJOR respectively). The three compounds are isostructural but only SC-XRD data and structures were reported for the iodide and bromide compounds. Contrary to the diammonium cations discussed above, the 1,6-diammonium cations are centrosymmetric and only half of the molecule is in the asymmetric unit. The molecules pack around inversion centres

located within the unit cell. The carbon atoms form a plane with the nitrogen atoms bent out of the plane. The unit cell contains only one complete layer per unit cell, i.e. two halves at x = 0 and 1 (See Figure 2.24). Synthesized but not structurally characterized are the Sn equivalents $[(H_3N(CH_2)_6NH_3)SnX_4]$ (X = Br and I). All five layered perovskite-type hybrids show excitonic peaks when optical absorption spectra were recorded and the peak positions are shifted to lower energies in the order I < Br < Cl (Mousdis et al, 1999). The lead(II) iodide hybrid shows a very large exciton binding energy of 0.33 eV, below room temperature, and this is correlated with the fact that it does not undergo any structural phase transitions below room temperature (Goto et al, 2001).

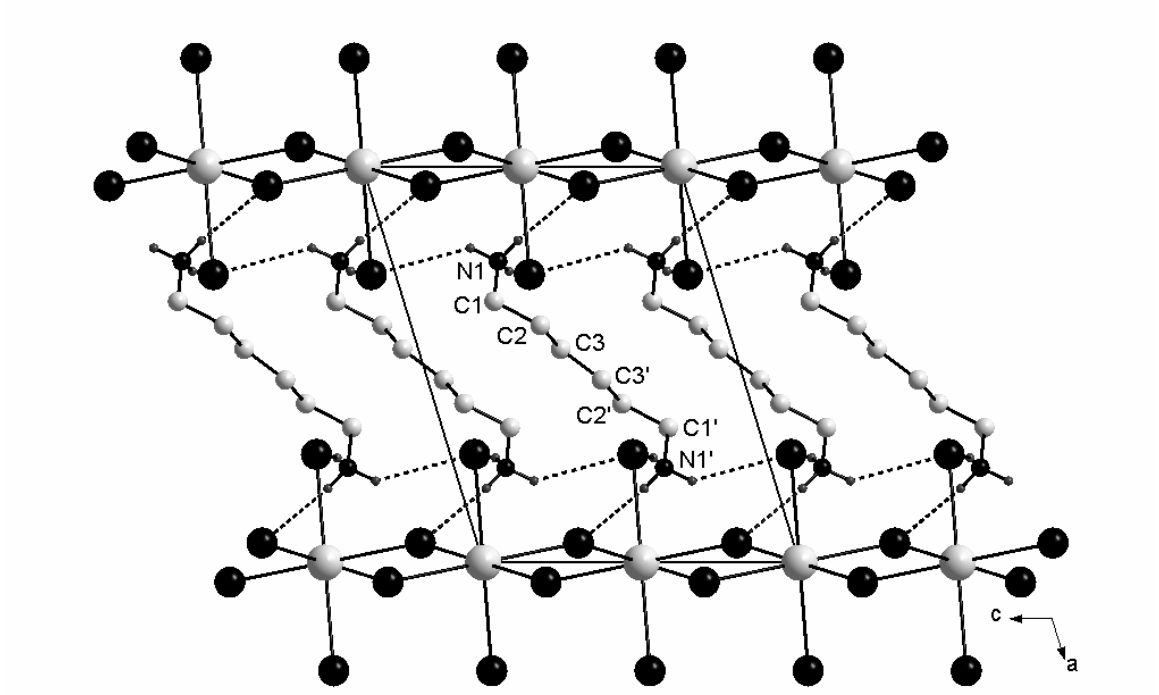


Figure 2.24: The structure of $[(H_3N(CH_2)_6NH_3)PbI_4]$. The cation is centrosymmetric and the two halves are related by the symmetry operator (1-x, 1-y, 1-z), shown as atoms marked with apostrophes (').

The optical absorption spectra of the series of compounds $[(H_3N(CH_2)_nNH_3)PbBr_4]$ (n = 4, 6, 8 and 10) (Matsui et al, 2002) were also measured. The structure of the compounds was deduced from P-XRD and confirmed to have the layered perovskite-type motif. The position of the exciton peak is independent of the length of the alkyldiammonium cation and is centred around

390 nm. The interlayer spacing ranges from 10.2 Å (n = 4) to 15.0 Å (n = 10) and separates the inorganic layers sufficiently to cause a quantum confinement effect.

In an attempt to enhance the electroluminescence and photoluminescence properties of the inorganic-organic layered perovskite-type hybrids compared to simple alkyl chains and aromatic moieties, a specially synthesized oligothiophene chromophore was incorporated into the layered perovskite-type motif employing the three lead(II) halides (Mitzi et al, 1999b). The molecule, shown in Figure 2.25 below and abbreviated AEQT, has a long, narrow profile and four α-linked thiophene rings. The ethylammonium groups provide flexibility and anchorage points to the inorganic layer via the hydrogen bonds of the ammonium group. Only the compound [(AEQT)$PbCl_4$] shows relatively efficient room-temperature electroluminescence (Chondroudis and Mitzi, 1999) and strong photoluminescence (Mitzi et al, 1999b).

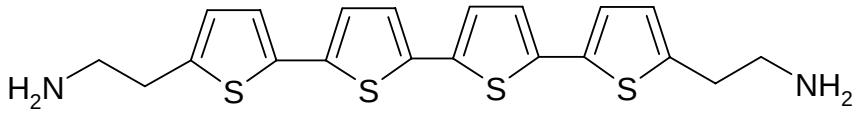


Figure 2.25: The molecule 5,5'''-bis-(aminoethyl)-2,2':5', 2'':5'',2'''-quaterthiophene, AEQT.

Of the three compounds synthesized and characterised by optical absorption spectra, only [(AEQT)$PbBr_4$] (CSD ref. code: QEKGES) was structurally characterized by SC-XRD. An interesting feature of this inorganic-organic layered perovskite-type hybrid is that it has the $2a_p$ x $2a_p$ superstructure. The packing of the compound has a herringbone arrangement of the organic dye molecules. The conformation of the quaterthiophene backbone is *syn-anti-syn* and each ring is essentially planar. The ethylammonium anchors are bent out of the plane formed by the quarterthiophene backbone and adopt a conformation suitable to hydrogen bonding interactions (Figure 2.26).

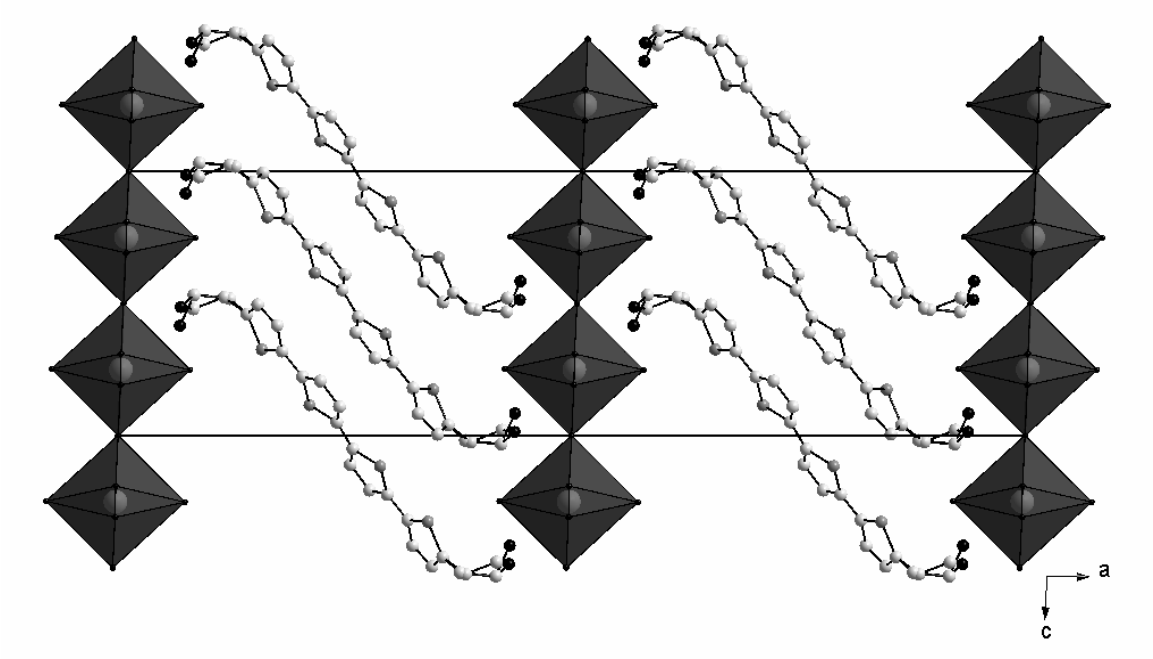


Figure 2.26: The unit cell of [(AEQT)$PbCl_4$]. The ethylammonium groups and the bridging bromides are disordered over two positions.

A related compound that has a bithiophene backbone instead of the quaterthiophene has also been synthesized and characterized (Zhu et al, 2003), the organic cation being 5,5'-bis(ammoniumethylsulfanyl-2,2'-bithiophene, abbreviated BAESBT, and is shown in Figure 2.27. The crystal structure of [(BAESBT)PbI_4] (CSD ref. code: BAYHAL) has the $\sqrt{2}a_p$ x $\sqrt{2}a_p$ superstructure (Mitzi, 1999b). The packing is similar to the above mentioned layered perovskite-type hybrid and has an exciton peak at 504 nm.

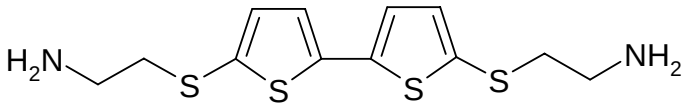


Figure 2.27: The molecule BAESBT.

Yet another compound has two thiophene units separated by a hexane chain and two ethylammonium groups on either end similar to AEQT. The compounds name is then 1,6-bis[5'-(2''-aminoethyl)-2'-thienyl]-[hexane], abbreviated AETH, and is shown in Figure 2.28. The hydrocarbon chain lends flexibility to the molecule and has the long, narrow profile the authors deem necessary (Chondroudis et al, 2000) (Figure 2.28). The optical properties of the inorganic-

organic layered perovskite-type hybrids [(AETH)PbX_4] (X = Br and I) were measured on thin films that were deposited using a single source thermal ablation method (SSTA). No SC-XRD data was reported but the layered perovskite-type motif was confirmed from P-XRD data.

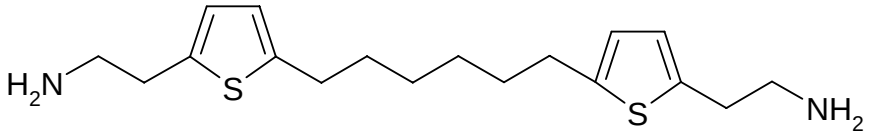


Figure 2.28: The molecule AETH.

2.4.2 Other divalent metals reported to form inorganic-organic layered perovskite-type hybrids [$(H_3N(CH_2)_nNH_3)MX_4$] with diammonium alkyl chains

A number of inorganic-organic hybrid materials containing short (n < 6) diammonium alkyl chains have been reported with mercury(II) chloride. The two inorganic-organic layered perovskite-type hybrids, [$(H_3N(CH_2)_3NH_3)HgCl_4$] (Spengler et al, 1998) (CSD ref. code: PUVLUN) and [$(H_3N(CH_2)_4NH_3)HgCl_4$] (Amami et al, 2002) (CSD ref. code: LOYBEG), both have eclipsed inorganic layers. One would expect the interlayer spacing to be greater for the 1,4-diammoniumbutane compound compared to the 1,3-diammoniumpropane compound but the reverse is observed, where the spacing is 0.4 Å longer in the latter compound. This is due to the conformation of the cations between the layers as the $H_3N(CH_2)_4NH_3$ chain has a *gauche-trans-gauche* conformation and $H_3N(CH_2)_3NH_3$ is *gauche-trans*. The shorter cation is also tilted more towards the perpendicular to the layers. The two compounds also differ significantly in their hydrogen bonding configuration. [$(H_3N(CH_2)_3NH_3)HgCl_4$] has a terminal halogen configuration and [$(H_3N(CH_2)_4NH_3)HgCl_4$] has a bridging halogen configuration (Figure 2.29).

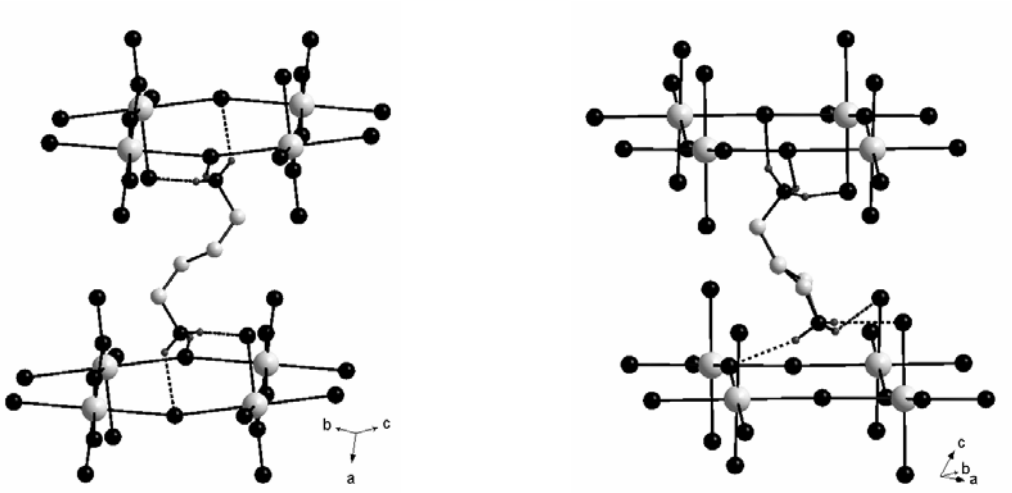


Figure 2.29: The hydrogen bonding configurations of $[(H_3N(CH_2)_4NH_3)HgCl_4]$ (left) and $[(H_3N(CH_2)_3NH_3)HgCl_4]$ (right).

The most frequently reported metal halide inorganic-organic layered perovskite-type hybrids contain the metals Cu, Mn, Cd, Hg and Ni and the halides Cl and Br. The crystal structures of most of them have been determined via SC-XRD and are listed in Table 2.10.

Table 2.10: Structures of compounds that appear in the CSD. Numbers the last column refer to the references listed at the end of the table.

Compound	Arrangement of Layers	Conformation of Cation	CSD ref. code	Hydrogen Bonding Configuration	Ref.
$[(H_3N(CH_2)_2NH_3)NiCl_4]$	Eclipsed	*trans*	NICLEN	Terminal	5
$[(H_3N(CH_2)_2NH_3)MnCl_4]$	Eclipsed	*trans*	ENDAMN10	Terminal	6
$[(H_3N(CH_2)_3NH_3)MnCl_4]$	Eclipsed	*trans*	PYDAMN03, PYDAMN	Terminal	8, 10
$[(H_3N(CH_2)_4NH_3)MnCl_4]$	Eclipsed	*trans*	BUCLMN BUCLMN01	Terminal	7
$[(H_3N(CH_2)_2NH_3)CuCl_4]$	Eclipsed	*trans*	EDIACU11	Terminal	6, 9
$[(H_3N(CH_2)_3NH_3)CuCl_4]$	Eclipsed	*trans*	PAMTCC	Terminal	3
$[(H_3N(CH_2)_4NH_3)CuCl_4]$	Eclipsed	*trans-gauche-trans*	JEPDUK	Bridging Bridging	2
$[(H_3N(CH_2)_5NH_3)CuCl_4]$	Eclipsed	*trans-trans-trans-gauche*	JEPLEV	Terminal Terminal	2
$[(H_3N(CH_2)_3NH_3)CdCl_4]$	Eclipsed	*trans-trans*	PRDACD	N/A	4
$[(H_3N(CH_2)_3NH_3)FeCl_4]$	Eclipsed	*trans-trans*	PYDAFE	N/A	10
$[(H_3N(CH_2)_2NH_3)CuBr_4]$	Eclipsed	*trans*	VABDUX	Terminal Terminal	1
$[(H_3N(CH_2)_3NH_3)CuBr_4]$	Eclipsed	*trans-gauche*	VABFAF	Terminal Bridging	1
$[(H_3N(CH_2)_4NH_3)CuBr_4]$	Eclipsed	*trans-gauche-trans*	JEPLAR	Bridging Bridging	2
$[(H_3N(CH_2)_5NH_3)CuBr_4]$	Eclipsed	*trans-trans-trans-gauche*	JEPLIZ	Terminal Terminal	2

Key to references in Table 2.10

1) Halvorsen and Willett, 1988.
2) Garland et al, 1990.
3) Phelps et al, 1976.
4) Willett, 1977.
5) Skaarup and Berg, 1978.
6) Tichý et al, 1978.
7) Tichý et al, 1980.
8) Crowley, et al, 1982.
9) Birrell and Zaslow, 1972
10) Willett and Riedel, 1975.

2.4.3 Structural phase transitions of inorganic-organic layered perovskite-type hybrids $[(H_3N(CH_2)_nNH_3)MCl_4]$ (M = Cd and Mn) with diammonium alkyl chains

The alkyldiammonium compounds have been intensely investigated to understand the mechanism of their structural phase changes, if any. The two most discussed systems are cadmium(II) chloride and manganese(II) chloride. The structural transitions were not always analysed only via SC-XRD but through other techniques.

The possible phase transitions of $[(H_3N(CH_2)_nNH_3)CdCl_4]$ (n = 2-5), abbreviated C_nN_2CdCl, were followed via ^1H NMR (Blinc et al, 1977) and changes in the dielectric constant (Levstik et al, 1976) as a function of temperature. The unit cell parameters of the room temperature phases of n = 2 and 4 were found to be monoclinic with space group $P2_1/b$ and orthorhombic for n = 3 and 5 (space group *Imma*) (Peterson and Willett, 1975; Arend and Gränicher, 1976). The compound C_2N_2CdCl shows no phase transitions between -150°C and +100°C, probably due to the rigidity of the cation between the layers due to the double hydrogen bonding interactions on both ends of the molecule and the short chain length, which does not allow for much freedom of movement. The longer chain compounds do have transitions at 103°C (C_3N_2CdCl), 68°C (C_5N_2CdCl) and multiple transitions at 68°C, 88°C and 91°C (C_4N_2CdCl). Enthalpies and entropy values for these transitions were determined by a calorimetric study done by Tello et al (1977). The transitions were detected by changes in the second moments M_2 of the NMR absorption spectra and the spin relaxation times T_1. In summary, Blinc et al (1977) found the transitions to be due to changes in the hydrogen bonding configurations, in conjunction with rotation and motion of the alkyl chains. The single phase transitions of C_3N_2CdCl and C_5N_2CdCl were also studied by a variety of techniques, including ^{35}Cl NMR and deuteron quadrupole resonance spectroscopy, and found to be order-disorder transitions (Kind et al, 1981). The motion of the diammonium chains could be followed more accurately as they were deuterated.

The manganese analogues, $[(H_3N(CH_2)_nNH_3)MnCl_4]$ (n = 2-5), abbr. C_nN_2MnCl, show a very similar phase behaviour compared to cadmium. The same odd / even effect of the room temperature unit cells is seen (Arend et al, 1976b). Again, there are no phase transitions for n = 2 but they exist for C_3N_2MnCl (33°C and 63°C), C_4N_2MnCl (110°C) and C_5N_2MnCl (28°C). The

space groups and crystal structures of C_3N_2MnCl were determined by SC-XRD and reveal the following phase sequence with increasing temperature: Phase **III** (*Pnma*) → Phase **II** (*Fmmm*) → Phase **I** (*Imma*) (Crowley et al, 1982). The results are in agreement with studies done using ^{35}Cl NQR measurements and deuterated NMR-NQR (Kind et al, 1978) where both phase transitions are first-order. Phase **III** and phase **I** both have a terminal hydrogen bonding configuration and only differ by a two-fold disorder of the cation in phase **I**, where the cation tilts by about 40° around the long axis compared to phase **III**. Phase **II** has a predominant terminal halogen configuration as one hydrogen bonds to both a bridging and a terminal chloride, also known as a bifurcated hydrogen bond. Phase **II** has the chain tilted by 20° relative to the inorganic layer, intermediate compared to phase **III** and phase **I**. Only the single crystal structure of phase **III** has been reported (CSD ref. code: PYDAMN03).

C_4N_2MnCl has only one phase transition compared to the three for C_4N_2CdCl and it is second-order. Complete SC-XRD crystal structures were reported for both the monoclinic room temperature phase **II** (CSD ref. code: BUCLMN) and the orthorhombic high temperature phase **I** (CSD ref. code: BUCLMN01) (Tichý et al, 1980). The cation in phase **II** is very nearly planar and all-*trans* with a centre of symmetry at the midpoint of the chain. In phase **I**, the position of the cation is split between two equivalent positions across a mirror plane. The connectivity of the resulting ten atoms, all of them half occupied, and the conformation of the cation can not be determined (See Figure 2.30). ^{35}Cl NMR and NQR measurements on deuterated samples again confirm the order-disorder transition behaviour (Kind et al, 1981).

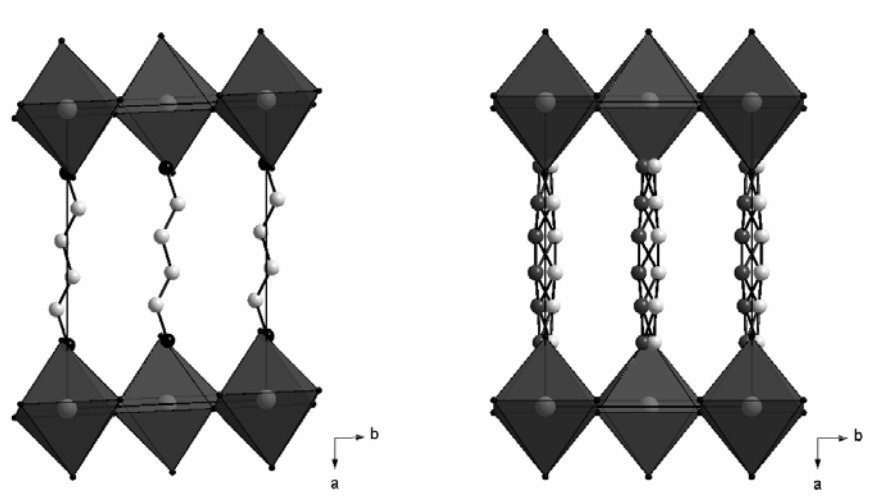


Figure 2.30: The packing diagrams of phase **II** (left) and phase **I** (right) of $[(H_3N(CH_2)_4NH_3)MnCl_4]$. The two equivalent positions of the atoms are shown as light grey and dark grey spheres in phase **I**.

2.5 Inorganic-organic layered perovskite-type hybrids $[(H_3N\text{-}R\text{-}NH_3)MX_4]$ containing aromatic diammonium cations

Diammonium compounds with aromatic R groups are rare. The simplest structure has a single benzene ring, as in 1,4-phenylenediammonium. The ammonium groups have to be *para* to each other; otherwise they will not be able to hydrogen bond to adjacent layers. Only three such structures have been reported, $[(H_3N\text{-}C_6H_4\text{-}NH_3)CdCl_4]$ (Ye et al, 1996) (CSD ref. code: ZITTOL) (eclipsed inorganic layers), $[(H_3N\text{-}C_6H_4\text{-}NH_3)CdBr_4]$ (Ishihara et al, 1996) (CSD ref code. NOJQIM) (staggered inorganic layers) and $[(H_3N\text{-}C_6H_4\text{-}NH_3)CuCl_4]$ (Bourne and Mangombo, 2004) (CSD ref. code: HAJSOB) (eclipsed inorganic layers. The phenyl rings themselves are almost perpendicular to the plane of the inorganic layers (See Figure 2.31). Both the cadmium(II) chloride and copper(II) chloride hybrids have weak edge-to-face C-H...π interactions between adjacent phenyl rings (Hydrogen...centroid distance is 3.134(17) Å for Cu compound and 3.034(66) Å for Cd compound).

The next cation of interest would have two benzene rings connected in a *para*-fashion, so that the ammonium groups are still *para* to each other. This organic compound is called benzidine. Only one reported structure of an inorganic-organic layered perovskite-type hybrid exists for this cation. $[(H_3N\text{-}C_6H_4\text{-}C_6H_4\text{-}NH_3)CuCl_4]$ (CSD ref. code: HAJTES) has eclipsed inorganic layers with an interlayer spacing of 14.3769(2) Å. For comparison, the interlayer spacing for the single aromatic case is 10.007(5) Å. The hydrogen bonding interactions are the same as those for the previous structures (terminal halogen configuration). The Cu compound with the benzidine cation has two edge-to-face C-H...π interactions which are closer than in the previous compound (H...centroid distance 2.985(2) Å and 3.074(2) Å) (Bourne and Mangombo, 2004) thus further stabilizing the overall structure. The same benzidine cation with lead(II) chloride does not form the layered perovskite structure type but rather a hybrid material with isolated $PbCl_6$ octahedra. This structure is discussed in Section 2.10.1 below.

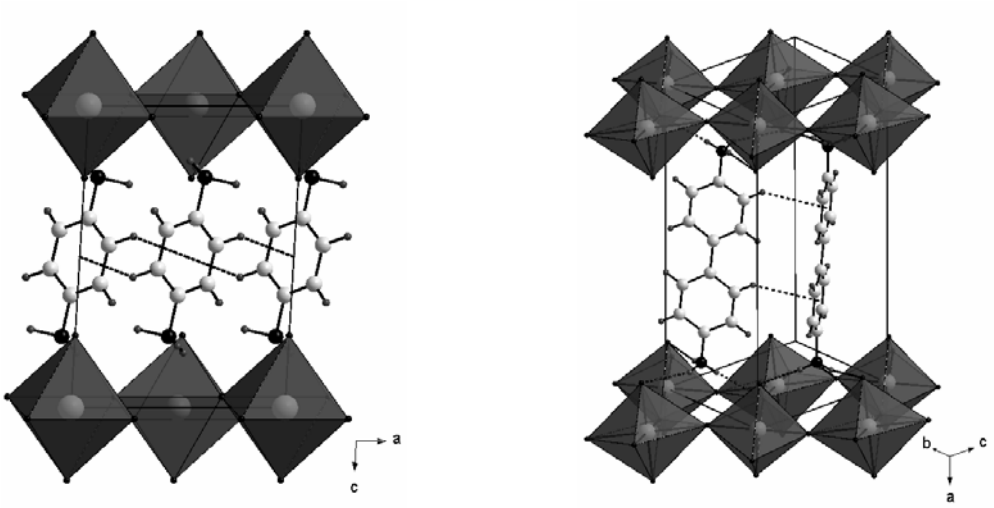


Figure 2.31: The packing diagrams of [(H_3N-C_6H_4-NH_3)$CdCl_4$] (left) and [(H_3N-C_6H_4-C_6H_4-NH_3)$CuCl_4$] (right). The C-H...π interactions are shown as dashed black lines.

2.6 Inorganic-organic layered perovskite-type hybrids with triammonium cations

The compound [(($H_3NCH_2CH_2$)$_2NH_2$)$CuCl_4$]·Cl (Ferguson and Zaslow, 1971) (CSD ref. code: AEATCU10) is unique as it contains not only layers of corner-sharing $CuCl_6$, but in between the layers, it has isolated chloride ions as well (See Figure 2.32). The two equivalent ethylammonium groups, consisting of the N2 atom, sit in the holes shaped by the four bridging and four terminal chlorides in the usual manner associated with the layered perovskite-type motif. The NH_2 group, to which the ethylammonium groups are attached and contains atom N1, is found on a mirror plane at y = 1/4 together with the chloride anion, Cl(3). There is a short N1...Cl3 distance of 3.06(3) Å, which is indicative of hydrogen bonding. The position of the hydrogen atoms were not reported in this structure. For this reason, a more accurate structure determination was done by Greenhough and Ladd (1977) at room temperature. An accurate crystallographic study of this compound at different temperatures would be useful as it undergoes thermochromic behaviour above and below room temperature, suggested to be due to shifts in the position of the hydrogen atoms involved in hydrogen bonding. The compound also undergoes a phase transition from a paramagnetic to an antiferromagnetic state when cooling to below 11.8 K (Losee and Hatfield, 1974).

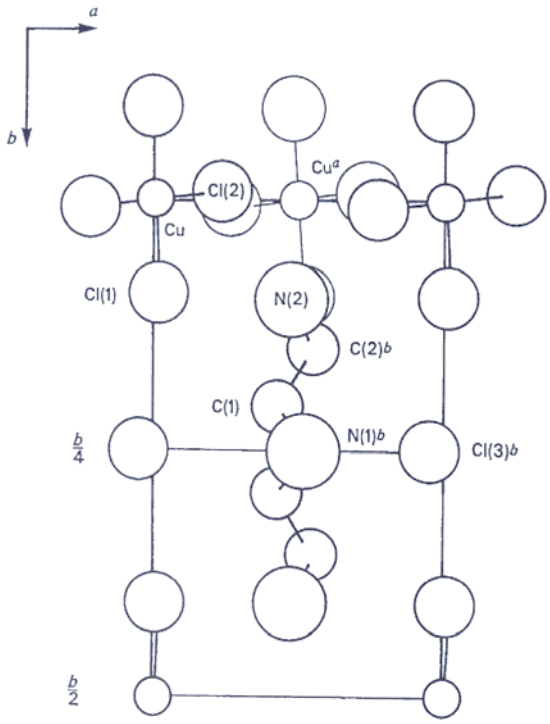


Figure 2.32: Half of the unit cell of $[((H_3NCH_2CH_2)_2NH_2)CuCl_4]\cdot Cl$. Figure is taken from Ferguson and Zaslow (1971).

The same amine was also crystallized with manganese(II) chloride and gave the same geometry as the copper(II) chloride inorganic-organic layered perovskite-type hybrid (See Figure 2.33). The compound $[(H_3NCH_2CH_2)_2NH_2)MnCl_4]\cdot Cl$ (CSD ref. code: ETRAMN) shows no structural phase transitions as the hydrogen bonding to the isolated interlayer chloride reduces the mobility of the organic chain (Breneman and Willett, 1981).

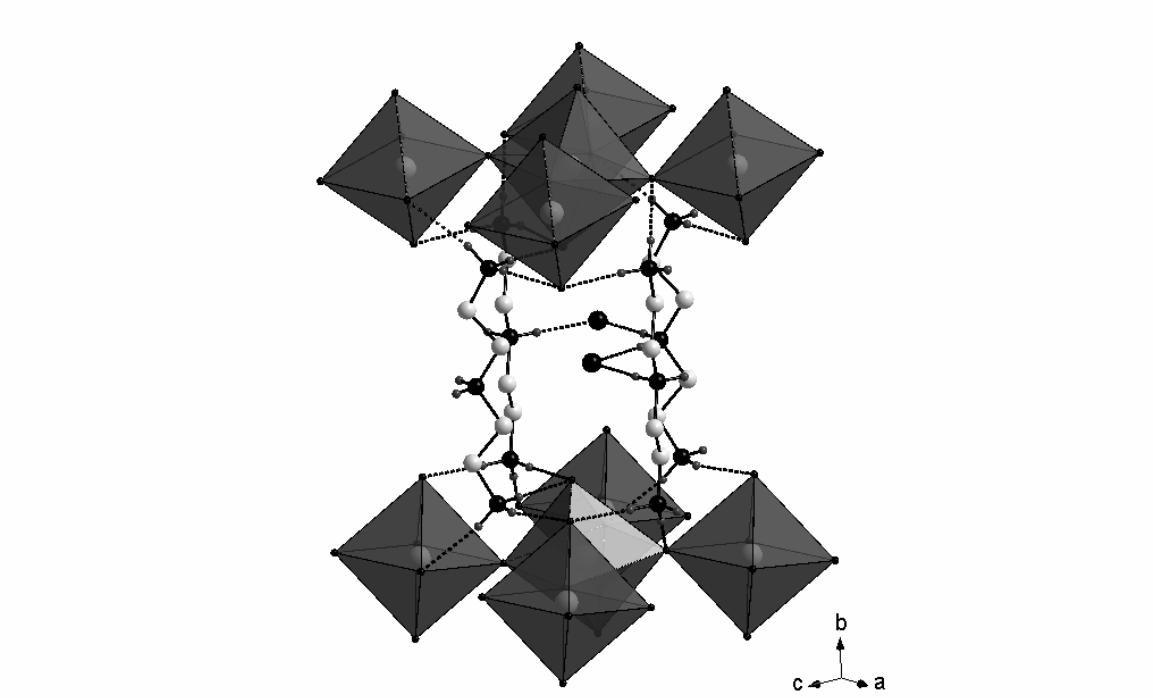


Figure 2.33: Half of the unit cell of $[((H_3NCH_2CH_2)_2NH_2)MnCl_4]\cdot Cl$. The hydrogen bonds to the interlayer chloride are shown as dashed black lines.

2.7 Other metals and more complex ammonium cations contained in inorganic-organic layered perovskite-type hybrids

In this section, we look at the compounds that contain unusual metals or that have specially designed cations resulting from crystal engineering type principles. These cations are often only characterized by non-crystallographic techniques to investigate the effect the metal(II) halide and the ammonium cation have on their optical properties. The most studied R group is based on the 2-phenylethylammonium backbone, abbr. PEA.

The use of non-transition metals, that are divalent, is an idea that follows on after much work has been done using the metals Cu, Pb, Mn, Fe, Cd, Sn, etc as discussed in the previous sections. The only divalent rare-earth metal reported so far has been europium (Mitzi and Liang, 1997). The synthesis of the inorganic-organic layered perovskite-type hybrid with butylammonium, Eu(II) and I is not trivial as the metal has a tendency to coordinate the solvent molecules to itself when in solution. Single crystals of the inorganic-organic layered perovskite-type hybrids are mostly

obtained from slow cooling or evaporation of solutions using acid halides and some alcohol or other common solvents (See Chapter 3). Furthermore, slow oxidation of Eu(II) is often seen in solution and this does not allow for a long enough crystallization period. Thus, the compound $[(C_4H_9NH_3)_2EuI_4]$ was prepared by solid state reaction in an inert atmosphere of Argon. The resulting polycrystalline samples were analysed by Powder X-Ray diffraction and the orthorhombic unit cell dimensions determined to be a = 8.913(3) Å, b = 8.759(3) Å and c = 27.793(6) Å. These values are very close to the room temperature unit cell of $[(C_4H_9NH_3)_2PbI_4]$ (Mitzi, 1996) and confirm that it has corner-sharing layers of EuI_6 octahedra. The compound shows a strong blue photoluminescence at 460 nm.

The group IVB metals Pb and Sn have been extensively studied. Mitzi (1996) has also prepared $[(C_4H_9NH_3)_2GeI_4]$ and characterized it by SC-XRD, and additionally shows photoluminescence at 690 nm. The crystal structure is similar to the analogues structures with Pb, Sn and Eu.

The conscious design of a particular structure in the inorganic-organic layered perovskite-type hybrids was performed on the system $[(C_6H_5C_2H_4NH_3)_2SnI_4]$. This parent structure has been used to change its electronic properties by changing the organic cation. This was achieved by Mitzi et al (2001) by substituting one of the aromatic hydrogens for a fluorine atom and then changing its position on the ring between the 2, 3 and 4 positions.

Table 2.11 summarizes the trends observed in the electronic properties and crystal structures of [(x-flourophenylethylammonium)$_2$SnI$_4$] for x = 2, 3, 4. There is a noticeable correlation between the bridging angle I-Sn-I and the shift of the peak position of the exciton band. The dependence of the absorption and photoluminescence spectra of spin coated films of these three compounds on the position of the fluorine atom was confirmed by Kikuchi et al (2004). The idea was then carried further by exchanging the halide for Br and Cl on the 2-position only and observing the effect of the halide on the peak position. These results are summarized in Table 2.12.

Table 2.11: $[(x\text{-}F\text{-}C_6H_4C_2H_4NH_3)_2SnI_4]$, x = 2, 3, 4.

x	F...F distance / Å	Bridging angle I-Sn-I/ °	Peak of Exciton / nm	Superstructure	Interlayer Spacing / Å	CSD ref. code
0	N/A	156.48	609	a_p x a_p	16.30	POFKOK (1)
2	> 6.0	153.28(3)	588	a_p x $2a_p$	17.535(3)	BAKHAX (2)
3	3.02(1)	154.16(3)	599	a_p x $2a_p$	17.297(4)	BAKHEB (2)
4	3.516(2)	156.375(8)	609	$\sqrt{2}a_p$ x $\sqrt{2}a_p$	16.653(2)	BAKHIF (2)

1) Papavassiliou et al, 1994.

2) Mitzi et al, 2001b.

Table 2.12: $[(2\text{-}X\text{-}C_6H_4C_2H_4NH_3)_2SnI_4]$ (X = Cl and Br) (1).

X	I...X distance / Å	Bridging angle I-Sn-I / °	Exciton Peak / nm	Superstructure	Interlayer Spacing / Å	CSD ref. code
Cl	3.98	154.76(6)	586	a_p x a_p	16.891(7)	RUYDUK
Br	4.29	148.71(1)	557	$\sqrt{2}a_p$ x $\sqrt{2}a_p$	18.540(2)	RUYDOE

(1) Xu et al, 2003a.

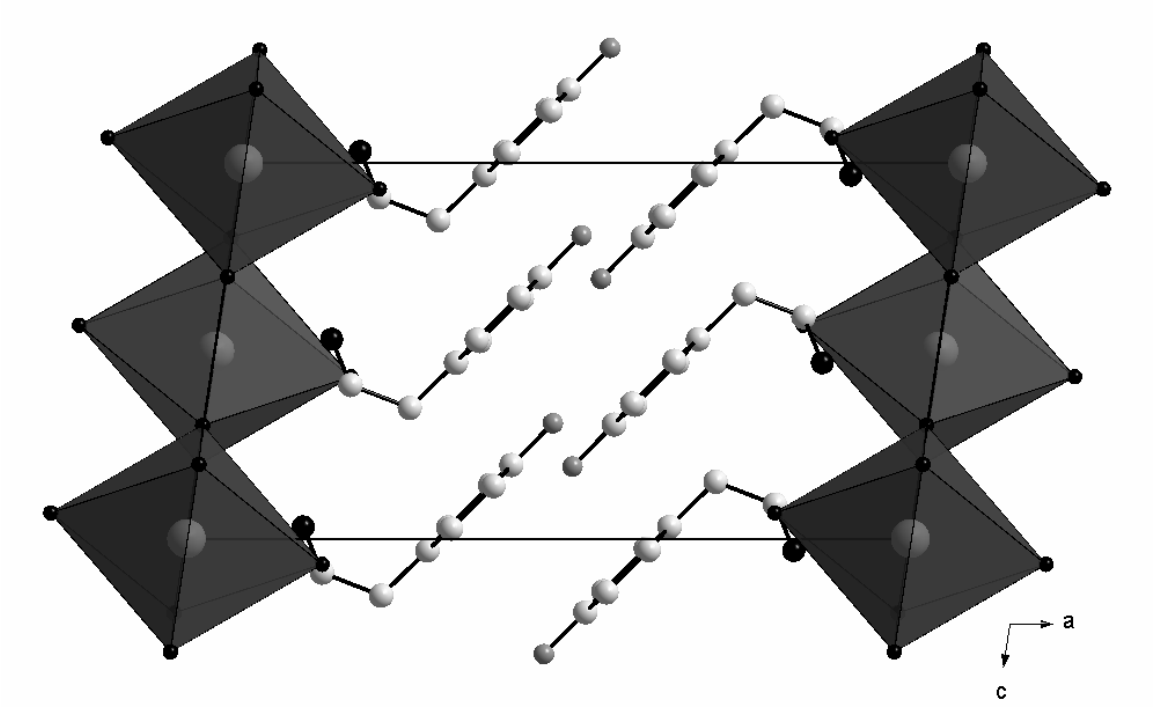


Figure 2.34: The packing diagram of $[(4\text{-}F\text{-}C_6H_4C_2H_4NH_3)_2SnI_4]$. The aromatic rings are parallel to each other.

In another example, an organic chromophore was used as the R group. In principle it can add hole-transporting capability to the overall inorganic-organic layered perovskite-type structure (Era et al, 2005). The distance between the ammonium group and the chromophore was varied by hydrocarbon chains of varying length (Figure 2.35). The inorganic layers were composed of $PbBr_6$ octahedra and the interlayer spacing was determined by P-XRD. The absorption spectra of spin coated films peaked at around 400nm for n > 3 and varied only slightly with the increasing values of n. No exciton absorption peak was seen for n = 3.

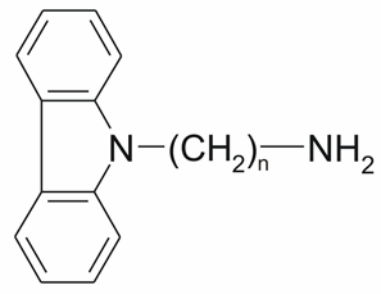


Figure 2.35: The carbozole chromophore, n = 3-8, 12.

Another comparatively common R group has a naphthalene backbone, $C_{10}H_7$, and the ammonium group on its 1-position. The inorganic-organic layered perovskite-type hybrids $[(C_{10}H_7\text{-}(CH_2)_nNH_3)_2PbBr_4]$ (n = 1 and 2) and $[(C_{10}H_7\text{-}O(CH_2)_nNH_3)_2PbBr_4]$ (n = 3, 4 and 8) show phosphoresence for all compounds and exciton emission for all compounds except where n = 1 (Era et al, 1998a). Another studied chromophore has azobenzene-linked ammonium molecules, $[(C_6H_5\text{-}N{=}N\text{-}C_6H_4\text{-}O(CH_2)_nNH_3)_2PbBr_4]$ (n= 3, 4 and 6). The absorption peaks for the three compounds are centered around 390 nm (Era et al, 1998b). The 1-naphthalene backbone has also been used to prepare copper(II) chloride inorganic-organic layered perovskite-type hybrids, $[(R\text{-}NH_3)_2CuCl_4]$, where R is $C_6H_5CH_2$-, $C_{10}H_7\text{-}CH_2$-, $C_{10}H_7\text{-}O(CH_2)_3$- and $C_{10}H_7\text{-}O(CH_2)_4$- (Shikoh et al, 2001). These complexes show ferromagnetism. The values of the Curie temperatures, Tc, are independent of the interlayer spacing but change with the identity of the R group. The absorption spectra show two peaks, around 290 nm and 370-400 nm, which are indicative of Jahn-Teller type distortion.

One of the largest chromophores, reported in the literature, has pyrene as the backbone and methylammonium on the 1-position. Three inorganic-organic layered perovskite-type hybrids were made, $[(C_{16}H_9\text{-}CH_2\text{-}NH_3)_2PbX_4]$ (X = Cl, Br and I), by slow evaporation of the DMF solvent containing a 2:1 ratio of the cation salt and PbX_2 (Braun et al, 1999b). The identity of the halide affects the emission spectra and phosphorescence decay times. The authors also investigated the inorganic-organic layered perovskite-type hybrids with mixed halide inorganic layers, $[(C_{16}H_9\text{-}CH_2\text{-}NH_3)_2PbCl_nBr_{4-n}]$ (n = 0-4). The compounds were prepared as spin-coated films on quartz substrates. The ratio of the two halides again affects the peak position of the absorption spectra (Braun et al, 1999b).

A significant achievement in the crystal engineering of inorganic-organic layered perovskite-type hybrids was achieved in the compound $[(C_6F_5C_2H_4NH_3{\cdot}C_{10}H_7C_2H_4NH_3)SnI_4]$ (CSD ref. code: AQIMOC), which contains two different ammonium cations in the same structure, the molecules 2,3,4,5,6-pentaflourophenethylammonium (5FPEA) and 2-naphthylenethylammonium (NEA) (Xu and Mitzi, 2003). The structural model was deduced from SC-XRD data. The bilayers of organic molecules within the 2-D inorganic layers each contain one of these molecules, so that the sequence of molecules perpendicular to the layers is [NEA-5FPEA-PbI_4-NEA-5FPEA-PbI_4-NEA] as the flouroaryl-aryl interactions seem to occur perpendicular to the layers. Hence, both the 5FPEA and NEA molecules hydrogen bond to the layers.

The second reported case of mixed organic molecules within the perovskite-type layers involves the compounds $[(C_6F_5C_2H_4NH_3)SnI_4]{\cdot}(C_6H_6)$ (CSD ref. code: XIYZEK) and $[(C_6H_5C_2H_4NH_3)_2SnI_4]{\cdot}(C_6F_6)$ (CSD ref. code: XIYZIO). In contrast to the compound described above, the benzene and flourinated benzene molecule do not have any ammonium groups and hence are intercalated between the bilayers of the 5FPEA and PEA organic cations. The sequence perpendicular to the layers is then [PbI_4-5FPEA-C_6H_6-5FPEA-PbI_4] and [PbI_4-PEA-C_6F_6-PEA-PbI_4]. The intercalated rings have strong face-to-face π-type interactions with the aromatic rings of the ammonium cations, thus stabilizing the overall structure (Mitzi et al, 2002). Also mentioned in the article is that when using separately either the flourinated or unflourinated compounds, no stable product compounds were formed. This highlights even further the significance of the flouroaryl-aryl interactions.

The only reported case of an inorganic-organic layered perovskite-type hybrid that has adjacent layers connected by covalent bonds is the compound [$(Cu(O_2C\text{-}(CH_2)_3\text{-}NH_3)_2PbBr_4$] (CSD ref. code: EXUNUG), which has Br-Cu-Cu-Br linkages between adjacent layers. The organic cation 4-aminobutyric acid is zwitterionic and is covalently bonded to Cu atoms via the carboxylate groups. Four of these organic cations are bonded to the Cu atoms to form dimeric clusters. The Cu atoms are then covalently linked to the terminal bromides of the $PbBr_6$ layered perovskite layers and to adjacent clusters to form a "covalent bond pathway between adjacent perovskite layers" (Mercier and Riou, 2004) (See Figure 2.36). This makes the overall 3-D structure much stronger than before as the usual interactions observed until now between adjacent layers and cations are weak van der Waals forces. The ammonium groups hydrogen bond to both the three bromides of the inorganic perovskite-type layers and to one of the oxygen atoms intramolecularly.

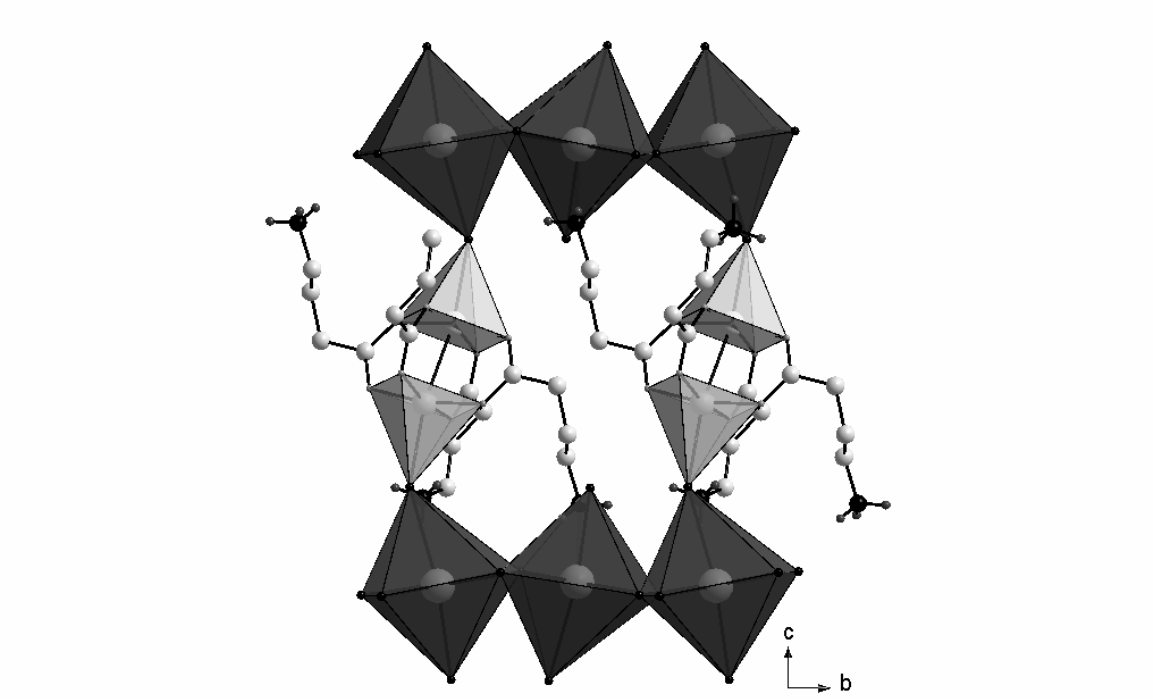


Figure 2.36: The packing diagram of [$(Cu(O_2C\text{-}(CH_2)_3\text{-}NH_3)_2PbBr_4$]. The $PbBr_6$ octahedra are shown as dark grey octahedra and the CuO_4Br square-planar pyramids are light grey.

The search for other non-covalent interactions between the R groups of the organic ammonium cations has had some success. The objective is to use functional groups that strengthen the

interactions between R groups without affecting the desired layered perovskite-type motif. This process is at the heart of crystal engineering. Previously, aromatic interactions between ring systems has shown positive results. However, a stronger interaction can be hydrogen bonds between alcohol and carboxylic acid functional groups. With this objective in mind, the layered perovskite-type hybrids $[(HO(CH_2)_2NH_3)_2PbX_4]$ (X = I and Br) were made, which have alcohol-based bifunctional ammonium cations (Mercier et al, 2004). There are three different hydrogen bonding interactions in these structures. The usual NH_3^+...X interaction, but with only two hydrogens bonding to the terminal halide and bridging halide. The second interaction is the one of interest as it involves the third ammonium hydrogen, which hydrogen bonds to the oxygen molecule of the adjacent cation to form hydrogen bonded dimers. The N-H...O bond distance is 2.23 Å in the lead iodide structure and brings the lead(II) iodide layers closer together. The nearest distance between I...I contacts is 4.279(2) Å, which is the second shortest reported for Group IVB divalent metals with the layered perovskite-type motif, helped by the fact that the inorganic layers are eclipsed. This causes a significant red shift of the exciton peak to 536 nm. The shortest Br...Br contact is 4.36(2) Å and the exciton peak is blue shifted to 417 nm. The layers are staggered. The third interaction has an O-H...I hydrogen bond, which means that both ends of the hydroxyethylammonium cations have hydrogen bonded interactions with the halides. The first reported structure with an alcohol functional group was $[(HO(CH_2)_2NH_3)_2CuCl_4]$ (CSD ref. code: TIRQOQ), which has a two-fold disorder of the $HOCH_2CH_2$- moiety (Halvorson et al, 2005).

Carboxylic acids form very strong hydrogen bonded dimers, stronger than the alcohols. The first inorganic-organic layered perovskite-type hybrids with carboxylic dimers reported were $[(\beta\text{-alaninium})_2CuCl_4]$ (Willett et al, 1981) (CSD ref. code: BEHXIV) and $[(\beta\text{-alaninium})_2CuBr_4]$ (Willett et al, 1983) (CSD ref. code: CAYPOH). The inorganic layers consist of square-planar CuX_4 anions separated by the organic cations. The cations from adjacent layers form dimeric pairs, adding a 3-D stability to the crystals not seen in other inorganic-organic layered perovskite-type hybrids. The O...O distance is 2.682(3) Å in the copper(II) chloride hybrid. Another inorganic-organic layered perovskite-type hybrid was prepared by Mercier (2005). The bifunctional cation is ammonium 4-butyric acid, which has a carboxylic acid group separated by a propane chain from the ammonium functional group. The compound is

$[(HO_2C(CH_2)_3NH_3)_2PbI_4]$ (CSD ref. code: QARWOW). The carboxylic acid groups form extended 1-D chains of hydrogen bonds. Adjacent cations point in opposite directions to form a ladder-like motif of O-H...O chains (See Figure 2.37).

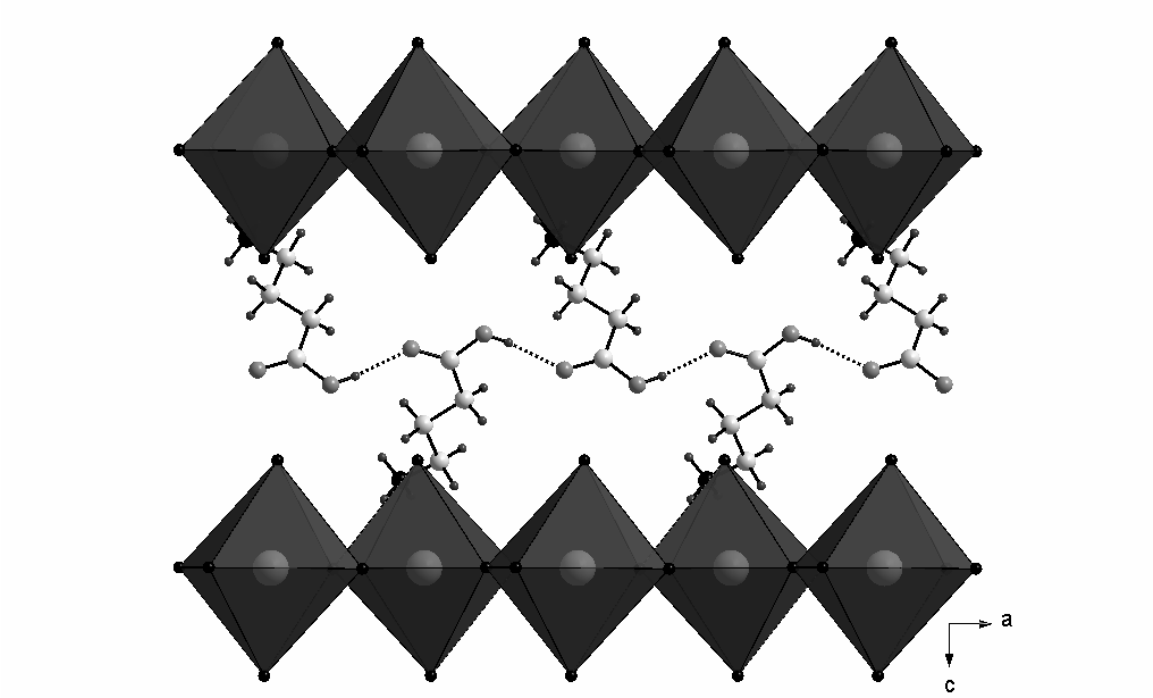


Figure 2.37: The packing diagram of $[(HO_2C(CH_2)_3NH_3)_2PbI_4]$. The R groups have a carboxylic functional group that interacts strongly with adjacent R groups via O-H...O (d(O...H) = 1.8 Å) hydrogen bonds to strengthen the overall structure.

The rare case of an inorganic-organic layered perovskite-type hybrid that does not have a primary ammonium head group is demonstrated in the two isostructural compounds $[(C_6H_8N_4)PbI_4]$ (CSD ref. code: QUFBUO) and $[(C_6H_8N_4)SnI_4]$ (CSD ref. code: QUFCAV) (Tang et al, 2001). The protonated cation has only one hydrogen on each of the four nitrogen atoms, as seen in Figure 2.38 below. Nonetheless, the molecule can move far enough into the "box" to hydrogen bond to both sandwiching layers akin to the primary, diammonium cations discussed previously.

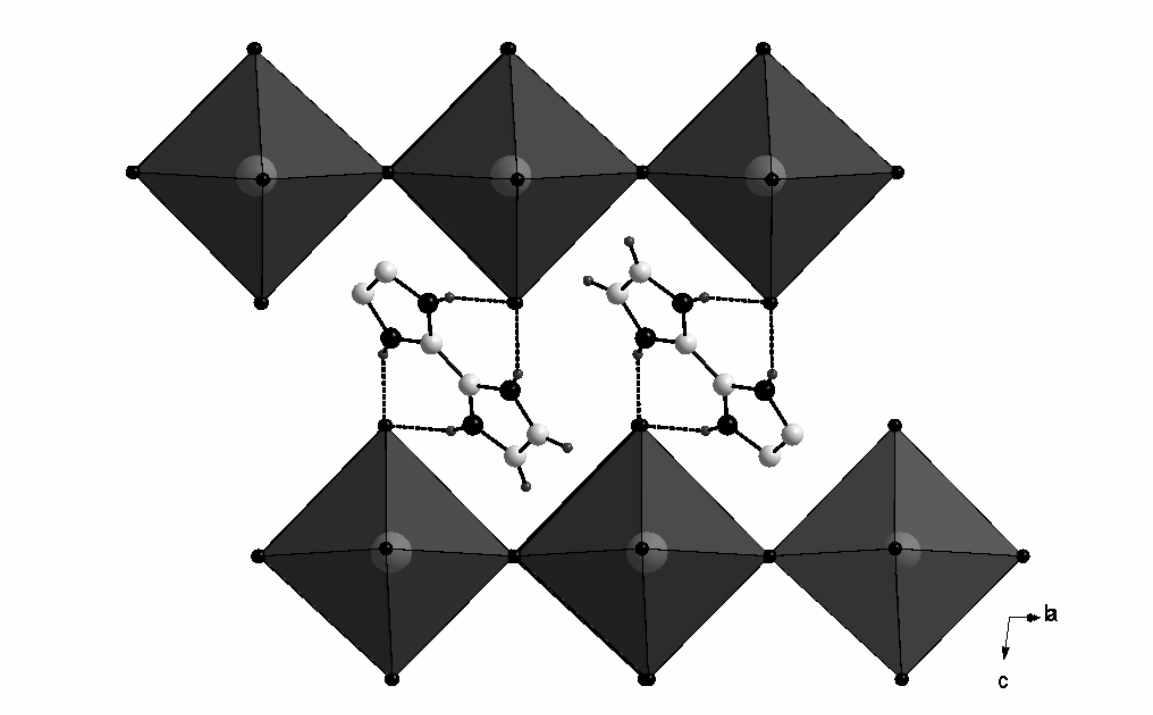


Figure 2.38: The packing diagram of $[(C_6H_8N_4)PbI_4]$. There are only four hydrogen bonds between the individual cations and the inorganic layers.

The inorganic-organic layered perovskite-type hybrid with the shortest interlayer spacing, and hence shortest I...I contact between adjacent layers, is $[((CH_3)_3N(CH_2)_2NH_3)SnI_4]$ (Xu et al, 2003b) (CSD ref. code: LUXJET). It has quaternary and primary ammonium cations and a I...I distance of 4.19 Å. The absorption peak is 630 nm. The structural consequence of the two ammonium cations can be seen in the corrugation of the SnI_6 layers. The terminal iodides are bent inward when the NH_3 group is in the hole and outward when the $N(CH_3)_3$ group is in the hole formed by the four bridging and terminal iodides (See Figure 2.39).

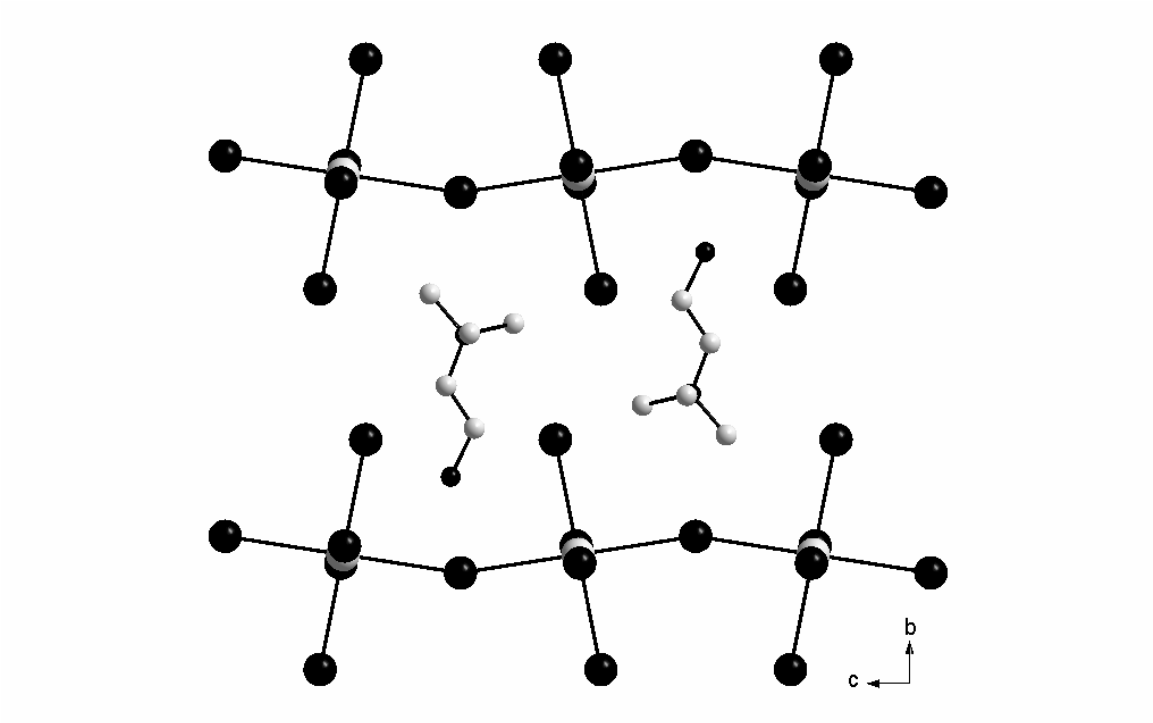


Figure 2.39: The packing diagram of $[((CH_3)_3N(CH_2)_2NH_3)SnI_4]$.

2.8 Multilayer inorganic-organic layered perovskite-type hybrids

A different structural variation of the cubic perovskite structure type is seen in the compounds of general formula $[(CH_3NH_3)_{m-1}(R\text{-}NH_3)_2M_mX_{3m+1}]$ (M = Sn or Pb; X = Cl, Br and I; R = C_nH_{2n+1}- or phenethylammonium; m = 1, 2, 3,…). If m = 1, then the hybrids have a monolayer of corner-sharing octahedra, which is then the layered perovskite-type motif already described extensively. If m > 1, then the monolayer is replaced by a bilayer (m = 2) (Figure 2.40 below), a trilayer (m = 3) (Figure 2.41 below), and so forth until m = ∞, which is again the 3-D cubic perovskite structure type of $[(CH_3NH_3MX_3]$. In the bilayer structure type, two monolayers are bonded by one of the formerly terminating iodides. Within the bilayer, the methylammonium cation occupies the cavities in the same manner as in the 3-D $[CH_3NH_3MX_3]$ inorganic-organic hybrid structures, i.e. it fits in the centre of eight corner-shared MX_6 octahedra. The bilayers are separated by any other ammonium cation, $R\text{-}NH_3$, which is larger than the methylammonium molecule, which fits on the periphery of a set of four corner-shared MX_6 octahedra (Tabuchi et al, 2000). Similarly, a trilayer has three monolayers stacked upon each other. Both ammonium

cations form hydrogen bonds to the halides in the usual manner described for the monolayer inorganic-organic layered perovskite-type hybrids.

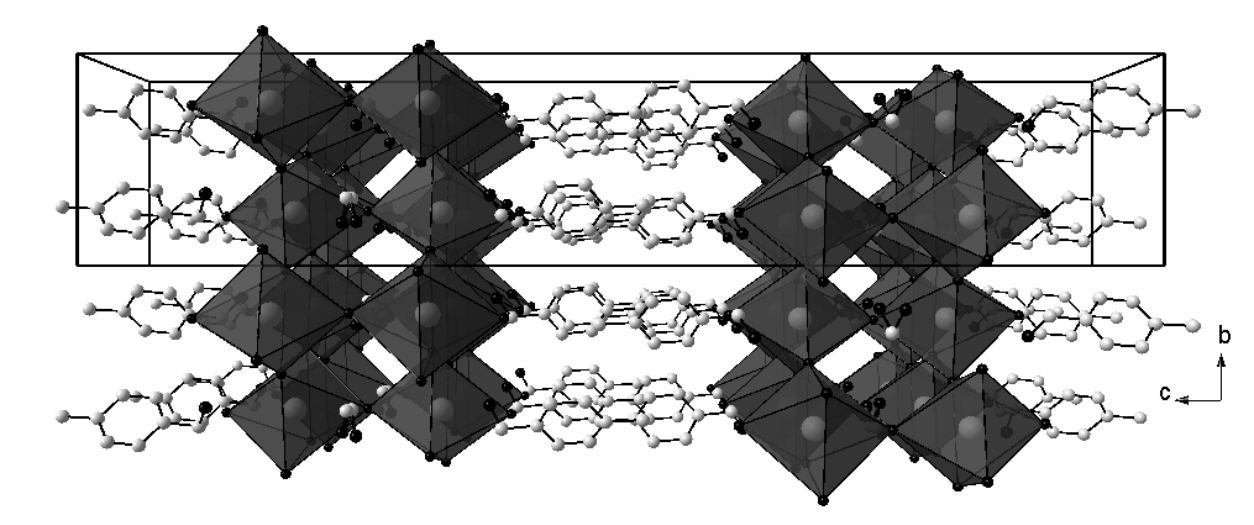


Figure 2.40: The packing diagram of the bilayer hybrid $[(CH_3NH_3)(H_3CC_6H_5(CH_2)NH_3)_2Pb_2I_7]$ (Papavassiliou et al, 2000; CSD ref. code: MEMYAE).

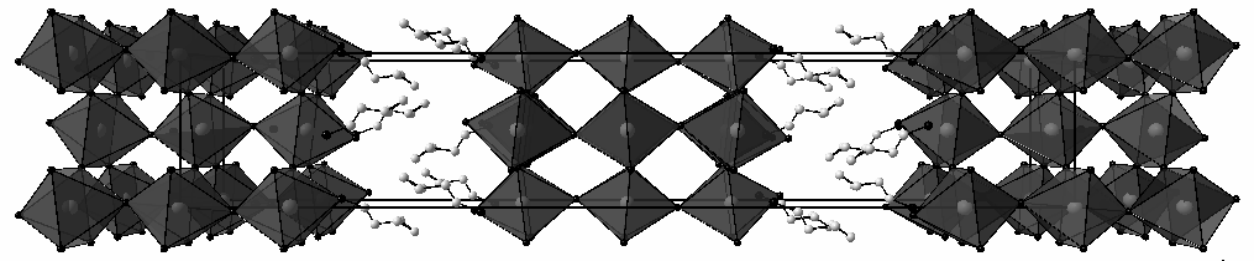


Figure 2.41: The packing diagram of the trilayer hybrid $[(CH_3NH_3)_2(C_4H_9NH_3)_2Pb_3I_{10}]$. The CH_3NH_3 cations are not shown as their positions were not accurately determined in the crystal structure (Mitzi et al, 1994; CSD ref. code: PIVCUS).

As the value for m increases, the behaviour of the hybrid goes from semiconducting to metallic (Mitzi et al, 1994). The electrical properties of these multilayer inorganic-organic layered perovskite-type hybrids can be further modified by varying the length of the alkylammonium chain from n = 2 - 12 and simultaneously varying the thickness of the inorganic layers, as in $(CH_3NH_3)_{m-1}(C_nH_{2n+1}NH_3)_2[Sn_mI_{3m+1}]$ (n = 2 - 12, m = 2, 3, 4, …) (Mitzi et al, 1994) and $(CH_3NH_3)_{m-1}(C_nH_{2n+1}NH_3)_2Pb_mBr_{3m+1}$ (m = 1 and n = 2, 3, 4, 6, 10; m = 2 and n = 2, 3, 4, 6; m = 3 and n = 6) (Tabuchi et al, 2000). In the latter study, the exciton absorption peak undergoes a red

shift as m increases. Only three other single crystal structures of various multilayer perovskites were found in the CSD (Table 2.13).

Table 2.13: Other bilayer inorganic-organic layered perovskite-type hybrids with their reported single crystal structures if reported.

Compound	CSD ref. code	Reference
$[(CH_3NH_3)(C_6H_5(CH_2)_2NH_3)_2Pb_2I_7]$	JIMDIS	Calabrese et al, 1991.
$[(CH_3NH_3)(HO_2C(CH_2)_3NH_3)_2Pb_2I_7]$	QARWIQ	Mercier, 2005.
$[(CH_3NH_3)(C_4H_3SCH_2NH_3)_2Pb_2I_7]$	MUBHEW	Zhu et al, 2002.
$[(CH_3NH_3)(C_6H_{13}NH_3)_2Pb_2I_7]$	N/A	Kataoka et al, 1994.

2.9 Photopolymerization

An exciting possibility in inorganic-organic layered perovskite-type hybrids is solid-state polymerization by irradiating the crystals with an external energy source. Simple alkyl chains that contain triple bonds are brought into close contact and photodimerize, as shown schematically in Figure 2.42 below (taken from Takeoka et al, 2001). The distance between closest triple bonds should be ideally between 3.6 and 4.1 Å (Schmidt, 1964) to form the polyene organic system.

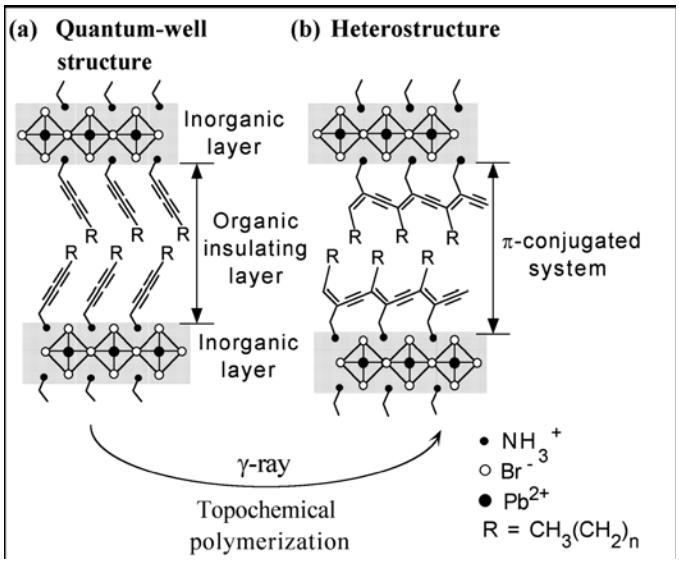


Figure 2.42: The basic idea of solid-state polymerization within layered type structures. Taken from Takeoka et al, 2001.

The simplest ammonium cation that has been investigated for possible solid-state reactivity is propargylammonium; it forms the layered perovskite-type structure with cadmium(II) chloride, $[(HC{\equiv}C\text{-}CH_2\text{-}NH_3)_2CdCl_4]$ (Lartigue-Bourdeau et al, 1992) (CSD Ref. code: LAPDIP). The cations form bilayers between the inorganic layers. The $-CH_2-$ spacer is important as it raises the unsaturated part of the cation above the level of the terminal halides, here chlorine, and angles the terminal HC≡C- groups within the bilayers towards each other (See Figure 2.43). The distances between the two closest terminal carbon atoms are 3.44 Å and 3.48 Å. When irradiated by u.v. or ^{60}Co-γ radiation, the colourless crystals display photoreactivity by changing colour (not specified by the authors). The authors surmise that the observed photoreactivity can possibly be due to a polymerization reaction of the triple bonds.

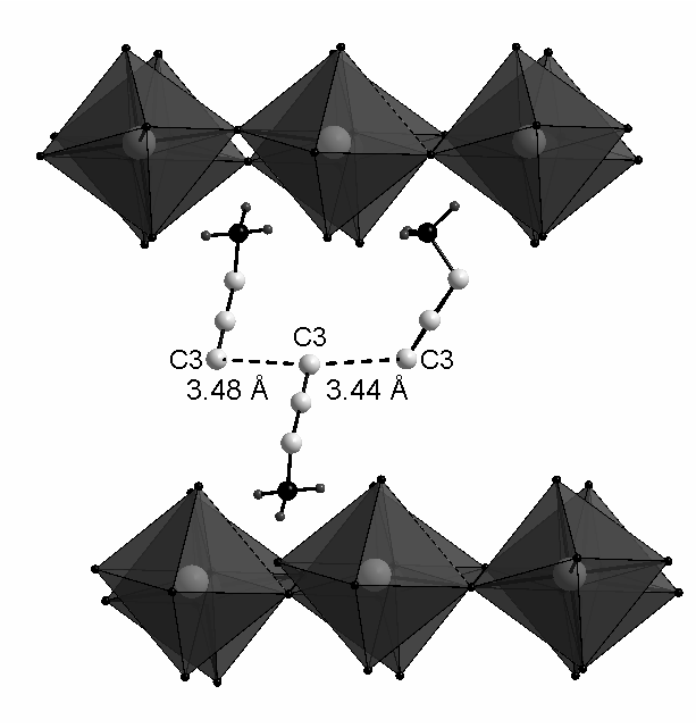


Figure 2.43: The geometries of the closest propargylammonium cations in the hybrid structure that undergoes possible photopolymerization. The octahedra consist of $CdCl_6$.

Longer alkyl chains with butadiyne moieties, $H_3C(CH_2)_{m-1}C{\equiv}C\text{-}C{\equiv}C(CH_2)_9NH_3$ (m = 6 and 14), have also formed inorganic-organic layered perovskite-type hybrids with cadmium(II) chloride. Thin films of both these hybrids were irradiated by a 4-W UV lamp at 254 nm and formed π-conjugated polymers (Kosuge et al, 2002a). P-XRD patterns of the thin films before and after irradiation show an increase in the interlayer spacing of 0.2 Å and 2.3 Å respectively for m = 6 and 14. The polymerization reactions were also followed by the changes in the absorption spectra of the spin-coated films. The maximum absorption wavelengths after irradiation are 528 nm (m = 6) and 635 nm (m = 14).

Takeoka and co-workers (2001) investigated a series of inorganic-organic layered perovskite-type hybrids with lead bromide, $[(H_3C(CH_2)_nC{\equiv}C\text{-}C{\equiv}C(CH_2)_mNH_3)_2PbBr_4]$, where n-m = 1-1, 2-1, 13-1, 15-1, 11-3. The source for the γ radiation was ^{60}Co. They found that photopolymerization only occured when n-m was 13-1 and 15-1, shown schematically in Figure 2.42. If the 11-3 cation is used, where the spacer consist of three methylene units, no reaction took place, even though the total length of the cation is the same as for the 13-1 cation. From this they concluded

that the ideal spacer distance between the butadiyne moiety and the ammonium group should be a single methylene group. The organic cations with n-m equal to 1-1 and 2-1 did not react, i.e. the longer alkyl chains in 13-1 and 15-1 help to orient the butadiyne moieties so that they can undergo a topochemical polymerization. The optical absorption spectra of the layered hybrid, $[(H_3C(CH_2)_{13}C{\equiv}C\text{-}C{\equiv}C(CH_2)_1NH_3)_2PbBr_4]$ was further investigated using spin-coated films on a SiO_2 substrate (Takeoka et al, 2002). The inorganic-organic layered perovskite-type hybrid in monomer form is colourless and changes colour to red after γ-irradiation. The exciton peak due to the 2-D quantum well structure of the monomer hybrid is at 378 nm and remains even after irradiation. A second, broad peak appears at 550 nm is attributed to the π*-π transitions of the formed polydiacetylene. The length of the polymer is estimated to be 22 monomer units, which the authors estimated from the π*-π peak using an adopted method of Exarhos et al (1976).

2.10 Two-dimensional inorganic motifs

2.10.1 Two-dimensional motifs - NET

Most 2-D inorganic motifs seen in the hybrid structures consist purely of corner-sharing octahedra. However, 2-D motifs can also be created by a combination of corner-, edge- and face-sharing. Most common of this type in the literature is the so-called net type motif which has trimeric units of *trans* face-sharing octahedra, summarised by the formula $(M_nX_{3n+1})^{(n+1)-}$. The 2-D layers are separated by monolayers or bilayers of organic cations containing primary, secondary or quaternary amine groups. The trimeric units are connected to each other via two corner-shared halides on both ends. To my knowledge, only one structure with n = 2 has been reported in the CSD, $[(Me_3N\text{-}C_2H_4\text{-}NMe_3)_2Pb_2I_7 \cdot I]$ (CSD ref. code: GEQHAL), which has isolated I^- anions between the lead iodide layers (Krautscheid et al, 1998). The organic cation is a quaternary diammonium group and forms a monolayer between two adjacent nets and interacts with the anionic layers purely through coulombic forces. There are numerous cases with n = 3 and this motif has been observed with both lead bromide as in $[(PhNMe_3)_4Pb_3Br_{10}]$ (Wiest et al, 1999) (CSD ref. code: CAQVIZ) and tin iodide $[(PhNMe_3)_4Sn_3I_{10}]$ (Lode and Krautscheid, 2001) (CSD ref. code: RAJMUK). Since the organic cation has only one nitrogen atom, both structures have bilayers of $PhNMe_3$ cations between the inorganic layers. Furthermore, these structures

have the individual building blocks *cis* related. The 2-D nets can also be corrugated if the trimeric units connect in an alternating *trans* fashion as seen in $[(C_6H_5NH_3)_4Cd_3Br_{10}]$ (Ishihara et al, 1994) (CSD ref. code: POPHAD), $[(C_6H_5CH_2SC(NH_2)_2)_4Pb_3I_{10}]$(Raptopoulou et al, 2002) (CSD ref. code: IGECIG) and $[(AESBT)_4Pb_3I_{10}]$ (Zhu et al, 2003) (CSD ref. code: BAYHEP), where AESBT is 5-ammoniumethylsulfanyl-2,2'-bithiophene. These three compounds have primary and secondary ammonium groups and are stacked head-to-tail between the inorganic layers to form a bilayers of organic cations. The bilayers interact with the inorganic layers in the same way as the 2-D layered perovskites via hydrogen bonds to the iodine atoms.

A net-type motif which has no face-sharing but only edge- and corner-sharing SnI_6 octahedra is found in $[(Me_2HN\text{-}C_2H_4\text{-}NHMe_3)Sn_3I_8]$ (Lode and Krautscheid, 2001) (CSD ref. code: RAJNEV) (Figure 2.44).

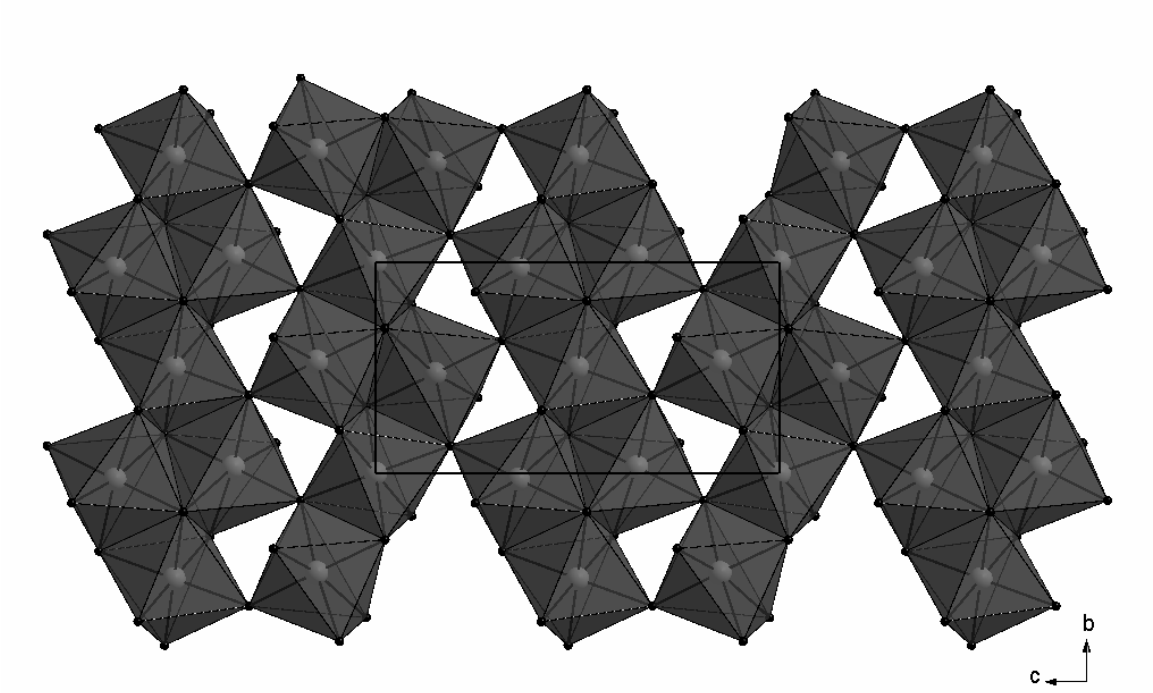


Figure 2.44: The 2-D net of $[(Me_2HN\text{-}C_2H_4\text{-}NHMe_3)Sn_3I_8]$. The cations are omitted for clarity.

Another net-type motif that has only been reported once is that formed in the compound $[(Pr_3N\text{-}C_2H_4\text{-}NPr_3)Pb(dmf)_6Pb_5I_{14}] \cdot DMF$ (Krautscheid et al, 1998) (CSD ref. code: GEQGUE), which has pentameric units of five face-sharing PbI_6 octahedra, $[Pb_5I_{15}]^{4-}$, that are connected to each other via a shared face to form S-shaped chains along the *b*-axis. These chains are then connected

to each other via corner-shared iodides along the *c*-axis to form the 2-D net as shown in Figure 2.45. In between the layers, there are $[Pb(dmf)_6]^{2+}$ and $(Pr_3N\text{-}C_2H_4\text{-}NPr_3)^{2+}$ cations as well as a DMF solvent molecule.

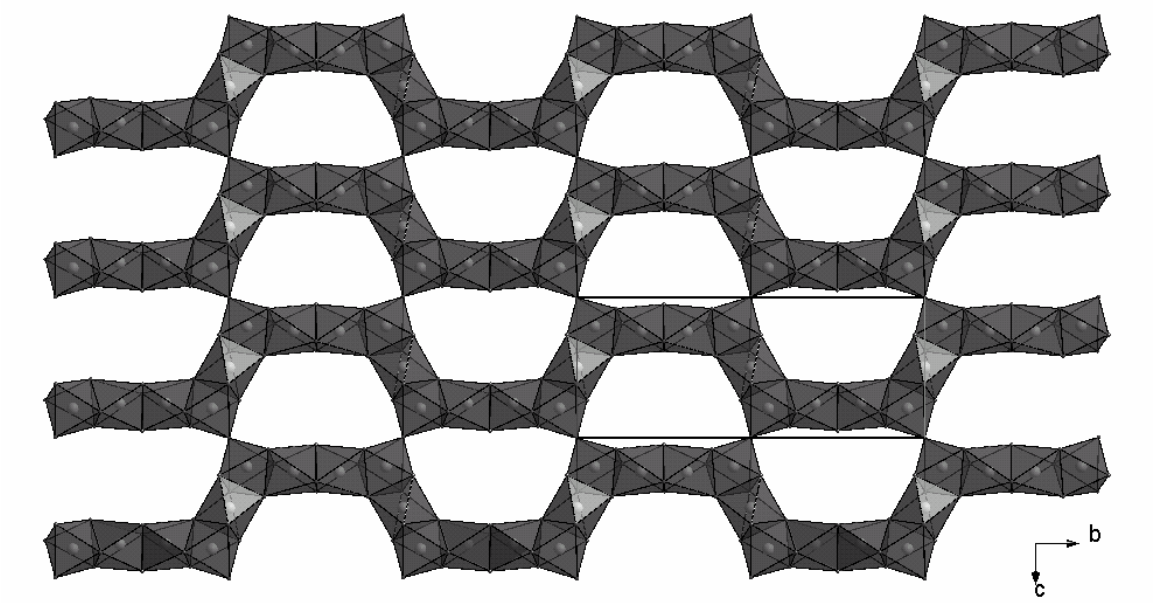


Figure 2.45: 2-D net of $[(Pr_3N\text{-}C_2H_4\text{-}NPr_3)Pb(dmf)_6Pb_5I_{14}] \cdot DMF$. The cations and $[Pb(dmf)_6]$ anions are omitted for clarity.

The only reported net-type motif that involves all three types of sharing is found in the compound $[(Me_3N\text{-}C_3H_6\text{-}NMe_3)_3Pb_3I_9]_2$ (Krautscheid and Vielsack, 1996) (CSD ref. code: TIDVOR). The $[Pb_3I_9]^{3-}$ units consist of three face-sharing octahedra shaped as an almost equilateral triangle. The lead atoms are at the vertices of the triangle and the distances between the three lead atoms are in the range 4.2191(9) Å to 4.3046(8) Å (Krautscheid and Vielsack, 1996). These trimeric units are connected via corner-sharing to form 1-D chains along the *b*-axis. The chains are then further connected via edge-sharing along the *c*-axis to eventually form the 2-D net-type layers (See Figure 2.46). By changing the identity of the counterion from $(Me_3N\text{-}C_3H_6\text{-}NMe_3)^{2+}$ to $(Me_3N\text{-}C_2H_4\text{-}NMe_3)^{2+}$, the chains of face-sharing and corner-sharing units are not connected via edge-sharing so that the inorganic motif simply consists of 1-D zig-zag chains. The molecular formula then becomes $[(Me_3N\text{-}C_2H_4\text{-}NMe_3)Pb_3I_{10}]$ (CSD ref. code: TIDVIL).

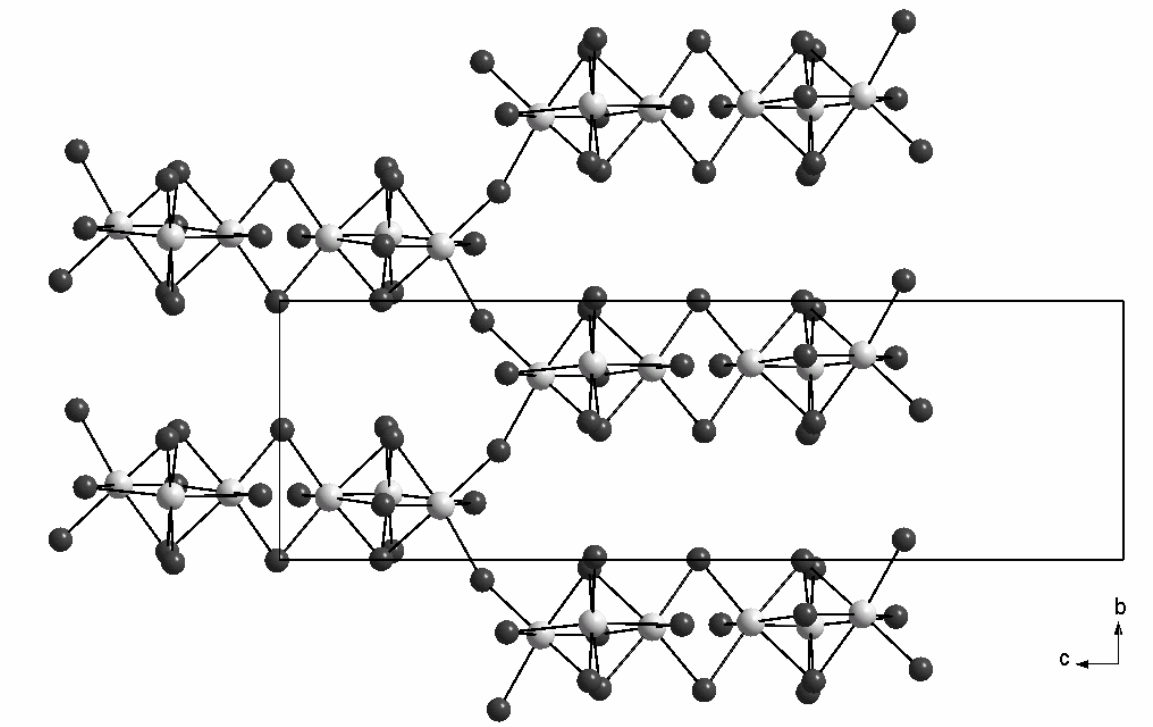


Figure 2.46: The 2-D net of $[(Me_3N\text{-}C_3H_6\text{-}NMe_3)_3Pb_3I_9]$. The cations are omitted for clarity.

2.10.2 Two-dimensional motifs - based on corner-sharing layers

A 2-D motif that is closely related to the layered perovskite-type motif has corrugated sheets of $[SnI_4]^{2-}$ corner-sharing octahedra. The layered perovskite-type motif has the corner-shared iodides always trans to each other. In this new motif, every third octahedron has *cis* shared iodides in the sequence -*trans-trans-cis-trans-trans-cis*- as described by the authors (Guan et al, 1999) (CSD Ref. code: DONDUF) (Figure 2.47). The organic counterion is $(H_3N(CH_2)_5NH_3)^{2+}$ and is linked to the inorganic tin(II) iodide sheets via hydrogen bonds.

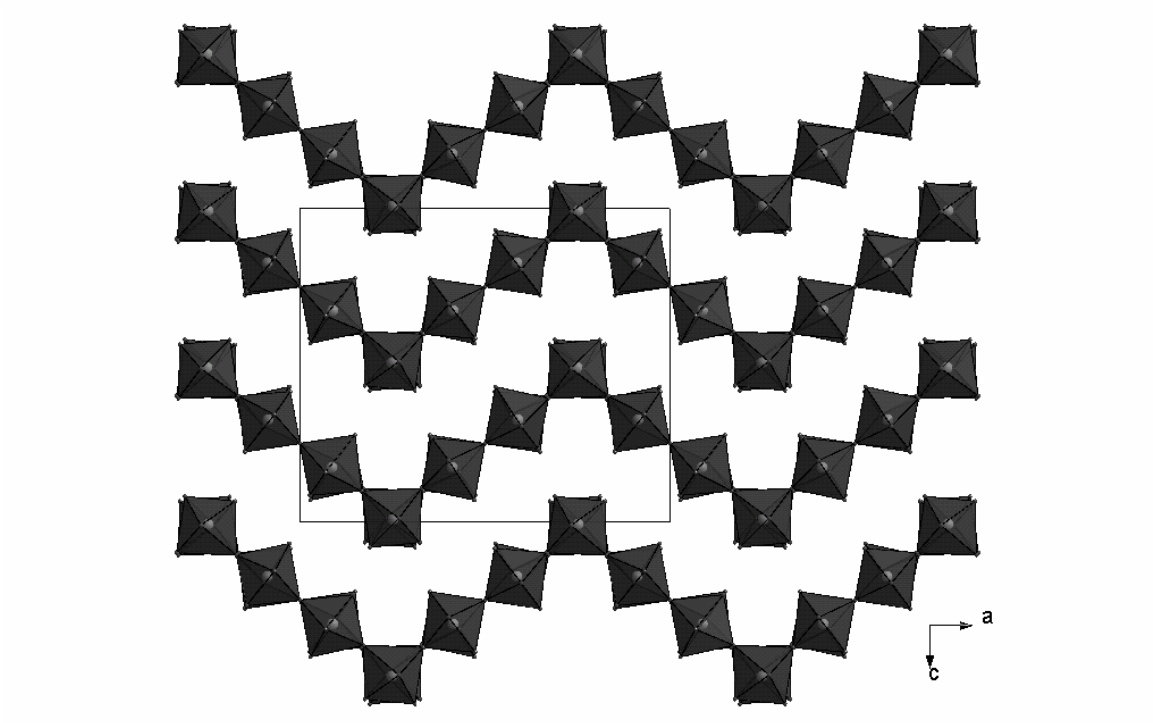


Figure 2.47: The $[SnI_4]^{2-}$ 2-D layers. The cations are omitted for clarity.

2.10.3 Two-dimensional motifs - based on face-sharing

One of the few reported cases of lead(II) halide inorganic-organic hybrids that does not have octahedral coordination is found in the compound $[(H_3N\text{-}C_6H_4\text{-}NH_3)(PbCl_3)_2]$ (CSD ref. code: HAJSUH) (Figure 2.48). Here, there are twin 2-D layers of purely-face-sharing eight-coordinate $PbCl_8$. The coordination geometry is square antiprismatic but the geometry is distorted with the bond lengths to the chloride ligands in the range from 2.805(2) to 3.388(2) Å (Bourne and Mangombo, 2004).

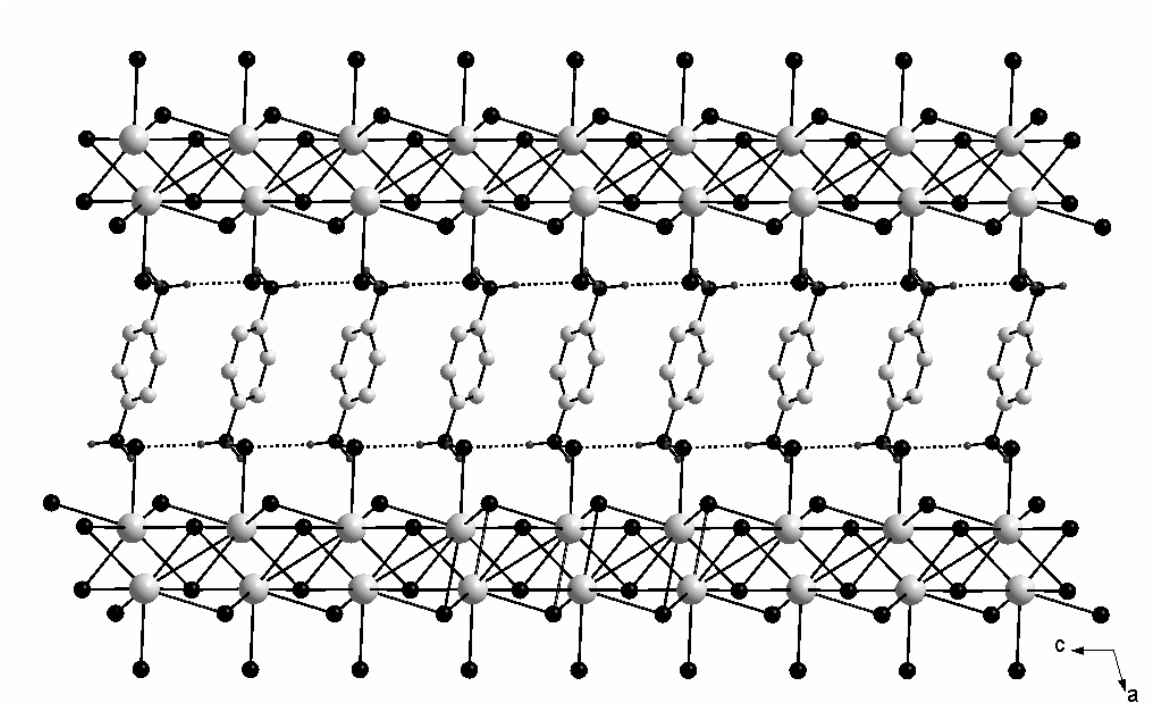


Figure 2.48: The twin 2-D layers of face-sharing $PbCl_8$ square antiprisms, separated by a monolayer of *p*-phenylenediammonium. The hydrogen bonds are shown as dashed black lines.

Another face-sharing 2-D motif has eight-coordinate lead(II) chloride but this time, there are three unique lead atoms in the asymmetric unit compared to the single one in the compound $[(H_3N\text{-}C_6H_4\text{-}NH_3)(PbCl_3)_2]$ discussed above. In the compound $[(H_3N(CH_2)_2NH_3)(Pb_2Cl_6)]$ (Löfving, 1976) (CSD ref. code: EDAPBC), Pb(1) and Pb(3) each form distorted bicapped trigonal prisms and Pb(2) forms a square antiprism. The mono layers are parallel to the *bc*-plane. The three lead atoms are at sites with different point symmetries, *1*, *2* and *m* respectively for Pb(1), Pb(2) and Pb(3) (Löfving, 1976). The layers are separated by diammonium ethylene ions and interact in the usual way via N-H...Cl hydrogen bonds (See Figure 2.49). There are two unique cations in the asymmetric unit. Cation I has all the atoms in a plane and is perpendicular to the layers as it is on a mirror plane at z = 1/4. Cation II is on a two-fold axis and is almost parallel to the layers.

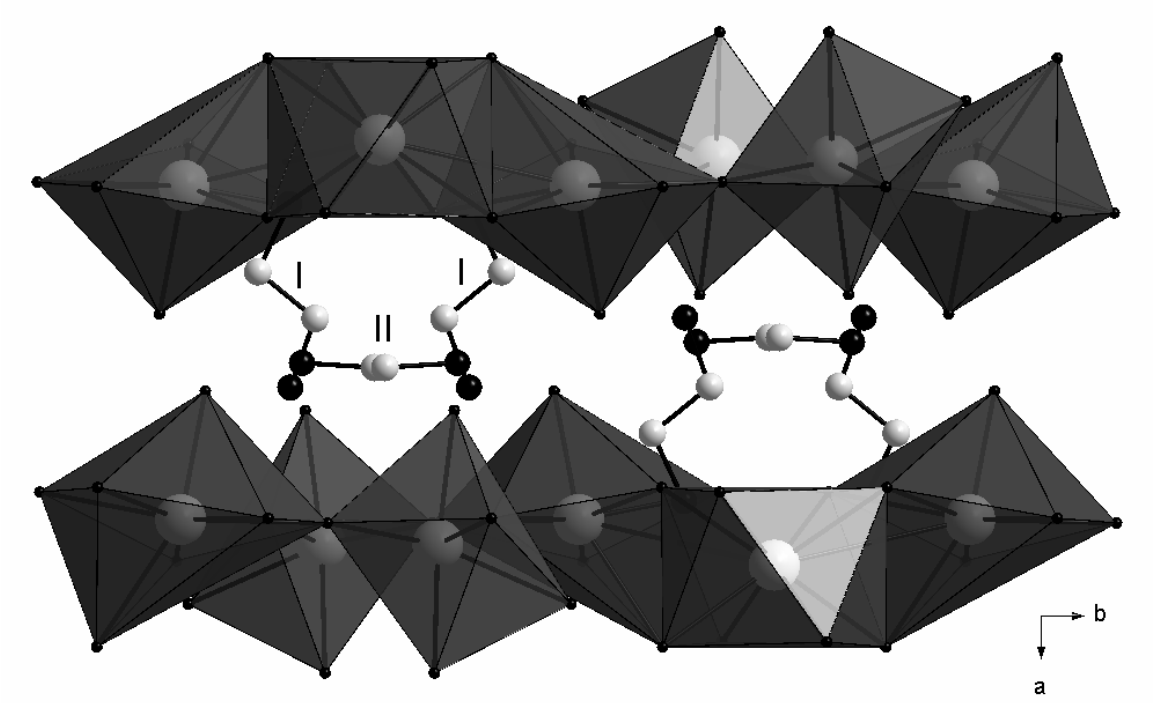


Figure 2.49: The mono 2-D layers of face-sharing [$PbCl_8$], separated by bilayers of H_3N-C_2H_4-NH_3. The two different orientations of the cations are labelled I and II.

2.11 One-dimensional inorganic motifs

2.11.1 Purely corner-sharing, edge-sharing and face-sharing

2.11.1.1 Motifs based on *trans* corner-sharing

Another very common inorganic motif after the layered perovskite-type, are 1-D chains of either purely corner-sharing or face-sharing octahedra. In the corner-sharing series, the two bridging halides that are shared to adjacent octahedra can either be *trans* to each other or *cis*. All the compounds that undergo *trans* corner-sharing have secondary ammonium groups, $=NH_2^+$. The octahedra themselves can be very distorted due to stereochemical activity of the Pb and Sn lone pairs. The compound [$(CH_3SC(=NH_2)NH_2)_3SnI_5$] (Raptopoulou et al, 2002) (CSD ref. code: IGEBUR) has the most distorted octahedral geometry and can be considered quasi-zero dimensional as the lead iodide bond lengths to the shared halides are 2.921(1) Å and 4.042(1) Å. The related compound, [$(CH_3SC(=NH_2)NH_2)_3PbI_5$] (Mousdis et al, 1998) (CSD ref. code: HIWMOP), has a similar distorted geometry, where the two bridging I-Pb-I bond lengths are

3.037(2) Å and 3.882(2) Å. When the halide is chloride, the extreme distortion is absent. This compound, $[(CH_3SC(=NH_2)NH_2)_3PbCl_5CH_3SC(=NH_2)NH_2Cl]$ (CSD ref. code: HIWNAC), has two unique inorganic chains in the asymmetric unit. The chains are similar to those in the lead(II) iodide case but the bond lengths to the bridging chlorides are 2.863(12) Å and 2.893(12) Å for the first chain and 2.811(12) Å and 2.941(12) Å for the second chain (Mousdis et al, 1998). The cation, $(CH_3SC(=NH_2)NH_3)^+$, has a resonance delocalised structure in all three compounds as the two C-N bonds are of almost equal length.

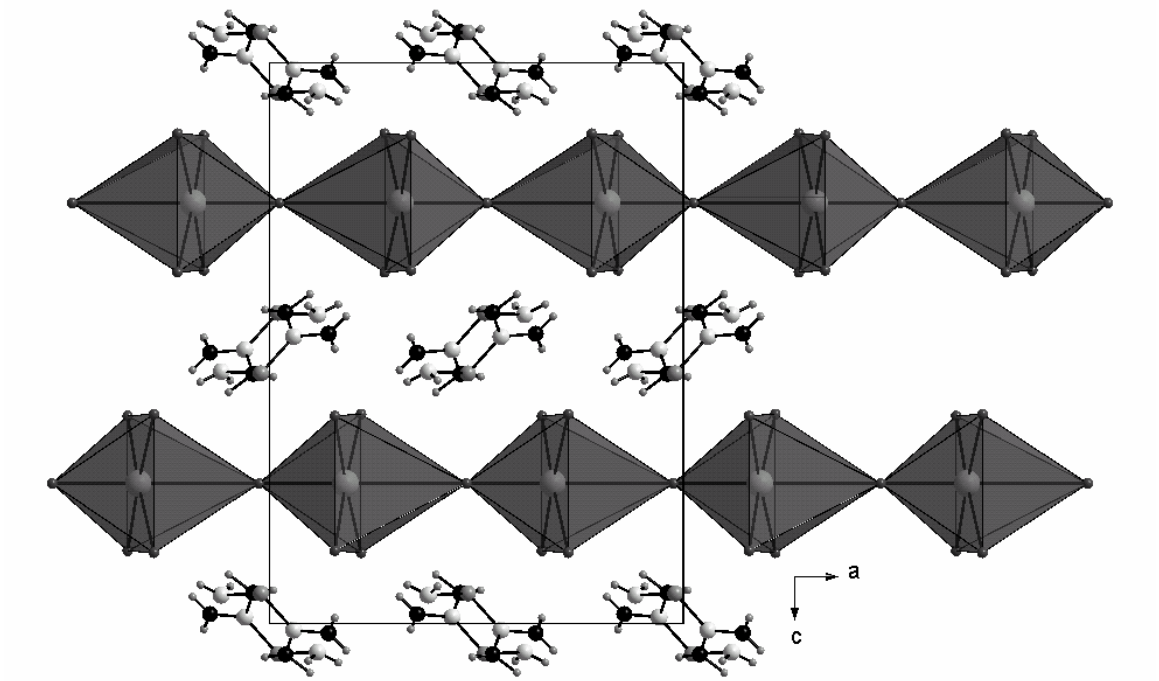


Figure 2.50: The quasi 0-D chains of $[(CH_3SC(=NH_2)NH_2)_3SnI_5]$. The activity of the stereochemical lone pair is in the direction of the chains.

Another cation that forms hybrids with *trans* corner-sharing octahedra is iodoformamidinium, $(H_2NC(I)=NH_2)^+$. In the paper by Wang et al (1995), the effect of the stereochemical lone pair was investigated in the compound $[(H_2NC(I)=NH_2)_3MI_5]$ (M = Sn and Pb, CSD ref. codes: YUVFIE and YUVFOK). Both compounds are isostructural and the three cations in the asymmetric unit are resonance stabilised. In the Sn analogue, the most distortion occurs along the direction of the chains, which is along the $(I\text{-}Sn\text{-}I)_n$ chain. The bridging bond lengths are 2.957(1) Å and 3.484(1) Å. The range decreases to 3.182(3) Å to 3.243(3) Å for $(I\text{-}Pb\text{-}I)_n$. An interesting phenomenon is observed in the Sn analogue. The compound is made by dissolving cyanamide,

H_2N-C≡N, and tin(II) iodide in hot, concentrated aqueous hydroiodic acid. If the solution is cooled immediately from 70 to -20 °C at 2 °C/h, cyanamide undergoes an addition reaction to form the iodoformamidinium cation and ultimately the compound $[(H_2NC(I)=NH_2)_3SnI_5]$ results (Mitzi, et al, 1998). If the same solution is prepared but left at 80 °C for 24 hours before the same cooling regime, some of the iodoformamidinium is reduced to formamidinium and both cations can be crystallized out in the structure $[(H_2NC(I)=NH_2)_2(H_2NCH=NH_2)SnI_5]$ (Mitzi, et al, 1998) (CSD ref. code: POXNEV). The mixed cations reduce the distortion of the SnI_6 octahedra so that the bond lengths range only from 3.140(8) Å to 3.210(6) Å.

2.11.1.2 Motifs based on *cis* corner-sharing

The motif of cis-corner-sharing chains can be considered to be a layered perovskite but with PbI_2 deficient sites as shown in Figure 2.51.

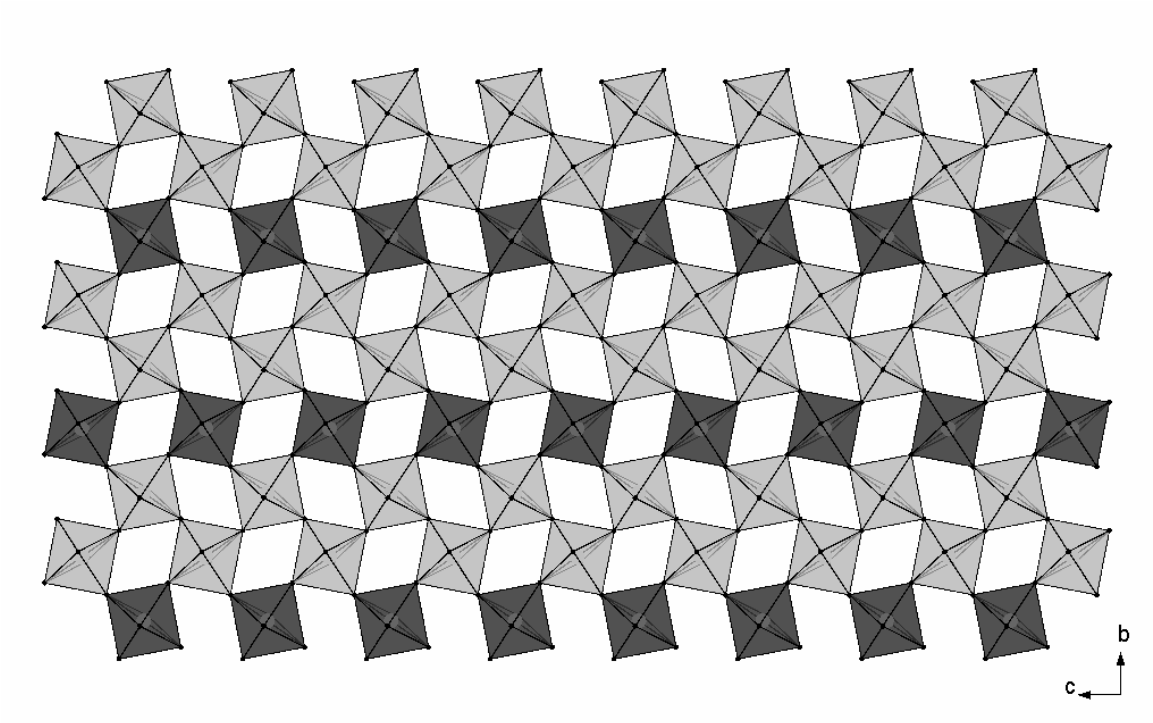


Figure 2.51: The 1-D chain of corner-sharing octahedra is shown in light grey as cut-outs of the layered perovskite-type structure, i.e. every row of dark grey octahedra is effectively omitted. The PbI_2 deficient sites repeat themselves every third row along the *b*-axis.

The packing diagram of $[(C_6H_5CH_2CH_2SC(NH_2)_2)_3PbI_5]$ (Papavassiliou et al, 1999b) (CSD ref. code: COTVOW) consists of anionic zig-zag chains of corner-sharing PbI_6 octahedra, which are formed via *cis* iodine bridges. This inorganic motif is encountered for a variety of simple cations and metal halides such as $[(H_3N(CH_2)_6NH_3)BiX_5]$ (X = I, Cl) and $[(H_3N(CH_2)_6NH_3)SbX_5]$ (X = I, Br) (Mousdis et al, 1998a) (CSD ref codes: SOWNUN, SOWPAV, SOWQAW, SOWQEA). The equatorial halides, including the two bridging halides, are equiplanar, i.e. when looking down the chains, every second octahedron is eclipsed. These four compounds show excitonic absorption bands in the blue region due to their 1-D character.

A more complex cation has been used together with lead(II) iodide, which can form either the layered perovskite-type hybrid $[(H_3N\text{-}R\text{-}NH_3)PbI_4]$, where R = 5,5'-bis(ethylsulfanyl)-2,2'-bithiophene or the 1-D hybrid $[(H_3N\text{-}R\text{-}NH_3)(H_3N\text{-}R\text{-}NH_2)PbI_5]$ (Zhu et al, 2004). Both compounds were prepared from the same solution mixture of $(H_3N\text{-}R\text{-}NH_3)Cl_2$, KI, PbI_2 and water. The ratio of the two forms is 1/1 and can be easily identified by the orange colour of the layered perovskite-type hybrid and the yellow colour of the corner-sharing hybrid. $[(H_3N\text{-}R\text{-}NH_3)PbI_4]$ becomes the sole product if a few drops of HI are added. The 1-D compound, CSD ref. code: EWAZOR, has two unique cations in the asymmetric unit. There are two additional interactions between the R moieties that are unique to this hybrid compound. The distances between S...S atoms on the individual cations is less than 3.9 Å, good evidence for charge transport properties. In addition, there are $NH_3^+...NH_2$ hydrogen bond interactions between molecules in addition to the usual $NH_3^+...I$ interaction between the inorganic and organic components.

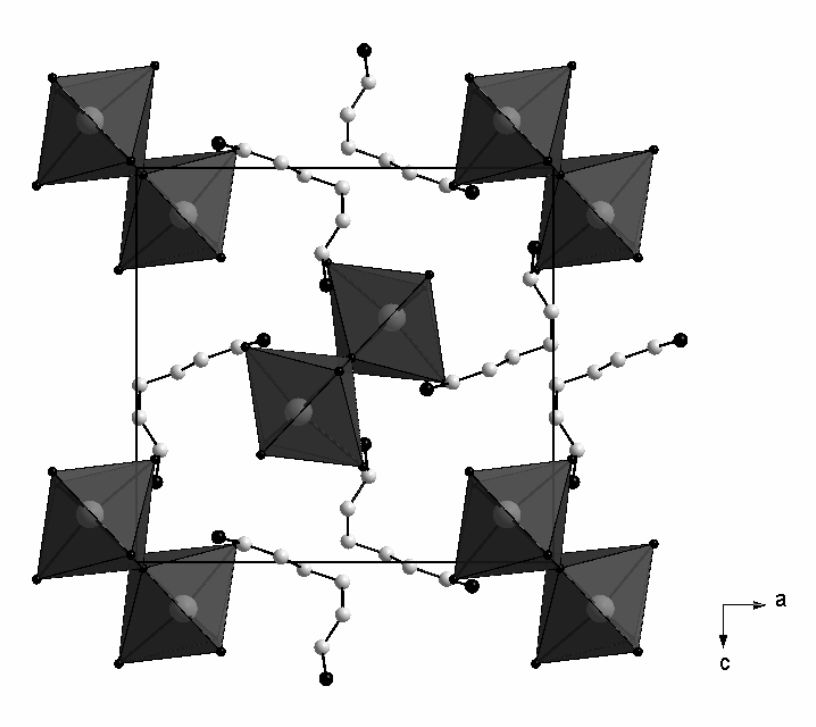


Figure 2.52: The 1-D chains of $[(H_3N(CH_2)_6NH_3)BiX_5]$.

The optical properties of inorganic-organic hybrids based on bismuth(III) iodides depend on the dimensionality of the inorganic motif and to this effect, Mitzi and Brock (2001) have investigated more complex organic cations and their effect on the overall structure and properties. Two corner-sharing inorganic-organic bismuth iodide hybrids with the amines 1,6-bis[5'-(2''-aminoethyl)-2'-thienyl]hexane (abbr. AETH) and 1,12-dodecanediamine (abbr. DDDA) were crystallized and their optical absorption spectra measured as thin films. The crystal structures of $[(H_3NC_{18}H_{24}S_2NH_3)BiI_5]$ (CSD ref. code: MIKZOV) and $[(H_3N(CH_2)_{12}NH_3)BiI_5]$ (CSD ref. code: MIKZOB) have similar Bi(III) coordination. The six Bi-I bond lengths can be subdivided into three pairs according to their lengths. The iodides that bridge the adjacent octahedra, I1, and form the backbone of the inorganic chain are the longest, 3.230(2) Å to 3.2711(4) Å, the iodides that are *trans*, I4 and I5, the shortest, 2.942(3) Å to 2.9290(6) Å, and the iodides in the axial positions, I2 and I3, which are *cis* to the long bonds, intermediate in length, 2.989(2) Å to 3.187(2) Å. This distribution of bond lengths is typical of purely corner-sharing compounds of this kind.

1-D chains that contain no six-coordinate metal(II) halide hybrids are also found. The compound $[(H_3NOC\text{-}C_5H_4N\text{-}CH_3)CdI_3]$ has corner-sharing CdI_4 tetrahedra, which is a rarely reported 1-D inorganic motif, according to the authors (Kosuge et al, 2002b). The deposited cif file in the CSD, AKOKIU, contains no 3-D coordinates.

2.11.1.3 Motifs based on face-sharing

Structures containing motifs based on purely face-sharing metal halide octahedra have been reported for a variety of metals, halides and counter ions. Generally, the adjacent octahedra share faces that are *trans*-related, as in $[(H_3C\text{-}C_5H_4N\text{-}CH_3)PbBr_3]$ (Raptopoulou et al, 2002) (CSD ref. code: IGECEC), $[(Na_4(dmf)_{14})PbI_3]_4$ (Krautscheid et al, 2001) (CSD ref. code: XEPDOL), $[(C_8H_4S_6)_2PbI_3]\cdot H_2O$ (Devic et al, 2004) (CSD ref. code: ARUWEP), $[(Me_4N)PbI_3]$ (Contreras et al, 1983) (CSD ref. code: CERBUW) and $[(Ph_4P)PbI_3]\cdot DMF$ (Krautscheid et al, 1996) (CSD ref. code: TOPZIH). Hybrids that have face-sharing octahedra have been demonstrated to undergo structural phase transitions, as in the compounds $[(Me_4N)PbBr_3]$ (Vaněk et al, 1992) (CSD ref. code: KUBBIS), $[(Et_4N)PbBr_3]$ and $[(Bu_4N)PbBr_3]$ (Goldstein and Tok, 1975). The nature of the phase transitions in $[(Me_4N)PbBr_3]$ was investigated by DSC, polarizing microscopy and dielectric measurements and found to depend on the reorganization of the tetramethylammonium anions (Vaněk et al, 1992). All of the anionic counterions described above have quaternary nitrogens, i.e. no hydrogen atoms that can undergo hydrogen bonding interactions with the halides of the extended inorganic chains.

MX_6 metal halide units can have mixed 6-membered coordination geometries within the face-shared chain. This is observed in the lead(II) iodide hybrid with 1,1'-dimethyl-4,4'-bipyridinium (CSD ref. code: HINYUY), which has four lead atoms in the asymmetric unit, labelled Pb1, Pb2, Pb3 and Pb4. Pb1 and Pb4 have a nearly regular octahedral coordination, Pb2 has a more distorted coordination geometry and leads up to the trigonal prismatic coordination of Pb3 (Tang and Guloy, 1999). The sequence of octahedral (O) and trigonal prismatic (TP) coordination of the *trans* face-sharing chain is described by the authors as [O-O-TP-O-TP-O]. The ligands bonded to the metal can be different. In the hybrid compound with the cation $(Na_3(OCMe_2)_{12})^+$ and the anion $[Pb_4I_{11}(OCMe_2)]^{3-}$ (CSD ref. code: TOPYUS), every fourth lead atom has an acetone

molecule replacing an iodide atom. The oxygen atom now bridges two lead atoms in the same way the iodide atom would (See Figure 2.53) (Krautscheid et al, 1996).

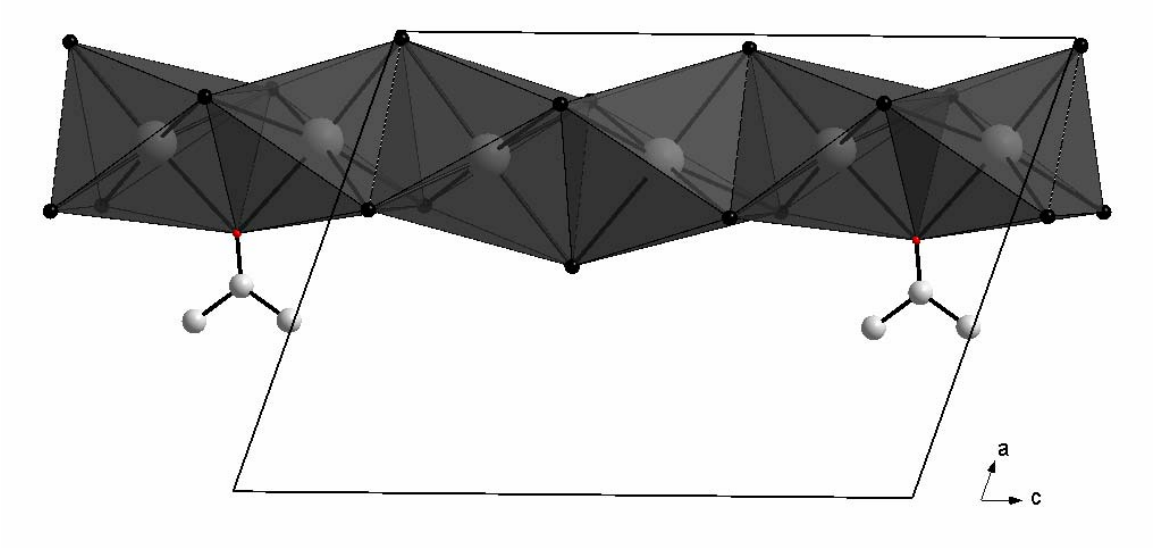


Figure 2.53: The 1-D chains of $[(Na_3(OCMe_2)_{12})Pb_4I_{11}(OCMe_2)]^{3-}$, which has face-sharing involving three I atoms or alternately, two I atoms and one O atom from an acetone solvent molecule.

The 1-D inorganic motif need not necessarily consist of only one chain. There is a reported structure of a compound that has two parallel chains of *trans* face-sharing octahedra, similar to the ones described above, which are then joined by additional Pb atoms so that they themselves undergo face-sharing again. These linkages are spaced apart regularly as shown in Figure 2.54 below. The molecular formula then becomes $[(Ph_4P)_2Pb_5I_{12}]$ (Krautscheid et al, 1996) (CSD ref. code: TOPZAZ).

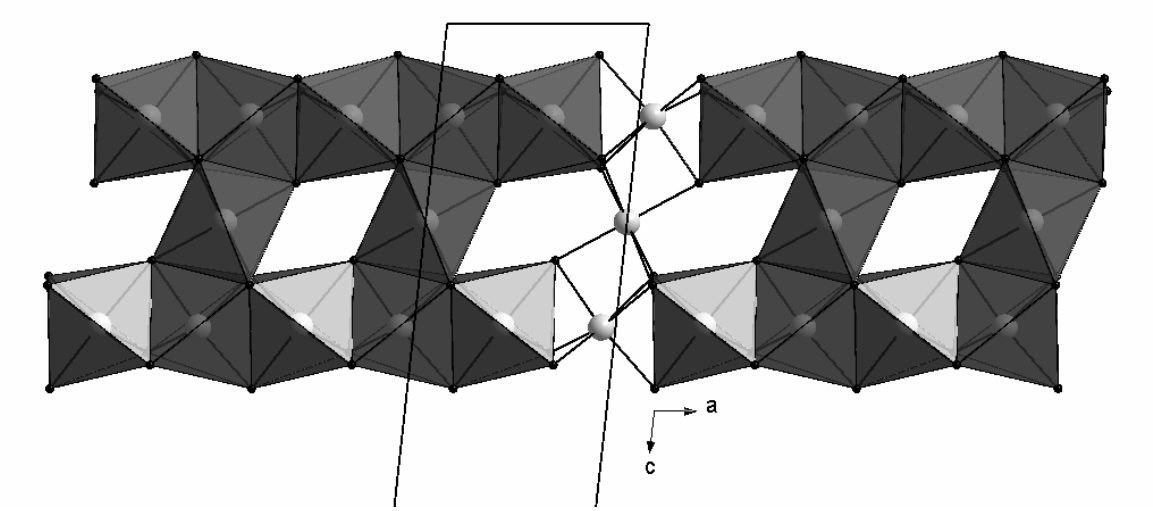


Figure 2.54: The twin 1-D chain of face-sharing PbI_6 octahedra.

There is no reported case of purely *cis*-related face-sharing octahedral chains. However, the compound $[(Me_3N(CH_2)_6NMe_3)PbI_3]_2$ (CSD ref. code: XEPDEB) contains *trans* face-shared octahedra and *cis* face-shared octahedra in the same chain linked along the crystallographic *a*-axis in the manner [*cis-trans-cis-trans-cis-trans*] as shown in Figure 2.55 below (Krautscheid et al, 2001).

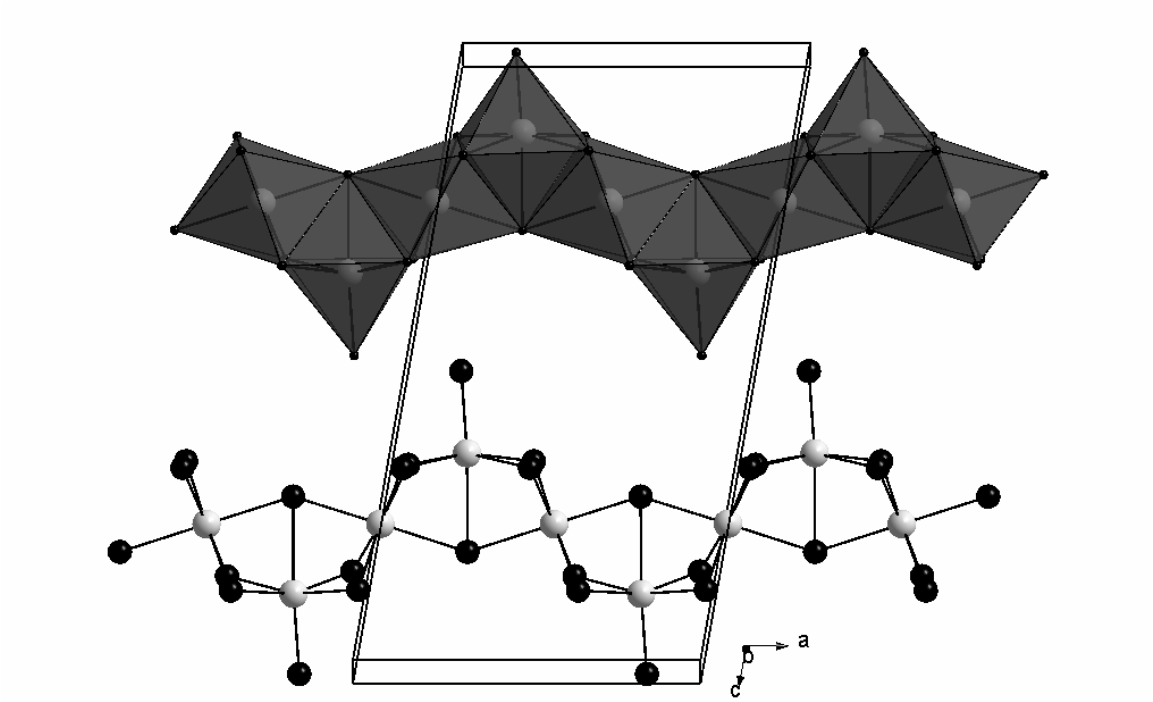


Figure 2.55: The 1-D chain of $[(Me_3N(CH_2)_6NMe_3)PbI_3]_2$. The face-shared octahedra are alternatively *cis* and *trans* related.

2.11.1.4 Motifs based on edge-sharing

As in the corner-sharing and face-sharing one dimensional chains, the edges that are shared between adjacent metal halide units can be purely *trans*, *cis* or a combination of both. To the best of my knowledge, only two cases of trans edge-sharing exist for lead(II) iodide, where square pyramidal PbI_5 units are connected to form infinite 1-D chains with the counterion either tetrahedral $(Pr_4N)^+$ (CSD ref. Code: GIYREL01) or octahedral $Mg(dmf)_6^{2+}$ (CSD ref. Code: GOGNAR) (Krautscheid and Vielsack, 1999). The bridging Pb-I bond distances cover a larger range with the former counterion, 3.1017(9) Å to 3.4553(9) Å, compared to the more symmetrical bond length range of 3.1836(5) Å to 3.2407(6) Å when the latter, bulkier counterion is included in the hybrid structure (Krautscheid and Vielsack, 1998).

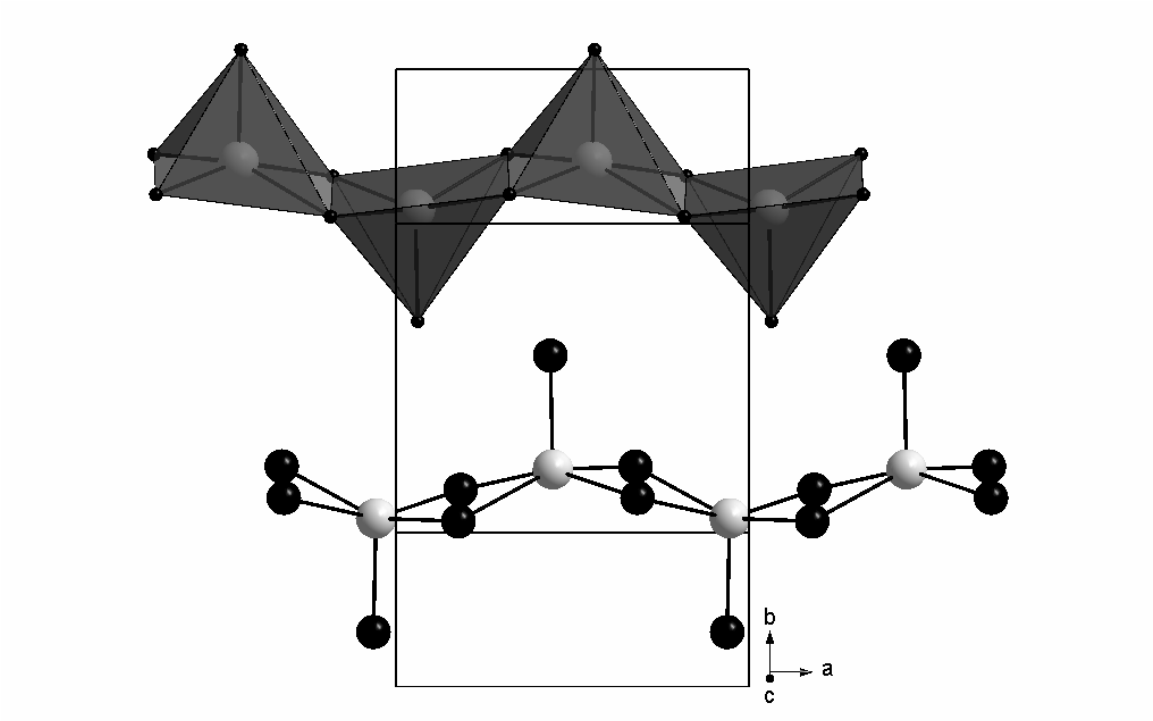


Figure 2.56: The 1-D chain of the hybrid $[(Pr_4N)PbI_3]$.

A similar compound that has purely edge-sharing chains is $(4\text{-}(CH_3)C_5H_3NH)CdBr_3$ (CSD ref. code: POPHED). The geometry of the cadmium(II) bromide is tetragonal pyramidal. The authors, Ishihara et al (2006), feel that the pentagonal coordination of the metal halide moiety, instead of octahedral, is due to the hydrogen bond between the basic 4-methyl-pyridinium and the bromine at the top of the pyramid (See Figure 2.57).

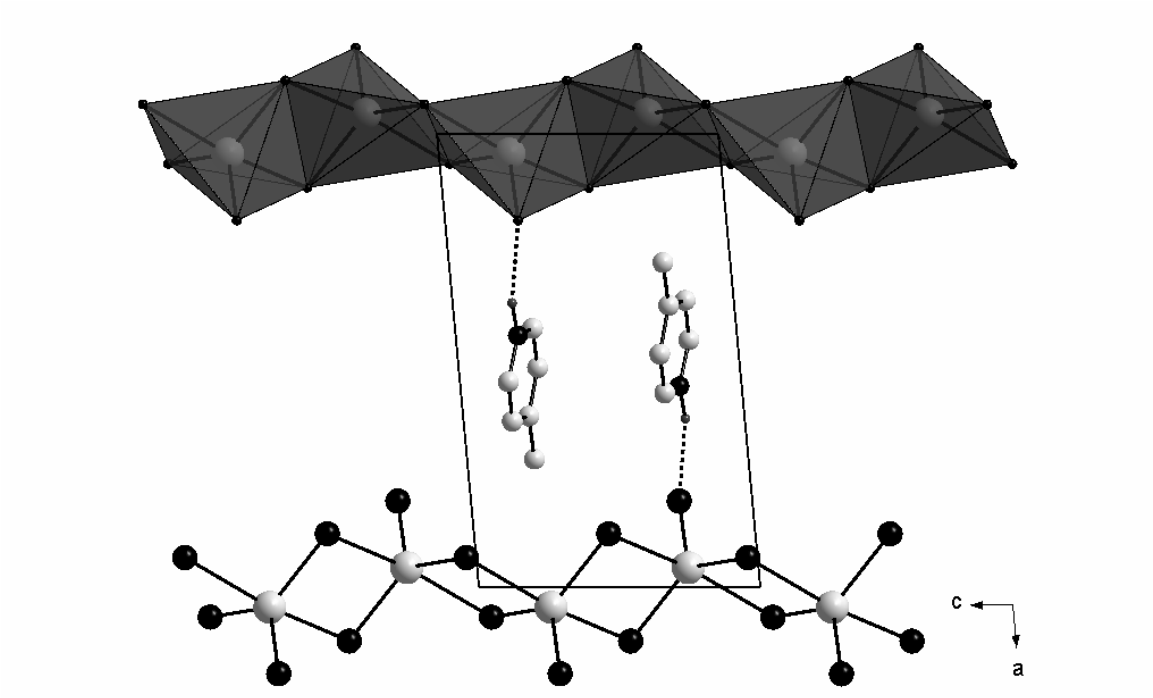


Figure 2.57: The 1-D chain of the hybrid [(4-$(CH_3)C_5H_3NH)CdBr_3$], which has a single hydrogen bond between the anionic chain and the organic cation.

The other metal that exhibits *trans* edge-sharing is mercury. Here, the 1-D chain has alternating octahedral and tetrahedral mercury(II) chloride units (Salah et al, 1983b) (Figure 2.58). The counterion is $(CH_3)_3NH^+$ and hydrogen bonds via the single hydrogen to the chlorides (CSD ref. code: CEGMOQ).

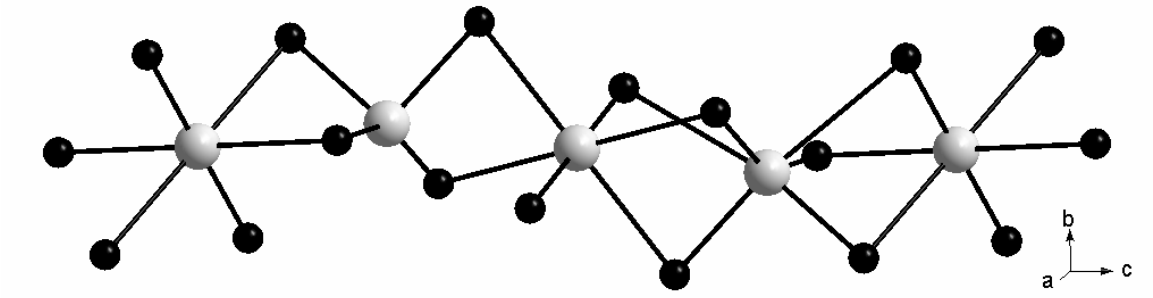


Figure 2.58: The 1-D chain of the hybrid [$((CH_3)_3NH)HgCl_3$].

2.11.2 Motifs based upon combinations of edge- and face-sharing

This 1-D motif based on edge- and face-sharing octahedra, has been observed most often with lead(II) iodide. The motif can be described by the shorthand notation $(f_me)_n$ for m adjacent face-sharing octahedra , f, connected by octahedra sharing an edge, denoted e. Structures with m = 3 have been synthesized based on lead iodide with the counterions $(C_{13}H_7O_2(CH_2)_2NH_3)^+$ (Maxcy et al, 2003) (CSD Ref. code.: WADMAQ), $(Me_3N\text{-}C_3H_6\text{-}NMe_3)^{2+}$ (Krautscheid and Vielsack, 1997) (CSD Ref. code.: TIDVUX) and $(H_3NCH_2CH(CH_3)CH_2CH_2CH_2NH_3)^{2+}$ (Corradi et al, 1999) (CSD Ref. code.: CAJZIW) and for tin iodide octahedra (Lode and Krautscheid, 2001) (CSD Ref. code: RAJNAR) octahedra with the counter ion containing a tertiary ammonium group $(Me_2HN\text{-}(CH_2)_2\text{-}NMe_2H)^{2+}$. The case with m = 1, $[((PhCH_2)_4P)Pb_3I_8]$ (CSD Ref. code.: XEPDAX) has PbI_6 octahedra that share a face with PbI_5 square pyramids, which in turn share an edge (Krautscheid et al, 2001).

2.11.3 One-dimensional "Ribbon" type motifs

Connecting many 1-D chains of either corner-, edge- or face-sharing octahedra together gives 1-D motifs with a certain width, resembling polymeric "ribbons". The most common inorganic ribbon motif has extended chains of *trans* edge-sharing octahedra, which are connected to each other again via *cis* related edges. This inorganic motif is based on strips of the CdI_2-type structure along the <100> direction (Pohl et al, 1987) (See Fig. 2.59). The simplest case has two chains connected, as shown in Figure 2.60 below, to form 1-D extended double-chains.

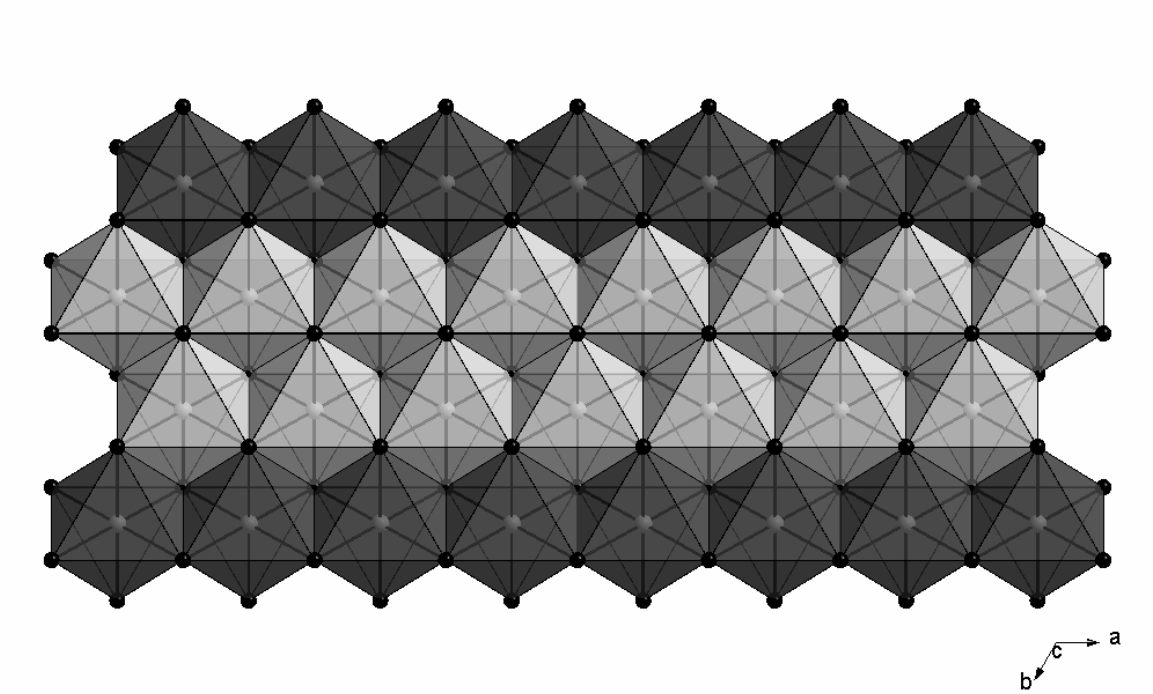


Figure 2.59: A single layer cutout of the CdI_2-Structure type. The octahedra in light grey show the twin anionic chains seen in lead iodide inorganic-organic hybrids.

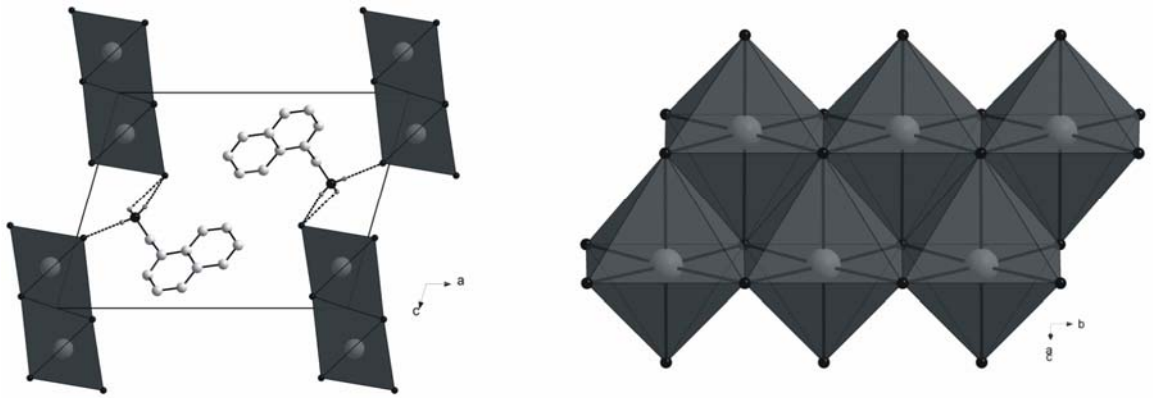


Figure 2.60: The packing diagram of $[(C_{10}H_7CH_2NH_3)PbI_3]$ is shown on the left together with the hydrogen bonds in dashed lines. On the right is an illustration of the anionic twin chains of edge-sharing PbI_6 octahedra (Papavassiliou et al, 1999b; CSD ref. code: COTVUC).

The width of the 1-D ribbon can vary. The compound $[(Pr_3N\text{-}C_2H_4\text{-}NPr_3)Pb_6I_{14}(dmf)_2] \cdot 4$ DMF (CSD ref. code: GEQGOY) has three parallel rows of lead atoms, octahedral PbI_6 in the centre and in the two outer rows of Pb atoms, all the Pb atoms are coordinated to five bridging iodides, as well as in an alternating fashion, a single dmf and a single iodide ligand in the terminal position in the manner [PbI_6-PbI_5dmf-PbI_6-PbI_5dmf] (Krautscheid et al, 1998). The dmf molecule

is a solvent molecule that gets incorporated into the anionic inorganic chain. This happens again in the closely related compound $[(Ph_4P)_4Pb_{15}I_{34}(dmf)_6]$ (Krautscheid et al, 1996) (CSD ref. code: TOPZED), which also has iodide and dmf molecules coordinated to lead. The anionic chain has the same middle row of PbI_6 octahedra as the structure above but the sequence of the two outer lead rows is $[PbI_6$-PbI_5dmf-PbI_5dmf-$PbI_6]$.

There is another motif of polymeric ribbons of edge-sharing octahedra that can be regarded as different band-shaped sections of the CdI_2 structure (Pohl et al, 1986). The two compounds are $[(Ph_4P)Sb_3I_{10}]$ (Pohl et al, 1987) (CSD ref. code: GANSET) and $[((Me_2N)_3C_3)Sb_3I_{10}]$ (Pohl et al, 1986) (CSD ref. code: FAFGUO) and their polymeric anionic structures are shown in Figure 2.61.

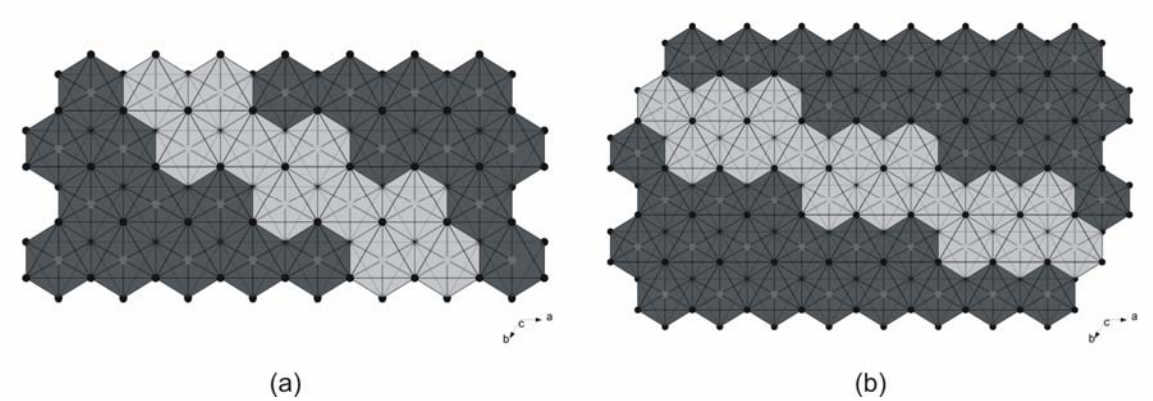


Figure 2.61: The anionic polymeric chains of $[(Ph_4P)Sb_3I_{10}]$ (a) and $[((Me_2N)_3C_3)Sb_3I_{10}]$ (b) shown schematically (light grey octahedra) as cutouts of the layer structure of CdI_2 (dark grey octahedra).

Just as individual edge-sharing chains can interconnect to form 1-D ribbons that are several octahedra wide, so do corner-sharing chains. This inorganic motif is closely related to the layered perovskite-type type motif, as shown in Figure 2.62 below, were a single row of *trans* corner-sharing chains is absent at regular intervals. The motif was first seen in a paper in 1999 and the authors claim it was then a heretofore never before seen structural archetype and coined the term "polymeric inorganic ribbons" (Corradi et al, 1999). The formula for the compound is $[(H_3N(CH_2)_3NH_3)_2Pb_{1.5}Br_7].H_20$ (CSD ref. code: CAKDIB). The authors contend that it is the water of hydration that prevents the formation of the 2-D layered perovskite-type motif as it is uncoordinated and replaces the missing row of octahedra. It does however hydrogen bond to the

bromides between the ribbons in the crystallographic *b* direction and hence forms pseudo 2-D layers (See Figure 2.63). The diammonium cation hydrogen bonds to adjacent layers in the crystallographic *a* direction, similar to the layered perovskites.

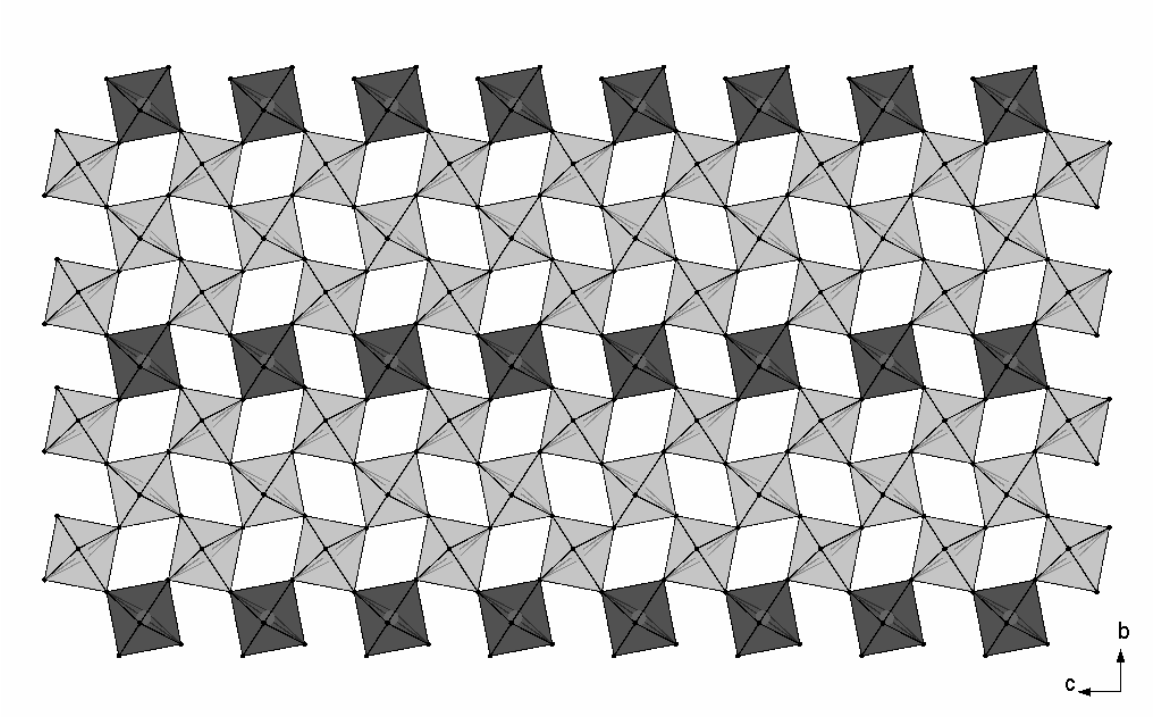


Figure 2.62: The cut-out of the layered perovskite-type inorganic motif that gives rise to the 1-D inorganic ribbons, shown as light grey octahedra. Every fourth row is missing, shown as dark grey octahedra.

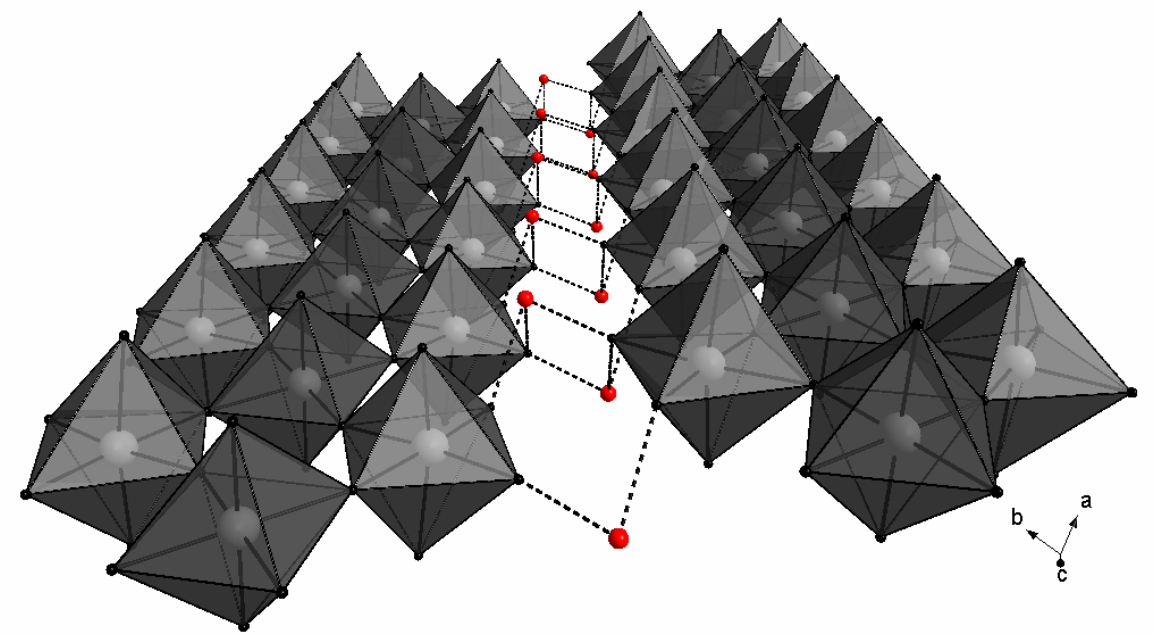


Figure 2.63: Two inorganic ribbons, connected by hydrogen bond interactions between the terminal bromides and the oxygen molecules between them.

Finally, it is possible to have ribbons of double chains that have three or two types of sharing within the ribbon. For example, $[(Na(dmf)_3)_4Pb_6I_{16}]$ has $[Pb_6I_{16}]^{4-}$ (CSD ref. code: XEPDIF) has building blocks consisting of a 2 x 3 array of three face-sharing and two edge-sharing PbI_6 octahedra (Krautscheid et al, 2001) (Figure 2.64). Adjacent units are linked by four common I atoms. This inorganic motif can also be described as double chains of the $(f_3e)_n$ motif described previously. $[(CH_3SC(NH_2)_2)(HSC(NH_2)_2)SnBr_4]$ (CSD ref. code: IGECAY) has double chains of two edge-sharing octahedra which are corner connected to each other (Raptopoulou et al, 2002) (Figure 2.65).

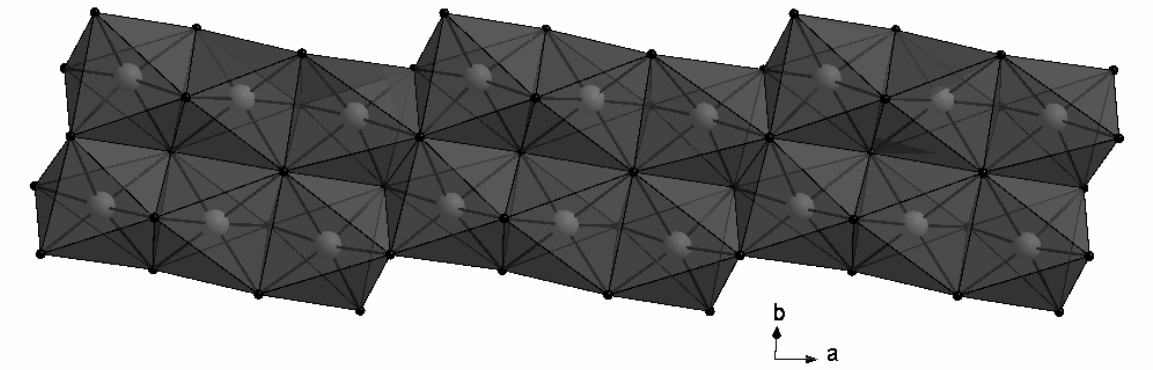


Figure 2.64: Twin anionic chains of face- and edge-sharing lead(II) iodide.

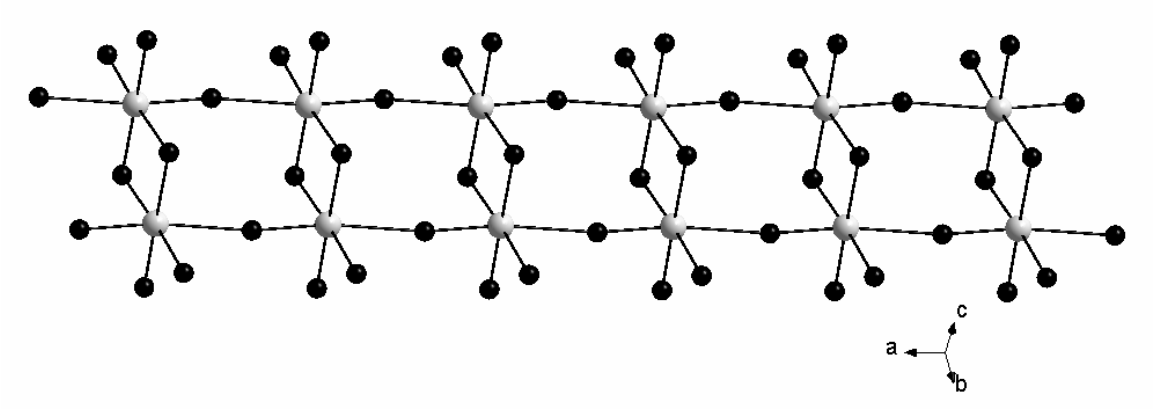


Figure 2.65: Twin anionic chains of edge- and corner-sharing Sn(II) bromide.

The compound [$(PrN(C_2H_4)_3NPr)Pb_2I_6$] (CSD ref. code: XEPDUR) combines face-, edge- and corner-sharing in twin anionic chains (Krautscheid et al, 2001) (Figure 2.67).

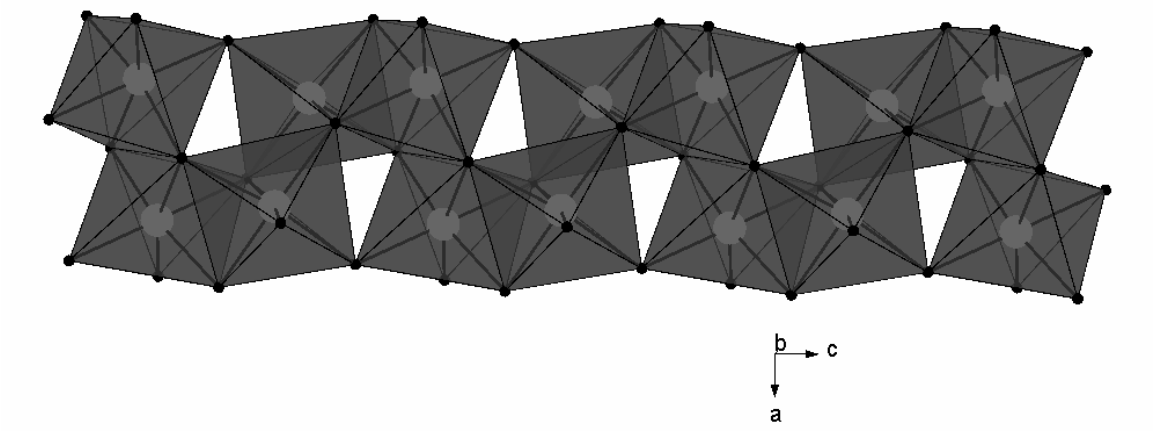


Figure 2.67: Twin anionic chains of lead(II) iodide, that has the three types of sharing in one structure.

2.12: Zero-dimensional inorganic motifs

Isolated compounds are classified as those that have no 1-D or 2-D inorganic motif. The isolated compounds can exist as either isolated, individual metal halide units or be isolated clusters consisting of several connected metal halide units. Hydrogen bonding interactions between the organic and inorganic moieties can form 1-D or even 2-D hydrogen bonded networks and those are included in this section.

Only three inorganic-organic hybrids have been found with isolated octahedra. The organic cations all contain primary ammonium groups and an extensive hydrogen bonded network exists. Even though the compound $[(H_3N\text{-}C_6H_4\text{-}C_6H_4\text{-}NH_3)_2PbCl_6]$ (Bourne and Mangombo, 2004) (CSD ref. code: HAJTIW) has no extended 1-D or 2-D lead(II) chloride inorganic motif, it has alternating inorganic and organic layers that are connected via hydrogen bonds to form a chain of hydrogen bonded interactions along the *a*-axis. Along the *b*-axis, adjacent isolated octahedra are bridged by the ammonium groups on both sides of the organic cation so that a 2-D system of hdrogen bonds results (See Figure 2.68). A secondary interaction occurs between the rings on one end of the benzidine molecules as they are parallel to each other with a separation of 3.7 Å between them. The use of the same ammonium cation but exchanging the lead atom for copper, gives the layered perovskite.

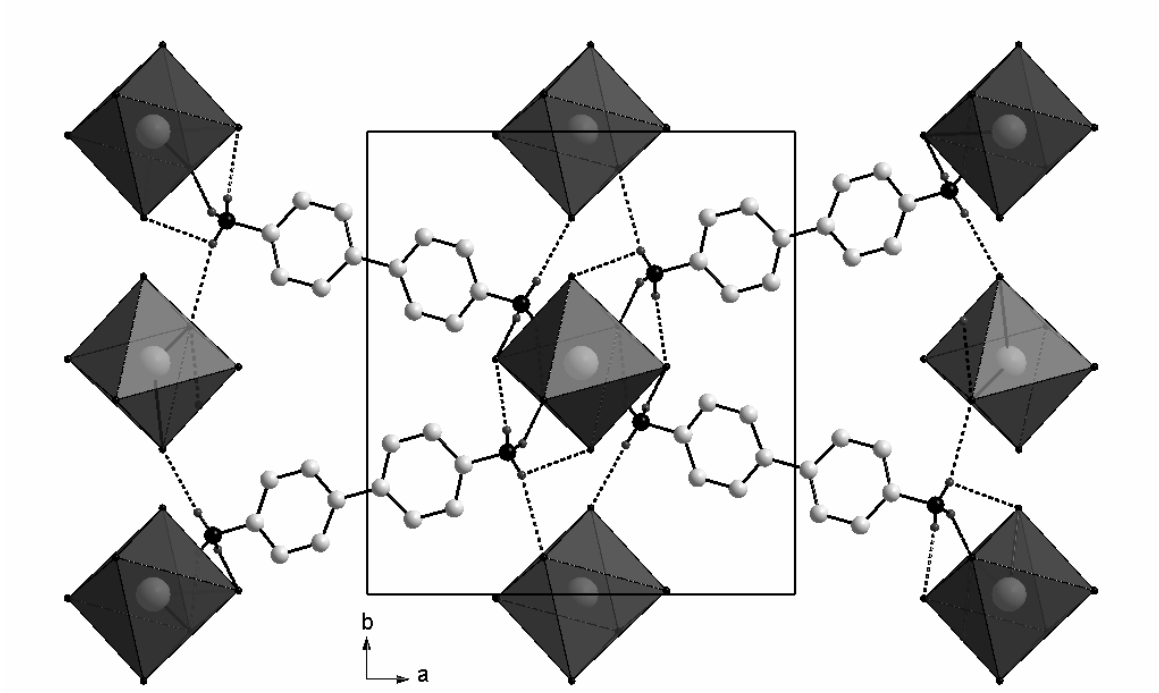


Figure 2.68: Alternating organic and inorganic layers bridged by hydrogen bonds in $[(H_3N\text{-}C_6H_4\text{-}C_6H_4\text{-}NH_3)_2PbCl_6]$.

The other case of isolated lead chloride octahedra is seen with the cation 2-chloro-ethylamine, $Cl\text{-}C_2H_4\text{-}NH_3^+$, which contains isolated chloride anions (Geselle and Fuess, 1995) (CSD ref. code:

HIBTIV). The three individual units are linked via hydrogen bonds to form a 1-D "ribbon" along the crystallographic *b*-axis (See Figure 2.69).

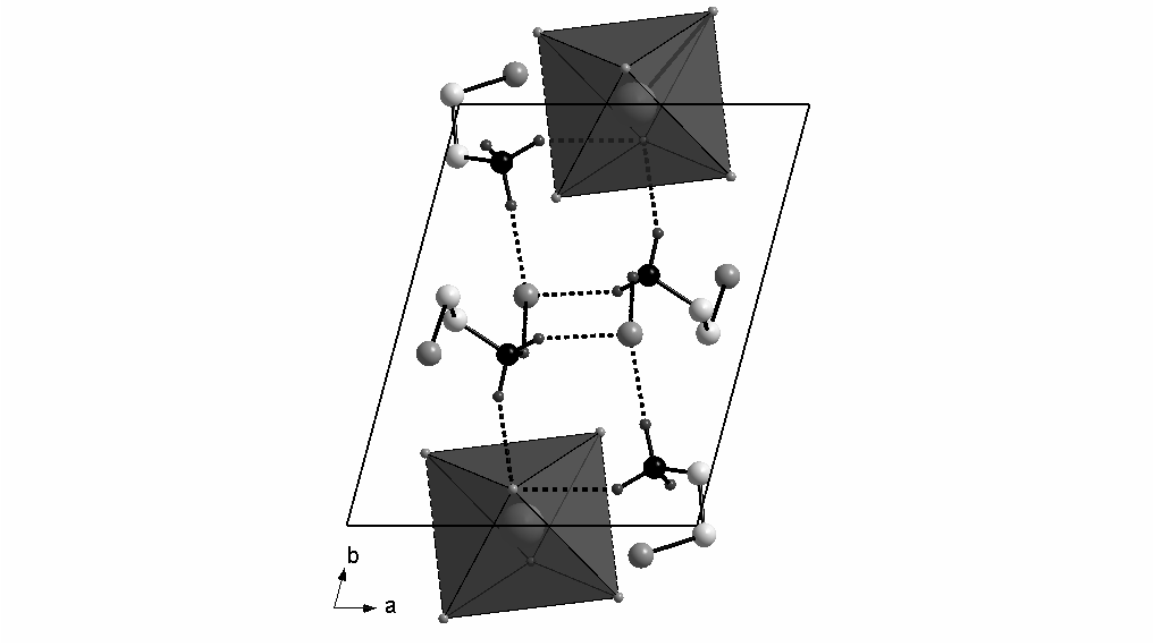


Figure 2.69: Incomplete part of the unit cell of $[(Cl\text{-}C_2H_4\text{-}NH_3)_6PbCl_6]\cdot 2Cl$, showing only a single ribbon of the hydrogen bonded interactions between the alternating $PbCl_6$ octahedra and the cations.

The only reported case of lead(II) iodide forming isolated octahedra is the compound $[(CH_3NH_3)_4PbI_6]\cdot 2H_2O$ (Vincent et al, 1987) (CSD ref. code: FOLLIB). The occurrence of this compound is important as it was prepared from the same solution that produced crystals of the hybrid with a 3-D perovskite structure, $CH_3NH_3PbI_3$, discussed in the layered perovskite section 2.2.4.1 above. The crystals were prepared by adding drop wise aqueous $Pb(NO_3)_2$ to an aqueous solution of CH_3NH_3I. When the temperature at which this was carried out was above 40°C, the product was black coloured $CH_3NH_3PbI_3$. Below this temperature, the product was yellow $[(CH_3NH_3)_4PbI_6]\cdot 2H_2O$, which has a 0-D structure. Furthermore, if one takes the solution containing the black precipitate and cools it down, a conversion to the yellow precipitate occurs spontaneously. The asymmetric unit of the isolated case contains PbI_6^{4-} ions, two $CH_3NH_3^+$ cations and a single water molecule. Each iodide ligand acts as an acceptor atom for two hydrogen bonded interactions and each water molecule is hydrogen bonded to the two cations to

form centrosymmetric pairs. Overall, the authors contend that a 3-D network of hydrogen bonds exist in the packing of the hybrid, shown in Figure 2.70.

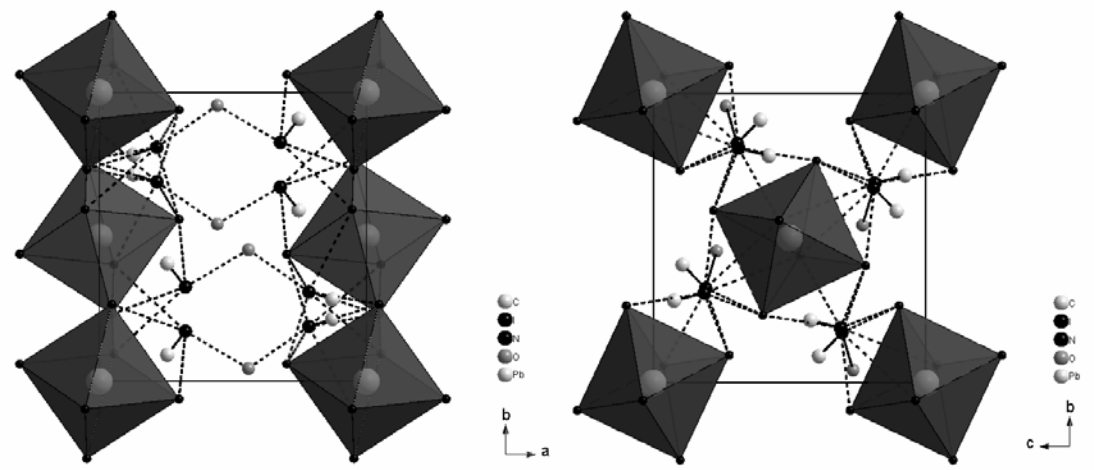


Figure 2.70: Two views of a filled unit cell of $[(CH_3NH_3)_4PbI_6]\cdot 2H_2O$. The cif file did not contain any hydrogen atom coordinates so the interactions are shown as dashed lines between the various acceptor and donor atoms.

Four-coordinate lead(II) iodide is seen only in the isolated structures (Figure 2.71). The coordination geometry of these anions can be regarded as incomplete octahedra. $[(Ph_4P)_2Pb_2I_6]$ (CSD ref. code: GOGNEV) (Krautscheid and Vielsack, 1999) has $[Pb_2I_6]^{2-}$ clusters connected by sharing a single edge. The individual lead atoms have only four iodide ligands, arranged in a pseudo-octahedral coordination, as two of the octahedral positions are not occupied. The angle between *cis* ligands are in the range 85.22(2)° to 97.69(2)°. Single, isolated $[PbI_4]^{2-}$ four-coordinate pseudo-octahedra are seen in only two hybrids, both with quaternary ammonium cations, $[(Bu_3N\text{-}(CH_2)_3\text{-}NBu_3)PbI_4]$ (Krautscheid and Vielsack, 1999) (CSD ref. code: GOGNIZ) and $[(Pr_4N)_2PbI_4]$ (Geselle and Fuess, 1997) (CSD ref. code: GIYRIP).

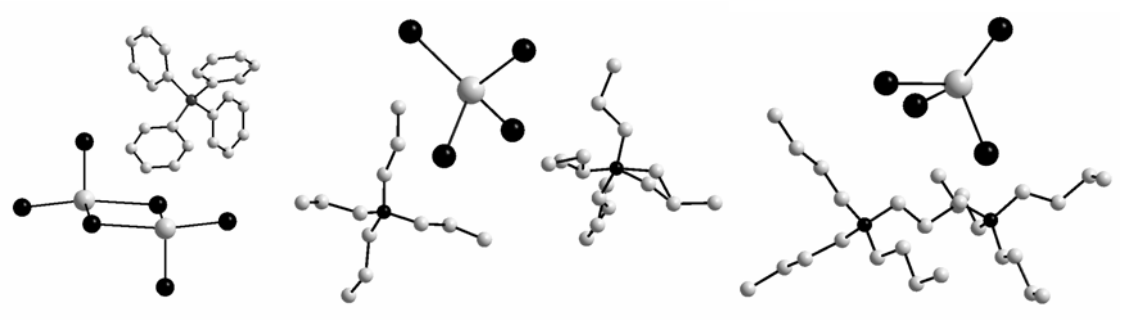


Figure 2.71: The anions and cations of $[(Ph_4P)_2Pb_2I_6]$ (left), $[(Pr_4N)_2PbI_4]$ (middle) and $[(Bu_3N\text{-}(CH_2)_3\text{-}NBu_3)PbI_4]$ (right) that contain tetra-coordinated lead atoms.

Larger lead(II) iodide clusters have also been reported, which consist of purely edge-sharing PbI_6 octahedra, as in $[(Bu_4N)_8Pb_{18}I_{44}]$ (Krautscheid and Vielsack, 1995) (CSD ref. code: ZETLIT). The $[Pb_{18}I_{44}]^{8-}$ anion is shown in Figure 2.72 below and has alternating Pb and I layers stacked on top of each other.

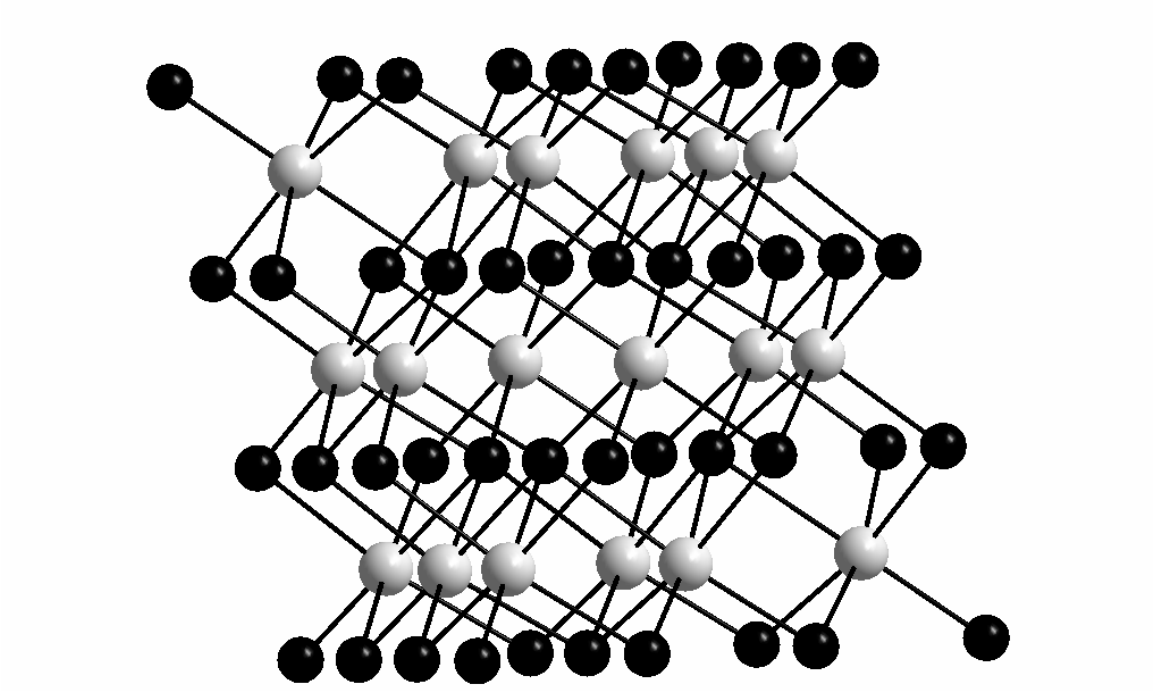


Figure 2.72: The cluster anion $[Pb_{18}I_{44}]^{8-}$.

2.13: Summary and Conclusion

The field of inorganic-organic hybrids exhibits a large range of inorganic motifs, from 3-D to 0-D. The 2-D layered perovskite-type motif has a rich literature of phase transitions when using alkylammonium chains and various optical and electronic properties for a variety of organic ammonium cations. Review articles that have touched on these phenomena include: *Templating and structural engineering in organic-inorganic perovskites* (Mitzi, 2001); *Synthesis, Structure, and Properties of Organic-Inorganic Perovskites and Related Materials* (Mitzi, 1999a), *Organic-Inorganic Layer Compounds: Physical Properties and Chemical Reactions* (Day, 1985) and *Crystal Structures of Three New Copper(II) Halide Layered Perovskites: Structural, Crystallographic, and Magnetic Correlations* (Willett et al, 1988). However, little SC-XRD work has been done on the phase transitions of the layered perovskite-type hybrids $[(C_nH_{2n+1}NH_3)_2PbI_4]$ (n = 4 - 18) and one of the objectives of this work is to determine the nature of the structural changes and compare them to the previously investigated phase transitions. A second objective is to investigate the changes in the crystal structures of the lead(II) halide inorganic-organic hybrids as a function of cation and halide identity, in other words, other possible structural motifs.

Chapter 3 Experimental Methods

3.1 Synthesis

The major obstacles to overcome in preparing crystals suitable for characterization via SCX-RD of these inorganic-organic hybrids with a layered perovskite-type motif all relate to the different solubilities of the inorganic metal halide and the organic amine components. The synthesis of the layered perovskite-type hybrids with either a monoamine or diamine is given by the following reaction schemes:

$$PbX_2 + 2R\text{-}NH_2 + 2HX \rightarrow (R\text{-}NH_3)_2PbX_4$$

$$PbX_2 + H_2N\text{-}R\text{-}NH_2 + 2HX \rightarrow (H_3N\text{-}R\text{-}NH_3)PbX_4$$

Generally, the ratio of metal halide to monoamine to acid halide is 1 to 2 to 2. Generally, the two most successful techniques for growing crystals are solution growth (SG) and slow cooling (SC) (Arend et al, 1978). All compounds used were obtained commercially and used without further purification. Detailed information on the experimental preparation can be found in the chapters to follow.

3.1.1 Slow cooling

Within this project, this technique proved to be the most successful in overcoming the differing solubility issue. The metal halide and amine are weighed out into a glass sample vial and 5 to 10 ml of the required acid halide is added. Generally, a precipitate would form that would not dissolve at room temperature even after being submersed in an ultrasound bath. The vial is then heated in an oil bath that is controlled by a programmable temperature controller (Fig. 3.1). The oil bath is heated to between 80 and 100°C, and then held constant at that temperature until all the precipitate dissolves (usually between 1 hr and 24 hrs). The sample vial is then sealed with its polytop lid and the height of the vial in the oil bath adjusted such that the vial is only immersed

up to the level of the solution inside the vial. This is to allow the vapour to condense in the upper half of the vial.



Figure 3.1: The basic experimental setup used to grow crystals of the inorganic-organic hybrids.

After the precipitate dissolves, the oil bath is cooled at a rate of 2°C/hr. Well-formed crystals generally appear during the cooling process (See Figure 3.2).

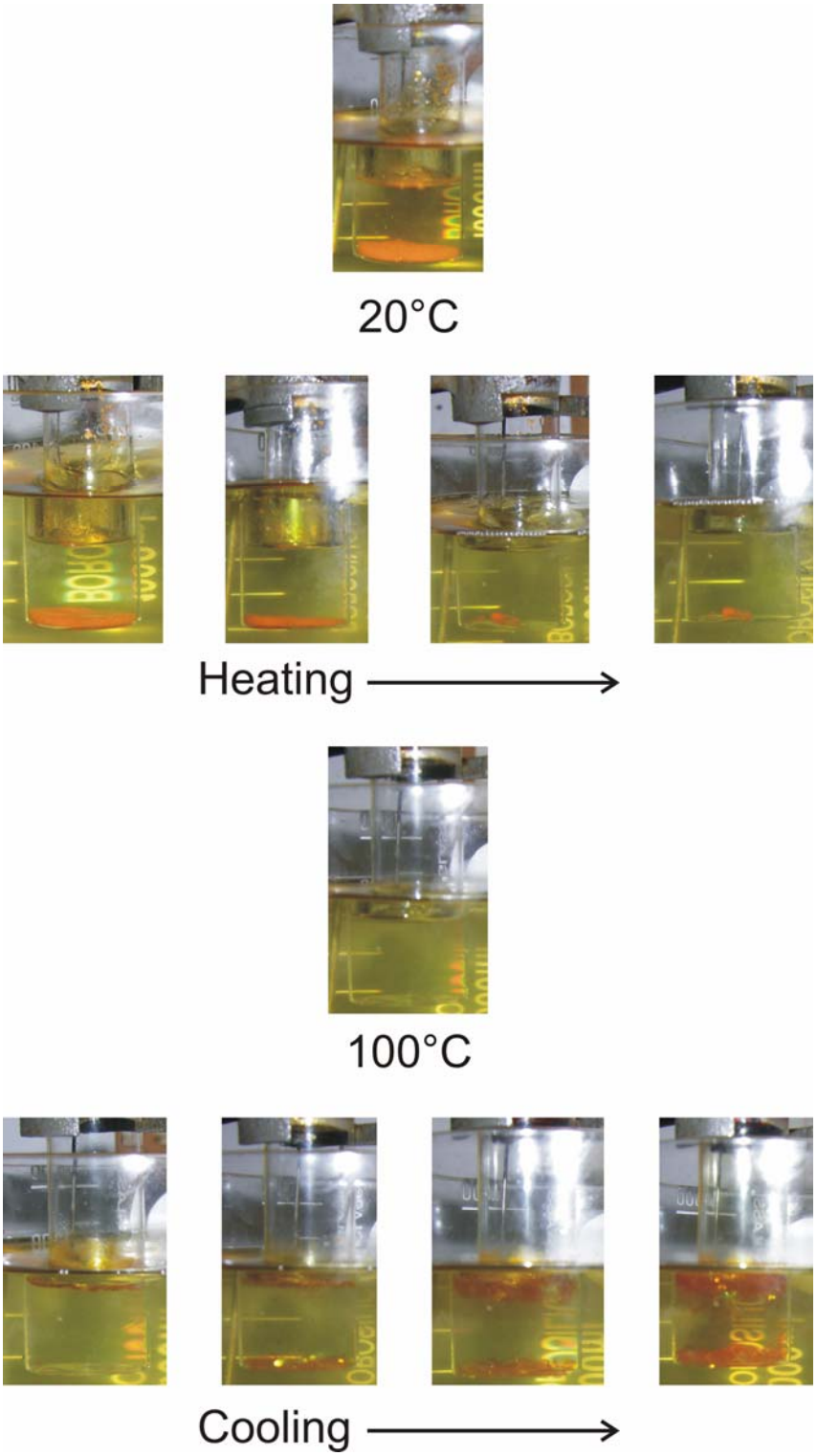


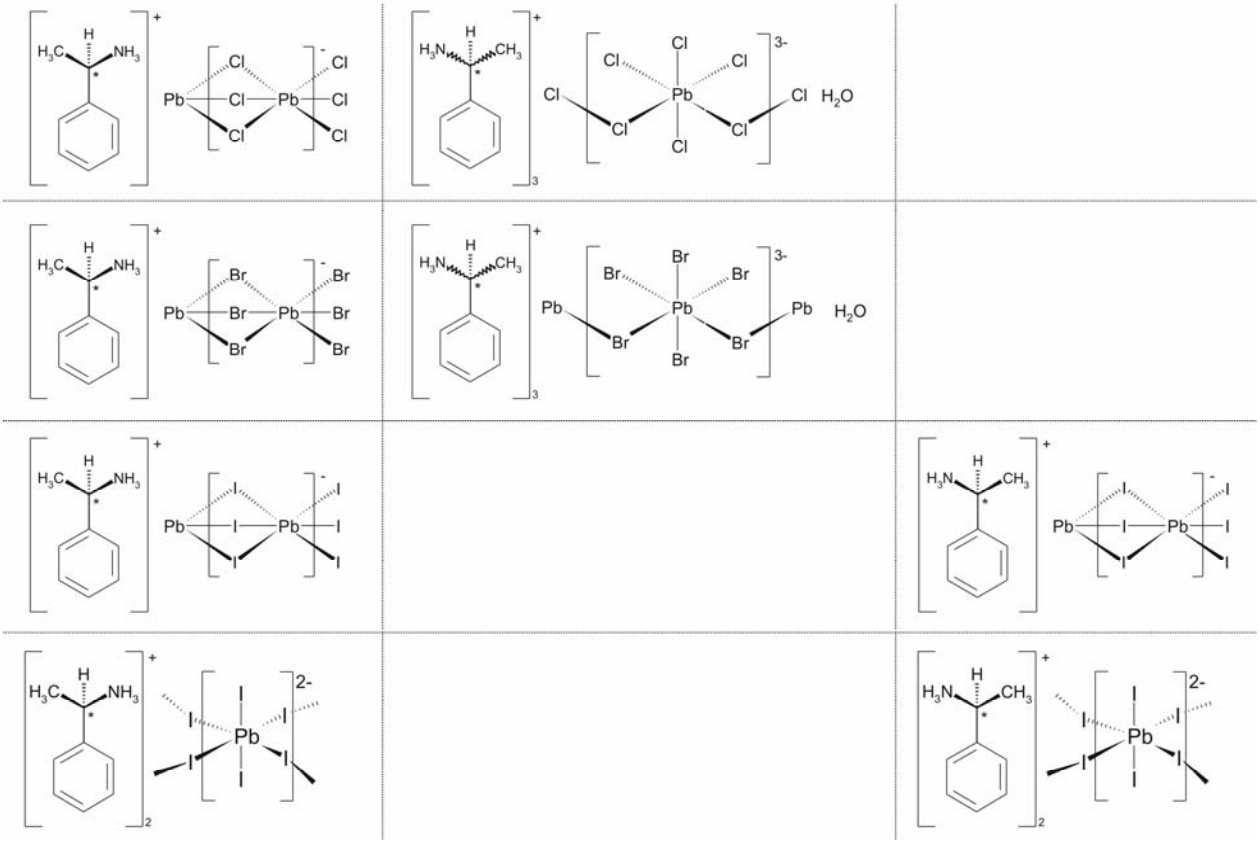
Figure 3.2: The pictures show the important stages of the slow cooling technique. An orange precipitate of the layered perovskite-type hybrid $[(C_8H_{17}NH_3)_2PbI_4]$ at room temperature slowly dissolves as the temperature of the solution increases to 100°C and then becomes a clear solution after a few hours. As the cooling takes place, orange plate-like crystals grow first at the surface of the solution and then at the bottom.

3.1.2 Slow evaporation

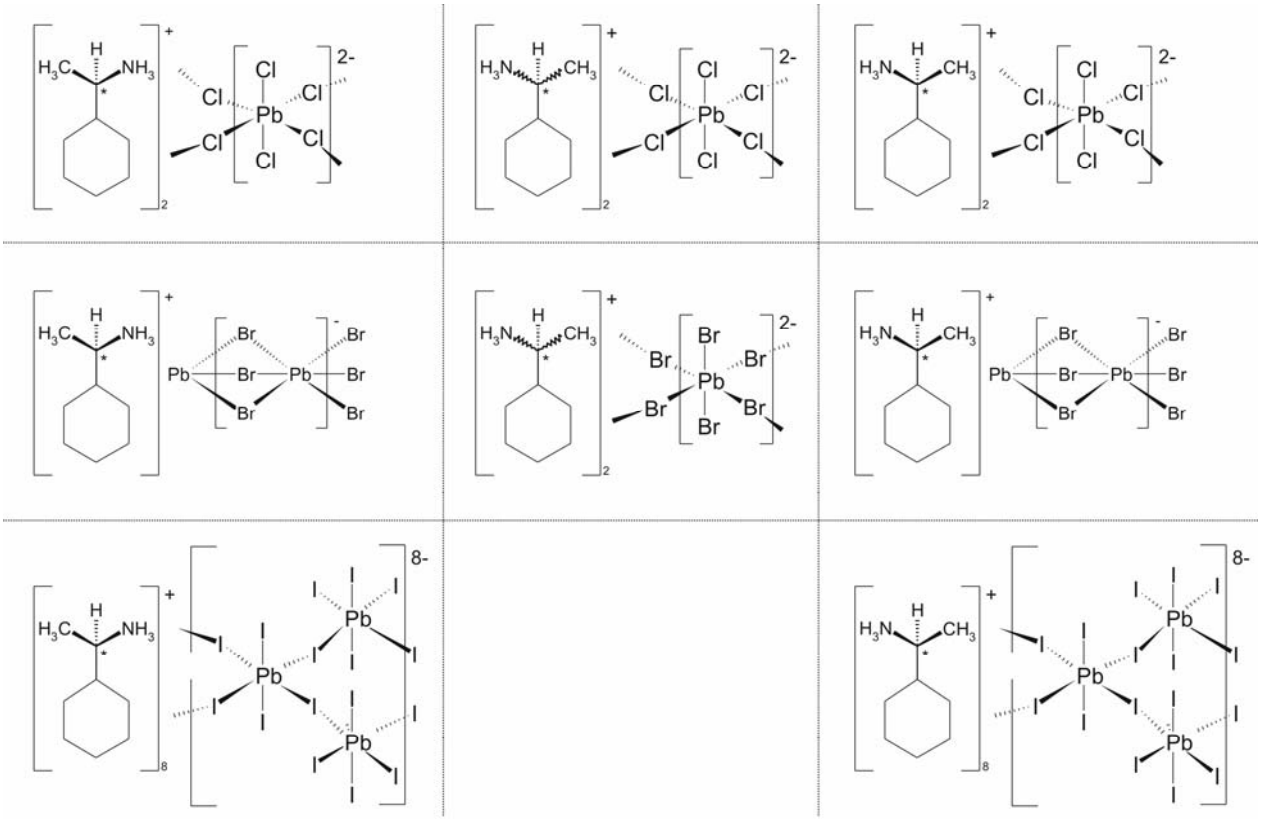
If the precipitate does not dissolve after 24 hrs at an elevated temperature, then adding a suitable solvent to the vial until dissolution occurs is preferred. The procedure is then to use less of the acid halide, of the order of 1 to 2 ml as the acid halide dissolves the metal halide easily. The resulting precipitate then needs to be dissolved and a choice of solvents is available. These include methanol, ethanol, acetone, acetonitrile, DMF, water and ethyl acetate. The latter has been particularly useful in dissolving the long chain alkylammonium hybrids. The sample vial is left open to the atmosphere in a fume hood and crystals grow by the evaporation of the given solvent.

3.1.3 List of compounds prepared with corresponding chapter reference in this thesis

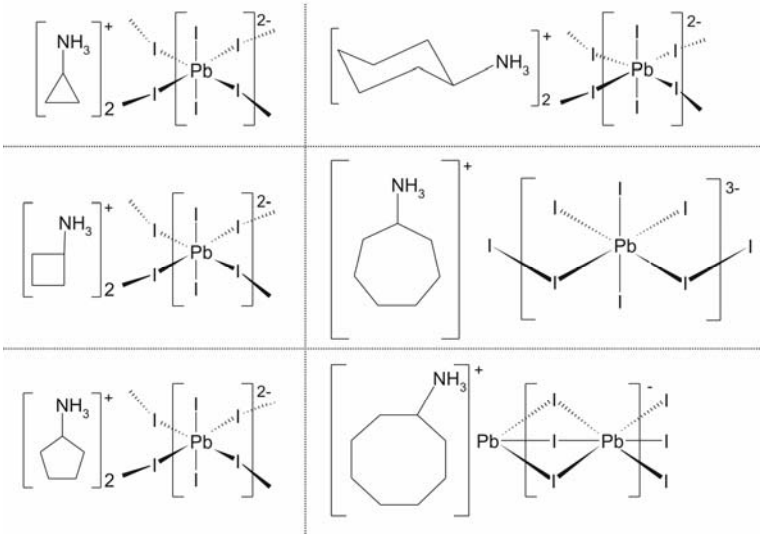
Section 4.2



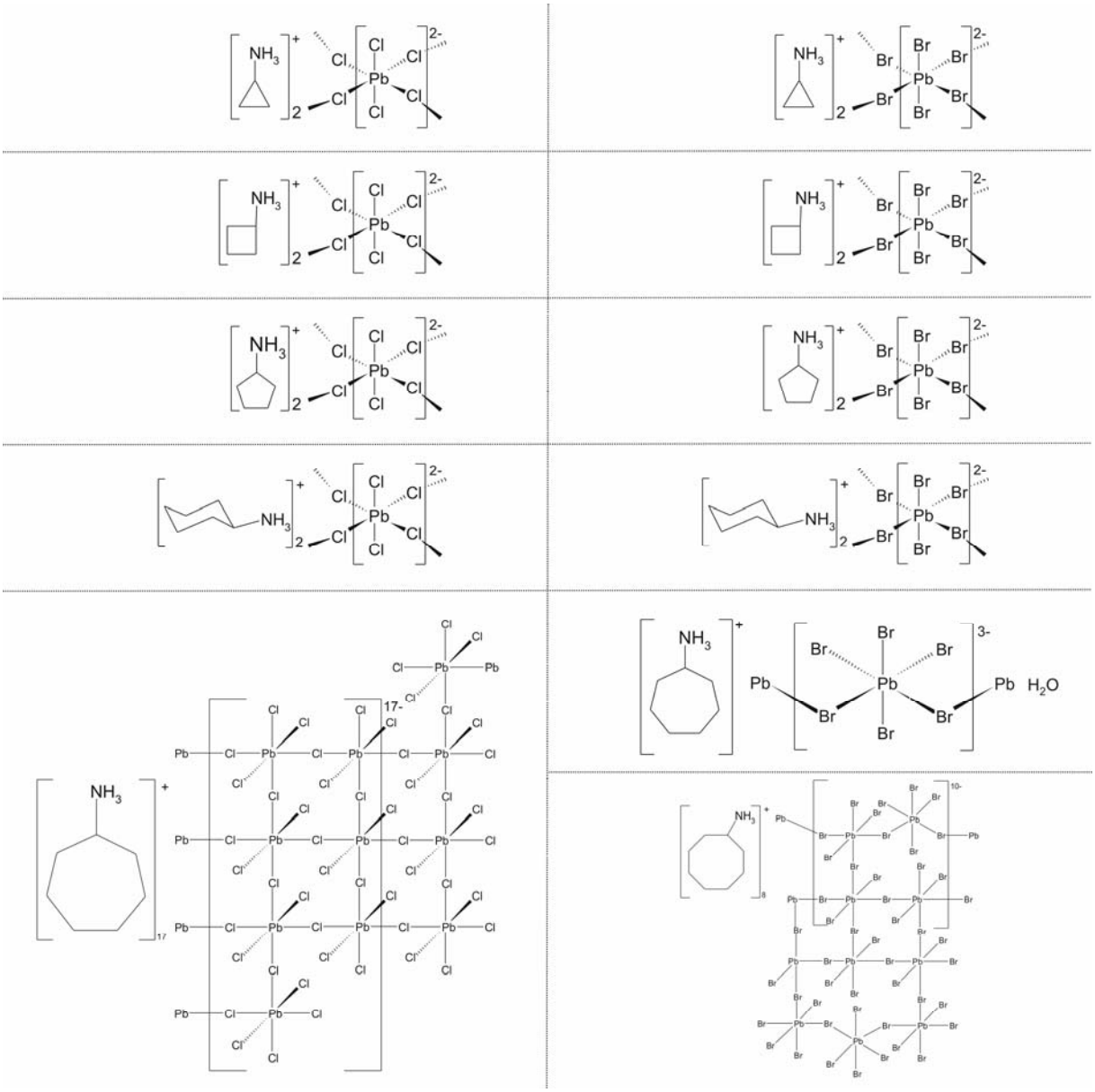
Section 4.3



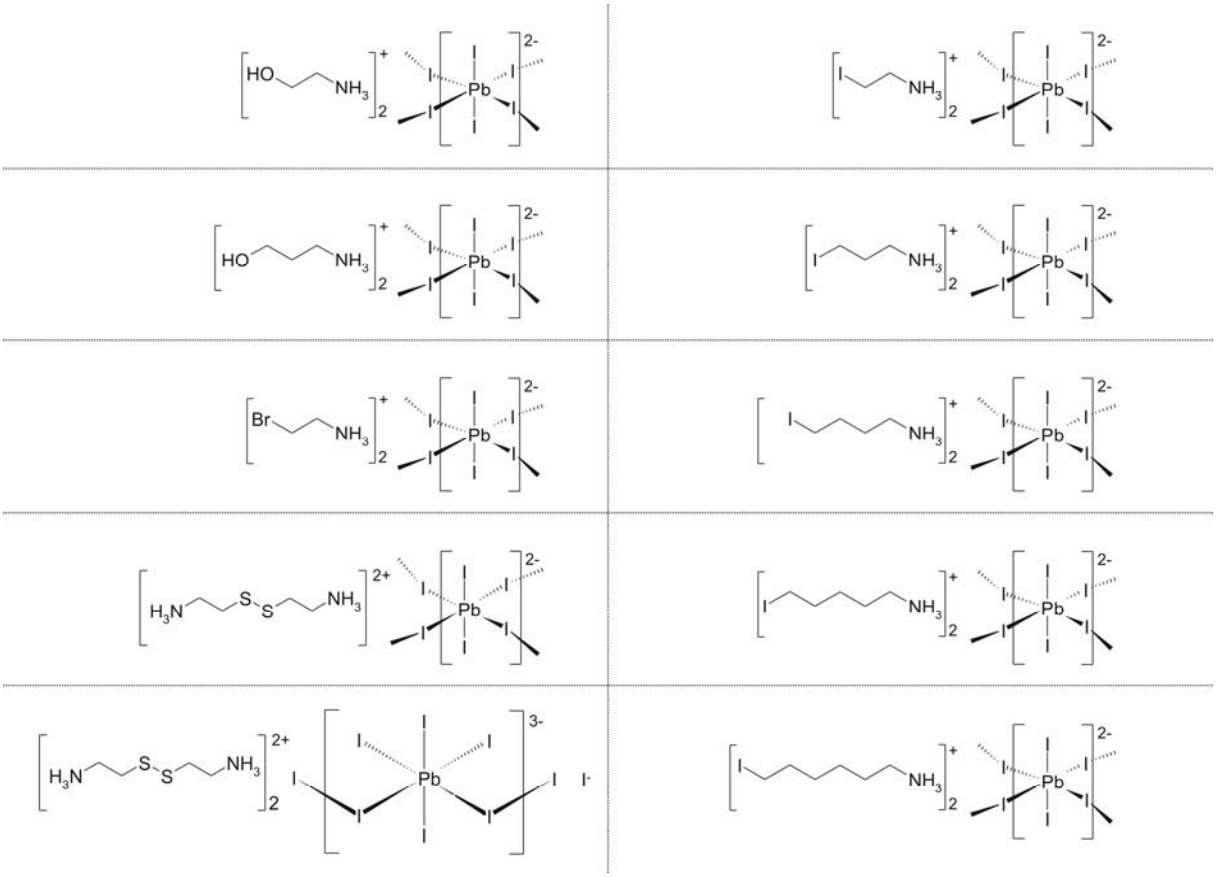
Section 4.4



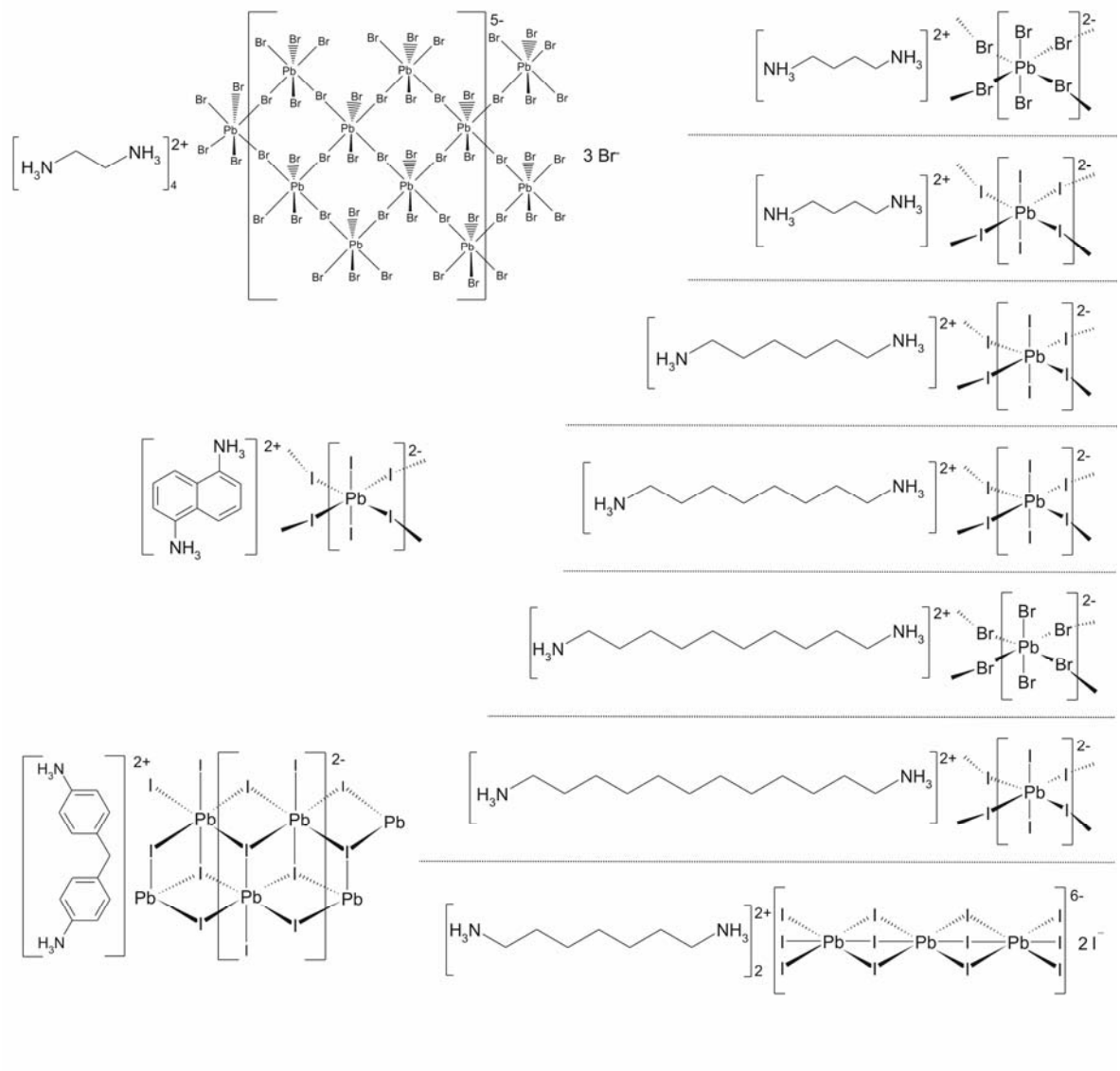
Section 4.5



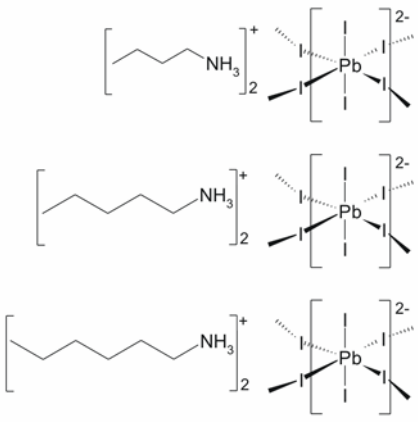
Section 4.6


HO
NH3
2
+
2-
Pb
I
I
NH3
2
+
2-
Pb
I
HO
NH3
2
+
2-
Pb
I
NH3
2
+
2-
Pb
Br
NH3
2
+
2-
Pb
I
NH3
2
+
2-
Pb
H3N
S
S
NH3
2+
2-
Pb
I
NH3
2
+
2-
Pb
H3N
S
S
NH3
2+
2
3-
Pb
I-
I
NH3
2
+
2-
Pb

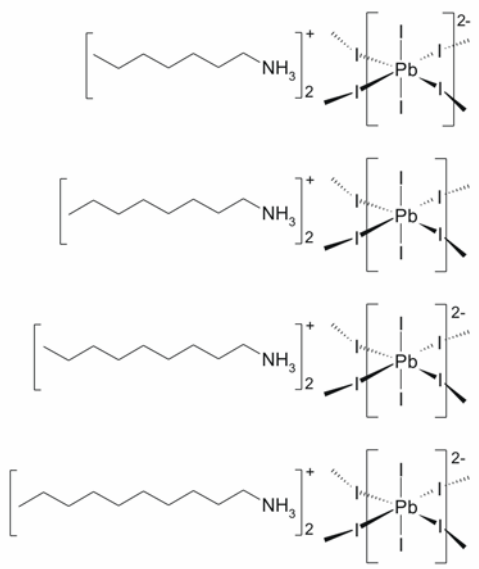
Section 4.7



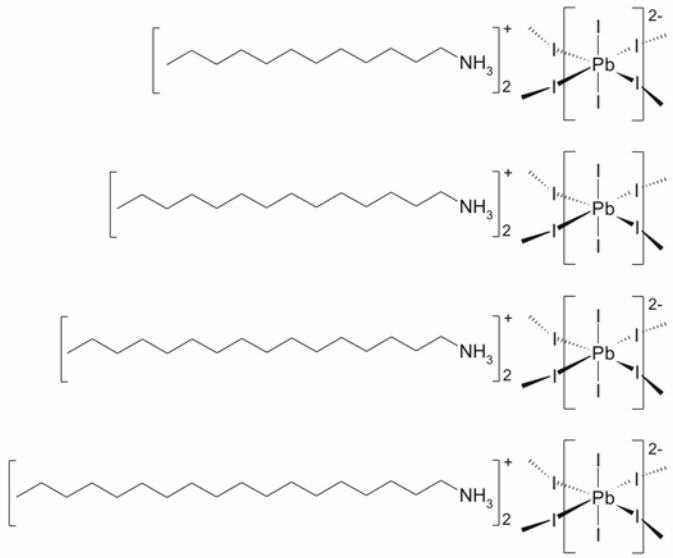
Section 5.2



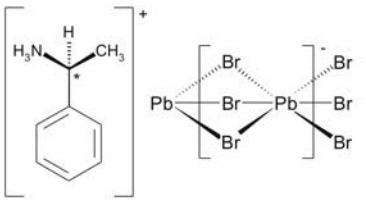
Section 5.3



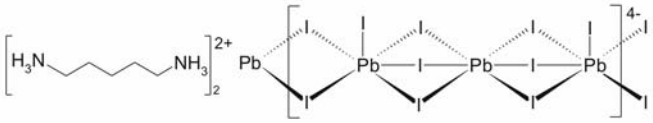
Section 5.4



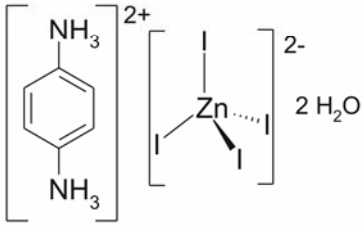
Chapter 6



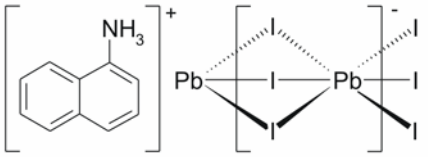
Section 6.2



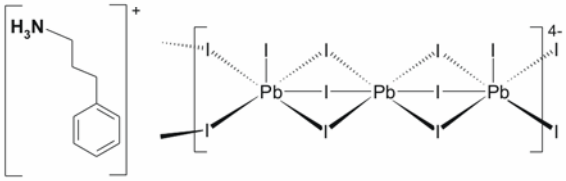
Section 6.3



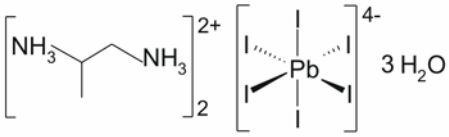
Section 6.4



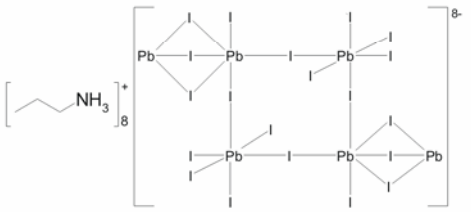
Section 6.5



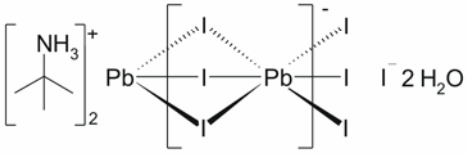
Section 6.6



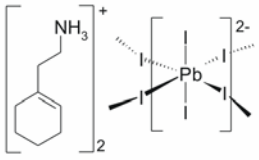
Section 6.7



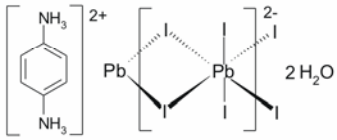
Section 6.8

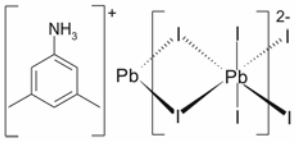


Section 6.9



Section 6.10





Section 6.11

3.2 X-ray Diffraction

Once crystals have been obtained and harvested, they are glued onto a thin glass fibre with 10 minute epoxy under a microscope (Figure 3.3).

3.2.1 Instruments used

Redundant sets of diffraction data were collected on a Siemens SMART 1K Single Crystal Diffractometer (Figure 3.3). All the intensity data were collected initially at room temperature and then at -100°C to improve the quality of the data. The crystals were often plate-like and would fracture if they were cooled too rapidly. This is especially true of the layered perovskite-like hybrids with long alkylammonium chains, as they would fracture easily when cooled. To investigate the phase transitions of the layered perovskite-type hybrids with alkylammonium chains, the crystals had to be both cooled and heated simultaneously. A newer model of the SMART system, the Bruker APEX II, was fitted with an Oxford CRYOSTREAM 700 that is designed for operation in the temperature range of -150°C to 120°C (Figure 3.3).

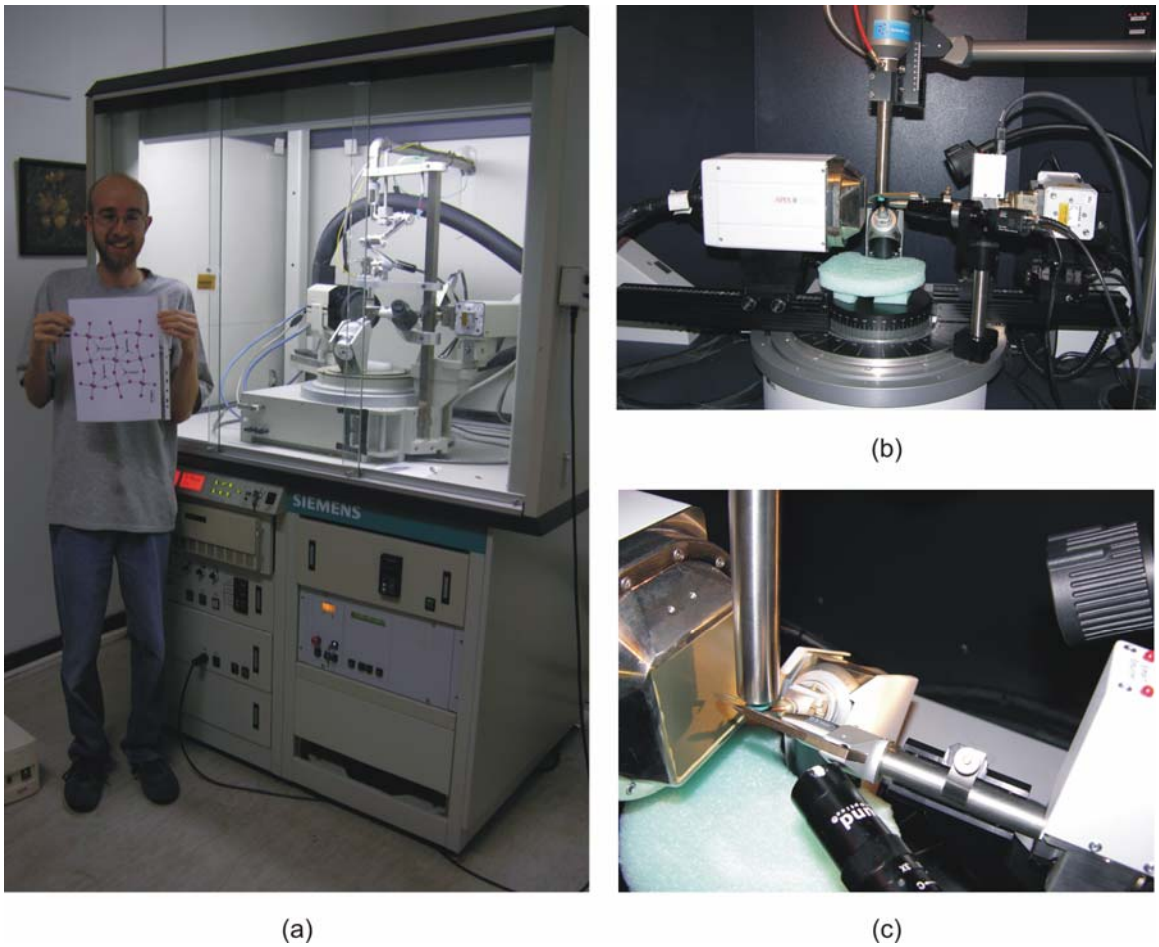


Figure 3.3: The CCD instruments used. (a) Siemens SMART 1K with Kryoflex. (b) The Bruker APEX II with an Oxford Cryostream. (c) Close-up picture of the APEX II showing the centering video camera, CCD detector plate, collimator and heating tube.

3.2.2 Face-indexed absorption corrections

A major problem encountered in SC-XRD with "heavy atoms" is absorption of the X-ray beams by the crystal, thereby reducing the intensity of the incoming and diffracted beam. The drop off in intensity of the diffracted beam I is given by

$$I = I_0 e^{-\tau\rho(\mu/\rho)_\lambda}$$

where I_0 is the intensity of the incident beam, τ the thickness of the absorber and $(\mu/\rho)_\lambda$ the mass absorption coefficient of the material (Stout and Jensen, 1989). The mass absorption coefficient is dependent on the wavelength used. Hence, the bigger the crystal and the greater the absorption

coefficient of the material, the greater the drop-off in intensity. A secondary problem is that the pathlengths of the incident and diffracted beam can vary considerably depending on the particular reflection and the shape of the crystal. For weakly absorbing crystals, such as those of purely organic molecules, that have a uniform size, the effect is not great and semi-empirical methods such as SADABS (Siemens, 1996) can address the problem satisfactorily. However, heavy atoms, such as lead and iodine, have large mass absorption coefficients, and semi-empirical methods proved inadequate. Analytical methods are used in these instances, which require the exact shape of the crystals. This is done by indexing the faces of the crystals and measuring the distances between the faces (Figure 3.4). Once the shape is known, programs such as *XPREP2* (Bruker, 2003) can calculate the path lengths of the incident and diffracted beams through the crystal and correct for the decrease in intensity. For materials with a $\mu > 2$ mm^{-1} (EUHEDRAL, http://www.crystal.chem.uu.nl/distr/euhedral/index.html), this is the recommended method. The range in μ for the inorganic-organic hybrids studied varied from 14.4 mm^{-1} to 21.7 mm^{-1}. Furthermore, the shapes of the crystals studied in this project were often plate-like, with the thickness of the plates no more than 0.01 mm and the width in excess of 0.30 mm. Hence, depending on if the crystal is face-on or edge-on to the incident beam, large discrepancies in the diffracted intensities has to be corrected for.

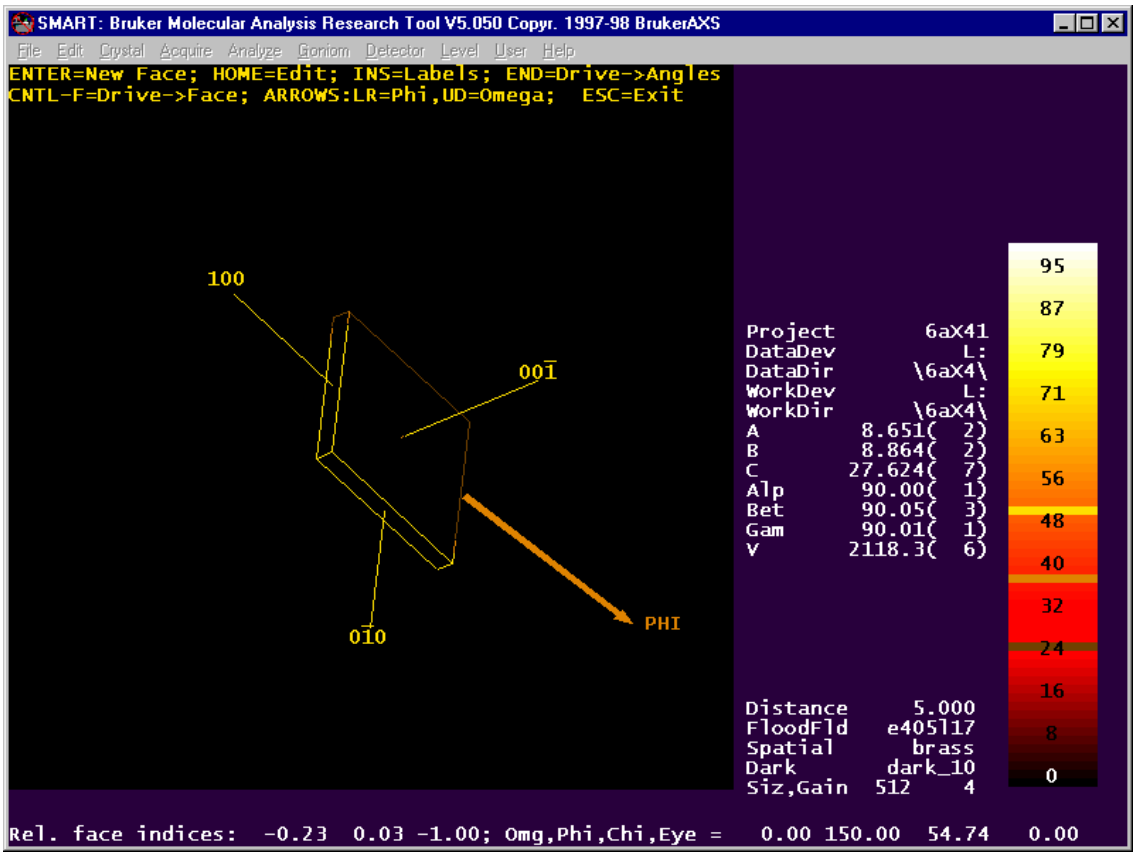


Figure 3.4: Typical crystal shape of hybrid with the layered perovskite-type motif.

3.3 Thermal Analysis

Differential Scanning Calorimetry was used to determine the transition temperatures of the phase transitions and their enthalpies. The device used was a Mettler Toledo 822e calorimeter, which was fitted with a cold finger to increase its range from -50°C to 400°C and further allows for controlled heating and cooling scans. This was sufficient to monitor all the phase transitions of the layered perovskite-type hybrids.

3.4 Elemental analysis

Elemental analysis of all the compound was performed by the Institute of Soil, Climate and Weather (Pretoria, South Africa). The instrument used was a Carlo Erba Instruments, model NA 1500, Nitrogen/Carbon/Sulphur Analyser. The instrument was modified to do CHN elemental analyses as well (Philpott, 2002).

3.5 Hot Stage Microscopy

The thermochromic phase transitions of the alkylammonium hybrids displayed colour changes and were easily observed by heating up the crystals to be determined on a hot plate under a microscope (Figure 3.5).



Figure 3.5: Locally modified Koffler Hot Stage.

Chapter 4 Structural Motifs of Inorganic-Organic Hybrids

4.1 Introduction

In this chapter I present the structures of 54 inorganic-organic hybrids that did not display any phase transitions. The essence of this chapter deals with the structural trends observed in the structure of the inorganic-organic hybrid as a function of the cation identity and the halide identity. Six separate investigations were carried out on various systems.

4.2 Synthesis and crystal structures of inorganic-organic hybrids incorporating an aromatic amine with a chiral functional group

Journal: CrystEngComm

Date Submitted: 17 May 2006

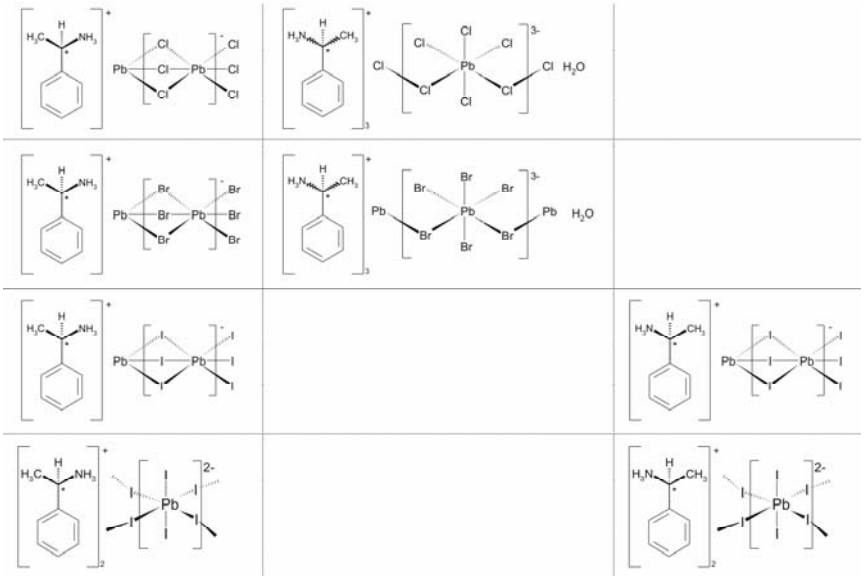
Reference Code of Submitted Article: B606987H

Date Accepted: 7 July 2006

Final Reference: Billing, D.G., Lemmerer, A. (2006). *CrystEngComm*, **8**, 686-695.

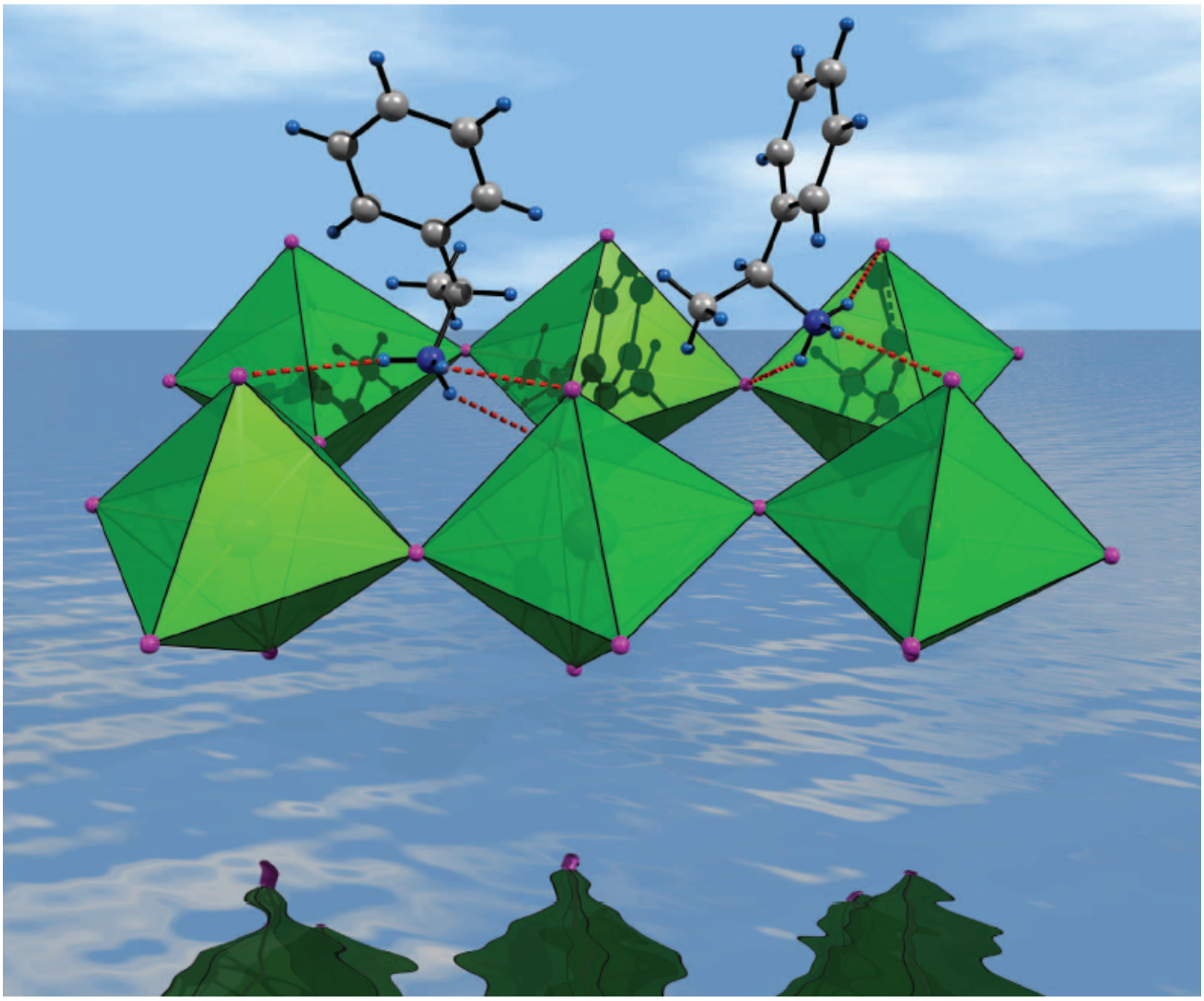
Brief Synopsis

In this paper, eight inorganic-organic hybrids were made using the metal lead and the halides chloride, bromide and iodide. The counter cations were the *R*, *S* and racemic forms of 1-phenethylammonium. The objective was to observe the inorganic motif obtained for various inorganic-organic hybrids. The work discussed in this paper was featured on the cover of the journal



CrystEngComm

www.rsc.org/crystengcomm Volume 8 | Number 9 | September 2006 | Pages 651–728



RSC Publishing

COVER ARTICLE
Billing and Lemmerer
Synthesis and crystal structures of inorganic–organic hybrids incorporating an aromatic amine with a chiral functional group

HOT ARTICLE
Datta *et al.*
Molecular and supramolecular structures of benzil dihydrazone, an organic helical molecule. Comparison with diacetyl dihydrazone

COMMUNICATION
Janiak *et al.*
Can a single C–H•••F–C hydrogen bond make a difference? Assessing the H•••F bond strength from 2-D ^{1}H–^{19}F CP/MAS NMR

PAPER www.rsc.org/crystengcomm | CrystEngComm

Synthesis and crystal structures of inorganic–organic hybrids incorporating an aromatic amine with a chiral functional group

David G. Billing* and Andreas Lemmerer

Received (in CAMBS) 17th May 2006, Accepted 7th July 2006
First published as an Advance Article on the web 27th July 2006
DOI: 10.1039/b606987h

In this paper we report the synthesis and the crystal structure of inorganic–organic hybrids containing various lead halides as the inorganic motif and a primary amine as the organic constituent. The organic molecule investigated is ($C_6H_5C^*H(CH_3)NH_2$) and both the *R* and *S* as well as the racemic (±) forms were used. Within the structures obtained, three different inorganic motifs are displayed by the lead halide octahedra: 1-D polymeric face-sharing chains of formula $PbCl_3((R)$–$C_6H_5CH(CH_3)NH_3)$, $PbBr_3((R)$–$C_6H_5CH(CH_3)NH_3)$, $PbI_3((R)$–$C_6H_5CH(CH_3)NH_3)$ and $PbI_3((S)$–$C_6H_5CH(CH_3)NH_3)$; 1-D polymeric corner-sharing chains of formula $PbCl_5((\pm)$–$C_6H_5CH(CH_3)NH_3)_3$ and $PbBr_5((\pm)$–$C_6H_5CH(CH_3)NH_3)_3$; and 2-D corner-sharing layers of formula $PbI_4((S)$–$C_6H_5CH(CH_3)NH_3)_2$ and $PbI_4((R)$–$C_6H_5CH(CH_3)NH_3)_2$. The changes in geometry and intermolecular interactions such as hydrogen bonding and pi stacking are discussed and compared between the eight structures.

Introduction

Organic–inorganic hybrid structures are able to combine excellent features from both types of constituents. Inorganic compounds have different band gaps and hence their electrical properties can vary from conducting to semiconducting right the way through to superconducting or insulating. Furthermore, they supply the hybrid structure with thermal stability and hardness as well as magnetic and dielectric properties. Organic materials offer highly efficient luminescence and can show superconducting and conducting properties. They also contribute a structural diversity that enables us to synthesize a large range of different compounds to suit our needs.

In recent years, a significant number of organic–inorganic hybrid materials, based on lead halide units, have been studied. Six coordinate lead halides can arrange themselves in three-, two- and one-dimensional networks through sharing of the halides in the PbX_6 octahedra, which are separated by organic cations.[1,2] One-dimensional (1-D) extended chains can be formed by one, two or three bridging halides and combinations thereof. Use of one bridging halide can form two types of chains: if the two bridging halides connecting the central octahedra to its neighbour are related *cis*, we get a zig-zag pattern; if they are *trans*, the chain is linear. The case with three bridging halides is described as face-sharing and is the most common linkage encountered. The octahedra can share faces that are either only *trans* to each or they can alternate between *trans* and *cis* related faces. The pure *trans* case gives long, straight chains whereas the latter case is wave-shaped with the amplitude perpendicular to the direction of the chain.[3]

2-D hybrids are based on the K_2NiF_4 structure type and result from replacing the potassium cations with bulkier ammonium cations. The organic cation can form bilayers between these organic layers if it has only one amine or a monolayer for two amines. The inorganic layer consists of MX_4^{2-} corner-sharing metal halide octahedra. To keep these larger cations effectively in place, there must exist hydrogen bonding between one end of the organic molecule and the halide on the metal. This "head" of the molecule is the primary amine, $-NH_3^+$, and the rest of the molecule –R is the tail. Weak van der Waals forces between the tails hold the sandwich together. The general formula then becomes $(R–NH_3)_2MX_4$ or $(NH_3–R–NH_3)MX_4$, where R can be aliphatic or aromatic.

The inorganic layers can occur in one of two conformations: The lead atoms can be either directly above each other in each adjacent layer (eclipsed) or they can be offset in each adjacent layer (staggered). In the staggered conformation, every second layer is eclipsed. The eclipsed configuration is seen in monoclinic unit cells whereas the staggered configuration comes about with a change to an orthorhombic crystal system.

The hydrogen bonding scheme in organic–inorganic hybrids between the ammonium hydrogens and the halides can have two possible scenarios: if there are more bonds to the axial halides than to equatorial halides, it is called axial halide configuration and the reverse case with more equatorial than axial acceptors, bridging halide configuration.

The objective of this study was two-fold. Firstly, to investigate what effect, if any, varying the identity of the halide would have on the inorganic motif within the hybrid structure. And secondly, we wanted to observe what impact the chiral and racemic nature of the organic compound has.

Molecular Sciences Institute, School of Chemistry, University of the Witwatersrand, PO Wits 2050, Johannesburg, South Africa. E-mail: dave@chem.wits.ac.za; Fax: 27 11 7176749; Tel: 27 11 7176759

 This journal is © The Royal Society of Chemistry 2006

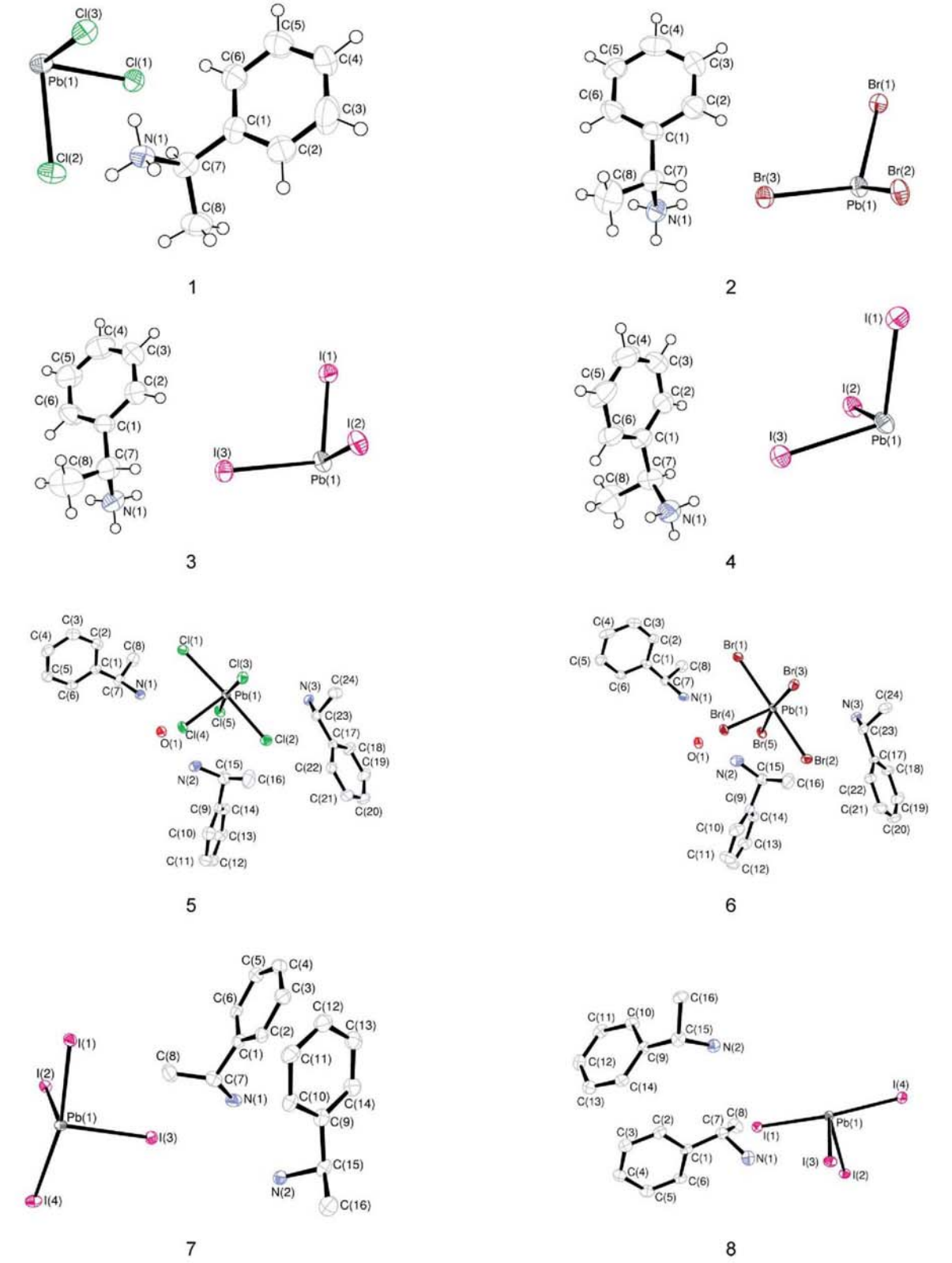


Fig. 1 The asymmetric units of compounds **1–8**, showing the atomic numbering scheme. Displacement ellipsoids are shown at the 50% probability level.

Results and discussion

Crystallographic description of the metal halide inorganic motifs

$PbCl_3((R)\text{–}C_8H_{12}N)$, **1**, (abbreviated $PbCl_3R$), $PbBr_3((R)\text{–}C_8H_{12}N)$, **2**, (abbr. $PbBr_3R$), $PbI_3((R)\text{–}C_8H_{12}N)$, **3**, (abbr. PbI_3R) and $PbI_3((S)\text{–}C_8H_{12}N)$, **4**, (abbr. PbI_3S) have essentially the same packing arrangement and crystallize in the space group $P2_12_12_1$. Each structure consists of chains of polymeric octahedral haloplumbates as seen previously in $PbBr_3((S)\text{–}C_8H_{12}N)$.[4] There is little structural variation in the octahedra and counter-ion if the halide is Br or I, and hence the structures of **2** and **3** can be considered isostructural but the conformation of the counterion $C_6H_5CH(CH_3)NH_3$ as well as the distortion of the octahedra in $PbCl_6$ is different in the chloride case. The cell volume increases by 108 $Å^3$ from the bromide to the chloride and by 176 $Å^3$ to the iodide as the ionic radius of the halides increase.

The inorganic network in **1** consists of 1-D chains running along the *b*-axis, in which six chlorides are bonded to lead to form severely distorted octahedra (Fig. 2). Two consecutive lead atoms are bonded *via* three bridging chlorides. The bond distances between the symmetry equivalent chlorides and the central lead atom are characterised by short and long distances. The equatorial chloride Cl(1) has the shortest and longest bond to the lead atoms of 2.6890(14) Å and 3.2910(14) Å. The axial halides Cl(2) and Cl(3) are less extreme, ranging from 2.7372(14) Å to 3.1334(15) Å for Cl(3), with Cl(2) the least, 2.8216(15) Å to 2.9480(14) Å. The bond angles also deviate from ideal octahedral values due to the uneven bond lengths. The axial *trans* angle for Cl(1)–Pb(1)–Cl(1) is 149.66(4)°, which deviates greater than for the two almost alike equatorial *trans* angles of 162.42(4)° and 163.84(3)° for Cl(3) and Cl(2), respectively. This geometry is seen in other face-sharing analogues with chloride as the halide. A similarly distorted structure is seen in $PbCl_3(C_4H_{10}NO)$,[2] which has morpholinium as the counter-ion. Close interactions between chlorides on adjacent chains are Cl(2)···Cl(3) [3.724(2) Å], slightly more than twice the ionic radii of Cl^- (1.81 Å).[5] The chiral counterion sits in the channels formed by the chains and through hydrogen bonds connects adjacent chains. The cation shows an unusual geometry in the chiral group attached to the benzene ring. The torsion angle C(6)–C(1)–C(7)–H(7) is 32.27(81)° which is far from the expected *cis* angle. This is unique and not seen in the organic cations with the other lead halides reported in this study and may explain why crystals with the opposite chirality, the *S* enantiomer, were never obtained. The atomic numbering scheme and thermal displacement ellipsoids are given in Fig. 1 for all eight hybrids discussed.

$PbBr_3R$, **2**, crystallizes with the *R* isomer in a smiliar fashion to the previously reported $PbBr_3((S)\text{–}C_8H_{12}N)$[4] and hence the structures are enantiomorphs of one another. Bond distances are in the range 2.8530(9) Å to 3.3208(9) Å for the axial halide Br(2) which are comparable to the previously reported values.[4] The geometry around the lead atom is not as extreme as in **1** with the axial *trans* angle 154.87(2)° for Br(2)–Pb(1)–Br(2). The equatorial *trans* angles are ~2° greater than in **1**. The distance between two adjacent chains increases to 3.893(1) Å, close to double the ionic radius of Br^- (1.96 Å).[5]

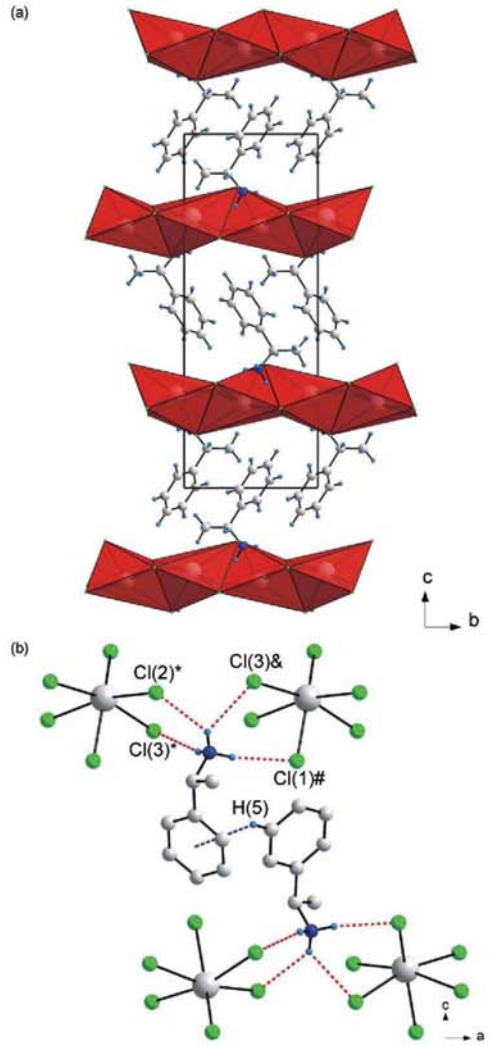


Fig. 2 (a) Packing diagram of **1**, viewed along the *a*-axis. The severely distorted $PbCl_6$ octahedra are shown in red. (b) Packing diagram view parallel to the chains, along the *b*-axis, showing the face-to-edge σ–π interaction between the cations (dashed blue lines) and the hydrogen bonds (dashed red lines) between the inorganic chain and the organic cations, which form a 3-D system. Atoms marked with an asterisk (*), hash (#) and ampersand (&) are at the symmetry positions (−1/2 + *x*, ½ − *y*, 1 − *z*), (1/2 + *x*, ½ − *y*, 1 − *z*) and (3/2 − *x*, −*y*, ½ + *z*), respectively.

The range between the longest and shortest Pb–I bond lengths are the least in PbI_3R, **3**, and PbI_3S, **4**. These two compounds are enantiomorphs of one another, as shown in Fig. 3. The values, respectively, for **3** and **4** are 3.1170(6) Å to 3.3870(6) Å and 3.1223(6) Å to 3.3928(6) Å. Both ranges are the bonds to the equatorial halide I(3). The *trans* angles are all closer to 180°, in agreement with the least distorted octahedra of the three lead halides that adopt the face-sharing motifs. The *R* and *S* enantiomers for **3** and **4** have the most regular geometry with torsion angles of −178.67(71)° and 178.19(55)°, respectively, for C(6)–C(1)–C(7)–H(7). The distance between

 This journal is © The Royal Society of Chemistry 2006

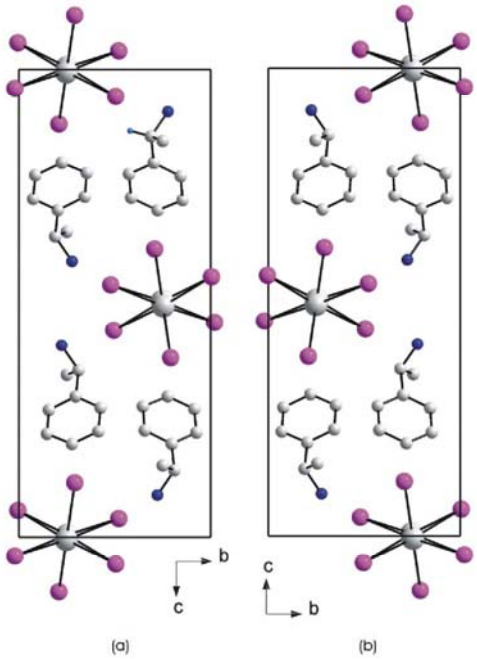


Fig. 3 Packing diagrams of the enantiomorphs PbI_3R **3** (a) and PbI_3S **4** (b). Both unit cells are non-superimposable mirror images of each other.

iodides on two adjacent chains, I(2)···I(3), are 4.140(1) Å and 4.148(1) Å for **3** and **4**, respectively, significantly shorter than twice the ionic radius of the iodide ion (2.20 Å).[5]

$PbCl_5((\pm)\text{–}C_6H_5CH(CH_3)NH_3)_3$, **5**, (abbr. $PbCl_5\pm_3$), has five unique chlorides surrounding the lead atom in the asymmetric unit. Chlorides Cl(1) and Cl(2) are in axial positions and alternate positions in each subsequent octahedra. Cl(3) and its symmetry equivalent Cl(3)′ [1/2 − *x*, −1/2 + *y*, 1/2 − *z*] lie in the equatorial plane and are shared between the octahedra. They are *cis* related and hence the overall pattern of the chains is zig-zag (Fig. 4b). The bond lengths of the shared chloride are 2.9180(10) Å and 3.1404(11) Å between two octahedra. The terminal halides Cl(4) and Cl(5) are *trans* to the bridging halides and have the shortest bond lengths. Four chains run along the *b*-axis and divide the unit cell into four quarters (Fig. 4a). Each chain has the organic cations arranged radially around it with the ammonium heads pointing inwards to engage in hydrogen bonding interactions. The water molecules are located between neighboring chains.

The organic cations are labelled cat1 (containing atom N(1)), cat2 (containing atom N(2)) and cat3 (containing atom N(3)). Cat1 is located above and below the gaps between the chains and the water molecule. Cat2 and cat3 fit above the gaps created by three bonded octahedra. Cat1 and cat3 are both *R* enantiomers and cat2, an *S* enantiomer. The symmetry operators then generate the opposite enantiomer for all three organic cations so that a racemic ratio is ensured. The three cations have three different conformations around the aromatic carbon and the methine carbon. Cat1 has a torsion angle of 16.61(47)° (C(6)–C(1)–C(7)–H(7)), cat2 a torsion

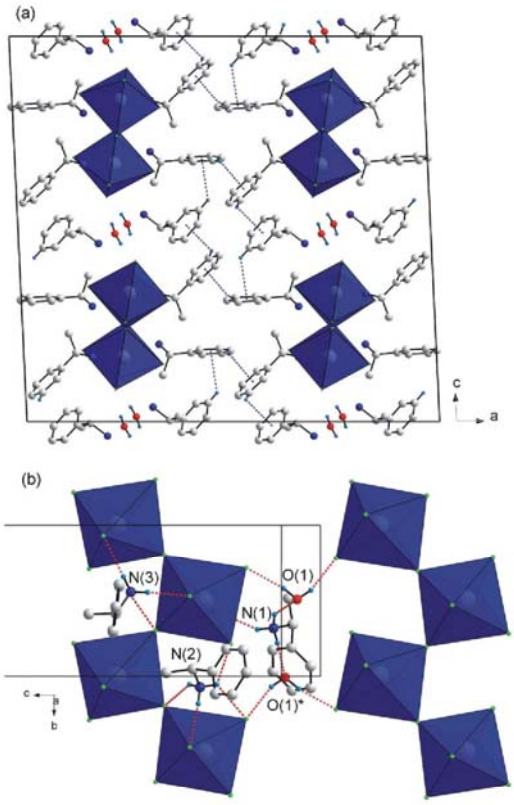


Fig. 4 (a) Packing diagram of **5**, viewed along the *b*-axis. The four corner-sharing chains of $PbCl_6$ octahedra that run through the unit cell are shown in blue. The dashed blue lines show the face-to-edge σ–π interactions between the three cations. (b) Packing diagram view perpendicular to the chains, along the *a*-axis, showing the three hydrogen bonding interactions of cat1 (N1), cat2 (N2) and cat3 (N3) with the chlorides and the waters of hydration. Atoms marked with asterisk (*) are at the symmetry position (1/2 − *x*, 3/2 − *y*, −*z*).

angle of 3.69(52)° (C(14)–C(9)–C(15)–H(15)) and cat3 a torsion angle of −36.74(41)° (C(22)–C(17)–C(23)–H(23)).

$PbBr_5((\pm)\text{–}C_6H_5CH(CH_3)NH_3)_3$, **6**, (abbr. $PbBr_5\pm_3$), has a similar packing arrangement to **5** and the two compounds can be considered isostructural. Br(3), Br(4) and Br(5) are equatorial with Br(3) the bridging halide. Bridging bond distances are longer at 3.0600(7) Å and 3.2014(7) Å than in the chloride case. The *trans* angles between the halides in the octahedra are similar in **5** and **6** but with both closer to 180° compared to the more irregular geometry in the face-sharing haloplumbates. The bridging angles are 161.92(4)° and 163.56(2)°, respectively, for **5** and **6** so that the octahedra are tilted relative to each other in the *bc*-plane. Cat1 is located above and below the gaps between the chains and the water molecule. Cat2 and cat3 fit above the area created by three bonded octahedra. The chiral functional groups are rotated at different angles to the benzene ring. The angles are 20.07(63)° (cat1, C(6)–C(1)–C(7)–H(7)), 6.84(66)° (cat2, (C(14)–C(9)–C(15)–H(15)) and −35.81(62)° (Cat3, C(22)–C(17)–C(23)–H(23)).

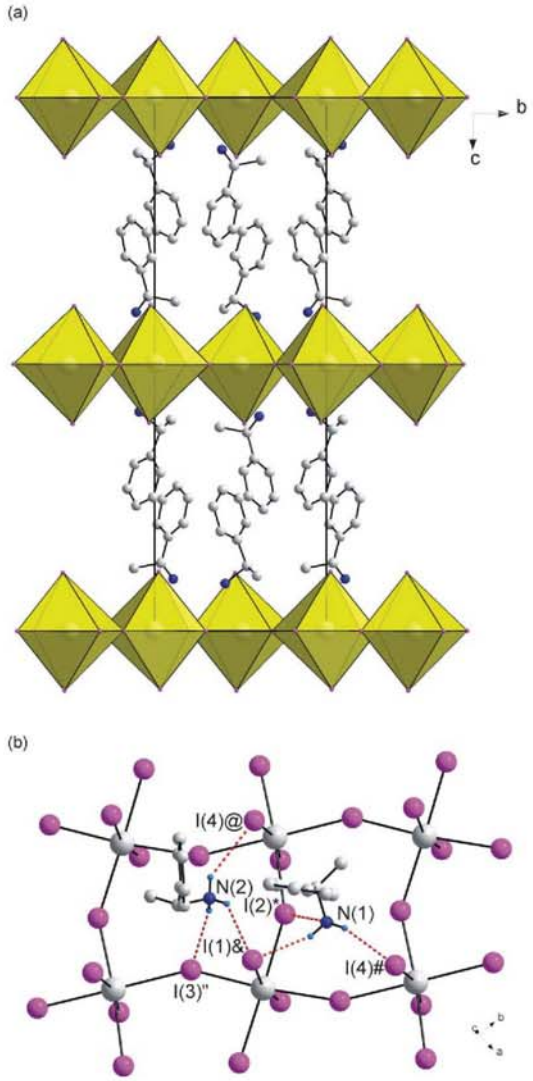


Fig. 5 (a) Packing diagram of the chiral hybrid PbI_4R_2 (**7**) that adopts the K_2NiF_4 type system. There are two complete inorganic layers in the unit cell. The structure of PbI_4S_2 (**8**) is isomorphous. (b) The view perpendicular to the layers, showing the rotation of adjacent corner-sharing octahedra to each other and the two unique cations in the asymmetric unit and their respective hydrogen bonding scheme. Atoms marked with asterisk (*), hash (#), ampersand (&), 'at' sign (@) or double prime (″) are at the symmetry positions $(-1/2 + x, 3/2 - y, -z)$, $(1/2 + x, 3/2 - y, -z)$, $(x, -1 + y, z)$, $(-1/2 + x, 3/2 - y, -z)$ and $(-1/2 + x, ½ - y, -z)$, respectively.

$PbI_4((R)$–$C_6H_5CH(CH_3)NH_3)_2$, **7**, (abbr. PbI_4R_2) and $PbI_4((S)$–$C_6H_5CH(CH_3)NH_3)_2$, **8**, (abbr. PbI_4S_2) are examples of the hybrid perovskite motif, seen in $PbI_4((\pm)$–$C_6H_5CH(CH_3)NH_3)_2$.[6] These two structures are the first reported cases of chiral amines in the hybrid perovskite motif. The PbI_6^{4-} octahedra share all four of its equatorial halides to form infinite sheets in the *ab*-plane. Each gap made by four-corner-sharing octahedra is occupied above and below by the two unique cations (Fig. 5b). The remaining two halogen ions, occupying the axial positions in the octahedra, together with one of the bridging iodides, hydrogen bond with the ammonium head, which form organic sheets sandwiching the inorganic layers (Fig. 5b).

The asymmetric unit of **7** contains two independent R-phenylethylammonium ions and the PbI_4^{2-} moiety. The lead atom does not occupy a special position as in $PbI_4(\pm)_2$ and has six unique bond lengths. Iodides I(1) and I(4) occupy the axial positions in the octahedra whereas I(2), I(3) and their symmetry equivalents are the bridging halides in the equatorial positions. The Pb–I bond lengths to the axial halides are on average shorter than the bridging bond lengths. The two unique bridging halides also introduce two bridging angles of 150.78(2)° (Pb(1)–I(3)–Pb(1)) and 156.41(2)° (Pb(1)–I(2)–Pb(1)). The former angle is considerably more acute compared to the latter angle and the one reported in the racemate structure (155.425(11)°).[6] The *trans* angles between the four bridging halides are 175.07(2)° and 177.93(3)°, close to the ideal case of 180° as the bonding to the adjacent octahedra has an ordering influence. The two axial halides in contrast are related by a *trans* angle of 167.72(2)°.

The crystal structure of compound PbI_4S_2, **8**, is isomorphous to **7** but has the opposite handedness as the asymmetric unit contains two cations with *S* chirality. The bond lengths and angles in the octahedra are similar to **7**. The most significant difference between the hybrid perovskite containing a racemic mixture and the pure enantiomers in **7** and **8** is the conformation of the layers. The perovskite with the racemic mixture of enantiomers crystallizes in the spacegroup $P2_1/a$ and has a monoclinic unit cell. The inorganic layers are parallel to the *ab*-plane and when viewed down the long *c*-axis, the layers overlap perfectly. The unit cell has only two layers at $z = 0$ and $z = 1$. The hybrid perovskites with the *R* and *S* enantiomers on the other hand have three layers in the unit cell. The layers at $z = 0$ and $z = 1$ are eclipsed and the extra layer at $z = 1/2$ is staggered relative to the other two. To accommodate the extra layer, the unit cell is double in **7** and **8** to that of $PbI_4(\pm)_2$.[6]

Intermolecular interactions: π–σ bonds and hydrogen bonding

Two additional interactions assist in stabilizing the complete 3-D structure of the hybrids: hydrogen bonding between the inorganic and organic moieties, shown in all compounds and listed in Table 4, and C–H···π interactions between the organic moieties themselves, seen in compounds **1**, **2**, **5** and **6**.

Fig. 2b shows the interaction between two aromatic rings of **1**. The centroid to centroid distance is 5.158(1) Å which is close enough to enable a C(5)–H(5)···Cg interaction to occur with a distance of 3.017(2) Å. The geometry of the interaction is the same in **2** with a slightly longer distance of 3.234(2) Å. The increase in distance must be caused by the greater ionic radius of the halide Br *versus* Cl. Compounds **3** and **4** have no interactions as the distance between H(5) and the nearest centroid is 4.064(1) Å in **3** and between H(3) and the nearest centroid for **4** is 3.632(1) Å.

No less than three separate π interactions are evident in both **5** and **6**. The corner-sharing compounds have three unique centroids in the asymmetric unit labelled Cg1, Cg2 and Cg3 for

 This journal is © The Royal Society of Chemistry 2006

Table 1 Details of C–H···Cg interactions

D–H···Cg	D–H/Å	H···Cg/Å	Cg···Cg/Å	∠(D–H···Cg)/°	Symmetry transformations
1					
C(5)–H(5)···Cg(1)	0.93	3.017(2)	5.158(1)	152.13(52)	$3/2 - x, 1 - y, -1/2 + z$
2					
C(5)–H(5)···Cg(1)	0.93	3.233(2)	5.363(1)	149.44(32)	$1 - x, -1/2 + y, 3/2 - z$
5					
C(3)–H(3)···Cg(3)	0.95	2.978(1)	4.830(15)	130.22(15)	$½ - x, ½ + y, ½ - z$
C(13)–H(13)···Cg(1)	0.95	2.904(4)	4.686(3)	126.35(15)	$½ - x, 3/2 - y, -z$
C(21)–H(21)···Cg(2)	0.95	2.872(4)	4.895(5)	139.57(15)	$-x, y, ½ - z$
6					
C(3)–H(3)···Cg(3)	0.95	3.009(3)	5.018(4)	139.18(25)	$-x, y, ½ - z$
C(13)–H(13)···Cg(1)	0.95	2.964(3)	4.771(2)	127.84(24)	$½ - x, ½ - y, -z$
C(21)–H(19)···Cg(2)	0.95	3.015(1)	4.867(4)	130.38(23)	$½ - x, -1/2 + y, ½ - z$

cat1, cat2 and cat3, respectively. Fig. 4a shows the simple C–H···Cg interactions for compound **5**. One interaction is in the direction of the *a*-axis, between cat2 and cat3. This interaction links the corner-sharing chains that are stacked above each other. The remaining two interactions are between the cations sitting between the chains, cat1, and the cations above the gaps of the chains, cat2 and cat3. Compound **6** has a similar arrangement and Table 1 summarizes the interactions for all the compounds.

The face-sharing compounds have a similar hydrogen bonding geomery regardless of the enantiomer chosen or the halide. One organic amine sits in between two chains and interacts with the halides in the chains on either side. The hydrogens form simple hydrogen bonds to the halides in the axial positions and bifurcated bonds to the halides in the equatorial positions. **1** has four hydrogen bonds, two simple and one bifurcated (Fig. 2b). The bifurcated distances Cl(2)···H(1C)···Cl(3) are 2.59 and 2.76 Å, respectively, with similar D–H–A angles of 136.6 and 135.1°. The simpler H(1A)···Cl(3) and H(1B)···Cl(1) bond to an equatorial and an axial halide on separate chains and it is this bonding that holds the chains in close proximity. The four bonds give an average H···Cl distance of 2.59 Å, longer than the average quoted by Steiner[7] of 2.247(5) Å.

Compound **2** has bromine as the halide and the average hydrogen acceptor distance increases to 2.81 Å. The increase in ionic radius adds an extra interaction so that two bifurcated and only one simple hydrogen bond exists (Fig. 6). The bifurcated bond to the equatorial halides Br(2)···H(1A)···Br(3) has the same geometry as in **1** with distances of 2.79 and 2.85 Å and angles of 138.5 and 131.9°. The second bifurcated interaction Br(2)···H(1B)···Br(3) are 2.67 and 3.06 Å. The latter interaction is longer by 0.30 Å and subsequently much weaker. The remaining simple hydrogen bond N(1)–H(1B)···Br(3) is the most linear, (∠(DHA) = 163.8°) and hence no bifurcation is possible. The previously reported crystal strucure with the *S* enantiomer, $PbBr_3S$ has only one bifurcated and two simple hydrogen bonds.[4] The very linear DHA bond angles of 159.8 and 161.7° for the simple hydrogen bonds interactions prevent any further bifurcation from take place. The average hydrogen acceptor distance in $PbBr_3S$ is 2.75 Å and if one excludes the hydrogen acceptor distance of 3.06 Å in **2**, the same average is calculated. This is some 0.26 Å greater than the average H···Br distance given by Steiner.[7]

The large ionic radius of iodine in PbI_3R and PbI_3S enables five hydrogen bonding interactions to occur. H(1A) in both structures **3** and **4** has the bifurcation seen in the previous structures with DHA angles in the range 132.2–133.7°. The second bifurcated bonds, I(3)···H(1B)···I(2) in **3** and I(3)···H(1C)···I(2) in **4**, have much larger differences in DHA angles as their respective hydrogen atoms point more directly towards the iodide I(3). The bifurcate distances are in the range 2.97–3.21 Å. The simple hydrogen bonds, N(1)–H(1C)···I(1) in **3** and N(1)–H(1B)···I(1) in **4** are shorter than the hydrogen acceptor distances of the bifurcated interactions.

The corner-sharing compounds, **5** and **6**, have, in addition to the usual halide acceptor and nitrogen donors, an oxygen atom which acts as an acceptor atom to the halides on the inorganic chains and as a donor atom to the nitrogens on the ammoniums. The three unique ammoniums on the cations show variable hydrogen bonding compared to each other. The first cation forms two bonds to oxygen and one to the halide, the second cation has one bifurcated bond to two equatorial halides and then one each to an axial and an equatorial halide and the third cation has two axial and one bridging halide. These three bonding schemes are the same in both cases with X = Cl and Br.

Fig. 4b shows the detailed hydrogen bonding scheme of all three cations for **5**. Cat1 has three simple hydrogen bonds. As

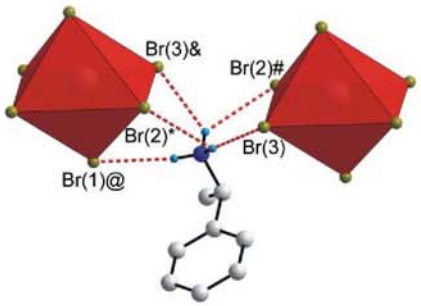


Fig. 6 Hydrogen bonding interactions between the bromine atoms and the hydrogen atoms on the organic cation in **2**. Note the additional bifurcated hydrogen bond not seen in **1**. Atoms marked with asterisk (*), hash (#), ampersand (&) and 'at' sign (@) are at the symmetry positions $(x, -1 + y, z)$, $(1/2 + x, 3/2 - y, 1 - z)$, $(1/2 + x)$, $½ - y$, $1 - z)$ and $(1 + x, -1 + y, z)$ respectively.

mentioned above, cat1 has two different acceptor atoms: oxygen O(1) on the water molecule and the axial atom Cl(1) on the chains. The hydrogen acceptor distances are 1.97 Å and 2.08 Å to oxygen and 2.37 Å to the larger chloride atom. The water molecule in turn acts as a donor when bonding to the inorganic chain. The H(1D)···Cl(5) and H(1E)···Cl(5) distances are 2.21 Å and 2.31 Å, respectively, well below the average of 2.349(9) Å for chloride acceptors bonded to transition metals.[8] Cat2 has two hydrogen bonds of almost equal distance from H(2A) to the equatorial chlorides Cl(4) and Cl(5) of 2.63 Å and 2.64 Å. H(2B) bonds to the bridging chloride and H(2C) to the axial halide Cl(2). Cat3 has two short bonds of 2.27 and 2.35 Å between N(3)–H(3B)···Cl(2) and N(3)–H(3B)···Cl(1) and a longer bond to the bridging chloride Cl(3).

The second corner-sharing compound **6** has bromine as acceptor atom and this increases the average N–H···Br distances to 2.63 Å from the average of 2.46 Å in the chloride case for the same number of bonds (eight). Cat1 has only simple hydrogen bonds but is split between O and Br acceptor atoms. The H(1C)···Br(1) length of 2.60 Å is considerably longer than the N(1)–H(1B)···O(1) and N(1)–H(1A)···O(1) lengths of 1.97 and 2.08 Å. This is in line with the smaller ionic radius of oxygen (1.32 Å) compared to bromide (1.95 Å)[5] Furthermore, the lengths fall in the range given by Steiner[8] of 1.71–2.17 Å for C–NH_3···O_w distances. Cat2 in **6** has the same equatorial bridging configuration as in **5**. The bifurcated distances to the equatorial halides are 2.74 and 2.77 Å. The remaining two hydrogens bond to the bridging halide, N(2)–H(2B)···Br(3) (2.63 Å) and to the axial halide N(2)–H(2C)···Br(2) (2.48 Å). Cat3 has three simple hydrogen bonds to two axial and one equatorial bond as it occupies the gaps above the chains.

The hydrogen bonding pattern has an axial bridging configuration for both **7** and **8** but with major differences between cat1 and cat2 in their distances and geometry. Cat1 in both **7** and **8** has three distances which are very far apart. The two terminal bonds to I(1) and I(2) are the shortest (2.61 and 2.81 Å for **7** and 2.64 and 2.85 Å for **8**) with the distance to the bridging halide the longest (3.16 Å for **7** and 3.09 Å for **8**). In cat2, the terminal distances are 2.82 and 3.01 Å for **7** and 2.78 and 3.01 Å for **8** with the bridging distances much shorter than in cat1 (2.89 Å for **7** and 2.84 Å for **8**).

Conclusions

Organic–inorganic hybrids that incorporate primary ammonium cations and metal halide octahedra can form a variety of packing arrangements. Table 2 summarizes the results obtained in this study, in which two of the three components present in the hybrids were systematically varied. Also included in Table 2 are two previously reported,[4,6] and related structures.

Table 2 Summary of structure types for the hybrid $MX(C_6H_5CH(CH_3)–NH_3)$

M = Pb	Cl	Br	I
R	F	F[4]	F, P
S	—	F	F, P
±	C	C	P[6]

[a] F = face-sharing chains; C = corner-sharing chains, P = K_2NiF_4 type 2-D layers.

Due to its demonstrated ability to impart electromagnetic properties to these structures, the most desirable and studied motif within this class of hybrids is the 2-D structure type, based on the K_2NiF_4 perovskite-type system. This 2-D motif is however not observed at all when the halide is chlorine or bromine. Structures **1** and **2** exhibit 1-D chains of face-sharing PbX_6 octahedra when the cation is the pure enantiomer. 1-D chains of corner-sharing PbX_6 octahedra are observed when the racemic cation is used (structures **5** and **6**).

The iodide case is however considerably more interesting. The 2-D layered motif being observed for all three iodides: $[PbI_4(\pm\text{-}C_6H_5CH(CH_3)NH_3)_2]$, has eclipsed inorganic layers. And structures **7** and **8** contain 2-D layers of staggered corner-sharing PbI_6 layers, different to those of the racemate. In addition, the asymmetric unit contains two moieties of the *R* isomer in **7** and two moieties of the *S* isomer in **8**.

Additionally, enantiopure iodide hybrids with a different structure can be obtained. The motif in these structures consist of 1-D chains of face-sharing PbI_6 octahedra. These hybrids crystallise from hot solutions. Once the solution temperature is cooled to below 60 °C, then crystals containing the layered 2-D structure appear. Also all 1-D crystals present at that stage will undergo a solution assisted interconversion to the 2-D structure type.

Experimental

Synthesis

Crystals used in this study were obtained either by slow evaporation of acidic alcoholic solutions of the metal halide or lead oxide and the amine or by slow cooling of saturated acidic solutions.

$[PbCl_3((R)–C_8H_{12}N)]$, 1. 0.100 g of PbO (0.448 mmol) and 0.087 g of (*R*)–$C_8H_{11}N$ (0.718 mmol) were added to 6 ml of HCl and then heated until all precipitate dissolved. After a few weeks, large irregular crystals of **1** where harvested at room temperature, together with crystals of $PbCl_2$. A colourless crystal of size 0.4 × 0.32 × 0.15 mm^{-3} was mounted on a glass fibre for crystallographic analysis. Elemental analysis (%). Found: C 22.10, H 2.94, N 3.19. Calc. for $PbCl_3C_8H_{12}N$: C 22.50, H 2.78, N 3.21.

$[PbBr_3((R)–C_8H_{12}N)]$, 2. 0.450 g of $PbBr_2$ (1.23 mmol) and 0.298 g of (*R*)–$C_6H_5C_2H_4NH_2$ (2.46 mmol) was dissolved in 10 ml of ethanol and 5 ml of HBr. After two days, large colourless cubes of **2** were harvested at room temperature. A crystal of size 0.44 × 0.26 × 0.08 mm^{-3} was mounted on a glass fibre for crystallographic analysis. Elemental analysis (%). Found: C 17.06, H 2.07, N 2.51. Calc. for $PbBr_3C_8H_{12}N$: C 16.89, H 2.13, N 2.46.

$[PbI_3((R)–C_8H_{12}N)]$, 3, and $[PbI_4((R)–C_8H_{12}N)_2]$, 7. 0.166 g of PbO (0.744 mmol) and 0.150 g of (*R*)–$C_6H_5C_2H_4NH_2$ (1.24 mmol) were added to 4 ml of HI. The orange precipate

 This journal is © The Royal Society of Chemistry 2006

dissolved after refluxing at 100 °C for 3 h. Slow cooling over four days produced yellow crystals of **3** and some were removed from the solution. A crystal of size 0.40 × 0.25 × 0.17 mm^{-3} was mounted on a glass fibre for crystallographic analysis. Elemental analysis (%). Found: C 13.56, H 1.77, N 1.97. Calc. for $PbI_3C_8H_{12}N$: C 13.53, H 1.70, N 1.97. Below 60 °C, orange crystals of the hybrid perovskite **7** started forming and eventually only those remained. A crystal of size 0.26 × 0.14 × 0.08 mm^{-3} was mounted on a glass fibre for crystallographic analysis. Elemental analysis (%). Found: C 19.82, H 2.58, N 2.88. Calc. for $PbI_4C_{16}H_{24}N_2$: C 20.04, H 2.52, N 2.92.

[PbI_3((*S*)–$C_8H_{12}N$)], 4, and [PbI_4((*S*)–$C_8H_{12}N)_2$], 8. 0.100 g of PbO (0.448 mmol) and 0.042 g of (*R*)–$C_6H_5C_2H_4NH_2$ (3.47 mmol) were added to 4 ml of HI. Slow cooling over four days produced yellow crystals of **4** and some were removed from the solution. A crystal of size 0.23 × 0.20 × 0.06 mm^{-3} was mounted on a glass fibre fibre for crystallographic analysis. Elemental analysis (%). Found: C 13.53, H 1.70, N 1.97. Calc. for $PbI_3C_8H_{12}N$: C 13.48, H 1.76, N 1.98. Upon cooling to room temperature, orange needles of the hybrid perovskite **8** formed exclusively. A crystal of size 0.27 × 0.13 × 0.06 mm^{-3} was mounted on a glass fibre for crystallographic analysis. Elemental analysis (%). Found: C 19.91, H 2.44, N 2.91. Analysis calculated for $PbI_4C_{16}H_{24}N_2$: C 20.04, H 2.52, N 2.92

[$PbCl_5$((±)–$C_8H_{12}N)_3$·H_2O], 5. 0.140 g of $PbCl_2$ (0.503 mmol) and 0.123 g of (±)-$C_6H_5C_2H_4NH_2$ (1.01 mmol) were added to 5 ml of HCl and then heated until all the white precipitate was dissolved at 90 °C. The solution was then placed in a freezer and after one week, waferlike colourless crystals of **6** appeared. A crystal of size 0.39 × 0.31 × 0.05 mm^{-3} was mounted on a glass fibre for crystallographic analysis. Elemental analysis (%). Found: C 37.72, H 5.14, N 5.48. Calc. for $PbCl_5C_{24}H_{38}N_3O$: C 37.48, H 4.98, N 5.46.

[$PbBr_5$((±)–$C_8H_{12}N)_3$·H_2O], 6. 0.447 g of $PbBr_2$ (1.22 mmol) and 0.312 g of (±)-$C_6H_5C_2H_4NH_2$ (2.57 mmol) was dissolved in 10 ml of ethanol and 5 ml of HBr. The solution was then placed in a freezer and after one week, waferlike colourless crystals of **7** appeared. A crystal of size 0.34 × 0.15 × 0.05 mm^{-3} was mounted on a glass fibre for crystallographic analysis. Elemental analysis (%). Found C 29.02, H 3.91, N 4.21. Calc. for $PbBr_5C_{24}H_{38}N_3O$: C 29.08, H 3.86, N 4.24.

Crystal data and X-ray structure analysis

Intensity data were collected on a Bruker SMART 1K CCD area detector diffractometer with graphite monochromated Mo Kα radiation (50 kV, 30 mA). The collection method involved ω-scans of width 0.3°. Data reduction was carried out using the program SAINT+, version 6.02.[9] and face indexed absorption corrections were made using the program XPREP.[9]

The crystal structure was solved by direct methods using SHELXS-97.[10] Non-hydrogen atoms were first refined isotropically followed by anisotropic refinement by full matrix

Table 3 Crystal data for all compounds

	1	2	3	4	5	6	7	8
Empirical Formula	$PbCl_5$(*R*-$C_8H_{12}N$)	$PbBr_5$(*R*-$C_8H_{12}N$)	PbI_5(*R*-$C_8H_{12}N$)	PbI_3(*S*-$C_8H_{12}N$)	$PbCl_5$((±)-$C_8H_{12}N)_3$·H_2O	$PbBr_5$((±)-$C_8H_{12}N)_3$·H_2O	PbI_4((*R*)-$C_8H_{12}N)_2$	PbI_4((*S*-$C_8H_{12}N)_2$
M	435.73	569.11	710.08	710.08	769.01	991.31	959.16	959.16
Crystal system	Orthorhombic	Orthorhombic	Orthorhombic	Orthorhombic	Monoclinic	Monoclinic	Orthorhombic	Orthorhombic
Space group (no.)	$P2_12_12_1$ (19)	$P2_12_12_1$ (19)	$P2_12_12_1$ (19)	$P2_12_12_1$ (19)	*C*2/*c* (15)	*C*2/*c* (15)	$P2_12_12_1$ (19)	$P2_12_12_1$ (19)
T/K	293	293	293	293	173	173	173	173
a/Å	7.6917(15)	7.9199(11)	8.0814(12)	8.0950(12)	28.826(5)	29.171(4)	8.868(5)	8.8531(17)
b/Å	7.7273(15)	8.1392(11)	8.6983(13)	8.7141(13)	7.8120(13)	8.1095(12)	9.247(5)	9.2312(18)
c/Å	20.524(4)	20.555(3)	21.337(3)	21.368(3)	27.055(5)	27.656(4)	28.729(5)	28.650(6)
α/°	90	90	90	90	90	90	90	90
β/°	90	90	90	90	92.684(4)	92.234(3)	90	90
γ/°	90	90	90	90	90	90	90	90
V/Å^3	1219.8(4)	1325.0(3)	1499.9(4)	1507.3(4)	6086.0(17)	6537.5(17)	2355.8(19)	2341.4(8)
Z	4	4	4	4	8	8	4	4
D_{calc}/g cm^{-3}	2.373	2.853	3.145	3.129	1.679	2.014	2.704	2.721
μ/mm^{-1}	14.446	21.741	17.391	17.305	6.005	11.294	12.405	12.481
F(000)	800	1016	1232	1232	3024	3744	1712	1712
Scan range (θ)/°	1.98–28.00	2.69–28.00	1.91–28.00	1.91–28.00	1.51–28.00	1.40–28.00	2.31–28.00	2.32–25.49
Total reflections	8272	9027	10282	10283	20019	21393	12963	13643
Unique reflections [*R*(int)]	2922 [0.0755]	3157 [0.0852]	3626 [0.0440]	3645 [0.0498]	7326 [0.0552]	7843 [0.0721]	4381 [0.0514]	4142 [0.0415]
Parameters	119	107	119	107	271	279	184	184
*R*1 [$I > 2\sigma(I)$]	0.0254	0.0295	0.0276	0.0274	0.0305	0.0387	0.0405	0.0316
*wR*2 (all data)	0.0619	0.0675	0.0608	0.0565	0.0655	0.0877	0.0851	0.0776
Flack parameter[15]	−0.011(7)	−0.010(11)	−0.009(5)	−0.008(6)	—	—	0.095(16)	0.057(13)

least-squares calculations based on F^2 using SHELXL-97.[10] Hydrogen atoms were first located in the difference map then positioned geometrically and allowed to ride on their respective parent atoms. Diagrams and publication material were generated using WinGx,[11] ORTEP,[12] PLATON[13] and DIAMOND.[14] Crystal structures of compounds **1–4** were done at 20 °C and had reasonable thermal ellipsoids. Compounds **5–8** were done at −100 °C as their room temperature structures gave unsatisfactory thermal ellipsoids. Further crystallographic data are summarised in Table 3.

Table 4 Hydrogen bonding details of all compounds

D–H···A	D–H/Å	H···A/Å	D···A/Å	∠(D–H···A)/°	Symmetry *trans*formations
1					
N(1)–H(1A)···Cl(3)	0.89	2.53	3.369(5)	151.5	—
N(1)–H(1B)···Cl(1)	0.89	2.47	3.326(5)	160.7	$x + 1, y, z$
N(1)–H(1C)···Cl(2)	0.89	2.59	3.290(5)	136.6	—
N(1)–H(1C)···Cl(3)	0.89	2.76	3.449(5)	135.1	−x + 2, y + 1/2, −z + 1/2
2					
N(1)–H(1A)···Br(2)	0.89	2.79	3.450(7)	131.9	$x + 1/2, -y + 3/2, -z + 1$
N(1)–H(1A)···Br(3)	0.89	2.85	3.562(7)	138.5	$x + 1/2, -y + 1/2, -z + 1$
N(1)–H(1B)···Br(1)	0.89	2.67	3.533(6)	163.8	—
N(1)–H(1C)···Br(3)	0.89	3.06	3.430(6)	107.4	$x, y - 1, z$
N(1)–H(1C)···Br(2)	0.89	2.69	3.524(6)	157.2	$x + 1, y - 1, z$
3					
N(1)–H(1A)···I(2)	0.89	3.03	3.702(6)	133.7	$x + 1/2, -y + 3/2, -z + 1$
N(1)–H(1A)···I(3)	0.89	3.18	3.842(6)	132.8	$x + 1/2, -y + 1/2, -z + 1$
N(1)–H(1B)···I(3)	0.89	2.98	3.821(7)	158.7	—
N(1)–H(1B)···I(2)	0.89	3.19	3.678(7)	116.9	$x, y - 1, z$
N(1)–H(1C)···I(1)	0.89	2.97	3.827(7)	161.1	$x + 1, y - 1, z$
4					
N(1)–H(1A)···I(2)	0.89	3.03	3.700(7)	133.6	$x - 1/2, -y + 1/2, -z + 1$
N(1)–H(1A)···I(3)	0.89	3.19	3.850(7)	132.2	$x - 1/2, -y + 3/2, -z + 1$
N(1)–H(1B)···I(1)	0.89	2.98	3.837(7)	161.7	$x, y + 1, z$
N(1)–H(1C)···I(3)	0.89	3.00	3.838(7)	158.6	—
N(1)–H(1C)···I(2)	0.89	3.21	3.705(7)	117.5	$x, y + 1, z$
5					
N(1)–H(1A)···O(1)	0.91	2.08	2.844(4)	141.3	—
N(1)–H(1B)···O(1)	0.91	1.97	2.879(4)	172.7	$-x + 1/2, -y + 3/2, -z$
N(1)–H(1C)···Cl(1)	0.91	2.37	3.208(3)	152.5	—
N(2)–H(2A)···Cl(4)	0.91	2.63	3.206(4)	121.9	—
N(2)–H(2A)···Cl(5)	0.91	2.64	3.247(4)	124.4	$x, y + 1, z$
N(2)–H(2B)···Cl(3)	0.91	2.46	3.238(3)	144.2	$-x + 1/2, y + 1/2, -z + ½$
N(2)–H(2C)···Cl(2)	0.91	2.32	3.221(4)	168.9	$x, y + 1, z$
N(3)–H(3A)···Cl(3)	0.91	2.64	3.260(4)	125.7	—
N(3)–H(3B)···Cl(2)	0.91	2.27	3.178(3)	175.0	—
N(3)–H(3C)···Cl(1)	0.91	2.35	3.239(4)	166.4	$-x + 1/2, y - 1/2, -z + 1/2$
O(1)–H(1D)···Cl(5)	0.93	2.21	3.123(3)	168.6	—
O(1)–H(1E)···Cl(5)	0.93	2.31	3.209(3)	163.3	$-x + 1/2, -y + 1/2, -z$
6					
N(1)–H(1A)···O(1)	0.91	2.08	2.856(7)	142.0	—
N(1)–H(1B)···O(1)	0.91	1.97	2.874(6)	171.6	$-x + 1/2, -y + 3/2, -z$
N(1)–H(1C)···Cl(1)	0.91	2.60	3.406(5)	148.2	—
N(2)–H(2A)···Cl(4)	0.91	2.77	3.366(5)	124.1	—
N(2)–H(2A)···Cl(5)	0.91	2.74	3.391(5)	129.8	$x, y + 1, z$
N(2)–H(2B)···Cl(3)	0.91	2.63	3.396(5)	142.4	$-x + 1/2, y + 1/2, -z + 1/2$
N(2)–H(2C)···Cl(2)	0.91	2.48	3.372(5)	168.1	$x, y + 1, z$
N(3)–H(3A)···Cl(3)	0.91	2.80	2.390(5)	123.5	—
N(3)–H(3B)···Cl(2)	0.91	2.45	3.358(5)	174.2	—
N(3)–H(3C)···Cl(1)	0.91	2.51	3.411(5)	168.5	$-x + 1/2, y - 1/2, -z + 1/2$
O(1)–H(1D)···Cl(5)	0.95	2.33	3.280(4)	174.6	—
O(1)–H(1E)···Cl(5)	0.95	2.45	3.369(4)	163.0	$-x + 1/2, -y + 1/2, -z$
7					
N(1)–H(1A)···I(2)	0.91	3.16	3.823(14)	131.6	$x - 1/2, -y + 3/2, -z$
N(1)–H(1B)···I(1)	0.91	2.61	3.472(15)	157.7	$x, y - 1, z$
N(1)–H(1C)···I(4)	0.91	2.81	3.686(15)	161.3	$x + 1/2, -y + 3/2, -z$
N(2)–H(2A)···I(1)	0.91	2.82	3.546(13)	137.2	$x, y - 1, z$
N(2)–H(2B)···I(4)	0.91	3.01	3.750(12)	139.5	$x - 1/2, -y + 3/2, -z$
N(2)–H(2C)···I(3)	0.91	2.89	3.694(12)	147.7	$x - 1/2, -y + 1/2, -z$
8					
N(1)–H(1A)···I(2)	0.91	3.09	3.758(10)	132.0	$x + 1/2, -y + 1/2, -z + 2$
N(1)–H(1B)···I(4)	0.91	2.85	3.714(10)	159.1	$x - 1/2, -y + 1/2, -z + 2$
N(1)–H(1C)···I(1)	0.91	2.64	3.488(10)	155.4	$x, y + 1, z$
N(2)–H(2A)···I(1)	0.91	2.78	3.502(10)	137.5	$x, y + 1, z$
N(2)–H(2A)···I(3)	0.91	2.84	3.660(9)	151.0	$x, y + 1, z$
N(2)–H(2C)···I(4)	0.91	3.01	3.757(9)	140.5	$x + 1/2, -y + 1/2, -z + 2$

This journal is © The Royal Society of Chemistry 2006

CCDC reference numbers 607734–607741. For crystallographic data in CIF or other electronic format see DOI: 10.1039/b606987h

References

1 D. B. Mitzi, *Prog. Inorg. Chem.*, 1999, **48**, 1.
2 A. B. Corradi, S. Bruni, F. Cariati, A. M. Ferari, A. Saccani, F. Sandrolini and P. Sgarabotto, *Inorg. Chim. Acta*, 1997, **254**, 137.
3 H. Krautscheid, C. Lode, F. Vielsack and H. Vollmer, *J. Chem. Soc., Dalton Trans.*, 2001, 1099.
4 D. G. Billing and A. Lemmerer, *Acta Crystallogr., Sect. A: Found. Crystallogr.*, 2003, **E59**, m381.
5 R. D. Shannon, *Acta Crystallogr., Sect. A* , 1976, **A32**, 751.
6 D. G. Billing, *Acta Crystallogr., Sect. A: Found. Crystallogr.*, 2002, **E58**, m669.
7 T. Steiner, *Acta Crystallogr., Sect. A: Found. Crystallogr.*, 1998, **B54**, 456.
8 T. Steiner, *Angew. Chem., Int. Ed.*, 2002, **41**, 48.
9 Bruker, SAINT+, version 6.02 (including XPREP), Bruker AXS Inc., Madison, WI, USA, 1999.
10 G. M. Sheldrick, SHELX, release 97-2 (includes SHELXS and SHELXL), University of Göttingen, 1997.
11 L. J. Farrugia, WinGX, *J. Appl. Crystallogr.*, 1999, **32**, 837–838.
12 L. J. Farrugia, *J. Appl. Crystallogr.*, 1997, **30**, 565.
13 A. L. Spek, *J. Appl. Crystallogr.*, 2003, **36**, 7–13.
14 K. Brandenburg, Diamond. Version 2.1e., Crystal Impact GbR, Bonn, Germany.
15 H. D. Flack, *Acta Crystallogr., Sect. A: Found. Crystallogr.*, 1983, **39**, 876–881.

ReSourCe

Lighting your way through the publication process

A website designed to provide user-friendly, rapid access to an extensive range of online services for authors and referees.

ReSourCe enables **authors** to:

- Submit manuscripts electronically
- Track their manuscript through the peer review and publication process
- Collect their free PDF reprints
- View the history of articles previously submitted

ReSourCe enables **referees** to:

- Download and report on articles
- Monitor outcome of articles previously reviewed
- Check and update their research profile

Register today!

RSCPublishing

www.rsc.org/resource

02030508

4.3 Inorganic-organic hybrids incorporating a chiral cyclic ammonium cation

Journal: CrystEngComm

Date Submitted: Pending, before 30 April 2007

Reference Code of submitted article:

Date Accepted:

Final Reference:

Brief Synopsis

In this paper, eight inorganic-organic hybrids were made using the metal lead and the halides chloride, bromide and iodide. The counter cations were R, S and racemic forms of 1-cyclohexylethylammonium. This is a similar study to the one discussed in Chapter 4.2.

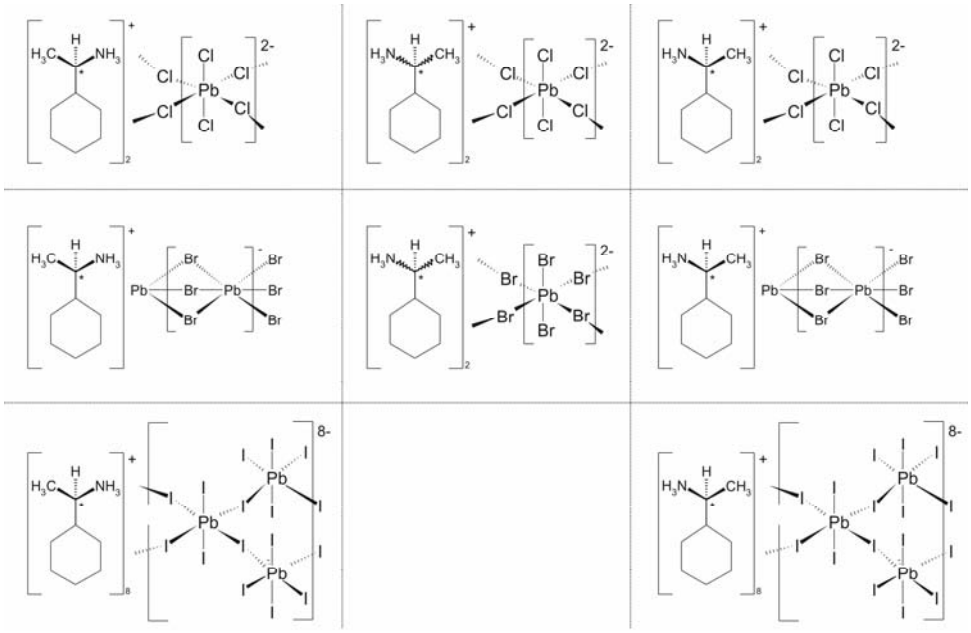
CREATED USING THE RSC ARTICLE TEMPLATE - SEE WWW.RSC.ORG/ELECTRONICFILES FOR FURTHER DETAILS

Inorganic-organic hybrids incorporating a chiral cyclic ammonium cation

David G. Billing and Andreas Lemmerer

Receipt/Acceptance Data **[DO NOT ALTER/DELETE THIS TEXT]**
Publication data **[DO NOT ALTER/DELETE THIS TEXT]**
DOI: 10.1039/b000000x [DO NOT ALTER/DELETE THIS TEXT]

In this paper we report the synthesis and the crystal structure of inorganic-organic hybrids containing various lead halides as the inorganic motif and a chiral, primary ammonium cation as the organic constituent. The organic molecule investigated is ($C_6H_{11}C^*H(CH_3)NH_3$) and both the *R* and *S* as well as the racemic (±) forms were used. Within the structures obtained, three different inorganic motifs are displayed by the lead halide octahedra: 1-D polymeric face-sharing chains of formula ((*R*)-$C_6H_5CH(CH_3)NH_3)PbBr_3$ and ((*S*)-$C_6H_5CH(CH_3)NH_3)PbBr_3$; 1-D polymeric corner-sharing ribbons based on the terminated-K_2NiF_4 type structure of formula ((*R*)-$C_6H_5CH(CH_3)NH_3)_8Pb_8I_{14}$ and ((*S*)-$C_6H_5CH(CH_3)NH_3)_8Pb_8I_{14}$; and 2-D corner-sharing layers based on the K_2NiF_4 perovskite structure type of formula ((±)-$C_6H_5CH(CH_3)NH_3)_2PbBr_4$, ((±)-$C_6H_5CH(CH_3)NH_3)_2PbCl_4$, ((*R*)-$C_6H_5CH(CH_3)NH_3)_2PbCl_4$ and ((*S*)-$C_6H_5CH(CH_3)NH_3)_2PbCl_4$.



[a] *Molecular Sciences Institute, School of Chemistry, University of the Witwatersrand, PO WITS 2050, Johannesburg, South Africa. Fax:27 11 717 6749; Tel:27 11 717 6759; E-mail:andy@hobbes.gh.wits.ac.za.*

† Electronic Supplementary Information (ESI) available: [details of any supplementary information available should be included here]. See http://dx.doi.org/10.1039/b000000x/

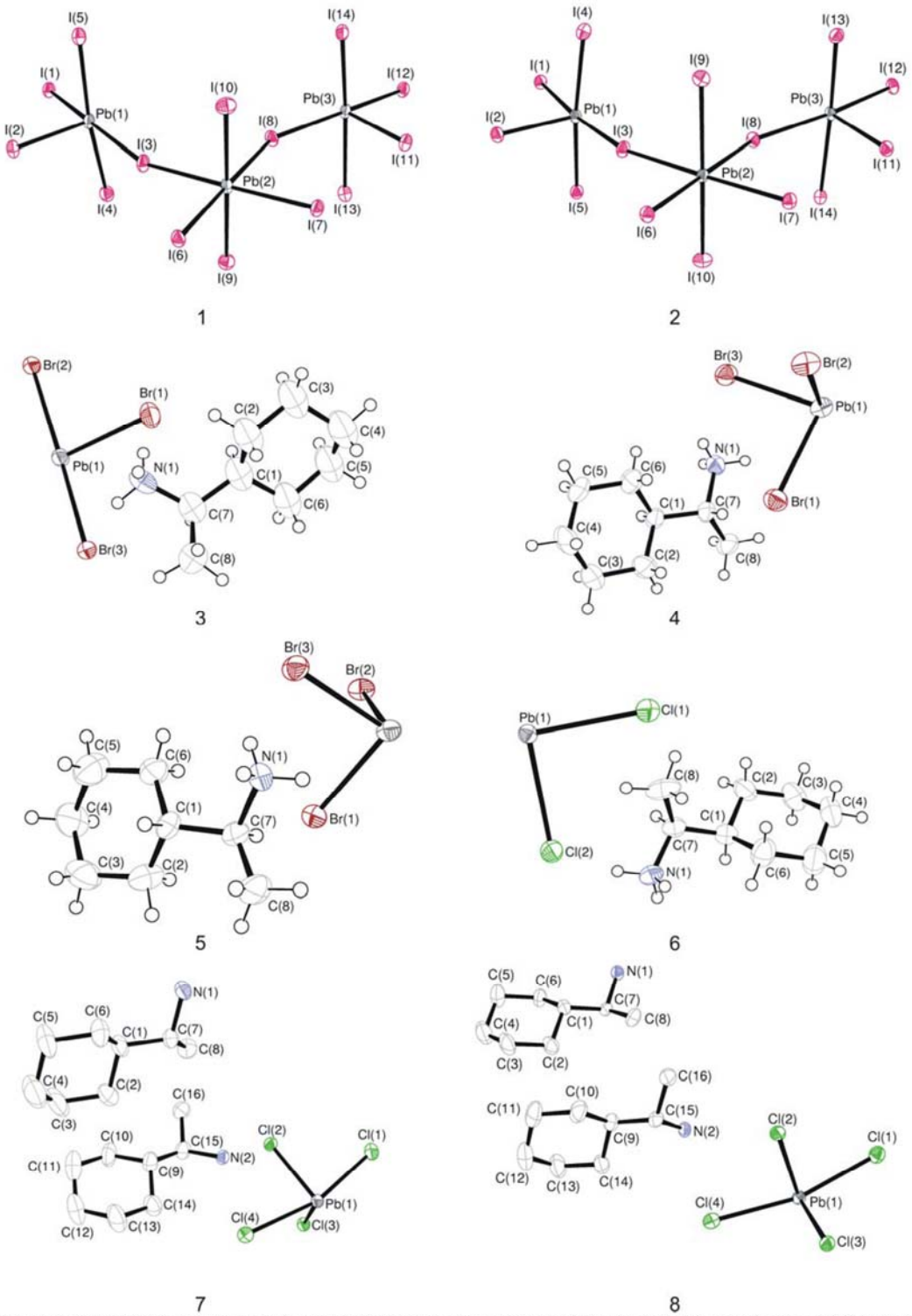


Fig. 1 The asymmetric units of compounds **1-8**, showing the atomic numbering scheme. Displacement ellipsoids are shown at the 50% probability level. Only the inorganic component of the compounds **1** and **2** are shown for clarity.

CREATED USING THE RSC ARTICLE TEMPLATE (VER. 2.0) - SEE WWW.RSC.ORG/ELECTRONICFILES FOR DETAILS

[JOURNAL NAME HERE] | www.rsc.org/[JOURNAL] Article

Introduction

Inorganic-organic hybrids with the general formula $[(R\text{-}NH_3)_x(M_yX_z]$, where M is any divalent metal and X = Cl, Br, I) have shown a great propensity for structural diversity. The choice of the ammonium cation, which can be anything from long alkylammonium chains to complex aromatic structures influences the motif of the inorganic component. The K_2NiF_4 type motif, also refered to as the layered perovskite-type motif in the literature, is the most sought after as these compounds form natural quantum well materials that show photoluminescence, electroluminescence and nonlinear optical properties.[1] By using the same metal, in this case lead, and only varying the identity of the halide and the R group, we have found a great variety of structures already.[2] When the organic moiety is chiral, the choice of racemic or pure enantiomeric forms in the crystal structure modifies the packing of the layers in the hybrid system. Similiarly, by varying the halide between chlorine, bromine and iodine and using the same enantiomer has an effect on which inorganic motif is prefered. This idea was first put into effect recently and three different inorganic motifs were observed.[3] The ammonium cation chosen in that study had an aromatic ring system and a chiral functional group as a ring substituent. In this study, we exchange the benzene for a cyclohexane ring as the R component.

Hybrids that have the 2-D layered perovskite-type motif, with general formula $[(R\text{-}NH_3)_2MX_4]$, are based on the K_2NiF_4 or $RbAlF_4$ structure type and result from replacing the K^+ and Rb^{2+} cations with the bulkier ammonium cations. The organic cation can form bilayers between these organic layers if it has only one ammonium group or a monolayer for two ammonium groups. The inorganic layer consists of MX_4^{2-} corner-sharing metal halide octahedra. Successive inorganic layers can either be staggered relative to each other as in the K_2NiF_4 structure or be eclipsed, where it is then related to the $PbAlF_4$ structure.[4] To keep these larger cations effectively in place, there must exist hydrogen bonding between one end of the organic molecule and the halide on the metal. This "head" of the molecule is the primary ammonium group, $-NH_3^+$, and the rest of the molecule -R is the tail. Weak van der Waals forces between the tails hold the sandwich organic-inorganic-organic together.

The hydrogen bonding involves all three of the primary ammonium hydrogens. In the 2-D case, two hydrogens can bond to the axial (bridging) halides and the third to the terminal halide (bridging halide configuration) or the reverse case with two terminal and one bridging halide (terminal halide configuration).

The alternative inorganic motif commonly seen are 1-D chains of inorganic metal halides with different connectivities. The adjacent octahedra in the chains can either share out a singe halide (corner-sharing), two halides (edge-sharing) or three halides (face-sharing). The degree of sharing can cause distortion of the geometry of the octahedra with respect to bond angles and bond lengths.

The objective of this study was to observe the effect on the inorganic motif in the hybrid structure by varying the identity of the halide between chlorine, bromine and iodine and simultaneously, the identity of the chiral organic component. The Pb atom remains unchanged.

Results and Discussion

The crystal structures of $[((R)\text{-}C_6H_{11}CH(CH_3)NH_3)_8Pb_8I_{14}]$ (1) and $[((S)\text{-}C_6H_{11}CH(CH_3)NH_3)_8Pb_8I_{14}]$ (2): The ribbon motif based on the K_2NiF_4 structure type

The enantiomorphic pair of compounds, abbreviated $[(R)_8Pb_8I_{14}]$ and $[(S)_8Pb_8I_{14}]$, where expected to give layered perovskite-type hybrids as the ammonium cation is sterically similiar to the aromatic equivalent, $C_6H_5CH(CH_3)NH_3$ which gave hybrid perovskites for the *R*, *S* and racemic species together with lead iodide.[3] Instead, the connectivity has been retained but instead of forming layers, the octahedra form infinite polymeric ribbons, which are three lead atoms abreast, i.e. every fourth row of corner-sharing octahedra is missing from the K_2NiF_4 structure type (Fig. 2). These chains run along the *a*-axis. Either side of these chains, there is a gap of 8.3(4) Å between the boundary lead atoms and 4.1(4) Å between the iodides to the next chain in the *c*-direction. These are characteristic of distances between adjacent corner-sharing PbI_6 octahedra within the 2-D layered perovskite-type motif. It is these two boundary lead atoms that are surprisingly not bridged by an iodide atom which would then have formed the two-dimensional layer motif (Fig. 3). The organic cations occupy positions above and below the gaps formed by three or four corner-sharing octahedra and the space in between the chains. The chains in **1** and **2** are offset to each other and separated by 4.0560(8) Å and 4.0517(8) Å respectively in the direction of the *b*-axis. This motif has been seen before only once to the best of our knowledge in the compound $[(H_3N(CH_2)_3NH_3)_2Pb_{1.5}Br_7{\cdot}H_2O]$.[5]

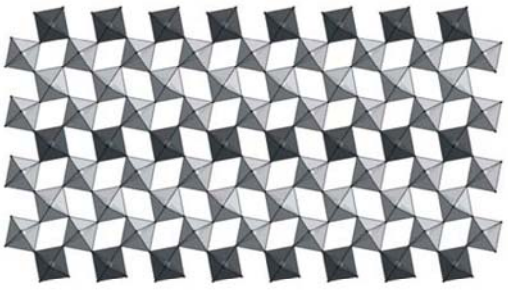


Fig. 2 The cut-out of the K_2NiF_4 type inorganic motif that gives rise to the 1-D inorganic ribbons, shown as light grey octahedra. Every fourth row is missing, shown as dark grey octahedra.

The two structures are enantiomorphs as the inorganic motif is the same regardless of which enantiomer is the counter cation. Compound **1** has three lead atoms in the asymmetric unit which span the breadth of the one-dimensional chain. Each lead atom is bonded to six iodides in

CREATED USING THE RSC ARTICLE TEMPLATE (VER. 2.0) - SEE WWW.RSC.ORG/ELECTRONICFILES FOR DETAILS

a non-ideal octahedral geometry. All six distances to the iodides are different and the cis and trans angles deviate from 90° and 180°. Pb(1) and Pb(3) occupy the borders of the chain whereas Pb(2) is sandwiched in between and runs along the centre of the chains. Hence, Pb(2) has four bridging halides as seen in the hybrid perovskite motif while Pb(1) and Pb(3) have only two bridging halides cis to each other. Pb(2) bonds to Pb(3) via I(7) and I(8) and similiarly to Pb(1) via I(3) and I(6). The bridging distances to the outer octahedra are in the range 3.1866(10) Å to 3.2122(10) Å between Pb(2) and I(3), I(6), I(7) and I(8) for structure **1** and 3.1913(15) Å to 3.2200(14) Å for structure **2**. In contrast, the bridging distances for the outer octahedra inwards towards Pb(2) are longer. The distance between Pb(1) and I(3) is 3.3731(10) Å **1** and 3.3751(15) Å **2** and to I(6) 3.4425(11) Å **1** and 3.4483(15) (**2**). Pb(3) has similiar distances of 3.3862(9)Å **1** and 3.3967(15) Å **2** and 3.3959(10) Å **1** and 3.4047(15) Å **2** respectively for I(7) and I(8). The iodides that are *trans* to the bridging halides on Pb(1) and Pb(3), and hence form the boundary of the chain, are shorter, i.e. I(12) is *trans* to I(8) and has a distance of 3.0541(10)Å **1** and 3.0585(15) Å **2**. The same effect is seen in the remaining terminal halides, i.e. I(1) (3.1127(10) Å **1** and 3.1182(15) **2**), I(2) (3.0201(11) Å **1** and 3.0305(16) Å **2**) and I(11) (3.0487(9) Å **1**, 3.0580(15) Å **2**). The remaining six halides, I(4) and I(5); I(9) and I(10); I(13) and I(14), occupy the axial positions of the octahedra with distances in the range 3.2096(10) Å to 3.3280(12) Å for **1** and 3.1377(18) Å to 3.4483(15) Å for **2**

An important geometric parameter of layered perovskite-type hybrids is the angle formed by the bridging halide and the two lead atoms it connects. The lead atoms do not occupy positions associated with inversion centres forcing all four bridging angles around Pb(2) to be different. There is a difference between the angles that bridge to either side of the chain. The greatest angle is 156.46(3)° to Pb(1) with a slightly shorter angle of 153.46(3)° via the other halide to the same lead atom. The corresponding angles to Pb(3) are shorter and differ by 3.65°.

No less than eight (*R*)-$C_6H_{11}CH(CH_3)NH_3$ ammonium cations are in the asymmetric unit. The organic cations are labelled cat1 (containing atom N1), cat2 (N2), etc. The cyclohexane rings exist in the chair configuration for all eight, whereas the torsion angles between the rings and the chiral functional groups are all different which explains the lack of higher symmetry elements between the eight moieties. One ammonium cation is disordered over two positions at right angles to another. The two rings both share the common atoms C(8C) and C(8F).

The interplanar angle between a meanplane formed the layer of lead and equatorial iodides and a meanplane through the six carbons of the cylohexanes vary between seven of the eight amines. There is a correlation between the torsion angle and the angle between the meanplanes. If the torsion angles are close to 180°, the cations are tilted at a greater angle away from the inorganic layer. Cation 3, 4 and 6 have torsion angles of -177.6(10)°, 174.0(1))° and -169.0(13)° and respectively tilt at angles of 76.01(38)°, 62.31(42)° and 79.03(46)° to the layers. The remaining four cations (1, 2, 5 and 7) have torsion angles in the range 52.6(17)° to 89.5(15)° and subsequently their tilt angles are close to perpendicular (79.49(47)° to 87.71(43)°).

The hydrogen bonding can be classified in two categories: if the number of hydrogen bonds to equatorial halides dominate, it is called equatorial halogen configuration and if the number of hydrogen bonds to axial halides dominate, it is called axial halogen configuration.

Cat1 and cat8 occupy the central gaps formed by four corner-sharing PbI_6 octahedra. This void is characteristic of the hybrid perovskite motif. Both NH_3^+ groups favour the axial halogen configuration. Cat3 and cat6 sit in the channels between two chains and sit closer to the plane of the chains as there is less steric hindrance. The equatorial configuration is adopted. The remaining four cations (2, 4, 5, 7) occupy the outer voids formed by three PbI_6 octahedra only as they sit on the edge of the chains and both apical (2, 5) and equatorial (4, 7) configurations are observed. The hydrogen bonding details for **1** and **2** are given as supplementary information and shown in Fig. 4 for **1**.

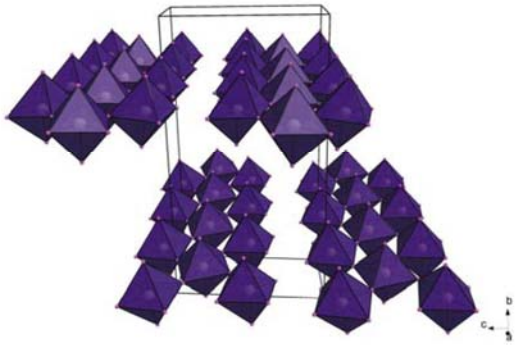


Fig. 3 Perspective view of the packing diagram of **1**. The infinite chains of corner-sharing ribbons run along the a-axis. The cations are excluded for clarity.

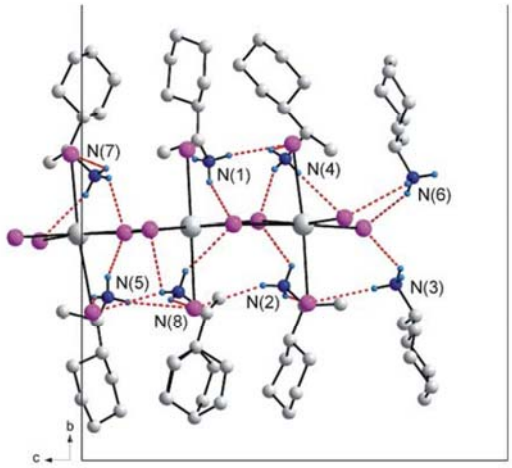


Fig. 4 Hydrogen bonding interactions between the cations and iodide atoms in **1**. Cat3 and cat6 hydrogen bond to adjacent slabs. The hydrogens on the carbon atoms are omitted for clarity. Cat3 and Cat6 occupy the space between the ribbons.

This journal © Royal Society of Chemistry

CREATED USING THE RSC ARTICLE TEMPLATE (VER. 2.0) - SEE WWW.RSC.ORG/ELECTRONICFILES FOR DETAILS

The crystal structure of [((±)-$C_6H_{11}CH(CH_3)NH_3)_2PbBr_4$] (3): The K_2NiF_4 motif with staggered inorganic layers

Figure 5a clearly underlines a bidimensional arrangement in which a double layer of (*R*)-1-cyclohexylethylammonium and (*S*)-1-cyclohexylethylammonium molecules are embedded between two consecutive inorganic [$PbBr_6$] sheets, forming an alternated inorganic-organic layered structure. The lead atoms are not aligned from layer to layer, resulting in a staggered arrangement of adjacent layers. In the direction perpendicular to the layers, the crystal cohesion is achieved by N-H...Br hydrogen bonds, In the direction parallel to the layers, the cohesion is achieved by strong ionic bonds between equatorial bromide and lead atoms.

The inorganic layer is built up from characteristic corner-sharing $PbBr_6$ octahedra. The asymmetric unit consists of a lead atom on a special position and three bromide atoms, Br(1) occupying the axial position and Br(2) and Br(3) occupying the equatorial position in the octahedra, with the same special position as the lead atom. The spacegroup is *Pnma*. The individual $PbBr_6$ octahedra are rotated by 149.92(11)° and 155.49(11)° relative to each other. Furthermore, the perovskite layers are corrugated in the *c*-direction by an angle of 6.39(5)° with respect to the *ac*-plane. The coordination geometry around the Pb atom shows axial compression of the octahedral geometry, with the average bridging Pb(1)-Br(2) and Pb(1)-Br(3) distances longer than the axial distances Pb(1)-Br(1). The angle between *cis* and *trans* related bromide atoms deviate from 90° and 180° respectively. The 1-cyclohexylethylammonium molecule sits on a general position. The atomic numbering scheme is shown in Fig 1. The cyclohexane rings are ordered within the layers and adopt the chair configuration. The cyclohexane rings of adjacent molecules are almost parallel (0.4(2)°). The torsion angle H(7)-C(7)-C(1)-H(1) is -53.2(3) so that the chiral functional group is bent out of the plane of the rings. The angle between adjacent molecules is 44.0(1)° (plane defined by all eight atoms). The hydrogen bonds between the organic and inorganic entities adopt the terminal halogen configuration (See Table 3). The hydrogen acceptor distances to the terminal halide Br1 are 2.48 Å and 2.52 Å and to the bridging halide Br3 2.69 Å.

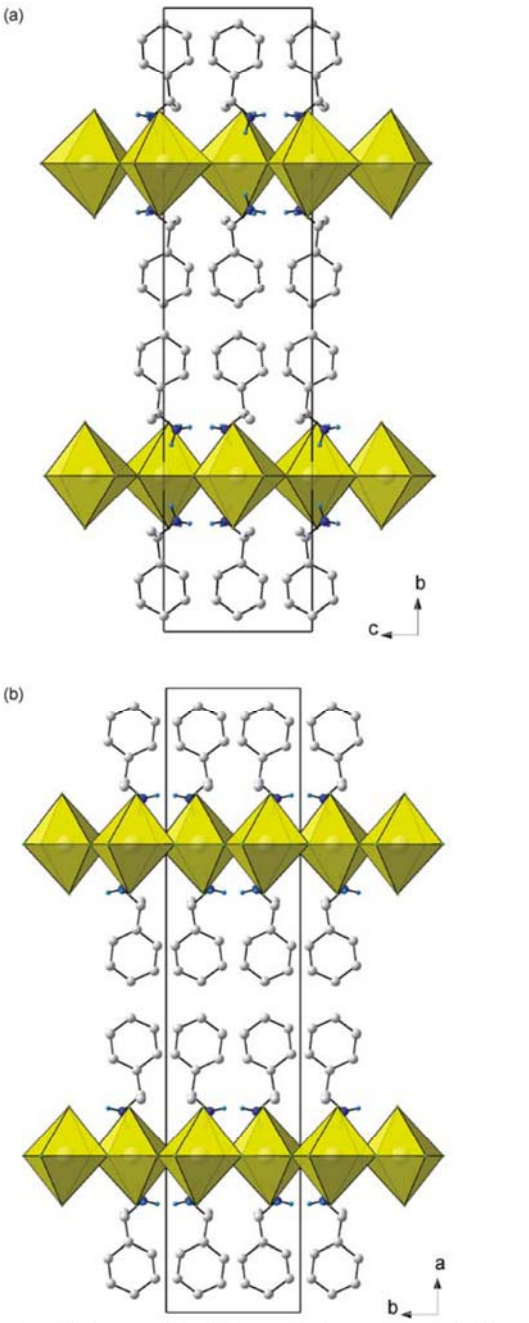


Fig. 5 (a) Packing diagram of **3**, which contains layers of corner-sharing $PbBr_6$ octahedra. The unit cell contains two unique layers, which are staggered relative to each other. (b) shows the similar packing of **6**, which has $PbCl_6$ octahedra. The hydrogens on the carbon atoms are excluded for clarity.

The crystal structures of [((*R*)-$C_6H_{11}CH(CH_3)NH_3)PbBr_3$] (4) and [((*S*)-$C_6H_{11}CH(CH_3)NH_3)PbBr_3$] (5): The face-sharing motif

These two compounds, abbreviated [(*R*)$PbBr_3$] (**4**) and [(*S*)-$PbBr_3$] (**5**), are enantiomorphs and possess the same inorganic motif and a similiar packing arrangement of their organic

CREATED USING THE RSC ARTICLE TEMPLATE (VER. 2.0) - SEE WWW.RSC.ORG/ELECTRONICFILES FOR DETAILS

cations. Figure 6a clearly underlines the one-dimensional arrangement of **4**, in which four chains of face-sharing $PbBr_6$ octahedra run along the four corners of the unit cell, parallel to the b-axis. In total, there is one complete chain in each unit cell. The channels in between the chains are occupied by (*R*)-$C_6H_{11}CH(CH_3)NH_3$ molecules in **4** and (*S*)-$C_6H_{11}CH(CH_3)NH_3$ in **5**. In the direction perpendicular to the chains, the crystal cohesion is achieved by N-H...Br hydrogen bonds. In the direction parallel to the layers, the cohesion is archieved by strong ionic bonds between the bromide and lead atoms.

The inorganic motif is built up from characteristic face-sharing $PbBr_6$ octahedra, which form extended chains along the b-axis. The asymmetric unit consists of a lead atom and three bromide atoms, Br(1) occupying the axial position with Br(2) and Br(3) occupying the equatorial positions in the octahedra (Fig. 6b). Within the chains, the shared face consists of these three halides. The octahedra are severely distorted with all lead bromide distances different, ranging from 2.8455(14) Å to 3.3251(14) Å. in **4** and from 2.8502(11) Å to 3.3236(12) Å in **5**. The bond angles between *cis* ligands vary from 77.78(4)° to 116.22(4)° in **4** and from 78.25(3)° to 116.15(3)° in **5**. Since the lead atom lies on a general position unlike in structure **3**, the three *trans* angles do not equal 180° but range from 160.67(4)° to 169.22(4)° in **4** and from 160.71(3)° to 169.22(3)° in **5**.

The (*R*)-1-cyclohexylethylammonium molecule sits on a general position. The atomic numbering scheme is shown in Fig 1. The unit cell contains two molecules and the dihedral angle formed by planes through the rings is 3.029° (**4**) and 3.279° (**5**). The cyclohexane ring adopts the chair conformation. The chiral functional group is aligned with the ring. This is evidenced by a torsion angle of -179.4(1) ° and 178.7(8)° for H(7)-C(7)-C(1)-H(1) respectively for **4** and **5**. The plane formed by the cyclohexane rings is in line with the chains of lead atoms. This was measured by measuring the angle between the vector connecting the lead atoms and a least-squares plane through the ring atoms. The angles are 89.326(473)° for **4** and 88.596(364)° for **5**. In the similar study with the benzene as the R group, the same inorganic motif was observed for the lead bromides but the R groups are angled differently to the chains. The benzene rings are angled at 43.0(1)° for [((*R*)-1-phenethylammonium)$PbBr_3$][3] and 42.595(177)° for [((*S*)-1-phenethylammonium)$PbBr_3$][1b] to the face-sharing chains. A possible reason is the possibility of weak σ-π interactions between the π systems of adjacent rings, which is absent in the saturated hydrocarbon rings used in this study. The hydrogen bonds between the organic and inorganic entities adopt the equatorial configuration (See Fig. 6b). Two hydrogens bond to the equatorial halides Br(2) and Br(3) and the third hydrogen bonds to the axial halide Br(1). Details of the hydrogen bonding are given in Table 2 for **4** and **5**. Due to the geometry of the NH_3 group, the hydrogen bonds to the equatorial halides are to one chain and to the axial halide on an adjacent chain.

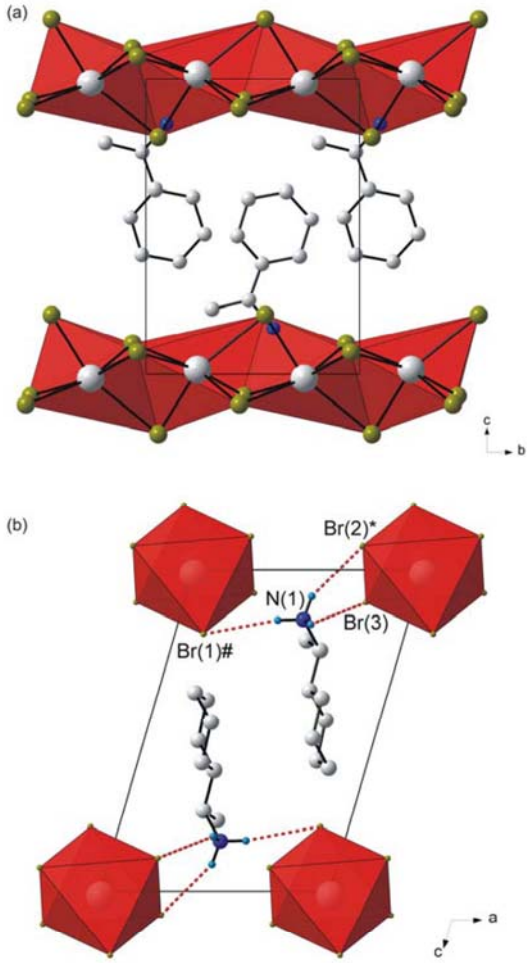


Fig. 6 (a) The chains of face-sharing $PbBr_6$ octahedra are shown superimposed over the drawn polyhedra, shown in red for the compound (*R*)$PbBr_3$ (**4**). (b) Hydrogen bonding interactions between one cation and two inorganic chains. Atoms marked with asterisk (*) and hash (#) are at the symmetry positions (2-x,1/2+y,-z) and (1+x,1+y,z) respectively. The hydrogens on the carbon atoms are excluded for clarity.

The crystal structure of [((±)-$C_6H_{11}CH(CH_3)NH_3)_2PbCl_4$] (6): The K_2NiF_4 motif with staggered inorganic layers

The crystal structure of **6** has the same layered perovskite-type motif to **3** as the unit cell contains two complete inorganic layers, i.e. adjacent inorganic layers are staggered.

Figure 5b clearly underlines a bidimensional arrangement in which a double layer of (*R*)-1-cyclohexylethylammonium and (*S*)-1-cyclohexylethylammonium molecules are embedded between two consecutive inorganic [$PbCl_6$] sheets, forming an alternated inorganic-organic layered structure. The lead atoms are not aligned from layer to layer, resulting in a staggered arrangement of adjacent layers.

The inorganic layer is built up from characteristic corner-sharing $PbCl_6$ octahedra. The asymmetric unit consists of a lead atom on a special position and two chloride atoms, Cl(1) occupying the axial position and Cl(2) occupying the equatorial position in the octahedra. Both chlorides are on general positions. There is one less halide in the asymmetric

 This journal © Royal Society of Chemistry

CREATED USING THE RSC ARTICLE TEMPLATE (VER. 2.0) - SEE WWW.RSC.ORG/ELECTRONICFILES FOR DETAILS

unit than in **3**. This means that there is only one unique bridging halide. The spacegroup is now *C2/c*. The $PbCl_6$ octahedra are rotated by 153.40(8)° relative to each other. Furthermore, the perovskite layers are corrugated in the *b*-direction by an angle of 5.261° with respect to the *bc*-plane. The coordination geometry around the Pb atom shows axial compression of the octahedral geometry, with the bridging Pb(1)-Cl(2) distances longer (2.9202(19) Å and 2.958(2) Å) than the axial distances Pb(1)-Cl(1) (2.845(2) Å). The angle between *cis* related chloride atoms range from 83.555(19)° to 96.445(19)°, with all *trans* angles equal to 180°, unlike the range of *trans* angles seen in **3**.

The 1-cyclohexylethylammonium molecule sits on a general position. The atomic numbering scheme is shown in Fig 1. The cyclohexane rings are ordered within the layers and adopt the chair configuration. Adjacent molecules are rotated at an angle of 12.283(404)° to each other; however the cyclohexane rings themselves are almost parallel to each other as measured by planes through the cyclohexane rings between adjacent molecules (0.146(406))°) as the torsion angle H(7)-C(7)-C(1)-H(1) is -61.539(957)°. The hydrogen bonds between the organic and inorganic entities adopt the terminal halogen configuration (See Table 2).

The crystal structures of $[((R)\text{-}C_6H_{11}CH(CH_3)NH_3)_2PbCl_4]$ (7) and $[((S)\text{-}C_6H_{11}CH(CH_3)NH_3)_2PbCl_4]$ (8): The $RbAlF_4$ motif with eclipsed inorganic layers

The two compounds with pure enantiomers crystallized in the layered perovskite-type motif based on the $RbAlF_4$ structure type in an almost identical fashion. The two structures, abbreviated $[(R)_2PbCl_4]$ (**7**) and $[(S)_2PbCl_4]$ (**8**), are enantiomorphic and only differ in the stereochemistry of the ammonium cation. The detailed crystal structure of **7** will be given and deviations and similiarities between the two structures commented on.

Figure 7a clearly underlines a bidimensional arrangement in which a double layer of (*R*)-1-cyclohexylethylammonium molecules are embedded between two consecutive inorganic $[PbCl_6]$ sheets, forming an alternated inorganic-organic layered structure. The lead atoms are aligned from layer to layer, resulting in an eclipsed arrangement of adjacent layers, typical of monoclinic unit cells. Here lies the main difference between the hybrid perovskite motif adopted in **7** and **8** to the structures **3** and **6**, which crystallized in orthorhombic unit cells. Instead of a single unique organic moiety, the use of a single enantiomer instead of the racemate as in **6**, forces double moieties in the asymmetric unit. The inorganic layer is built up from characteristic corner-sharing $PbCl_6$ octahedra. The asymmetric unit consists of a lead atom Pb(1) and four chloride atoms on general positions, Cl(1) and Cl(4) occupying the axial positions and Cl(2) and Cl(3) occupying the equatorial position in the octahedra. As a result of the lead atom not occupying a special position, the lead atoms do not sit on a plane but deviate by 0.252 Å from the *ab*-plane in **7** and by 0.223 Å in **8**. As shown in the projection perpendicular to the layers, along the *a*-axis in Fig. 7b, the $PbCl_6$ octahedra are rotated by 146.12(7)° and 155.57(7)° relative to each other when bridging by Cl(2) and Cl(3) respectively (145.99(5)° and 155.40(6)° in **8**). The layers are corrugated by 8.179(32)° (**7**) and 8.011(30)° (**8**) along the *a*-axis, about 3° more than in the racemic layered hybrids **3** and **6**. The coordination geometry around the Pb atom shows only a slight axial compression of the octahedral geometry, with the average bridging distances (3.0245(17) Å) longer than the average axial distances (2.8894(17) Å). However, the octahedra are severely distorted in the equatorial plane as there are two long and two short Pb-Cl bond lengths between *trans* related bridging chlorides (Fig. 8). The difference in the bond lengths are 0.5432(17) Å and 0.7272(18) Å in the same direction. The same phenomena is seen in **8**, where the differences are 0.5150(14) Å and 0.7708(14) Å. Such a severe disparity is rarely seen in other lead chloride perovskite-type hybrids. A search on the Cambridge Structural database (Version 5.27, November 2005 release[6]) evidenced three other compounds that have the layered perovskite-type motif: $[(C_2H_5NH_3)_2PbCl_4]$[7], $[(C_3H_7NH_3)_2PbCl_4]$[8] and $[(C_6H_5C_2H_4NH_3)_2PbCl_4]$.[9] The maximum ranges of bond lengths in the lead chloride octahedra are 0.645 Å, 0.064 Å and 0.280 Å respectively for those three compounds. It is surprising that the smallest cation of the three, $C_2H_5NH_3^+$, would have the most distorted octahedral geometry. The bond angles between *cis* and *trans* related chlorides within the octahedra all deviate from ideality for both **7** and **8**. The *cis* angles in the former structure vary from 81.25(5)° to 98.85(5)°. The *trans* angles between the bridging chlorides Cl(2) and Cl(3) deviate less from 180° (172.52(5)° and 177.65(5)°) than between the axial chlorides Cl(1) and Cl(4) (163.60(6)°). In the latter case, the *cis* angles in **8** vary from 81.15(4)° to 99.10(4)°. The *trans* angles between the bridging chlorides Cl(2) and Cl(3) deviate less from 180° (172.67(4)° and 177.51(4)°) than between the axial chlorides Cl(1) and Cl(4) (163.33(5)°).

The (*R*)-1-cyclohexylethylammonium molecules in **7** sit on general positions. The atomic numbering scheme is shown in Fig 1. The molecules are labelled cat1 (containing atom N(1)) and cat2 (N2)). The two molecules in the asymmetric unit are not quite perpendicular to each other (82.2(2)°) to coincide with the two orientations of the voids. The cyclohexane rings are ordered within the layers and adopt the chair configuration. The chiral functional groups are parallel to the cyclohexane rings. The torsion angles are -178.6(7)° (cat1: H(7)-C(7)-C(1)-H(1)) and 178.6(7)° (cat2: H(15)-C(15)-C(9)-H(9)).

The hydrogen bonds between the organic and inorganic entities adopt the terminal configuration for both chiral molecules, typical of hybrid perovskites with a monoclinic unit cell (See Table 2). The hydrogen acceptor distances to the terminal halides are longer (2.50 Å and 2.52 Å) and (2.57 Å and 2.57 Å) than to the bridging halides (2.42 Å and 2.54 Å) respectively for cat1 and cat2 (Fig. 7b).

The (*S*)-1-cyclohexylethylammonium molecule in **8** sits on a general position. The atomic numbering scheme is shown in Fig 1. The two molecules in the asymmetric unit are not quite perpendicular to each other (84.5(2)°) to coincide with the two orientations of the voids. The cyclohexane rings are ordered within the layers and adopt the chair configuration. The chiral functional groups are parallel to the cyclohexane rings. The

CREATED USING THE RSC ARTICLE TEMPLATE (VER. 2.0) - SEE WWW.RSC.ORG/ELECTRONICFILES FOR DETAILS

torsion angles are 179.3(5)° (cat1: H(7)-C(7)-C(1)-H(1)) and -179.2(5)° (cat2: H(15)-C(15)-C(9)-H(9)).

The hydrogen bonding between the organic and inorganic entities adopt the terminal halogen configuration for both chiral molecules, typical of layered perovskite-type hybrds with a monoclinic unit cell (See Table 2). The hydrogen acceptor distances to the terminal halides are longer (2.51 Å and 2.54 Å) and (2.56 Å and 2.58 Å) than to the bridging halides (2.41 Å and 2.56 Å) respectively for cat1 and cat2.

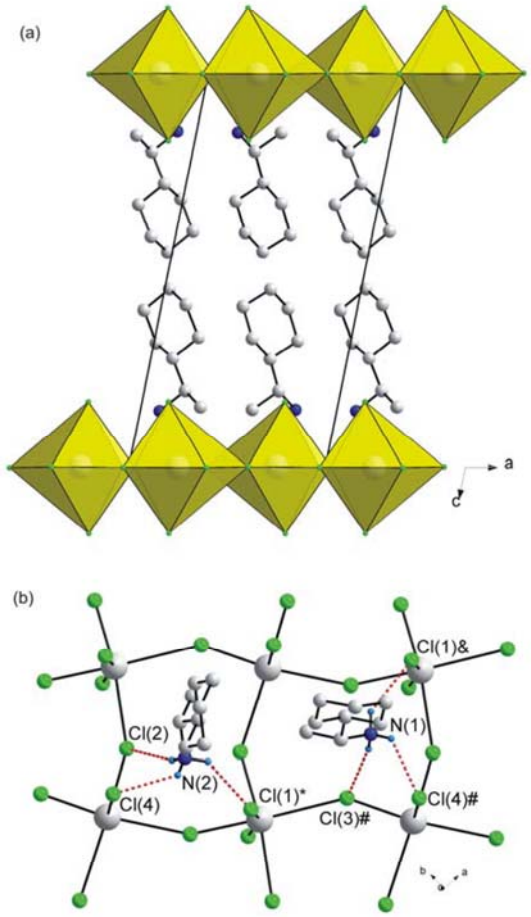


Fig. 7 (a) The same bidimensional arrangement of the cations in between the inorganic layers that is seen in **3** and **6** is displayed in the packing diagram of **8**. The difference is that only one unique inorganic layer exists in the unit cell and hence the layers are eclipsed. (b) The terminal halogen configuration of the two unique cations. Compound **7** has an isomorphous packing arrangement. Atoms marked with asterisk (*), hash (#) and ampersand (&) are at the symmetry positions (-x,-1/2+y,-z), (1+x,-1+y,z) and (1-x, -1/2+y,-z) respectively. The hydrogens on the carbon atoms are excluded for clarity.

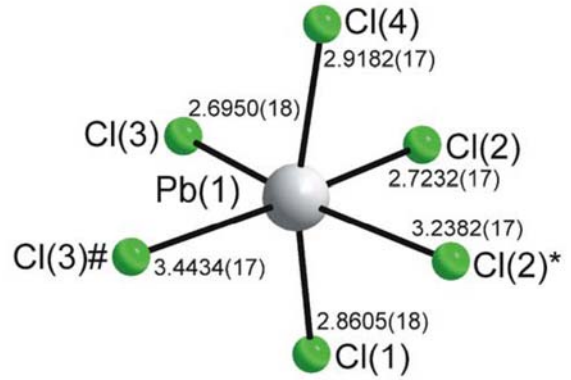


Fig. 8 A magnified view of the distorted $PbCl_6$ octahedra in compound **7**. The bridging chlorides Cl(2) and Cl(3) and their symmetry equivalents Cl(2)* and Cl(3)# show a large range of bond lengths to the lead atom, whereas the bond lengths to the terminal chlorides Cl(1) and Cl(4) are similar. The atoms with an asterisk (*) and a hash (#) are at the symmetry positions (-x,-1/2+y,-z) and (-1-x,1/2+y,-z) respectively. All bond lengths are given in Å.

Conclusion

A different pattern of the type of inorganic motifs that are templated by the choice of halide and chirality of the organic cation was found in this study, summarized in Table 3. In the previous study,[3] the layered perovskite-type motif, based on the K_2NiF_4 structure type, was adopted when using lead(II) iodide and the *R* and *S* cation and the $RbAlF_4$ structure type in the racemic cation. Here, the compounds **6**, **7** and **8**, which consist of lead(II) chloride octahedra, have the desired 2-D motif. However, the racemic cation produced eclipsed inorganic layers in lead iodide and staggered layers in lead chloride, with the reverse scenario observed for the pure enantiomers: staggered in lead iodide and eclipsed in lead chloride.

The motif adopted by lead iodide in this study is still related to the K_2NiF_4 motif. Here corner-sharing, 1-D ribbons form chains along one of the axes for both *R* and *S* enantiomers, respectively compounds **1** and **2**. Attempts at growing crystals of the racemic cation and lead iodide, $[((\pm)\text{-}C_6H_{11}CH(CH_3)NH_3)_2PbI_4]$, gave orange crystals of poor quality. The authors surmise that the colour is indicative of the layered perovskite-type motif.

The only common motif observed in both studies was 1-D chains of face-sharing octahedra, observed in both studies for lead bromide and the pure enantiomers, *R* (**4**) and *S* (**5**). Lead bromide with the racemic cation, compound **3**, has an isostructural packing arrangement and motif to the lead chloride compound, both having staggered inorganic layers. In contrast, the previous study had isostructural 1-D corner-sharing chains for both lead chloride and lead bromide. This study, in conjunction with the previous one, highlight again the unpredictability of and diversity within the field of inorganic-organic hybrids.

Experimental

Materials

This journal © Royal Society of Chemistry

CREATED USING THE RSC ARTICLE TEMPLATE (VER. 2.0) - SEE WWW.RSC.ORG/ELECTRONICFILES FOR DETAILS

[JOURNAL NAME HERE] | www.rsc.org/[JOURNAL] Article

All reagents and solvents employed were commercially avalable and used as received without further purification.

Synthesis

Preparation of [((*R*)-$C_6H_{11}CH(CH_3)NH_3)_8Pb_3I_{14}$], 1. 0.059 g PbI_2 (0.130 mmol) was dissolved in 2 ml 47% HI in a large sample vial. Thereafter, 0.025 g (R)-$C_6H_5C(H)(CH_3)NH_2$ (0.196 mmol) was added and the precipitate dissolved by refluxing for 12 hours at 80°C. The solution was slowly cooled to room temperature by 2 °C/h. A yellow single crystal suitable for X-ray diffraction analysis was selected and studied. Elemental analysis (%). Found: C 22.39, H 4.21, N 3.44. Calc. for $C_{64}H_{144}I_{14}N_8Pb_3$: C 22.45, H 4.24, N 3.27.

Preparation of [((S)-$C_6H_{11}CH(CH_3)NH_3)_8Pb_3I_{14}$], 2. 0.080 g PbI_2 (0.174 mmol) was dissolved in 3 ml 47% HI in a large sample vial. Thereafter, 0.040 g (S)-$C_6H_5CH(CH_3)NH_2$ (0.314 mmol) was added and the precipitate dissolved by refluxing for 12 hours at 80°C. The solution was slowly cooled to room temperature by 2 °C/h. A yellow single crystal suitable for X-ray diffraction analysis was selected and studied. Elemental analysis (%). Found: C 21.58, H 4.07, N 3.33. Calc. for $C_{64}H_{144}I_{14}N_8Pb_3$: C 22.45, H 4.24, N 3.27.

Preparation of [(±)-$C_6H_{11}CH(CH_3)NH_3)_2PbBr_4$], 3 0.072 g $PbBr_2$ (0.196 mmol) was dissolved in 3 ml 48% HBr in a large sample vial. Thereafter, 0.014 g (R)-$C_6H_{11}CH(CH_3)NH_2$ (0.109 mmol) and 0.014 g (S)-$C_6H_{11}CH(CH_3)NH_2$ (0.109 mmol) was added and the precipitate dissolved by ultrasound. The solution was left at room temperature and crystals grown by slow evaporation. A single colorless crystal suitable for X-ray diffraction analysis was selected and studied. Elemental analysis (%): calc. for $Br_4C_{16}H_{36}N_2Pb_1$: C 24.53, H 4.63, N 3.58. Found: C , H , N .

Preparation of [((*R*)-$C_6H_{11}CH(CH_3)NH_3)_1PbBr_3$], 4. 0.090 g $PbBr_2$ (0.245 mmol) was dissolved in 2 ml 48% HBr in a large sample vial. Thereafter, 0.030 g (R)-$C_6H_{11}C(H)(CH_3)NH_2$ (0.234 mmol) was added and the precipitate dissolved by refluxing for 1 hour at 80°C. The solution was slowly cooled at 2°C/hour to room temperature. A single colourless crystal suitable for X-ray diffraction analysis was selected and studied. Elemental analysis (%). Found: C , H , N . Calc. for $Br_3C_8H_{18}N_1Pb_1$: C 16.71, H 3.51, N 2.44.

Preparation of [((*S*)-$C_6H_{11}CH(CH_3)NH_3)_1PbBr_3$], 5. 0.081 g $PbBr_2$ (0.221 mmol) was dissolved in 2 ml 48% HBr in a large sample vial. Thereafter, 0.038 g (S)-$C_6H_{11}C(H)(CH_3)NH_2$ (0.296 mmol) was added and the precipitate dissolved by refluxing for 1 hour at 80°C. The solution was slowly cooled at 2°C/hour to room temperature. A single colourless crystal suitable for X-ray diffraction analysis was selected and studied. Elemental analysis (%). Found: C , H , N . Calc. for $Br_3C_8H_{18}N_1Pb_1$: C 16.71, H 3.51, N 2.44.

Preparation of [((±)-$C_6H_{11}CH(CH_3)NH_3)_2PbCl_4$], 6. 0.090 g $PbCl_2$ (0.324 mmol) was dissolved in 2 ml 33% HCl in a large sample vial. Thereafter, 0.030 g (R)-$C_6H_{11}C(H)(CH_3)NH_2$ (0.234 mmol) and 0.030 g (S)-$C_6H_{11}C(H)(CH_3)NH_2$ (0.234 mmol) was added and the precipitate dissolved by refluxing for 1 hour at 80°C. The solution was slowly cooled at 2°C/hour to room temperature. A single colorless crystal suitable for X-ray diffraction analysis was selected and studied. Elemental analysis (%). Found: C , H , N . Calc. for $C_{16}H_{36}Cl_4N_2Pb_1$: C 31.74, H 5.99, N 4.63.

Preparation of [((*R*)-$C_6H_{11}CH(CH_3)NH_3)_2PbCl_4$], 7. 0.040 g $PbCl_2$ (0.144 mmol) was dissolved in 3 ml 33% HCl in a large sample vial. Thereafter, 0.038 g (*R*)-$C_6H_5CH(CH_3)NH_2$ (0.296 mmol) was added and the precipitate dissolved by ultrasound. The solution was left at room temperature and crystals grown by slow evaporation. A single colorless crystal suitable for X-ray diffraction analysis was selected and studied. Elemental analysis (%). Found: C , H , N . Calc. for $C_{16}H_{36}Cl_4N_2Pb_1$: C 31.74, H 5.99, N 4.63.

Preparation of [((*S*)-$C_6H_{11}CH(CH_3)NH_3)_2PbCl_4$], 8. 0.050 g $PbCl_2$ (0.180 mmol) was dissolved in 4 ml 33% HCl in a large sample vial. Thereafter, 0.047 g (S)-$C_6H_5C(H)(CH_3)NH_2$ (0.369 mmol) was added and the precipitate dissolved by ultrasound. The solution was left at room temperature and crystals grown by slow evaporation. A single colourless crystal suitable for X-ray diffraction analysis was selected and studied. Elemental analysis (%). Found: C , H , N . Calc. for $C_{16}H_{36}Cl_4N_2Pb_1$: C 31.74, H 5.99, N 4.63.

Crystal Data and X-Ray structure analysis

Intensity data were collected on a Bruker SMART 1K CCD area detector diffractometer with graphite monochromated Mo K_α radiation (50kV, 30mA). The collection method involved ω-scans of width 0.3°. Data reduction was carried out using the program *SAINT+*, version 6.02.[10] and face indexed absorption corrections were made using the program XPREP.[10]

The crystal structure was solved by direct methods using SHELXS-97.[11] Non-hydrogen atoms were first refined isotropically followed by anisotropic refinement by full matrix least-squares calculations based on F^2 using SHELXL-97.[11] Hydrogen atoms were first located in the difference map then positioned geometrically and allowed to ride on their respective parent atoms. Diagrams and publication material were generated using WinGx[12], ORTEP[13], PLATON[14] and DIAMOND[15].

The conformational disorder around the cyclohexane ring of cat8 in structures **1** and **2** was resolved by finding alternate positions from the difference Fourier map for the respective atoms. Four of the atoms of the six-membered ring are disordered, with the remaining two atoms, C8C and C8F, common to both ring systems. The atoms were then refined anisotropically together with their site occupancy such that the sum of the occupancies for the eight alternate atom positions equaled one. Hydrogen atom positions were then calculated for the respective atoms using a riding model. The

CREATED USING THE RSC ARTICLE TEMPLATE (VER. 2.0) - SEE WWW.RSC.ORG/ELECTRONICFILES FOR DETAILS

ratio of major component, consisting of the atoms C(8D), C(8E), C(8G) and C(8H), to minor component, consisting of the atoms C(8I), C(8J), C(8K) and C(8L), is 58.65 to 41.35% in **1** and 54.73 to 45.27% in **2**.

The 20°C structures of compounds **1**, **2**, **3**, **6**, **7** and **8** were considered to be not good enough for publication. These were subsequently repeated at -100°C. Comparison of the 20°C and -100°C structures of these compounds reveal that no phase changes took place upon cooling. Further crystallographic data are summarised in Table 1.

References

1 (a) D.B. Mitzi, Prog. *Inorg. Chem.* 1999, 1; (b) G.C. Papavassiliou, G. A. Mousdis and I. B. Koutselas, *Adv. Mater. Opt. Electron.*, 1999, **8**, 265; (c) S.A. Bourne and Z. Mangombo, *CrystEngComm*, 2004, **6**, 437.

2 (a) D. G. Billing, *Acta Crystallogr. E*, 2002, **58**, m669; (b) D. G. Billing and A. Lemmerer, *Acta Crystallogr. E*, 2003, **59**, m381; (c) D. G. Billing and A. Lemmerer, *Acta Crystallogr. C*, 2004, **60**, m224; (d) A. Lemmerer and D. G. Billing, *Acta Crystallogr.* E, 2006, 62, m779; (e) A. Lemmerer and D. G. Billing, *Acta Crystallogr.* E, 2006, 62, m904; (f) D. G. Billing and A. Lemmerer, *Acta Crystallogr. C*, 2006, **62**, m174; (g) D. G. Billing and A. Lemmerer, *Acta Crystallogr. E*, 2006, **62**, m1103; (h) D. G. Billing and A. Lemmerer, *Acta Crystallogr. C*, 2004, **62**, m238; (i) D. G. Billing and A. Lemmerer, *Acta Crystallogr. C*, 2004, **62**, m264; (j) D. G. Billing and A. Lemmerer, *Acta Crystallogr. C*, 2004, **62**, m269.

3 D. G. Billing and A. Lemmerer, *CrystEngComm*, 2006, **8**, 686.

4 D. M. Hatch and H. T. Stokes, *Phys. Rev. B*, 1987, **35**, 8509.

5 A.B. Corradi, A.M. Ferrari, G.C. Pellacani, A. Saccani, F. Sandrolini and P. Sgarabotto, *Inorg. Chem.*, 1999, **38**, 716.

6 F.H. Allen, *Acta Crystallogr.*. B, 2002, **58**, 380.

7 M. Geselle and H. Fuess, *Z. Kristallogr.-New Cryst.Struct.* (1997), **212**, 241.

8 A. Meresse and A. Daoud, *Acta Crystallogr.* C, 1989, **45**, 194.

9 D.B. Mitzi, *J. Solid State Chem.*, 1999, **145**, 694.

10 Bruker, SAINT+. Version 6.02 (includes XPREP and SADABS). Bruker AXS Inc., Madison, Wisconsin, USA.

11 G. M. Sheldrick, SHELX, release 97-2 (includes SHELXS and SHELXL), University of Göttingen, 1997

12 L. J. Farrugia, *J. Appl. Crystallogr.*, 1997, **30**, 565.

13 L. J. Farrugia, WinGX. *J. Appl., Cryst.*, 1999, **32**, 837.

14 A. L. Spek, *J. Appl. Crystallogr.* 2003, **36**, 7.

15 K. Brandenburg, Diamond. Version 2.1e., Crystal Impact GbR, Bonn, Germany.

16 H. D. Flack, *Acta Cryst. A*, 1983, **39**, 876-881.

Table 3 Summary of structure types observed for the hybrids $(C_6H_{11}CH(CH_3)NH_3)MX$

M = Pb	Cl	Br	I
R	P	F	R
S	P	F	R
±	P	P	N/A

F = face-sharing 1-D chains, P = layered perovskite-type 2-D layers, R = 1-D ribbons based on the K_2NiF_4 motif

This journal © Royal Society of Chemistry

CREATED USING THE RSC ARTICLE TEMPLATE (VER. 2.0) - SEE WWW.RSC.ORG/ELECTRONICFILES FOR DETAILS

Table 1 Crystal data for **1**, **2**, **3** and **4**

	1	**2**	**3**	**4**
Formula	$C_{64}H_{144}I_{14}N_8Pb_3$	$C_{64}H_{144}I_{14}N_8Pb_3$	$Br_4C_{16}H_{36}N_2Pb$	$Br_3C_8H_{18}NPb$
Mr	3424.04	3424.04	783.30	575.15
Temperature/K	173	173	173	293
Crystal size/mm	0.30 x 0.16 x 0.08	0.46 x 0.12 x 0.05	0.17 x 0.17 x 0.05	0.50 x 0.30 x 0.14
Crystal system	Monoclinic	Monoclinic	Orthorhombic	Monoclinic
Space group	$P2_1$	$P2_1$	$Pnma$	$P2_1$
a/Å	9.0390(18)	9.0623(8)	8.5404(10)	7.9812(4)
b/Å	32.391(7)	32.422(3)	34.835(4)	8.0531(5)
c/Å	17.385(4)	17.4115(16)	8.2699(9)	11.6409(6)
α/°	90	90	90	90
β/°	95.013(4)	94.970(5)	90	106.155(3)
γ/°	90	90	90	90
V/Å^3	5070.7(18)	5096.6(8)	2460.4(5)	718.66(7)
Z	2	2	4	2
Dc/g cm^{-3}	2.243	2.231	2.115	2.658
μ(Mo-Ka)/mm^{-1}	9.265	9.218	13.355	20.044
Theta range/°	1.18 to 28.00	0.63 to 28.00	1.17 to 25.25	1.82 to 28.00
Total reflections	51031	59437	26066	9180
No. unique data [R(int)]	24253 [0.0563]	24431 [0.0673]	2270 [0.0675]	3473 [0.0809]
No. data with $I \geq 2s(I)$	18252	17663	1835	3301
$R1$	0.0455	0.0682	0.0777	0.0497
$wR2$ (all data)	0.1123	0.1761	0.2506	0.1346
Flack parameter[16]	0.012(4)	0.038(7)	-	0.039(3)

Table 1 contd. Crystal data for **5**, **6**, **7** and **8**

	5	**6**	**7**	**8**
Formula	$Br_3C_8H_{18}NPb$	$C_{16}Cl_4H_{36}N_2Pb$	$C_{16}Cl_4H_{36}N_2Pb$	$C_{16}Cl_4H_{36}N_2Pb$
Mr	575.15	605.46	605.46	605.46
Temperature/K	293	173	173	173
Crystal size/mm^3	0.40 x 0.18 x 0.14	0.20 x 0.20 x 0.16	0.36 x 0.16 x 0.07	0.40 x 0.28 x 0.05
Crystal system	Monoclinic	Monoclinic	Monoclinic	Monoclinic
Space group	$P2_1$	$C2/c$	$P2_1$	$P2_1$
a/Å	7.9833(13)	35.497(3)	8.4344(9)	8.4460(14)
b/Å	8.0524(12)	7.6096(8)	8.1132(6)	8.0983(14)
c/Å	11.6404(19)	8.5437(8)	17.2796(17)	17.184(3)
α/°	90	90	90	90
β/°	106.200(4)	90.405	101.400(7)	100.502(4)
γ/°	90	90	90	90
V/Å^3	718.6(2)	2307.7(4)	1159.11(19)	1155.7(3)
Z	2	4	2	2
Dc/g cm^{-3}	2.658	1.743	1.735	1.740
μ(Mo-Ka)/mm^{-1}	20.045	7.775	7.740	7.763
Theta range/°	2.77 to 28.00	1.15 to 28.00	2.40 to 28.00	2.40 to 28.00
Total reflection	6715	6151	12418	14639
No. unique data [R(int)]	3471 [0.0774]	2767 [0.0614]	5600 [0.0733]	5526 [0.0615]
No. data with $I \geq 2s(I)$	3114	2144	4269	4404
$R1$	0.0358	0.0402	0.0336	0.0281
$wR2$ (all data)	0.0879	0.1313	0.0927	0.0844
Flack parameter[16]	0.031(13)	-	0.068(11)	0.035(9)

Table 2 Hydrogen bonding details of some compounds

D-H…A	D-H (Å)	H…A (Å)	D…A (Å)	<(D-H…A) (°)	Symmetry transformations
3					
N(1)-H(1B)…Br(1)	0.91	2.48	3.34(2)	155.7	x-1/2,y,-z+5/2
N(1)-H(1A)…Br(1)	0.91	2.52	3.35(3)	151.5	-
N(1)-H(1C)…Br(2)	0.91	2.69	3.46(2)	142.3	-
4					
N(1)-H(1B)…Br(1)	0.89	2.64	3.523(12)	170.3	x-1,y,z
N(1)-H(1A)…Br(2)	0.89	2.63	3.466(12)	155.9	-x+2,y-1/2,-z
N(1)-H(1C)…Br(3)	0.89	2.81	3.549(12)	141.8	-
5					
N(1)-H(1C)…Br(1)	0.89	2.63	3.512(9)	170.2	x+1,y,z
N(1)-H(1B)…Br(2)	0.89	2.65	3.478(9)	155.0	-x,y+1/2,-z+2
N(1)-H(1A)…Br(3)	0.89	2.81	3.548(9)	141.5	-
6					
N(1)-H(1A)…Cl(1)	0.91	2.29	3.177(7)	166.0	x,y,z+1
N(1)-H(1C)…Cl(1)	0.91	2.35	3.247(8)	169.0	x,-y,z+1/2
N(1)-H(1B)…Cl(2)	0.91	2.60	3.320(7)	136.1	-x+1/2, -y+1/2,-z+1
7					
N(1)-H(1C)…Cl(3)	0.91	2.42	3.292(6)	159.7	x+1,y-1,z
N(1)-H(1A)…Cl(4)	0.91	2.50	3.141(6)	127.5	x+1,y-1,z
N(1)-H(1B)…Cl(1)	0.91	2.52	3.237(7)	136.1	-x+1,y-1/2,-z
N(2)-H(2C)…Cl(2)	0.91	2.54	3.415(6)	161.3	-
N(2)-H(2B)…Cl(1)	0.91	2.57	3.240(6)	130.5	-x,y-1/2,-z
N(2)-H(2A)…Cl(4)	0.91	2.57	3.123(6)	119.4	-
8					
N(1)-H(1B)…Cl(3)	0.91	2.42	3.291(5)	161.3	x-1,y+1,z
N(1)-H(1A)…Cl(4)	0.91	2.50	3.136(5)	127.7	x-1,y+1,z
N(1)-H(1B)…Cl(1)	0.91	2.52	3.238(5)	135.4	-x+1,y+1/2,-z+2
N(2)-H(2C)…Cl(1)	0.91	2.55	3.224(5)	130.9	-x+2,y+1/2,-z+2
N(2)-H(2B)…Cl(2)	0.91	2.57	3.439(5)	160.6	-
N(2)-H(2A)…Cl(4)	0.91	2.58	3.123(5)	119.1	-

690

This journal © Royal Society of Chemistry

4.4 Inorganic-organic hybrid materials incorporating primary cyclic ammonium cations: The lead iodide series

Journal: CrystEngComm

Date Submitted: 17 May 2006

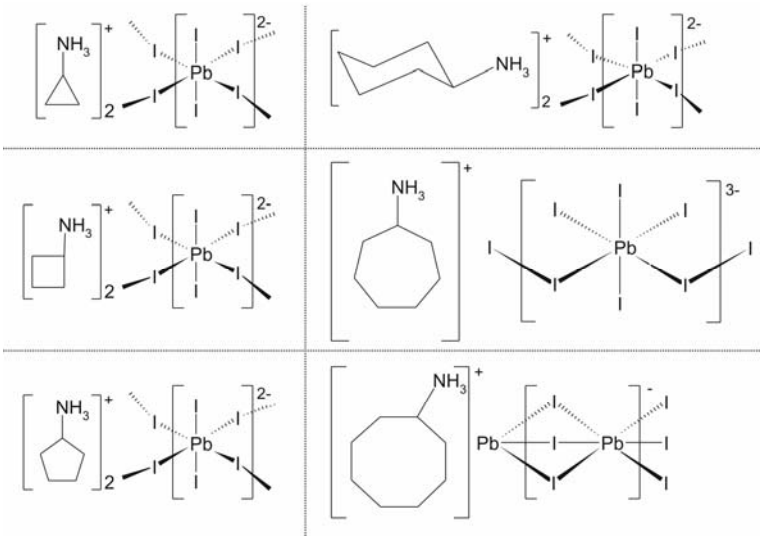
Reference Code of Submitted Article: B618196A

Date Accepted: 19 December 2006

Final Reference: Billing, D.G., Lemmerer, A. (2006). *CrystEngComm*, **9**, 236-244.

Brief Synopsis

In this paper, six hybrids were made using the metal lead and the halide iodide. The counter cations were six cyclic hydrocarbons with increasing ring size. The effect of the ring size on the inorganic motif was analyzed.



PAPER www.rsc.org/crystengcomm | CrystEngComm

Inorganic–organic hybrid materials incorporating primary cyclic ammonium cations: The lead iodide series†

David G. Billing* and Andreas Lemmerer

Received 13th December 2006, Accepted 19th December 2006
First published as an Advance Article on the web 8th January 2007
DOI: 10.1039/b618196a

Six inorganic–organic hybrids have been synthesized and characterised by single-crystal X-ray diffraction experiments. The inorganic component is based on lead(II) iodide units and the organic component various cyclic hydrocarbons with only a primary ammonium group as a ring substituent. If the organic component is cyclopropylammonium, cyclobutylammonium, cyclopentylammonium and cyclohexylammonium, the inorganic motif observed is based on the cubic perovskite structure type and consists of 2-D layers of corner-sharing octahedra, in the ratio of 1 : 2 inorganic–organic. lead(II) iodide and cycloheptylammonium combined to give 1-D chains of corner-sharing lead iodide octahedra and similarly, lead(II) iodide and cyclooctylammonium gave 1-D chains of face-sharing octahedra. A quantitative measure of the steric effects of the size of the cyclic rings on the tilting of the inorganic layers is proposed.

Introduction

Inorganic–organic hybrid structures, with the general formula $(R–NH_3)_2MX_4$, where R is any hydrocarbon group, are able to combine desirable characteristics from both types of constituents into a molecular scale composite.[1] Inorganic compounds have varying band gaps and hence their electrical properties can vary from insulators to semiconductors right the way through to superconductors. Furthermore, they supply the hybrid structure with thermal stability and hardness as well as magnetic and dielectric properties. In addition to structural diversity, organic materials offer highly efficient luminescence. These hybrids form natural quantum well structures and have been extensively studied for their excitonic and magneto-optical properties, in particular the compound $(C_6H_5C_2H_4NH_3)_2PbI_4$.[2] Significantly, a thin-film field-effect transistor has been made using the same organic amine, 2-phenylethylamonium, and substituting the metal centre for tin(II).[3]

These hybrids form 2-D layers conceptually derived from the basic AMX_3 perovskite structure, which consists of corner-sharing octahedral MX_6, where M is a divalent metal and X a halide. The cation A sits in the voids of this 3-D network (Fig. 1) and has a limited allowed radius. The formula that determines this maximum radius is

$$R_A + R_x = t\sqrt{2}\,(R_M + R_x)$$

where R_A, R_M and R_X are the ionic radii for the spheres in contact and assumes that we have a perfect cubic perovskite structure.[4] The parameter t is the Goldschmidt tolerance factor and occurs in the range $1.05 > t > 0.78$ for compounds in the perovskite family.[5] If the octahedra are tilted as in $CaTiO_3$,[6,7] then t is close to 1. The geometric limit imposed on R_A is then R_A = 2.60 Å, for the largest possible scenario for a metal and halide being Pb and I (R_{Pb} = 1.19 Å and R_I = 2.20 Å[8]). Hence, if A were to be an

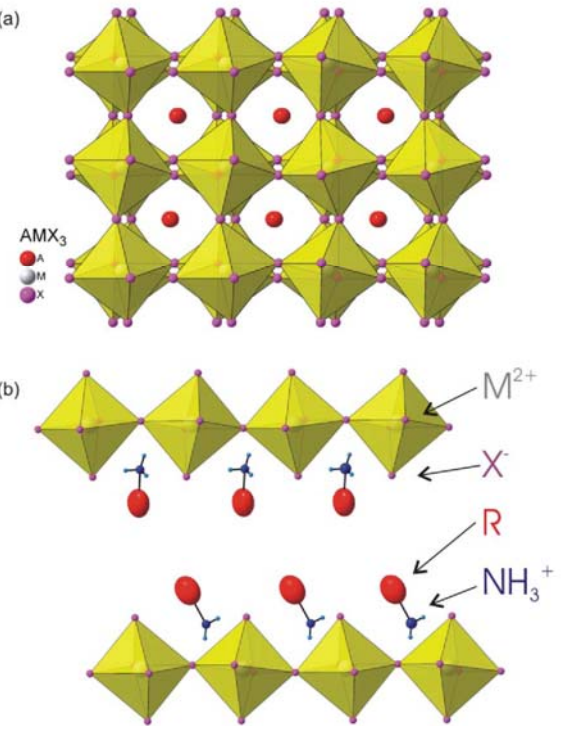


Fig. 1 (a) The 3-D basic cubic perovskite structure, showing the tilted, corner-sharing octahedra. (b) Schematic drawing of the 2-D layered structure of the $(R–NH_3)_2PbI_4$ hybrids. The increased size of the R group causes the transition to the lower dimensional structure.

Molecular Sciences Institute, School of Chemistry, University of the Witwatersrand, PO WITS 2050, Johannesburg, South Africa. E-mail: dave@chem.wits.ac.za; Fax: 27 11 717 6749; Tel: 27 11 717 6759
† Electronic supplementary information (ESI) available: Derivation of the calculation of the area defined by four terminal halides. See DOI: 10.1039/b618196a

 This journal is © The Royal Society of Chemistry 2007

organic ammonium cation, it can only consist of at maximum two C–C or C–N bonds. This restriction is only fulfilled by the methylammonium cation and compounds with the general formula $CH_3NH_3MX_3$, where M is Sn or PB and X is Cl, Br and I have been synthesized.[9] If A is larger, the 3-D arrangement is destroyed and the inorganic–organic hybrid structure will form well-defined 2-D layers of purely corner-sharing $[PbI_2I_{4/2}]^{2-}$ octahedra, where the four equatorial iodides are shared, called bridging iodides, and the two axial iodides are unshared, called terminal iodides. The inorganic layers correspond to a <100> cut out of the cubic perovskite structure. This inorganic layer is sheathed on both sides by the $R–NH_3$ ammonium cations, which form hydrogen bridges to three of the iodides, and stacking of these "sandwiches" creates a bilayer between each inorganic layer. The resulting crystal structure will then have a laminar arrangement, shown schematically in Fig. 1. The ammonium cations then sits in the holes formed by four corner-shared octahedra and the size of this organic ammonium cation depends on the cross sectional area defined by the four terminal iodides. The size of this area is twice the length of the average metal halide bond length, here 40 $Å^2$ for lead iodide.[10] If the molecule is smaller than the limit, the octahedra can tilt around the normal to the layer plane, reflected in the Pb–I–Pb bridging angle being no longer linear and the area is then reduced. This angle has been defined as a θ tilt previously.[11] A second reduction of the area comes about from puckering or corrugation of the octahedra in one crystallographic direction, defined as a Ψ tilt.[11]

Another effect that the cation size can have on the hybrid structure is the relative displacement of adjacent inorganic layers. When viewed perpendicular to the layers, they can either be eclipsed relative to each other, where all the lead atoms are directly above each other or staggered, where the lead atoms are then offset. For small R cations, the eclipsed configuration is seen often.[10]

Yet another pattern derivable from the cubic perovskite structure is shown in Fig. 2. This results in 1-D chains of *cis*-corner-sharing octahedra. This packing arrangement compensates for large *R* groups by increasing the distance between adjacent chains. A further possible structure variation due to the size of the ammonium cation changes the connectivity from corner-sharing to chains of face-sharing octahedra.

The *R* group can be large if there are linkages to the ammonium NH_3^+ head that raises the *R* group sufficiently above the layers to negate the influence of the iodide atoms. For example, Era *et al* prepared a series of layered perovskites using naphthalene-linked ammonium molecules ($C_{10}H_7–C_nH_{2n}NH_3$), n = 1 and 2, and ($C_{10}H_7–OC_nH_{2n}NH_3$), n = 3, 4 and 8, and lead(II) bromide.[12]

In this study, we wanted to investigate the steric effect of the *R* group, here a cyclic ring, by systematically increasing the size of the cyclic ring from three to eight carbon atoms, on the inorganic lead(II) iodide motif that is adopted in the hybrid structure. To the best of our knowledge, there are no reports explicitly discussing the factors determining whether a particular hybrid will have 2-D layers or 1-D chains.

Results and discussion

To better describe the structural trends observed, we describe the position of the ammonium group and its effect on the geometry of the hydrogen bridges between the ammonium group and the iodides. In the 2-D case, two hydrogens can bridge to the axial (terminal) halides and the third to the equatorial (bridging) halide (bridging halogen configuration) or the reverse case with two terminal and one bridging halide (terminal halogen configuration). This classification is taken from Mitzi.[10] There are two subtypes in the terminal halogen configuration and bridging halogen configuration, depending on the position of the nitrogen atom within a parallelogram defined by the four bridging halides. If the nitrogen atom is close to a corner of the parallelogram that has an oblique angle, the three halides would be at the corners of an equilateral triangle. This subtype is called the equilateral halogen subtype and means that the organic cation is aligned with the short diagonal of the parallelogram (Fig. 3a). The other possibility, when the nitrogen atom is close to an acute angled corner of the parallelogram, the three halides form a right-angled triangle. This is called the right-angled halogen subtype (Fig. 3b) and the organic cation is aligned with the long diagonal. This position allows for larger *R* groups. The intermediate position is when the nitrogen atom is at the centre of the parallelogram, where the two diagonals intersect. This position can either have the equilateral halogen or right-angled halogen subtype.

If the inorganic motif consists of 1-D chains, a different classification of the hydrogen bridging geometry is necessary.

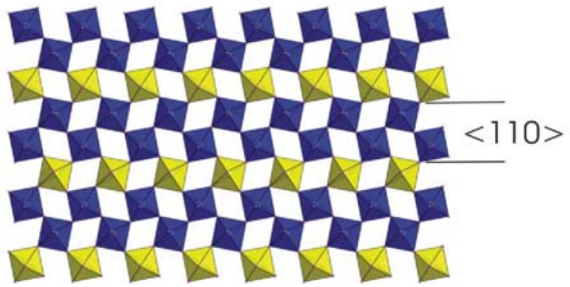


Fig. 2 The 1-D chains of corner-sharing octahedra are shown in blue and are cut-outs of the layered perovskite structure along the <110> direction. The row of yellow octahedra is replaced by the cycloheptylammonium cations in compound **5**.

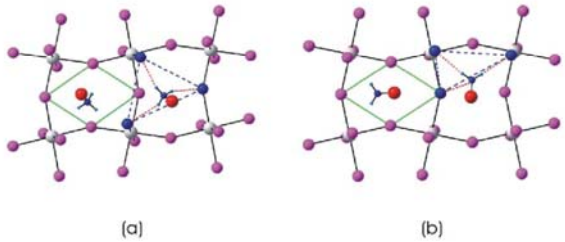


Fig. 3 The subtypes in the terminal halogen configuration. On the left, the nitrogen atom is in the oblique angled corner of the parallelogram, shown in green, and adopts the equilateral halogen subtype, shown in blue. The picture on the right shows the right-angled halogen subtype seen when the nitrogen atom is in the acute angled corner of the parallelogram.

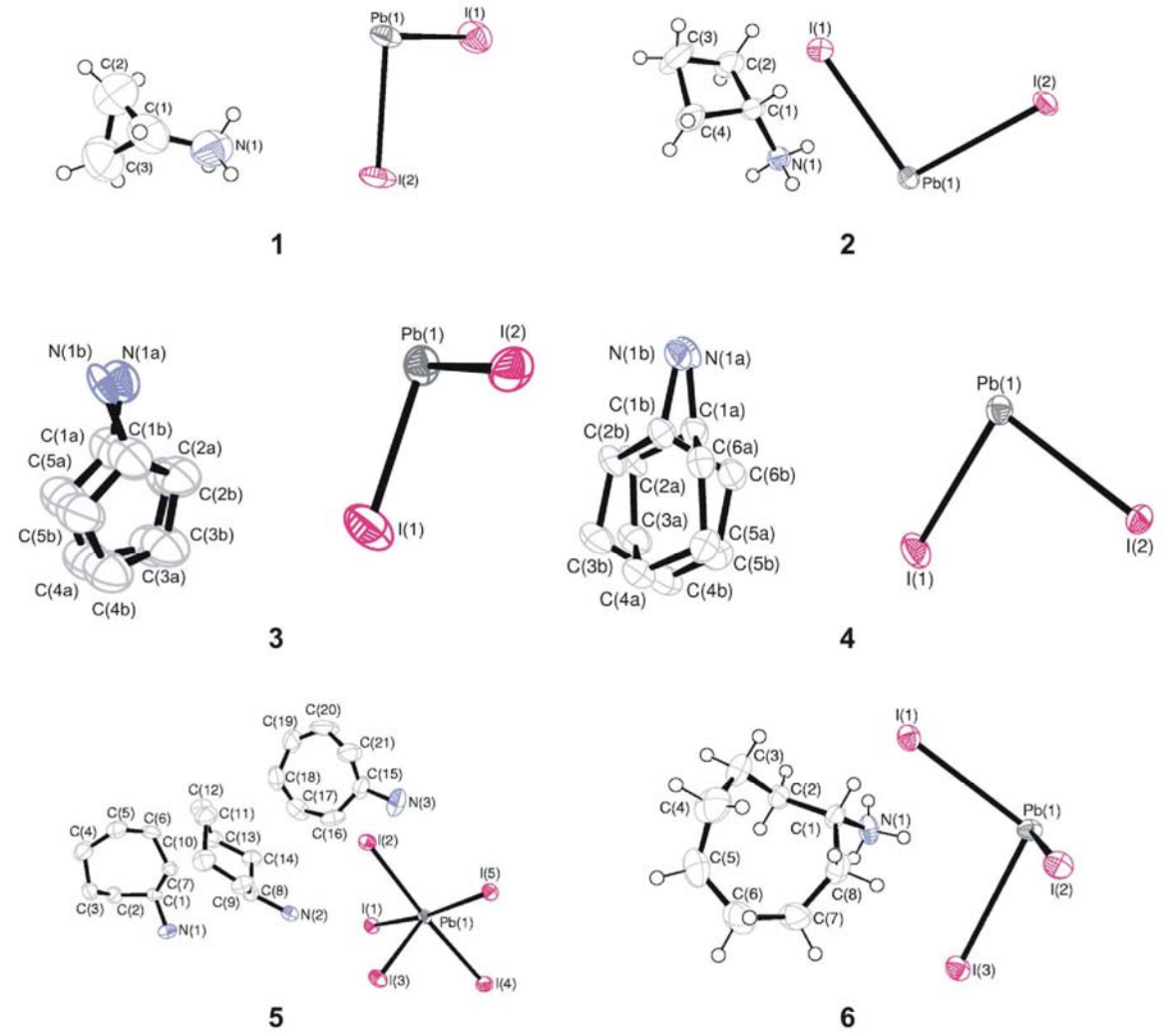


Fig. 4 The contents of the asymmetric unit for structures **1–6**, showing the atomic numbering scheme. Displacement ellipsoids are shown at the 50% probability level. H atoms are omitted in **3–5** for clarity.

If the majority of the hydrogen bridges are to halides occupying the equatorial positions in the octahedra, it is called equatorial halogen configuration, and similarly for the reverse case, where the halides are in the axial positions, axial halogen configuration.

The atomic numbering scheme for all six compounds to be discussed is shown in Fig. 4.

Crystallographic description of the hybrids incorporating cyclopropylammonium, cyclobutylammonium, cyclopentylammonium and cyclohexylammonium: $[(C_3H_5NH_3)_2PbI_4]$ (1), $[(C_4H_7NH_3)_2PbI_4]$ (2), $[(C_5H_9NH_3)_2PbI_4]$ (3) and $[(C_6H_{11}NH_3)_2PbI_4]$ (4)

The structures of the compounds **1**, **2** and **3** are similar and adopt the same 2-D layered motif, with all the inorganic layers eclipsed. The overall structure remains the same; however there are changes in the packing of the ammonium cations between the layers, and changes in the tilting of the PbI_6 octahedra within the layers themselves. Compound **4**, too, has a 2-D layered motif, but with staggered inorganic layers.

The crystal structure of 1

Fig. 5a clearly underlines a bidimensional arrangement in which two layers of non-interdigitated cyclopropylammonium molecules are embedded between two consecutive inorganic $[PbI_2I_{4/2}]$ sheets, forming an alternated inorganic–organic layered structure. The lead atoms are aligned from layer to layer, resulting in an eclipsed arrangement of adjacent layers, typical of 2-D layered hybrids with monoclinic unit cells. In the direction perpendicular to the layers, the crystal cohesion is achieved by N–H···I hydrogen bridges, related to the NH_3 polar groups. There are no van der Waals forces between

This journal is © The Royal Society of Chemistry 2007

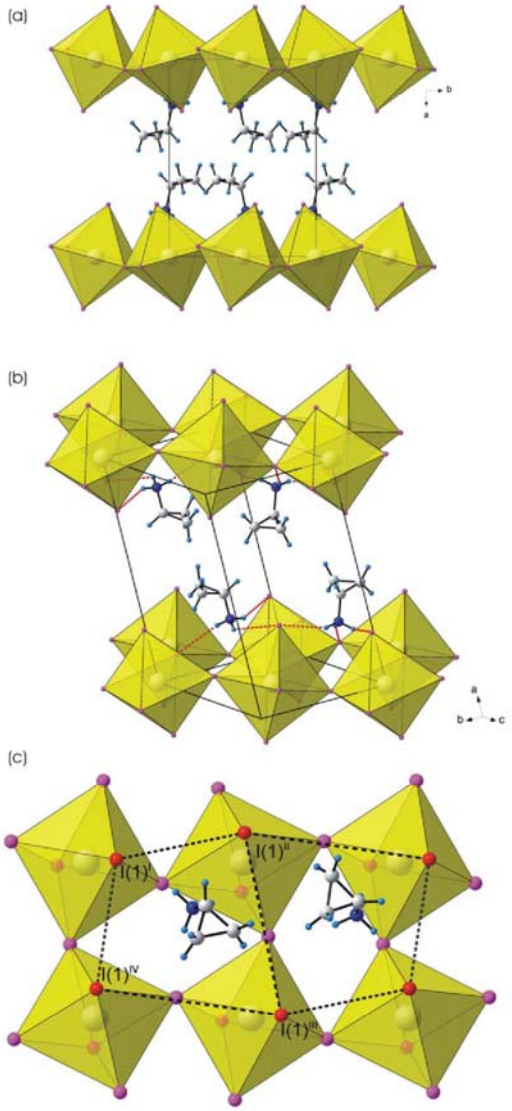


Fig. 5 (a) The crystal structure of the organic–inorganic hybrid $(C_3H_5NH_3)_2PbI_4$ (**1**) adopting the 2-D layered structure type. (b) The hydrogen bridges between the ammonium group and the iodides are shown as red, dashed lines. The terminal halogen configuration is shown. (c) The view perpendicular to the layer. The irregular quadrilateral, shown as dashed black lines, is created by the four terminal iodides I(1), shown in red. The area of the quadrilateral can adjust to the size of the ammonium cation, here cyclopropylammonium. Atoms marked with superscripts (i), (ii), (iii) and (iv) are at the symmetry positions $(1 + x, ½ - y, -1/2 + z)$, $(1 + x, -1 + y, -1 + z)$, $(1 + x, 3/2 - y, -1/2 + z)$ and $(1 + x, -1 + y, z)$, respectively.

two adjacent molecules (nearest neighbour distances is 4.407(13) Å). In the direction parallel to the layers, the cohesion is achieved by strong ionic bonds between equatorial iodide and lead atoms.

The inorganic layer is built up from characteristic corner-sharing PbI_6 octahedra. The asymmetric unit consists of a lead atom on a special position (centre of inversion) and two iodide atoms, I(1) occupying the terminal position and I(2) occupying the bridging position in the octahedra. As shown in the projection normal to the layers in Fig. 5c, along the *a*-axis, the PbI_6 octahedra are tilted relative to each other. The tilt angle θ is equal to 32.84(3)°, which is calculated by subtracting the Pb(1)–I(2)–Pb(1) bridging angle, 147.16(3)°, from 180°. Furthermore, the octahedra are corrugated along the b-direction by an angle of 14.09(2)° with respect to the *bc*-plane (Fig. 5a). This angle is the Ψ tilt and measured by the angle between the normal to the inorganic layers and the vector connecting the lead atom Pb(1) and one of the terminal iodides I(1). The net effect of these two tilts is a decrease in the area, thus maximising the packing efficiency. The four terminal halides, I(1), are no longer arranged in a perfect square but in an irregular quadrilateral, shown as dashed black lines (See Fig. 5c). The area of this quadrilateral is now 37.87(5) $Å^2$, less than the possible maximum of 40 $Å^2$. The coordination geometry around the Pb atom shows axial compression of the octahedral geometry, with the bridging Pb(1)–I(2) distances (3.2055(15) Å and 3.2102(16) Å) longer than the axial distances Pb(1)–I(1) (3.1794(15) Å). The angle between *cis* related iodide atoms deviate from 90°, with all *trans* angles equal to 180° by virtue of the centre of inversion.

The cyclopropylammonium molecule occupies a general position. The chains are ordered within the inorganic layer and the three-membered ring is planar. The ring is tilted at an angle of 15.2(9)° to the inorganic layer. This tilt angle α of the ring is defined as the dihedral angle between a plane containing all the C atoms of the ring and the lead atoms of the inorganic layers. The NH_3 ammonium group itself is tilted at an angle of 12.4(7)°. This tilt angle, β, is the angle between a vector connecting atoms N(1) and C(1) and the plane of the lead atoms. The hydrogen bridges between the organic and inorganic entities adopt the terminal halogen configuration with the equilateral halogen subtype. The hydrogen acceptor distances to the terminal halide I(1) are 2.69 Å and 3.00 Å and to the bridging halide I(2) 2.79 Å (See Table 1).

The crystal structures of 2, 3 and 4

Compounds **2** and **3** have the same bidimensional arrangement, with cyclobutyl- and cyclopentylammonium molecules respectively, between the eclipsed $[PbI_2I_{4/2}]$ sheets. The inorganic layers consist of the same asymmetric unit as **1**, where the Pb atom is on a centre of inversion and the iodides all on general positions.

The cyclobutylammonium molecule in **2** sits on a general position and adopts the equilateral halogen subtype (see Table 1). The chains are ordered within the inorganic layer and the four-membered ring adopts the crown form.

The cyclopentylammonium molecule in **3** sits on a general position but the entire molecule is disordered over two positions, labelled Ring A and Ring B. The closest puckering descriptor for both rings is envelope.[13] Ring A adopts the bridging halogen configuration, whereas Ring B has the terminal halogen configuration. Both rings however have the right-angled halogen subtype (see Table 1).

Table 1 Hydrogen bridging details of all compounds

D–H···A	D–H/Å	H···A/Å	D···A/Å	∠(D–H···A)/°	Symmetry transformations
1					
N(1)–H(1A)···I(1)	0.91	2.69	3.517(13)	151.5	$-x, y + 1/2, -z + 3/2$
N(1)–H(1B)···I(1)	0.91	3.00	3.592(11)	124.1	$-x, -y + 2, -z + 2$
N(1)–H(1C)···I(2)	0.91	2.79	3.668(12)	162.6	$-x, -y + 2, -z + 1$
2					
N(1)–H(1C)···I(1)	0.91	2.70	3.602(4)	174.1	$x, y - 1, z$
N(1)–H(1B)···I(1)	0.91	2.74	3.606(5)	158.3	$x, -y + 3/2, z - 1/2$
N(1)–H(1A)···I(2)	0.91	2.85	3.668(5)	150.0	$-x + 2, -y + 2, -z + 2$
3					
N(1A)–H(1A1)···I(1)	0.89	3.19	3.98(7)	149.7	$x, -y + 3/2, z + 1/2$
N(1A)–H(1A3)···I(2)	0.89	2.79	3.59(7)	149.5	$-x, y - 1/2, -z + 1/2$
N(1A)–H(1A2)···I(2)	0.89	2.80	3.58(7)	146.9	$x, -y + 3/2, z - 1/2$
N(1B)–H(1B2)···I(1)	0.89	2.82	3.57(4)	142.8	$x, y - 1, z$
N(1B)–H(1B1)···I(1)	0.89	2.85	3.56(3)	138.0	$x, -y + 3/2, z + 1/2$
N(1B)–H(1B3)···I(2)	0.89	2.92	3.73(3)	151.5	$-x, y - 1/2, -z + 1/2$
4					
N(1A)–H(1A2)···I(1)	0.91	2.51	3.38(5)	161.0	$-x + 1/2, y - 1/2, z$
N(1A)–H(1A1)···I(2)	0.91	2.85	3.75(6)	169.4	$x - 1, y, z$
N(1A)–H(1A3)···I(2)	0.91	2.87	3.56(6)	133.5	$-x + 1, -y, -z + 1$
N(1B)–H(1B2)···I(1)	0.91	2.65	3.51(3)	157.9	$x - 1, y, z$
N(1B)–H(1B3)···I(1)	0.91	2.83	3.72(2)	165.9	$-x + 1/2, y - 1/2, z$
N(1B)–H(1B1)···I(2)	0.91	3.06	3.69(3)	128.0	$x - 1, y, z$
5					
N(1)–H(1C)···I(4)	0.91	2.98	3.839(6)	158.0	$-x + 3/2, -y + 3/2, -z + 2$
N(1)–H(1A)···I(3)	0.91	3.08	3.860(6)	145.0	$-x + 3/2, -y + 3/2, -z + 2$
N(1)–H(1B)···I(5)	0.91	2.91	3.753(6)	154.4	$x, -y + 1, z + 1/2$
N(2)–H(2B)···I(2)	0.91	2.72	3.627(5)	175.8	—
N(2)–H(2C)···I(1)	0.91	2.86	3.648(5)	146.3	$-x + 3/2, -y + 3/2, -z + 2$
N(2)–H(2A)···I(5)	0.91	2.88	3.637(6)	140.9	$-x + 3/2, -y + 3/2, -z + 2$
N(3)–H(3B)···I(2)	0.91	2.73	3.615(7)	163.4	—
N(3)–H(3C)···I(4)	0.91	2.82	3.639(9)	161.9	$-x + 3/2, y - 1/2, -z + 3/2$
N(3)–H(3A)···I(5)	0.91	3.14	3.558(6)	110.5	$-x + 3/2, y - 1/2, -z + 3/2$
6					
N(1)–H(1A)···I(1)	0.91	2.82	3.691(10)	160.5	$x, y - 1, z$
N(1)–H(1C)···I(2)	0.91	2.85	3.671(9)	150.8	$x + 1/2, -y + 3/2, -z + 2$
N(1)–H(1B)···I(2)	0.91	2.86	3.706(9)	155.8	$x + 1, y - 1, z$

Compound **4** has the same bidimensional arrangement as **2** and **3** but the lead atoms are not aligned from layer to layer, resulting in a staggered arrangement of adjacent layers, typical of 2-D layered hybrids with orthorhombic unit cells. As a consequence, the unit cell direction perpendicular to the layers is double that of the eclipsed compounds **1**–**3** (see Fig. 6a). Again, the lead atom is on a centre of inversion.

The cyclohexylammonium molecule in **4** is disordered within the inorganic layer. The two parts of the disorder are interlinked and labelled Ring A and Ring B. Both six-membered rings adopt the chair configuration. The two parts of the disordered cyclohexylammonium molecule adopt the same terminal halogen configuration, with the right-angled halogen subtype (see Fig. 6b and Table 1).

Effect of the size of the ammonium cations on the structure of the lead(II) iodide motif

In Table 2, the important geometric parameters mentioned so far are summarized for the four layered perovskites. There exists a correlation between the ring size and the θ and Ψ tilts of the individual octahedra, as observed in Fig. 7. The four hybrids can be subdivided into two groups, one containing compounds **1** and **2**, and the second compounds **3** and **4**.

The θ and Ψ tilts for **1** and **2** are approximately the same and only differ by about 0.11° and 1.68°, respectively. Both compounds have the same equilateral halogen subtype, eclipsed inorganic layers and almost identical areas (37.87(5) and 37.84(2) Å^2). The most substantial difference is in the orientation of the rings. In **1**, the cyclopropylammonium cation is almost parallel to the layers, whereas in **2**, the cyclobutylammonium cation is tilted almost perpendicular. This is further reflected in the β tilt angle, which is closer to the normal to the layers in **1** (12.4(7)°) than in **2** (38.4(2)°).

The tilt angles change substantially in the second grouping, decreasing to 5.03(2)° and 6.51(9)° for the Ψ tilt and increasing to 25.25(5)° and 25.21(5)° for the θ tilt. The net effect of these changes is an increase in the areas to 39.95(1) and 40.03(2) Å^2, respectively, for **3** and **4**, as a result of the octahedra becoming less tilted and the ring size of the cations increasing. The areas are now at the limit of the lead(II) iodide structure. The cyclopentylammonium and cylcohexylammonium cations are both tilted perpendicular to the inorganic layers, evidenced by their α tilt angles.

In general, the organic ammonium cations migrate from the oblique-angled position to the acute-angled position as the ring size increases (see Fig. 7). The larger rings in **3** and **4** now lie along the long-diagonal of the parallelogram, by virtue of their greater size. The interlayer spacing between the eclipsed layers increases from **1** to **3** and then decreases again in **4**, as the inorganic layers are now staggered and hence the cations can interdigitate more.

This journal is © The Royal Society of Chemistry 2007

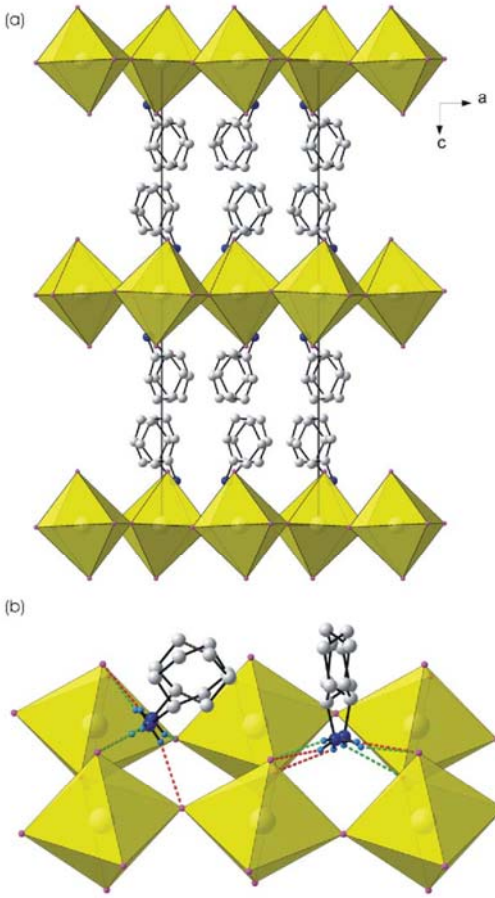


Fig. 6 (a) View of **4**, parallel to the inorganic sheets of a single unit cell. The cyclohexane rings are disordered between the staggered layers. (b) The right-angled halogen subtype of both disordered components.

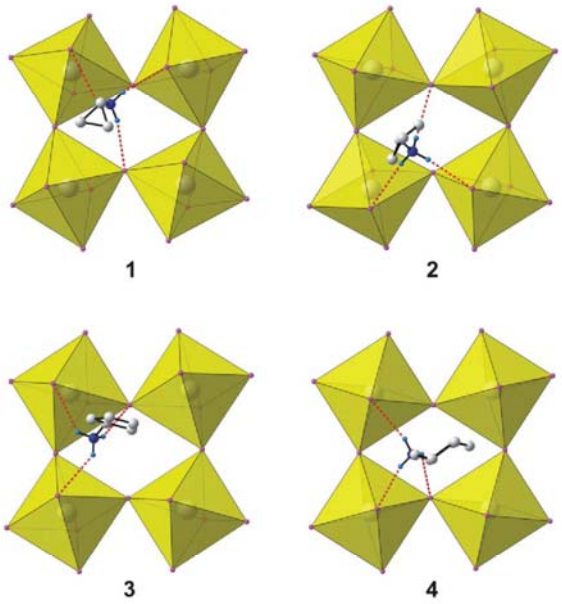


Fig. 7 Magnified top views of the hydrogen bridging geometries of compounds **1–4**, showing the more tilted octahedra of **1** and **2** compared to **3** and **4** and the position of the cations relative to the corner-sharing octahedra. Only the major component of the disordered cations in **3** and **4** is shown.

Crystallographic description of the hybrid complexes that incorporate cycloheptylamine and cyclooctylamine: $[(C_7H_{13}NH_3)_3PbI_5]$ (5) and $[(C_8H_{15}NH_3)PbI_3]$ (6)

The structure of **5** consists of alternating ionic and hydrocarbon layers. The ionic layer contains four chains of corner-sharing $[PbI_6]$ octahedra running along the *b*-axis and the hydrocarbon layer is comprised of cycloheptylammonium moieties (Fig. 8a). The alternating layers are similar to the 2-D layered motif of the previous hybrids, but adjacent chains are not connected along the *c*-axis and hence the adopted lead(II) iodide motif is 1-D, shown schematically in Fig. 2. The asymmetric unit consists of a lead atom and five iodide atoms, all occupying general positions. I(1), I(3) and I(5) occupy the axial positions and I(2) and I(4) the equatorial positions. I(5) and I(5) $(-x+3/2,\ y-1/2,\ -z+3/2)$, complete the octahedral coordination sphere. The octahedra share corners *via* two iodides, here I(5), and since they are *cis* to each other, the chain zig-zags. The bridging angle between two octahedra is almost linear (166.266(13)°). The coordination geometry around the Pb atom is characterized by short and long Pb–I bonds. The

Table 2 Effect of ring size on the packing of the 2-D layered hybrids with lead(II) iodide

	$(C_3H_5NH_3)_2PbI_4$	$(C_4H_7NH_3)_2PbI_4$	$(C_5H_9NH_3)_2PbI_4$	$(C_6H_{11}NH_3)_2PbI_4$
Interlayer spacing/Å	12.475(5)	13.355(3)	14.00(2)	13.638(5)
Space group	$P2_1/c$	$P2_1/c$	$P2_1/c$	Pbca
Conformation of layers	Eclipsed	Eclipsed	Eclipsed	Staggered
Average Pb–I (terminal) bond/Å	3.1794(15)	3.2015(7)	3.193(6)	3.1752(7)
Average Pb–I (bridging) bond/Å	3.2079(15)	3.2110(6)	3.240(4)	3.2437(6)
Bridging angle Pb–X–Pb, θ tilt/°	147.16(3), 32.84(3)	147.27(1), 32.73(1)	154.75(5), 25.25(5)	154.79(1), 25.21(5)
Corrugation or Ψ tilt/°	14.09(2)	12.41(1)	5.03(2)	6.51(9)
Area/Å^2	37.87(5)	37.84(2)	39.95(1)	40.03(2)
Position of nitrogen atom	Oblique	Oblique	Acute	Acute
Hydrogen bonding subtype	Equilateral	Equilateral	Right-Angled	Right-Angled
Tilt angle of NH_3 group β/°	12.4(7), N(1)–C(1)	38.4(2), N(1)–C(1)	35.4(3), N(1A)–C(1A) 44.0(2), N(1B)–C(1B)	42.1(2), N(1A)–C(1A) 39.5(7), N(1B)–C(1B)
Tilt of ring to inorganic layer α/°	15.2(9)	82.6(3)	88.4(2), Ring A 88.3(2), Ring B	85.9(5), Ring A 89.7(3), Ring B

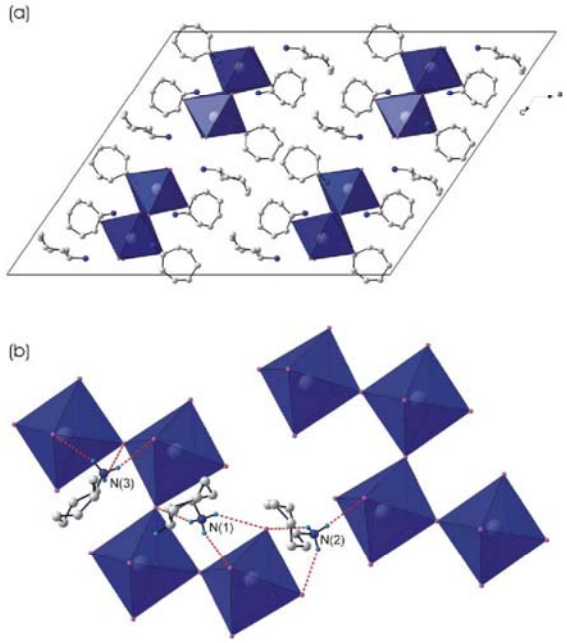


Fig. 8 (a) Packing of **5**, showing the four corner-sharing chains extending along the *b*-axis. (b) The view above the chains illustrating the hydrogen bridging scheme of the three unique cycloheptylammonium molecules.

bond distances to the bridging iodides are the longest, 3.3634(5) Å and 3.3931(5) Å, and to the iodides trans to the bridging iodides the shortest, 3.0999(5) Å and 3.0644(5) Å. The Pb–I distances to the axial iodides are intermediate, with Pb(1)–I(2) longer than Pb(1)–I(4). The angle between *cis* related iodide atoms deviate from 90°, and the *trans* angles from 180°.

The three cycloheptylammonium molecules in the asymmetric unit occupy general positions. The rings are labelled cat1 (containing atom N1), cat2 (N2) and cat3 (N3). Cat1 and cat3 sit above the chains in the holes formed by the corner-shared octahedra. Cat2 occupies the gaps between the chains. The molecules are well ordered and all adopt the twist-chair ring conformation. The hydrogen bridges between the organic and inorganic entities adopt two different hydrogen bonding geometries with iodide atoms (Fig. 8b). N(1) and N(2) have an equatorial halogen configuration, whereas N(3) has an axial halogen configuration.

The crystal packing of **6**, shown in Fig. 9a, clearly displays a 1-D arrangement in which three chains of characteristic face-sharing PbI_6 octahedra run along the unit cell, parallel to the *a*-axis. The channels in between the chains are occupied by cyclooctylammonium molecules. The inorganic motif is built up from characteristic face-sharing PbI_6 octahedra that form infinite chains along the *a*-axis. The positions of the three chains in the unit cell are at $z \approx 0, 0.5, 1$. The asymmetric unit consists of a lead atom and three iodide atoms, all on general positions, I(1) occupying the axial position with I(2) and I(3) occupying the equatorial positions in the octahedra. Within the chains, the shared face consists of these three halides. The

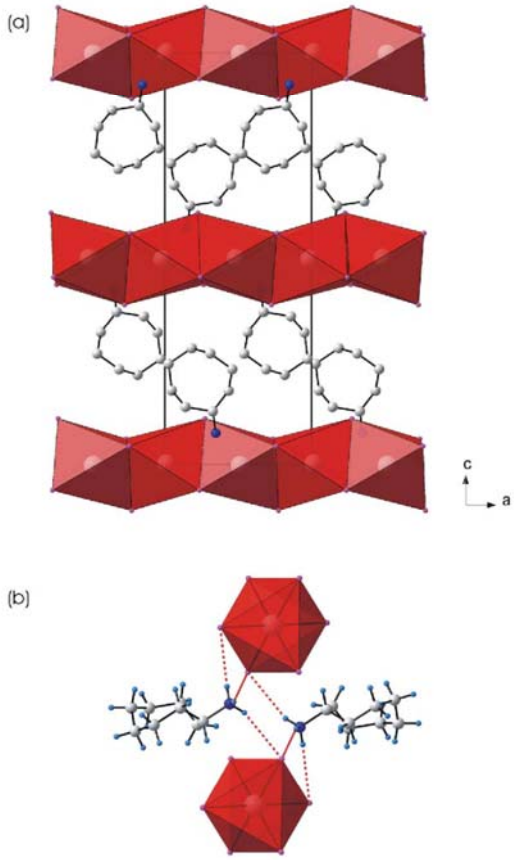


Fig. 9 (a) Packing of **6**, viewed along the b-axis. (b) Magnified view of the face-sharing $[PbI_6]$ octahedra and axial hydrogen bridging scheme (red dashed lines).

octahedra are severely distorted with all lead iodide distances different, ranging from 3.1078(8) Å to 3.3505(9) Å. The bond angles between *cis* ligands vary from 76.334(17)° to 100.83(2)° and *trans* angles from 172.91(2)° to 177.59(2)°.

The cyclooctylammonium molecule sits on a general position and adopts the boat-chair conformation. The hydrogen bridges between the organic and inorganic entities adopt the equatorial halogen configuration (see Fig. 9b). The hydrogen acceptor distances to the equatorial halides I(2) of two adjacent chains are 2.85 and 2.86 Å and to the axial halide I(1) 2.82 Å.

Conclusion

In a previous study, we investigated the effect that the identity of the halide Cl, Br and I had on the inorganic motif by keeping the identity of the metal atom and organic ammonium cation constant.[14] In this study, we kept the metal and halide atom constant and varied the identity of the organic ammonium cation. As a consequence, we have determined a cut-off point where inorganic–organic lead(II) iodide hybrid compounds convert from a 2-D system of corner-sharing octahedra to a 1-D system of corner-sharing and face-sharing

This journal is © The Royal Society of Chemistry 2007

Table 3 Summary of structure types for the hybrid $[(C_nH_{2n-1}NH_3)PbI]$

n	3	4	5	6	7	8
Motif	P	P	P	P	C	F

[a] F = face-sharing chains; C = corner-sharing chains; P = 2-D corner-sharing layers

octahedra (See Table 3). If the ring contains six or less carbon atoms, the organic moieties can fit between the four terminal halides and hence the layered motif is adopted as in structures **1–4**. In these cases, the cross sectional area defined by the four terminal halides are approximately the same, when the rings are cyclopropane or cyclobutane (37.87(5) and 37.84(5) $Å^2$, respectively) and when the rings are cyclopentane or cyclohexane (39.95(1) and 40.03(1) $Å^2$ respectively). In the cycloheptane or cyclooctane cases, the 2nd and 7th or 8th carbon atoms in the ring sterically prevents the formation of the perovskite layers, as is the case in **5** and **6**. The tilting of the octahedra also decreases with increasing the size of the organic ammonium cations. A similar trend is observed in the lead(II) bromide and lead(II) chloride hybrids.[15]

Experimental

Materials

All reagents and solvents employed were commercially available and used as received without further purification.

Crystal growth

Preparation of $[(C_3H_5NH_3)_2PbI_4]$, 1. 0.056 g PbI_2 (0.121 mmol) was dissolved in 2 ml 47% HI in a sample vial. Thereafter, 0.034 g $C_3H_5NH_2$ (0.595 mmol) was added and the precipitate dissolved by refluxing for 1 h at 80 °C. The solution was slowly cooled at 2 °C h^{-1} to room temperature. A yellow single crystal suitable for X-ray diffraction analysis was selected and studied. Elemental analysis (%). Found: C 8.98, H 2.16, N 3.55. Calc. for $C_6H_{16}I_4N_2Pb_1$: C 8.67, H 1.94, N 3.37.

Preparation of $[(C_4H_7NH_3)_2PbI_4]$, 2. 0.059 g PbI_2 (0.128 mmol) was dissolved in 2 ml 47% HI in a sample vial. Thereafter, 0.024 g $C_4H_7NH_2$ (0.337 mmol) was added and the precipitate dissolved by refluxing for 1 h at 80 °C. The solution was slowly cooled at 2 °C h^{-1} to room temperature. An orange single crystal suitable for X-ray diffraction analysis was selected and studied. Elemental analysis (%). Found: C 11.33, H 2.50, N 3.39. Calc. for $C_6H_{20}I_4N_2O_2Pb_1$: C 11.19, H 2.35, N 3.26.

Preparation of $[(C_5H_9NH_3)_2PbI_4]$, 3. 0.091 g PbI_2 (0.197 mmol) was dissolved in 3 ml 46% HI in a sample vial. Thereafter, 0.033 g $C_5H_9NH_2$ (0.388 mmol) was added and the precipitate dissolved by refluxing at 80 °C. The solution was slowly cooled at 2 °C h^{-1} to room temperature. An orange single crystal suitable for X-ray diffraction analysis was selected and studied. Elemental analysis (%). Found: C 13.87, H 2.95, N 3.21. Calc. for $C_{10}H_{24}I_4N_2Pb_1$: C 13.54, H 2.73, N 3.16.

The crystals were of poor quality and twined. The twin law applied, as suggested by PLATON,[7] is [1.00 0.00 1.00 0.00 −1.00 0.00 0.00 0.00 −1.00] and the batch scale factor is 0.36. The entire molecule is disordered within the inorganic layer. The conformational disorder around the five carbon atoms, C(1), C(2), C(3), C(4), C(5), and the nitrogen atom N(1) was resolved by finding alternate positions from the difference Fourier map for the respective atoms. These atoms were then refined anisotropically together with their site occupancy such that the sum of the occupancies for the two alternate atom positions equalled one. The ratio of major to minor component is 60 to 40%. The bond lengths and bond angles were restrained using the SADI instruction in SHELX to be within 0.01 Å of each other for the two parts, labelled Ring A and Ring B, respectively. Hydrogen atom positions were then calculated for the respective atoms using a riding model.

Preparation of $[(C_6H_{11}NH_3)_2PbI_4]$, 4. 0.176 g PbI2 (0.382 mmol) was dissolved in 6 ml 47% HI in a round bottom flask. Thereafter, 0.075 g $C_6H_{11}NH_2$ (0.756 mmol) was added and the precipitate dissolved by refluxing for 12 h at 105 °C. The solution was slowly cooled at 2 °C h^{-1} to room temperature. An orange single crystal suitable for X-ray diffraction analysis was selected and studied. Elemental analysis (%). Found: C 16.09, H 3.22, N3.18. Calc. for $C_{12}H_{28}I_4N_2Pb_1$: C 15.75, H 3.08, N 3.06.

The conformational disorder around the six carbon atoms, C(1), C(2), C(3), C(4), C(5) and C(6), and the nitrogen atom N(1) was resolved by finding alternate positions from the difference Fourier map for the respective atoms. These atoms were then refined anisotropically together with their site occupancy such that the sum of the occupancies for the two alternate atom positions equalled one. The ratio of major to minor component is 69 to 31%. The bond lengths and bond angles were restrained using the SADI instruction in SHELX to be within 0.01 Å of each other for the two parts, labelled Ring A and Ring B, respectively. Hydrogen atom positions were then calculated for the respective atoms using a riding model.

Preparation of $[(C_7H_{13}NH_3)_3PbI_5]$, 5. 0.056 g PbI_2 (0.121 mmol) was dissolved in 6 ml 47% HI in a glass vial. Thereafter, 0.046 g $C_7H_{13}NH_2$ (0.414 mmol) was added and the precipitate dissolved by heating for 12 hour at 90 °C. The solution was slowly cooled at 2 °C h^{-1} to room temperature. A yellow single crystal suitable for X-ray diffraction analysis was selected and studied. Elemental analysis (%). Found: C 21.11, H 4.02, N 3.51. Calc. for $C_{21}H_{48}I_5N_3Pb_1$: C 21.30, H 4.08, N 3.55.

Preparation of $[(C_8H_{15}NH_3)PbI_3]$, 6. 0.066 g PbI_2 (0.143 mmol) was dissolved in 6 ml 47% HI in a glass vial. Thereafter, 0.035 g $C_8H_{15}NH_2$ (0.275 mmol) was added and the precipitate dissolved by refluxing for 3 hours at 113 °C. The solution was slowly cooled at 2 °C h^{-1} to room temperature. A yellow single crystal suitable for X-ray diffraction analysis was selected and studied. Elemental analysis (%). Found: C 13.77, H 2.60, N 1.95. Calc. for $C_8H_{18}I_3N_1Pb_1$: C 13.42, H 2.53, N 1.97.

X-Ray crystallography

Intensity data were collected on a Bruker SMART 1K CCD area detector diffractometer with graphite monochromated

Table 4 Crystal data for **1**, **2**, **3**, **4**, **5** and **6**

	1	2	3	4	5	6
Formula	$C_6H_{16}I_4N_2Pb$	$C_8H_{20}I_4N_2Pb$	$C_{10}H_{24}I_4N_2Pb$	$C_{12}H_{28}I_4N_2Pb$	$C_{21}H_{48}I_5N_3Pb$	$C_8H_{18}I_3NPb$
M_r	831.00	867.03	887.10	915.15	1184.31	716.12
Temperature/K	173	173	293	173	173	173
Crystal size/mm	0.20 × 0.06 × 0.04	0.36 × 0.28 × 0.05	0.38 × 0.24 × 0.04	0.34 × 0.22 × 0.05	0.43 × 0.40 × 0.17	0.30 × 0.11 × 0.03
Crystal system	Monoclinic	Monoclinic	Monoclinic	Orthorhombic	Monoclinic	Orthorhombic
Space group	$P2_1/c$	$P2_1/c$	$P2_1/c$	$Pbca$	$C2/c$	$P2_12_12_1$
a/Å	12.475(5)	13.355(3)	14.00(2)	9.1677(15)	34.587(5)	7.9889(12)
b/Å	8.656(5)	8.3560(17)	8.928(14)	8.7335(14)	8.7821(12)	8.6291(13)
c/Å	8.750(5)	9.0583(18)	8.949(15)	27.276(5)	26.662(3)	22.455(3)
α/°	90	90	90	90	90	90
β/°	110.275(5)	107.747(4)	108.57(4)	90	124.255(2)	90
γ/°	90	90	90	90	90	90
V/Å^3	886.3(8)	962.7(3)	1060(3)	2183.9(6)	6693.8(15)	1548.0(4)
Z	2	2	2	4	8	4
D_{calc}/g cm^{-3}	3.114	2.963	2.778	2.783	2.350	3.073
μ(Mo Ka)/mm^{-1}	16.459	15.158	13.765	13.373	9.666	16.851
θ range/°	1.74 to 28.00	1.60 to 28.00	1.53 to 28.00	1.49 to 28.00	1.58 to 28.00	1.81 to 27.99
No. unique data	2105	2297	1864	2633	8054	3743
No. data with $I \geqslant 2\sigma(I)$	1466	1962	1625	1986	6809	3313
$R1$	0.0386	0.0264	0.0930	0.0315	0.0351	0.0423
$wR2$ (all data)	0.1034	0.0573	0.2610	0.0748	0.0870	0.1019
Absolute parameter[22]	—	—	—	—	—	0.286(9)

Mo Kα radiation (50 kV, 30 mA). The collection method involved ω-scans of width 0.3°. Data reduction was carried out using the program SAINT+, version 6.02[16] and face indexed absorption corrections were made using the program XPREP.[16]

The crystal structure was solved by direct methods using SHELXS-97.[17] Non-hydrogen atoms were first refined isotropically followed by anisotropic refinement by full matrix least-squares calculations based on F^2 using SHELXL-97.[17] Hydrogen atoms were first located in the difference map then positioned geometrically and allowed to ride on their respective parent atoms. Diagrams and publication material were generated using WinGx,[18] ORTEP,[19] PLATON[20] and DIAMOND.[21] Further crystallographic data are summarised in Table 4.

CCDC reference number 609992. For crystallographic data in CIF or other electronic format see DOI: 10.1039/b618196a

Acknowledgements

The University of the Witwatersrand and the National Research Fund (GUN: 2069064) is thanked for the award of a research grant and for providing the infrastructure required to do this work. The authors thank Mike F. Philpott for elemental analysis work.

References

1 (*a*) D. B. Mitzi, K. Chondroudis and C. R. Kagan, *IBM J. Res. Dev.*, 2001, **45**, 29; (*b*) I. B. Koutselas, L. Ducasse and G.C. Papavassiliou, *J. Phys.: Condens. Matter*, 1996, **8**, 1217; (*c*) P. Day, *Philos. Trans. R. Soc. London, A*, 1985, **314**, 145; (*d*) D. B. Mitzi, *J. Mater. Chem.*, 2004, **14**, 2355; (*e*) R. Willett, H. Place and M. Middleton, *J. Am. Chem. Soc.*, 1988, **110**, 8639; (*f*) K. Matsuishi, T. Ishihara, S. Onari, Y. H. Chang and C. H. Park, *Phys. Status Solidi B*, 2004, **241**, 3328.
2 X. Hong, T. Ishihara and A. V. Nurmikko, *Solid Sate Commun.*, 1992, **84**, 657.
3 C. R. Kagan, D. B. Mitzi and C. D. Dimitrakopoulos, *Science*, 1999, **286**, 945.
4 V. M. Goldschmidt, *Naturwissenschaften*, 1926, **21**, 477.
5 P. M. Woodward, *Acta Crystallogr., Sect. B: Struct. Sci.*, 1997, **53**, 44.
6 A. M. Glazer, *Acta Crystallogr., Sect. B: Struct. Crystallogr. Cryst. Chem.*, 1972, **28**, 3384.
7 H. F. Kay and P. C. Bailey, *Acta Crystallogr.*, 1957, **10**, 219.
8 R. D. Shannon, *Acta Crystallogr., Sect. A*, 1976, **32**, 751.
9 A. Poglitsch and D. Weber, *J. Chem. Phys.*, 1987, **87**, 6373.
10 D. B. Mitzi, *Prog. Inorg. Chem.*, 1999, **48**, 1.
11 D. M. Hatch, H. T. Stokes, K. S. Aleksandrov and S. V. Miguel, *Phys. Rev. B: Condens. Matter Mater. Phys.*, 1989, **39**, 9282.
12 M. Era, K. Maeda and T. Tsutsui, *Chem. Phys. Lett.*, 1998, **296**, 417.
13 D. Cremer and J. A. Pople, *J. Am. Chem. Soc.*, 1975, **97**, 1354.
14 D. G. Billing and A. Lemmerer, *CrystEngComm*, 2006, **8**, 686.
15 A. Lemmerer and D. G. Billing, unpublished result.
16 Bruker, SAINT+. Version 6.02 (includes XPREP and SADABS). Bruker AXS Inc., Madison, WI, USA.
17 G. M. Sheldrick, SHELX, release 97-2 (includes SHELXS and SHELXL), University of Göttingen, 1997.
18 L. J. Farrugia, *J. Appl. Crystallogr.*, 1997, **30**, 565.
19 L. J. Farrugia, *J. Appl. Crystallogr.*, 1999, **32**, 837.
20 A. L. Spek, *J. Appl. Crystallogr.*, 2003, **36**, 7.
21 K. Brandenburg, Diamond. Version 2.1e., Crystal Impact GbR, Bonn, Germany.
22 H. D. Flack, *Acta Crystallogr., Sect. A: Found. Crystallogr.*, 1983, **39**, 876–881.

This journal is © The Royal Society of Chemistry 2007

4.5 Inorganic-organic hybrid materials combining primary cyclic ammonium cations with bromoplumbate and chloroplumbate anions

Journal: CrystEngComm

Date Submitted: Pending, before 30 April 2007

Reference Code of Submitted Article:

Date Accepted:

Final Reference:

Brief Synopsis

This paper, presenting the structures of 12 inorganic-organic hybrids, is a continuation of the work started in Chapter 4.4. In this paper, the same metal and counter cations are used as in Chapter 4.4 but using the halides bromide and chloride instead. This paper discusses the trends observed in the bromide and chloride series and then summarizes the results together with the iodide series.

CREATED USING THE RSC ARTICLE TEMPLATE (VER. 2.0) - SEE WWW.RSC.ORG/ELECTRONICFILES FOR DETAILS

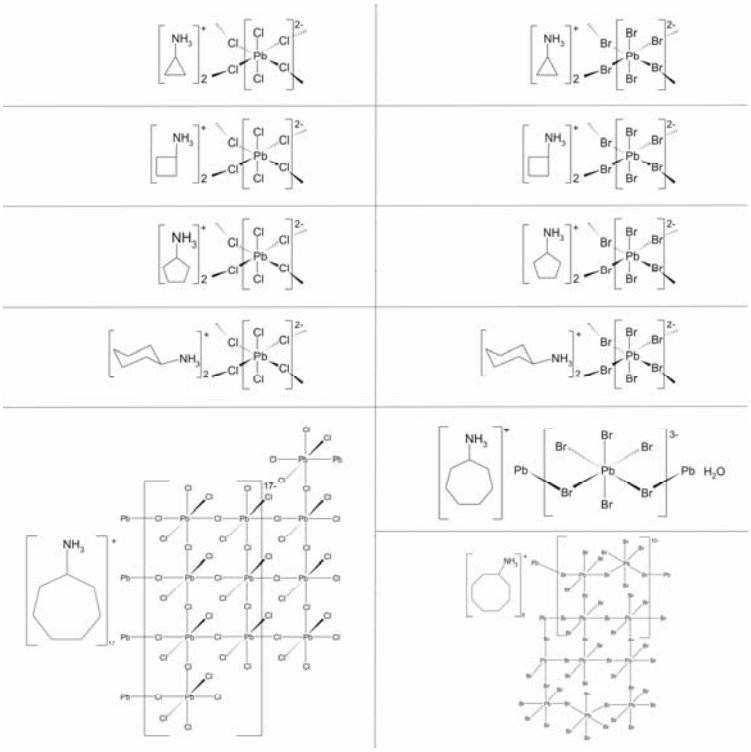
[JOURNAL NAME HERE] | www.rsc.org/[JOURNAL] Article

Inorganic-organic hybrid materials combining primary cyclic ammonium cations with bromoplumbate and chloroplumbate anions

David G. Billing and Andreas Lemmerer

Receipt/Acceptance Data **[DO NOT ALTER/DELETE THIS TEXT]**
Publication data **[DO NOT ALTER/DELETE THIS TEXT]**
DOI: 10.1039/b000000x [DO NOT ALTER/DELETE THIS TEXT]

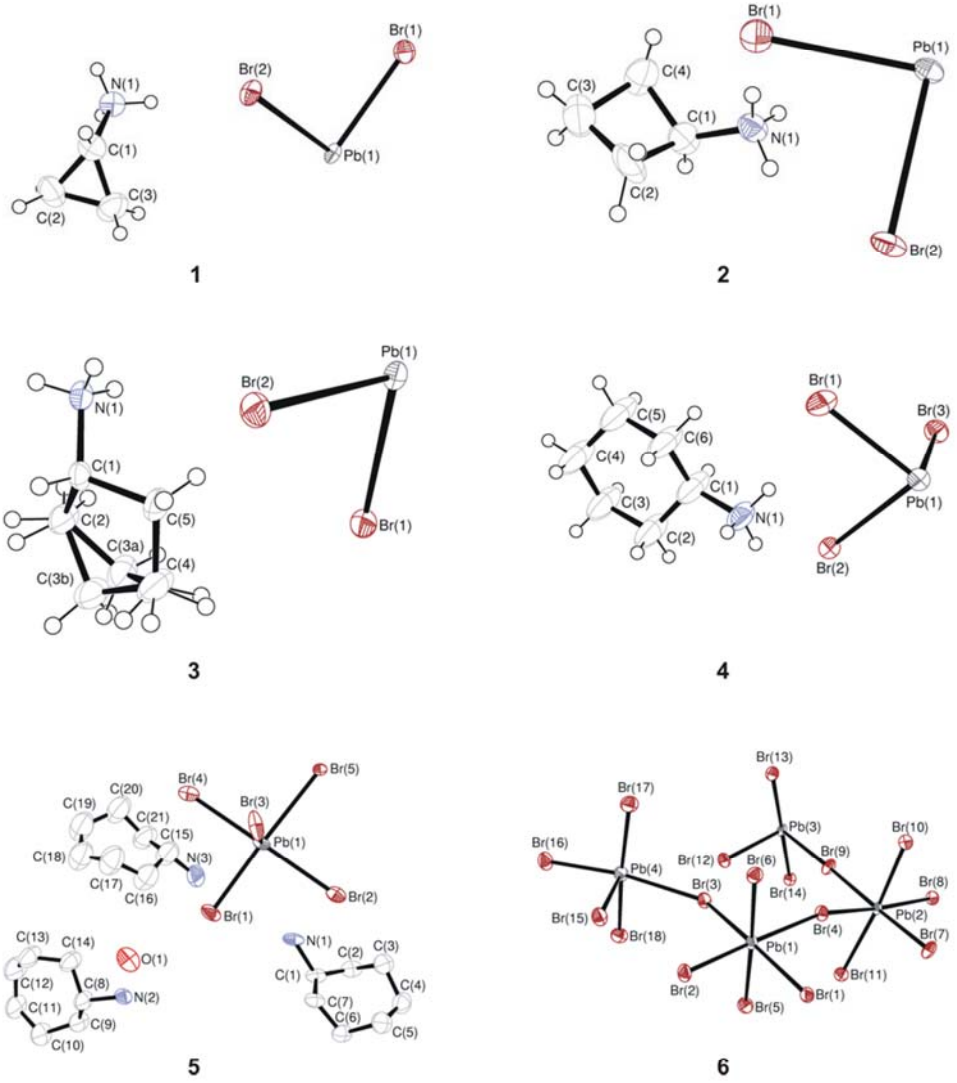
12 inorganic-organic hybrids have been synthesized and characterised by Single-crystal X-Ray diffraction experiments. The inorganic component is based on lead(II) bromide and lead(II) chloride units and the organic component various cyclic hydrocarbons with only a primary ammonium group as a ring substituent. If the organic component is cyclopropylammonium, cyclobutylammonium, cyclopentylammonium and cyclohexylammonium, the inorganic motif observed is based on the cubic perovskite structure type and consists of 2-D layers of corner-sharing octahedra, in the ratio of 1:2 inorganic-organic. Lead(II) bromide and cycloheptylammonium combined to give 1-D chains of corner-sharing $PbBr_6$ octahedra and similarly, lead(II) bromide and cyclooctylammonium gave 1-D ribbons of corner-sharing $PbBr_6$ octahedra. Lead(II) chloride and cycloheptylammonium has a ribbon motif and lead(II) chloride and cyclooctylammonium has 2-D layers of corner-, edge- and face-sharing octahedra. These results are compared with a similar study involving lead(II) iodide units and the same set of six cations. General trends and conclusions are discussed.



Molecular Sciences Institute, School of Chemistry, University of the Witwatersrand, PO WITS 2050, Johannesburg, South Africa.. E-mail: dave@hobbes.gh.wits.ac.za; Fax: 27 11 7176749; Tel: 27 11 717 6759

Electronic Supplementary Information (ESI) available: Table of hydrogen bonding details for compounds **6**, **11** and **12**. See http://dx.doi.org/10.1039/b000000x/

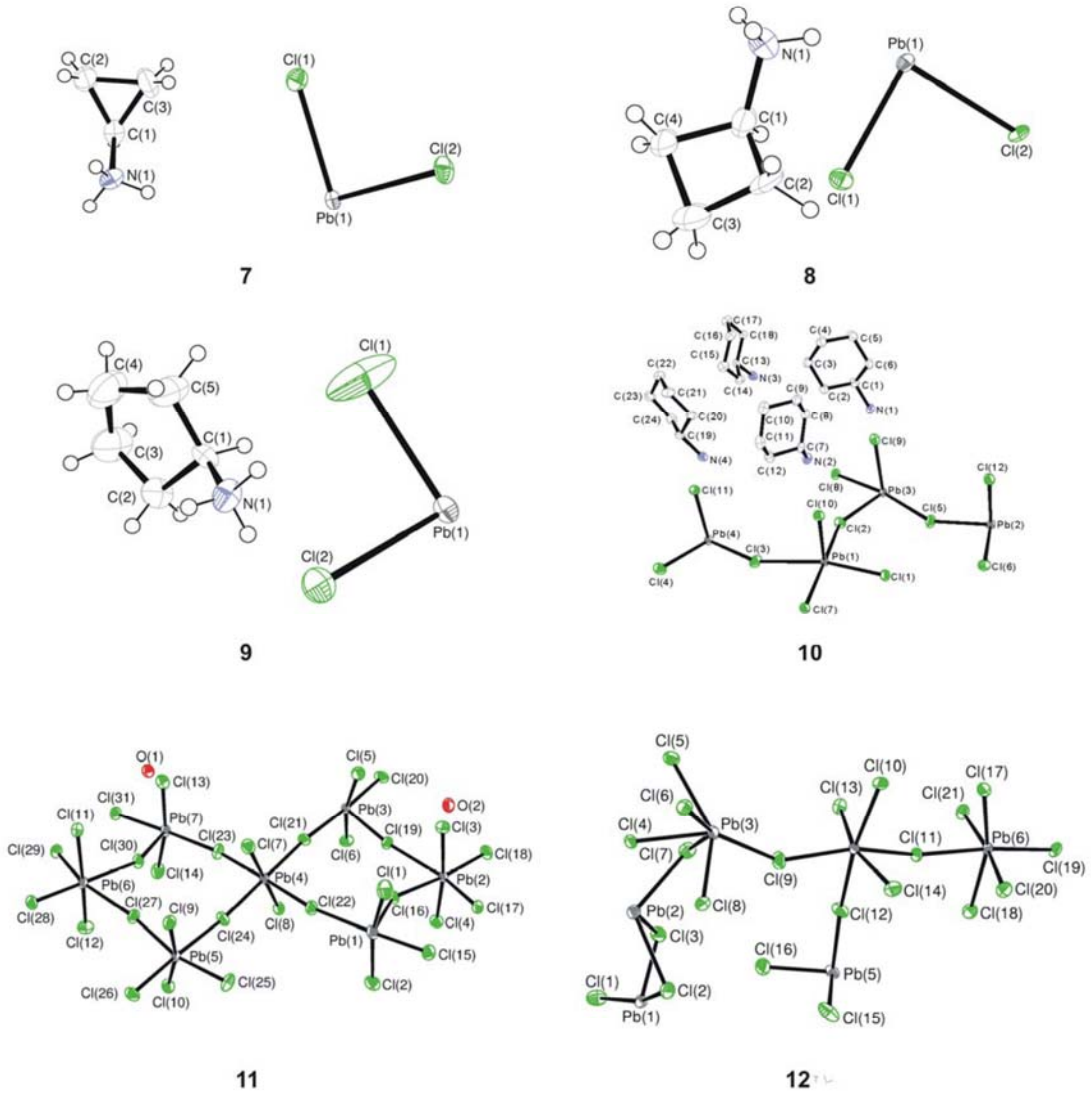
CREATED USING THE RSC ARTICLE TEMPLATE (VER. 2.0) - SEE WWW.RSC.ORG/ELECTRONICFILES FOR DETAILS



25 **Fig. 1** The contents of the asymmetric unit for structures **1**-**6**, showing the atomic numbering scheme. Displacement ellipsoids are shown at the 50% probability level. The H atoms are omitted for clarity in **5** and only the asymmetric unit of the inorganic part is shown for compound **6**.

 This journal © Royal Society of Chemistry

CREATED USING THE RSC ARTICLE TEMPLATE (VER. 2.0) - SEE WWW.RSC.ORG/ELECTRONICFILES FOR DETAILS



30 **Fig. 2** The contents of the asymmetric unit for structures **7**-**12**, showing the atomic numbering scheme. Displacement ellipsoids are shown at the 50% probability level. Only the inorganic part is shown for compounds **11** and **12**. Hydrogen atoms are excluded for clarity in compound **10**.

CREATED USING THE RSC ARTICLE TEMPLATE (VER. 2.0) - SEE WWW.RSC.ORG/ELECTRONICFILES FOR DETAILS

Introduction

Inorganic-organic hybrids with the general formula $[(R\text{-}NH_3)_2MX_4]$, where M is any divalent metal and X = Cl, Br and I, have shown a great propensity for structural diversity. The choice of the ammonium cation, which can be anything from long alkylammonium chains to complex aromatic structures influences the motif of the inorganic component. If the inorganic part has 2-D layers of corner-sharing MX_6 octahedra, otherwise known as a layered perovskite-type motif, then these compounds form natural quantum well materials that show photoluminescence, electroluminescence and nonlinear optical properties.[1]

Organic ammonium cations with cyclic hydrocarbon rings are able to template the structure or motif of the inorganic moiety. The compounds $[(C_nH_{2n-1}NH_3)_2PbI_4]$, where the size of the ring is increased from three carbon atoms, n = 3, to eight, n = 8, generate such a templating effect.[2] If n = 3 - 6, the lead(II) iodide units have the layered perovskite-type motif, and when n = 7 or 8, the corresponding motif has 1-D chains of corner-sharing and face-sharing PbI_6 octahedra respectively. The relationship between the various motifs was introduced in the previous article. In this study, the effect of halide identity on the same system is investigated by crystallizing out 12 new compounds with general formula $[(C_nH_{2n-1}NH_3)_2PbX_4]$, X = Br and Cl, n = 3-8.

Results and Discussion

The lead bromide series

Crystallographic description of the layered perovskite-type hybirds with cyclopropylammonium, cyclobutylammonium, cyclopentylammonium and cyclohexylammonium: $[(C_3H_5NH_3)_2PbBr_4]$ (1), $[(C_4H_7NH_3)_2PbBr_4]$ (2), $[(C_5H_9NH_3)_2PbBr_4]$ (3) and $[(C_6H_{11}NH_3)_2PbBr_4]$ (4)

The asymmetric unit of **1**, **2** and **3** consists of one lead atom, on a special position in the space group $P2_1/c$ and two bromides, Br(1) and Br(2), on general positions. The two bromides are cis to each other with the terminal bromide Br(1) facing in the a direction whereas the single unique bridging bromide Br(2) lies in the *bc*-plane. The bromides *trans* to Br(1) and Br(2) are completed via the inversion centre at the special position and the bromides *cis* via the 2-fold screw axis. The shared halides on each octahedra bridge to the adjacent octahedra to form the infinite organic sheets. The unit cell consists of two layers at x = 0 and 1 that eclipse each other when viewed down the a-axis. The lead halide distance to the terminal bromides decrease from 3.0005(11) Å (**1**) to 2.8859(11) Å (**3**). The bridging bromides *cis* to each other have similiar bond distances to the central lead atom and are slightly longer than the terminal distances. The ammonium groups sit in 'boxes' defined by four corner-sharing octahedra and are held in place by hydrogen bonding to two terminal bromides and one bridging bromide. This type of hydrogen bonding is classified as terminal halogen configuration and is the same for **1-4** (See Table 2 and Fig. 6). Adjacent octahedra are rotated relative to each other with bridging angles far from 180°. The bridging angles Pb(1)-Br(2)-Pb(1) are 146.29(3)°, 148.60(3)° and 153.50(3)° for **1**, **2** and **3** respectively. This rotation is also known as a θ tilt of the octahedra and is the deviation from 180°.[3] The octahedra experience another tilt that is perpendicular to the θ tilt. The Ψ tilt[3] quantifies the degree of corrugation of the inorganic layers along one unique direction, in compunds **1-3** along the *b*-axis, and is greatest in **1** and **2** and decreases in **3**. The bilayers of the organic cyclic cations determine the interlayer spacing and inceases from 12.400(3) Å to 13.429(3) Å as the ring size increases from three to five-membered. The position of the ammonium group in the hole depends on minimizing the interaction between the carbons closest to the nitrogen and the terminal bromides. The atomic numbering scheme for the cations is shown in Fig. 1. The organic cations are well ordered between the inorganic layers in **1** and **2** but the cyclopentylammonium molecule in **3** is disordered within the inorganic layer as one of the carbon atoms, C(3), flips above and below the plane of the other ring atoms. The ratio of major to minor is 52 to 48% and the five-membered ring has an envelope conformation in the major component and a planar conformation in the minor component.

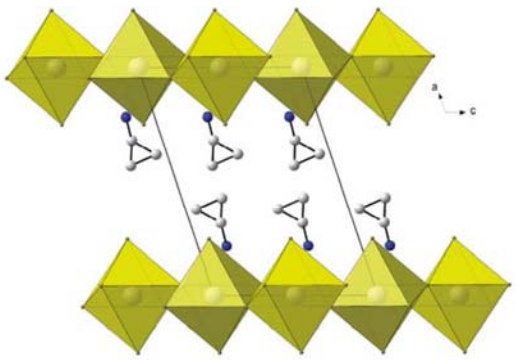


Fig. 3 View of **1** parallel to the inorganic layers.

The first three hybrids have an isomorphous packing arrangements of the inorganic layer, i.e. the three oganic cations used have little effect on the inorganic motif. A change occurs when the organic cation is cyclohexylammonium. In structure **4**, the asymmetric unit consists of $PbBr_3^-$ units in the space group $Cmc2_1$. The lead atom and both bridging bromides Br(2) and Br(3) lie on special positions on the *bc*-plane with the terminal Br(1) on a general position. Whereas the previous layered perovskite-type hybrids had only one complete layer per unit cell (Fig. 3), **4** has two complete layers (Fig. 4). This is achived by doubling the unit cell along the *a*-axis and inserting a layer at x = 0.5. This middle layer is staggered relative to the layers at x = 0 and 1. The doubling of the unit cell is accompanied by a change from a monoclinic unit cell to an orthorhombic one. The number of unique lead bromide bond distances in the octahedra has increased to five. The terminal Pb(1)-Br(1)

This journal © Royal Society of Chemistry

CREATED USING THE RSC ARTICLE TEMPLATE (VER. 2.0) - SEE WWW.RSC.ORG/ELECTRONICFILES FOR DETAILS

distance is 2.9686(11) Å and the four bridging Pb(1)-Br(2) and Pb(1)-Br(3) distances range from 3.0049(17) Å to 3.1176(15) Å.

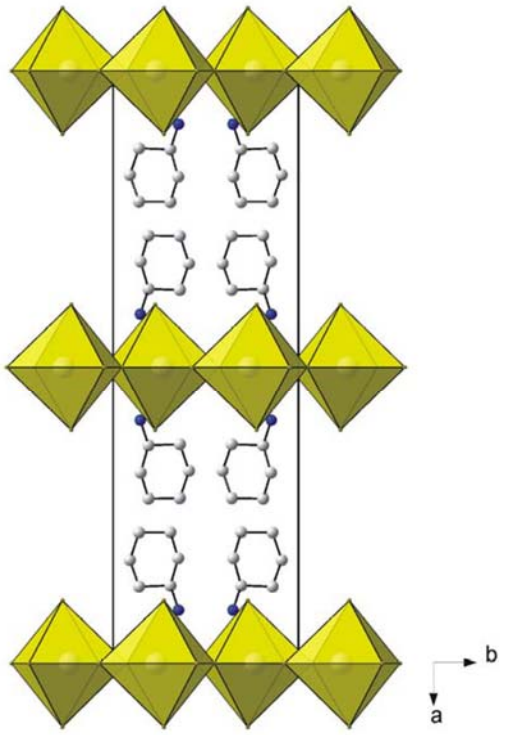


Fig. 4 View of **4** parallel to the inorganic sheets of a single unit cell.

The ammonium group is situated in different positions within the holes generated by the four corner-shared $PbBr_6$ octahedra. The position also determines the geometry of the hydrogen bonding of the ammonium group. A way of describing the position is to consider the four bridging bromides as arranged in a parallelogram and projecting the position of the ammonium group on this parallelogram (See Fig. 5). If the ammonium group is close to the corner of the parallelogram that has an obtuse angle, one hydrogen will bond to the bridging bromide at the opposite corner and hydrogen bond to the two terminal iodides that would be at the corners of an equilateral triangle. This subtype is called the equilateral configuration (Fig 5a). The other extreme, when the ammonium group is close to an acute angled corner of the parallelogram, the two terminal iodides and the bridging iodide form a right-angled triangle. This is called the right-angled configuration (Fig 5b). The intermediate position is when the ammonium group is at the centre of the parallelogram, where the diagonals intersect. This position can either have the equilateral or right-angled configuration.

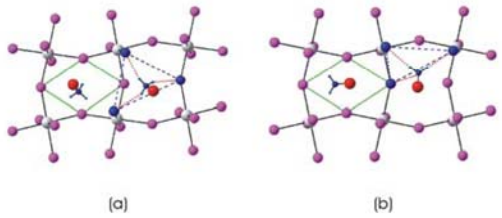


Fig. 5 The obtuse angled position is shown on the left with the parallelogram, consisting of the bridging halides at the corners, in green and the equilateral configuration, in blue. The picture on the right shows the right-angled configuration when the ammonium group is in the acute angled position.

In **1**, the ammonium group of the cyclopropylammonium cation is in the obtuse position whereas the cyclobutylammonium in **2** sits in the centre of the parallelogram, not far from where the diagonals would intersect. Both compounds have the equilateral configuration (See Table 2 for hydrogen bonding details). The change-over to the acute angled position is observed when the ring is larger than four carbon atoms. The five- and six-membered rings in **3** and **4** have now aligned themselves along the long diagonal of the parallelogram (Fig. 6) and the rings are able to move closer to the inorganic layer. The cations now have the right-angled configuration (See Table 2). This is further evidenced by comparing the tilt of the ammonium groups in all four hybrids. The angle $\angle_\beta$ between a vector connecting the nitrogen atom N(1) and the carbon atom it is attached to on the ring, C(1), is 35.5(4)° and 36.5(4)° away from the normal to the inorganic layers for cyclopropylammonium and cyclobutylammonium respectively. The tilt angle reaches a maximum in **3**, where cyclopentylammonium is tilted at the greatest angle away from the normal, 45.1(3)°. The angle decreases to 38.9(5)° in **4** as the chair conformation of the cyclohexane ring takes up more space than the envelope or flat conformation of the cyclopentane ring.

CREATED USING THE RSC ARTICLE TEMPLATE (VER. 2.0) - SEE WWW.RSC.ORG/ELECTRONICFILES FOR DETAILS

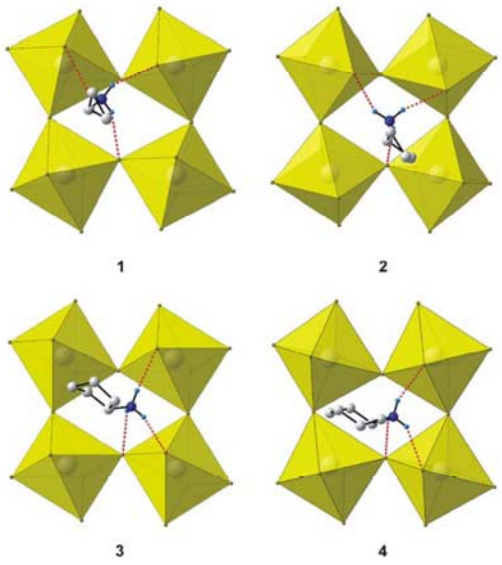


Fig. 6 Magnified top views of the hydrogen bonding geometries of compounds **1**-**4**, showing the more tilted octahedra of **1** and **2** compared to **3** and **4** and the position of the ammonium group relative to the corner-sharing octahedra.

Crystallographic description of the zig-zag motif with cycloheptylammonium: $[(C_7H_{13}NH_3)_3PbBr_5 \cdot H_20]$ (5)

In a previous paper, where the lead iodide series was investigated, we postulated that the increased size of the seven-membered ring sterically prevented the lead(II) iodide hybrid from forming 2-D layers of corner-shared octahedra. Instead, every third row of corner-shared octahedra is missing, resulting in a 1-D inorganic motif. The same motif is observed in compound **5**, which has the iodide atom replaced by bromide. The structure of **5** has the same bidimensional arrangement as $[(C_7H_{13}NH_3)_3PbI_5]$, in which two layers of non-interdigitated cycloheptylammonium molecules are embedded between two consecutive inorganic $[PbBr_6]$ chains, forming an alternated organic-inorganic structure (Fig. 7). The inorganic layer contains four chains of corner-sharing $[PbBr_6]$ octahedra running along the *a*-axis and the hydrocarbon layer is comprised of both cyclohepylammonium moieties and water molecules. In the direction perpendicular to the chains, the crystal cohesion is achieved by N-H...Br, N-H…O and O-H…Br hydrogen bonds, related to the NH_3 polar groups on one end and by van der Waals forces between the hydrocarbon rings on the opposite end (nearest neighbour distance is 3.716(1) Å). In the direction parallel of the chains, the cohesion is archieved by strong ionic bonds between bromide and lead atoms.

The asymmetric unit consists of a lead atom and five bromide atoms occupying general positions. Br(1), Br(3) and Br(5) occupy the axial positions and Br(2) and Br(4) the equatorial positions. Br(5) and its symmetry related equivalent Br(5)' [symmetry operator: x+1/2,-y+1/2,-z] complete the octahedral coordination sphere. The octahedra share corners via two bromides, here Br(5), and since they are cis to each, the chain zig-zags. The bridging angle between two octahedra is almost linear, 165.72(9)°. The bond distances to the bridging bromides Br(5) and Br(5) are the longest, 3.160(3) Å and 3.168(3) Å, and to the bromides trans to the bridging bromides the shortest, Br(1) (2.907(3) Å) and Br(3) (2.908(3) Å). The Pb-Br distances to the axial bromides are intermediate at 3.012(4) Å and 3.036(3) Å. The angle between cis related bromide atoms deviate from 90°, and the trans angles from 180°.

The three cycloheptylammonium molecules in the asymmetric unit occupy general positions. The atomic numbering scheme is shown in Fig. 1. The rings are labeled cat1 (containing atom N(1)), cat2 (N(2)) and cat3 (N(3)) similar to the nitrogen atoms. Cat1 and cat3 sit above the chains in the gaps formed by the corner-shared octahedra. Cat2 occupies the space between the chains. The molecules are well ordered and all the seven-membered rings have a chair conformation.

The hydrogen bonds between the organic and inorganic entities adopt two different hydrogen bonding configurations with bromide atoms. N(1) has an axial configuration whereas N(3) has an equatorial configuration. The hydrogen acceptor distances from N(1) to the axial halides Br(3) and Br(5) are 2.53 Å and 2.81 Å and to the equatorial halide Br(2) 2.49 Å. The hydrogen acceptor distances from N(3) to the equatorial halides Br(4) and Br(2) are 2.46 Å and 2.54 Å and to the axial halide Br(5) 2.86 Å. N(2) occupies the space between the chains and forms one hydrogen bridge each to the two chains. The distances to the chains are 2.66 Å and 2.77 Å. The water molecules are in between the chains and so the oxygen molecule acts as an acceptor atom to the third hydrogen on N(2). The N(2)-H(2A)...O(1) distance is the shortest of all distances (1.91 Å) as the radius of the oxygen atom is smaller than the bromide atoms. The water molecule itself bonds to the equatorial halides Br(3) and Br(1) on neighbouring chains, 2.43 Å and 2.53 Å respectively.

This journal © Royal Society of Chemistry

CREATED USING THE RSC ARTICLE TEMPLATE (VER. 2.0) - SEE WWW.RSC.ORG/ELECTRONICFILES FOR DETAILS

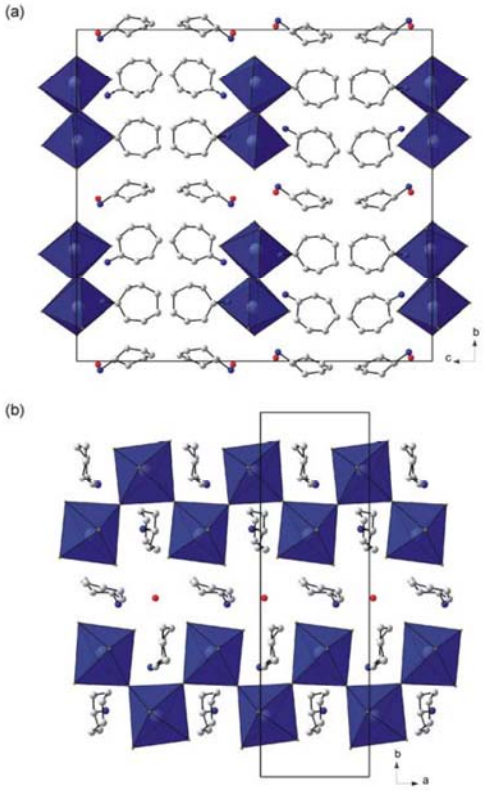


Fig. 7 (a) Packing of 5, showing the four corner-sharing chains extending along the *a*-axis. (b) The view above the chains.

Crystallographic description of the ribbon motif with cyclooctylammonium: $[(C_8H_{15}NH_3)_{10}Pb_4Br_{18}]$ (6)

Both lead iodide and lead bromide do not form the layered perovskite-type motif with cyclooctylammonium. In the former case, the inorganic motif consisted of 1-D chains of face-sharing octahedra and one unique cyclooctylammonium moiety in the asymetric unit.[2] The latter case has a never before seen inorganic motif that has layers of corner-shared octahedra similar to the layered perovskite-type motif but instead of extending in two dimensions, every fifth row is missing and hence only one-dimensional ribbons of octahedra extend along the *a*-axis (Fig. 8). The border of the ribbon has alternating octahedral and trigonal-prismatic shaped lead bromide units.

There are three types of corner-sharing octahedra involving $PbBr_6$ units: Pb(1) and Pb(3) share three of their equatorial bromides to adjacent octahedra. They have similiar distortions from the ideal octahedral geometry as the cis angles between the bromides range from 83.98(4)° to 95.41(4)°. The maximum deviation from 180° for the trans angles is 172.38(4)° (Pb(1)) and 176.93(4)° (Pb(3)). Pb(2) shares all four of its equatorial bromides and hence has the same connectivity as the octahedra in the layered perovskite-type hybrids seen in **1**, **2**, **3** and **4**. The cis angles range from 81.18(4)° to 91.20(4)° and the trans angles from 170.19(4)° to 175.87(4)°. Pb(4) shares only two of its bromides and both of them to Pb(1). However, the bromides that Pb(1) shares to Pb(4) are trans related whereas the bromides on Pb(4) are cis related to form a chain in the manner [cis-trans-cis-trans] as the repeating unit. To accomodate this type of sharing, the cis angles between the corner-sharing bromides in Pb(4) is 113.86(3)°. Pb(4) defines the outer boundary of the one-dimensional slabs as it is not in line with Pb(1) but deviates by 1.77 Å along the c-direction. Pb(2) and Pb(3) occupy the centres of the slabs. The lead bromide bond lengths are in a narrow range for the $PbBr_6$ octahedra that share three or four corners [2.8465(14) Å to 3.2168(14) Å]. Due to the unusual sharing of Pb(4), the result is a lengthening of the lead bromide distances to the particular bromides that are shared [Pb(4)-Br(1): 3.4549(14) Å and Pb(4)-Br(3): 3.3619(14) Å].

There are ten unique cyclooctylammonium cations in the asymmetric unit, labelled cat1(containing atom N(1)), cat2 (N(2)), etc. These can be subdivivded into five pairs, each pair runs along the a-axis and is associated exclusively with a particular row above the chains (See Fig. 8). The hydrocarbon rings of two of the ten cations, cat8 and cat9, are not well ordered in the crystal structure and the conformation of their eight membered rings do not appear in any of the ten canonical forms that exist.[4] The remaining eight rings have the thermodynamically preferred boat-chair conformation.

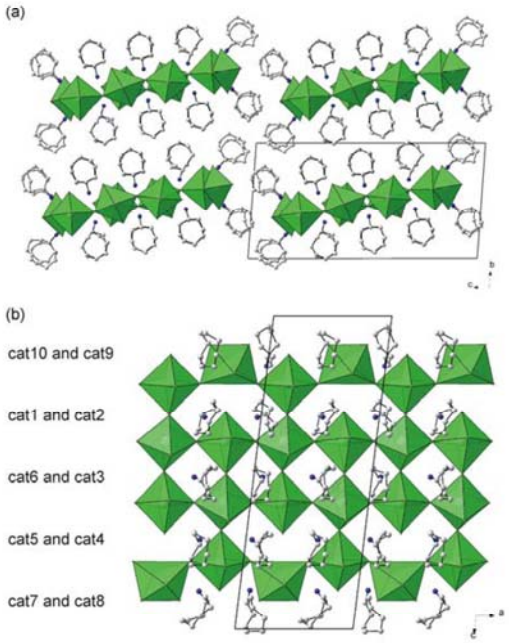


Fig. 8 (a) Each unit cell contains one 1-D ribbon motif in **6**. In between the ribbons, the cyclooctylammonium cations form bilayers. (b) Magnified top view of the structure of the 1-D ribbons, and the regular positions of the ten cations.

CREATED USING THE RSC ARTICLE TEMPLATE (VER. 2.0) - SEE WWW.RSC.ORG/ELECTRONICFILES FOR DETAILS

The lead chloride series

Crystallographic description of the hybrids with cyclopropylammonium and cyclobutylammonium: $[(C_3H_5NH_3)_2PbCl_4]$ (7) and $[(C_4H_7NH_3)_2PbCl_4]$ (8)

Compounds **7** and **8** are isomorphous to **1** and **2** and to $[(C_3H_5NH_3)_2PbI_4]$ and $[(C_4H_7NH_3)_2PbI_4]$ described previously.[2] All six structures crystallize in the same space group, $P2_1/c$, and have similar cell dimensions. The atomic numbering scheme for **7** and **8** is shown in Fig. 2. The lead halide series is now complete for the inoganic-organic hybrids with cyclopropylammonium and cyclobutylammonium cations and a comparison of the effect of halide on the crystal strucutres and packing can be discussed.

Discussion of all six layered perovskite-type hybrids with general formula $[(C_nH_{2n-1}NH_3)_2PbX_4]$, n = 3 and 4 and X = Cl, Br and I.

Table 3 summarises the most important structural features that can be measured in these inorganic-organic hybrids that have the layered perovskite-type motif. The interlayer spacing is the distance between two consecutive inorganic corner-sharing layers and is the length of the *a*-axis of the unit cell. There is an increase as the radius of the halide increases from chloride to bromide to iodide and when the size of the ring goes from three- to four-membered. The size of the ring has the largest effect as the spacing increases by an average of 0.92 Å, regardless of the identity of the halide. The inorganic layers are eclipsed in all structures.

The octahedral coordination of the PbX_6 octahedra remains invariant right throughout the series. The average Pb-X bond lengths change as the halide atom is changed. The cyclopropyl- or cyclobutylammonium molecules have no effect on the θ and Ψ tilts of the octahedra. There is little steric influence as the cations are small. This is most evident when comparing the areas that the corner-shared octahedra provide to accomodate the cations. They are generally the same for each halide, even if the cation is different and only increase as the bond lengths increase. For example, the areas for $[(C_3H_5NH_3)_2PbBr_4]$ and $[(C_4H_7NH_3)_2PbBr_4]$ differ by only 0.78 $Å^2$, even though the ring size is different.

At the interface where the inorganic and organic components interact there is some deviation. The position of the cations relative to the octahedra is different in $[(C_3H_5NH_3)_2PbBr_4]$ and $[(C_3H_5NH_3)_2PbI_4]$. These two compounds have their ammonium group at the obtuse corner of the parallelogram whereas the remaing four are all at the centre. The hydrogen bonding configuration is the same nonetheless (equilateral). The most outstanding feature however is the angle that the organic cations make to the plane of the inorganic layers. The cyclobutylammonium series has the three angles ina narrow range and average out to 86.(2)°. The cations are almost perpendicular to the layers. The cyclopropylammonium series has angles of 60.760° and 61.945° when the halide is chloride and bromide but this drops to 15.225(221)° when the halide is iodide. The cyclopropylammonium ring is the most parallel to the layers compared to any of the other ring sizes chosen in this study. This must be due to the combination of the smallest cation and the largest halide in terms of size and radius.

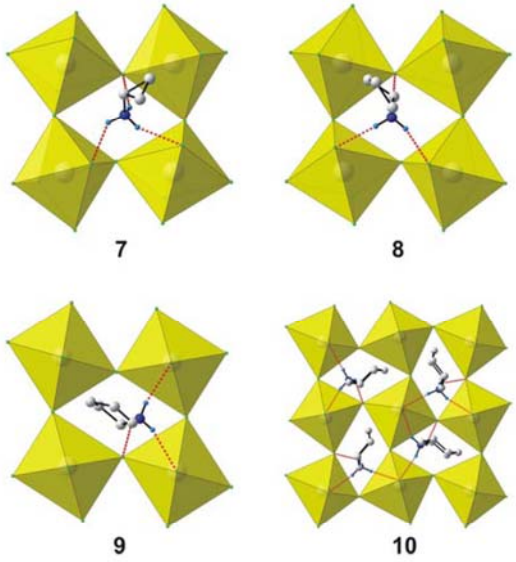


Fig. 9 Magnified top views of the hydrogen bonding geometries of the lead chloride series of compounds **7-10**, showing the more tilted octahedra of **7** and **8** compared to **9** and **10** and the position of the cations relative to the corner-sharing octahedra.

Crystallographic description of the layered perovskite-type hybrids with cyclopentylammonium and cyclohexylammonium: $[(C_5H_9NH_3)_2PbCl_4]$ (9) and $[(C_6H_{11}NH_3)_4Pb_2Cl_8]$ (10)

The crystal structure of 9.

The hybrid $[(C_5H_9NH_3)_2PbCl_4]$ is unique as the inorganic layer is situated on a mirror plane and is not corugated at all. Figure 10 clearly underlines a bidimensional arrangement in which two layers of non-interdigitated cyclopentylammonium molecules are embedded between two consecutive inorganic $[PbCl_6]$ sheets, forming an alternated organic-inorganic layered structure. The lead atoms are not aligned from layer to layer, resulting in a staggered arrangement of adjacent layers.

The inorganic layer is built up from characteristic corner-sharing $PbCl_6$ octahedra. The asymmetric unit consists of a lead atom on a special position and two chloride atoms, Cl(1) occupying the axial position and Cl(2) occupying the equatorial position in the octahedra. Both chlorides are on special positions as well. Pb(1) and Cl(2) sit on a mirror plane perendicular to the *a*-axis, parallel to the plane of the inorganic layers. Hence, the octahedra are not tilted (Ψ tilt = 0°) and the vector joining the two chlorides in the axial positions of the octahedra is parallel to the *a*-axis. However, adjacent octhaedra are still rotated relative to each other by 154.80(12)° (θ tilt = 25.20(12)°). The coordination geometry around the Pb atom shows axial compression of the octahedral

 This journal © Royal Society of Chemistry

CREATED USING THE RSC ARTICLE TEMPLATE (VER. 2.0) - SEE WWW.RSC.ORG/ELECTRONICFILES FOR DETAILS

geometry, with the bridging Pb(1)-Cl2 distances longer than the axial distances Pb(1)-Cl1 (Table 3). The angles between Cl(1) and Cl(2) are all 90° and between individual bridging chlorides 95.66(2)° and 84.34(2)°, with all trans angles 180°.

The cyclopentylammonium molecule is disordered over two positions, each at a half occupancy. The two parts of the disorder are related by the two-fold rotation axis parallel to the a-axis. The atomic numbering scheme is shown in Fig 2. The five-membered ring has a half-chair conformation. The ring is tilted at an angle of 77.7(4)° to the inorganic layer. The hydrogen bridges between the organic and inorganic entities adopt the terminal configuration (See Table 3). Both halves of the disorder are in the acute angled corner of the parallelogram and hence adopt the right-angled configuration.

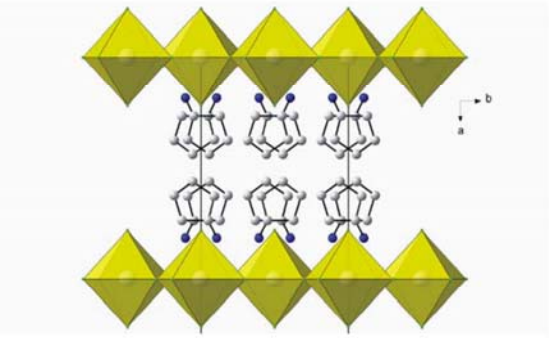


Fig.10 Half of the unit cell of **9**, which has bilayers of disordered cyclopentylammonium cations.

The crystal structure of 10.

An interesting feature of this layered perovskite-type hybrid is that the monoclinic unit cell dimensions parallel to the perovskite layers are twice the simple cubic perovskite lattice parameter of $[(CH_3NH_3)PbCl_3]$ (a_p = 5.657(2) Å).[5] All of the hybrids discussed so far and the many found in the literature have the $\sqrt{2}a_p$ x $\sqrt{2}a_p$ superstructure, not the unusual $2a_p$ x $2a_p$ observed here.[6] This rarely seen superstructure is also observed and discussed in the related compound, $[(C_6H_5C_2H_4NH_3)_2PbCl_4]$, which crystallizes out in the triclinic spacegroup P-1.[7] A consequence is that the asymmetric unit is the largest of all 12 layered perovskite-type hybrids synthesized in this body of work.

The inorganic layer is built up from characteristic corner-sharing $PbCl_6$ octahedra. The asymmetric unit consists of four lead atoms on special positions and twelve chloride atoms, Cl(1) to Cl(8) occupying the terminal positions and Cl(9) to Cl(12) occupying the bridging positions in the octahedra. This large number of atoms in the asymmetric unit (4 + 12) requires the $2a_p$ x $2a_p$ superstructure. As shown in the projection perpendicular to the layers in Fig. 9, along the *b*-axis, the $PbCl_6$ octahedra are rotated relative to each other. The degree of rotation varies from 140.64(11)° to 160.06(10)° as there are eight different bridging chlorides and hence eight different Pb-Cl-Pb bridging angles. Furthermore, each Pb atom in the asymmetric unit is corrugated at a different angle, ranging from 6.22(4)° to 8.56(4)°. The coordination geometry around the Pb atom shows axial compression of the octahedral geometry, with the average bridging Pb-Cl distances longer than the distances to the axial chlorides. The angle between cis related chloride atoms deviate from 90°, with all trans angles 180°.

There are four unique cyclohexylammonium molecules in the asymmetric unit and four unique boxes asoociated with them. This ratio goes hand in hand with the four unique octahedra in the inorganic layer. The atomic numbering scheme is shown in Fig 2. All four cations are well ordered between the layers and have a chair conformation. The cyclohexylammonium molecules are almost perpendicular to the layers. The rings are tilted at angles ranging from 84.4(1)° to 88.1(2)° to the inorganic layer.

The hydrogen bonding between the organic and inorganic entities adopt the terminal halogen configuration and the equilateral configuration for all four unique ammonium cation moieties (See Table 3 for details of the hydrogen bonding).

Discussion of all six layered hybrids with general formula $[(C_nH_{2n-1}NH_3)_2PbX_4]$, n = 5 and 6 and X = Cl, Br and I.

This series of six compounds, where the two cations are cyclopentylammonium and cyclohexylammonium and the three halides chloride, bromide and iodide show more structural diversity than the related series discussed above, as summarized in Table 4. There are five different space groups and both monoclinic and orthorhombic crystal systems. The most significant variation from the cyclopropyl and cyclobutylammonium series is the conformation of the layers. All the layered perovskite-type hybrids with cyclohexylammonium have their consecutive layers staggered. This is in agreement with the expected trend, where cations with bulky R groups can be better accomodated between the layers if adjacent cations and layers are staggered. In the corresponding case with cyclopentylammonium, the five membered ring forces the staggered conformation on the lead chloride inorganic layers but when the halide is bromide or iodide, the eclipsed conformation is still favoured. Interestingly, the interlayer spacing in the cyclohexylammonium series decreases as the halide radius increases. This is contrary to the trend observed for all three other ring sizes. A possible explanation would be the increased area afforded by the terminal halides, which allows the rings that sandwich the inorganic layers to move closer towards them, thus shrinking the overall structure perpendicular to the layers.

The bond lengths in the octahedra still show the axial compression seen in the previous series. Hence, the identity of the cation has little effect on the bond lengths of the individual octahedra. However, the bridging angle of all six compounds averages out to 152.48(9)°, which is about 5° more than the average bridging angle seen in the series with the smaller rings (147.38(5)°). Hence, the five and six-membered rings force a more regular arrangement on the way adjacent octahedra are connected. The areas of the holes defined by the terminal halides of four corner-shared octahedra are the same for the individual halides regardless if

CREATED USING THE RSC ARTICLE TEMPLATE (VER. 2.0) - SEE WWW.RSC.ORG/ELECTRONICFILES FOR DETAILS

the cation is cyclopentyl- or cyclohexylammonium, i.e. the areas do not change for those ring sizes. The same phenomenon was seen in the previous series, where the three or four-membered rings had the same value for the areas. However, the areas increase by approximately 2.23 Å^2 on average between the two series for each of the three halides. For example in the case with lead chloride, $[(C_3H_5NH_3)_2PbCl_4]$ and $[(C_4H_7NH_3)_2PbCl_4]$ have similar magnitudes of their areas of 30.24(2) and 30.83(3) Å^2 respectively and $[(C_5H_9NH_3)_2PbCl_4]$ and $[(C_6H_{11}NH_3)_2PbCl_4]$ have areas of 32.95(2) and 32.96(26) Å^2 respectively.

There is little variation in the position of the ammonium group, which is acute for all six compounds and concurrently, the hydrogen bonding configuration is right-angled. The angle at which the rings are inclined to the inorganic layers is in the range from 77.671(351)° to 88.702(26)°, which includes the range seen in the cyclobutylammonium compounds. In general, the four, five and six-membered rings are almost perpendicular to the inorganic layers.

Crystallographic description of the hybrids with cycloheptylammonium and cycloocytlammonium: $[(C_7H_{13}NH_3)_{17}Pb_7Cl_{31}]$ (11) and $[(C_8H_{15}NH_3)_{18}Pb_{11}Cl_{40}]$ (12)

Discussion of the 1-D ribbons of 11.

The crystal packing of compound **5** is non-centrosymmetric even though none of the individual moieties are chiral. The chiral space group is $P2_1$ and the Flack[8] parameter is 0.019(5). The inorganic motif has one-dimensional ribbons of purely corner-sharing octahedra. Figure 11 clearly underlines a one-dimensional arrangement in which the ribbons are surrounded by cycloheptylammonium molecules. The individual ribbons are tilted at 33.4(1)° to each other along the *b*-axis to create a washboard-like packing. Above and below the ribbons, the crystal cohesion is achieved by N-H...Cl hydrogen bonds. In the direction parallel to the slabs, the cohesion is archieved by strong ionic bonds between chloride and lead atoms.

The individual $PbCl_6$ octahedra share four, three or two of their chlorides with adjacent octahedra (See Fig. 11). There are seven unique lead atoms in the asymmetric unit, labelled Pb(1) through to Pb(7), and 31 unique chloride atoms, labelled Cl(1) to Cl(31) and all are on general positions in the unit cell. The slabs are built up by two building blocks that alternate along the a-axis. The first building block has a row of three corner-shared octahedra and the second building block has a row of four corner-shared octahedra. The former block consists of the lead atoms Pb(1), Pb(4) and Pb(7) and are connected in that sequence, i.e. Pb(4) is sandwiched by Pb(1) and Pb(7). Similarly, the latter block has the sequence Pb(2)-Pb(3)-Pb(5)-Pb(6). The lead atoms Pb(3), Pb(4) and Pb(5) are in the centre of the slabs and share out all four of their chlorides that are in the equatorial positions of the octahedra. The bond lengths to their chlorides are in the narrowest range of all lead atoms and vary from 2.747(4) Å (Pb(2)-Cl(19)) to 3.082(4) Å (Pb(2)-Cl(21)). The outermost perimeter of the slab is then defined by Pb(2) and Pb(6), which only share out two of their equatorial chlorides. The bond lengths to the non bridging chlorides are the shortest (2.682(4) Å to 2.729(4) Å) and to the bridging chlorides the longest (3.077(3) Å to 3.273(4) Å). Pb(1) and Pb(7) share out three of their chlorides and have a large range of leach chloride bond lenghts, as seen in Pb(2) and Pb(6) (2.704(4) Å to 3.261(4) Å).

An amazing part of this structure is the large number of molecules in the asymmetric unit in both the inorganic and organic part. The inorganic part had 38 individual atoms and the organic component has 17 unique cycloheptylammonium cations and two waters of hydration. The cations are labelled consistently after the N atoms in the same manner is in **5**. The rings of the cations have their conformations split between chair and twist-chair in the ratio 5:12. As in the layered perovskite-type hybrids, the cations are directly above the boxes shaped by the corner-shared octahedra with the N atoms in close contact with the equatorial and axial chlorides. The three hydrogens on the ammonium groups all have simple or bifurcated hydrogen bonds. The majority of the acceptor chlorides are in the axial positions. The hydrogen bonding distances and angles are given as supplementary information.

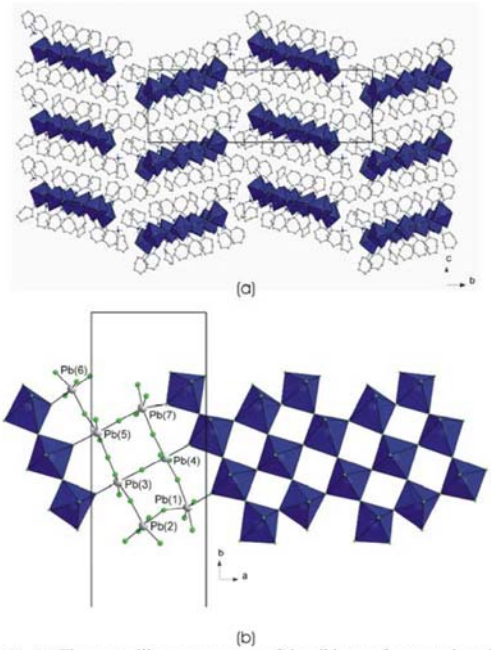


Fig. 11 (a) The wave-like arrangement of the ribbons of corner-shared $PbCl_6$ octahedra in **11**. (b) A magnified view of a single ribbon.

Discussion of the new two-dimensional layered motif of 12.

This hybrid combines the largest hydrocarbon ring and the smallest lead halide combination in this study. All the other compounds with seven or eight-membered rings had one-dimensional extended motifs. The motif observed here has the same bidimensional arrangement of organic and inorganic components seen in the layered perovskite-type hybirds (See Fig. 12). The difference lies in the connectivity of the lead chloride octahedra that make up the two-dimensional layers, using corner-, edge- and face-sharing simultaneously of the chloride ligands. The individual chloride atoms themselves can either be bonded to two, three or four lead atoms. The

 This journal © Royal Society of Chemistry

CREATED USING THE RSC ARTICLE TEMPLATE (VER. 2.0) - SEE WWW.RSC.ORG/ELECTRONICFILES FOR DETAILS

[JOURNAL NAME HERE] | www.rsc.org/[JOURNAL] Article

large variation requires a large number of atoms in the asymmetric unit: six lead and 21 chloride atoms and nine cyclooctylammonium cations. The simplest repeating unit can best be seen in Figure 12. The structure has a central chloride atom, Cl(4), that is bonded to four lead atoms, Pb(2) and Pb(3), which then form a ring of face-sharing octahedra. The bond lengths between the lead atoms and Cl(4) are 3.0665(8) and 3.0829(8) Å respectively for Pb(2) and Pb(3). The other chlorides that partake in the face-sharing, Cl(5) to Cl(8), contain both the shortest (2.747(4) Å) and longest (3.394(4) Å) bond lengths in the structure. The geometry of the seven-coordinate Pb(3) is capped octahedral. Pb(2) undergoes face-sharing again outwards of the ring to Pb(1) and corner-sharing to atom Pb(6). Pb(3) undergoes corner-sharing to both Pb(4) and Pb(6). Two Pb(1) octahedra are connected to each other via edge-sharing and to Pb(6) via corner-sharing. Pb(6) itself only undergoes corner-sharing to the atoms Pb(1), Pb(2), Pb(3) and Pb(4). The lead atom Pb(5) undergoes corner-sharing via trans related chlorides with Pb(4) to form a linear chain of $PbCl_6$ octahedra, similar to the lead bromide hybrid with cyclooctylammonium. Since Pb(5) only bonds to Pb(4), there are large gaps on both sides of the linear chain, which are only filled by one cation. The perimeter of this gap is a ring made up of all the lead atoms in the asymmetric unit plus an extra Pb(4) lead atom. The sequence is Pb(1)-Pb(2)-Pb(3)-Pb(4)-Pb(5)-Pb(4)-Pb(6). A search of the Cambridge Structural Database[9] (Version. 5.27, November 2005) for other seven- or eight-coordinate lead(II) chloride complexes gave only one result. The compound $[(H_3NC_2H_4NH_3)Pb_2Cl_6]$ has infinite two-diemnsional layers of $(Pb_2Cl_6^{2-})_n$ parallel to the *bc*-plane.[10] The two lead atoms in the asymmetric unit have eight chlorides atoms coordinated to them and the polyhedra can be described as distorted bicapped trigonal prisms and square antiprism respectively.

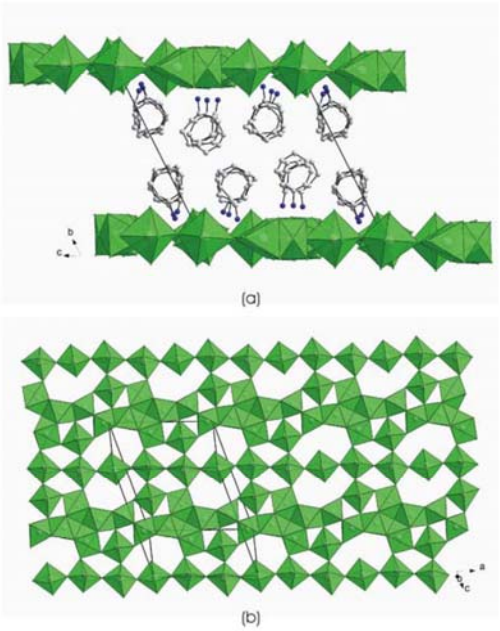


Fig. 12 (a) The bidimensional arrangement of cycloheptylammonium cations in between the 2-D layers of lead(II) chloride in hybrid **12**. (b) Magnified view of the connectivity of the 2-D layers.

The cations are linked to the layers by N-H...Cl hydrogen bonds. The three hydrogens on the N atoms are all involved in the bonding interactions except for cat9, which forms no hydrogen bonds between H(1B) and the chlorides. The reason is that cat9 sits above the large hole within the layers as described above. The summary of the hydrogen bonding geometry is given as supplementary information.

The nine cycooctylammonium cations in the aymmetric unit are aligned along the b-axis. The cations are labelled accoriding the to the labelling of the nitrogen atoms, i.e. cat1 contains atom N(1), etc. The overall three-dimensional structure is held together by van der Waals forces between the ring moieties and the hydrogen bridging interactions (See Supplemenary info for hydrogen bridging details). The eight-membered rings have two conformations. Cat6 and cat8 have a twist-boat-chair conformation and the remaining cations the thermodynamically favoured boat-chair conformation.

Discussion of all six hybrids with cycloheptylammonium and cyclooctylammonium and PbX_6, X = Cl, Br and I.

There is little conformity in the adopted inorganic motif when the rings are larger. There are five diffferent motifs in the six structures: two one-dimensional chains of corner-sharing octahedra, one-dimensional chains of face-sharing, two ribbon motifs and one 2-D motif.

Conclusion

We have demonstrated that the identity of the halide has little influence on the motif adopted by the inorganic-organic hybrids

CREATED USING THE RSC ARTICLE TEMPLATE (VER. 2.0) - SEE WWW.RSC.ORG/ELECTRONICFILES FOR DETAILS

when the size of the cation remains below heptylamonium. The detailed packing of the inorganic layers and their relative geometry is however dependant on the specific size of the rings, and subsequntly can be divided into two classes: The six hybrids with cyclopropylammonium and cyclobutylammonium all have eclipsed inorganic layers and crystallize in the same space group and approximate unit cell dimensions. All the cations have the same equilateral configuration. The six hybrids with cyclopentylammonium and cyclohexylammonium can have both staggered and eclipsed layers and have exclusively the right-angled configuration.

Experimental

Materials

All reagents and solvents employed were commercially avalable and used as received without further purification.

Synthesis

$[(C_3H_5NH_3)_2PbBr_4]$, 1: 0.122 g PbBr2 (0.332 mmol) was dissolved in 2 ml 48% HBr in a sample vial. Thereafter, 0.050 g C3H5NH2 (0.856 mmol) was added and the precipitate dissolved by refluxing for 1 hour at 80°C. The solution was slowly cooled at 2°C/hour to room temperature. Crystals where grown from slow evaporation of the cooled solution. A colourless single crystal suitable for X-ray diffraction analysis was selected and studied. Elemental analysis (%). Found: C 11.23, H 2.48, N 4.35. Calc for $Br_4C_6H_{16}N_2Pb$: C 11.21, H 2.51, N 4.36.

$[(C_4H_7NH_3)_2PbBr_4]$, 2: 0.067 g $PbBr_2$ (0.183 mmol) was dissolved in 2 ml 48% HBr in a sample vial. Thereafter, 0.031 g $C_4H_7NH_2$ (0.436 mmol) was added and the precipitate dissolved by refluxing for 1 hour at 80°C. The solution was slowly cooled at 2°C/hour to room temperature. Crystals formed by slow evaporation at room temperature of the cooled solution. A colourless single crystal suitable for X-ray diffraction analysis was selected and studied. Elemental analysis (%). Found: C 14.30, H 3.00, N 4.41. Calc. for $Br_4C_8H_{20}N_2Pb$: C 14.32, H 3.00, N 4.17.

$[(C_5H_9NH_3)_2PbBr_4]$, 3: 0.090 g $PbBr_2$ (0.245 mmol) was dissolved in 2 ml 48% HBr in a sample vial. Thereafter, 0.054 g $C_5H_9NH_2$ (0.634 mmol) was added and the precipitate dissolved by refluxing at 80°C. The solution was slowly cooled at 2°C/hour to room temperature. A colourless single crystal suitable for X-ray diffraction analysis was selected and studied. Elemental analysis (%). Found: C 17.47, H 3.56, N 4.00. Calc. for $Br_4C_{10}H_{24}N_2Pb$: C 17.18, H 3.46, N 4.01.

The conformational disorder around the carbon atom C3 was resolved by finding alternate positions from the difference Fourier map for the respective atom. These atoms, C(3A) and C(3B), were then refined anisotropically together with their site occupancy such that the sum of the occupancies for the two alternate atom positions equaled one. Hydrogen atom positions were then calculated for the respective atoms using a riding model. The ratio of major to minor component is 52 to 48%.

$[(C_6H_{11}NH_3)_2PbBr_4]$, 4: 0.200 g $PbBr_2$ (0.545 mmol) was dissolved in 4 ml 48% HBr in a round bottom flask. Thereafter, 0.106 g $C_6H_{11}NH_2$ (0.545 mmol) was added and the precipitate dissolved by refluxing for 12 hours at 105°C. The solution was slowly cooled at 2°C/hour to room temperature. An orange single crystal suitable for X-ray diffraction analysis was selected and studied. Elemental analysis (%). Found: C 19.88, H 3.92, N 3.74. Calc. for $Br_4C_{12}H_{28}N_2Pb$: C 19.82, H 3.88, N 3.85.

$[(C_7H_{13}NH_3)_3PbBr_5]$, 5: 0.076 g $PbBr_2$ (0.207 mmol) was dissolved in 3 ml 46% HBr in a glass vial. Thereafter, 0.066 g $C_7H_{15}NH_2$ (0.573 mmol) was added and the precipitate dissolved by refluxing at 90°C. The solution was cooled to room temperature and then placed in a fridge, whereupon long colourless needle-shaped crystals grew. A single crystal suitable for X-ray diffraction analysis was selected and studied. Elemental analysis (%). Found: C 26.38, H 5.10, N 4.34. Calc. for $Br_5C_{21}H_{50}N_3Pb$: C 26.57, H 5.10, N 4.43.

$[(C_8H_{15}NH_3)_{10}Pb_4Br_{18}]$, 6: 0.050 g $PbBr_2$ (0.136 mmol) was dissolved in 2 ml 48% HBr in a glass vial. Thereafter, 0.030 g $C_8H_{15}NH_2$ (0.236 mmol) was added and the precipitate dissolved by refluxing for 3 hours at 88°C. The solution was slowly cooled at 2°C/hour to room temperature. No crystals formed. Thereafter, slow evaporation of the solution at room temperature gave colourless needles. A colourless single crystal suitable for X-ray diffraction analysis was selected and studied. Elemental analysis (%). Found: C 27.24, H 5.04, N 4.19. Calc. for $Br_{18}C_{80}H_{180}N_{10}Pb_4$: C 27.07, H 5.11, N 3.95.

$[(C_3H_5NH_3)_2PbCl_4]$, 7. 0.071 g $PbCl_2$ (0.255 mmol) was dissolved in 3 ml 33% HCl in a sample vial. Thereafter, 0.041 g $C_3H_5NH_2$ (0.718 mmol) was added and the precipitate dissolved by refluxing for 1 hour at 80°C. The solution was slowly cooled at 2°C/hour to room temperature. Thereafter, the solution was left to evaporate at room temperature. A colourless single crystal suitable for X-ray diffraction analysis was selected and studied. Elemental analysis (%): calc. for $Cl_4C_6H_{16}N_2Pb_1$: C 15.49, H 3.47, N 6.02. Found: C 11.50, H 2.64, N 6.02.

$[(C_4H_7NH_3)_2PbCl_4]$, 8. 0.062 g PbCl2 (0.223 mmol) was dissolved in 4 ml 33% HCl in a sample vial. Thereafter, 0.029 g $C_4H_7NH_2$ (0.408 mmol) was added and the precipitate dissolved by refluxing for 1 hour at 80°C. The solution was slowly cooled at 2°C/hour to room temperature. Thereafter, the solution was left to evaporate at room temperature. A colourless single crystal suitable for X-ray diffraction analysis was selected and studied. Elemental analysis (%). Found: C 19.02, H 3.87, N 5.50. Calc. for $C_8H_{20}C_{14}N_2Pb$: C 19.48, H 4.09, N 5.68.

$[(C_5H_9NH_3)_2PbCl_4]$, 9. 0.034 g PbCl2 (0.122 mmol) was dissolved in 2 ml 33% HCl in a sample vial. Thereafter, 0.060 g $C_5H_9NH_2$ (0.705) was added and the precipitate dissolved by refluxing for 1 hour at 80°C. The solution was slowly cooled

This journal © Royal Society of Chemistry

CREATED USING THE RSC ARTICLE TEMPLATE (VER. 2.0) - SEE WWW.RSC.ORG/ELECTRONICFILES FOR DETAILS

[JOURNAL NAME HERE] | www.rsc.org/[JOURNAL] Article

at 2°C/hour to room temperature. Thereafter, the solution was left to evaporate at room temperature. A colourless single crystal suitable for X-ray diffraction analysis was selected and studied. Elemental analysis (%). Found: C 23.10, H 4.51, N 5.31. Calc. for $Cl_4C_{10}H_{24}N_2Pb$: C 23.04, H 4.64, N 5.37.

$[(C_6H_{11}NH_3)_4Pb_2Cl_8]$, 10 0.200 g $PbCl_2$ (0.545 mmol) was dissolved in 4 ml 33% HCl in a round bottom flask. Thereafter, 0.106 g $C_6H_{11}NH_2$ (0.545 mmol) was added and the precipitate dissolved by refluxing for 12 hours at 105°C. The solution was slowly cooled at 2°C/hour to room temperature. A colourless single crystal suitable for X-ray diffraction analysis was selected and studied. Elemental analysis (%). Found: C 24.06, H 4.58, N 4.61. Calc. for $C_{24}H_{56}Cl_8N_4Pb_2$: C 26.24, H 5.14, N 5.10.

$[(C_7H_{13}NH_3)_{17}Pb_7Cl_{31}]$, 11. 0.050 g $PbCl_2$ (0.180 mmol) was dissolved in 2 ml 33% HCl in a sample vial. Thereafter, 0.055 g $C_7H_{13}NH_2$ (0.486 mmol) was added and the precipitate dissolved by refluxing for 1 hour at 80°C. The solution was slowly cooled at 2°C/hour to room temperature. Thereafter, the solution was left to evaporate at room temperature. A colourless single crystal suitable for X-ray diffraction analysis was selected and studied.Elemental analysis (%) Found: C 31.51, H 5.71, N 5.19. Calc. for $C_{119}H_{276}Cl_{31}N_{17}Pb_7$: C 31.58, H 6.15, N 5.26.

$[(C_8H_{15}NH_3)_{18}Pb_{11}Cl_{40}]$, 12. 0.050 g $PbCl_2$ (0.180 mmol) was dissolved in 2 ml 33% HCl in a sample vial. Thereafter, 0.055 g $C_8H_{15}NH_2$ (0.477 mmol) was added and the precipitate dissolved by refluxing for 1 hour at 80°C. The solution was slowly cooled at 2°C/hour to room temperature. Thereafter, the solution was left to evaporate at room temperature. A colourless single crystal suitable for X-ray diffraction analysis was selected and studied. Elemental analysis (%). Found: C 30.72, H 5.65, N 4.50. Calc. for $C_{144}H_{324}Cl_{40}N_{18}Pb_{11}$: C 28.80, H 5.44, N 4.20.

X-ray structure analysis

Intensity data were collected on a Bruker SMART 1K CCD area detector diffractometer with graphite monochromated Mo K_α radiation (50kV, 30mA). The collection method involved ω-scans of width 0.3°. Data reduction was carried out using the program *SAINT+*, version 6.02.[11] and face indexed absorption corrections were made using the program XPREP.[11]

The crystal structure was solved by direct methods using SHELXS-97.[12] Non-hydrogen atoms were first refined isotropically followed by anisotropic refinement by full matrix least-squares calculations based on F^2 using SHELXL-97.[12] Hydrogen atoms were first located in the difference map then positioned geometrically and allowed to ride on their respective parent atoms. Diagrams and publication material were generated using WinGx, [13] ORTEP, [14] PLATON[15] and DIAMOND.[16] Crystal structures of all compounds except 10 were done at -100 °C. Crystals of compound **10** would fracture upon cooling and the structure was done at 20 °C. Further crystallographic data are summarised in Table 1.

References

1 (a) G. C. Papvassiliou, G. A. Mousdis and I. B. Koutselas, *Adv. Mater. Opt. Electron, 1999.* **9**, , *265*; (b) D. B. Mitzi, *J. Chem. Soc., Dalton Trans.*, 2001. 1; (c) J. Calabrese, N. L. Jones, R. L. Harrow, N. Herron, D. L. Thornand Y. Wang, *J. Am. Chem. Soc.*, 1991, **113**, 2328; (d) R.-Z. Yin and C. H. Yo, *Bull. Korean Chem. Soc.*, 1998, **19**, 947; (e) D. B. Mitzi, C. A. Field, W. T. A. Harrison and A. M. Guloy, *Nature,* 1994, **369**, 467; I. B. Koutselas, L. Ducasse and G. C. Papavassiliou, *J. Phys.: Condens. Matter*, 1996, **8**, 1217.

2 A. Lemmerer and D. G. Billing, *CrystEngComm*, 2006, in press.

3 D. M. Hatch, H. T. Stokes, K. S. Aleksandrov and S. V. Miguel, *Phys. Rev. B*, 1998, **39**, 9282.

4 D. G. Evans and J. C. A. Boeyens, *Acta Crystallogr. B*, 1988, **44**, 663.

5 O. Knop, R. E. Wasylishen, M. A. White, T. S. Cameron and M. J. M. Van Oort, *Can J. Chem.*, 1990, **68**, 412.

6 D. B. Mitzi, *Prog. Inorg. Chem.*, 1999, **48**, 1.

7 D.B. Mitzi, *J. Solid State Chem.*, 1999, **145**, 694

8 H. D. Flack, *Acta Cryst. A*, 1983, **39**, 876.

9 F. H. Allen, *Acta Cryst. B*, 2002, **58**,380.

10 I. Löfving, *Acta Chem. Scand. A*, 1976, **30**, 715.

11 Bruker, SAINT+. Version 6.02 (includes XPREP and SADABS). Bruker AXS Inc., Madison, Wisconsin, USA.

12 G.M. Sheldrick, SHELX, release 97-2 (includes SHELXS and SHELXL), University of Göttingen, 1997.

13 L.J. Farrugia, WinGX. *J. Appl., Cryst.*, 1999, **32**, 837.

14 L. J. Farrugia, *J. Appl. Crystallogr.* 1997, **30**, 565.

15 A. L. Spek, J. Appl. Crystallogr. 2003, **36**, 7.

16 K. Brandenburg, Diamond. Version 2.1e., Crystal Impact GbR, Bonn, Germany.

CREATED USING THE RSC ARTICLE TEMPLATE (VER. 2.0) - SEE WWW.RSC.ORG/ELECTRONICFILES FOR DETAILS

Article www.rsc.org/[JOURNAL] | [JOURNAL NAME HERE]

Table 1 Crystal Data for **1**, **2**, **3**, **4**, **5** and **6**

	1	**2**	**3**	**4**	**5**	**6**
Formula	$C_6H_{16}Br_4N_2Pb$	$C_8H_{20}Br_4N_2Pb$	$C_{10}H_{24}Br_4N_2Pb$	$C_{12}H_{28}Br_4N_2Pb$	$C_{21}H_{50}Br_5N_3OPb$	$C_{80}H_{180}Br_{18}N_{10}Pb_4$
Mr	643.04	671.09	699.14	727.19	967.38	3549.48
Temperature/K	173	173	173	173	173	173
Crystal size/mm	0.40 x 0.21 x 0.06	0.20 x 0.10 x 0.04	0.40 x 0.36 x 0.13	0.22 x 0.19 x 0.05	0.40 x 0.10 x 0.05	0.21 x 0.08 x 0.06
Crystal system	Monoclinic	Monoclinic	Monoclinic	Orthorhombic	Orthorhombic	Triclinic
Space group	$P2_1/c$	$P2_1/c$	$P2_1/c$	$Cmc2_1$	$Pbca$	$P\bar{1}$
a/Å	12.400(3)	13.278(3)	13.429(3)	27.788(5)	8.0888(4)	11.7861(11)
b/Å	7.8407(19)	7.9463(18)	7.9862(19)	8.6541(14)	27.1707(15)	16.0354(16)
c/Å	8.385(2)	8.4703(19)	8.800(2)	8.2367(13)	28.9932(16)	31.135(3)
a/°	90	90	90	90	90	92.891(4)
b/°	108.177(4)	108.430(4)	106.163(4)	90	90	96.420(4)
c/°	90	90	90	90	90	100.267(4)
V/Å^3	774.5(3)	847.9(3)	906.4(4)	1980.8(6)	6372.1(6)	5739.0(10)
Z	2	2	2	4	8	2
Dc/g cm^{-3}	2.757	2.629	2.562	2.438	2.017	2.054
μ(Mo-Ka)/mm^{-1}	21.178	19.352	18.108	16.578	11.584	12.157
Theta range/°	1.73 to 28.00	1.62 to 28.00	1.58 to 28.00	1.47 to 27.99	1.40 to 25.50	0.66 to 28.00
No. unique data	1867	2050	2169	2346	5927	27362
No. data with $I \geq 2\sigma(I)$	1577	1514	1959	2163	4811	14506
$R1$	0.0450	0.0374	0.0409	0.0360	0.1401	0.0572
$wR2$ (all data)	0.1206	0.0875	0.1146	0.0922	0.2700	0.1569

This journal © Royal Society of Chemistry

CREATED USING THE RSC ARTICLE TEMPLATE (VER. 2.0) - SEE WWW.RSC.ORG/ELECTRONICFILES FOR DETAILS

Table 1 contd. Crystal Data for **7**, **8**, **9**, **10**, **11** and **12**.

	7	**8**	**9**	**10**	**11**	**12**
Formula	$C_6H_{16}Cl_4N_2Pb$	$C_8H_{20}Cl_4N_2Pb$	$C_{10}H_{24}Cl_4N_2Pb$	$C_{24}H_{56}Cl_8N_4Pb_2$	$C_{119}H_{276}Cl_{31}N_{17}O_2Pb_7$	$C_{144}H_{324}Cl_{40}N_{18}Pb_{11}$
Mr	465.20	493.25	521.30	1098.71	4526.85	6005.30
Temperature/K	173	173	293	173	173	173
Crystal size/mm	0.38 x 0.28 x 0.04	0.24 x 0.16 x 0.03	0.42 x 0.23 x 0.03	0.24 x 0.22 x 0.16	0.28 x 0.28 x 0.26	0.32 x 0.22 x 0.08
Crystal system	Monoclinic	Monoclinic	Orthorhombic	Monoclinic	Monoclinic	Triclinic
Space group	$P2_1/c$	$P2_1/c$	$Cmca$	$P2_1/m$	$P2_1$	$P\bar{1}$
a/Å	12.187(5)	13.219(5)	25.8420(10)	11.4446(11)	12.7667(15)	17.365(3)
b/Å	7.508(3)	7.618(3)	8.5174(3)	28.306(3)	46.043(5)	19.016(4)
c/Å	8.054(3)	8.093(3)	7.6956(3)	11.5206(10)	14.9592(15)	19.357(4)
a/°	90	90	90	90	90	63.476(3)
b/°	109.141(6)	106.828(7)	90	90.031(6)	94.385(5)	70.493(4)
c/°	90	90	90	90	90	88.146(4)
V/Å^3	696.3(4)	780.1(5)	1693.85(11)	3732.1(6)	8767.6(16)	5339.0(17)
Z	2	2	4	4	2	1
Dc/g cm^{-3}	2.219	2.100	2.044	1.955	1.715	1.868
μ(Mo-Ka)/mm^{-1}	12.848	11.474	10.575	9.605	7.214	9.182
Theta range/°	1.77 to 27.49	1.61 to 27.99	1.58 to 28.00	0.72 to 25.50	0.88 to 25.00	1.28 to 25.00
No. unique data	1601	1885	1051	6980	29908	28276
No. data with $I \geq 2\sigma(I)$	1332	1726	817	6348	21702	18557
$R1$	0.0308	0.0771	0.0411	0.0320	0.0457	0.0581
$wR2$ (all data)	0.0914	0.1942	0.1127	0.0767	0.1069	0.1668
Absolute Parameter[8]	-	-	-	-	0.019(5)	-

Table 2 Hydrogen bonding details of compounds **1**, **2**, **3**, **4** and **5.**

D-H…A	D-H (Å)	H…A (Å)	D…A (Å)	<(D-H…A) (°)	Symmetry transformations
1					
N(1)-H(1B)...Br(1)	0.91	2.52	3.357(7)	152.5	-x+2,y-1/2,-z+3/2
N(1)-H(1A)...Br(1)	0.91	2.73	3.362(9)	127.0	-x+2,-y+1,-z+1
N(1)-H(1C)…Br(2)	0.91	2.55	3.392(9)	153.6	-
2					
N(1)-H(1C)...Br(1)	0.91	2.49	3.353(7)	159.0	-
N(1)-H(1A)...Br(1)	0.91	2.71	3.409(7)	134.1	x,-y+1/2,z+1/2
N(1)-H(1B)…Br(2)	0.91	2.60	3.427(7)	152.0	-x+2,y+1/2,-z-1/2
3					
N(1)-H(1A)...Br(1)	0.91	2.46	3.338(6)	162.3	x,y,z+1
N(1)-H(1B)...Br(1)	0.91	2.47	3.378(7)	174.0	x,-y+5/2,z+1/2
N(1)-H(1C)…Br(2)	0.91	2.70	3.392(7)	133.6	x,-y+3/2,z+1/2
4					
N(1)-H(1C)…Br(2)	0.91	2.52	3.381(10)	157.8	x,-y+1,z+1/2
N(1)-H(1A)...Br(1)	0.91	2.56	3.365(10)	147.4	-
N(1)-H(1B)...Br(1)	0.91	2.79	3.506(9)	136.1	-
5					
N(1)-H(1A)...Br(5)	0.91	2.81	3.59(3)	143.7	x-1,y,z
N(1)-H(1B)...Br(2)	0.91	2.49	3.40(2)	174.3	-
N(1)-H(1C)...Br(3)	0.91	2.53	3.33(3)	146.4	x-1,y,z
N(2)-H(2A)...O(1)	0.91	1.91	2.80(3)	164.2	-
N(2)-H(2B)...Br(4)	0.91	2.66	3.55(3)	165.2	x-1,y,z
N(2)-H(2C)...Br(1)	0.91	2.78	3.45(3)	130.6	-
N(3)-H(3A)...Br(2)	0.91	2.54	3.44(3)	173.1	x-1/2,-y+1/2,-z
N(3)-H(3B)...Br(4)	0.91	2.46	3.37(3)	177.6	x-1,y,z
N(3)-H(3C)...Br(5)	0.91	2.86	3.47(3)	125.3	x-1/2,-y+1/2,-z
O(1)-H(11)...Br(1)	0.95	2.53	3.48(2)	179.5	-
O(1)-H(12)...Br(3)	0.95	2.43	3.38(2)	179.6	-x+2,-y+1,-z

This journal © Royal Society of Chemistry

CREATED USING THE RSC ARTICLE TEMPLATE (VER. 2.0) - SEE WWW.RSC.ORG/ELECTRONICFILES FOR DETAILS

[JOURNAL NAME HERE] | www.rsc.org/[JOURNAL] Article

Table 3 Hydrogen bonding details of compounds **7**, **8**, **9** and **10**

D-H…A	D-H (Å)	H…A (Å)	D…A (Å)	<(D-H…A) (°)	Symmetry transformations
7					
N(1)-H(1B)…Cl(1)	0.91	2.38	3.194(5)	149.1	x,-y+1/2,z-1/2
N(1)-H(1A)…Cl(1)	0.91	2.59	3.214(8)	125.9	x,y,z-1
N(1)-H(1C)…Cl(2)	0.91	2.41	3.244(7)	151.7	-x,-y,-z
8					
N(1)-H(1B)…Cl(1)	0.91	2.29	3.193(17)	175.5	x,y-1,z
N(1)-H(1C)…Cl(1)	0.91	2.41	3.239(18)	150.6	x,-y+3/2,z-1/2
N(1)-H(1A)…Cl(2)	0.91	2.41	3.277(18)	159.8	-x,y-1/2,-z+1/2
9					
N(1)-H(1B)...Cl(1)	0.89	2.52	3.402(12)	168.7	x,y+1/2,-z+1/2
N(1)-H(1C)...Cl(1)	0.89	2.58	3.435(12)	160.8	-
N(1)-H(1A)...Cl(2)	0.89	2.57	3.252(11)	133.7	-x,-y+1/2,z-1/2
10					
N(1)-H(1B)…Cl(9)	0.91	2.32	3.229(7)	176.7	-
N(1)-H(1C)…Cl(10)	0.91	2.35	3.236(7)	164.1	x,y,z+1
N(1)-H(1A)…Cl(3)	0.91	2.55	3.259(7)	135.1	x,y,z+1
N(2)-H(2C)…Cl(12)	0.91	2.32	3.217(7)	170.7	x+1,y,z
N(2)-H(2B)…Cl(9)	0.91	2.35	3.231(7)	163.0	-
N(2)-H(2A)…Cl(2)	0.91	2.55	3.259(7)	135.1	x,y,z+1
N(3)-H(3B)…Cl(11)	0.91	2.34	3.241(7)	172.8	x,y,z+1
N(3)-H(3C)…Cl(10)	0.91	2.37	3.243(7)	160.4	x+1,y,z+1
N(3)-H(3A)…Cl(7)	0.91	2.63	3.309(7)	131.9	x+1,y,z+1
N(4)-H(4B)…Cl(12)	0.91	2.33	3.219(7)	167.0	x+1,y,z
N(4)-H(4A)…Cl(11)	0.91	2.43	3.247(7)	149.3	-
N(4)-H(4C)…Cl(1)	0.91	2.57	3.323(7)	139.9	x+1,y,z

Table 4 Effect of Halide and Ring size on the packing of the layered perovskite-type hybrids with cyclopropylammonium and cyclobutylammonium cations

Parameter	$(C_3H_5NH_3)_2PbCl_4$	$(C_3H_5NH_3)_2PbBr_4$	$(C_3H_5NH_3)_2PbI_4$	$(C_4H_7NH_3)_2PbCl_4$	$(C_4H_7NH_3)_2PbBr_4$	$(C_4H_7NH_3)_2PbI_4$
Interlayer Spacing/Å	12.187(5)	12.400(3)	12.475(5)	13.219(5)	13.278(3)	13.355(3)
Space Group	$P2_1/c$	$P2_1/c$	$P2_1/c$	$P2_1/c$	$P2_1/c$	$P2_1/c$
Conformation of Layers	Eclipsed	Eclipsed	Eclipsed	Eclipsed	Eclipsed	Eclipsed
Average Pb-X(terminal) bond/Å	2.8625(16)	3.0005(11)	3.1794(15)	2.849(4)	2.9876(11)	3.2015(7)
Average Pb-X(bridging) bond/Å	2.8732(15)	2.9989(9)	3.2079(15)	2.889(4)	3.0161(9)	3.2110(6)
Bridging angle Pb(1)-X(2)-Pb(1)/°	146.71(5)	146.29(3)	147.16(3)	148.22(16)	148.60(3)	147.27(1)
θ tilt/	33.29(5)	33.71(3)	32.84(3)	31.78(16)	31.40(3)	32.73(1)
Corrugation or Ψ tilt/°	14.24(3)	13.45(2)	14.09(2)	13.47(8)	13.02(2)	12.41(1)
Area/Å²	30.24(3)	32.87(2)	37.87(5)	30.83(3)	33.65(2)	37.84(2)
Position of ammonium group	Centre	Obtuse	Obtuse	Centre	Centre	Centre
Hydrogen Bonding Configuration	Equilateral	Equilateral	Equilateral	Equilateral	Equilateral	Equilateral
Tilt angle of NH_3 group $\angle_\beta$/°	34.7(3)	35.6(4)	12.4(7)	34.4(1)	36.5(4)	38.4(2)
Angle of Ring to Inorganic Layer $\angle_\alpha$/°	60.8(3)	61.9(5)	15.2(9)	84.5(1)	82.2(5)	82.6(3)

This journal © Royal Society of Chemistry

CREATED USING THE RSC ARTICLE TEMPLATE (VER. 2.0) - SEE WWW.RSC.ORG/ELECTRONICFILES FOR DETAILS

[JOURNAL NAME HERE] | www.rsc.org/[JOURNAL] Article

Table 5 Effect of Halide and Ring size on the packing of the layered hybrids with cyclopentylammonium and cyclohexylammonium

Parameter	$(C_5H_9NH_3)_2PbCl_4$	$(C_5H_9NH_3)_2PbBr_4$	$(C_5H_9NH_3)_2PbI_4$	$(C_6H_{11}NH_3)_2PbC_4$	$(C_6H_{11}NH_3)_2PbB_4$	$(C_6H_{11}NH_3)_2PbI_4$
Interlayer Spacing/Å	12.921(1)	13.429(3)	14.00(2)	14.153(3)	13.894(5)	13.638(5)
Space Group	*Cmca*	$P2_1/c$	$P2_1/c$	$P2_1/m$	$Cmc2_1$	*Pbca*
Conformation of Layers	Staggered	Eclipsed	Eclipsed	Staggered	Staggered	Staggered
Average Pb-X(terminal) bond /Å	2.826(4)	2.9959(11)	3.193(6)	2.841(2)	2.9686(11)	3.1752(7)
Average Pb-X(bridging) bond /Å	2.941(3)	3.0516(9)	3.240(4)	2.973(3)	3.1440(15)	3.2437(6)
Bridging angle Pb-X-Pb/°	154.80(12)	153.60(3)	154.75(5)	140.64(11) to 160.06(10)	145.90(6) and 158.86(5)	154.79(1)
θ tilt/°	25.20(12)	26.40(3)	25.25(5)	39.36(11) to 19.40(10)	34.10(6) and 21.12(5)	25.21(1)
Corrugation or Ψ tilt/°	None	5.97(1)	5.03(2)	6.22(4) to 8.56(4)	7.55(3)	6.51(9)
Area/Å^2	32.95(2)	35.14(2)	39.95(15)	32.96(26)	35.64(1)	40.03(2)
Position of ammonium group	Acute	Acute	Acute	Acute	Acute	Acute
Hydrogen Bonding Configuration	Right-Angled	Right-Angled	Right-Angled	Right-Angled	Right-Angled	Right-Angled
Tilt angle of NH_3 group $\angle_\beta$ /°	45.0(4)	45.1(3)	35.4(3) and 44.0(2)	35.1(2) to 39.5(3)	38.9(5)	42.1(2) and 39.5(7)
Tilt of Ring to Inorganic Layer $\angle_\alpha$/°	77.7(4)	82.8(4)	86.7(1) and 88.7(1)	84.4(1) to 88.1(2)	87.3(3)	85.9(5) and 89.7(3)
	This work	This work	Ref. 2	This work	This work	Ref. 2

4.6 Effect of heteroatoms in the layered perovskite-type system $[(XC_nH_{2n}NH_3)_2PbI_4]$, n = 2, 3, 4, 5, 6; X = OH, Br and I; and $[(H_3NC_2H_4S_2C_2H_4NH_3)PbI_4]$.

Journal: CrystEngComm

Date Submitted: Pending, before 30 April 2007

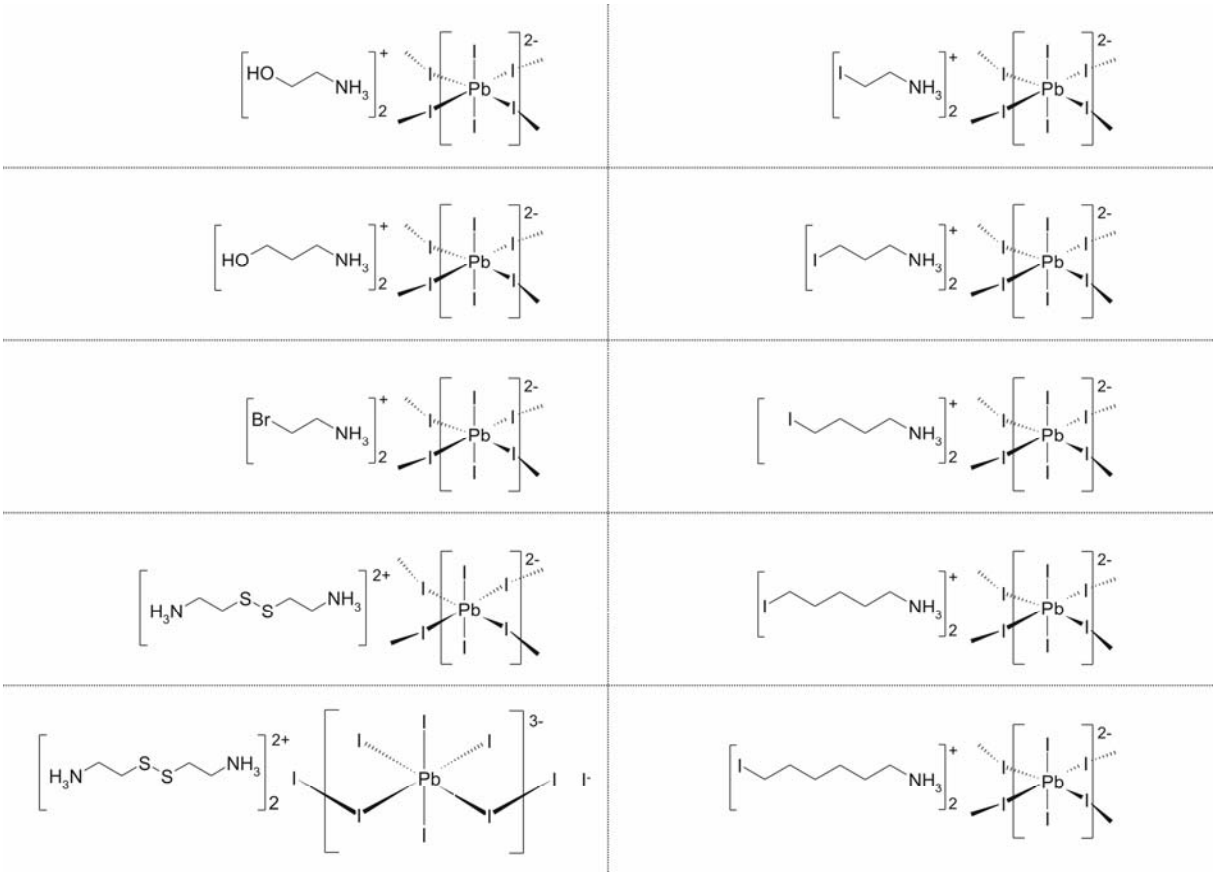
Reference Code of submitted article:

Date Accepted:

Final Reference:

Brief Synopsis

In this paper, ten inorganic-organic hybrids were made, nine of which have the layered perovskite-type motif. The objective was to observe how the inorganic layered perovskite-type motif changes by changing the identity of the heteroatoms and the length of the alkylammonium chain within the hybrid structure.


HO
NH3
2
+
Pb
I
2-
I
NH3
2
+
Pb
I
2-
HO
NH3
2
+
Pb
I
2-
I
NH3
2
+
Pb
I
2-
Br
NH3
2
+
Pb
I
2-
I
NH3
2
+
Pb
I
2-
H3N
S
S
NH3
2+
Pb
I
2-
I
NH3
2
+
Pb
I
2-
H3N
S
S
NH3
2+
2
I
Pb
I
3-
I
I-
I
NH3
2
+
Pb
I
2-

CREATED USING THE RSC ARTICLE TEMPLATE (VER. 2.0) - SEE WWW.RSC.ORG/ELECTRONICFILES FOR DETAILS

[JOURNAL NAME HERE] | www.rsc.org/[JOURNAL] Article

Effect of heteroatoms in the inorganic-organic layered perovskite-type hybrids $[(XC_nH_{2n}NH_3)_2PbI_4]$, n = 2, 3, 4, 5, 6; X = OH, Br and I; and $[(H_3NC_2H_4S_2C_2H_4NH_3)PbI_4]$.

Andreas Lemmerer and David G. BIlling*

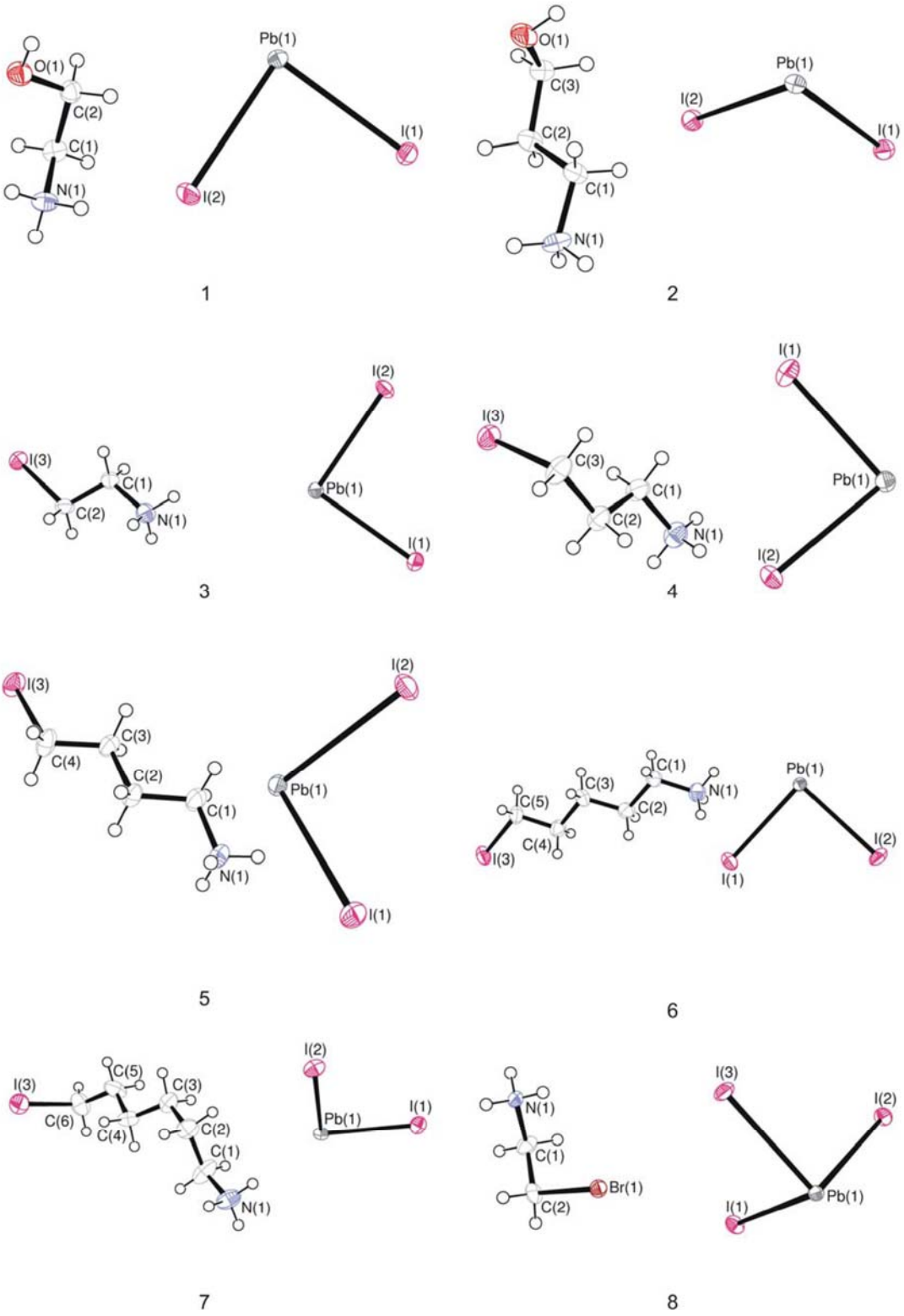
Receipt/Acceptance Data **[DO NOT ALTER/DELETE THIS TEXT]**
Publication data **[DO NOT ALTER/DELETE THIS TEXT]**
DOI: 10.1039/b000000x [DO NOT ALTER/DELETE THIS TEXT]

Nine inorganic-organic hybrids have been synthesized and characterised by Single-crystal X-Ray diffraction experiments. The inorganic component is based on lead(II) iodide units and four different types of alkylammonium cations. The motif of the inorganic component has 2-D layers of corner-sharing PbI_6 octahedra, which are closely related to the K_2NiF_4 and $RbAlF_4$ structure types. This motif is observed with alkylammonium cations, $(XC_nH_{2n}NH_3)$, that have three different heteroatoms : $[(HOC_2H_4NH_3)_2PbI_4]$ and $[(HOC_3H_6NH_3)_2PbI_4]$, $[(BrC_2H_4NH_3)_2PbI_4]$ and $[(IC_nH_{2n}NH_3)_2PbI_4]$ (n = 2-6). Both of the hybrids with diammonium cations, $[(H_3NC_2H_4S_2C_2H_4NH_3)PbI_4]$ and $[(NH_3C_2H_4S_2C_2H_4NH_3)_2PbI_5{\cdot}I]$, crystallized out of the same solution but have different inorganic motifs, the former has 2-D layers of corner-sharing octahedra and the latter 1-D chains of corner-sharing octahedra. The identity of the heteroatom and the chain length have an effect on the overall packing of the hybrid structures.

Molecular Sciences Institute, School of Chemistry, University of the Witwatersrand, PO WITS 2050, Johannesburg, South Africa.. E-mail: dave@hobbes.gh.wits.ac.za; Fax: 27 11 7176749; Tel: 27 11 717 6759

Electronic Supplementary Information (ESI) available: Table of hydrogen bonding details for compound **10**. See http://dx.doi.org/10.1039/b000000x/

CREATED USING THE RSC ARTICLE TEMPLATE (VER. 2.0) - SEE WWW.RSC.ORG/ELECTRONICFILES FOR DETAILS



20

Fig. 4 The contents of the asymmetric unit for structures **1**-**8**, showing the atomic numbering scheme. Displacement ellipsoids are shown at the 50% probability level.

This journal © Royal Society of Chemistry

CREATED USING THE RSC ARTICLE TEMPLATE (VER. 2.0) - SEE WWW.RSC.ORG/ELECTRONICFILES FOR DETAILS

[JOURNAL NAME HERE] | www.rsc.org/[JOURNAL] Article

Introduction

Inorganic-organic hybrid structures, with the general formula $[(R\text{-}NH_3)_2MX_4]$, where R is any alkyl or aromatic group, are able to combine desirable characteristics from both types of constituents into a molecular scale composite.[1] Inorganic compounds have varying band gaps and hence their electrical properties can vary from insulators to semiconductors right the way through to superconductors. Furthermore, they supply the hybrid structure with thermal stability and hardness as well as magnetic and dielectric properties. In addition to structural diversity, organic materials offer highly efficient luminescence. These hybrids form natural quantum well structures and have been extensively studied for their excitonic and magneto-optical properties, in particular the compound $[(C_6H_5C_2H_4NH_3)_2PbI_4]$.[2] Significantly, a thin-film field-effect transistor has been made using the same organic amine, 2-phenylethylamonium, and substituting the metal centre for tin(II).[3]

The iodoplumbate hybrids, where M = Pb and X = I, in particular have demonstrated a propensity for forming a great variety of crystalline structures by varying the identity of the R group. It has been shown that their structures can vary considerably, ranging from systems based on isolated inorganic octahedra, $[(NH_3CH_2CH(NH_3)CH_3)_2PbI_6{\cdot}3H_2O]$[4], to ones containing extended chains, $[(CH_3)_3C(H)NH_3)_2PbI_3{\cdot}I{\cdot}2H_2O]$[5], right up to 2-D networks, $[(C_6H_5(CH_2)_3NH_3)_2Pb_3I_{10}]$[6]. The most desired structure type has 2-D layers of corner-sharing PbI_6 octahedra, separated by the organic ammonium cations, as in $[(C_6H_9(CH_2)_2NH_3)_2PbI_4]$.[7] Successive inorganic layers can have the octahedra directly above each other, giving eclipsed inorganic layers, or the octahedra can be offset, resulting in a staggered conformation. In the former conformation, the inorganic structure is closely related to the K_2NiF_4 structure type[8] and in the latter conformation, the strucure is based on the $RbAlF_4$ structure type.[9] The tilting of the octahedra relative to each other is a further variable that can be modified. The iodides in the equatorial plane of the octahedra are called the bridging halides as they bond to the adjacent octahedra and the iodides in the axial positions are called the terminal halides as they undergo no sharing. This desired motif as also known as the layered perovskite-type motif. Within this desired motif, subtle changes in the organic ammonium cation can change the physical properties of the inorganic-organic hybrid and the crystal packing. This type of crystal engineering within the layered perovskite-type hybrids was first done on the system $[(C_6H_5C_2H_4NH_3)_2SnI_4]$.[10] The authors subtly changed the electronic properties by substituting one of the aromatic hydrogens for a flourine atom and then changing its position on the ring between the 2, 3 and 4 positions. There is a noticeable correlation between the bridging angle between adjacent SnI_6 octahedra and the position of the exciton band in the absorption spectra. The dependence of the absorption and photoluminescence spectra of spin coated films of these three compounds on the position of the flourine atom was confirmed by Kikuchi and co-workers.[11] The idea was then carried further by exchanging the halide for Br and Cl on the 2-position only and observing the effect of the halide on the peak position.

In this study, we wanted to investigate the effect of the heteroatom X on various alkylammonium chains, here a iodide, bromide, alcohol or sulfur group, has on the inorganic lead(II) iodide motif that is adopted in the layered perovskite-type hybrids.

Results and Discussion

To better describe the structural trends to be observed, we need to describe the position of the ammonium group and its effect on the geometry of the hydrogen bonds between the ammonium group and the halides. The "box" containing the ammonium groups are defined by the four equatorial, or bridging iodides, and the four axial, or terminal iodides that protrude above the layer. In projection, the ammonium group is contained within a parallelogram defined by the four bridging iodides (See Fig. 2). By projection onto this parallelogram the ammonium group is found in proximity to either an acute or an obtuse angle of the parallelogram. It has been found that the three hydrogens associated with the ammonium group either hydrogen bond to two terminal iodides and one bridging iodide (terminal halogen configuration) or to two bridging iodides and one terminal iodide (bridging halogen configuration).[12] All the compounds described here adopt the terminal halogen configuration. However, there are two ways that the hydrogens can adopt the terminal halogen configuration: The three iodides to which the hydrogens bond can be at the vertices of either an equilateral triangle or a right-angle triangle (See Fig. 2). There is a correlation between the position of the ammonium group and the type of terminal halogen configuration: If the ammonium group is in the acute angled position, the ammonium group has the right-angled configuration and if the ammonium group is in the obtuse angled position, the ammonium group has the equilateral configuration. If the inorganic motif consists of 1-D chains, a different classification of the hydrogen bonding geometry is necessary. If the majority of the hydrogen bonds are to halides occupying the equatorial positions in the octahedra, it is called equatorial halogen configuration, and similarly for the reverse case, where the halides are in the axial positions, axial halogen configuration. The atomic numbering scheme for all six compounds to be discussed is shown in Fig. 4.

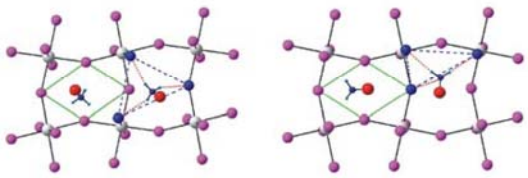


Fig. 2 The obtuse angled position is shown on the left with the parallelogram, consisting of the bridging halides at the corners, in green and the equilateral configuration, in blue. The picture on the right shows the right-angled configuration when the ammonium group is in the acute angled position.

CREATED USING THE RSC ARTICLE TEMPLATE (VER. 2.0) - SEE WWW.RSC.ORG/ELECTRONICFILES FOR DETAILS

Crystallographic description of the hybrid with the $RbAlF_4$ strucure type and alcohol ammonium cations: $[(HOC_nH_{2n}NH_3)_2PbI_4]$, n = 2 (1) and n = 3 (2)

The first objective of our study was to see the effect of chain length on the packing of the $HOC_nH_{2n}NH_3$ organic cations within the gaps of the corner-shared PbI_6 octahedra and the hydrogen bonding arrangement. The layered perovskite-type hybrid $[(HOC_2H_4NH_3)_2PbI_4]$ (**1**) was first prepared and characterised by Mercier and co-workers.[13] The unit cell parameters reported by Mercier and the ones found in this study are almost identical, even though the latter was performed at -100°C, except for a slightly smaller cell volume. The spacegroup is $P2_1/a$ in the structure by Mercier and $P2_1/c$ in this study. We left the unit cell untransformed so that it can be compared to the other layered perovskite-type hybrids in this paper. The packing of the two structures are similar, with the chain lying parallel to the plane of the inorganic layer and only the alcohol group protruding above the level of the terminal iodides. The hydrogen bonding arrangement has two extra interactions in **1**, which can be classified as weak interactions as the hydrogen acceptor distances are long (3.07 Å and 3.22 Å).

Comparison between compounds 1 and 2.

Both structures where collected at 173 K and are isomorphous. Fig. 3 clearly underlines a bidimensional arrangement in which two layers of 2-hydroxyethylammonium (**1**) and 3-hydroxypropylammonium (**2**) molecules are embedded between two consecutive inorganic $[PbI_6]$ sheets, forming an alternated inorganic-organic layered structure. The lead atoms are aligned from layer to layer, resulting in an eclipsed arrangement of adjacent layers, typical of layered perovskite-type hybrids with monoclinic unit cells. In the direction perpendicular to the layers, the crystal cohesion is achieved on one end of the organic molecule by N-H...I hydrogen bonds, related to the NH_3 polar groups; and on the other end by O-H...I hydrogen bonds, related to the alcohol group. The 2-hydroxyethylammonium molecules are stacked head-to-tail enabling N-H...O hydrogen bonds. In the direction parallel to the layers, the cohesion is archieved by strong ionic bonds between equatorial iodide and lead atoms.

The 2-hydroxyethylammonium molecule sits on a general position and is ordered within the inorganic layer. The atomic numbering scheme is shown in Fig 1. The molecule lies along the long diagonal of the parallelogram and is contained completely in the void. The molecule is twisted along the C(1)-C(2) bond (torsion angle -59.6(5)°) so that the hydroxyl groups point towards the layer above and can accept a hydrogen bond from the ammonium group of the molecule above. Similiarly, the 3-hydroxypropylammonium molecule sits along the long diagonal and is twisted along the C2-C3 bond (torsion angle -67.8(7)°). The nitrogen and carbon atoms are aligned in a plane at an angle of 18.604(7)° **1** and 29.833(4)° **2** to the inorganic layer.

The hydrogen bonds between the ammonium group and the iodides adopt the terminal halogen configuration in **1**. The hydrogen acceptor distances to the terminal halide I(1) are 2.75 Å and 3.07 Å and to the bridging halide I(2) 2.90 Å. The alcohol group itself bonds to the terminal halide I(1) of the same layer as the ammonium group with a hydrogen acceptor distance of 2.95 Å and to the layer above via a long hydrogen bond (3.22 Å), also to a terminal iodide. Two 2-hydroxyethylammonium molecules form dimers as they are connected on either end by N(1)-H(1B)...O(1) hydrogen bonds (2.31 Å). This extra hydrogen bond joins the 2-D layers to form a 3-D system not usually seen in the layered perovskite-type hybrids that have only ammonium groups on one end. In structure **2**, the same hydrogen bonding configuration is seen albeit with differing distances and angles (See Table 2). Significant is the much shorter N(1)-H(1C)...O(1) bond distance of 1.93 Å. This implys a much closer arrangement of the dimers in **2**. Both cations are in the in the acute position and have the righ-angled configuration.

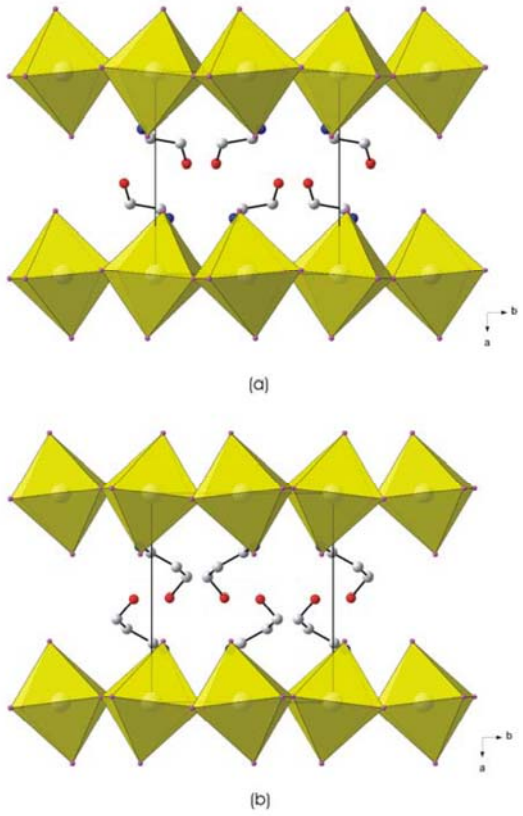


Fig. 3 The packing diagram of the compounds (a) $(HOC_2H_4NH_3)_2PbI_4$ **1** and (b) $(HOC_3H_6NH_3)_2PbI_4$ **2**. Hydrogen atoms are excluded for clarity.

The inorganic layer for both structures **1** and **2** is built up from characteristic corner-sharing PbI_6 octahedra. The asymmetric unit consists of a lead atom on a special position and two iodide atoms, I(1) occupying the terminal position and I(2) occupying the bridging position in the octahedra. As shown in the projection perpendicular to the layers in Fig. 3, along the c-axis, the PbI_6 octahedra in **1** are rotated by 153.099(12)° relative to each other, which is the bridging angle Pb(1)-I(2)-Pb(1). This angle is larger in **2** (163.679(13)°) to accommodate the longer chain and to enable

 This journal © Royal Society of Chemistry

CREATED USING THE RSC ARTICLE TEMPLATE (VER. 2.0) - SEE WWW.RSC.ORG/ELECTRONICFILES FOR DETAILS

the 3-propanolammonium molecule to fit perfectly within the gaps of four adjacent octahedra (See Fig. 4). Furthermore, the perovskite layers are corrugated in the b-direction by an angle of 7.123(8)° and 10.675(8)° respectively for **1** and **2** with respect to the *bc*-plane (See Fig. 5). The coordination geometry around the Pb atom shows axial compression of the octahedral geometry, with the bridging Pb(1)-I(2) distances longer than the terminal distances Pb(1)-I(1). The angle between *cis* related iodide atoms deviate from 90°, with all *trans* angles 180°.

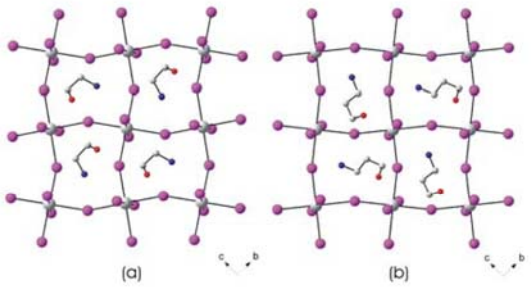


Fig. 4 Top view of a single layer of corner-sharing octahedra and its associated organic cation of the hybrids **1** and **2**. The 2-hydroxyethylammonium (a) and 3-hydroxypropylammonium (b) molecules are completely contained in the gaps formed by four corner-shared PbI_6 octahedra.

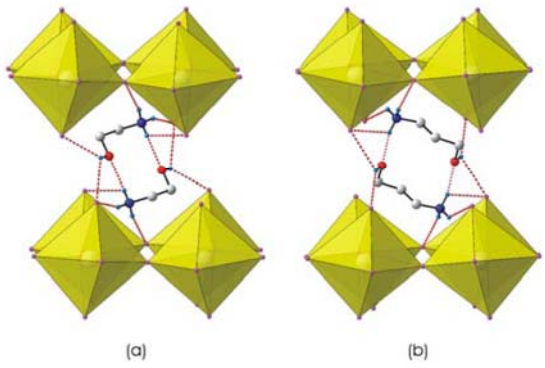


Fig. 5 The hydrogen bonding scheme of compounds **1** (a) and **2** (b). The ammonium group adopts the usual terminal bonding configuration often seen in hybrid perovskites and additionally forms a hydrogen bonded dimer to the molecule in the same layer. The alcohol group hydrogen bonds to both inorganic layers that sandwich it.

Crystallographic description of the layered perovskite-type hybrids with iodo ammonium cations: $[(IC_nH_{2n}NH_3)_2PbI_4]$, n = 2, 3, 4, 5 and 6 (3-7) and bromo ammonium cations $[(BrC_2H_4NH_3)_2PbI_4]$ (8)

The structures with chain lengths from ethane to pentane are isomorphous. The structure of compound $[(C_2H_4NH_3)_2PbI_4]$ (**3**) can be considered a model for the other structures and will be discussed in greater detail. The structure of the inorganic layers in $[(IC_6H_{12}NH_3)_2PbI_4]$ (**7**) is significantly different to warrant a separate description.

Crystal Packing of 3.

Fig. 6a clearly underlines the same bidimensional arrangement seen in the compounds **1** and **2** in which two layers of interdigitated 2-iodoethylammonium molecules are embedded between two consecutive inorganic $[PbI_6]$ sheets, forming an alternated organic-inorganic layered structure. The lead atoms are aligned from layer to layer, resulting in an eclipsed arrangement of adjacent layers, typical of layered perovskite-type hybrids with monoclinic unit cells. The unit cell contains two half layers at x = 0 and 1 to give a total number of one complete inorganic layer per unit cell. In the direction perpendicular to the layers, the crystal cohesion is achieved on one end of the organic molecules by N-H...I hydrogen bonds.

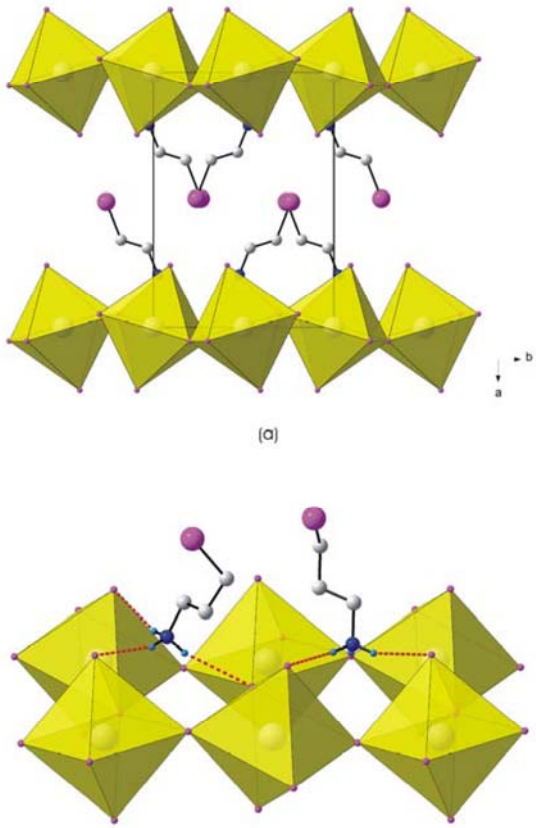


Fig. 6 (a) The packing arrangement of **3** has only one complete inorganic layer per unit cell. (b) The iodide atom is bent out of the plane of the hydrocarbon chain by 73.3(5)° in **4**.

The inorganic layer is built up from characteristic corner-sharing PbI_6 octahedra. The asymmetric unit consists of a lead atom on a special position and two iodide atoms, I(1) occupying the axial or terminal position and I(2) occupying the equatorial or bridging position in the octahedra. The bridging angle Pb(1)-I(2)-Pb(1) between adjacent corner-shared octahedra is 147.251(15)°, i.e. the PbI_6 octahedra are rotated relative to each other in the *bc*-plane. Furthermore, the perovskite layers are corrugated in the *b*-direction by an angle

CREATED USING THE RSC ARTICLE TEMPLATE (VER. 2.0) - SEE WWW.RSC.ORG/ELECTRONICFILES FOR DETAILS

of 15.239(7)° with respect to the *bc*-plane. The coordination geometry around the Pb atom shows axial compression of the octahedral geometry, with the bridging Pb(1)-I(2) distances longer than the axial distances Pb(1)-I(1). The angle between *cis* related iodine atoms deviate from 90°, with all *trans* angles 180°.

The 2-iodoethylammonium molecule sits on a general position and is ordered within the inorganic layer. The atomic numbering scheme is shown in Fig 1. The tilt of the organic cation to the inorganic layer is approximately 46.8(2)° measured through a line connecting the nitrogen atom, N(1), and the last carbon atom in the chain, C(2), and the plane of the lead atoms. The carbon atoms and the nitrogen atom in the chain are *trans* to each other as the torsion angle, N(1)-C(1)-C(2)-I(3), is 180.0(5)°. The chains are ordered within the inorganic layer and interdigitated up to the I atom of the chain next to it. The plane of the chain is angled at 60.7(3)° to the inorganic layer. The ammonium group is in the obtuse angled position (See Fig. 7). The angle of the ammonium group to the inorganic layers is 29.5(3)°, measured by the vector connecting atoms N(1) and C(1) and the plane of the lead atoms.

The hydrogen bonds between the organic and inorganic entities adopt the terminal halogenconfiguration and has the equilateral configuration (See Table 2 and Fig. 8). The hydrogen acceptor distances to the terminal halide I(1) are 2.67 Å and 2.71 Å and to the bridging halide I(2) 2.89 Å.

Crystal packing of 7.

$[(IC_6H_{12}NH_3)_2PbI_4]$ has a similiar bidimensional arrangement to **3** in which two layers of interdigitated 6-iodo-hexylammonium molecules are embedded between two consecutive inorganic $[PbI_6]$ sheets, forming an alternated organic-inorganic layered structure. The lead atoms however are now offset from layer to layer, resulting in a staggered arrangement of adjacent layers, typical of layered perovskite-type hybrids with orthorhombic unit cells. The unit cell contains two complete layers (Fig. 7) instead of only one complete inorganic layer, as seen in **3**. Subsequently, the unit cell is twice the volume in **7**.

The inorganic layer has the same characteristic corner-sharing PbI_6 octahedra and asymmetric unit as **3**. However, the spacegroup is now *Pbca* and hence the layers are parallel to the *ab*-plane. The perovskite layers are corrugated in the *a*-direction by an angle of 9.793(8)° with respect to the *ab*-plane and the PbI_6 octahedra are rotated by 160.984(18)° relative to each other, along the *c*-axis. The coordination geometry around the Pb atom shows axial compression of the octahedral geometry.

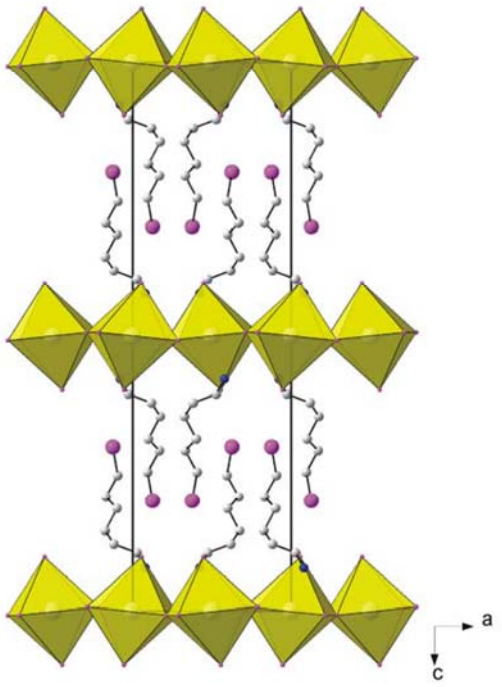


Fig. 7 The packing diagram of **7**. The unit cell contains two complete inorganic layers per unit cell. The layers at z = 0 and 1 are eclipsed relative to each other and are half occupied. The second layer, in the middle of the unit cell at z = 0.5, is staggered relative to the layers adjacent to it and is corrugated in the opposite direction.

Comparison of structures 3-7.

Similiarities and differences within the series $[(IC_nH_{2n}NH_3)_2PbI_4]$, n = 2, 3, 4, 5, 6 are summarized in Table 3. The most significant feature is that the inorganic layers are eclipsed relative to each other for n = 2-5 ($RbAlF_4$ structure-type), regardless of the chain length, and staggered for n = 6 (K_2NiF_4 structure-type). The degree of corrugation of the PbI_6 octahedra decreases with increasing chain length. The tilt of the chains relative to the inorganic sheets, measured by a line connecting the nitrogen atom and the last carbon atom in a chain, decreases from n = 2 to n = 3 by approx. 6° and then remains the same for the longer chain lengths.

 This journal © Royal Society of Chemistry

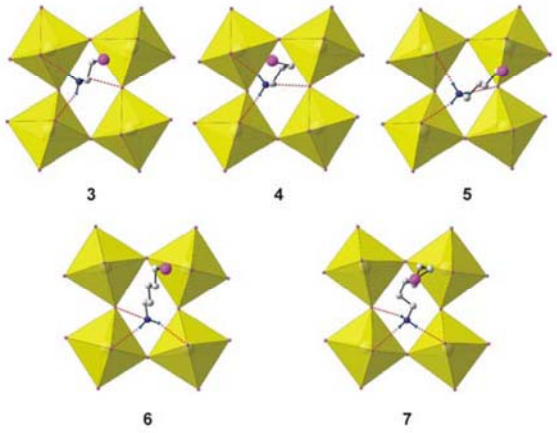


Fig. 8 Compounds **3-7** adopt the terminal halogen configuration but the first three have the equilateral configuration and the last two the right-angled configuration. As the chain length and the size of the organic cations increases, the position of the molecules changes from obtuse (**3-5**) to acute (**6** and **7**).

The tilt of the ammonium group normal to the layers remains about the same for n = 2, 3 and 4. The position of the ammonium group is in the obtuse angled corner and the chains lie along the short diagonal of the space of the parallelogram (Fig. 8). The tilt of the NH_3 group to the inorganic layers remains the same. The packing of the cations changes in the structures with n = 5 and 6. The case with n = 5 has the ammonium group significantly tilted further away from the plane of the layers (64.6(6)°) and this is because the ammonium group is now positioned in the acute angled corner of the parallelogram, similiar to n = 6. To accommodate the longer chains, the cations are now aligned with the long diagonal. The octahedra are rotated to a lesser extent in the hybrids with n = 5 and 6 as a consequence of the different packing, observed in the bridging angles being closer to 180°

Only the structures **4** and **7** have the iodide atoms bend out of the plane of the hydrocarbon chains. In $[(IC_3H_6NH_3)_2PbI_4]$, the iodide atom I(3) is bent by 31.6(3)° from the plane of the hydrocarbon chain (Fig. 6b) and in $[(IC_6H_{12}NH_3)_2PbI_4]$ by 33.0(4)° (Fig. 7). The hydrocarbon chains are all co-planar except for n = 6, which has a +syn-clinal angle around the C(2)-C(3) bond. The bend of the hydrocarbon chains influences the interlayer spacing in **7** as it is shorter by 0.2685(15) Å compared to the five-membered chain in $[(IC_5H_{10}NH_3)_2PbI_4]$; in contrast to the trend observed, where interlayer spacing inceases continuously as the chain length increases from n = 2 to 5 (Table 3).

The structure of compound 8

After studying the effect that chain length had on the inorganic layers, where the chains had an iodide atom on the one end of the chain, $(IC_nH_{2n}NH_3)$, an investigation on the effect of radius of the atom X would be warranted. The compound $[(BrC_2H_4NH_3)_2PbI_4]$ (**8**) is the same as compound **3** except for the Br atom replaced by an I atom. Fig. 9a clearly underlines the same bidimensional arrangement as **3**, in which two layers of 2-bromoethylammonium molecules are embedded between two consecutive inorganic $[PbI_6]$ sheets, forming an alternated organic-inorganic layered structure. The inorganic layers are slightly offset from layer to layer, resulting in a semi-staggered arrangement of adjacent layers. The 2-bromoethylammonium molecules are stacked head-to-tail enabling intermolecular as well as intramolecular hydrogen bonds.

The asymmetric unit is different to the previous layered-perovskite-type hybrids discussed and consists of a lead atom on a special position and three iodide atoms, I(1) occupying the terminal position and I(2) and I(3), both on special positions, occupying the bridging position in the octahedra. As shown in the projection perpendicular to the layers, along the b-axis, the PbI_6 octahedra in each layer have a very regular chessboard type pattern, (See Fig. 8b), similar to the K_2NiF_4 structure-type. The bridging angle I(2)-Pb(1)-I(2) is 175.70(5)° and I(3)-Pb(1)-I(3) is 172.94(2)°. The coordination geometry around the Pb atom shows axial compression of the octahedral geometry. The angle between *cis* and *trans* related iodide atoms deviate from 90° and 180° respectively.

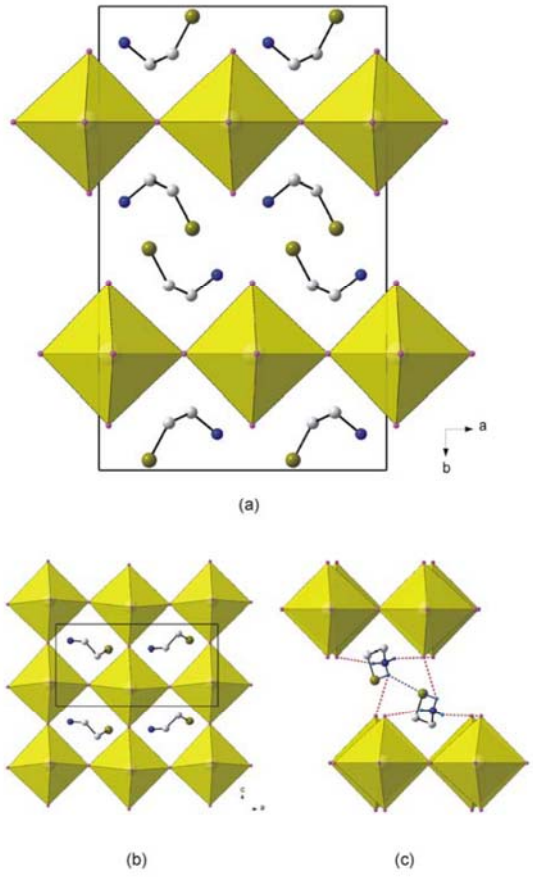


Fig. 9 (a) shows the staggered inorganic layers that are offset from each other along the a-axis. (b) is a topview of a single layer of corner-shared octahedra. The PbI_6 octahedra are only rotated by 5° and 7° relative to each other. (c) The ammonium group hydrogen bonds to two inorganic

CREATED USING THE RSC ARTICLE TEMPLATE (VER. 2.0) - SEE WWW.RSC.ORG/ELECTRONICFILES FOR DETAILS

layers (dashed red lines). The intramolecular and intermolecular hydrogen bonds between the ammonium group and the bromine atoms are shown in dashed blue lines and the hydrogen bonds between the ammonium group and the $PbBr_6$ octahedra in dashed red lines.

The 2-bromoethylammonium molecule is in a general position and is ordered within the inorganic layer. The atomic numbering scheme is shown in Fig 1. The molecule is contained completely in the area between the corner-shared octahedra (Fig. 9b). The two carbon atoms are closer to the inorganic layers than the nitrogen atom and the bromine atom, a type of packing only seen once before in the layered perovskite-type. The hybrids $[(C_6H_8N_4)[PbI_4]$ (CSD ref. code: QUFBUO) and $(C_6H_8N_4)[SnI_4]$ (CSD ref. code: QUFCAV) have the aromatic rings of the organic cation penetrating "into the perovskite 'bay region' formed" by the terminal iodides (Fig. 10).[14] These two hybrids also display the rare case of a layered perovskite stucture that does not have a primary ammonium head group. The protonated cation has only one hydrogen on each of the four nitrogen atoms, as seen in Fig. 10, and form only hydrogen bonds to the terminal iodides.

The molecule in **8** is twisted along the C(1)-C(2) bond (torsion angle = 67.9(13)°). The nitrogen and carbon atoms are aligned in a plane at an angle of 29.833(4)° to the inorganic layer. The hydrogen bonds between the ammonium group and the iodides can not be classified as either the terminal or bridging halogen configuration (Fig. 9c). Two hydrogens bond to the terminal halide I(1) of one layer via simple N-H...I bonds with distances of 2.74 and 2.79 Å. The third hydrogen has a trifurcated geometry. It bonds to the terminal halide of the layer above with a long hydrogen bond of 3.11 Å. It then has an intermolecular bond to the bromine atom of the molecule above, 2.77 Å, and an intramolecular hydrogen bond to the bromine atom on the end of the molecule (2.90 Å).

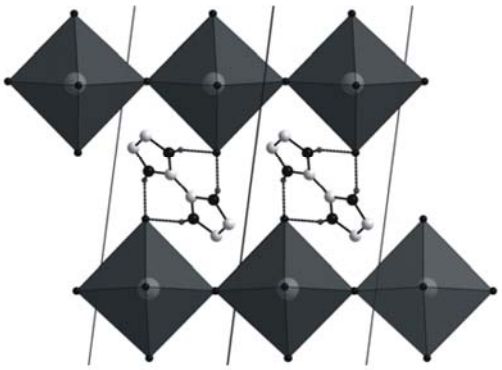


Fig. 10 The packing diagram of $(C_6H_8N_4)[PbI_4]$.[14] There are only four hydrogen bonds between the individual cations and the inorganic layers.

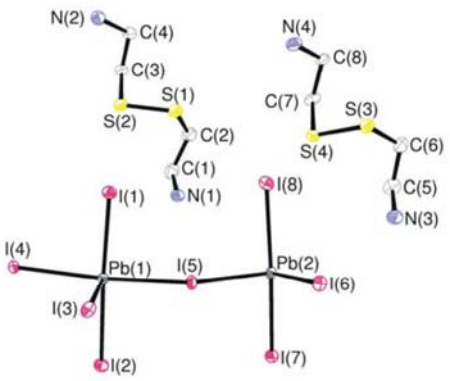
Crystallographic description of the layered perovskite-type hybrid perovskite with sulfur ammonium cations $[(NH_3C_2H_4S_2C_2H_4NH_3)PbI_4]$ (9) and the 1-D hybrid $[(NH_3C_2H_4S_2C_2H_4NH_3)_2PbI_5 \cdot I^-]$ (10)

The compound where X = SH was attempted with the ammonium cation $HSC_2H_4NH_3$ to compare the influence of the donor atom on the hydrogen bonding scheme with that of the alcohol derivative $HOC_2H_4NH_3$. However, in solution, all the cations reacted with another to form sulfur-sulfur linkages, creating the new diammonium cation $(H_3NC_2H_4S\text{-}SC_2H_4NH_3)$. Two different crystal structures crystallized out of the same solution: orange crystals of the hybrid $[(NH_3C_2H_4S_2C_2H_4NH_3)PbI_4]$ (**9**), which has 2-D layers of corner-sharing octahedra; and yellow cystals of the 1-D hybrid with chains of corner-sharing octahedra $[(NH_3C_2H_4S_2C_2H_4NH_3)_2PbI_5 \cdot I^-]$ (**10**).

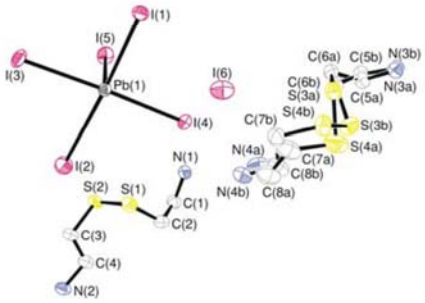
Obtaining more than product out of the same solution mixture has been observed with the cation R = 5,5'-bis(ethylsulfanyl)-2,2'-bithiophene. It can form either the layered perovskite-type hybrid $[(H_3N\text{-}R\text{-}NH_3)PbI_4]$ or the 1-D hybrid $[(H_3N\text{-}R\text{-}NH_3)(H_3N\text{-}R\text{-}NH_2)PbI_5]$. Both compounds are made from the same solution mixture of $(H_3N\text{-}R\text{-}NH_3)Cl_2$, KI, PbI_2 and water. The ratio of the two forms is 1/1 and can be easily identified by the orange colour of the layered hybrid and the yellow colour of the corner-sharing. $[(H_3N\text{-}R\text{-}NH_3)PbI_4]$ can be the sole product if a few drops of HI are added. The 1-D compound has $NH_3^+ \ldots NH_2$ hydrogen bond interactions between molecules, in addition to the usual $NH_3^+ \ldots I$ interaction between the inorganic and organic components.

This journal © Royal Society of Chemistry

CREATED USING THE RSC ARTICLE TEMPLATE (VER. 2.0) - SEE WWW.RSC.ORG/ELECTRONICFILES FOR DETAILS



9



10

Fig. 11 The contents of the asymmetric unit for structures **9** and **10**, showing the atomic numbering scheme. Anisotropic displacement parameters are shown at the 50% probability level. H atoms are omitted for clarity.

The crystal strucure of 9

Figure 12 clearly underlines a monodimensional arrangement in which a single layer of 2,2'-dithiodiethanammonium molecules are embedded between two consecutive inorganic [PbI_6] sheets, forming an alternated inorganic-organic layered structure. The lead atoms are slightly offset from layer to layer and rotated in opposite directions, resulting in a semi-eclipsed arrangement of adjacent layers.

The inorganic layer is built up from characteristic corner-sharing PbI_6 octahedra. The asymmetric unit consists of two lead atoms on general positions and eight iodide atoms, I(1), I(2), I(7) and I(8) occupying the terminal positions and I(3), I(4), I(5) and I(6) occupying the bridging positions in the inorganic layers. The four unique bridging halides instead of the usual single one, seen so far in the structures **1-7**, results in four different bridging angles to neighbouring octahedra, the smallest 142.906(18)° and the largest 157.254(17)°. The Pb atoms are not on special positions as in the previous hybrids and hence the Pb atoms do not lie on a common plane. Instead, the Pb atoms are displaced from the centers of the octahedra by 0.061 Å (Pb1) and 0.062 Å (Pb2). Furthermore, the perovskite layers are corrugated on average in the *a*-direction by an angle of 7.3(1)° with respect to the *ab*-plane. The coordination geometry around the Pb atom shows the typical axial compression of the octahedral geometry. The angle between *cis* and *trans* related iodine atoms deviate from 90° and 180° respectively.

There are two unique 2,2'-dithiodiethanammonium molecules in the asymmetric unit, labeled cat1 (containing atoms N(1) and N(2)) and cat2 (N(3) and N(4)). Both sit on general positions and the atomic numbering scheme is shown in Fig. 11. The tilt of the two cations is approximately 27.46(5)° (cat1) and 35.54(6)° (cat2) measured through a line connecting the nitrogen atoms and the plane of the lead atoms. The two chains have torsion angles in the range -48.4(5)° to -75.0(5)° and hence spiral along the *c*-axis. The two chains themselves are exactly at right angles to each other. The angle between least squares planes through all eight atoms on each chain is 90.000°.

The hydrogen bonds between the organic and inorganic entities adopt the right-angled configuration. The hydrogen acceptor distances to the terminal iodides are in the range 2.70 to 2.89 Å and to the bridging halides 2.79 to 3.02 Å. See Table 3 for the complete list. Figure 12 shows the hydrogen bonding pattern.

The crystal strucure of 10

The structure consists of alternating inorganic and organic layers. The inorganic layer contains two chains of corner-sharing [PbI_6] octahedra running along each half of the unit cell, parallel to the b-axis, and the organic layer is comprised of 2,2'-dithiodiethanammonium moieties. The channels in between the chains are occupied by isolated iodide atoms as well (See Fig. 13). In the direction parallel to the layers, the cohesion is archieved by strong ionic bonds between the iodide and lead atoms.

The asymmetric unit consists of a lead atom and five iodide atoms occupying general positions. I(1) and I(2) occupy the axial positions and I(3), I(4) and I(5) the equatorial positions. I(3) and its symmetry related equivalent, I(3)' [symmetry operator: -x+1, y-1/2, -z+5/2], complete the octahedral coordination sphere. The octahedra share corners via two iodides, here I(3), and since they are *cis* to each other, the chain zig-zags in the *ab*-plane. The bridging angle between two octahedra is almost linear, 166.22(2)°. Within the chain, the octahedra are severely distorted with all lead iodide distances different, ranging from 3.1200(5) Å to 3.2541(6) Å. The bond angles between *cis* ligands vary from 83.409(16)° to 97.090(17)° and *trans* angles from 173.554(16)° to 177.079(16)°.

The two 2,2'-dithiodiethanammonium molecules in the asymmetric unit occupy general positions. The molcules are labeled cat1 (containing atoms N(1) and N(2)) and cat2 (N(3) and N(4)) and the atomic numbering scheme shown in Fig 1. Cat1 sits above the chains in the holes formed by the corner-shared octahedra. Cat2 occupies the space between the chains. Cat1 is well ordered within the chains and has small displacement ellipsoids. Cat2 on the other hand had very large thermal ellipsoids, especially the S atoms, when singly occupied. Subsequently, a disorder model was applied to the entire chain with occupancies of 54% and 46%. The sulfur

CREATED USING THE RSC ARTICLE TEMPLATE (VER. 2.0) - SEE WWW.RSC.ORG/ELECTRONICFILES FOR DETAILS

atoms S(3) and S(4) are split over two positions, labeled S(3A), S(3B), S(4A) and S(4B), in a cross-shaped pattern (See Ortep diagram in Fig. 11).

The hydrogen bonds between the organic and inorganic entities adopt two different hydrogen bonding configurations with the iodide atoms. Cat1, which is not disordered, has its nitrogen atoms in the "boxes" formed by the corner-sharing octahedra. N(1) has an axial halogen configuration. The distances to the axial halides I(2) and I(1) are 3.06 Å and 3.09 Å respectively and to the bridging halide I(3) 3.06 Å. The second nitrogen atom on cat1, N(2), bonds to the isolated iodide I(6) (2.66 Å), the axial iodide I(2) (3.04 Å) and lastly to the equatorial halide I(5) (3.04 Å). Cat2, since it has its two nitrogen atoms each disordered over two positions, has an extensive hydrogen bonding geometry. All the iodides, except for the bridging I(3), act as acceptor atoms. The hydrogen-acceptor distances are in the range 2.70 Å to 3.13 Å See supplementary information for hydrogen bonding details for compound **10**.

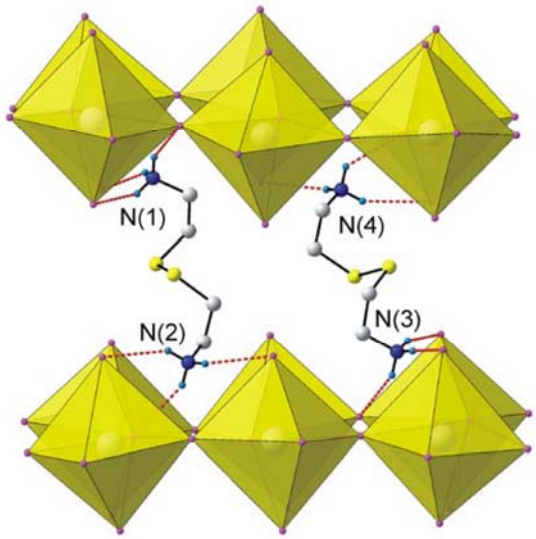
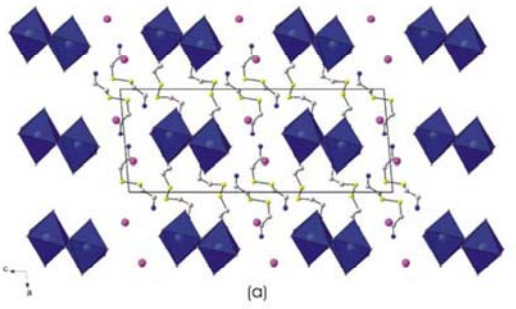


Fig. 12 Packing diagram of **9**. The two organic cations that make up the asymmetric unit are twisted along their chains. The crystals of this compound were orange coloured.



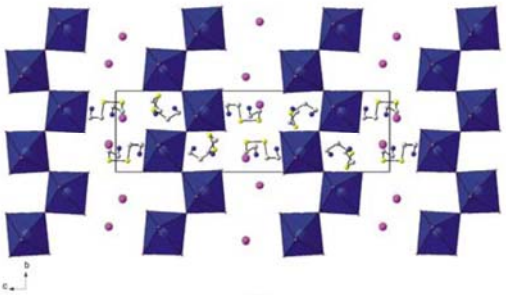


Fig. 13 The one-dimensional motif of corner-sharing chains of **10**. The crystals of this compound were yellow in colour.

Conclusion

We synthesized nine inorganic-organic hybrids of general formula $[(XC_nH_{2n}NH_3)_2PbI_4]$ that have a layered perovskite-type motif. The organic mono-ammonium cations had various heteratoms attached at the opposite terminal end of the chains. Intermolecular hydrogen bonding interactions between the organic cations in between the layers and between the inorganic and organic moieties helped stabilize the layered perovskite-type structures **1** and **2**, which had alcohol groups. Compound **8** has a Br atom on an ethylammonium cation, which then forms an intramolecular hydrogen bond between the ammonium group and the Br atom. The chain is twisted as a consequence so that the ammonium group forms only hydrogen bonds to the terminal iodides. Replacing the Br atom with an I atom causes the structure to revert to the classical layered perovskite-type motif for all chain lengths from n = 2-6, where the ammonium group hydrogen bonds to both terminal and bridging iodides. There are neither intermolecular nor intramolecular hydrogen bonds involving the I atoms on the chains. The length of the hydrocarbon chain influences the geometry and packing of the inorganic layers, being eclipsed in compounds **3-6** (n = 2-5) and staggered in **7** (n = 6). Finally, replacing the -OH group by a -SH group on the ethylammonium cation caused a reaction between two cations to form a S-S linkage. Out of this solution, both the layered perovskite-type hybrid was formed, **9**, and a hybrid with 1-D chains of corner-sharing octahedra. **10**. The factor

 This journal © Royal Society of Chemistry

CREATED USING THE RSC ARTICLE TEMPLATE (VER. 2.0) - SEE WWW.RSC.ORG/ELECTRONICFILES FOR DETAILS

that influences the crystallisation of both compounds out of one solution is unknown.

Experimental

Materials

All reagents and solvents employed were commercially avalable and used as received without further purification. Differential Scanning Calorimetry (DSC) data were collected on a Mettler Toledo 822^e at a scan rate of 5 °C/min in sealed aluminium pans under air.

Synthesis

Preparation of $[(HOC_2H_4NH_3)_2PbI_4]$, 1. 0.150 g PbI_2 (0.325 mmol) was dissolved in 2 ml 47% HI in a sample vial. Thereafter, 0.080 g $HOC_2H_4NH_2$ (1.31 mmol) was added and the precipitate dissolved by ultrasound at room temperature. The solution was placed in a fridge at 5°C. A red single crystal suitable for X-ray diffraction analysis was selected and studied. Elemental analysis (%). Found: C 5.77, H 1.86, N 3.34. Calc. for $C_4H_{16}I_4N_2O_2Pb_1$: C, 5.73, H, 1.93, N, 3.34.

Preparation of $[(HOC_3H_6NH_3)_2PbI_4]$, 2 0.228 g PbI_2 (0.495 mmol) was dissolved in 1 ml 47% HI in a sample vial. Thereafter, 0.128 g $HOC_3H_6NH_2$ (1.70 mmol) was added and the precipitate dissolved by refluxing for 1 hour at 90°C. The solution was slowly cooled at 2°C/hour to -7°C. A red single crystal suitable for X-ray diffraction analysis was selected and studied. Elemental analysis (%). Found: C 8.49, H 2.44, N 3.25. Calc. for $C_6H_{20}I_4N_2O_2Pb_1$: C 8.31, H 2.32, N 3.23.

Preparation of $[(IC_2H_4NH_3)_2PbI_4]$, 3.. 0.200 g PbI_2 (0.434 mmol) was dissolved in 2 ml 47% HI in a round bottom flask. Thereafter, 0.036 g $HOC_2H_4NH_2$ (0.798 mmol) was added and the precipitate dissolved by heavy refluxing for 12 hours. In solution, the amine underwent a substitution reaction where the alcohol group was substituted by an iodide atom. The solution was slowly cooled at 2°C/hour to room temperature. A yellow single crystal suitable for X-ray diffraction analysis was selected and studied. Elemental analysis (%). Found: C 4.61, H 1.36, N 2.60. Calc. for $C_4H_{14}I_6N_2Pb$: C 4.54, H 1.33, N 2.65.

Preparation of $[(IC_3H_6NH_3)_2PbI_4]$, 4 0.281 g PbI_2 (0.610 mmol) was dissolved in 1.5 ml 47% HI in a sample vial. Thereafter, 0.071 g $HOC_3H_6NH_2$ (0.945 mmol) was added and the precipitate dissolved by refluxing for 2 hours at 90°C. The solution was slowly cooled at 2°C/hour to room temperature. In solution, the amine underwent a substitution reaction where the alcohol group was substituted by an iodide atom. A yellow single crystal suitable for X-ray diffraction analysis was selected and studied. Elemental analysis (%). Found: C 6.67, H 1.76, N 2.53. Calc. for $C_6H_{18}I_6N_2Pb$: C 6.63, H 1.67, N 2.58.

Preparation of $[(IC_4H_8NH_3)_2PbI_4]$, 5. 0.082 g PbI_2 (0.178 mmol) was dissolved in 1 ml 47% HI in a sample vial. Thereafter, 0.040 g $HOC_4H_8NH_2$ (0.449 mmol) was added and the precipitate dissolved with 3 ml ethylacetate. The solution was left standing at room temperature. In solution, the amine underwent a substitution reaction where the alcohol group was substituted by an iodide atom. A yellow single crystal suitable for X-ray diffraction analysis was selected and studied.

Elemental analysis (%). Found: C 8.84, H 2.06, N 2.53. Calc. for $C_8H_{22}I_6N_2Pb$: C 8.62, H 1.99, N 2.51.

Preparation of $[(IC_5H_{10}NH_3)_2PbI_4]$, 6. 0.236 g PbI_2 (0.325 mmol) was dissolved in 2 ml 47% HI in a sample vial. Thereafter, 0.130 g $HOC_5H_{10}NH_2$ (1.26 mmol) was added and the precipitate dissolved by ultrasound at room temperature. The solution was placed in a fridge at 5°C. In solution, the amine underwent a substitution reaction where the alcohol group was substituted by an iodide atom. An orange single crystal suitable for X-ray diffraction analysis was selected and studied. Elemental analysis (%). Found: C 10.75, H 2.39, N 2.47. Calc. for $C_{10}H_{26}I_6N_2Pb$: C 10.51, H 2.29, N 2.45.

Preparation of $[(IC_6H_{12}NH_3)_2PbI_4]$, 7 0.200 g PbI_2 (0.434 mmol) was dissolved in 2 ml 47% HI in a sample vial. Thereafter, 0.108 g $HOC_6H_{12}NH_2$ (0.922 mmol) was added and the precipitate dissolved by ultrasound at room temperature. The solution was placed in a fridge at 5°C. In solution, the amine underwent a substitution reaction where the alcohol group was substituted by an iodide atom. An orange single crystal suitable for X-ray diffraction analysis was selected and studied. Elemental analysis (%). Found: C 12.43, H 2.74, N 2.37. Calc. for $C_{12}H_{30}I_6N_2Pb$: C 12.31, H 2.58, N 2.39.

Preparation of $[(BrC_2H_4NH_3)_2PbI_4]$, 8 0.052 g PbI_2 (0.113 mmol) was dissolved in 2 ml 47% HI in a sample vial. Thereafter, 0.077 g $BrC_2H_4NH_2 \cdot HBr$ (0.376 mmol) was added and the precipitate dissolved by ultrasound at room temperature. The solution was placed in a fridge. A red single crystal suitable for X-ray diffraction analysis was selected and studied. Elemental analysis (%). Found: C 5.07, H 1.46, N 2.85. Calc. for $Br_2C_4H_{14}I_4N_2Pb_1$: C 4.98, H 1.46, N 2.90.

Preparation of $[(NH_3C_2H_4S_2C_2H_4NH_3)[PbI_4]$, 9 0.116 g PbI_2 (0.252 mmol) was dissolved in 4 ml 47% HI in a sample vial. Thereafter, 0.100 g $HSC_2H_4NH_2 \cdot HCl$ (0.880 mmol) was added forming a yellow precipitate. Upon heating, a reaction occurs whereby the S-S linkage is made and the solution clears within a few minutes at 90°C. The solution was slowly cooled at 2°C/hour to room temperature forming yellow and orange crystals. An orange single crystal suitable for X-ray diffraction analysis was selected and studied. The yellow crystals are of compound **10**. Elemental analysis (%). Found: C 5.51, H 1.55, N 3.11, S 7.44. Calc. for $C_4H_{14}I_4N_2Pb_1S_2$: C 5.53, H 1.62, N 3.22, S 7.38.

Preparation of $[(NH_3C_2H_4S_2C_2H_4NH_3)_2PbI_5 \cdot I^-]$, 10. Elemental analysis (%). Found: C 7.50, H 2.18, N 4.27, S 10.27. Calc. for $C_8H_{28}I_6N_4PbS_4$: C 7.52, H 2.21, N 4.39, S 10.04.

X-ray structure analysis

CREATED USING THE RSC ARTICLE TEMPLATE (VER. 2.0) - SEE WWW.RSC.ORG/ELECTRONICFILES FOR DETAILS

Intensity data were collected on a Bruker SMART 1K CCD area detector diffractometer with graphite monochromated Mo K_α radiation (50kV, 30mA). The collection method involved ω-scans of width 0.3°. Data reduction was carried out using the program *SAINT+*, version 6.02.[16] and face indexed absorption corrections were made using the program XPREP.[16]

The crystal structure was solved by direct methods using SHELXS-97[17]. Non-hydrogen atoms were first refined isotropically followed by anisotropic refinement by full matrix least-squares calculations based on F^2 using SHELXL-97[17]. Hydrogen atoms were first located in the difference map then positioned geometrically and allowed to ride on their respective parent atoms. Diagrams and publication material were generated using WinGx[18], ORTEP[19], PLATON[20] and DIAMOND[21]. Further crystallographic data are summarised in Table 1.

References

1 (a) D. B. Mitzi, K. Chondroudis and C. R. Kagan, *IBM J. Res. & Dev.*, 2001, **45**, 29; (b) I. B. Koutselas, L. Ducasse and G.C. Papavassiliou, *J. Phys.: Condens. Matter*, 1996, **8**, 1217; (c) P. Day, *Phil. Trans. R. Soc. Lond. A*, 1985, **314**, 145; (d) D. B. Mitzi, *J. Mater. Chem.*, 2004, **14**, 2355; (e) R. Willett, H. Place and M. Middleton, *J. Am. Chem. Soc.*, 1988, **110**, 8639; (f) K. Matsuishi, T. Ishihara, S. Onari, Y. H. Chang and C. H. Park, *phys. stat. sol. (b)*, 2004, **241**, 3328.

2 X. Hong, T. Ishihara and A. V. Nurmikko, *Solid Sate Commun.*, 1992, **84**, 657.

3 C. R. Kagan, D. B. Mitzi and C. D. Dimitrakopoulos, *Science*, 1999, **286**, 945.

4 D. G. Billing and A. Lemmerer, *Acta Crystallogr.* E, 2006, **62**, m1103.

5 D. G. Billing and A. Lemmerer, *Acta Crystallogr.* C, 2006, **62**, m264.

6 D. G. Billing and A. Lemmerer, *Acta Crystallogr.* C, 2006, **62**, m174.

7 D. G. Billing and A. Lemmerer, *Acta Crystallogr.* C, 2006, **62**, m269.

8 D. M. Hatch, H. T. Stokes, K. S. Aleksandrov and S. V. Misyul, *Phys. Rev.* B, 1989, **39**, 9282.

9 D. M. Hatch and H. T. Stokes, *Phys. Rev. B*, 1987, **35**, 8509.

10 D. B. Mitzi, C. D. Dimitrakopoulos and L. L. Kosbar, *Chem. Mater.* 2001, **13**, 3728.

11 K. Kikuchi, Y. Takeoka, M. Rikukawa and K. Sanui, *Current Appl. Phys.*, 2004, **4**, 599.

12 D. B. Mitzi, *Prog. Inorg. Chem.*, 1999, **48**, 1.

13 N. Mercier, S. Poiroux, A. Riou and P. Batail, *Inorg. Chem.*, 2004, **43**, 8361.

14 Z. Tang, J. Guan and A. M. Guloy, *J. Mater. Chem.*, 2001, **11**, 479.

15 X.-H. Zhu, N. Mercier, M. Allain, P. Frère, P. Blanchard, J. Roncali and A. Riou, *J. Solid State Chem.*, 2004, **177**, 1067.

16 Bruker, SAINT+. Version 6.02 (includes XPREP and SADABS). Bruker AXS Inc., Madison, Wisconsin, USA.

17 G.M. Sheldrick, SHELX, release 97-2 (includes SHELXS and SHELXL), University of Göttingen, 1997.

18 L.J. Farrugia, WinGX. *J. Appl., Cryst.*, 1999, **32**, 837.

19 L. J. Farrugia, *J. Appl. Crystallogr.* 1997, **30**, 565.

20 A. L. Spek, J. Appl. Crystallogr. 2003, **36**, 7.

21 K. Brandenburg, Diamond. Version 2.1e., Crystal Impact GbR, Bonn, Germany.

 This journal © Royal Society of Chemistry

CREATED USING THE RSC ARTICLE TEMPLATE (VER. 2.0) - SEE WWW.RSC.ORG/ELECTRONICFILES FOR DETAILS

[JOURNAL NAME HERE] | www.rsc.org/[JOURNAL] Article

Table 1 Crystal Data for **1**, **2**, **3**, **4** and **5**.

	1	**2**	**3**	**4**	**5**
Formula	$C_4H_{16}I_4N_2O_2Pb$	$C_6H_{20}I_4N_2O_2Pb$	$C_4H_{14}I_6N_2Pb$	$C_6H_{18}I_6N_2Pb$	$C_8H_{22}I_6N_2Pb$
Mr	838.98	867.03	1058.76	1086.81	1114.87
Temperature/K	173	173	173	173	173
Crystal size/mm	0.40 x 0.20 x 0.06	0.44 x 0.40 x 0.04	0.626 x 0.395 x 0.161	0.54 x 0.22 x 0.10	0.515 x 0.25 x 0.032
Crystal system	Monoclinic	Monoclinic	Monoclinic	Monoclinic	Monoclinic
Space group	*P2₁/c*	*P2₁/c*	*P2₁/c*	*P2₁/c*	*P2₁/c*
a/Å	10.167(3)	10.631(3)	12.5520(9)	14.0739(15)	15.3677(8)
b/Å	9.038(3)	9.199(3)	8.7614(6)	9.0379(10)	8.2431(4)
c/Å	8.930(3)	9.207(3)	8.6441(6)	8.4723(10)	9.0441(4)
α/°	90	90	90	90	90
β/°	100.572(5)	93.057(6)	97.994(2)	99.246(5)	91.9050(10)
γ/°	90	90	90	90	90
V/Å^3	806.6(4)	899.1(4)	941.38(11)	1063.7(2)	1145.05(10)
Z	2	2	2	2	2
Dc/g cm^{-3}	3.454	3.202	3.735	3.393	3.234
μ(Mo-Ka)/mm^{-1}	18.096	16.239	18.775	16.622	15.445
Theta range/°	2.04 to 28.00	1.97 to 27.99	1.64 to 28.00	1.47 to 28.00	1.33 to 28.00
No. unique data	1944	2160	2274	2571	2756
No. data with $I \geq 2s(I)$	1855	2047	2150	2385	2554
*R*1	0.0234	0.0296	0.0319	0.0251	0.0213
*wR*2 (all data)	0.0583	0.0807	0.0791	0.0582	0.0731

.

Table 1 contd. Crystal Data for **6**, **7**, **8**, **9** and **10**.

	6	**7**	**8**	**9**	**10**
Formula	$C_{10}H_{26}I_6N_2Pb$	$C_{12}H_{30}I_6N_2Pb$	$Br_2C_4H_{14}I_4N_2Pb$	$C_8H_{28}I_8N_4Pb_2S_4$	$C_8H_{28}I_6N_4Pb_2S_4$
Mr	1142.92	1170.97	964.78	1738.16	1277.17
Temperature/K	173	173	173	173	173
Crystal size/mm	0.20 x 0.14 x 0.016	0.36 x 0.28 0.04	0.45 x 0.28 x 0.02	0.24 x 0.18 x 0.03	0.24 x 0.12 x 0.06
Crystal system	Monoclinic	Orthorhombic	Orthorhombic	Monoclinic	Monoclinic
Space group	*P2₁/c*	*Pbca*	*Pnma*	*P2₁/n*	*P2₁/c*
a/Å	16.2583(11)	9.2206(4)	12.8543(7)	17.7950(10)	11.3748(2)
b/Å	8.9028(5)	8.8513(4)	20.7714(13)	8.5195(7)	8.72900(10)
c/Å	8.6261(6)	31.9795(15)	6.4866(4)	23.1666(15)	29.2867(4)
α/°	90	90	90	90	90
β/°	90.071	90	90	98.719(5)	95.0040(10)
γ/°	90	90	90	90	90
V/Å^3	1248.58(14)	2610.0(2)	1731.93(18)	3471.6(4)	2896.81(7)
Z	2	4	4	4	4
Dc/g cm^{-3}	3.040	2.980	3.700	3.326	2.928
μ(Mo-Ka)/mm^{-1}	14.168	13.560	21.459	17.048	12.510
Theta range/°	1.25 to 28.00	1.27 to 28.00	1.96 to 27.99	1.35 to 28.00	1.40 to 28.00
No. unique data	3017	3145	2152	8376	6980
No. data with $I \geq 2s(I)$	2751	2684	1855	6373	6041
*R*1	0.0359	0.0334	0.0538	0.0354	0.0381
*wR*2 (all data)	0.1002	0.1032	0.1485	0.0705	0.0921

Table 2 Hydrogen bonding details of all compounds except **10**.

D-H…A	D-H (Å)	H…A (Å)	D…A (Å)	<(D-H…A) (°)	Symmetry transformations
1					
O(1)-H(1)…I(1)	0.84	2.95	3.665(4)	144.2	-x+2,-y+2,-z+2
O(1)-H(1)…I(1)	0.84	3.22	3.802(4)	128.9	x-1,y,z
N(1)-H(1B)…O(1)	0.91	2.31	2.916(5)	123.9	-x+1,-y+1,-z+2
N(1)-H(1A)…I(1)	0.91	2.75	3.581(5)	152.4	-x+2,-y+1,-z+2
N(1)-H(1B)…I(1)	0.91	3.07	3.697(4)	127.6	-x+2,y-1/2,-z+5/2
N(1)-H(1C)…I(2)	0.91	2.90	3.772(4)	161.3	-
2					
O(1)-H(1)…I(1)	0.84	2.83	3.567(5)	148.0	-x,-y,-z
O(1)-H(1)…I(1)	0.84	3.20	3.613(4)	113.1	x+1,y,z
N(1)-H(1C)…O(1)	0.91	1.93	2.808(7)	162.1	-x+1,-y,-z+1
N(1)-H(1A)…I(1)	0.91	2.85	3.538(5)	133.0	-x,y-1/2,-z+1/2
N(1)-H(1C)…I(1)	0.91	3.29	3.750(5)	113.8	-x,-y,-z+1
N(1)-H(1B)…I(2)	0.91	2.90	3.793(5)	166.0	x,-y+1/2,z+1/2
3					
N(1)-H(1C)…I(1)	0.91	2.67	3.576(7)	176.6	-x+2,y+1/2,-z+3/2
N(1)-H(1A)…I(1)	0.91	2.71	3.492(6)	145.0	-x+2,-y,-z+2
N(1)-H(1B)…I(2)	0.91	2.89	3.623(7)	139.0	x,y+1,z
4					
N(1)-H(1A)…I(1)	0.91	2.67	3.529(5)	157.2	x,-y+1/2,z-1/2
N(1)-H(1B)…I(1)	0.91	2.72	3.592(5)	164.9	x,-y+3/2,z-1/2
N(1)-H(1C)…I(2)	0.91	2.84	3.721(5)	164.3	-
5					
N(1)-H(1A)…I(1)	0.91	2.85	3.616(5)	143.0	-x,y+1/2,-z+1/2
N(1)-H(1B)…I(1)	0.91	2.70	3.607(5)	172.9	-x,-y+2,-z+1
N(1)-H(1C)…I(2)	0.91	2.76	3.656(5)	169.7	-x,-y+1,-z+1
6					
N(1)-H(1B)…I(1)	0.91	2.77	3.637(10)	160.9	x,-y+3/2,-z
N(1)-H(1C)…I(1)	0.91	2.77	3.623(11)	156.5	-
N(1)-H(1A)…I(2)	0.91	2.94	3.658(11)1	137.4	-x,-y+2,-z
7					
N(1)-H(1B)…I(1)	0.91	2.78	3.532(7)	141.1	x+1/2,-y+1/2,-z
N(1)-H(1C)…I(1)	0.91	2.84	3.656(7)	150.2	-x,-y+1,-z
N(1)-H(1A)…I(2)	0.91	2.87	3.718(7)	156.4	-x-1/2,y+1/2,z
8					
N(1)-H(1C)…Br(1)	0.91	2.77	3.480(12)	136.1	-x+3/2,-y+1,z-1/2
N(1)-H(1C)…Br(1)	0.91	2.90	3.325(12)	110.3	-
N(1)-H(1A)…I(1)	0.91	2.74	3.631(11)	168.3	-x+3/2,-y+1,z+1/2
N(1)-H(1B)…I(1)	0.91	2.79	3.620(11)	152.1	-x+3/2,-y+1,z-1/2
N(1)-H(1C)…I(1)	0.91	3.11	3.758(15)	129.9	x+1/2,y,-z+1/2
9					
N(1)-H(1C)…I(8)	0.91	2.75	3.564(6)	149.5	-
N(1)-H(1B)…I(1)	0.91	2.85	3.620(6)	142.9	-
N(1)-H(1A)…I(4)	0.91	2.79	3.578(6)	145.3	-x+1/2,y+1/2,-z+3/2
N(2)-H(2C)…I(7)	0.91	2.79	3.644(6)	156.8	x-1/2,-y+3/2,z+1/2
N(2)-H(2B)…I(8)	0.91	2.84	3.628(6)	146.0	-x+1,-y+1,-z+2
N(2)-H(2A)…I(5)	0.91	2.87	3.699(6)	152.8	-x+1,-y+1,-z+2
N(3)-H(3C)…I(2)	0.91	2.70	3.590(6)	165.2	-x+3/2,y+1/2,-z+3/2
N(3)-H(3B)…I(7)	0.91	2.82	3.685(6)	158.3	-x+3/2,y-1/2,-z+3/2
N(3)-H(3A)…I(6)	0.91	2.97	3.697(6)	138.0	-
N(4)-H(4C)…I(1)	0.91	2.72	3.561(6)	154.2	-x+1,-y+1,-z+2
N(4)-H(4B)…I(2)	0.91	2.89	3.713(6)	151.3	x+1/2,-y+1/2,z+1/2
N(4)-H(4A)…I(3)	0.91	3.02	3.710(6)	133.9	x+1/2,-y+1/2,z+1/2

This journal © Royal Society of Chemistry

CREATED USING THE RSC ARTICLE TEMPLATE (VER. 2.0) - SEE WWW.RSC.ORG/ELECTRONICFILES FOR DETAILS

Table 3 Selected Geometric parameters of the series $[(IC_nH_{2n}NH3)_2PbI_4]$, n = 2, 3, 4, 5 and 6

n	2	3	4	5	6
Compound	**3**	**4**	**5**	**6**	7
Interlayer Spacing/Å	12.5520(9)	14.0739(15)	15.3677(8)	16.2583(11)	15.9898(15)
Conformation of adjacent layers	Eclipsed	Eclipsed	Eclipsed	Eclipsed	Staggered
Roatation of Octahedra/°	147.251(15)	148.755(11)	147.024(12)	154.36(3)	160.984(18)
Angle of Corrugation	15.239(7)	12.113(7)	11.238(7)	5.61(2)	9.793(8)
Compression of Pb-I bond lengths	Axial	Axial	Axial	Bridging	Axial
Tilt of chain $\angle_\varphi$/° (atoms used to define vector)	46.8(2) (N(1)…C(2))	40.8(1) (N(1)…C(3))	40.8(1) (N(1)…C(4))	39.3(1) (N(1)…C(5))	39.6(1) (N(1)…C(6))
Tilt of NH_3 group $\angle_\beta$/° (vector N(1)-C(1))	29.5(3)	25.7(3)	25.7(2)	64.6(6)	55.0(4)
Plane tilt of chain $\angle_\alpha$/° (atoms used to define plane)	60.7(3) (N(1)-C(1)-C(2)-I(3))	63.6(3) (N(1)-C(1)-C(2)-C(3))	79.4(2) (N(1)-C(1)-C(2)-C(3)-C(4)-I(3))	69.0(2) (N(1)-C(1)-C(2)-C(3)-C(4)-C(5)-I(3))	60.0(3) (C(2)-C(3)-C(4)-C(5)-C(6))
Interdigitation	I(3)	C(3)	C(4)	C(4)	C(4)
I-I contacts/Å	4.327(1)	4.445(3)	4.998(0)	4.843(1)	4.988(0)
Conformation of hydrocarbon chain	Flat	Bent	Flat	Flat	Bent
Non co-planar Torsion angles/°	-	73.3(5) C(1)-C(2)-C(3)-I(3)	-	-	67.2(11) C(1)-C(2)-C(3)-C(4) 69.7(9) C(4)-C(5)-C(6)-I(3)
Position of ammonium group	Obtuse	Obtuse	Obtuse	Acute	Acute
Hydrogen bonding configuration	Equilateral	Equilateral	Equilateral	Right-Angled	Right-Angled

855

860

4.7 Inorganic-organic hybrids incorporating diammonium cations

Journal: CrystEngComm

Date Submitted: Pending, before 30 April 2007

Reference Code of Submitted Article:

Date Accepted:

Final Reference:

Brief Synopsis

In this paper, nine inorganic-organic hybrids were made using the metal lead and the halides iodide and bromide. The counter cations were different alkyldiammonium chains. Some structural trends are discussed.

CREATED USING THE RSC ARTICLE TEMPLATE (VER. 2.0) - SEE WWW.RSC.ORG/ELECTRONICFILES FOR DETAILS

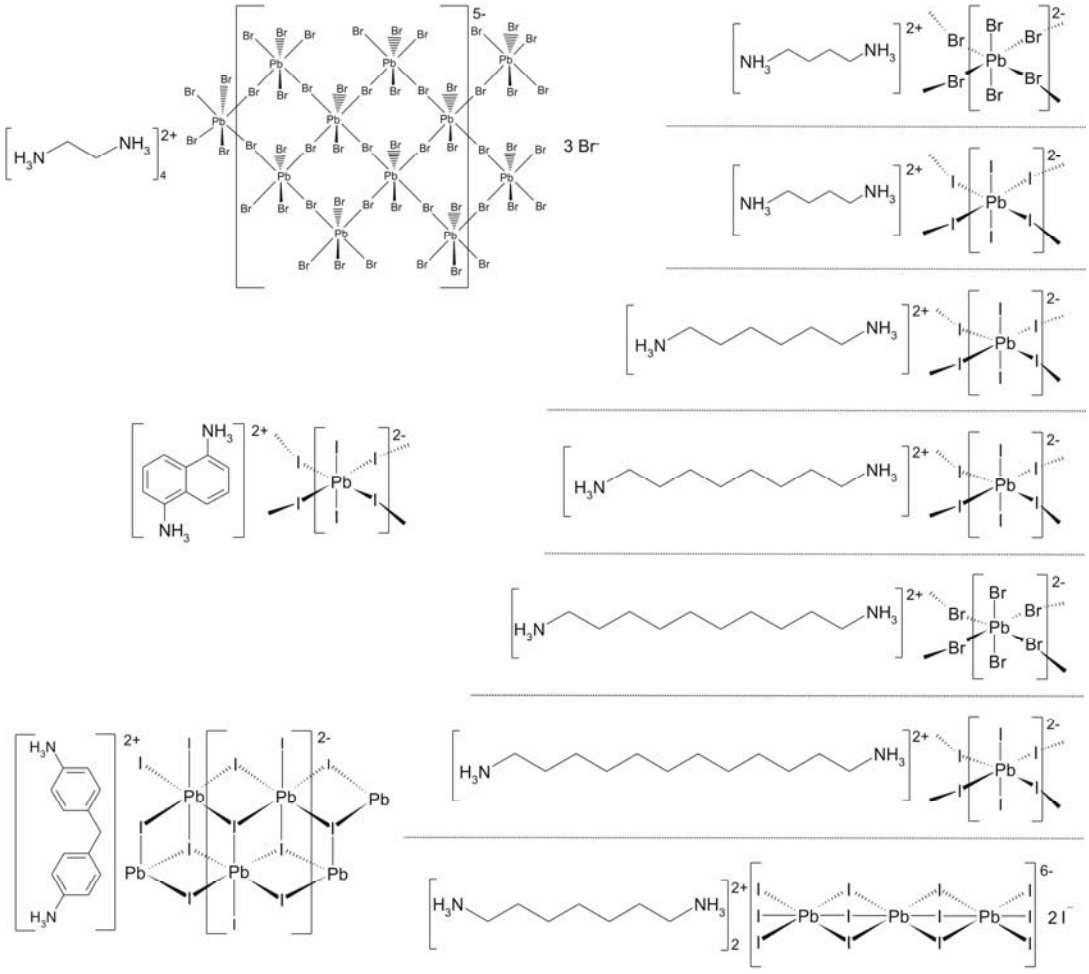
[JOURNAL NAME HERE] | www.rsc.org/[JOURNAL] Article

Inorganic-organic hybrids incorporating diammonium cations

David G. Billing and Andreas Lemmerer

Receipt/Acceptance Data **[DO NOT ALTER/DELETE THIS TEXT]**
Publication data **[DO NOT ALTER/DELETE THIS TEXT]**
DOI: 10.1039/b000000x [DO NOT ALTER/DELETE THIS TEXT]

Diammonium cations of general formula (H_3N-R-NH_3), have been used as templating moieties on lead(II) halide motifs, forming a variety of inorganic-organic nanocomposites. The R group can have simple, straight alkyl chains, which if even-membered and greater than ethane, form 2-D layers based on the $RbAlF_4$ structure type, as found in $[(H_3N(CH_2)_4NH_3)PbBr_4]$, $[(H_3N(CH_2)_4NH_3)PbI_4]$, $[(H_3N(CH_2)_8NH_3)PbI_4]$, $[(H_3N(CH_2)_{10}NH_3)PbBr_4]$, and $[(H_3N(CH_2)_{12}NH_3)PbI_4]$. If the R group has fused aromatic rings like naphthalene, the 2-D layered perovskite-type motif is still adopted, as in $[(H_3NC_{10}H_6NH_3)PbI_4]$. If the chain is odd-membered, a 0-D inorganic motif, consisting of isolated blocks of face-sharing PbI_6 octahedra and isolated iodide anions, is seen in $[(H_3N(CH_2)_7NH_3)_4Pb_3I_{12}\cdot 2I^-]$. 1-D motifs, which have corner-sharing ribbons or edge-sharing twin-anionic chains, are also observed in the compounds $[(H_3NC_6H_4CH_2C_6H_4NH_3)PbI_6]$ and $[(H_3NC_2H_4NH_3)_4PbBr_4]$ respectively.



Molecular Sciences Institute, School of Chemistry, University of the Witwatersrand, PO WITS 2050, Johannesburg, South Africa. E-mail: dave@chem.wits.ac.za; Fax: 27 11 7176749; Tel: 27 11 7176759

CREATED USING THE RSC ARTICLE TEMPLATE (VER. 2.0) - SEE WWW.RSC.ORG/ELECTRONICFILES FOR DETAILS

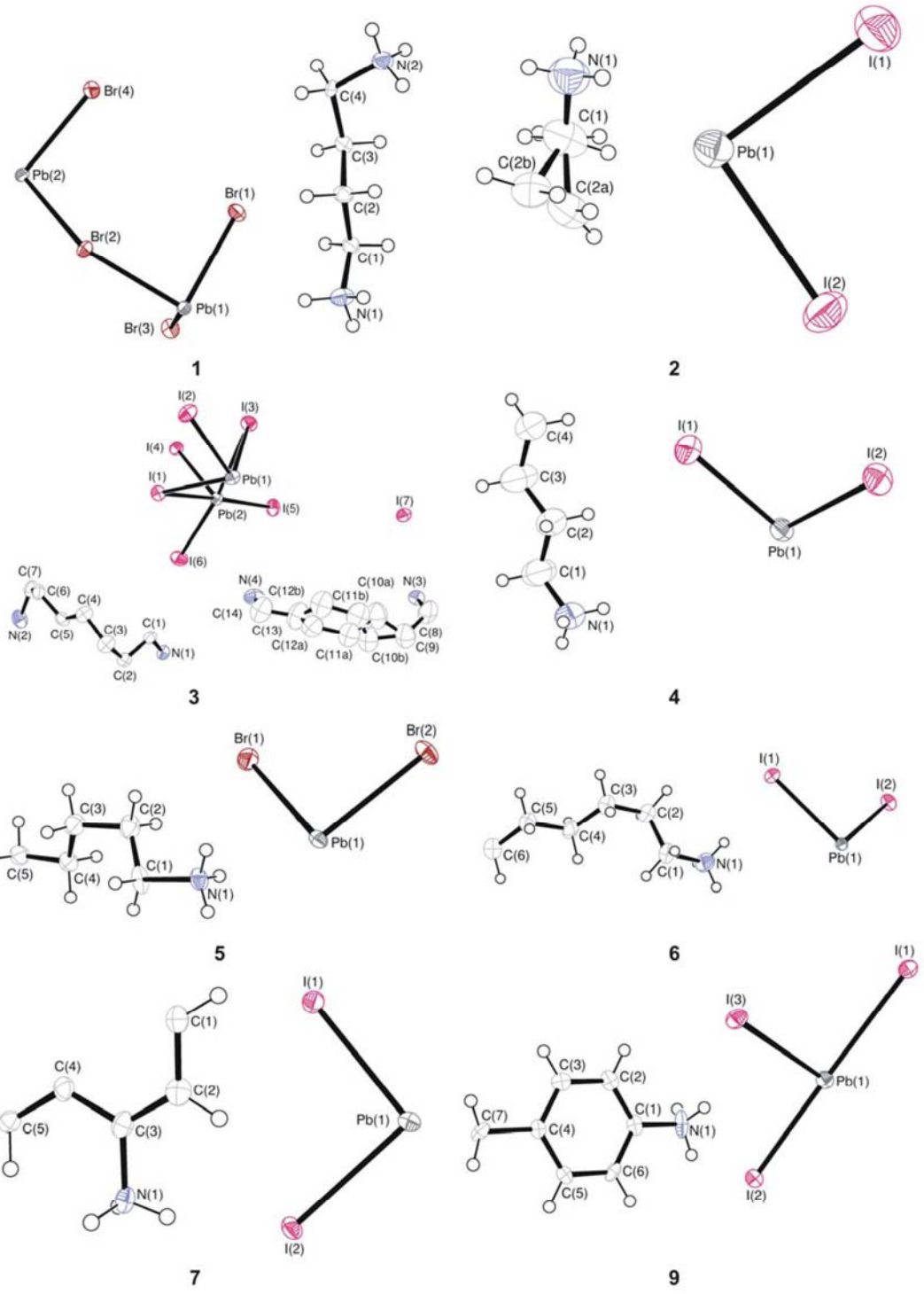


Fig. 1 The asymmetric units of compounds **1**-**7** and **9**, showing the atomic numbering scheme. Displacement ellipsoids are shown at the 50% probability level.

20

CREATED USING THE RSC ARTICLE TEMPLATE (VER. 2.0) - SEE WWW.RSC.ORG/ELECTRONICFILES FOR DETAILS

Introduction

Inorganic-organic hybrids with the general formula [(R-$NH_3)_2MX_4$] or [(H_3N-R-NH_3)MX_4], where M is any divalent metal and X = Cl, Br and I, have shown a great propensity for structural diversity. The choice of the ammonium cation, which can be anything from long alkylammonium chains to complex aromatic structures influences the motif of the inorganic component. If the inorganic part has a 2-D motif, then these compounds form natural quantum well materials that show photoluminescence, electroluminescence and nonlinear optical properties.[1]

Hybrids that have a 2-D inorganic motif are based on the $RbAlF_4$ structure type, which has AlF_6 octahedra corner linked in the *ab*-plane and successive layers are stacked on top of each other along the *c*-axis, separated by the Rb cation.[2] The structure of the hybrids results from replacing the Rb^{2+} cations with a monolayer of the bulkier diammonium cations and the inorganic layer consists of MX_6 corner-sharing metal halide octahedra. The four halides lying on the equatorial plane are shared out and refered to as bridging halides. The two halides in the axial position of the octahedra undergo no sharing and are called terminal halides. To keep these larger cations effectively in place, there exists hydrogen bonds between the ammonium groups on both ends of the organic cation and the halide on the metal. If two of the hydrogens bond to terminal halides and the third to a bridging halide, the hydrogen bonding is often refered to as having the terminal halogen configuration.[1] The reverse case, with hydrogen bonds to two bridging halides and one terminal halide, is called the bridging halogen configuration. Since the corner-sharing of the inorganic layers is confined to two dimensions, this motif is commonly known as layered perovskite-type. Few inorganic-organic hybrids with this layered perovskite-type motif have been synthesized and characterized with diammonium cations. The length of the simple straight alkyl chain studied is generally quite short with the maximum being ten carbon atoms, as seen in the compound [($H_3N(CH_2)_{10}NH_3$)$PbBr_4$].[3] Structural phase transitions in the compounds [($H_3N(CH_2)_nNH_3$)MX_4] (M = Mn or Cd; X = Cl and Br; n = 2-5) have been intensely invesigated and are due to conformational changes of the diammonium alkyl chains and their motion relative to the inorganic layers.[4]

An advantage to hybrids with diammonium groups is that even complex R groups are more likely to adopt the layered perovskite-type motif compared to having only one ammonium group. These complex R groups have been used to enhance the electroluminescence and photoluminescence properties of the layered perovskite-types hybrids compared to simple alkyl chains and aromatic moieties. Much work has been done on using organic molecules that show optical properties by themselves. For example, a specially synthesized oligothiophene chromophore was crystallized together with PbX_6, X = Cl, Br and I, out of solution and successfully gave the layered perovskite motif.[5] The molecule, 5,5'''-bis-(aminoethyl)-2,2':5',5",2'"-quaterthiophene, abbreviated AEQT, has a long, narrow profile and four α-linked thiophene rings. The two ethylammonium groups on either end of the R group act as anchorage points to the inorganic layer via the hydrogen bonds of the ammonium group, thus favouring the layered perovskite-type motif. Of the three compounds synthesized and characterised by optical absorption spectra, only [(AEQT)$PbBr_4$] was structurally characterized by Single-crystal X-ray diffraction. The packing of the compound has a herringbone arrangement in the monolayer of organic dye molecules. The conformation of the quaterthiophene backbone is syn-anti-syn and each ring is essentially planar. The ethylammonium anchors are bent out of the plane and adopt a conformation suitable to undergo the hydrogen bonding interactions. Only the compound [(AEQT)$PbCl_4$] shows relatively efficient room-temperature electroluminescence.[6]

Other examples of complex R goups that have been attempted with the various lead halides are 5,5'-bis(ammoniumethylsulfanyl-2,2'-bithiophene, abbr. AESBT, [7] and 1,6-bis[5'-(2"-aminoethyl)-2'-thienyl]-[hexane].[8]

In this study, we set out to investigate the affect of the R-group on the inorganic motif of the inorganic-organic hybrids where R is either a simple alkyl chain of increasing length, contains an aromatic fused system or has joined aromatic rings.

Results and Discussion

Crystallographic description of the layered perovskite-type hybrids with 1,4-diammoniumbutane: [($H_3NC_4H_8NH_3$)$PbBr_4$] (1) and [($H_3NC_4H_8NH_3$)PbI4] (2)

Fig. 2 clearly underlines a monodimensional arrangement for **1**, in which a single layer of 1,4-diammoniumbutane molecules are embedded between two consecutive inorganic [$PbBr_6$] sheets, forming an alternated inorganic-organic layered structure. The lead atoms are aligned from layer to layer, resulting in an eclipsed arrangement of adjacent layers. In the direction perpendicular to the layers, the crystal cohesion is achieved on both ends of the organic molecules by N-H...Br hydrogen bonds, related to the NH_3 polar groups. In the direction parallel to the layers, the cohesion is archieved by strong ionic bonds between equatorial bromide and lead atoms, giving the classical perovskite structural arrangement.

The inorganic layer is built up from characteristic corner-sharing $PbBr_6$ octahedra. The asymmetric unit consists of two lead atoms on special positions and four bromide atoms, Br(1) and Br(4) occupy the axial (terminal) positions and Br(2) and Br(3) occupy the equatorial (bridging) positions in the octahedra. In the projection perpendicular to the layers, along the *c*-axis, the $PbBr_6$ octahedra are rotated by 147.28(4)° and 149.42(3)° relative to each other. Furthermore, the perovskite layers are corrugated in the *a*-direction by an angle of 12.419(7)° with respect to the *bc*-plane. The coordination geometry around the Pb atom shows the typical axial compression of the octahedral geometry, with the bridging Br(3)-Pb(1)-Br(2) and Br(3)-Pb(1)-Br3 distances marginally longer than the axial distances Pb(1)-Br(1) and Pb(2)-Br(4). The angle between *cis* related bromide atoms deviate from 90°, with all *trans* angles 180°.

The 1,4 diammoniumbutane molecule sits on a general position and hence the asymmetric unit contains the complete

CREATED USING THE RSC ARTICLE TEMPLATE (VER. 2.0) - SEE WWW.RSC.ORG/ELECTRONICFILES FOR DETAILS

chain. The atomic numbering scheme is shown in Fig 1. The alkyl chains span half the length of the unit cell, orientated along the *b*-direction. The degree of rotation is approximately 33.9(1)° measured through a vector connecting the nitrogen atoms and the plane of the lead atoms. The chains are well ordered within the inorganic layer. The N(1) terminal end has a *trans* geometry so that the torsion angle for N(1)-C(1)-C(2)-C(3) is 171.3(8)°. There is a kink on the other terminal end with a torsion angle of 84.1(10)° for C(2)-C(3)-C(4)-N(2). This means that individual chains are situated over voids that are offset and at right-angles to each other. The hydrogen bonds between the inorganic and organic entities adopt the terminal halogen configuration, typical of layered perovskite-type hybrids with a monoclinic unit cell (See Table 2). A very similar cation conformation is seen in the closely related hybrid $[(H_3N(CH_2)_4NH_3)_2PbCl_4]$ (CSD ref. code: YOVXAI), which has staggered inorganic layers.[9] The 1,4-diammoniumbutane cation is non-centrosymmetric and has a "left-hand" conformation at one extremity. The atoms N(1), C(1), C(2), C(3), C(4) form a quasi-perfect all-trans configuration and Fig. 3 shows that N(2) is clearly bent out of the plane of those atoms.

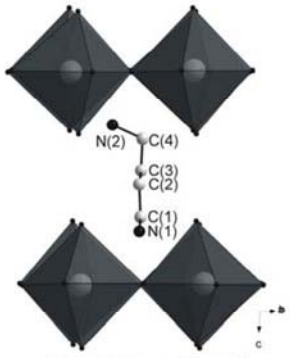


Fig. 3 Packing diagram of $[(H_3NC_4H_8NH_3)PbCl_4]$.[9]

Compound **2** has the same monodimensional arrangement as **1**, in which a single layer of 1,4-diammoniumbutane molecules are embedded between two consecutive inorganic $[PbI_6]$ sheets, forming an alternated organic-inorganic layered structure. The lead atoms are offset from layer to layer, resulting in a staggered arrangement of adjacent layers, identical to the hybrid with lead(II) chloride but different to compound **1**. Hence, the unit cell contains an extra layer compared to **1**. In the direction perpendicular to the layers, the crystal cohesion is achieved on both ends of the organic molecules by N-H...I hydrogen bonds, related to the NH_3 polar groups. In the direction parallel to the layers, the cohesion is archieved by strong ionic bonds between equatorial iodine and lead atoms, giving the classical perovskite structural arrangement.

The inorganic layer is built up from characteristic corner-sharing PbI_6 octahedra. The octahedra in $[(NH_3C_4H_8NH_3)PbI_4]$ sit on inversion centres and near 2-fold screw axis in the spacegroup $P2_1/c$. In the bromide case described above, the compound crystallizes in the triclinic spacegroup *P-1*, which has only got inversion centres. Hence, there are two unique bridging halides instead of the single one in **2**. Now, the asymmetric unit consists of one lead atom on a special position and two iodide atoms, I(1) occupying the axial position and I(2) occupying the equatorial position in the octahedra. In the projection perpendicular to the layers, along the *a*-axis, the PbI_6 octahedra are rotated by 147.175(19)° relative to each other. Furthermore, the perovskite layers are corrugated in the *b*-direction by an angle of 12.079(7)° with respect to the *bc*-plane. The coordination geometry around the Pb atom shows the typical axial compression of the octahedral geometry, with the bridging Pb(1)-I(2) distances longer than the axial distances Pb(1)-I(1). The angle between *cis* related iodide atoms deviate from 90°, with all *trans* angles equal to 180°.

The 1,4 diammoniumbutane molecule sits near a two fold axis and hence the asymmetric unit contains half the molecule only. The atomic numbering scheme is shown in Fig 1. The alkyl chains span half the length of the unit cell, orientated along the c-direction. The degree of rotation is approximately 33.73(9)° measured through a line connecting the nitrogen atoms and the plane of the lead atoms. The chains are disordered within the inorganic layer. The ammonium are well ordered by the hydrogen bonds to the halides and act as anchorage points around which the carbon chain flips. The second carbon atom in the chain is disordered over two positions, labelled C(2A) and C(2B). The second half of the complete chain is generated by a two fold rotation so that C(2A) is connected to C(2B) [symmetry operator: -x,y,-z+3/2] and vice versa. Subsequently, the chain has two unique torsion angles depending on which chain conformation is chosen: 99.8(16)° and 176.2(12)°.

The hydrogen bonds between the organic and inorganic entities adopt the same terminal halogen configuration as **1**. The hydrogen acceptor distances to the terminal halides I(1) are 2.71 Å and 2.89 Å and the bridging halide I(2) in between the two 2.81 Å (Fig 4).

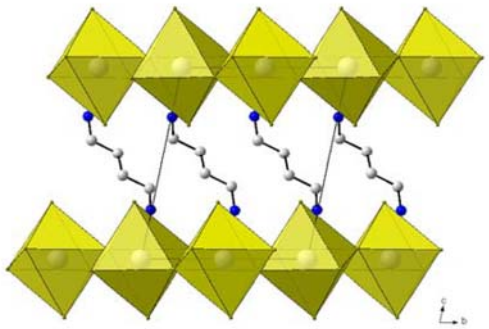


Fig. 2 Packing diagram of $[(H_3NC_4H_8NH_3)PbBr_4]$ (**1**).

This journal © Royal Society of Chemistry

CREATED USING THE RSC ARTICLE TEMPLATE (VER. 2.0) - SEE WWW.RSC.ORG/ELECTRONICFILES FOR DETAILS

[JOURNAL NAME HERE] | www.rsc.org/[JOURNAL] Article

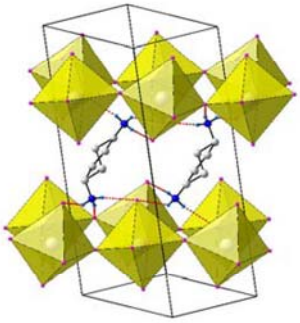


Fig. 4 Packing diagram and hydrogen bonding between the disordered 1,4-diammonium butane molecules and the staggered inorganic layers in $[(H_3NC_4H_8NH_3)PbI_4]$ (**2**).

Crystallographic description of the hybrid compound with 1,7-diammoniumheptane: $[(H_3NC_7H_{14}NH_3)_4Pb_3I_{12}\cdot 2I^-]$ (3)

The packing diagram consists of isolated $[Pb_3I_{12}]^{6-}$ blocks stacked parallel to the *ab*-plane (Fig. 5a). The spaces between these blocks are filled by isolated iodide atoms and 1,7-diammoniumheptane molecules, with the general direction of the carbon chain perpendicular to the *ab*-plane. The crystal cohesion is achieved on both ends of the organic molecules by N-H...I hydrogen bonds, related to the NH_3 polar groups, to the iodides on the blocks and the isolated iodides. There are van der Waals forces between two adjacent molecules (nearest neighbour carbon distance is 3.790(12) Å). In the direction parallel to the layers, the cohesion is archieved by strong ionic bonds between equatorial and axial iodine and lead atoms.

The inorganic motif is built up from characteristic face-sharing PbI_6 octahedra. The asymmetric unit contains two crystallographically independent Pb atoms, viz. atom Pb(1) and Pb(2). Each block consists of two Pb(2) octahedra and one Pb(1) octahedron, where the central Pb(1) octahedron is connected to the Pb(2) octahedra by shared faces. Atom Pb(1) is located on a centre of inversion and is bonded to only three unique halide atoms, viz. I(1), I(2) and I(3), which then complete the full octahedron through the inversion centre. Pb(2) is located on a general position and shares the same halides with Pb(1) to create the face-sharing connection. The full octahedron for Pb(2) is completed by the halides I(4), I(5) and I(6). The second Pb(2) octahedron is generated via the inversion centre on Pb(1) so that a Pb(2) octahedra is at the end of each block. A similar motif has been observed in the compound $[(AESBT)_3Bi_2I_9]$, which has blocks of two face-shared octahedra.[7]

Atom Pb(1) has a more regular coordination geometry, as it lies on an inversion centre, which ensures that all *trans* angles are exactly 180°. The angles between *cis* iodides are in the range 84.182(19)° to 95.818(19)°. The bond distances are in a narrow range from 3.2150(9) Å to 3.2260(10) Å. Atom Pb(2), in contrast, has a more distorted environment, with *cis* angles ranging from 79.85(2)° to 103.35(2)° and *trans* angles from 165.02(2)° to 176.02(2)°. Bond distances follow the same trend as the bond angles (3.0493(11) Å to 3.5047(12) Å).

There are two 1,7-diammoniumheptane molecules in the asymmetric unit, labeled cat1 (containing atom N(1) and N(2)) and cat2 (N(3) and N(4)). Both chains are parallel to the *c*-axis and are curved like a 'C'. Cat1 is ordered whereas cat2 is disordered. The three carbon atoms in the middle of the chain (C10, C11 and C(12)) are disordered over two positions, with the ratio of major to minor component being 61% to 39%.

The hydrogen bonds between the inorganic and organic entities are different for the four ammonium groups at the ends of the two unique 1,7-diammoniumheptane molecules (See Fig 5b). Two hydrogens and one hydrogen respectively on N(1) and N(2) bond to the isolated iodide I(7) (2.74 Å, 2.83 Å and 2.93 Å). The remaining three hydrogens bond to the iodides I(5), I(2) and I(1) of neighbouring blocks (2.82 Å, 2.86 Å and 2.96 Å). N(3) on cat2 bonds to equatorial iodides I(4) on different blocks (2.78 Å and 2.82 Å) and to I(7) (3.13 Å). N(4) does not bond to the isolated iodide I(7) at all. Two hydrogens bond to axial I(6) and equatorial I(5) on one block (2.87 Å and 2.88 Å). The last hydrogen bond to I(3) on another block (2.97 Å).

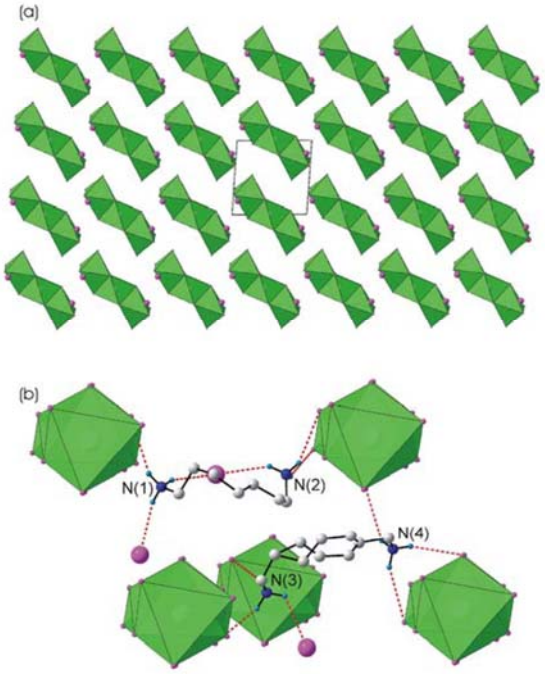


Fig. 5 (a) Packing diagram of the inorganic motif adopted in $[(H_3NC_7H_{14}NH_3)_4Pb_3I_{12}\cdot 2I^-]$ (**3**). The individual blocks are made up of three face-shared octahedra. (b) The two 1,7-diammoniumheptane cations hydrogen bond to the iodides of the PbI_6 octahedra and to the two isolated iodide atoms.

CREATED USING THE RSC ARTICLE TEMPLATE (VER. 2.0) - SEE WWW.RSC.ORG/ELECTRONICFILES FOR DETAILS

Crystallographic description of the layered perovskite-type hybrids with 1,8-diammoniumoctane, 1,10-diammoniumdecane and 1,12-diammoniumdodecane: $[(H_3NC_8H_{16}NH_3)PbI_4]$ (4), $[(H_3NC_{10}H_{20}NH_3)PbBr_4]$ (5) and $[(H_3NC_{12}H_{24}NH_3)PbI_4]$ (6)

The structure of $[(H_3NC_6H_{12}NH_3)PbI_4]$ was reported previously[10] and is similar to **4**, **5** and **6**. All of the compounds have centrosymmetric diammonium cations. A comprehensive description of **4** will be given and the differences and similiarities between all three subsequently summarized. Attempts at crystallizing lead iodide with 1,10-diammoniumdecane gave poor quality crystals, whereas the crystals of the lead bromide analogue gave twinned plates that could be resolved.

The crystal structure of **4** has a monodimensional arrangement in which a single layer of 1,8-diammoniumoctane molecules are embedded between two consecutive inorganic $[PbI_6]$ sheets, forming an alternated organic-inorganic layered structure. The lead atoms are aligned from layer to layer, resulting in an eclipsed arrangement of adjacent layers. The asymmetric unit consists of a lead atom on a special position and two iodide atoms, I(1) occupying the axial position and I(2) occupying the equatorial position in the octahedra. Along the *a*-axis, the PbI_6 octahedra are rotated by 147.62(2)° relative to each other. Furthermore, the perovskite layers are corrugated in the *b*-direction by an angle of 11.825(11)° with respect to the *bc*-plane. The coordination geometry around the Pb atom shows the typical axial compression of the octahedral geometry, with the bridging Pb(1)-I(2) distances longer than the axial distances Pb(1)-I(1). The angle between *cis* related iodine atoms deviate from 90°, with all *trans* angles 180°.

The greatest change structurally in the inorganic layers is the corrugation of the octahedra in the *b*-direction. The angle decreases to 2.479(8)° in **4** and to 0.231(62)° in **5**. The angle of rotation btween adjacent octahedra does not change much for **5** (148.85(5)°) and **6** (148.30(3)°).

The 1,8 diammoniumoctane molecule sits near the centre of inversion and hence the asymmetric unit contains half the molecule only. The atomic numbering scheme is shown in Fig 1. The alkyl chains span the length of the unit cell, orientated along the *c*-direction. The degree of rotation is approximately 39.32(7)° measured through a line connecting the two nitrogen atoms and the plane of the lead atoms (Figure 6a). The chains are ordered within the inorganic layer. The eight-membered alkyl chain has two conformations, *trans* and gauche. The four carbon atoms and nitrogen atom making up the asymmetric unit are all *trans* to each other and lie approximately in a plane. However, there is a kink in the middle of the chain which means the two halves form an approximate gauche angle of 63.7(18)° to each other.

The hydrogen bonds between the organic and inorganic entities adopt the terminal halogen configuration, typical of hybrid perovskites with a monoclinic unit cell (See Table 2). The hydrogen acceptor distances to the terminal halides I(1) are 2.75 Å and 2.93 Å and the bridging halide I(2) 2.80 Å.

Comparing the packing of the organic molecules among the three compounds **4**, **5**, and **6**, the major difference is the increase of the tilt angle of the chains to the inorganic layers and the conformation of the chains. The tilt of the 1,10 diammoniumdecane molecule in **5** is approximately 41.72(5)° and 45.73(6)° for 1,12-diammoniumdodecane in **6**. The alkyl chains have an all *trans* geometry except between the carbon atoms on the terminal end of the chain where the four carbon atoms C(1)-C(2)-C(3)-C(4) have a torsion angle of -69.6(16)°. In **6**, this torsion angle is -81(2)°. There are no gauche bonds between the two symmetry related parts of the cations as in **4**.

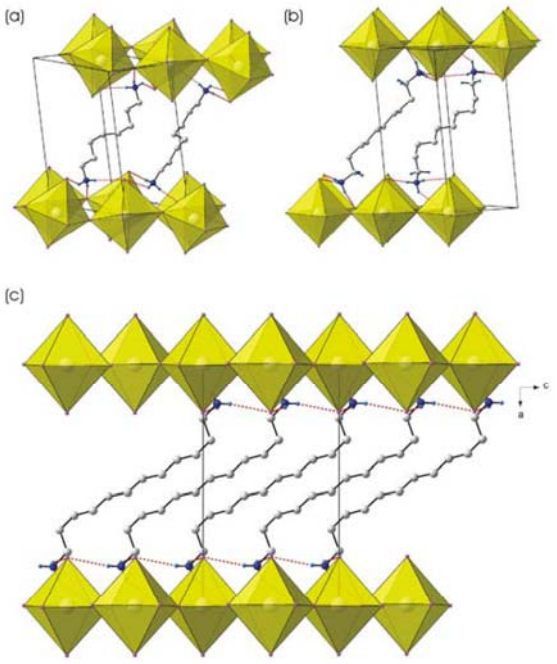


Fig. 6 The packing diagrams of **4** (a), **5** (b) and **6** (c). All of the compounds have centrosymmetric cations and eclipsed inorganic layers.

Crystallographic description of the layered perovkite-type hybrid with 1,5-diammoniumnaphthalene: $[(H_3NC_{10}H_6NH_3)PbI_4]$ (7)

Diammonium compounds with aromatic R groups are rarer than hybrids with simple diammonium alkyl chains. The simplest structure has a single benzene ring, as in 1,4-phenylenediammonium. The ammonium groups have to be *para* to each other, otherwise they will not be able to hydrogen bond to the adjacent layers at the same time. Only two such structures have been made, $(H_3N\text{-}C_6H_4\text{-}NH_3)[CdCl_4]$[11] (CSD ref. code: ZITTOL) and $(H_3N\text{-}C_6H_4\text{-}NH_3)[CuCl_4]$[1c] (CSD ref. code: HAJSOB). Both have eclipsed inorganic layers and the same terminal halogen configuration of hydrogen bonds. The phenyl rings themselves are almost perpendicular to the plane of the inorganic layers. Both compound have weak edge-to-face C-H...π interaction between adjacent phenyl rings (Hydrogen...centroid distance

 This journal © Royal Society of Chemistry

CREATED USING THE RSC ARTICLE TEMPLATE (VER. 2.0) - SEE WWW.RSC.ORG/ELECTRONICFILES FOR DETAILS

[JOURNAL NAME HERE] | www.rsc.org/[JOURNAL] Article

is 3.13(2) Å for the Cu compound and 3.03(7) Å for Cd compound). To investigate the effect of multiple fused phenyl rings on the inorganic motif, we decided to use for the R group a naphthalene backbone that still has the ammonium groups parallel to each other. The two aromatic pi systems might increase the strength of the C-H...π interactions.

Figure 7b clearly underlines a monodimensional arrangement in which a single layer of 1,5-diammoniumnaphthalene molecules are embedded between two consecutive inorganic [PbI_6] sheets, forming an alternated organic-inorganic layered structure. The lead atoms are aligned from layer to layer, resulting in an eclipsed arrangement of adjacent layers. As shown in the projection perpendicular to the layers, along the *a*-axis, the PbI_6 octahedra are rotated by 150.668(18)° relative to each other. Furthermore, the perovskite layers are corrugated in the *b*-direction by an angle of 5.857(8)° with respect to the *bc*-plane. The coordination geometry around the Pb atom shows the typical axial compression of the octahedral geometry, with the bridging Pb(1)-I(2) distances longer than the axial distances Pb(1)-I1. The angle between *cis* related iodine atoms deviate from 90°, with the *trans* angles equal to 180°.

The 1,5-diammonium naphthalene molecule sits near a centre of inversion and hence the asymmetric unit contains half the molecule only. The atomic numbering scheme is shown in Fig 1. The fused rings are tilted around their midpoint between the layers to maximise the interlayer spacing. The degree of rotation is approximately 21.5(1)° measured through the atoms N(1) and N(1)' [symmetry position: -x,-y,-z], and the plane of the lead atoms. The fused rings are ordered within the inorganic layer and orientated with the backbone of the ring lying along the longest diagonal of the parallelogram generated by four corner-shared octahedra (See Fig. 7a). The fused rings themselves are at right angles to the inorganic layer, parallel to the *a*-axis. Adjacent naphthalene rings have dihedral angles of 88.2(1)° to each other to create a edge-to-face packing arrangement with a centroid-to-centroid distance of 5.45(2) Å, too large to be considered as representing π-stacking interactions. The carbon and nitrogen atoms all lie in the plane of the ring. Even though the packing of the cations is the same as the Cd and Cu hybrids mentioned above, the distance between H atoms and the two nearest centroids are 3.305(1) Å and 3.799(1) Å, too large for C-H...π interactions. The large distance between the centroids is due to the larger ionic radii[12] of I^- (2.20 Å) and Pb^{2+} (1.19 Å) compared to Cl^- (1.81 Å), Cd^{2+} (0.95 Å) and Cu^{2+} (0.73 Å), which causes the "box" created by the corner-shared octahedra within which the cations sit to be further apart.

The hydrogen bonds between the organic and inorganic entities adopt the terminal halogen configuration, typical of hybrid perovskites with a monoclinic unit cell (See Table 2). The hydrogen acceptor distances to the terminal halides are significantly shorter (2.58 Å and 2.62 Å) than to the bridging halides (3.02 Å).

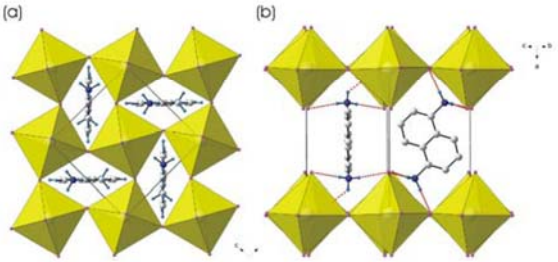


Fig. 7 (a) The 1,5-diammoniumnaphthalene molecules are almost perpendicular to each other. (b) The terminal halogen configuration and tilts of the fused rings.

Crystallographic description of the hybrid with the inorganic ribbon motif with 1,2-diammoniumethane: $[(H_3NC_2H_4NH_3)_4Pb_2Br_9{\cdot}3Br^-]$ (8)

The 1,2-diammoniumethane cation has formed many layered perovskite-type hybrids with a variety of divalent metals (Ni, Mn and Cu) and halides (Cl and Br).[13] The compound using lead(II) bromide does not give the 2-D layered perovskite-type motif but has infinite one-dimensional ribbons of corner-sharing $PbBr_6$ octahedra running along the *a*-axis. This ribbon motif is nonetheless closely related to the layered $RbAlF_4$ motif. Every fifth row of $PbBr_6$ octahedra is missing, i.e. each ribbon has a width of four corner-sharing octahedra (Fig. 8). These ribbons are then tilted relative to each other. Fig. 9 shows the atomic numbering scheme.

Figure 10 clearly underlines a one-dimensional arrangement in which the ribbons are surrounded by 1,2-diammoniumethane molecules and isolated bromide atoms. The individual ribbons are tilted at 75° to each other along the *b*-axis to create a washboard-like packing. Above and below the ribbons, the crystal cohesion is achieved on both ends of the organic molecules by N-H...Br hydrogen bonds. In the direction parallel to the slabs, the cohesion is archieved by strong ionic bonds between bromide and lead atoms.

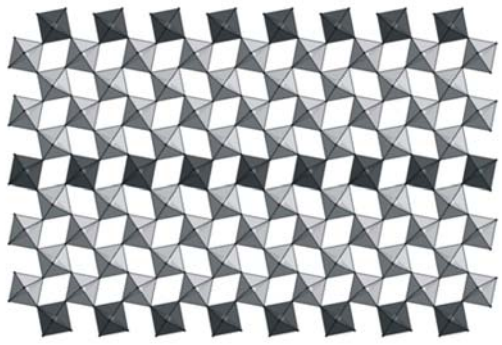


Fig. 8 The cut-out of the 2-D $RbAlF_4$ type inorganic motif that gives rise to the 1-D inorganic ribbons, shown as light grey octahedra. Every fifth row is missing, shown as dark grey octahedra.

The asymmetric unit contains two crystallographically independent lead atoms, viz. atom Pb(1) and Pb(2), that occupy general positions and thirteen bromide atoms. The ribbons have a width of four Pb atoms, with two Pb(1)

CREATED USING THE RSC ARTICLE TEMPLATE (VER. 2.0) - SEE WWW.RSC.ORG/ELECTRONICFILES FOR DETAILS

octahedra in the middle and the Pb(2) octahedra bordering the slabs on both sides. The bromides Br(11), Br(12) and Br(13) are isolated and occupy the space between adjacent slabs. Br(2), Br(3), Br(7) and Br(10) are in the four axial positions of the Pb(1) and Pb(2) octahedra. The axial bromides Br(4) and Br(5) are corner shared by the Pb(1) and Pb(2) octahedra and are hence classified as bridging bromides. Br(8) and Br(9) occupy the last two axial positions in Pb(2) to complete the full octahedron. These two bridged Pb(1) and Pb(2) units make up exactly half of the slabs. The complete slab is then created by connecting two units together via the bridging bromides Br(1) and Br(6). These two bromides complete the full octahedral geometry of Pb(1) and run through the exact centre of the slabs. Hence, they are the only atoms on special positions at (0,1/2,1/2) and (-1/2,1/2,1/2) respectively. This means that the bridging angles Pb(1)-Br(1)-Pb(1) and Pb(1)-Br(6)-Pb(1) are close to 180.0°. The other two bridging angles are 173.34(7)° and 161.23(7)° respectively for Pb(1)-Br(4)-Pb(2) and Pb(1)-Br(5)-Pb(2). The geometry around the Pb(1) and Pb(2) octahedra is severely distorted with *cis* angles deviating at most by 8.58(4)° from 90° for Pb(1) and by 10.06(5)° for Pb(2). *Trans* angles are equally far from ideal for Pb(1) (170.31(5)°) and Pb(2) (163.89(5°)).

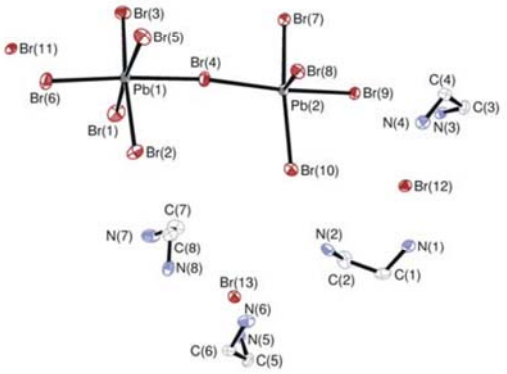


Fig. 9 The asymmetric unit of compound **8**, showing the atomic numbering scheme. Displacement ellipsoids are shown at the 50% probability level. The H atoms are omitted for clarity.

The asymmetric unit contains four 1,2-diammoniumethane molecules. The organic molecules follow a similar wave pattern as the inorganic component and sit in the holes formed by the corner-shared octahedra. All four unique amines are ordered and have the same staggered conformation. The general torsion angles N-C-C-N around the carbon atoms range from 66(2)° to 78.1(17)°.

The acceptor atoms for the hydrogen bonds are the bromide atoms in the axial and equatorial positions of the octahedra and to the three isolated bromide atoms. The four cations are labeled cat1 (containing atom N(1) and N(2)), cat2 (N(3) and N(4)), cat3 (N(5) and N(6)) and cat4 (N(7) and N(8)). N(1) hydrogen bonds only to isolated bromide atoms with hydrogen acceptor distances varying from 2.47 Å to 2.76 Å. N(2)-H(2B) has the second shortest distance to Br(13) (2.37 Å) with the remaining hydrogens bonding to Br(9) and Br(5), 2.52 Å and 2.69 Å respectively.

The second cation has the same hydrogen bonding configuration for N(3) and N(4), i.e. bridging to two axial and one isolated bromide. The distances to the acceptor atoms range form 2.38 Å to 2.79 Å.

N(5) on the third cation bonds to the equatorial bromide Br(8) and the bridging bromide Br(7) (2.49 Å and 2.53 Å) and one axial bromide Br(10) (2.49 Å). N(6) on the other hand bonds to three equatorial bromides, Br(9) twice and Br(8) once, and one isolated bromide Br(12).

Cat4 bonds on one end to Br(4) (bridging, 2.62 Å), Br(5) (bridging, 2.77 Å) and Br(11) (isolated, 2.49 Å) and on the opposite end to four isolated bromides, Br(12), Br(13) and Br (11) (twice). The distance to Br(13) is the shortest at 2.32 Å. A complete list of all the hydrogen bonds is given in Table 3.

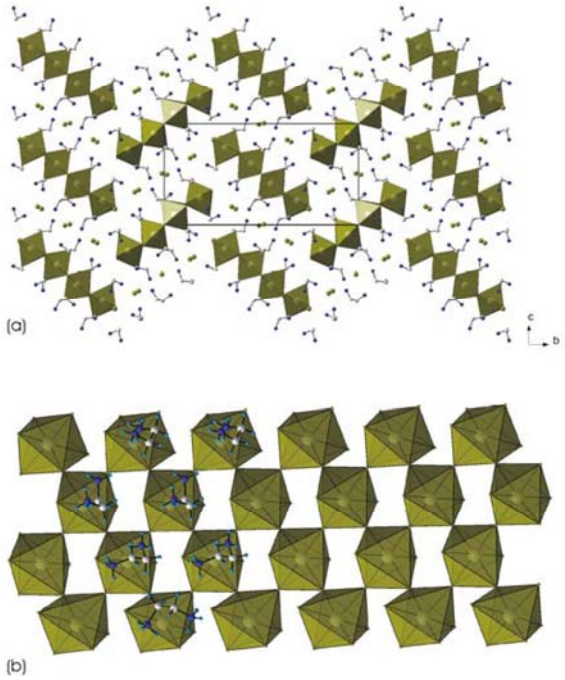


Fig. 10 (a) The wave-like arrangement of the ribbons of corner-shared $PbBr_6$ octahedra in **8**. (b) The ribbons form infinite 1-D chains along the *a*-axis.

Crystallographic description of the hybrid with the twin anionicchain motif with 4,4'-methylenedianilinium: $[(H_3NC_6H_4CH_2C_6H_4NH_3)Pb_2I_6]$ (9)

Instead of having two phenyl rings fused as in compound **7**, the next step up would have two phenyl rings connected in a *para*-fashion, so that the ammonium groups are still *para* to each other. This organic compound is readily available and called benzidine. Only one reported structure with the layered perovskite-type motif exists with this cation. $(H_3N\text{-}C_6H_4\text{-}C_6H_4\text{-}NH_3)[CuCl_4]$[1c] (CSD ref. code: HAJTES), which has eclipsed inorganic layers with an interlayer spacing of 14.3769(2) Å. The hydrogen bonding interactions are the same as for the mono-phenyl structures (terminal halogen configuration). The Cu compound with the benzidine cation

 This journal © Royal Society of Chemistry

CREATED USING THE RSC ARTICLE TEMPLATE (VER. 2.0) - SEE WWW.RSC.ORG/ELECTRONICFILES FOR DETAILS

[JOURNAL NAME HERE] | www.rsc.org/[JOURNAL] Article

has two edge-to-face C-H...π interactions (H...centroid distance 2.985(2) Å and 3.074(2) Å) and which further stabilize the overall structure. Inserting a CH_2 group between the phenyl rings has the ammonium groups no longer directly opposite each other. This makes the layered perovskite motif no longer favourable, as observed in the rarely seen motif (Fig. 11) of the reported hybrid $[(H_3NC_6H_4CH_2C_6H_4NH_3)Pb_2I_6]$ (**9**).

Figure 12a clearly underlines a checkerboard arrangement in which twin-anionic chains of edge-sharing PbI_6 octahedra are surrounded by protonated 4,4'-methylenedianiline molecules. This inorganic motif is based on strips of the CdI_2-type structure taken along the <100> direction.[14] The simplest case has two chains connected, as shown in Figure 11 below. In the direction perpendicular to the chains, the crystal cohesion is achieved on both ends of the organic molecules by N-H...I hydrogen bonds. In the direction parallel of the chains, the cohesion is archieved by strong ionic bonds between iodine and lead atoms and N-H...π hydrogen bonds between individual 4,4'-methylenedianilinium molecules.

The asymmetric unit consists of a lead atom and three iodide atoms (Fig. 1). I(1) occupies three positions in the octahedra, an axial position and two equatorial positions. All three I1 are *cis* to each other. I(2) occupies the remaining axial position in the octahedra and I(3) the other two equatorial positions. The octahedra share equatorial edges, made up of I(1) and I(3), on both sides. Hence, due to the arrangement of the sharing, I(1) can occupy both the equatorial and axial positions in two bonded octahedra (Fig. 12c). The two chains are then connected to each other via two axial edges to form a double-barrel. The coordination geometry around the Pb atom shows the equatorial bond distances to be similiar whereas the two axial bond distances are the longest and shortest. The angle between *cis* related iodide atoms deviate from 90°, and the *trans* angles from 180°. This motif has been seen in $[(C_{10}H_7CH_2NH_3)PbI_3]$.[15]

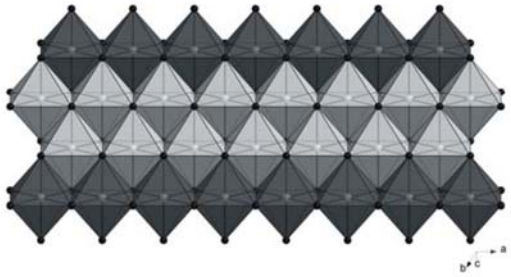


Fig. 11 A single layer cutout of the CdI_2-structure type. The octahedra in light grey show the twin anionic chains seen in the lead iodide organic-inorganic hybrid **9**.

The 4,4'-methylenedianilinium molecule sits on a mirror plane and hence the asymmetric unit contains half the molecule only. The atomic numbering scheme is shown in Fig 1. Adjacent molecules are stacked parallel to each other along the *c*-axis. The two aromatic rings connected bt the methylene carbon are not tilted relative to each other by virtue of the mirror plane. The methylene carbon atom linking the two rings has tetrahedral geometry as the bond angle between the rings is 111.3(9)°.

The hydrogen bonds to the inorganic moieties are via two of the hydrogens on the ammonium head group. One hydrogen has a bifurcated bond to I(3) and I(2) and the distances are 2.80 Å and 3.06 Å respectively. The other hydrogen bond is simple and bonds to I(2) as well (3.08 Å). The last hydrogen is unusual and bonds to the π centre of the aromatic rings on neighbouring 4,4'-methylenedianilinium molecules (Fig. 12b). The hydrogen-centroid distance is 2.58 Å.

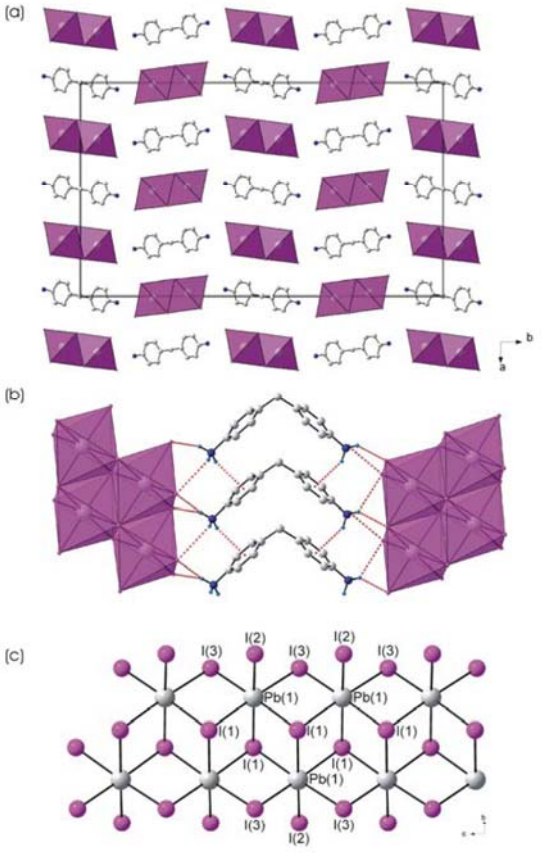


Fig. 12 (a) The packing diagram of **9**. The cations sit in channels created by the inorganic chains. (b) The hydrogen bonding pattern between the organic and inorganic moieties and the parallel stacking of the organic caations, strengthened by C-H...π interactions. (c) The atomic labelling scheme of the twin-anionic chains. Each PbI_6 octahedral unit shares out four edges.

Conclusion

The even-membered alkyl chains with ammonium groups at both ends gave layered perovskite-type hybrid structures, regardless if the halide is bromide or iodide (structures **1, 2, 4-6**). The chains that are sandwiched in between the 2-D layers have kinks in them so that the hydrogens on both ends of the organic molecules can hydrogen bond to the halides of the inorganic layers. The odd-membered alkyl chains behaved differently, and gave different inorganic motifs for lead

CREATED USING THE RSC ARTICLE TEMPLATE (VER. 2.0) - SEE WWW.RSC.ORG/ELECTRONICFILES FOR DETAILS

Article www.rsc.org/[JOURNAL] | [JOURNAL NAME HERE]

iodide. The compound $[(H_3NC_5H_{10}NH_3)_4Pb_3I_{10}]$[16] has 1-D chains of face- and edge-sharing lead iodide octahedra and structure **3** has a 0-D inorganic motif of isolated face-sharing blocks of lead iodide octahedra surrounded by $(H_3N(CH_2)_7NH_3)$ cations. A related templating effect by the organic cation has also been seen in the hybrids with tin as the metal.[17] Hence, the use of either even- or odd-membered diammonium alkyl chains may affect the motif of the inorganic layer.

The use of fused aromatic rings can also form the layered perovskite structure if the cation is able to tilt within the holes and hydrogen bond to the ioides (**7**). If the ammonium groups are fixed in their positions to the aromatic cations and have no degree of freedom, the layered perovskite motif is not favoured and 1-D motifs are observed (**9**). Lastly, even if the cation consists of C-C single bonds and has an even-membered chain, as in $(H_3N(CH_2)_2NH_3)$, the layered perovskite motif is predicted but not observed. Compound **8** has 1-D ribbons made up of corner-sharing $PbBr_6$ octahedra, which are still structurally closely related to the layered perovskite-type motif.

Experimental

Materials

All reagents and solvents employed were commercially available and used as received without further purification.

Synthesis

Preparation of $[(H_3NC_4H_8NH_3)PbBr_4]$, 1. 0.099 g $PbBr_2$ (0.270 mmol) was dissolved in 3 ml 48% HBr in a sample vial. Thereafter, 0.022 g $NH_2C_4H_8NH_2$ (0.250 mmol) was added and the precipitate dissolved by refluxing at 85°C. The solution was slowly cooled at 2°C/hour to room temperature. A colourless single crystal suitable for X-ray diffraction analysis was selected and studied. Elemental analysis (%). Found: C , H , N . Calc. for $C_4H_{14}Br_4N_2Pb_1$: C 7.79, H 2.29, N 4.54.

Preparation of $[(H_3NC_4H_8NH_3)PbI_4]$, 2 0.148 g PbI_2 (0.321 mmol) was dissolved in 3 ml 47% HI in a sample vial. Thereafter, 0.054 g $NH_2C_4H_8NH_2$ (0.680 mmol) was added and the precipitate dissolved by refluxing at 80°C. The solution was slowly cooled at 2°C/hour to room temperature. An orange single crystal suitable for X-ray diffraction analysis was selected and studied. Elemental analysis (%). Found: C 5.83, H 1.92, N 3.37. Calc. for $C_4H_{14}I_4N_2Pb_1$: C 5.97, H 1.75, N 3.48.

Preparation of $[(H_3NC_7H_{14}NH_3)_4Pb_3I_{12}{\cdot}2I^-]$, 3. 0.149 g PbO (0.323 mmol) was dissolved in 3 ml 47% HI in a sample vial. Thereafter, 0.167 g $NH_2C_7H_{14}NH_2$ (0.307 mmol) was added and the precipitate dissolved with slight heating. The orange crystals grew from slow evaporation at room temperature. A single crystal suitable for X-ray diffraction analysis was selected and studied. Elemental analysis (%). Found: C 11.71, H 2.99, N 3.86. Calc. for $C_{28}H_{80}I_{14}N_8Pb_3$: C 11.49, H 2.75, N 3.83.

Preparation of $[(H_3NC_8H_{16}NH_3)PbI_4]$, 4. 0.137 g PbI_2 (0.297 mmol) was dissolved in 3 ml 47% HI in a round bottom flask. Thereafter, 0.050 g $NH_2C_8H_{16}NH_2$ (0.342 mmol) was added and the precipitate dissolved by refluxing for 12 hours at 100°C. The solution was slowly cooled at 2°C/hour days to room temperature. A yellow single crystal suitable for X-ray diffraction analysis was selected and studied. Elemental analysis (%). Found: C 11.24, H 2.65, N 3.31. Calc. for $C_8H_{22}I_4N_2Pb_1$: C 11.16, H 2.58, N 3.25.

Preparation of $[(H_3NC_{10}H_{20}NH_3)PbBr_4]$, 5. 0.058 g $PbBr_2$ (0.158 mmol) was dissolved in 5 ml 48% HBr in a glass vial. Thereafter, 0.050 g $NH_2C_{10}H_{20}NH_2$ (0.290 mmol) was added and the precipitate dissolved by refluxing for 12 hours at 110°C. The solution was slowly cooled at 2°C/hour to room temperature. A colourless single crystal suitable for X-ray diffraction analysis was selected and studied. Elemental analysis (%). Found: C 16.99, H 3.64, N 3.91. Calc. for $C_{10}H_{26}Br_4N_2Pb_1$: C 17.13, H 3.74, N 4.00.

Preparation of $[(H_3NC_{12}H_6NH_3)PbI_4]$, 6. 0.049 g PbI_2 (0.106 mmol) was dissolved in 3 ml 47% HI / 3 ml acetone in a round bottom flask. Thereafter, 0.026 g $NH_2C_{12}H_{24}NH_2$ (0.130 mmol) was added and the precipitate dissolved by refluxing for 1 hour at 80°C. The solution was slowly cooled at 2°C/hour days to room temperature. A yellow single crystal suitable for X-ray diffraction analysis was selected and studied. Elemental analysis (%). Found: C 11.16, H 2.58, N 3.25. Calc. for $C_{12}H_{30}I_4N_2Pb_1$: C 15.71, H 3.30, N 3.05.

Preparation of $[(H_3NC_{10}H_6NH_3)PbI_4]$, 7. 0.060 g PbI_2 (0.130 mmol) was dissolved in 5 ml 47% HI in a sample vial. Thereafter, 0.011 g $C_{10}H_{10}N_2$ (0.070 mmol) was added and the precipitate dissolved by refluxing for 12 hours at 100°C. The solution was slowly cooled at 2°C/hour to room temperature. A yellow single crystal suitable for X-ray diffraction analysis was selected and studied. Elemental analysis (%). Found: C 13.78, H 1.56, N 3.05. Calc. for $C_{10}H_{12}I_4N_2Pb_1$: C 13.73, H 1.38, N 3.20.

Preparation of $[(H_3NC_2H_4NH_3)_4Pb_2Br_9{\cdot}3Br^-]$, 8. 0.070 g $PbBr_2$ (0.191 mmol) was dissolved in 10 ml 48% HBr in a glass vial. Thereafter, 0.021 g $NH_2C_2H_4NH_2$ (0.349 mmol) was added and the precipitate dissolved by refluxing for 3 hours at 88°C. The solution was slowly cooled at 2°C/hour to room temperature. No crystals formed. Thereafter, slow evaporation of the solution at room temp over sveral days gave colourless blocks. A colourless single crystal suitable for X-ray diffraction analysis was selected and studied. Elemental analysis (%). Found: C 5.93, H 2.35, N 6.96. Calc. for $C_8H_{40}Br_{12}N_8Pb_2$: C 5.93, H 2.49, N 6.91.

Preparation of $[(H_3NC_6H_4CH_2C_6H_4NH_3)Pb_2I_6]$, 9. 0.041 g PbI_2 (0.089 mmol) was dissolved in 5 ml 47% HI in a round bottom flask. Thereafter, 0.014 g $NH_2C_{13}H_{10}NH_2$ (0.071 mmol) was added and partially dissolved by refluxing for 12 hours at 90°C. The solution was slowly cooled at 2°C/hour to room temperature. A yellow single crystal suitable for X-ray diffraction analysis was selected and studied. Elemental

This journal © Royal Society of Chemistry

CREATED USING THE RSC ARTICLE TEMPLATE (VER. 2.0) - SEE WWW.RSC.ORG/ELECTRONICFILES FOR DETAILS

[JOURNAL NAME HERE] | www.rsc.org/[JOURNAL] Article

Analysis (%). Found: C 11.41, H 1.29, N 2.00. Calc. for $C_{13}H_{16}I_6N_2Pb_2$: C 11.35, H 1.17, N 2.04

Crystal Data and X-Ray structure analysis

Intensity data were collected on a Bruker SMART 1K CCD area detector diffractometer with graphite monochromated Mo K_α radiation (50kV, 30mA). The collection method involved ω-scans of width 0.3°. Data reduction was carried out using the program *SAINT+*, version 6.02.[18] and face indexed absorption corrections were made using the program XPREP.[18]

The crystal structure was solved by direct methods using SHELXS-97.[19] Non-hydrogen atoms were first refined isotropically followed by anisotropic refinement by full matrix least-squares calculations based on F^2 using SHELXL-97.[19] Hydrogen atoms were first located in the difference map then positioned geometrically and allowed to ride on their respective parent atoms. Diagrams and publication material were generated using WinGx[20], ORTEP[21], PLATON[22] and DIAMOND[23]. Further crystallographic data are summarised in Table 1.

The conformational disorder in compound **2** around the carbon atom C(2) was resolved by finding alternate positions from the difference Fourier map for the respective atoms. These atoms, C(2A) and C(2B), were then refined anisotropically together with their site occupancy such that the sum of the occupancies for the two alternate atom positions equaled one. Hydrogen atom positions were then calculated for the respective atoms using a riding model. The ratio of major to minor component is 59 to 41%.

The conformational disorder in compound **3** around the carbon atoms C(10), C(11) and C(12) was resolved by finding alternate positions from the difference Fourier map for the respective atoms. These six atoms were then refined anisotropically together with their site occupancy such that the sum of the occupancies for the two alternate atom positions equaled one. Hydrogen atom positions were then calculated for the respective atoms using a riding model. The ratio of major to minor component is 61 to 39%.

The 20°C structures of compounds **1**, **3**, **5**, **6**, **7**, **8** and **9** were considered to be not good enough for publication. These were subsequently repeated at -100°C. Comparison of the 20°C and -100°C structures of these compounds reveal that no phase changes took place upon cooling. Further crystallographic data are summarised in Table 1.

References

1 (a) D.B. Mitzi, Prog. *Inorg. Chem.* 1999, 1; (b) G.C. Papavassiliou, G. A. Mousdis and I. B. Koutselas, *Adv. Mater. Opt. Electron.*, 1999, **8**, 265; (c) S.A. Bourne and Z. Mangombo, *CrystEngComm*, 2004, **6**, 437.
2 D. M. Hatch and H. T. Stokes, *Phys. Rev. B*, 1987, **35**, 8509.
3 T. Matsui, M. Kawahara, K. Teshima, M. Rikukawa and K. Sanui, *Mol. Cryst. Liq. Cryst.*, 2002, **376**, 89.
4 (a) R. Blinc, M. Burgar, B. Ložar, J. Seliger, J. Slak, V. Rutar, H. Arend and R. Kind, *J. Chem. Phys.*, 1977, **66**, 278; (b) J. C. Crowley, H. W. Dodgen and R. D. Willett, *J. Phys. Chem.*, 1982, **86**, 4046; (c) R. Kind, S. Plesko and J. Roos, *Phys. Stat. Sol. (a)*, 1978, **47**, 233; (d) A. Levstik, C. Filipič, R. Blinc, H. Arend and R. Kind, *Solid State Commun.*, 1976, **20**, 127; (e) K. Tichý, J. Beneš, W. Hälg and H. Arend, *Acta Cryst. B*, 1978, **34**, 2970; (f) M. J. Tello, M. A. Arriandiaga and J. Fernãndez, *Solid State Commun.*, 1978, **24**, 299.
5 D. B. Mitzi, K. Chondroudis and C. R. Kagan, *Inorg. Chem.*, 1999, **38**, 6246.
6 K. Chondroudis and D. B. Mitzi, *Chem. Mater.*, 1999, **11**, 3028.
7 X.-H Zhu, N. Mercier, P. Frère, P. Blanchard, J. Roncali, M. Allain, C. Pasquier and A. Riou, *Inorg Chem.*, 2003, **42**, 5330.
8 K. Chondroudis, D. B. Mitzi, D.B and P. Brock, *Chem. Mater.*, 2000 **12**, 169.
9 C. Courseille, N. B. Chanh, Th. Maris, A. Daoud, Y. Abid and M. Laguerre, *Phys. Stat. Sol. (a)*, 1994, **143**, 203.. 316
10 G. A. Mousdis, G. C. Papavassiliou, C. P. Raptopoulou and A. Terzis, *J. Mater. Chem.*, 2000, 10, 515. 25
11 Q. Ye, Q. Meng, X. You and X. Huang, *Acta Cryst.C*, 1996, **52**, 33.
12 R.D. Shannon, *Acta Cryst. A*, 1976, **32**, 751.
13 (a) S. Skaarup and R.W. Berg, *J Solid State Chem.*, 1978, **26**, 59; (b) H. Arend, K. Tichý, K. Bàberschke and F. Rys, *Solid State Commun.*, 1978, **18**, 999; (c) K. Tichý, J. Beneš, W. Hälg and H. Arend, *Acta Cryst. B*, 1978, **34**, 2970; (d) G. B. Birrell and B. Zaslow, B., *J. Inorg. Nucl. Chem.*, 1978, **34**, 1751; (e) K. Halvorsen and R. D. Willett, *Acta Cryst. C*, 1988, 44, 2071; (f) E. R. Peterson and R. D. Willett, *J. Chem. Phys.*, 1972, **56**, 1879.
14 S. Pohl, W. Saak and D. Haase, *Z. Natur. B*, 1987, 42, 1493. 371
15 G.C. Papavasiliou, G.A. Mousdis, C.P. Raptopoulou and A. Terzis, *Z. Naturforsch.* B, 1999, **54**, 1405.
16 D. G. Billing and A. Lemmerer, *Acta Cryst. C*, 2004, 50, m224.
17 J. Guan, Z. Tang and A. M. Guloy, *Chem. Commun.*, 2005, 48.
18 Bruker, SAINT+. Version 6.02 (includes XPREP and SADABS). Bruker AXS Inc., Madison, Wisconsin, USA.
19 G. M. Sheldrick, SHELX, release 97-2 (includes SHELXS and SHELXL), University of Göttingen, 1997
20 L. J. Farrugia, *J. Appl. Crystallogr.*, 1997, **30**, 565.
21 L. J. Farrugia, WinGX. *J. Appl., Cryst.*, 1999, **32**, 837.
22 A. L. Spek, *J. Appl. Crystallogr.* 2003, **36**, 7.
23 K. Brandenburg, Diamond. Version 2.1e., Crystal Impact GbR, Bonn, Germany.
24 H. D. Flack, *Acta Cryst. A*, 1983, **39**, 876-881.

CREATED USING THE RSC ARTICLE TEMPLATE (VER. 2.0) - SEE WWW.RSC.ORG/ELECTRONICFILES FOR DETAILS

Article www.rsc.org/[JOURNAL] | [JOURNAL NAME HERE]

870

Table 1 Crystal Data for **1**, **2**, **3**, **4** and **5**.

	1	**2**	**3**	**4**	**5**
Formula	$C_4H_{14}Br_4N_2Pb$	$C_4H_{14}I_4N_2Pb$	$C_{28}H_{80}I_{14}N_8Pb_3$	$C_8H_{22}I_4N_2Pb$	$C_{10}H_{26}Br_4N_2Pb$
Mr	617.00	804.96	2927.17	861.07	701.16
Temperature/K	173	293	173	293	173
Crystal size/mm	0.27 x 0.26 x 0.12	0.44 x 0.30 x 0.16	0.40 x 0.20 x 0.06	0.38 x 0. 31 x 0.21	0.44 x 0.34 x 0.05
Crystal system	Triclinic	Monoclinic	Triclinic	Monoclinic	Monoclinic
Space group	$P\bar{1}$	$C2/c$	$P\bar{1}$	$P2_1/c$	$P2_1/c$
a/Å	8.0070(18)	21.119(4)	11.639(3)	13.815(3)	14.651(6)
b/Å	8.389(2)	8.5018(14)	11.877(3)	8.3815(15)	7.926(3)
c/Å	10.586(3)	8.8936(15)	13.828(3)	9.0264(16)	8.455(3)
α/°	78.572(7)	90	68.680(5)	90	90
β/°	70.445(7)	103.648(3)	71.022(5)	106.749(3)	96.709(8)
γ/°	89.192(7)	90	86.892(4)	90	90
V/Å^3	655.8(3)	1551.7(4)	16.79.5(7)	1000.8(3)	975.1(7)
Z	2	4	1	2	2
Dc/g cm^{-3}	3.125	3.446	2.894	2.857	2.388
μ(Mo-Ka)/mm^{-1}	25.007	18.796	13.959	14.581	16.833
Theta range/°	2.09 to 25.00	1.98 to 27.98	1.67 to 25.00	1.54 to 28.00	1.40 to 25.00
No. unique data	2276	1863	5863	2399	1710
No. data with $I \geq 2s(I)$	1909	1594	4930	2164	1551
$R1$	0.0346	0.0394	0.0369	0.0576	0.0588
$wR2$ (all data)	0.0918	0.1003	0.0948	0.1418	0.1667

Table 1 contd Crystal Data for **6**, **7**, **8** and **9.**

	6	**7**	**8**	**9**
Formula	$C_{12}H_{30}I_4N_2Pb$	$C_{10}H_{12}I_4N_2Pb$	$C_8H_{40}Br_{12}N_8Pb_2$	$C_{13}H_{16}I_6N_2Pb_2$
Mr	917.17	875.01	1621.78	1376.06
Temperature/K	173	173	173	173
Crystal size/mm	0.32 x 0.20 x 0.01	0.28 x 0.24 x 0.06	0.48 x 0.24 x 0.12	0.38 x 0.12 x 0.25
Crystal system	Monoclinic	Monoclinic	Monoclinic	Orthorhombic
Space group	$P2_1/c$	$P2_1/c$	$P2_1/n$	$Fdd2$
a/Å	15.8186(8)	11.163(3)	8.9023(8)	25.333(8)
b/Å	8.4304(4)	8.960(2)	27.727(2)	42.923(14)
c/Å	8.8539(4)	8.737(2)	14.7100(12)	4.5149(15)
α/°	90	90	90	90
β/°	90.213(3)	90.314(4)	102.226(6)	90
γ/°	90	90	90	90
V/Å^3	1180.72(10)	873.8(4)	3548.5(5)	4909(3)
Z	2	2	4	8
Dc/g cm^{-3}	2.580	3.326	3.036	3.724
μ(Mo-Ka)/mm^{-1}	12.368	16.704	23.004	21.246
Theta range/°	1.29 to 28.00	1.82 to 28.00	1.47 to 28.00	1.87 to 27.99
No. unique data	2840	2089	8504	2938
No. data with $I \geq 2s(I)$	2393	2015	6389	2706
$R1$	0.0577	0.0326	0.0610	0.0277
$wR2$ (all data)	0.1842	0.0758	0.1649	0.0633
Flack Parameter[24]	-	-	-	0.008(5)

This journal © Royal Society of Chemistry

CREATED USING THE RSC ARTICLE TEMPLATE (VER. 2.0) - SEE WWW.RSC.ORG/ELECTRONICFILES FOR DETAILS

[JOURNAL NAME HERE] | www.rsc.org/[JOURNAL] Article

Table 2 Hydrogen bonding details of all compounds except **8**.

D-H…A	D-H (Å)	H…A (Å)	D…A (Å)	<(D-H…A) (°)	Symmetry transformations
1					
N(1)-H(1C)…Br(1)	0.91	2.43	3.335(9)	171.3	x+1,y,z
N(1)-H(1A)…Br(4)	0.91	2.60	3.367(10)	141.9	x+1,y+1,z
N(1)-H(1C)…Br(3)	0.91	2.56	3.427(10)	160.5	-x+1,-y+1,-z
N(2)-H(2C)...Br(4)	0.91	2.46	3.325(8)	158.2	-x+1,-y,-z+1
N(2)-H(2A)...Br(1)	0.91	2.60	3.421(8)	150.7	-x+1,-y,-z+1
N(2)-H(2B)...Br(2)	0.91	2.60	3.452(9)	156.7	x,y,z+1
2					
N(1)-H(1C)…I(1)	0.89	2.71	3.583(9)	168.4	-x+1/2,y-1/2,-z+3/2
N(1)-H(1A)…I(1)	0.89	2.89	3.631(9)	141.7	-x+1/2,-y+1/2,-z+2
N(1)-H(1B)…I(2)	0.89	2.81	3.665(9)	162.3	x,-y+1,z+1/2
3					
N(1)-H(1A)...I(7)	0.91	2.74	3.613(9)	161.5	-x+1,-y+2,-z+1
N(1)-H(1B)...I(7)	0.91	2.83	3.700(9)	160.2	x+1,y,z-1
N(1)-H(1C)...I(1)	0.91	2.96	3.791(9)	152.6	x+1,y,z
N(2)-H(2A)...I(5)	0.91	2.82	3.596(10)	143.4	x+1,y,z-1
N(2)-H(2B)...I(2)	0.91	2.86	3.693(11)	153.1	-x+1,-y+1,-
N(2)-H(2C)...I(7)	0.91	2.93	3.645(12)	136.0	x+1,y,z-1
N(3)-H(3A)...I(4)	0.91	2.82	3.627(10)	149.2	x,y,z+1
N(3)-H(3B)...I(7)	0.91	3.13	3.628(10)	116.5	-
N(3)-H(3C)...I(4)	0.91	2.78	3.651(9)	160.5	-x+1,-y+2,-z+1
N(4)-H(4A)...I(6)	0.91	2.87	3.593(12)	137.7	-
N(4)-H(4B)...I(3)	0.91	2.97	3.760(10)	145.7	x+1,y,z
N(4)-H(4C)...I(5)	0.91	2.88	3.699(10)	151.0	-
4					
N(1)-H(1B)...I(1)	0.89	2.75	3.631(9)	169.1	x,-y+5/2,z-1/2
N(1)-H(1A)...I(1)	0.89	2.93	3.618(11)	135.2	-x,y-1/2,-z+3/2
N(1)-H(1C)...I(2)	0.89	2.80	3.678(11)	168.9	-x,-y+2,-z+2
5					
N(1)-H(1C)...Br(1)	0.91	2.51	3.393(12)	162.4	-
N(1)-H(1A)...Br(1)	0.91	2.54	3.395(12)	155.9	x,-y+1/2,z-1/2
N(1)-H(1B)...Br(2)	0.91	2.73	3.471(12)	138.7	x,y,z-1
6					
N(1)-H(1C)…I(1)	0.91	2.73	3.588(17)	157.0	x,-y+3/2,z-1/2
N(1)-H(1A)…I(1)	0.91	2.75	3.637(16)	165.2	-
N(1)-H(1A)…I(2)	0.91	2.88	3.657(16)	143.8	X,y,z-1
7					
N(1)-H(1A)...I(1)	0.91	2.58	3.485(8)	176.4	x,y+1,z
N(1)-H(1C)...I(1)	0.91	2.62	3.530(8)	174.7	x,-y+1/2,z+1/2
N(1)-H(1B)...I(2)	0.91	3.02	3.703(7)	133.3	-
9					
N(1)-H(1C)...π	0.91	2.58	?	?	?
N(1)-H(1B)...I(3)	0.91	2.80	3.596(8)	146.6	x,y,z+1
N(1)-(H1B)...I(2)	0.91	3.06	3.498(8)	111.2	-
N(1)-H(1A)...I(2)	0.91	3.08	3.574(7)	116.4	x,y,z+1

875

Table 3 Hydrogen bonding details of **8**.

D-H…A	D-H (Å)	H…A (Å)	D…A (Å)	<(D-H…A) (°)	Symmetry transformations
N(1)-H(1A)...Br(11)	0.91	2.56	3.371(14)	149.5	-
N(1)-H(1B)...Br(11)	0.91	2.68	3.302(13)	126.7	-x+1,-y,-z+1
N(1)-H(1B)...Br(13)	0.91	2.76	3.467(14)	135.0	x-1/2,-y+1/2,z+1/2
N(1)-H(1C)...Br(12)	0.91	2.47	3.380(13)	178.0	-
N(2)-H(2A)...Br(9)	0.91	2.52	3.385(15)	158.2	-
N(2)-H(2B)...Br(13)	0.91	2.37	3.233(14)	159.3	x-1/2,-y+1/2,z+1/2
N(2)-H(2C)...Br(5)	0.91	2.69	3.488(14)	146.5	x+1/2,-y+1/2,z-1/2
N(3)-H(3A)...Br(2)	0.91	2.38	3.261(12)	162.0	x+3/2,-y+1/2,z+1/2
N(3)-H(3B)...Br(10)	0.91	2.44	3.305(13)	159.6	x+1/2,-y+1/2,z+1/2
N(3)-H(3C)...Br(12)	0.91	2.41	3.255(14)	154.4	-
N(4)-H(4A)...Br(2)	0.91	2.50	3.324(14)	150.6	-
N(4)-H(4B)...Br(3)	0.91	2.50	3.407(14)	175.9	-x+1/2,y-1/2,-z+3/2
N(4)-H(4C)...Br(12)	0.91	2.79	3.485(14)	133.6	-
N(5)-H(5A)...Br(10)	0.91	2.49	3.341(13)	156.0	x+1/2,-y+1/2,z-1/2
N(5)-H(5B)...Br(8)	0.91	2.53	3.346(14)	150.1	x+1/2,-y+1/2,z-1/2
N(5)-H(5C)...Br(7)	0.91	2.49	3.363(13)	162.2	x,y,z-1
N(6)-H(6A)...Br(9)	0.91	2.87	3.373(14)	116.3	x-1/2,-y+1/2,z-1/2
N(6)-H(6B)...Br(8)	0.91	2.77	3.493(16)	137.3	x+1/2,-y+1/2,z-1/2
N(6)-H(6B)...Br(12)	0.91	2.88	3.444(15)	121.1	x-1/2,-y+1/2,z-1/2
N(6)-H(6C)...Br(5)	0.91	3.09	3.656(14)	122.2	x+1/2,-y+1/2,z-1/2
N(7)-H(7A)...Br(4)	0.91	2.62	3.437(17)	149.7	-x+1,-y+1,-z+1
N(7)-H(7B)...Br(5)	0.91	2.77	3.639(19)	160.2	-x,-y+1,-z+1
N(7)-H(7C)...Br(11)	0.91	2.49	3.360(17)	159.9	-x+3/2,y+1/2,-z+1/2
N(8)-H(8A)...Br(12)	0.91	2.52	3.341(14)	149.7	x-1/2,-y+1/2,z-1/2
N(8)-H(8B)...Br(13)	0.91	2.32	3.227(14)	174.8	-
N(8)-H(8C)...Br(11)	0.91	2.59	3.318(15)	137.8	x-1/2,-y+1/2,z-1/2
N(8)-H(8C)...Br(11)	0.91	2.92	3.586(15)	131.2	-x+3/2,y+1/2,-z+1/2

This journal © Royal Society of Chemistry

Chapter 5 Phase Transitions of Inorganic-Organic Layered Perovskite-type Hybrids

5.1 Introduction

In this chapter I present the SC-XRD structures of 11 inorganic-organic hybrids that have the layered perovskite-type motif. The counter cations are simple alkylammonium chains with chain lengths from 4 carbon atoms to 18. All of the compounds display phase transitions. The essence of this chapter deals with the SC-XRD structures of the different phases and from this information, discussing the structural changes that undergo at the phase transitions.

5.2 Synthesis, characterization and phase transitions in the inorganic-organic layered hybrids $[(C_nH_{2n+1}NH_3)_2PbI_4]$, n = 4, 5 and 6

Journal: Acta Crystallographica B, Structural Science

Date Submitted: 23 February 2007

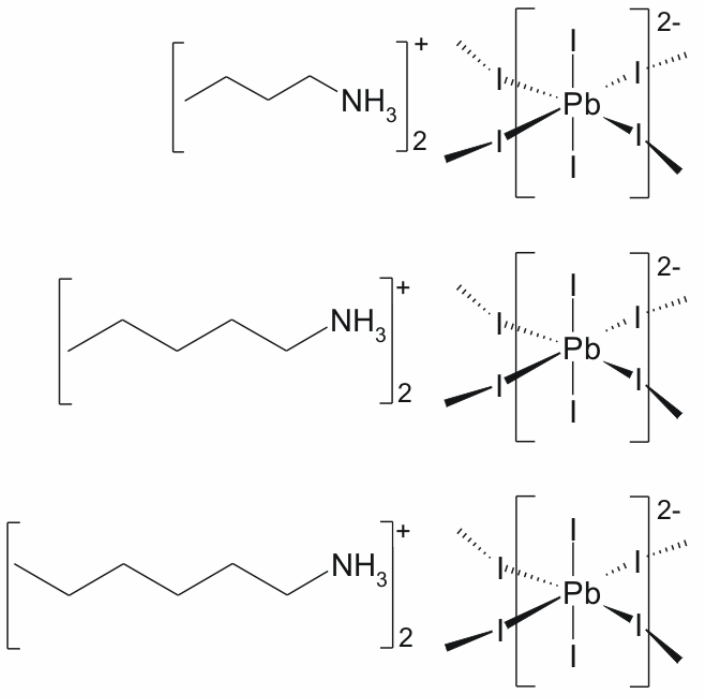
Reference Code of Submitted Article: BS5044

Date Accepted:

Final Reference:

Brief Synopsis

In this paper, the phase transitions of the inorganic-organic layered perovskite-type hybrids $[C_nH_{2n+1}NH_3)_2PbI_4]$ (n = 4, 5 and 6) are presented. The techniques used were SC-XRD, DSC and Hot Stage Microscopy (HSM).



Synthesis, characterization and phase transitions in the inorganic-organic layered perovskite-type hybrids $[(C_nH_{2n+1}NH_3)_2PbI_4]$, n = 4, 5 and 6

David G. Billing* **and Andreas Lemmerer**

Molecular Sciences Institute, School of Chemistry, University of the Witwatersrand, Johannesburg, South Africa. E-mail: dave.billing@wits.ac.za; Fax: 27 11 717 6749; Tel: 27 11 717 6759

Abstract The three inorganic-organic layered perovskite-type hybrids of general formula $[(C_nH_{2n+1}NH_3)_2PbI_4]$; n = 4, 5 and 6 display a number of reversible first-order phase transitions in the temperature range from -17°C to 120°C. $[(C_4H_9NH_3)_2PbI_4]$ has a single phase transition, $[(C_5H_{11}NH_3)_2PbI_4]$ has two phase transitions and $[(C_6H_{13}NH_3)_2PbI_4]$ has three phase transitions. In all three cases, the lowest temperature phase transition is thermochromic and the crystals change colour from yellow in their lowest temperature phase to orange in their higher temperature phase for $[(C_4H_9NH_3)_2PbI_4]$ and $[(C_6H_{13}NH_3)_2PbI_4]$, and from orange to red for $[(C_5H_{11}NH_3)_2PbI_4]$. The structural details associated with this phase transition has been investigated via single-crystal X-ray diffraction, SC-XRD, for all three compounds.

Keywords: Inorganic-organic hybrids, phase transitions, X-ray diffraction, thermochromism

1. Introduction

Structural phase changes and polymorphism are two of the more significant and enigmatic problems in modern structural chemistry. When coupled with our lack of understanding and control of these phenomena, it presents major obstacles to the successful design of compounds with specific chemical and physical properties (Fernandes et al, 2004; Dunitz, 1995). This phenomenon is seen especially in inorganic-organic layered hybrid structures, which are able to combine desirable features from both types of constituents (Mitzi, 2001). Inorganic compounds have different band gaps and hence their electrical properties can vary from insulators to semiconductors and right the way through to superconductors. Furthermore, they supply the hybrid structure with thermal stability and hardness as well as magnetic and dielectric properties. The layered hybrid materials have been extensively studied for their excitonic and magneto-optical properties as they form natural quantum well structures, especially the compound $[(C_6H_{13}NH_3)PbI_4]$ (Tanaka at al, 2002; Kataoka et al, 1993a; Kataoka et al, 1993b; Kondo et al, 1998a; Shibuya et al, 2002; Kondo et al, 1998b; Tanaka et al, 2005), $[(C_4H_9NH_3)PbBr_4]$ (Kato et al, 2003) and under high pressure $[(C_8H_{17}NH_3)PbI_4]$ (Matsuishi et al, 2004)

The two-dimensional hybrids, $[(R\text{-}NH_3)_2MX_4]$, where R is a long-chain hydrocarbon, M is a divalent metal, and X is a halogen, are based on the perovskite-like K_2NiF_4 or $RbAlF_4$ structure type. These inorganic compounds have staggered 2-D layers of corner-sharing NiF_6 octahedra or eclipsed 2-D layers of corner-sharing AlF_6 octahedra, which are separated by the K^+ or Rb^{2+} cations (Hatch and Stokes, 1987; Hatch et al, 1989). In the inorganic-organic hybrids studied here, the 2-D layers consist of MX_6 octahedra and the cations are replaced

by RNH_3^+ to form a laminar structure (Needham et al, 1984), also referred to as a layered perovskite-type motif. The organic cation can form bilayers between their organic layers if it has only one ammonium or a monolayer for two ammonium groups. Successive inorganic layers can either be staggered as in the K_2NiF_4 structure or they can be eclipsed, whereupon they are then based on the $RbAlF_4$ structure type. Weak hydrogen bonds between the ammonium group and the halides hold the inorganic-organic structure together.

Furthermore, the aliphatic materials $[(C_nH_{2n+1}NH_3)_2MX_4]$, here abbreviated as C_nMX, often exhibit a range of temperature-dependant structural phase transitions in the range from 235 K onwards for n = 4, 8, 9, 10 (Ishihara et al, 1990) and above room temperature for n = 12, 16 and 18 (Barman et al, 2003), associated with changes in the ordering and hydrogen bonding of the organic cations. The crystals change colour from yellow to orange at the first transition temperature. The structural phase transitions observed can be displasive phase transitions, associated with conformational changes within the ammonium chains or order-disorder transitions of the ammonium chains along their longitudinal axis. The latter ultimately leads to a "quasi-melting" of the hydrocarbon part (Chanh et al, 1989) in the highest temperature phases. The interlayer spacing between the layers increases with temperature as the rotational disordering increases (Barman et al, 2003). The order-disorder transition is the only one observed when $n \leq 2$ and both have been reported in chain lengths $n \geq 3$. The chain-melting transition is the major transition, usually the last one observed and with the highest enthalpy. Further, the conformation of the inorganic layers can change between eclipsed and staggered at the phase transitions and the degree of distortion of the octahedral geometry decrease with increasing temperature. The most obvious effect is often a change in the crystal system of the structure, from monoclinic to orthorhombic phase and finally tetragonal at the highest temperature (Mitzi, 1999). One of the most intensely studied series of compounds is $[(C_3H_7NH_3)_2MCl_4]$ (M = Cu, Cd and Mn). In these short chain compounds, the structural transitions can be associated with the motion of the rigid propylammonium cation (Doudin and Chapuis, 1988; Doudin and Chapuis, 1990; Depmeier et al, 1977; Chapuis, 1978).

The objective of the present study was to determine the single-crystal structures of all the phases of the short chain layered perovskite-type materials $[(C_nH_{2n+1}NH_3)_2PbI_4]$ (n = 4, 5 and 6) as identified by Differential Scanning Calorimetry and Hot Stage Microscopy.

$$(C_4H_9NH_3)_2PbI_4:\ \mathbf{II}\ (1a^*) \underset{-17.0^\circ C}{\overset{0.8^\circ C}{\rightleftharpoons}} \mathbf{I}\ (1b^*)$$

$$(C_5H_{11}NH_3)_2PbI_4:\ \mathbf{III}\ (2b^*) \underset{42.3^\circ C}{\overset{45.4^\circ C}{\rightleftharpoons}} \mathbf{II}\ (2c^*) \underset{116.8^\circ C}{\overset{118.1^\circ C}{\rightleftharpoons}} \mathbf{I}$$

$$(C_6H_{13}NH_3)_2PbI_4:\ \mathbf{IV}\ (3a^{\S}) \underset{-15.0^\circ C}{\overset{-5.0^\circ C}{\rightleftharpoons}} \mathbf{III}\ (3b^{\S}) \underset{76.1^\circ C}{\overset{81.7^\circ C}{\rightleftharpoons}} \mathbf{II}\ (3c) \underset{94.0^\circ C}{\overset{98.1^\circ C}{\rightleftharpoons}} \mathbf{I}\ (3d)$$

*Single crystal to single crystal

§Two different crystals

Scheme 1 Phase transitions as identified by DSC.

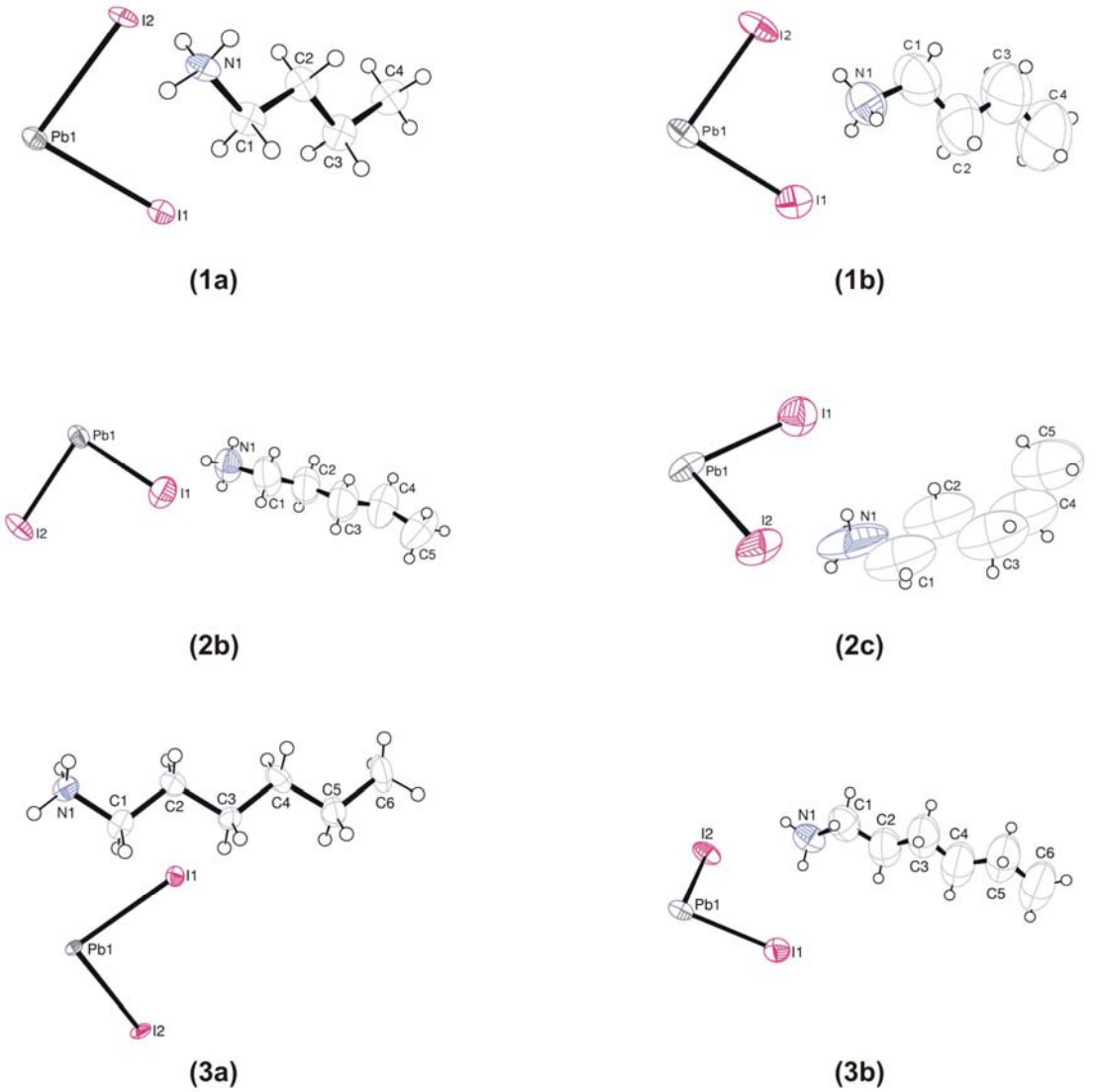


Figure 1 The asymmetric unit and atomic numbering scheme of the three compounds **1**-**3**. The structures of the compounds in their lowest temperature phase are shown in the left column, labelled **1a**, **2b** and **3a**, and their respective higher temperature phases shown on the right, labelled **1b**, **2c** and **3b**. The anisotropic displacement parameters are shown at the 50% probability level.

2. Experimental

2.1. Crystal Growth

2.1.1. Preparation of $[(C_4H_9NH_3)_2PbI_4]$ (1)

0.217 g PbI_2 (0.471 mmol) was dissolved in 3 ml 47% HI in a sample vial. Thereafter, 0.074 g $C_4H_9NH_2$ (1.01 mmol) was added and the precipitate dissolved by refluxing for 2 hours at 90°C. The solution was slowly cooled

at 2°C/hour to room temperature. An orange single crystal suitable for X-ray diffraction analysis was selected and studied. Elemental analysis (%): calc. for $C_8H_{24}I_4N_2Pb_1$: C 11.13, H 2.80, N 3.25. Found: C 11.14, H 2.91, N 3.22.

2.1.2. Preparation of $[(C_5H_{11}NH_3)_2PbI_4]$ (2)

0.138 g PbI_2 (0.065 mmol) was dissolved in 7 ml 47% HI in a sample vial. Thereafter, 0.015 g $C_5H_{11}NH_2$ (0.080 mmol) was added and the precipitate dissolved by refluxing for 2 hour at 90°C. The solution was slowly cooled at 2°C/hour to room temperature. An orange single crystal suitable for X-ray diffraction analysis was selected and studied. Elemental analysis (%): calc. for $C_{10}H_{28}I_4N_2Pb_1$: C 13.48, H 3.17, N 3.14. Found: C 13.61, H 3.14, N 3.13.

2.1.3. Preparation of $[(C_6H_{13}NH_3)_2PbI_4]$ (3)

0.138 g PbI_2 (0.065 mmol) was dissolved in 7 ml 47% HI in a sample vial. Thereafter, 0.015 g $C_6H_{13}NH_2$ (0.080 mmol) was added and the precipitate dissolved by refluxing for 2 hour at 90°C. The solution was slowly cooled at 2°C/hour to room temperature. An orange single crystal suitable for X-ray diffraction analysis was selected and studied. Elemental analysis (%): calc. for $C_{12}H_{32}I_4N_2Pb_1$: C 15.68, H 3.51, N 3.05. Found: C 15.98, H 3.35, N 3.11.

2.2. DSC measurements

Differential Scanning Calorimetry (DSC) data were collected on a Mettler Toledo 822^e at a scan rate of 5 °C/min in sealed aluminium pans under air.

2.3. X-Ray Crystallography

All diffraction data were collected on a Bruker Apex II CCD diffractometer (Bruker, 2005) with graphite-monochromated Mo-Kα radiation (α = 0.71073). Collections done at non-ambient temperatures were done using an Oxford Cryostream 700. Data reduction and cell refinement where done using *SAINT-PLUS* (Bruker, 2004) and space groups were determined from systematic absences by *XPREP* (Bruker, 2004) and further justified by the refinement results. Face indexed absorption corrections where performed on all crystals using *XPREP* (Bruker, 2004). In all cases, the structures were solved in the *WinGx* Suite (Farrugia, 1999) by direct methods using *SHELXS97* (Sheldrick, 1997a) and refined using full-matrix least squares calculations based on F^2 using *SHELXL97* (Sheldrick, 1997b). All non-hydrogen atoms were refined with anisotropic displacement parameters. Bond lengths and angles in the chains were restrained to ideal geometries. After that, all hydrogen atoms were placed at idealized positions and refined as riding atoms with the relative isotropic parameters of the heavy atoms to which they are attached (U_{iso}(H) = 1.2U_{eq}(C) or 1.5U_{eq}(N) or 1.5U_{eq}(C). The crystal structure of C_6PbI, **3a**, required a twin law.

The carbon distances in (**3b**), collected at room temperature, had very long and short carbon distances. All carbon distances where then restricted using SADI and the anisotropic displacement parameters restrained to be equal in the direction of the bonds. The carbon distances then averaged out to approximately 1.44 Å. The

thermal ellipsoids improve in the low temperature structure, (**3a**), so that no restrictions are necessary. The C-C distances refine in the range 1.50(2) to 1.52(3) Å.

Experimental details of the X-Ray analyses are provided in Table 1. Diagrams and publication material were generated using *ORTEP* (Farrugia, 1997), *PLATON* (Spek, 2003), *DIAMOND* (Brandenburg, 1999) and *WinGx* (Farrugia, 1999).

3. Results and Discussion

The series of compounds investigated in this paper show changes in the position of the alkylammonium chains relative to the inorganic layer as a consequence of phase changes. The compounds $[(C_5H_{11}NH_3)_2PbI_4]$, C_5PbI, and $[(C_6H_{13}NH_3)_2PbI_4]$, C_6PbI, additionally show relative movements of the inorganic layers, containing the corner-shared lead iodide octahedra. These shifts of the inorganic layers result in changes in the crystal system of the compounds. C_6PbI is monoclinic in phase **IV** and orthorhombic in phase **III**. Similarly, C_5PbI changes from monoclinic (**III**) to orthorhombic (**II**). $[(C_4H_9NH_3)_2PbI_4]$, C_4PbI, is the exception and is orthorhombic in both phases **II** and **I** and no observable shift in the layers. Only the first phase transition of each compound was investigated structurally. The last phase transition of C_5PbI was beyond the capabilities of the heating device. For C_6PbI, the phase transition at the higher temperatures unfortunately lead to fracturing of the crystals studied. As a consequence it was not feasible to collect data of a quality suitable for structure refinement, hence only unit cell dimensions were determined.

Doudin and Chapuis (1990) introduced a geometric quantity for their discussion of the phase changes of $[(C_3H_7NH_3)_2CuCl_4]$; the tilt $\angle_\varphi$ of the organic chains, "which defines the rotation angle of the N-C(3) axis". In this paper, we extend the definition of the tilt $\angle_\varphi$ to be the angle between a plane through the inorganic layers and a vector connecting the first and last atom of each chain, for example the nitrogen atom N1 and the carbon atom C4 in the case of C_4PbI. Two further quantities are required to track the motion of the alkylammonium chains before and after the phase transition: An angle $\angle_\alpha$, which is defined as the dihedral angle between a plane containing all the atoms of the alkylammonium chains and the plane formed by the lead atoms of the inorganic layers. And an angle $\angle_\beta$, which is defined as the angle between a vector connecting the atoms N1 and C1 and a plane through the lead atoms of the inorganic layers.

The position of the ammonium group by itself is affected by the phase changes and consequently effects the hydrogen bonding configuration. The "box" containing the ammonium groups are defined by the four equatorial, or bridging iodides, and the four axial, or terminal iodides that protrude above the layer. In projection, the ammonium group is contained within a parallelogram defined by the four bridging iodides (See Fig. 2). By projection onto this parallelogram the ammonium group is found in proximity to either an acute or an obtuse angle of the parallelogram.

It has been found that the three hydrogens associated with the ammonium group either bond to two terminal iodides and one bridging iodide (terminal halogen configuration) or to two bridging iodides and one terminal iodide (bridging halogen configuration) (Mitzi, 1999). All the compounds described here in all their phases adopt the terminal halogen configuration. However, there are two ways that the hydrogens can adopt the terminal halogen configuration: The three iodides to which the hydrogens bond can be at the vertices of either

an equilateral triangle or a right-angle triangle (See Fig. 2). There is a correlation between the position of the ammonium group and the type of terminal halogen configuration: If the ammonium group is in the acute angled position, it has the right-angled configuration and if the ammonium group is in the obtuse angled position, it has the equilateral configuration. The phase changes we observe for C_4PbI and C_5PbI are associated with the interconversion between these two geometries.

The corner-sharing PbI_6 octahedra that make up the 2-D layers are affected by the phase changes. For the layered perovskite-type hybrids, two out of a three possible tilts are encountered (Hatch et al, 1989. 237). Firstly, a tilt perpendicular to the inorganic sheets (θ tilt), so that adjacent corner-shared octahedra are rotated relative to each other. The angle of the θ tilt is mirrored in the bridging angle Pb-I-Pb, which deviates from 180°. The second kind of tilt is parallel to the layers (Ψ tilt), so that the layers are corrugated in one direction. The corrugation angle is measured by the angle between the normal to the inorganic layers and the vector connecting the Pb atom and the terminal I.

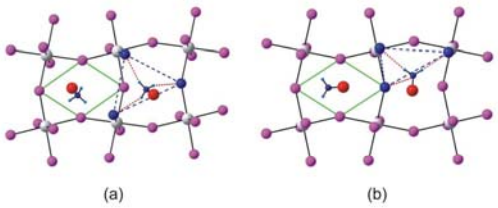


Figure 2 The picture on the left shows the position of the ammonium group near the obtuse angle of the parallelogram, shown in green, and the equilateral configuration, shown in blue. The picture on the right shows the alternative case.

3.1. Thermal Analysis Studies

All the three compounds studied showed multiple reversible phase transitions (Fig. 3) when studied by DSC. The phase transitions are numbered consecutively T_1, T_2, etc with increasing temperature. Hysteresis causes some variation in actual transition temperatures and hence the superscript ^{h} is added when the crystals were heated or the superscript ^{c} when the crystals were cooled.

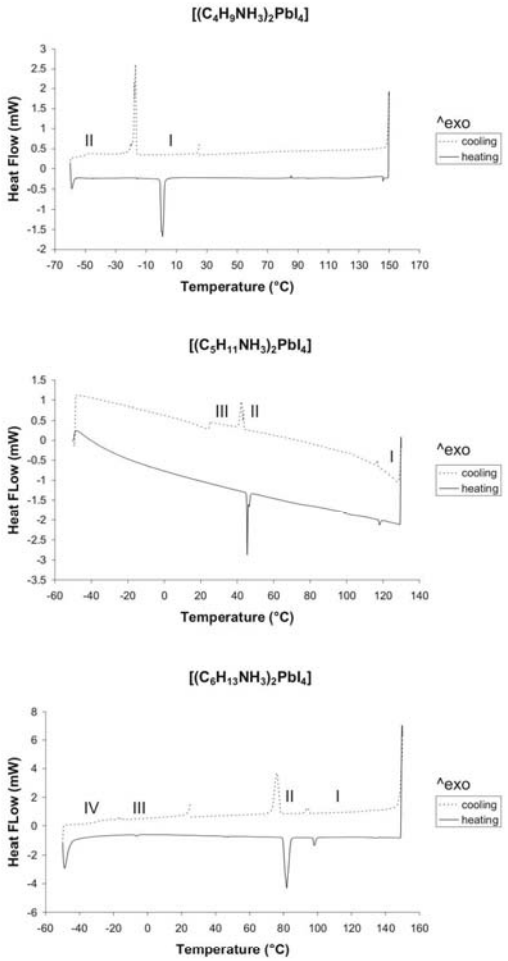
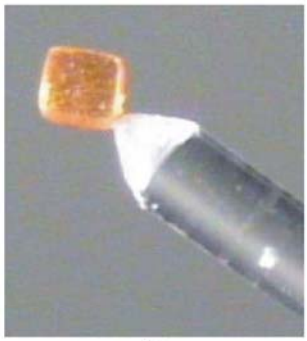


Figure 3 DSC scans of the reversible phase transitions for the compounds **1** (a), **2** (b) and **3** (c), including phase labelling.

3.1.1. $[(C_4H_9NH_3)_2PbI_4]$ (1)

Thermal analysis of C_4PbI via DSC revealed one endotherm when heating, at T_1^h = 0.8° and one exotherm when cooling, T_1^c = -17°C. The exothermic peak is shifted by almost 18°C lower compared to the endothermic peak, evidence of severe thermal hysteresis. The phase transition is accompanied by a change in crystal colour (See Fig. 4). The colour of the crystals is orange at room temperature. The colour remains unchanged until the phase transition. Then, the colour change is sudden and the crystal is yellow with significant fractures visible on the surface. C_4PbI shows no additional phase behaviour up to thermal decomposition.



(a)



(b)

Figure 4 The crystal of $[(C_4H_9NH_3)_2PbI_4]$ used in the diffraction experiment. (a) phase **I** (-3°C) and (b) **II** (-50°C)

3.1.2. $[(C_5H_{11}NH_3)_2PbI_4]$ (2)

Thermal analysis of C_5PbI via DSC revealed two endotherms at T_1^h = 45.4°C and T_2^h = 118.1°C, when heating the sample and two exotherms when cooling. The exothermic peaks are shifted to lower temperatures to the endothermic peaks, evidence of thermal hysteresis. The values of the enthalpies of the endotherms on the cooling cycle are slightly lower.

Hot stage microscope pictures were taken before and after the first phase transition. The colour of the crystal is orange at room temperature. The colour darkens with temperature until the first phase transition. Then, the colour change is sudden and the crystals turn reddish orange. When the rate of heating is slow, a distinct, red colour wave runs through the crystal (See Fig. 5). The enthalpy for this transition is much greater than for the second transition. The colour of the crystal after the last phase change becomes a more intense red.

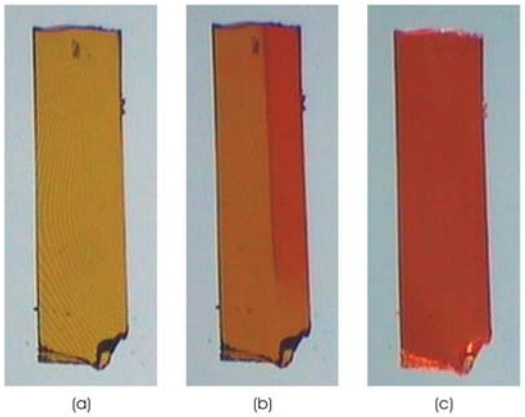


Figure 5 Hot stage microscope pictures of a crystal of $[(C_5H_{11}NH_3)_2PbI_4]$ under polarised light. Photograph (a) shows the crystal at room temperature (Phase **III**), (b) at the phase transition temperature of 45°C where the new phase is encroaching from the right, and (c) after the phase change is complete (Phase **II**).

3.1.3. $[(C_6H_{13}NH_3)_2PbI_4]$ (3)

Ishihara (1990) has investigated the optical spectra of $(C_6H_{13}NH_3)_2PbI_4$ (C_6PbI) and found no evidence suggesting the existence of any structural phase transitions between ambient and liquid-helium temperature. However, DSC scans done between -50° C and 160° show a series of small exothermic peaks starting at T_1^c = -15°C (See Fig. 6). These peaks result from the inorganic layers shifting relative to each other resulting in a change in symmetry from monoclinic to orthorhombic together with a doubling of the unit cell parameter perpendicular to the layer shift. Additional DSC characterisation revealed two further endotherms at T_2^h = 81.7°C and T_3^h = 98.1°C, when heating the sample and two exotherms when cooling. On average, the exotherms are 5 and 4°C lower than the endotherms.

Hot stage microscope pictures were taken before and after the second and third phase transitions. The crystals are orange at room temperature. The colour darkens with temperature until the second phase transition, where the colour suddenly changes to a reddish orange. When the rate of heating is slow, a wavefront propagating the newly formed phase is discernible (See Fig. 7). The enthalpy for this transition is much greater than that for the second transition. The colour of the crystal after the last phase change is again a more intense red, similar to C_5PbI. The colour change associated with the phase transition below room temperature is from orange to yellow.

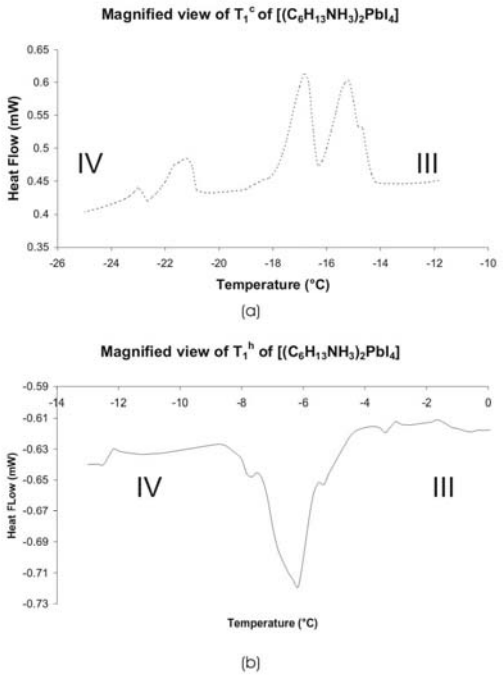


Figure 6 Magnified view of the first phase transition of C_6PbI in the cooling (a) and heating (b) cycle.



Figure 7 Optical Microscopy shows the visual evidence for the phase transitions of $(C_6H_{13}NH_3)_2PbI_4$ at 82°C (**III** to **II**) and 103°C (**II** to **I**).

3.2. Structural aspects of the thermochromic phase transitions of C_4PbI, C_5PbI and C_6PbI

3.2.1. Discussion of the phase transition of C_4PbI, II (1a) to I (1b)

The crystal structure of the lowest temperature phase, **II** of C_4PbI, designated **1a**, was determined at -50°C, and the room temperature structure of phase **I**, done at 20°C, is designated **1b**. Figure 8 clearly shows a bidimensional arrangement in which two layers of interdigitated butylammonium molecules are embedded between two consecutive inorganic $[PbI_6]$ sheets, forming an alternated inorganic-organic layered structure. The lead atoms are offset from layer to layer in both the phases **II** and **I**, resulting in a staggered arrangement of adjacent layers, thus displaying the K_2NiF_4 structure type. In the direction perpendicular to the layers, the crystal cohesion is achieved by N-H...I hydrogen bonds, related to the NH_3^+ ammonium groups. There are only weak van der Waals forces between two adjacent molecules (nearest neighbour distances are 4.236(0) Å for **II** and

4.073(2) Å for **I**. Within the inorganic layers, the crystal cohesion is achieved by strong ionic bonds between iodide and lead ions.

The inorganic layer of phase **II** (**1a**) is built up from characteristic corner-sharing PbI_6 octahedra. The asymmetric unit consists of a lead atom on a special position and two iodide atoms, I1 occupying the terminal position and I2 occupying the bridging position in the octahedra. As shown in the projection perpendicular to the layers in Fig. 8 (c), along the c-axis, the PbI_6 octahedra are rotated by 149.24(10)° relative to each other, increasing to 155.07(2)° in phase **I** (**1b**) (Fig. 8 (d)). The bridging angle translates directly into the θ tilt, being 30.76(10)° and 24.93(2)° respectively for **1a** and **1b**. Furthermore, the perovskite layers in phase **II** are more corrugated in the *a*-direction by an angle of Ψ = 12.92(4)° with respect to the *ab*-plane compared to the room temperature phase **I**, Ψ = 5.76(1)°. The coordination geometry around the Pb atom shows axial compression of the octahedral geometry at -50°C, with the bridging Pb1-I2 distances longer than the axial distances Pb1-I1. Phase **I** however has a terminal distance of 3.2028(7) Å, longer than the bridging distances to I2 (3.1780(5) Å and 3.1837(5) Å). The largest deviation from the ideal octahedral geometry is seen in the I(1)-Pb(1)-I(2) *cis* angles, which deviate by 3.86(7)° and 3.559(16)° for **II** and **I** respectively from 90°. The *trans* angles are all 180°, by virtue of the inversion centre at the lead atom. The structure at room temperature has been reported previously and the values for the lead iodide distances and angles agree well with those reported previously (Mitzi, 1996).

The butylammonium molecule is on a general position. The atomic numbering scheme is shown in Fig 5. During the course of the phase transition, the butylammonium molecule undergoes possibly the most striking rearrangement, as can be seen in Fig. 8 (c) and (d).

In phase **I**, the butylammonium molecule is orientated, in projection, along the long diagonal of the parallelogram formed by adjacent bridging iodide ions. The ammonium group is in close proximity of an acute angle and adopts the right-angled configuration. The hydrogen acceptor distances to the terminal halide I1 are 2.72 Å and 3.02 Å and to the bridging halide I2 2.80 Å (Table 3). Upon cooling, the butylammonium molecule moves relative to the parallelogram away from acute angle to an obtuse angle. The hydrogen bonding scheme is now equilateral and the hydrogen acceptor distances to the terminal halide I1 are 2.72 Å and 2.76 Å and to the bridging halide I2 3.05 Å. The change from the right-angled to the equilateral geometry goes hand in hand with an increase of the tilt angle of the ammonium head group. This angle $\angle_\beta$, almost doubles from 32.2(2)° to 61.2(5)°.

The movement also effects the general orientation of the butylammonium chain relative to the inorganic layers. In phase **I**, the general orientation of the molecule is perpendicular to the layers. The C1-C2 and C3-C4 bonds are almost normal to the layers. Upon conversion, the butylamonium molecule increases its tilt angle from $\angle_\varphi$ = 29.3(2)° to $\angle_\varphi$ = 39.9(4)° in phase **II**. Furthermore, the molecule also pivots around its own axis. The plane angle $\angle_\alpha$ decreases by 33.5° in going from phase **II** to **I**. The movement of the butylammonium molecular ions is accompanied by a decrease in the interlayer spacing by 1.368 Å. The molecular conformation of the butylammonium chain does not change during the phase transition, with the carbon atoms remaining in an all-*trans* conformation. Hence, this particular phase transition of C_4PbI is primarily due to the movement of the essentially rigid butylammonium cations relative to the inorganic layers.

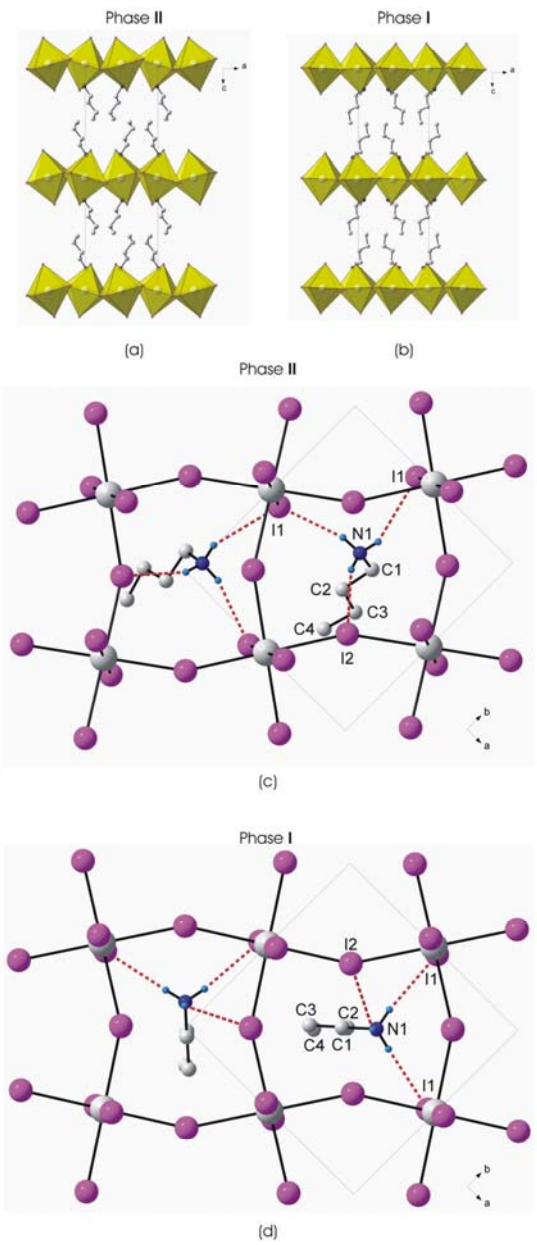


Figure 8 The two phases of C_4PbI are shown. Packing diagram of **II** at -50°C (a) and **I** at 20°C (b). The hydrogen bonding scheme and orientation of the butylammonium chains in phase **II** is shown in (c) and of phase **I** in (d). The equilateral and right-angled configuration is clearly seen in (c) and (d) respectively. H atoms on C atoms are omitted for clarity.

3.2.2. C_5PbI, III (2b) to II (2c)

Figure 9a and 9b again show a bidimensional arrangement in which two layers of interdigitated pentylammonium molecules are embedded between two inorganic [PbI_6] sheets, forming the familiar alternating

inorganic-organic layered structure. Within the range of temperatures studied, C_5PbI does not undergo any phase transitions below room temperature. The crystal structure of C_5PbI was determined at -100°C, designated (**2a**), and was found to be isostructural to its structure at room temperature, (**2b**), and the geometric parameters show no unexpected variation. In contrast to the phase transition of C_4PbI, where the inorganic layers retain their relative positions, the phase behaviour of C_5PbI is more complicated. It involves a movement of the layers as well as a conformational change within the pentylammonium chains. The lead atoms are aligned from layer to layer in phase **III** (**2b**), resulting in an eclipsed arrangement of adjacent layers, typical of layered perovskite-type hybrids with monoclinic unit cells. The space group is $P2_1/c$ and the structure type is based on $RbAlF_4$. The unit cell in **III** contains two half occupied inorganic layers at x = 0 and 1, equivalent to one complete inorganic layer. Consecutive layers are corrugated in the same direction, along the *b*-axis. The crystal structure of phase **II**, as determined at 60°C (**2c**), has the lead atoms offset from layer to layer, resulting in a staggered arrangement, typical of layered perovskite-type hybrids with orthorhombic unit cells. The space group of **2c** is *Pbca* and its structure type is based on K_2NiF_4. The unit cell has doubled in volume to 2356.0(5) $Å^3$ and now contains three inorganic layers, a complete one at z = 1/2 and the same two half layers at z = 0 and 1. The middle layer is corrugated in the opposite direction to the layers that sandwich it. To get adjacent layers to be staggered means that during the phase transition, every second layer in phase **III** has to move half a unit cell in the *b*-direction to get to the same staggered packing arrangement as in phase **II** (Fig. 9d). The interlayer spacing increases with an increase in temperature from 14.8805(13) Å to 14.978(4) Å.

The same changes in the octahedra in C_4PbI are observed for C_5PbI. The asymmetric unit again consists of a lead atom on a special position and two iodide atoms, I1 occupying the terminal position and I2 occupying the bridging position in the octahedra. The layers are parallel to the *bc*-plane in **III** and parallel to the *ab*-plane in **II**. The θ tilt of the octahedra relative to each other decreases from 26.32(3)° to 20.99(11)°. Furthermore, the inorganic layers are corrugated in the *b*-direction by an angle of 12.59(1)° with respect to the *bc*-plane in **III** and in the *a*-direction by 7.30(7)° in **II**. The bond lengths and angles in the individual PbI_6 octahedra behave similar to those in C_4PbI. Phase **III** has axial compression just as phase **II** in C_4PbI. The Pb-I1 bond distance in phase **III** is 3.1720(8) Å and the average Pb-I2 bond distance is 3.1958(7) Å. After the phase transition, phase **II** has bridging compression and the difference between the terminal and bridging distances is less (0.0115 Å) than in phase **III** (0.0238 Å). The *trans* angles are 180° and the *cis* angles deviate from 90° by 3.399(8)° and 2.76(10)° respectively for phase **II** and **III**.

As in C_4PbI, the pentylammonium molecules are ordered within the layers in both the C_5PbI phases. The atomic numbering scheme is shown in Fig. 1. At room temperature (phase **III**), the pentylammonium chain is planar and the torsion angles range from -170(2)° to -174.8(2)°. In phase **II**, the carbon atoms are no longer all in a plane. The atoms N1, C1, C2, C3 and C5 are approximately in a plane but atom C4 is bent out of it. The torsion angles C1-C2-C3-C4 and C2-C3-C4-C5 are now 138(9)° and 89(8)° respectively.

The pentylammonium chain in phase **III** faces towards the obtuse angled corner of the parallelogram and its hydrogen bonding has the equilateral configuration (See Fig. 10a). The hydrogen acceptor distances to the terminal halide I1 are 2.84 Å and 2.92 Å and to the bridging halide I2 2.88 Å. When the compound is heated, the pentylammonium chain aligns itself towards the acute angled position. The hydrogen bonding then displays

the right-angled configuration (See Fig. 10b). The average hydrogen acceptor distances to the terminal iodides increase to 2.85 Å and 3.04 Å as the D-H...A bridging angles decrease (the hydrogens no longer point directly towards the iodides) (Table 3). The angle $\angle_{\beta}$ at the same time increases from 24.9(1)° to 59.7(4)° (Table 4). The distance to the bridging iodide increases significantly to 3.07 Å. The angle $\angle_{\varphi}$ of the chains also changes from 28.8(2)° to 22.5(1)° upon heating, however the plane angle $\angle_{\alpha}$ does not change much (70.8(8)° to 77.8(3)°). In summary, the phase transition of C_5PbI at 45.4°C from phase **III** to **II** involves a conformational change within the pentylammonium cation as well as a displacement of the inorganic layers and the pentylammonium cation.

The last phase transition at 118.1°C from phase **II** to **I** was beyond the design specifications of the heating device on the diffractomer so no diffraction data is reported.

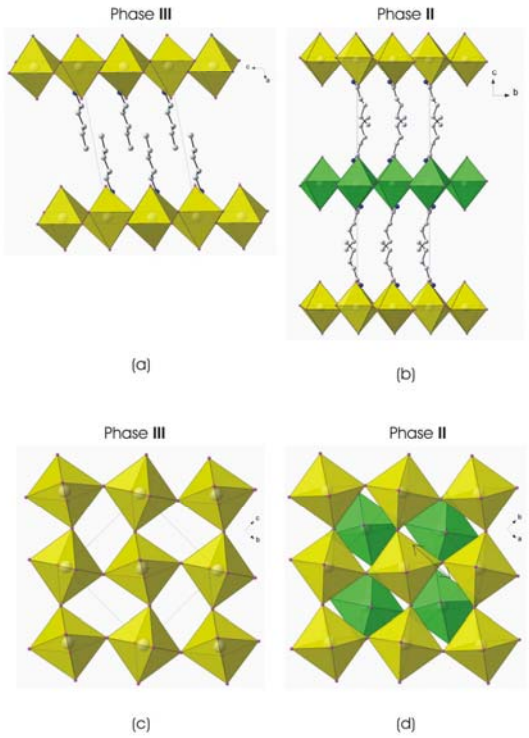


Figure 9 The first two phases of C_5PbI are shown. Diagram (a) shows the packing of phase **III** at 20°C. Diagram (b) illustrates the doubling of the unit cell and the change to an orthorhombic system in phase **II**. A further difference is the decreasing tilt of the pentylammonium chain in the higher temperature phase. Diagrams (c) and (d) are shown perpendicular to the layers. (c) shows the eclipsed arrangement of adjacent layers in **III** and (d) the staggered layers in **II**. In (b) and (d), the two adjacent layers that are staggered relative to each other are shown in yellow and green. The arrow indicates the offset of the lead atoms relative to each other. H atoms omitted for clarity.

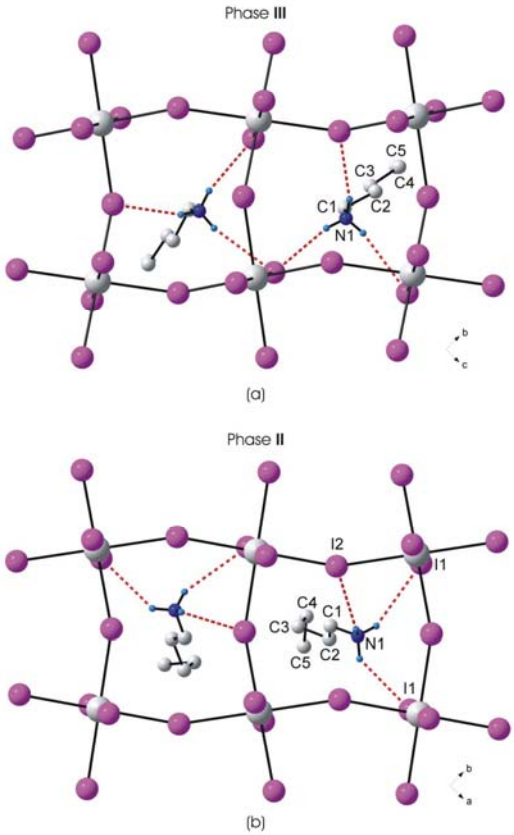


Figure 10 Projection of phase **III** of C_5PbI (a) and phase **II** (b). The pentylammonium chains are flat in **III** whereas C4 is bent out of the plane of the chain in **II**. H atoms on C atoms are omitted for clarity.

3.2.3. C_6PbI, IV (3a) to III (3b)

The phase behaviour of C_6PbI resembles that of C_5PbI. The crystal structure of the monoclinic phase **IV** of C_6PbI, (**3a**), was determined at -100°C and crystallizes in the $P2_1/c$ space group with monoclinic angle of 91.985(8)°. The asymmetric unit consists of a $Pb_{0.5}I_2$ unit (Pb atom sits on a special position) and a single $C_6H_{13}NH_3^+$ chain. The inorganic layers are then created by sharing the four corner iodides with adjacent octahedra. The lead atom is on a centre of inversion and has three unique bond distances to the iodides. I1 is terminal and has the longest bond distance of 3.2071(17) Å. The bridging halide I2 has shorter distances of 3.1608(14) and 3.1711(14) Å. The *trans* angles in the octahedra are all 180° with *cis* angles in the range 90.21(3)° to 94.59(3)°. The angle between two lead atoms bridged by I2 is 155.12(3)°.

The orthorhombic phase **III** of C_6PbI, **3b**, was collected at 20°C and crystallizes in the *Pbca* space group. The lead atom is again situated at a special position. The phase transition at T_1^c = -15°C can be associated with a lateral movement of the layers, perpendicular to the longest axis, relative to each other. This phase **IV** has a monoclinic unit cell and octahedra lie eclipsed above each other ($RbAlF_4$ structure type). In phase **III**, two successive layers are staggered and the octahedra in the adjacent layers are offset (See Fig. 11). The phase

change causes the inorganic-organic hybrid to convert from the K_2NiF_4 to the $RbAlF_4$ structure type. The interlayer spacing increases from 16.052(7) Å in phase **IV** to 16.372(1) Å in phase **III**.

The hexylammonium chain does not undergo any conformational changes during the phase transition. The plane of the hexylammonium chain changes its orientation relative to the layers, changing from $\angle_\alpha$ = 75.2(4)° (**IV**) to $\angle_\alpha$ = 89.6(8)° (**III**). Interestingly, there is no change in the position of the ammonium group and the hydrogen bonding has the right-angled configuration in both phases. The $\angle_\beta$ angle also remains similar being 66.6(8)° at -100°C (**IV**) and 61.3(1)°C at 20°C (**III**). The change in $\angle_\alpha$ has a slight effect on the hydrogen bonding geometry. The hydrogen bonds to the terminal iodides are more linear in phase **III**, seen in the D-H…A angles 169.7° and 171.7°, compared to phase **IV**, being 152.5° and 164.2°.

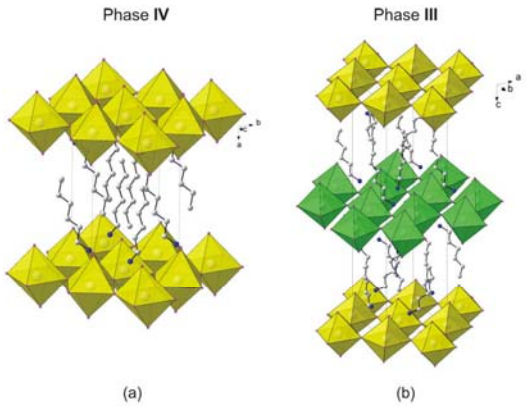


Figure 11 Packing diagrams of phase **IV** of C_6PbI (a) and phase **III** (b). The layers in yellow in both diagrams are eclipsed relative to each other whereas the green and yellow layers are shown staggered in (b). H atoms are omitted for clarity.

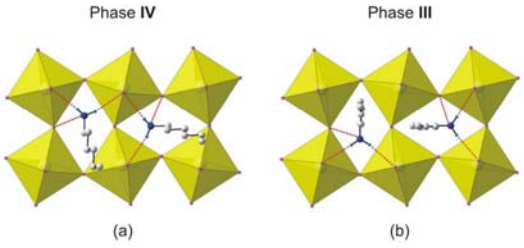


Figure 12 The slight orientation change between phase **IV** (a) and phase **III** (b) of C_6PbI. Both phases have the acute position and the right-angled configuration. H atoms on C atoms are omitted for clarity.

3.2.4. C_6PbI above room temperature, III (3b) to II (3c) to I (3d)

We attempted a study of the two phase changes that C6PbI undergoes above room temperature via SC-XRD, on the same crystal used for **3b**. The phase change at T_2^h = 81.7°C has the highest enthalpy and caused significant damage to the crystal. This is the major transition, where the hexylammonium cation becomes rotationally disordered. The crystal unfortunately fractured sufficiently, resulting in poor diffraction data that

was not suitable for structure solution and refinement. Hence, only the unit cell parameters are reported (**3c**). The crystal system, orthorhombic, remains the same in this phase as in phase **III**. There is an increase in the interlayer spacing from 16.3514(10) Å (phase **III**) to 17.6212(36) Å (phase **II**). The transition from **III** to **II** is presumed to be the chain melting transition. This conclusion comes from the model of the phase transitions put forward for the compound $[(C_6H_{13}NH_3)_2PbCl_4]$ (C_6PbCl), which has four phases (Kammoun and Daoud, 1997). In this compound, the lowest temperature phase, labelled **IV** by the authors, transforms to phase **III** via a first order, minor phase transition, similar to what is observed in C_6PbI. The major transition in C_6PbCl is from phase **II** to phase **I**, the final and highest temperature phase. The major transition was attributed to a conformational disorder of the chains, where gauche type kinks run through the chains. Furthermore, the orientation of the chains becomes more perpendicular to the inorganic layers as evidenced by the increase in the interlayer spacing from 17.56 Å to 19.01 Å, a change of 1.45 Å. The increase in the interlayer spacing in C_6PbI is less as the hexylammonium chains in C_6PbI are interdigitated, whereas in C_6PbCl, the chains are non-interdigitated. The same crystal of C_6PbI was then heated further, past the last phase transition at T_3^h = 98.1°C, and has a tetragonal unit cell (**3d**). The enthalpy for this phase transition from **II** to **I** is lower (1.1 kJ mol^{-1}) than for the previous phase transition from phase **III** to **II** (13.5 kJ mol^{-1}) and is presumably due to changes in the inorganic layers only.

4. Conclusion

The compounds $[(C_nH_{2n+1}NH_3)_2PbI_4]$ (n = 4, 5 and 6), which belong to the family of inorganic-organic layered perovskite-type hybrids, have one, two and three phase transitions respectively. Each phase transition is reversible. Only the first phase transition has been investigated by single crystal structures of the hybrids before and after the first transition. The phase transitions were single-to-single-crystal for C_4PbI (**1**) and C_5PbI (**2**), whereas two different crystals were needed for C_6PbI (**3**). Three major structural changes were observed: (1) the packing of the inorganic layers changes from staggered to eclipsed in C_5PbI and C_6PbI, (2) the position of the ammonium group changes relative to the layers from the obtuse to the acute angled position in C_4PbI and C_5PbI, and (3) the hydrogen bonding configuration changes from equilateral to right-angled in C_4PbI and C_5PbI. In C_6PbI, the cation does not change its position relative to the inorganic layers as drastically as the cations in C_4PbI and C_5PbI, which could explain why its phase transition enthalpy is the lowest of the three hybrids for that particular phase transition.

Table 1 Crystal Data for the compounds **1a**, **1b**, **2a**, **2b and 2c**.

Compound	**1a, II**	**1b, I**	**2a, III**	**2b, III**	**2c, II**
Crystal data					
Chemical formula	$2(C_4H_{12}N).I_4Pb$	$2(C_4H_{12}N).I_4Pb$	$2(C_5H_{14}N).I_4Pb$	$2(C_5H_{14}N).I_4Pb$	$2(C_5H_{14}N).I_4Pb$
M_r	863.08	863.08	891.13	891.13	891.13
Cell setting, space group	Orthorhombic, *Pbca*	Orthorhombic, *Pbca*	Monoclinic, *P*2(1)/*c*	Monoclinic, *P*2(1)/*c*	Orthorhombic, *Pbca*
Temperature (K)	223 (2)	293 (2)	173 (2)	293 (2)	333 (2)
a, *b*, *c* (Å)	8.428 (2), 8.986 (2), 26.233 (6)	8.87640 (10), 8.69250 (10), 27.6014 (5)	14.784 (3), 9.007 (2), 8.4716 (18)	14.8805 (13), 8.9297 (6), 8.6716 (7)	9.0078 (10), 8.7310 (10), 29.956 (4)
α, β, γ (°)	90, 90, 90	90, 90, 90	90, 100.881 (4), 90	90, 100.212 (2), 90	90, 90, 90
V (Å^3)	1986.7 (17)	2129.67 (5)	1107.8 (4)	1134.01 (15)	2356.0 (5)
Z	4	4	2	2	4
D_x (Mg m^{-3})	2.886	2.692	2.671	2.61	2.512
Radiation type	Mo *K*α	Mo *K*α	Mo *K*α	Mo *K*α	Mo *K*α
No. of reflections for cell parameters	3361	4303	843	4406	4614
θ range (°)	3.1–28.2	2.7–28.0	3.4–28.3	2.5–30.8	2.6–28.9
μ (mm^{-1})	14.69	13.71	13.18	12.87	12.39
Crystal form, colour	Cube, yellow	Cube, orange	plate, orange	Plate, orange	Plate, red
Crystal size (mm)	0.14 × 0.13 × 0.08	0.15 × 0.14 × 0.08	0.58 × 0.32 × 0.11	0.5 × 0.46 × 0.14	0.5 × 0.45 × 0.14
Data collection					
Diffractometer	Bruker Apex II CCD area detector	Bruker Apex II CCD area detector	Bruker Apex II CCD area detector	Bruker Apex II CCD area detector	Bruker Apex II CCD area detector
Data collection method	ω scans	ω scans	ω scans	ω scans	ω scans

Absorption correction	Integration	Integration	Integration	Integration	Integration
T_{min}	0.165	0.160	0.035	0.020	0.017
T_{max}	0.339	0.359	0.241	0.179	0.176
No. of measured, independent and observed reflections	7581, 1745, 1500	18996, 2568, 1744	7043, 2649, 2334	8718, 2734, 2259	11217, 2195, 1567
Criterion for observed reflections	$I > 2\sigma(I)$	$I > 2\sigma(I)$	$I > 2\sigma(I)$	$I > 2\sigma(I)$	$I > 2\sigma(I)$
R_{int}	0.083	0.084	0.080	0.055	0.066
θ_{max} (°)	25	28.0	28	28	25.5
Range of h, k, l	$-10 \rightarrow h \rightarrow 9$	$-11 \rightarrow h \rightarrow 11$	$-13 \rightarrow h \rightarrow 19$	$-19 \rightarrow h \rightarrow 19$	$-9 \rightarrow h \rightarrow 10$
	$-10 \rightarrow k \rightarrow 10$	$-11 \rightarrow k \rightarrow 10$	$-11 \rightarrow k \rightarrow 11$	$-7 \rightarrow k \rightarrow 11$	$-6 \rightarrow k \rightarrow 10$
	$-31 \rightarrow l \rightarrow 29$	$-36 \rightarrow l \rightarrow 35$	$-11 \rightarrow l \rightarrow 11$	$-10 \rightarrow l \rightarrow 11$	$-31 \rightarrow l \rightarrow 36$
Refinement					
Refinement on	F^2	F^2	F^2	F^2	F^2
$R[F^2 > 2\sigma(F^2)]$, $wR(F^2)$, S	0.102, 0.27, 1.38	0.039, 0.090, 1.13	0.038, 0.104, 1.14	0.044, 0.121, 1.07	0.125, 0.299, 1.31
No. of relections	1745 reflections	2568 reflections	2649 reflections	2734 reflections	2195 reflections
No. of parameters	70	71	79	79	79
H-atom treatment	Constrained to parent site	Constrained to parent site	Constrained to parent site	Constrained to parent site	Constrained to parent site
Weighting scheme	Calculated $w = 1/[\sigma^2(F_o^2) + (0.P)^2 + 568.7284P]$ where $P = (F_o^2 + 2F_c^2)/3$	Calculated $w = 1/[\sigma^2(F_o^2) + (0.0321P)^2 + 2.6863P]$ where $P = (F_o^2 + 2F_c^2)/3$	Calculated $w = 1/[\sigma^2(F_o^2) + (0.035P)^2 + 9.889P]$ where $P = (F_o^2 + 2F_c^2)/3$	Calculated $w = 1/[\sigma^2(F_o^2) + (0.057P)^2 + 5.6634P]$ where $P = (F_o^2 + 2F_c^2)/3$	Calculated $w = 1/[\sigma^2(F_o^2) + (0.0235P)^2 + 314.4561P]$ where $P = (F_o^2 + 2F_c^2)/3$
$(\Delta/\sigma)_{max}$	<0.0001	0.003	0.001	0.001	0.019
$\Delta\rho_{max}$, $\Delta\rho_{min}$ (e Å^{-3})	3.92, –5.67	0.86, –1.34	1.50, –2.69	1.87, –2.11	2.15, –2.78
Extinction method	None	SHELXL	None	None	None
Extinction coefficient		0.00350 (16)			

Table 1 contd Crystal Data for the compounds **1a**, **1b**, **2a**, **2b and 2c**.

Compound	**3a, IV**	**3b, III**	**3c, II**	**3d, I**
Crystal data				
Chemical formula	$2(C_6H_{16}N).I_4Pb$	$2(C_6H_{16}N).I_4Pb$	$2(C_6H_{16}N).I_4Pb$	$2(C_6H_{16}N).I_4Pb$
M_r	919.19	919.19	919.19	919.19
Cell setting, space group	Monoclinic, *P*2(1)/*c*	Orthorhombic, *Pbca*	Orthorhombic	Tetragonal
Temperature (K)	173 (2)	293 (2)	358(2)	378(2)
a, *b*, *c* (Å)	16.052 (7), 8.845 (4), 8.643 (4)	8.9413 (2), 8.6874 (2), 32.7027 (10)	8.6606(8), 8.8215(8), 35.2423(36)	8.7632(3), 8.7632(3), 34.0586(19)
α, β, γ (°)	90, 91.985 (8), 90	90, 90, 90	90, 90, 90	90, 90, 90
V (Å^3)	1226.4 (9)	2540.24 (11)	2692.50(77)	2615.47(32)
Z	2	4	4	4
D_x (Mg m^{-3})	2.489	2.403		
Radiation type	Mo *K*α	Mo *K*α	Mo *K*α	Mo *K*α
No. of reflections for cell parameters	866	5270	2465	1563
θ range (°)	3.3–28.2	2.6–29.9	2.3-28.3	3.3-28.1
μ (mm^{-1})	11.91	11.50		
Crystal form, colour	Plate, yellow	Plate, orange	Plate, red	Plate, red
Crystal size (mm)	0.32 × 0.16 × 0.02	0.46 × 0.28 × 0.05	0.46 × 0.28 × 0.05	0.46 x 0.28 x 0.05
Data collection				
Diffractometer	Bruker Apex II CCD area detector	Bruker Apex II CCD area detector	Bruker Apex II CCD area detector	Bruker Apex II CCD area detector
Data collection method	ω scans	ω scans		
Absorption correction	Integration	Integration		
T_{min}	0.147	0.058		
T_{max}	0.784	0.536		
No. of measured, independent and observed reflections	11777, 2954, 2562	12553, 3057, 2422		
Criterion for observed reflections	$I > 2\sigma(I)$	$I > 2\sigma(I)$		
R_{int}	0.092	0.045		
θ_{max} (°)	28	28		
Range of *h*, *k*, *l*	$-18 \rightarrow h \rightarrow 21$ $-11 \rightarrow k \rightarrow 11$ $-11 \rightarrow l \rightarrow 11$	$-9 \rightarrow h \rightarrow 11$ $-10 \rightarrow k \rightarrow 11$ $-42 \rightarrow l \rightarrow 43$		
Refinement				
Refinement on	F^2	F^2		
$R[F^2 > 2\sigma(F^2)]$, $wR(F^2)$, S	0.055, 0.135, 1.14	0.082, 0.177, 1.32		
No. of relections	2954 reflections	3057 reflections		
No. of parameters	91	88		
H-atom treatment	Constrained to parent site	Constrained to parent site		
Weighting scheme	Calculated $w = 1/[\sigma^2(F_o^2) +$	Calculated $w = 1/[\sigma^2(F_o^2) +$		

	$(0.0288P)^2$ + 44.4933P] where $P = (F_o^2 + 2F_c^2)/3$	$(0.0097P)^2$ + 113.3411P] where $P = (F_o^2 + 2F_c^2)/3$
$(\Delta/\sigma)_{max}$	0.006	0.001
$\Delta\rho_{max}$, $\Delta\rho_{min}$ (e Å^{-3})	4.91, –1.94	1.73, –1.95
Extinction method	None	None
Extinction coefficient		

Table 2 DSC scan details and values of the phase transitions after heating and cooling.

Chain Length	heating	cooling
n = 4		
T_1 (°C, K)	0.8 (274.0)	-17.0 (256.2)
ΔH (kJ mol^{-1})	9.5	12.5
n = 5		
T_1 (°C, K)	45.4 (318.6)	42.3 (315.4)
ΔH_1 (kJ mol^{-1})	6.0	7.8
T_2 (°C, K)	118.1 (391.2)	116.8 (390.0)
ΔH_2 (kJ mol^{-1})	0.56	0.71
n = 6		
T_1 (°C, K)	-4 to -8 (269-265)	-16 to -22 (257-251)
ΔH_1 (kJ mol^{-1})	0.435	0.539
T_2 (°C, K)	81.7 (354.9)	76.1 (349.3)
ΔH_2 (kJ mol^{-1})	13.5	12.7
T_3 (°C, K)	98.1 (371.3)	94.0 (367.2)
ΔH_3 (kJ mol^{-1})	1.1	1.2

Table 3 Hydrogen bonding details for compounds **1**, **2** and **3** in their various phases

D-H---A	D-H (Å)	H---A (Å)	D---A (Å)	<(D-H---A) (deg)	Symmetry transformations
1a, II					
N(1)-H(1C)-I(1)	0.90	2.72	3.58(3)	162	x+1,y,z
N(1)-H(1A)-I(1)	0.90	3.02	3.65(3)	120	-x+1/2,y+1/2,z
N(1)-H(1B)-I(2)	0.90	2.80	3.65(3)	158	-
1b, I					
N(1)-H(1C)…I(1)	0.89	2.72	3.604(8)	171	-
N(1)-H(1B)…I(1)	0.89	2.76	3.645(8)	172	-x+1/2,y-1/2,z
N(1)-H(1A)…I(2)	0.89	3.05	3.614(3)	123	-x,-y,-z+1
2a, III					
N(1)-H(1C)…I(1)	0.91	2.73	3.626(9)	167	-
N(1)-H(1A)…I(1)	0.91	2.84	3.595(9)	141	x,-y-1/2,z+1/2
N(1)-H(1B)…I(2)	0.91	2.81	3.657(9)	155	-x+2,-y,-z+1
2b, III					
N(1)-H(1A)…I(1)	0.89	2.84	3.599(12)	143	-
N(1)-H(1B)…I(1)	0.89	2.92	3.789(15)	165	x,-y+3/2,z-1/2
N(1)-H(1C)…I(2)	0.89	2.88	3.719(13)	158	x,-y+3/2,z+1/2
2c, II					
N(1)-H(1C)...I(1)	0.89	2.85	3.57(5)	139	-
N(1)-H(1B)...I(1)	0.89	3.04	3.81(8)	145	-x+1/2,y-1/2,z
N(1)-H(1A)...I(2)	0.89	3.07	3.80(6)	140	-x+1,-y,-z+2
3a, IV					
N(1)-H(1A)-I(1)	0.91	2.72	3.555(13)	153	x,y,z+1
N(1)-H(1C)-I(1)	0.91	2.76	3.646(13)	164	x,-y+1/2,z+1/2
N(1)-H(1B)-I(2)	0.91	2.84	3.594(12)	141	x,y,z+1
3b, III					
N(1)-H(1B)…I(1)	0.89	2.75	3.633(19)	172	-x+3/2,y+1/2,z
N(1)-H(1A)…I(1)	0.89	2.76	3.64(2)	170	-
N(1)-H(1C)…I(2)	0.89	3.07	3.70(2)	130	-x+3/2,y+1/2,z

Table 4 Geometric parameters for all compounds in their phases.

Geometric Parameter	**1a, II**	**1b, I**	**2a, III**	**2b, III**	**2c, II**	**3a, IV**	**3b, III**
Interlayer Spacing (Å)	13.117(5)	13.8007(5)	14.784(3)	14.881(1)	14.978(4)	16.052(7)	16.351(1)
Bridging Angle Pb1-I2-Pb1 (°)	149.24(10)	155.07(2)	150.22(2)	153.68(3)	159.01(11)	155.13(3)	155.65(5)
θ tilt (°)	30.76(10)	24.93(2)	29.78(2)	26.32(3)	20.99(11)	24.87(3)	24.35(5)
Corrugation Ψ tilt (°)	12.92(4)	5.76(1)	12.83(1)	12.59(1)	7.30(7)	5.71(2)	5.88(3)
Tilt of Chains $\angle_{\varphi}$ (°)	39.9(4)	29.3(2)	30.8(1)	28.8(2)	22.5(1)	32.7(1)	21.3(4)
Tilt of plane $\angle_{\alpha}$ (°)	56.4(9)	88.9(5)	67.4(4)	70.8(8)	77.8(3)	75.2(4)	89.6(8)
Tilt of NH_3 group $\angle_{\beta}$ (°)	33.2(2)	61.2(5)	27.5(5)	24.9(1)	59.7(4)	66.6(8)	61.3(1)
Position of ammonium group	Obtuse	Acute	Obtuse	Obtuse	Acute	Acute	Acute
Hydrogen Bonding Configuration	Equilateral	Right-angled	Equilateral	Equilateral	Right-angled	Right-angled	Right-angled
Torsion Angle (°)	Trans	Trans	Trans	Tans	138(9) C1-C2-C3-C4 89(8) C2-C3-C4-C5	Trans	Trans

Acknowledgements

The University of the Witwatersrand and the National Research Fund (GUN 2069064) are thanked for the award of a research grant and for providing the infrastructure required to do this work.

References

Barman, S., Venkatamaran, N. V., Vasudevan, S., Seshadri, R. (2003). *J. Phys. Chem. B* **107**, 1875-1883.

Brandenburg, K. (1999). DIAMOND. Version 2.1e. Crystal Impact GbR, Bonn, Germany.

Bruker (2004). SAINT-PLUS. Version 7.12 (including *XPREP*). Bruker AXS Inc., Madison, Wisconsin, USA.

Bruker 2005, *APEX2*. Version 1.27. Bruker AXS Inc., Madison, Wisconsin, USA.

Chanh, N. B., Houstry, J. R., Meresse, A., Ricard, L., Rey-Lafon, M. (1989). *J. Phys. Chem. Solids* **50**, 829-838.

Chapuis, G. (1978). *Acta Cryst.* B**34**, 1506-1512

Depmeier, W., Felsche, J., Wildermuth, G. (1977). *Journal of Solid State Chemistry* **21**, 57-65.

Doudin, B., Chapuis, G. (1988). *Acta Cryst.* **B44**, 495-502.

Doudin, B., Chapuis, G. (1990). *Acta Cryst.* **B46**, 175-180.

Dunitz, J. (1995). *Acta Cryst.* B 51, 619-631.

Farrugia, L. J. (1997) ORTEP-3 for Windows, *J. Appl. Cryst.* 30, 565.

Farrugia, L. J. (1999) WinGX, *J. Appl. Cryst.* **32**, 837-838.

Fernandes, M. A., Levendis, D. C., Schoening, F. R. L. (2004). *Acta Cryst. B* 60, 300-314.

Ishihara, T., Takahashi, J. and Goto, T. (1990). *Physical Review B***42**, 11099-11107.

Kammoun, S., Daoud, A. (1997). *phys. stat. sol. (a)* **162**, 575-586.

Kato, Y., Ichii, D., Ohashi, K., Kunugita, H., Ema, K., Tanaka, K., Takahashi, T., Kondo, T. (2003). *Solid State Commun.* **128**, 15-18.

Kataoka, T., Kondo, T., Ito, R., Sasaki, S., Uchida, K., Miura, N. (1993a). *Physical review B* **47**, 2010-2018.

Kataoka, T., Kondo, T., Ito, R., Sasaki, S., Uchida, K., Miura, N. (1993b). *Physica B* **184**, 132-136.

Kondo, T., Iwamoto, S., Hayase, S., Tanaka, K., Ishi, J., Mizuno, M., Ema, K., Ito, R. (1998a). *Solid State Commun.* **105**, 503-506.

Kondo, T., Azuma, T., Yuasa, T., Ito, R. (1998b). *Solid State Commun.* 105, 253-255.

Matsuishi, K., Ishihara, T., Onari, S., Chang, Y. H., Park, C. H. (2004). *phys. stat. sol. (b)* **241**, 3328-3333.

Mitzi, D. B. (1996). *Chemistry of Materials* **8**, 791-800.

Mitzi, D. B. (1999). *Progr. Inorg. Chem.* **48**, 1-121.

Needham, G. F., Willett, R. D., Franzen, H. F. (1984). *J. Phys. Chem.*, 88, 674-680.

Sheldrick, G. M. (1997a). *SHELXS97. Program for Crystal Structure Solution.* University of G\"ottingen, Germany.

Sheldrick, G. M. (1997b). *SHELXL97. Program for Crystal Structure Refinement*. University of G\"ottingen, Germany.

Shibuya, K., Koshimizu, M., Takeoka, T., Asai, K. (2002), *Nuclear Instruments and Methods in Physics Research B* **194**, 207-212

Spek, A. L. (2003). *J. Appl. Cryst*. **36**, 7-13.

Tanaka, K., Sano, F., Takahashi, T., Kondo, T., Ito, R., Ema, K. (2002). *Solid State Commun.* **122**, 249-252.

Tanaka, K., Takahashi, T., Kondo, T., Umebayashi, T., Asai, K., Ema, K. (2005). *Phys. Rev. B* **71**, 045312-1-6.

5.3 Synthesis, Characterisation and Phase Transitions of the inorganic-organic layered hybrids $[(C_nH_{2n+1}NH_3)_2PbI_4]$, n = 7, 8, 9 and 10

Journal: Crystal Growth and Design

Date Submitted: Pending, before 30 April 2007

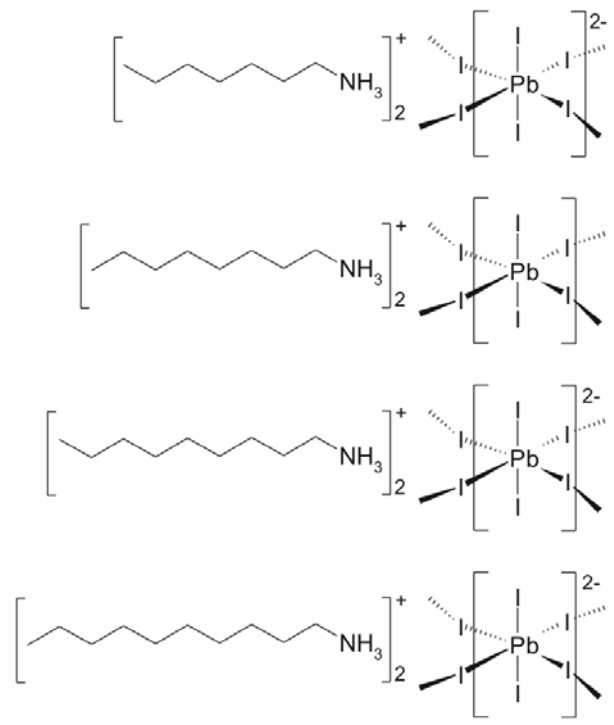
Reference Code of submitted article:

Date Accepted:

Final Reference:

Brief Synopsis

In this paper, the phase transitions of the inorganic-organic layered perovskite-type hybrids $[C_nH_{2n+1}NH_3)_2PbI_4]$ (n = 7, 8, 9 and 10) are presented. The techniques used were SC-XRD, DSC and Hot Stage Microscopy (HSM).



Synthesis, characterisation and phase transitions of the inorganic-organic layered perovskite-type hybrids $[(C_nH_{2n+1}NH_3)_2PbI_4]$, n = 7, 8, 9 and 10

David G. Billing and Andreas Lemmerer*

Molecular Sciences Institute, School of Chemistry, University of the Witwatersrand, Private Bag 3, Wits, 2050, South Africa; dave@chem.wits.ac.za

RECEIVED DATE (to be automatically inserted after your manuscript is accepted if required according to the journal that you are submitting your paper to)

ABSTRACT Four inorganic-organic hybrids that have 2-D layers of corner-sharing lead(II) iodide octahedra separated by alkylammonium chains have been crystallized and characterized via single-crystal XRD (SC-XRD). The four hybrids, given by the general formula $[(C_nH_{2n+1}NH_3)_2PbI_4]$, exhibit multiple reversible phase transition in a narrow temperature range. The number of transitions and the transition temperatures are dependant on the chain length; if n = 7 and 10, there are three transitions, and if n = 8 and 9, there are two transitions. The transition temperatures were determined with Differential Scanning Calorimetry experiments and Hot Stage Optical Microscopy. The SC-XRD structures of the various phases give clues to the structural changes that the compounds undergo at the phase transitions.

KEYWORDS Inorganic-organic hybrids, phase transitions, DSC, Single-crystal x-ray diffraction.

Introduction

Phase changes in crystals, the formation of different crystal structures from the same molecules, is a major unsolved problem in solid state chemistry. The occurrence of phase changes coupled with our lack of understanding and control of this phenomenon, is one of the major obstacles in successful design of compounds with specific chemical and physical properties.[1,2] This phenomenon is seen especially in inorganic-organic hybrid structures, which are able to combine excellent features from both types of constituents.[3, 4] Inorganic compounds have different band gaps and hence their electrical properties can vary from conductors to semiconductors right the way through to superconductors or insulators. Furthermore, they supply the hybrid structure with thermal stability and hardness as well as magnetic and dielectric properties. The hybrids have been extensively studied for their excitonic and magneto-optical properties as they form natural quantum well structures, especially $[(C_{10}H_{21}NH_3)_2PbI_4]$.[5, 6]

Two-dimensional hybrids, $[(R\text{-}NH_3)_2MX_4]$, where R is a long-chain hydrocarbon, M is a divalent metal, and X is a halogen, are based on the K_2MgF_4[7] or $RbAlF_4$[8] structure type. These inorganic compounds have staggered 2-D layers of corner-sharing MgF_6 octahedra or eclipsed 2-D layers of corner-sharing AlF_6 octahedra, which are separated by the K^+ or Rb^{2+} cations. In the inorganic-organic hybrids studied here, the 2-D inorganic layers consist of MX_6 octahedra and the cations are replaced by RNH_3^+ to form a laminar structure.[9] This packing arrangement will be referred to as a layered perovskite-type motif. The organic cation can form bilayers between these organic layers if it has only one ammonium or a monolayer for two ammonium groups. Successive inorganic layers can either be staggered as in the K_2MgF_4 structure or they can be eclipsed, whereupon they are then based on the $RbAlF_4$ structure type. Weak hydrogen bonds between the ammonium group and the halides hold the inorganic-organic structure together.

The $[(C_nH_{2n+1}NH_3)_2MX_4]$ materials, often abbreviated C_nMX, often exhibit a range of temperature-dependant structural phase transitions as a result of changes in the ordering and hydrogen bonding of the alkylammonium cations. The hybrid compounds $[(C_nH_{2n+1}NH_3)PbI_4]$ undergo multiple phase transitions above and below 298 K for n = 7 8, 9 and 10[10] and only above room temperature for n = 12, 16 and 18.[11] The structural phase transitions observed can be displasive phase transitions, associated with conformational changes within the ammonium chains or order-disorder transitions of the ammonium chains along their longitudinal axis. The interlayer spacing between the layers often increases with temperature as the rotational disordering of the alkylammonium chains increases,[11] that leads up to a "quasi-melting" of the hydrocarbon part at the highest temperature phase.[12] Furthermore, the arrangement of the inorganic layers themselves can change between eclipsed and staggered at the phase transitions and the degree of distortion of the octahedral geometry decreases with increasing

temperature. The most obvious effect is often a change in the crystal setting of the structure from a monoclinic low temperature phase to an orthorhombic room temperature phase and finally tetragonal at the highest temperature.[3] The objective of this study was to determine the single-crystal structures off all the phases of the medium chain layered perovskite-type hybrids $[(C_nH_{2n+1}NH_3)_2PbI_4]$ (n = 7, 8, 9 and 10). The phase transition temperatures were determined by Differential Scanning Calorimetry and Hot Stage Microscopy.

$[(C_7H_{15}NH_3)_2PbI_4]$: **III (1a)** $\underset{-21.6°C}{\overset{-2.4°C}{\rightleftharpoons}}$ **I (1b)** $\underset{10.4C}{\overset{12.7°C}{\rightleftharpoons}}$ **I (1c)** $\underset{35.9°C}{\overset{36.9°C}{\rightleftharpoons}}$ **I'**

$[(C_8H_{17}NH_3)_2PbI_4]$: **III (2a)** $\underset{-37.5°C}{\overset{-21.0°C}{\rightleftharpoons}}$ **II (2b)** $\underset{35.4°C}{\overset{38.0°C}{\rightleftharpoons}}$ **I (2c)**

$[(C_9H_{19}NH_3)_2PbI_4]$: **III (3a)** $\underset{-32.2°C}{\overset{-21.0°C}{\rightleftharpoons}}$ **II (3b)** $\underset{39.6°C}{\overset{40.8°C}{\rightleftharpoons}}$ **I**

$[(C_{10}H_{21}NH_3)_2PbI_4]$: **IV (4a)** $\underset{-24.1°C}{\overset{-14.6°C}{\rightleftharpoons}}$ **III (4b, 4c)** $\underset{3.5°C}{\overset{10.9°C}{\rightleftharpoons}}$ **II (4d, 4e)** $\underset{61.5°C}{\overset{64.1°C}{\rightleftharpoons}}$ **I (4f)**

Scheme 1. Summary of the transition temperatures of the phases for compounds **1-4**. The crystal structure for each phase is given in brackets.

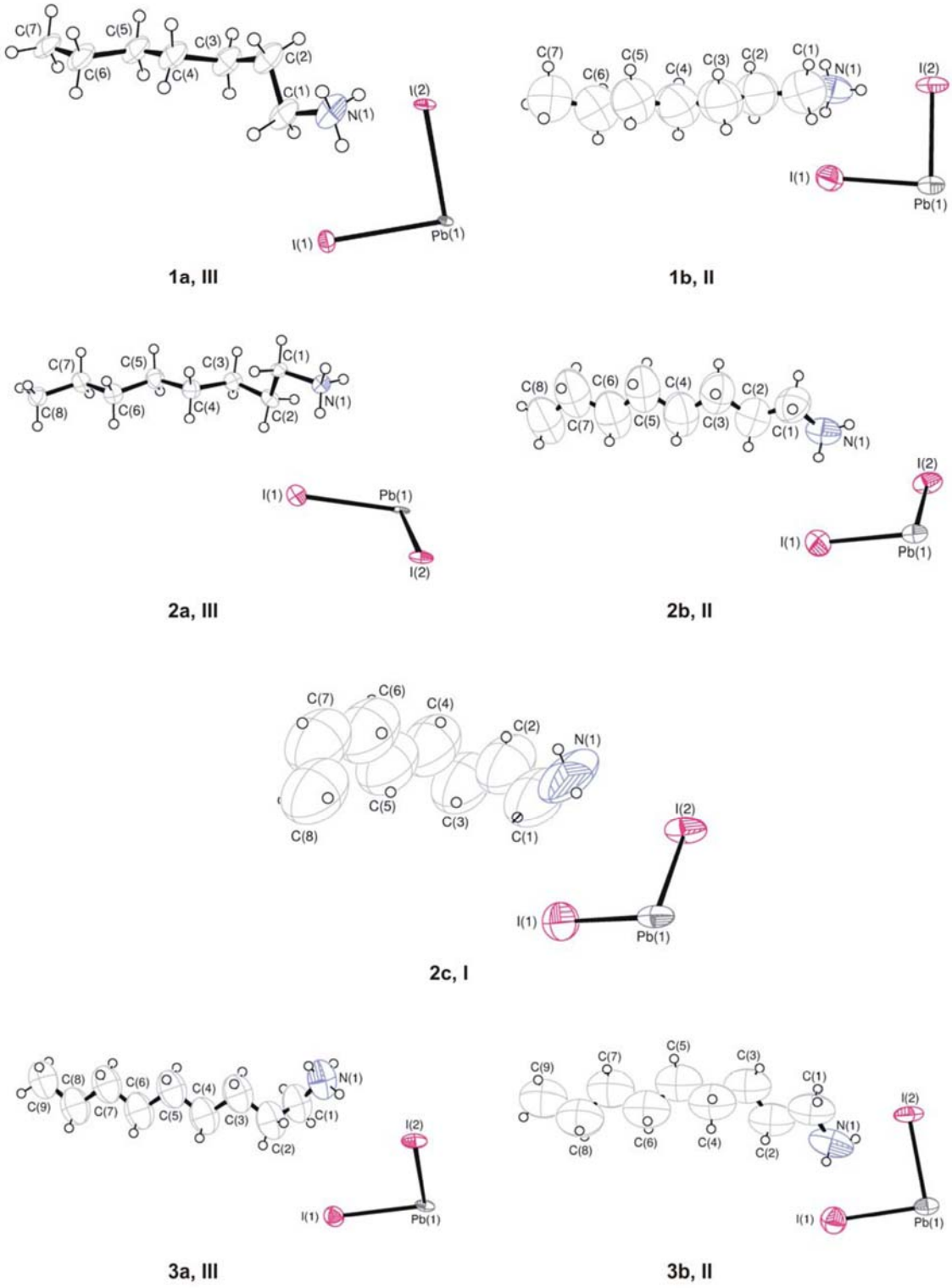


Figure 1. The contents of the asymmetric unit for the single-crystal structures of the different phases of compounds **1-3**, showing the atomic numbering scheme. Displacement ellipsoids are shown at the 50% probability level.

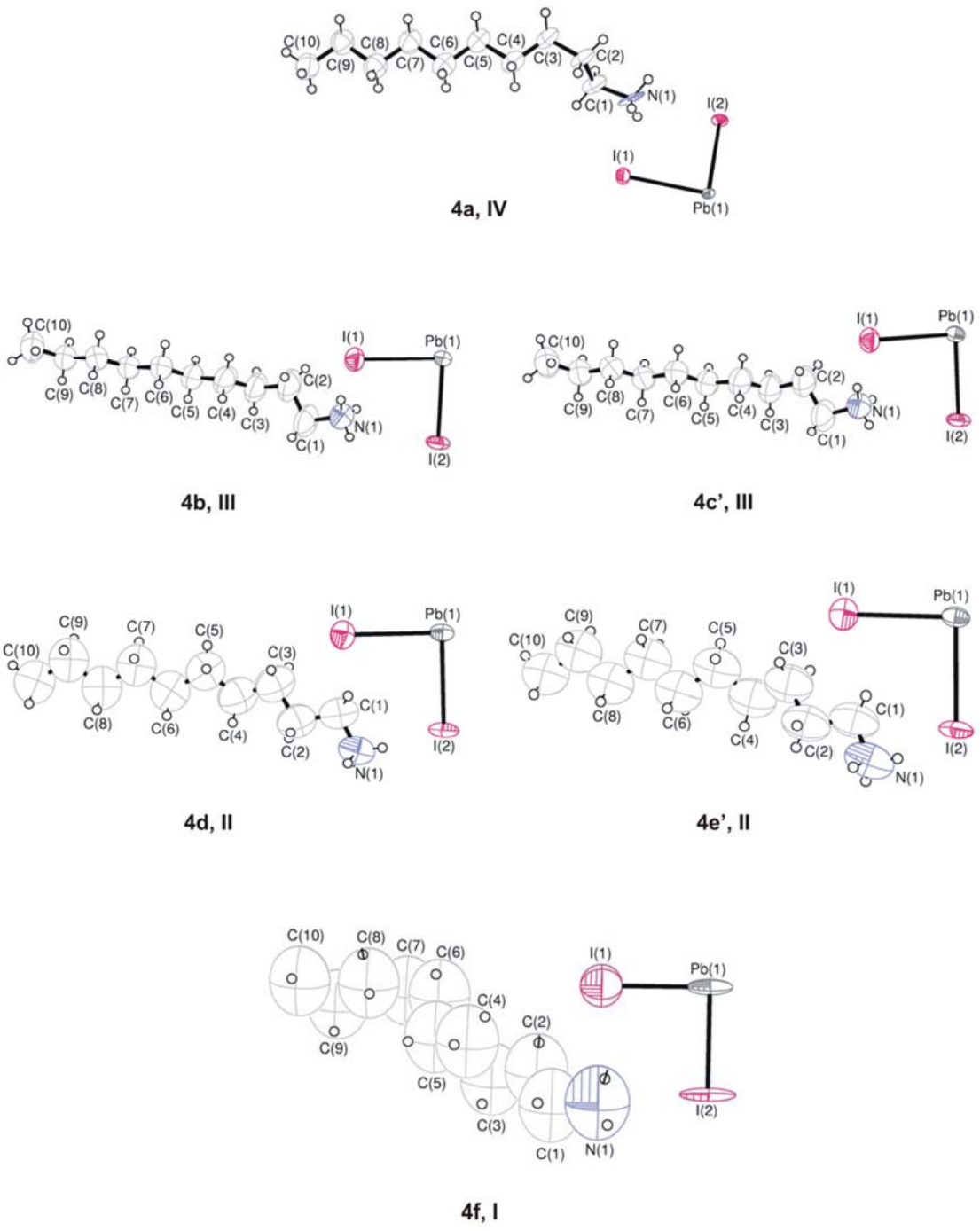


Figure 2. The contents of the asymmetric unit for the single-crystal structures of the different phases of compound **4**, showing the atomic numbering scheme. Displacement ellipsoids are shown at the 50% probability level.

Experimental Procedures

Compounds. All reagents were purchased from commercial sources and used without further purification.

Preparation of bis(heptylammonium)tetraiodoplumbate(II) (1). 0.105 g PbI_2 (0.228 mmol) was dissolved in 5 ml 47% HI in a sample vial. Thereafter, 0.047 g $C_7H_{15}NH_2$ (0.408 mmol) was added and the precipitate dissolved by refluxing for 2 hour at 100°C. The solution was slowly cooled at 2°C/hour to room temperature. An orange single crystal suitable for X-ray diffraction analysis was selected and studied. Elemental analysis (%): calc. for $C_{14}H_{36}I_4N_2Pb_1$: C 17.83, H 3.42, N 2.97. Found: C 17.88, H 3.64, N 2.98.

Preparation of bis(octylammonium)tetraiodoplumbate(II) (2). 0.138 g PbI2 (0.065 mmol) was dissolved in 7 ml 47% HI in a sample vial. Thereafter, 0.015 g C8H17NH2 (0.080 mmol) was added and the precipitate dissolved by refluxing for 2 hour at 90°C. The solution was slowly cooled at 2°C/hour to room temperature. An orange single crystal suitable for X-ray diffraction analysis was selected and studied. Elemental analysis (%): calc. for $C_{16}H_{40}I_4N_2Pb_1$: C 19.70, H 4.13, N 2.87. Found: C 19.91, H 4.03, N 2.95.

Preparation of bis(nonylammonium)tetraiodoplumbate(II) (3). 0.138 g PbI_2 (0.065 mmol) was dissolved in 7 ml 47% HI in a sample vial. Thereafter, 0.015 g $C_9H_{19}NH_2$ (0.080 mmol) was added and the precipitate dissolved by refluxing for 2 hour at 90°C. The solution was slowly cooled at 2°C/hour to room temperature. A yellow single crystal suitable for X-ray diffraction analysis was selected and studied. Elemental analysis (%): calc. for $C_{18}H_{44}I_4N_2Pb_1$: C 21.55, H 4.42, N 2.79. Found: C 21.80, H 4.27, N 2.68.

Preparation of bis(decylammonium)tetraiodoplumbate(II) (4). 0.138 g PbI_2 (0.065 mmol) was dissolved in 7 ml 47% HI in a sample vial. Thereafter, 0.015 g $C_{12}H_{25}NH_2$ (0.080 mmol) was added and the precipitate dissolved by refluxing for 2 hour at 90°C. The solution was slowly cooled at 2°C/hour to room temperature. A yellow single crystal suitable for X-ray diffraction analysis was selected and studied. Elemental analysis (%): calc. for $C_{20}H_{48}I_4N_2Pb_1$: C 23.29, H 4.69, N 2.72. Found: C 23.46, H 4.78, N 2.77.

Differential Scanning Calorimetry. Differential Scanning Calorimetry (DSC) data were collected on a Mettler Toledo 822^e at a scan rate of 5 °C/min in sealed aluminium pans under air. All the four compounds studied showed multiple reversible phase transitions (See Figure 3). The phase transitions are numbered consecutively T_1, T_2, etc with increasing temperature. The transition temperatures

themselves depended on the direction of the scan, hence the superscript ^{h} is added when the crystals were heated or the superscipt ^{c}, when the crystals were being cooled.

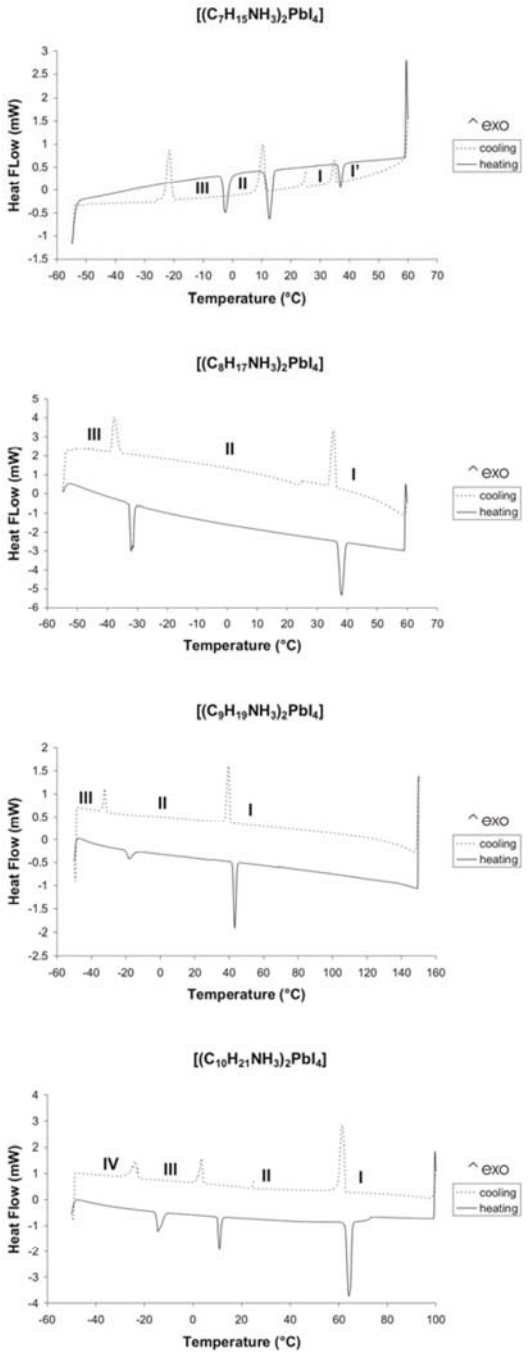


Figure 3. DSC thermograms of the hybrids $[(C_nH_{2n+1}NH_3)_2PbI_4]$ (n = 7, 8, 9 and 10). C_7PbI and $C_{10}PbI$ have three reversible phase transitions and C_8PbI and C_9PbI only two.

X-Ray Crystallography. All diffraction data were collected on a Bruker Apex II CCD diffractometer[14] with graphite-monochromated Mo-Kα radiation (λ = 0.71073) at room temperature and at high temperature using an Oxford Cryostream 700. Data reduction and cell refinement where done using SAINT-PLUS[15] and space groups of these compounds were determined from systematic absences by XPREP[16]and further justified by the refinement results. Face indexed absorption corrections where performed on all crystals using XPREP.[16] In all cases, the structures were solved in the WinGx[17] Suite by direct methods using SHELXS 97[18] and refined using full-matrix least squares/difference Fourier techniques using SHELXL 97.[19] After that, all hydrogen atoms were placed at idealized positions and refined as riding atoms with the relative isotropic parameters of the heavy atoms to which they are attached. Diagrams and publication material were generated using ORTEP,[20] PLATON[21] and DIAMOND.[22] Experimental details of the X-Ray analyses are provided in Table 1.

Table 1. Crystallographic data for compounds 1 and 2

	1a, III	**1b, II**	**1c, I**	**2a, III**	**2b, II**
Formula	$(C_7H_{15}NH_3)_2PbI_4$	$(C_7H_{15}NH_3)_2PbI_4$	$(C_7H_{15}NH_3)_2PbI_4$	$(C_8H_{17}NH_3)_2PbI_4$	$(C_8H_{17}NH_3)_2PbI_4$
M_r	947.24	947.24	947.24	975.29	975.29
Temperature (K)	253	278	293	173	293
Crystal size (mm^3)	0.38 x 0.33 x 0.02	0.28 x 0.24 x 0.01	0.28 x 0.24 x 0.01	0.55 x 0.20 x 0.02	0.55 x 0.20 x 0.02
Crystal system	Monoclinic	Orthorhombic	Orthorhombic	Monoclinic	Orthorhombic
Space group	*P2₁/c* (14)	*Pbca* (61)	*Pbca* (61)	*P2₁/c* (14)	*Pbca* (61)
a (Å)	17.243(9)	9.0126(2)	8.8549(15)	18.738(3)	8.9817(4)
b (Å)	8.942(4)	8.7087(2)	8.6840(19)	8.9916(10)	8.6886(3)
c (Å)	8.589(4)	34.5612(10)	36.612(13)	8.4542(9)	37.4821(18)
α (deg)	90	90	90	90	90
β (deg)	96.902(11)	90	90	96.301(8)	90
χ (deg)	90	90	90	90	90
V ($Å^3$)	1314.6(11)	2712.64(12)	2815.4(12)	1415.8(3)	2925.0(2)
Z	2	4	4	2	4
ρ(calcd) (Mgm^{-3})	2.393	2.319	2.235	2.288	2.215
μ(Mo-Ka) (mm^{-1})	11.112	10.771	10.378	10.322	9.992
Theta range (deg)	1.19 to 25.50	1.18 to 25.50	1.11 to 25.50	1.09 to 25.50	1.09 to 25.50
No. unique data	2412	2526	2621	2625	2725
No. data with I > 2σ(I)	2197	1784	805	2376	2081
final *R* (I > 2σ(I))	0.1449	0.0765	0.1837	0.1464	0.0720
final *wR2* (all data)	0.4367	0.2402	0.5286	0.4378	0.2118

Table 1 contd. Crystallographic data for compounds 2, 3 and 4

	2c, I	**3a, III**	**3b, II**	**4a, IV**
Formula	$(C_8H_{17}NH_3)_2PbI_4$	$(C_9H_{19}NH_3)_2PbI_4$	$(C_9H_{19}NH_3)_2PbI_4$	$(C_{10}H_{21}NH_3)_2PbI_4$
M_r	975.29	1003.34	1003.34	1031.39
Temperature (K)	314	223	293	243
Crystal size (mm^3)	0.55 x 0.20 x 0.02	0.35 x 0.30 x 0.02	0.20 x 0.20 x 0.02	0.64 x 0.28 x 0.08
Crystal system	Orthorhombic	Monoclinic	Orthorhombic	Monoclinic
Space group	*Cmca* (64)	$P2_1/c$ (14)	*Pbca* (61)	$P2_1/c$
a (Å)	40.0276(18)	19.791(3)	9.0232(2)	21.330(9)
b (Å)	8.7440(3)	8.8401(10)	8.7054(2)	8.950(4)
c (Å)	8.7436(3)	8.7054(11)	39.7578(9)	8.433(3)
α (deg)	90	90	90	90
β (deg)	90	96.376(9)	90	96.107(10)
χ (deg)	90	90	90	90
V ($Å^3$)	3060.3(2)	1513.6(3)	3123.00(12)	1600.7(11)
Z	4	2	4	2
ρ(calcd) (Mgm^{-3})	2.117	2.201	2.134	2.140
μ(Mo-Ka) (mm^{-1})	9.551	9.658	9.362	9.136
Theta range (deg)	1.02 to 25.50	1.04 to 25.50	1.02 to 25.50	0.96 to 25.0
No. unique data	1450	2789	2907	2824
No. data with I > 2σ(I)	1028	2180	2083	2562
final *R* (I > 2σ(I))	0.0470	0.0964	0.0711	0.1022
final *wR2* (all data)	0.1659	0.2858	0.2112	0.3024

Table 1 contd. Crystallographic data for compounds 4b, 4c, 4d, 4e, 4f

	4b, III	**4c, III**	**4d, II**	**4e, II**	**4f, I**
Formula	$(C_{10}H_{21}NH_3)_2PbI_4$	$(C_{10}H_{21}NH_3)_2PbI_4$	$(C_{10}H_{21}NH_3)_2PbI_4$	$(C_{10}H_{21}NH_3)_2PbI_4$	$(C_{10}H_{21}NH_3)_2PbI_4$
M_r	1031.39	1031.39	1031.39	1031.39	1031.39
Temperature (K)	268	268	293	293	343
Crystal size (mm^3)	0.64 x 0.28 x 0.08	0.28 x 0.24 x 0.08	0.36 x 0.18 x 0.02	0.28 x 0.24 x 0.08	0.28 x 0.24 x 0.08
Crystal system	Orthorhombic	Orthorhombic	Orthorhombic	Orthorhombic	Orthorhombic
Space group	*Pbca* (61)	*Pbca* (61)	*Pbca* (61)	*Pbca* (61)	*Cmca* (64)
a (Å)	8.8314(2)	8.8339(2)	8.9708(2)	8.9807(2)	47.479(11)
b (Å)	8.4871(2)	8.4845(2)	8.6733(2)	8.6742(2)	8.7115(19)
c (Å)	43.9491(13)	43.9647(8)	42.5696(12)	42.5253(14)	8.7152(18)
α (deg)	90	90	90	90	90
β (deg)	90	90	90	90	90
χ (deg)	90	90	90	90	90
V ($Å^3$)	3294.12(15)	3295.21(12)	3312.19(14)	3312.74(15)	3604.7(14)
Z	4	4	4	4	4
ρ(calcd) (Mgm^{-3})	2.080	2.079	2.068	2.068	1.900
μ(Mo-Ka) (mm^{-1})	8.879	8.876	8.830	8.829	8.114
Theta range (deg)	0.93 to 25.50	0.93 to 25.50	0.96 to 25.49	0.96 to 25.49	0.86 to 25.50
No. unique data	3070	3045	3086	3089	1716
No. data with $I > 2\sigma(I)$	2647	2595	2147	2476	985
final *R* ($I > 2\sigma(I)$)	0.0909	0.1061	0.0929	0.1530	0.1166
final *wR2* (all data)	0.2661	0.3092	0.2772	0.4187	0.3428

Table 2. Differential Scanning Calorimetry temperatures and enthalpies as a function of chain length.

Chain length	T_1 (°C, K)	ΔH_2 (kJ mol^{-1})	T_2 (°C, K)	ΔH_2 (kJ mol^{-1})	T_3 (°C, K)	ΔH_3 (kJ mol^{-1})
n = 7						
heating	-2.4 (270.7)	6.7	12.7 (285.8)	8.4	36.9 (310.1)	2.8
cooling	-21.6 (251.6)	8.9	10.4 (283.6)	8.0	35.9 (309.1)	2.8
n = 8						
heating	-21.0 (241.0)	14.6	38.0 (311.2)	21.2	-	-
cooling	-37.5 (235.6)	15.1	35.4 (308.6)	20.8	-	-
n = 9						
heating	-21.0 (252.1)	7.1	40.8 (314.0)	23.7	-	-
cooling	-32.2 (240.9)	7.8	39.6 (312.8)	22.9	-	-
n = 10						
heating	-14.6 (258.6)	10.1	10.9 (284.0)	8.4	64.1 (337.21)	32.4
cooling	-24.1 (249.1)	8.2	3.5 (276.6)	9.6	61.5 (334.65)	28.8

Results and Discussion

Previous work on phase transitions in the layered perovskite-type hybrids $[(C_3H_7NH_3)_2CuCl_4]$ introduced geometric quantities to describe quantitatively the different structures and the differences between them.[13] They were: "The tilt angle φ of the organic chains, which defines the rotation angle of the N-C(3) axis around b" and "the tilt angle ϕ of the inorganic bipyramids, which defines the rotation angle of the Cu-Cla direction around **b**". In this paper, we extend the definition of the tilt angle $\angle_\varphi$ to be the angle between a plane through the inorganic layers and a vector connecting the first and last atom of each chain, for example the nitrogen atom N1 and C10 in the case of $C_{10}PbI$. Two further quantities are required to track the motion of the alkylammonium chains before and after the phase transition: An angle $\angle_\alpha$, which is defined as the dihedral angle between a plane containing all the atoms of the alkylammonium chains and the plane formed by the lead atoms of the inorganic layers. And an angle $\angle_\beta$, which is defined as the angle between a vector connecting the atoms N1 and C1 and a plane through the lead atoms of the inorganic layers.

The position of the ammonium group by itself is affected by the phase changes and consequently effects the hydrogen bonding configuration. The "box" containing the ammonium groups are defined by

the four equatorial, or bridging iodides, and the four axial, or terminal iodides that protrude above the layer. In projection, the ammonium group is contained within a parallelogram defined by the four bridging iodides (See Fig. 4). By projection onto this parallelogram the ammonium group is found in proximity to either an acute or an obtuse angle of the parallelogram.

It has been found that the three hydrogens associated with the ammonium group either bond to two terminal iodides and one bridging iodide (terminal halogen configuration) or to two bridging iodides and one terminal iodide (bridging halogen configuration).[3] All the compounds described here in all their phases adopt the terminal halogen configuration. However, there are two ways that the hydrogens can adopt the terminal halogen configuration: The three iodides to which the hydrogens bond can be at the vertices of either an equilateral triangle or a right-angle triangle (See Fig. 4). There is a correlation between the position of the ammonium group and the type of terminal halogen configuration: If the ammonium group is in the acute angled position, it has the right-angled configuration and if the ammonium group is in the obtuse angled position, it has the equilateral configuration.

The corner-sharing PbI_6 octahedra that make up the 2-D layers are affected by the phase changes. For the layered perovskite-type hybrids, two out of a three possible tilts are encountered:[7] a tilt perpendicular to the inorganic sheets (θ tilt), so that adjacent corner-shared octahedra are rotated relative to each other. The angle of the θ tilt is mirrored in the bridging angle Pb-I-Pb, which deviates from the ideal 180°. The second kind of tilt is parallel to the layers (Ψ tilt), so that the layers are corrugated in one particular direction. The corrugation angle is measured by the angle between the normal to the inorganic layers and the vector connecting the Pb atom and the terminal I. The direction of the corrugation is determined by the terminal halogen configuration. The terminal iodides that are acceptor atoms for the hydrogen bonds are tilted towards the ammonium groups, influencing the Ψ tilt of the octahedra. In an identical manner, the bridging iodide that is an acceptor atom affects the θ tilt of adjacent octahedra.

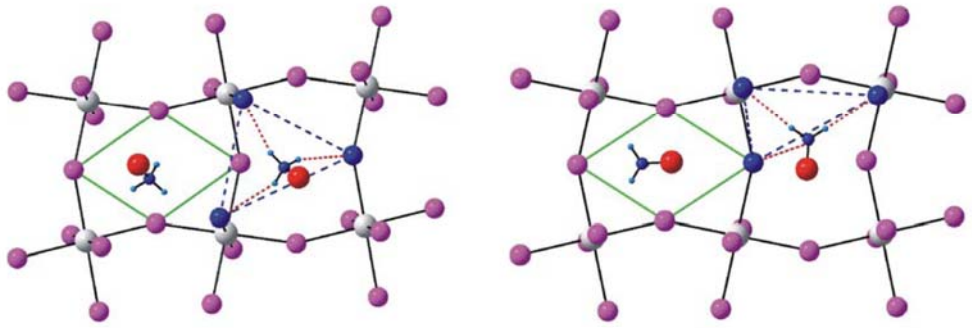


Figure 4. The subtypes in the terminal halogen configuration. On the left, the ammonium group is in the obtuse angled corner of the parallelogram, shown in green, and adopts the equilateral configuration, shown in blue. The picture on the right shows the right-angled configuration seen when the ammonium group is in the acute angled corner of the parallelogram.

The phase transition behaviour of the hybrid $[(C_{10}H_{21}NH_3)_2)PbI_4]$ (4). A study on the compound $[(C_{10}H_{21}NH_3)PbI_4]$, abbreviated $C_{10}PbI_4$, done by Xu and co-workers,[6] revealed the existence of three structural phase transitions, that are "associated with the change of the molecular states of the alkylammonium chains". The presence of the four phases was demonstrated by the temperature dependence of the interlayer spacing. The authors labeled the four phases **I** through **IV** with decreasing temperature, i.e. **I** is the phase stable at the highest temperature. To more accurately determine the transition temperatures between the four phases, a cyclic Differential Calorimetric Scan (DSC) was performed in this report (Figure 3). These three phase transitions are shown to be reversible by the DSC scan by performing a cooling and heating cycle on the same sample. The transition temperatures and enthalpies are summarized in Table 2. The enthalpies for the transitions from **IV** to **III** and **III** to **II** are approximately the same, and the **II** to **I** transition the highest. Previously, only the single-crystal structure of the phase stable at room temperature, phase **II**, has been determined.[10] The paper only reports the unit cell parameters (a = 8.968 Å, b = 8.667 Å, c = 42.51 Å, space group *Pbca*) and the fractional coordinates of the Pb and I atoms. The authors do not comment on the conformation of the decylammonium chain, which can give important clues on the mechanism of the phase transitions. The objective here was to determine the single-crystal structures of all four phases, compare the structural differences between them for clues on the details of the phase transition mechanism and to confirm their reversibilty by performing all diffraction experiments on a single crystal.

The single crystal structural phase transitions and the sequence of diffraction experiments that were carried out on a crystal of $C_{10}PbI$ are shown in Figure 5 and summarized in Table 6. The start point is the structure performed at room temperature of phase **II (4d),** and the end point is structure **4f** of phase

I. The structure of Phase **II** (**4d**) is in the orthorhombic spacegroup *Pbca*, and has similar unit cell parameters, given in Table 1, to the previously reported structure of the same hybrid at room temperature.

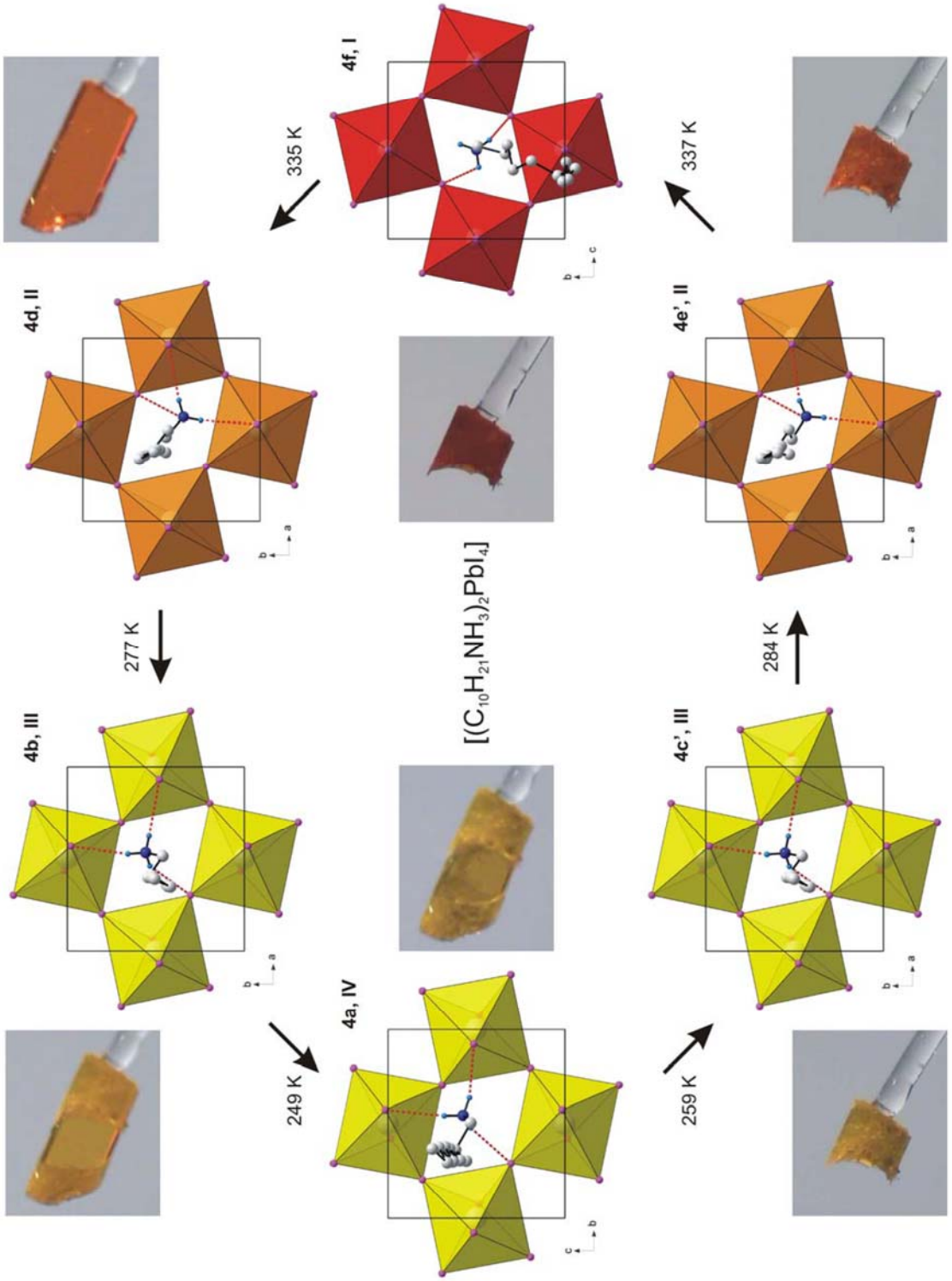


Figure 5. Hydrogen bonding views between the decylammonium chains and the PbI_6 octahedra of the inorganic layer. The direction of the arrows shows the sequence of data collections performed on the crystal shown, starting at structure **4d** and terminating at structure **4f**.

Figure 6 clearly underlines a bidimensional arrangement in which two layers of interdigitated decylammonium molecules are embedded between two consecutive inorganic [PbI_6] sheets, forming an alternated inorganic-organic layered structure. The lead atoms are offset from layer to layer, resulting in a staggered arrangement of adjacent layers, based on the K_2MgF_4 structure type. The unit cell contains two fully occupied inorganic layers per unit cell, two layers with an occupancy of 0.5 at z = 0 and 1, and a layer with an occupancy of 1 at z = 1/2. In the direction perpendicular to the layers, the crystal cohesion is achieved by N-H...I hydrogen bonds, related to the NH_3 polar groups. In the direction parallel to the layers, the cohesion is achieved by strong ionic bonds between equatorial I and Pb atoms. The inorganic layer is built up from characteristic corner-sharing PbI_6 octahedra. The asymmetric unit consists of a lead atom on a special position and two iodide atoms, I1 occupying the terminal position and I2 occupying the bridging position in the octahedra. As shown in the projection perpendicular to the layers in Figure 5, along the c-axis, the PbI_6 octahedra are rotated by 155.56(7)° relative to each other. The θ tilt corresponds to 24.44(7)°. Furthermore, the perovskite layers are corrugated in the *a*-direction by an angle of 6.02(3)° with respect to the *ab*-plane, henceforth known as the Ψ tilt. The coordination geometry around the Pb atom shows no axial compression of the octahedral geometry, with the bridging Pb1-I2 distances shorter than the terminal distances Pb1-I1. The angle between *cis* related I atoms deviate from 90°, with all *trans* angles 180°. The decylammonium molecule sits on a general position. The atomic numbering scheme is shown in Figure 2. The tilt of the chain to the inorganic layers is $\angle_\varphi$ = 11.2(3)°. The chains are ordered within the inorganic layer and interdigitated up to the seventh carbon atom of the chain next to it. The plane of the chain is angled at $\angle_\alpha$ = 89.8(4)° to the inorganic layer. The chain has a planar zig-zag arrangement as the moduli of the N-C-C-C and C-C-C-C torsion angles are in the 142(5)-180(6)° range. The hydrogen bonds between the organic and inorganic entities adopt the terminal halogen configuration and the right-angled configuration (See Figure 5). The hydrogen acceptor distances to the terminal halides I1 are 2.76 Å and 2.78 Å and to the bridging halide I2 3.12 Å (See Table 4). The ammonium group is in the acute angled corner and is tilted at an angle of $\angle_\beta$ = 64.2(2)°.

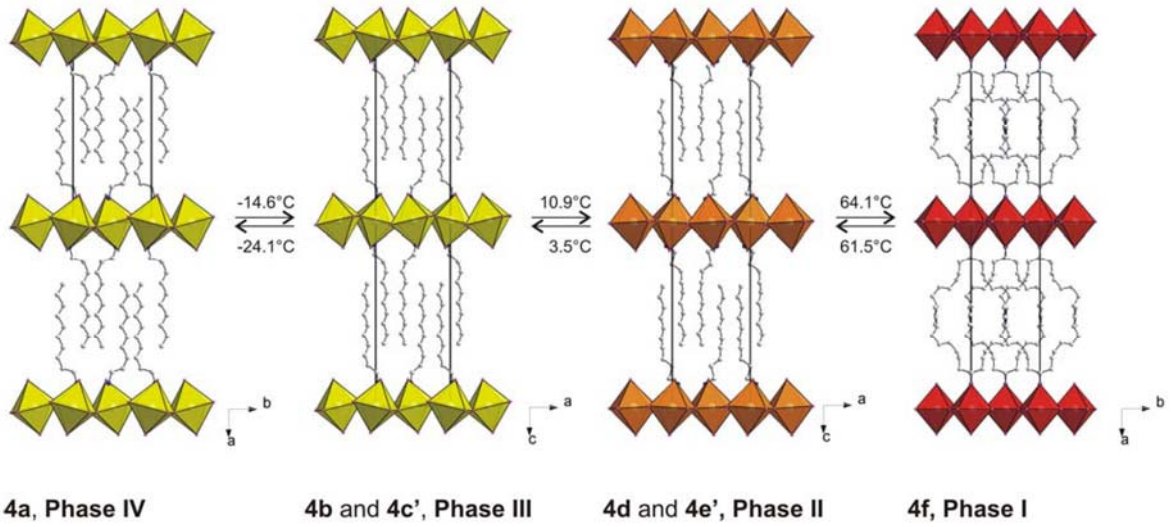


Figure 6. Packing diagrams of the unit cells of the four phases of $C_{10}PbI$. The colour of the inorganic layers mimic the colour of the crystal in that particular phase. The disordered decylammonium chain, related by a two-fold axis, is seen in the highest temperature phase OHT.

The crystal which structure **4d** was collected on fractured on cooling to phase **III** and deemed unsuitable for further experiments. A second crystal was used to continue the cycle and is shown in Figure 5. The unit cell of the new crystal was confirmed to be identical to the unit cell of **4d** and the structure was presumed to be isostructural. In the course of the crystal transformation to phase **III** (**4b**), the crystal changes colour from orange to yellow and has some fracturing at both ends. The middle portion of the crystal retains its integrity. The space group is still *Pbca* and the inorganic layers have the same K_2MgF_4 structure type. The change in colour is indicative of a conformational change of the decylammonium chain, which rotates around its C2-C3 bond by 37(4)° to form a torsion angle of 115(4)° for C1-C2-C3-C4. This means that the ammonium group has moved from the acute to the obtuse position and now adopts the equilateral halogen configuration. The ammonium group changes its tilt angle to the layers to $\angle_\beta$ = 35.0(1)°. The collection temperature was -5°C and an improvement in the size of the anisotropic displacement parameters is evident in Figure 2. The decrease in motion of the atoms is evident as the chain is more planar as the remaining torsion angles are now in a much narrower range from 173(3)-179(4)°. The changes in the inorganic layer are minimal. The Ψ and Ω tilts increase by 5.10 and 6.03° respectively.

The single-to-single-crystal transition to the lowest temperature phase **IV** (**4a**) shows no further colour change and only a small change in the alkylammonium chain. The torsion angle C1-C2-C3-C4 decreases further to 88(4)° and the range of torsion angles of the remainder of the chain varies from

171(3) to 180(5)°. The most significant change occurs at the inorganic layers, where every second layer moves by approximately 4 Å in the crystallographic *a* direction. The lead atoms are now aligned from layer to layer, resulting in an eclipsed arrangement of adjacent layers, typical of layered perovskite-type hybrids with monoclinic unit cells. The structure type is now based on $RbAlF_4$. This also means that there is only one complete layer per unit cell, two layers at x = 0 and 1, each one with an occupancy of 0.5. The unit cell axis halves perpendicular to the layers. This phase has a monoclinic crystal system and the space group changes from *Pbca* to $P2_1/c$.

The structures **4c'** and **4e'** were done at the same temperatures as **4b** and **4a** respectively and are isostructural, proving the structural reversibility of the phase transitions. The different geometric parameters for those four structures are similar and are summarized in Table 6. However, on transforming from phase **IV** back to phase **III**, the upper two thirds of the crystal broke off.

The final phase of $C_{10}PbI$, phase **I** (**4f**), shows a complete disordering of the entire $C_{10}H_{21}NH_3$ chain over two equivalent positions. The two disordered components are related by a two-fold axis and are half occupied. The space group is *Cmca* and the Pb atom and both iodides I1 and I2 occupy special positions. The structure of the high temperature phase of $C_{10}PbI$ is in agreement with another high temperature phase of an inorganic-organic hybrid, phase **I** of $C_{10}CdCl$.[23] The decylammonium chains in $C_{10}CdCl$ have conformational freedom, akin to diffusion of their gauche bonds through the whole chain. The decylammonium chains are disordered over two equivalent positions in this phase, related by a mirrorplane in the space group *Amaa*. The disordered chains in $C_{10}CdCl$ are tilted almost perpendicular to the inorganic layers, increasing the interlayer spacing by 1.5 Å. The electron density map in Figure 7 shows the probable positions of the carbon and nitrogen atoms in the alkylammonium chains of $C_{10}CdCl$. The interlayer spacing in the $C_{10}PbI$ analogue increases from 21.263(2) Å in phase **II** to 23.740(11) Å in phase **I**. The chains are no longer interdigitated up to atom C4 of the neighbouring chain as in phases **IV**, **III** and **II** but only up to atom C9. As in the $C_{10}CdCl$ structure, the positions of the N1 and C1 atoms are well-defined and the remainder of the chain splits. The position of the ammonium group is at the centre of the box. The closest N…I distance is 3.94(2) Å, too long to be considered a possible hydrogen bonding interaction. For a comparison between all six structures, see Table 5 for details.

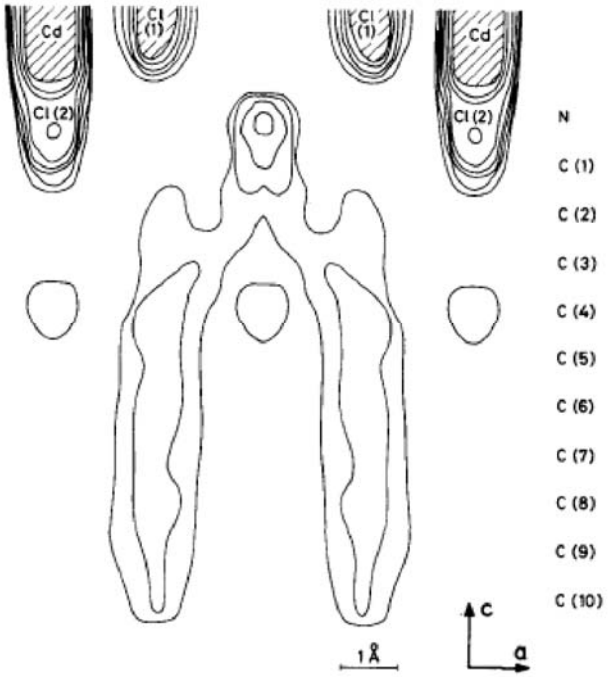


Figure 7. Electron density map of $C_{10}CdCl$ perpendicular to the a-axis. Figure taken from (23).

Table 3. Hydrogen bonding details for compounds 1, 2 and 3 in their various phases

D-H---A	D-H (Å)	H---A (Å)	D---A (Å)	<(D-H---A) (deg)	Symmetry transformations
1a, III					
N(1)-H(1A)-I(1)	0.89	2.78	3.52(5)	140.3	x,-y+3/2,z+1/2
N(1)-H(1B)-I(1)	0.89	2.79	3.67(5)	175.8	x,y,z+1
N(1)-H(1C)-I(2)	0.89	2.98	3.73(4)	142.6	-
1b, II					
N(1)-H(1B)…I(1)	0.89	2.71	3.59(2)	171.0	-x+3/2, y-1/2, z
N(1)-H(1A)…I(1)	0.89	2.80	3.67(3)	164.4	-
N(1)-H(1C)…I(2)	0.89	3.09	3.68(3)	125.3	x-1/2, -y+3/2, -z
2a, III					
N(1)-H(1A)…I(1)	0.91	2.63	3.46(3)	152.2	x,-y+1/2,z-1/2
N(1)-H(1C)…I(1)	0.91	2.73	3.62(4)	165.9	-
N(1)-H(1B)…I(1)	0.91	2.83	3.69(3)	157.1	-x,y+1/2,-z+3/2
2b, II					
N(1)-H(1C)…I(1)	0.89	2.75	3.63(2)	168.0	-x+3/2, y-1/2, z
N(1)-H(1A)…I(1)	0.89	2.78	3.66(2)	169.5	-
N(1)-H(1B)…I(2)	0.89	3.12	3.67(2)	122.3	x-1/2, -y+3/2, -z
2c, I					
N(1)-H(1B)...I(2)	0.89	3.36	3.84(2)	115.8	-
N(1)-H(1C)...I(2)	0.89	3.37	3.84(2)	115.2	-x+2,-y+1,-z+1
N(1)-H(1A)...I(1)	0.89	3.63	4.37(1)	143.7	x,y+1/2,-z+1/2
3a, III					
N(1)-H(1B)-I(1)	0.90	2.71	3.24(6)	119.0	x,y-1,z
N(1)-H(1A)-I(1)	0.90	3.29	4.03(6)	140.8	x,-y+3/2,z+1/2
N(1)-H(1C)-I(2)	0.90	2.91	3.70(5)	147.9	x,-y+3/2,z-1/2
3b, II					
N(1)-H(1B)…I(1)	0.89	2.73	3.59(2)	160.7	x-3/2, y-1/2, z
N(1)-H(1C)…I(1)	0.89	2.85	3.71(2)	162.5	-
N(1)-H(1A)…I(2)	0.89	3.10	3.71(2)	127.3	-

Table 4. Hydrogen bonding details and short contacts for compound 4 in its various phases

D-H---A	D-H (Å)	H---A (Å)	D---A (Å)	<(D-H---A) (deg)	Symmetry transformations
4a, IV					
N(1)-H(1B)-I(1)	0.90	2.61	3.42(4)	151.1	-
N(1)-H(1C)-I(1)	0.90	2.81	3.70(3)	170.8	x,-y+3/2,z+1/2
N(1)-H(1A)-I(2)	0.90	2.88	3.75(4)	162.3	-x,y-1/2,-z+1/2
4b, III					
N(1)-H(1C)-I(1)	0.89	2.76	3.62(3)	163.4	-
N(1)-H(1B)-I(1)	0.89	2.87	3.62(3)	142.2	-x+3/2,y-1/2,z
N(1)-H(1A)-I(2)	0.89	2.93	3.73(3)	150.6	-x+1,-y+1,-z
4c', III					
N(1)-H(1C)-I(1)	0.89	2.78	3.62(3)	162.7	-
N(1)-H(1B)-I(1)	0.89	2.89	3.62(4)	142.3	-x+3/2,y-1/2,z
N(1)-H(1A)-I(2)	0.89	2.92	3.72(4)	151.1	-x+1,-y+1,-z
4d, II					
N(1)-H(1C)…I(1)	0.89	2.76	3.63(3)	164.5	-x+3/2, y-1/2, z
N(1)-H(1B)…I(1)	0.89	2.78	3.66(3)	170.7	x,y-1,z
N(1)-H(1A)…I(1)	0.89	3.12	3.79(3)	133.3	-
4e', II					
N(1)-H(1B)...I(2)	0.89	2.77	3.61(6)	156.8	-x+3/2, y-1/2, z
N(1)-H(1C)...I(2)	0.89	2.79	3.67(7)	171.7	x,y-1,z
N(1)-H(1A)...I(1)	0.89	3.17	3.86(6)	135.2	-
4f, I					
N(1)-H(1C)-I(2)	0.89	3.18	3.94(2)	144.8	-x+2,-y+1,-z+1
N(1)-H(1B)-I(2)	0.89	3.54	3.94(2)	110.2	-

Table 5 Geometric Parameters of compound 4 in all of its phases

	4a, IV	**4b, III**	**4c', III**	**4d, II**	**4e', II**	**4f, I**
Interlayer Spacing (Å)	21.330(9)	21.9746(13)	21.9824(8)	21.2848(12)	21.263(2)	23.740(11)
Bridging Angle Pb(1)-I(2)-Pb(1) (deg)	150.01(9)	149.53(7)	149.55(9)	155.56(7)	155.91(12)	154.80(9)
θ tilt (°)	29.99(9)	30.47(7)	30.45(9)	24.44(7)	24.09(12)	25.20(9)
Corrugation Ψ tilt (°)	12.97(5)	11.12(5)	11.15(5)	6.02(3)	6.06(7)	0
Tilt of Chains $\angle_{\varphi}$ (°)	8.0(4)	6.5(3)	6.4(3)	11.2(3)	11.4(6)	25.9(1)
Tilt of plane $\angle_{\alpha}$ (°) (N1…C10)	88.2(3)	87.9(3)	88.0(4)	89.8(4)	89.4(7)	89.4(3)
Tilt of NH_3 group $\angle_{\beta}$ (°)	25.3(2)	35.0(1)	34.7(2)	64.2(2)	64.3(3)	7.3(5)
Position of ammonium group	Obtuse	Obtuse	Obtuse	Acute	Acute	Centre
Hydrogen bonding configuration	Equilateral	Equilateral	Equilateral	Right-Angled	Right-Angled	-
Torsion Angle: C(1)-C(2)-C(3)-C(4)	88(4)	116(4)	115(5)	152(4)	138(7)	121(7)

The phase behaviour of $[(C_8H_{17}NH_3)_2)PbI_4]$ (2). The hybrid C_8PbI has one fewer phase transition than $C_{10}PbI$ and the structures of all three phases were determined successfully on a single crystal. Figure 8 shows magnified views of the three different structures. The phases are labelled **III**, **II** and **I** with increasing temperature. The structure of the orthorhombic phase **II**, determined at room temperature, is isomorphous to the orthorhombic phase **II** of $C_{10}PbI$, with the tilts of the PbI_6 octahedra and the hydrocarbon chains similar (See Table 5 and 6). The only difference is the decrease in the interlayer spacing, due to the shorter octylammonium chain, and the difference in the C1-C2-C3-C4 torsion angles. In $C_{10}PbI$, the torsion angle is 152(4)°, whereas in C_8PbI, the angle of -172(3) is much closer to 180°. The entire octylammonium chain has an all-*trans*, planar conformation. The transition to the lowest temperature phase **III** that has a monoclinic crystal system in C_8PbI involves a concerted movement of the inorganic layers and a rotation around the C2-C3 bond to give a new torsion angle of 73(5)°, an absolute change of 99°. C_8PbI transforms from the K_2MgF_4 (staggered inorganic layers) to the $RbAlF_4$ (eclipsed inorganic layers) structure type in the same way $C_{10}PbI$ did previously when it transformed from the orthorhombic phase **III** to the monoclinic phase **IV**. However, the rotation around the C2-C3 bond was performed separately in $C_{10}PbI$ in an additional phase change form phase **II** to

phase **III**, i.e. $C_{10}PbI$ transforms from the same phase **II** as C_8PbI to the lowest temperature phase via an intermediate phase **III**. The detailed geometry of phase **III** in C_8PbI compares favourably to the observations made on phase **IV** of $C_{10}PbI$. Both the octylammonium and decylammonium chains have their ammonium groups in the obtuse position and the same equilateral configuration. The same crystal of C_8PbI was also heated to phase **I** and there undergoes an order-disorder transition. The space group is *Cmca* and the asymmetric unit is the same as phase **I** of $C_{10}PbI$. There is no corrugation of the inorganic layers ($\Psi = 0$) and the θ tilt is 1.50° more than in $C_{10}PbI$. The two halves of the disordered octylammonium chain, again related by a two-fold axis are shown in Figure 8. The conformation of the chain is non-planar, with the torsion angles ranging from -49(5)° to 165(5)°. For a comparison between all three structures, see Table 6 for details.

Table 6 Geometric Parameters of compounds 1 and 2 in some of their phases.

	1a, III	**1b, II**	**1c, I**	**2a, III**	**2b, II**	**2c, I**
Interlayer Spacing (Å)	17.243(9)	17.2806(10)	18.306(13)	18.738(3)	18.741(2)	20.014(2)
Bridging Angle Pb(1)-I(2)-Pb(1) (°)	149.61(10)	157.03(6)	154.96(16)	149.42(9)	156.05(5)	153.30(4)
θ tilt (°)	30.39(10)	22.97(6)	25.04(16)	30.58(9)	23.95(5)	26.70(4)
Corrugation Ψ tilt (°)	13.60(5)	6.85(3)	5.75(1)	13.10(5)	6.06(3)	0
Tilt of Chains $\angle_{\varphi}$ (°)	16.7(5)	22.9(4)	-	10.8(4)	15.2(3)	41.3(7)
Tilt of plane $\angle_{\alpha}$ (°)	88.3(8)	89.6(9)	-	87.1(4)	89.7(4)	90
Tilt of NH_3 group $\angle_{\beta}$ (°)	30.8(2)	65.7(1)	-	27.4(2)	64.4(1)	21.3(2)
Position of ammonium group	Obtuse	Acute	-	Obtuse	Acute	Centre
Hydrogen bonding configuration	Equilateral	Right-angled	-	Equilateral	Right-angled	-
Torsion Angle: C(1)-C(2)-C(3)-C(4)	98(5)	176(5)	-	73(5)	-172(3)	151(6)

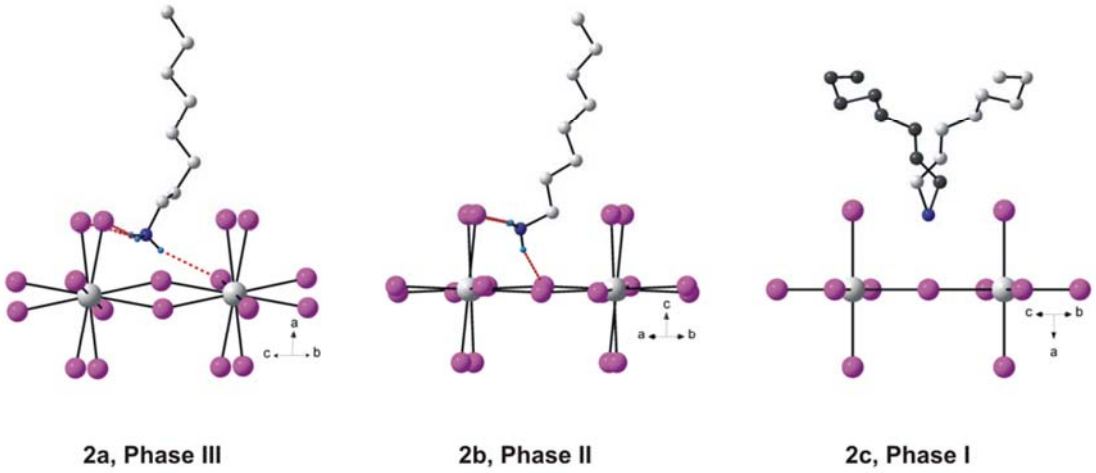


Figure 8. The packing of a single octylammonium chain relative to the inorganic layer. The monoclinic phase **III** has a kink at the ammonium end of the chain, which disappears in the orthorhombic phase **II**. The tilting of the octahedra decreases with increasing temperature. The two separate octylammonium chains that are related by the two-fold axis are shown as light grey and dark grey spheres in phase **I**.

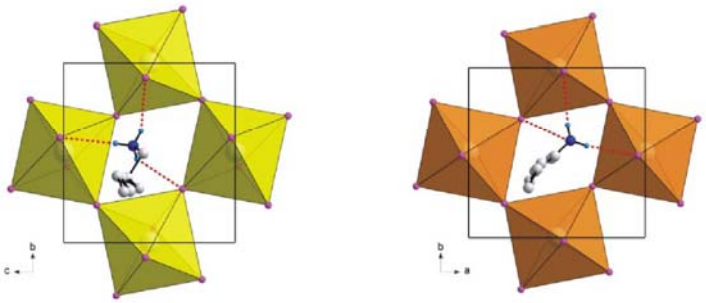
The phase behaviour of $[(C_9H_{19}NH_3)_2)PbI_4]$ (3). The hybrid C_9PbI has only two phase transitions (Table 2 and Figure 3). However, only the structures of the phases **III** and **II** were determined, and a separate crystal was required for each single-crystal structure collection. The detailed phase behaviour of C_9PbI can be compared to that of C_8PbI. As in the previous two hybrids, C_8PbI and $C_{10}PbI$, phase **II** of C_9PbI has orange coloured crystals at room temperature. The overall packing in this phase has staggered inorganic-organic layers and an orthorhombic crystal system. The nonylammonium chain is in its planar all-*trans* conformation. The transition to the lowest temperature phase **III** is the same as in C_8PbI. This monoclinic phase of C_9PbI has eclipsed inorganic layers and a kink develops at the ammonium end of the chain. The position of the ammonium group changes from the acute to the obtuse position as a consequence of the kink it undergoes from phase **II** to **III**. Repeated attempts at obtaining the single-crystal structure of the highest temperature phase **I** of C_9PbI were unsuccessful as the crystals did not survive the phase transition at $T_2^h = 40.8°C$. The transition enthalpy ΔH_2^h is 2.5 kJ mol^{-1} greater than for C_8PbI and we propose that the structure of phase **I** for C_9PbI is the same as for phase **I** of C_8PbI. For detailed geometric parameters, see Table 7.

The phase behaviour of $[(C_7H_{15}NH_3)_2)PbI_4]$ (1). The compound C_7PbI has three phase transitions but differs from the phase behaviour of the other three hybrids. The latter compounds record their highest transition enthalpies in going to their highest temperature phase **I**, respectively 21.2, 23.7 and 32.4 kJ

mol^{-1} for C_8PbI, C_9PbI and $C_{10}PbI$. C_7PbI however has a very low enthalpy for its highest phase transition, T_3^h = 2.8 kJ mol^{-1}. The phase behaviour can be explained if one assumes that the transition at T_3 is not the transition to phase **I** as encountered in the previous discussions and is labelled as **I'**. In fact, the structure at room temperature, **1c**, has the highest interlayer spacing between the inorganic layers, indicative of the structure already being in its highest temperature phase **I**, even though the temperature is in fact at room temperature. This is supported by not being able to determine the fractional coordinates of the heptylammonium chains at room temperature, in other words, the hybrid is undergoing rapid rotational disordering already at room temperature. The position of the Pb atom and the I atoms was determined in this phase and adjacent inorganic layers are found to be staggered. On cooling the same crystal below the phase transition at T_2^c = 10.4 °C, the heptylammonium molecule sandwiched between the layers becomes ordered and the interlayer spacing decreases from 18.306(13) Å to 17.2806(10) Å. The position of the heptylammonium molecule does *not* change its position during this phase transition. This phase **II**, structure **1b**, is the same as the other three hybrids in their phase **II**. The colour of the crystal remains orange for both phases **II** and **I**. The heptylammonium chain has a zig-zag planar conformation as the modulus of the torsion angles range from 174(6)° to 178(5)°. The ammonium group is in the acute position and the tilt of the NH_3 group is $\angle_\beta$ = 65.7(1)° (for comparison, C_8PbI: 64.4(1)°; C_9PbI: 65.8(1)°; $C_{10}PbI$: 64.2(2°). This is the disorder-order transition seen in other hybrids such as C_3CdCl, where the propylammonium chain oscillates by approximately 74° around the N…C3 axis.[24] The phase transition at 183 K is due to a freezing of this movement and only one position remains.[24] The lowest phase transition is from phase **II** to **III** and is identical to the transitions to the lowest temperature phase seen in all the previous hybrids, where the crystal changes colour from orange to yellow (Figure 9) and the position of the ammonium group changes from acute to obtuse (Figure 10). For a comparison between all three structures, see Table 6 for details.



Figure 9. The colour change of a crystal of C_7PbI. The structures of phase **I** (**1c**) and **II** (**1b**) were collected on this crystal. The same crystal was cooled to phase **III**, shown at -50°. However, a different crystal was used to collect the structure of phase **III** (**1a**).



1a, Phase III 1b, Phase II

Figure 10. The packing of a single heptylammonium chain relative to the inorganic layer in the two phases **III** and **II**. The kink around the C2-C3 bond is evident in the phase **III**, compared to phase **II**.

Table 7 Geometric Parameters of compound 3 in two of its phases.

	3a, III	**3b, II**
Interlayer Spacing (Å)	19.791(3)	19.8789(9)
Bridging Angle Pb(1)-I(2)-Pb(1) (°)	149.98(10)	157.24(5)
θ tilt (°)	30.02(10)	22.76(5)
Corrugation Ψ tilt (°)	14.03(5)	6.92(3)
Tilt of Chains $\angle_{\varphi}$ (°)	15.1(5)	15.5(3)
Tilt of plane $\angle_{\alpha}$ (°)	84.9(1)	89.5(4)
Tilt of NH_3 group $\angle_{\beta}$ (°)	51.4(1)	65.8(1)
Position of ammonium group	Obtuse	Acute
Hydrogen bonding configuration	Equilateral	Right-angled
Torsion Angle: C(1)-C(2)-C(3)-C(4)	110(4)	-146(3)

Conclusions

The compounds $[(C_nH_{2n+1}NH_3)_2PbI_4]$, n = 7, 8, 9 and 10, which belong to the family of inorganic-organic hybrids that have a layered perovskite-type packing, have multiple reversible phase transitions. The phase transitions are due to changes in the hydrocarbon chains and the relative arrangement of the inorganic layers. All four hybrids have a lowest temperature phase, labelled phase **III** for n = 7, 8 and 9 and phase **IV** for n = 10, which is the phase stable at the lowest temperature, where successive inorganic layers are eclipsed and the alkylammonium chains are kinked. This phase can be identified by the yellow colour of the crystals and the monoclinic crystal system. The next highest temperature phase depends on the chain length of the hybrid. If the chain length is 7, 8 or 9 C atoms, then the alkylammonium chains become planar and loose their kink. At the same time, the inorganic layers shift to change from the staggered to the eclipsed configuration. The crystal colour is orange and the crystal system is orthorhombic. This phase is labelled phase **II**. If the chain length is 10 C atoms long, then only the conformation of the hydrocarbon chain changes in going from phase **IV** to phase **III** and the layers remain eclipsed. $C_{10}PbI$ undergoes another phase transition to its phase **II**, where the layers then become staggered. The highest temperature phase, which is above room temperature for n = 8, 9 and 10, then features a disordering of the entire alkylammonium chain over two positions, described in detail for C_8PbI and $C_{10}PbI$. This phase has been designated phase **I**. Structurally, this phase was not determined for C_9PbI but is assumed to be similar. Phase **I** of C_7PbI already occurs at room temperature.

References

(1) Dunitz, J. *Acta Cryst. B* 1995, *51*, 619-631.

(2) Fernandes, M. A.; Levendis, D. C.; Schoening, F. R. L. *Acta Cryst. B* 2004, *60*, 300-314.

(3) Mitzi, D. B. *Progr. Inorg. Chem.* 1999, *48*, 1-121.

(4) Mitzi, D. B. *J. Chem. Soc., Dalton Trans*. 2001. 1-12.

(5) Ishihara, T.; Takahashi, J.; Goto, T. *Solid State Commun.* **1989**, *69*, 933. Xu, C.; Kondo, T.; Sakakura, H.; Kumata, K.; Takahashi, Y.; Ito, R. *Solid State Commun.* **1991**, *79*, 245. Xu, C.; Sakakura, H.; Kondo, T.; Takeyama, S.; Miura, N.; Takahashi, Y.; Kumata, K.; Ito, R. *Solid State Commun.* **1991**,*79*, 249. Hirasawa, M.; Ishihara, T.; Goto, T.; Sasaki, S.; Uchida, K.; Miura, N. *Solid State Commun.* **1993**, *86*, 479.

(6) Xu, C.; Fukuta, S.; Sakakura, H.; Kondo, T.; Ito, R.; Takahashi, Y.; Kumata, K. *Solid State Commun.* **1991**, *77*, 923.

(7) Hatch, D.; Stokes, H. T.; Aleksandrov, K. S.; Misyul, S. V. *Phys. Rev. B* **1989**, *39*, 9282.

(8) Hatch, D. M.; Stokes, H. T. *Phys. Rev. B* **1987**, *35*, 8509.

(9) Needham, G. F.; Willett, R. D.; Franzen, H. F. *J. Phys. Chem.* **1984**, *88*, 674.

(10) Ishihara, T.; Takahashi, J.; Goto, T. *Phys. Rev. B* **1990**, *42*, 11099.

(11) Barman, S.; Venkataraman, N. V.; Vasudevan, S.; Seshadri, R. *J. Phys. Chem.* B **2003**, *107*, 1875.

(12) Chanh, N. B.; Houstry, J. R.; Meresse, A.; Ricard, L.; Rey-Lafon, M. *J. Phys. Chem. Solids* **1989**, *50*, 829.

(13) Doudin, B.; Chapuis, G. *Acta Cryst. B* **1990**, *46*, 175.

(14) Bruker 2005, *APEX2*. Version 1.0-27. Bruker AXS Inc., Madison, Wisconsin, USA.

(15) Bruker 2005, *SAINT-PLUS*. Version 7.14. Bruker AXS Inc., Madison, Wisconsin, USA.

(16) Bruker 2003, *XPREP2*. Version 6.14. Bruker AXS Inc., Madison, Wisconsin, USA.

(17) Farrugia, L. J. WinGX, *J. Appl. Cryst.* **1997**, *30*, 565.

(18) Sheldrick, G. M. *SHELXS-97. Program for the Solution of Crystal Structure*; University of Gottingen: Germany, 1997.

(19) Sheldrick, G. M. *SHELXL-97. Program for the Refinement of Crystal Structure*; University of Gottingen: Germany, 1997.

(20) Spek, A. L. *J. Appl. Crystallogr.* **2003**, *36*, 7.

(21) Farrugia, L. J. WinGX, *J. Appl. Cryst.* **1999**, *32*, 837.

(22) Brandenburg, K. *Diamond*. Version 2.1e., Crystal Impact GbR, Bonn, Germany.

(23) Kind, R.; Pleško, S.; Arend, H.; Blinc, R.; Žekš, B.; Seliger, J.; Ložar, B.; Slak, J.; Levstik, A.; Filipič, C.; Žagar, V.; Lahajnar, G.; Milla, F.; Chapuis, G. J. Chem. Phys. **1979**, *71*, 2118.

(24) Chapuis, G. *Acta Cryst. B* **1978**, *34*, 1506.

Chapter 5.4 Structural transitions of the inorganic-organic layered perovskite-type hybrids $[(C_nH_{2n+1}NH_3)_2PbI_4]$; n = 12, 14, 16, 18

Journal: Dalton Transactions

Date Submitted: Pending, before 30 April 2007

Reference Code of submitted article:

Date Accepted:

Final Reference:

Brief Synopsis

In this paper, the phase transitions of the inorganic-organic layered perovskite-type hybrids $[C_nH_{2n+1}NH_3)_2PbI_4]$ (n = 12, 14, 16 and 18) are presented. The techniques used were SC-XRD, DSC and Hot Stage Microscopy (HSM).

CREATED USING THE RSC ARTICLE TEMPLATE (VER. 2.0) - SEE WWW.RSC.ORG/ELECTRONICFILES FOR DETAILS

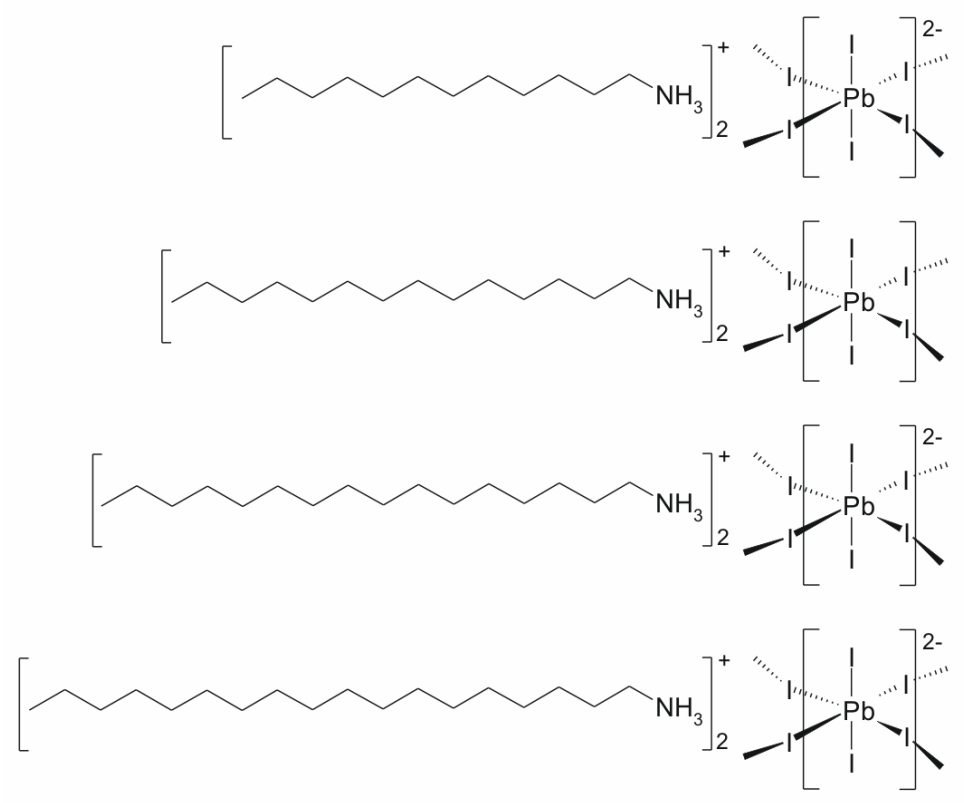
[JOURNAL NAME HERE] | www.rsc.org/[JOURNAL] Article

Structural transitions of the inorganic-organic layered perovskite-type hybrids $[(C_nH_{2n+1}NH_3)_2PbI_4]$; n = 12, 14, 16, 18

David G. Billing* and Andreas Lemmerer

Receipt/Acceptance Data **[DO NOT ALTER/DELETE THIS TEXT]**
Publication data **[DO NOT ALTER/DELETE THIS TEXT]**
DOI: 10.1039/b000000x [DO NOT ALTER/DELETE THIS TEXT]

The first single-crystal structures of the inorganic-organic layered perovskite-type hybrids of general formula $[(C_nH_{2n+1}NH_3)_2PbI_4]$; n = 12, 14, 16, 18, have been determined at room temperature. The four compounds each display two reversible phase transitions above room temperature, labelled phases **III**, **II** and **I**. The single-crystal structures of phase **II** have also been determined. The phase transition from phase **III** to phase **II** is a first-order transition and corresponds to a change in the conformation of the alkylammonium chains and a shift of the inorganic layers relative to each other.



[a] *Molecular Sciences Institute, School of Chemistry, University of the Witwatersrand, PO WITS 2050, Johannesburg, South Africa. E-mail: dave@chem.wits.ac.za; Fax: 27 11 717 6749; Tel: 27 11 717 6759*

† Electronic Supplementary Information (ESI) available: [details of any supplementary information available should be included here]. See http://dx.doi.org/10.1039/b000000x/

CREATED USING THE RSC ARTICLE TEMPLATE (VER. 2.0) - SEE WWW.RSC.ORG/ELECTRONICFILES FOR DETAILS

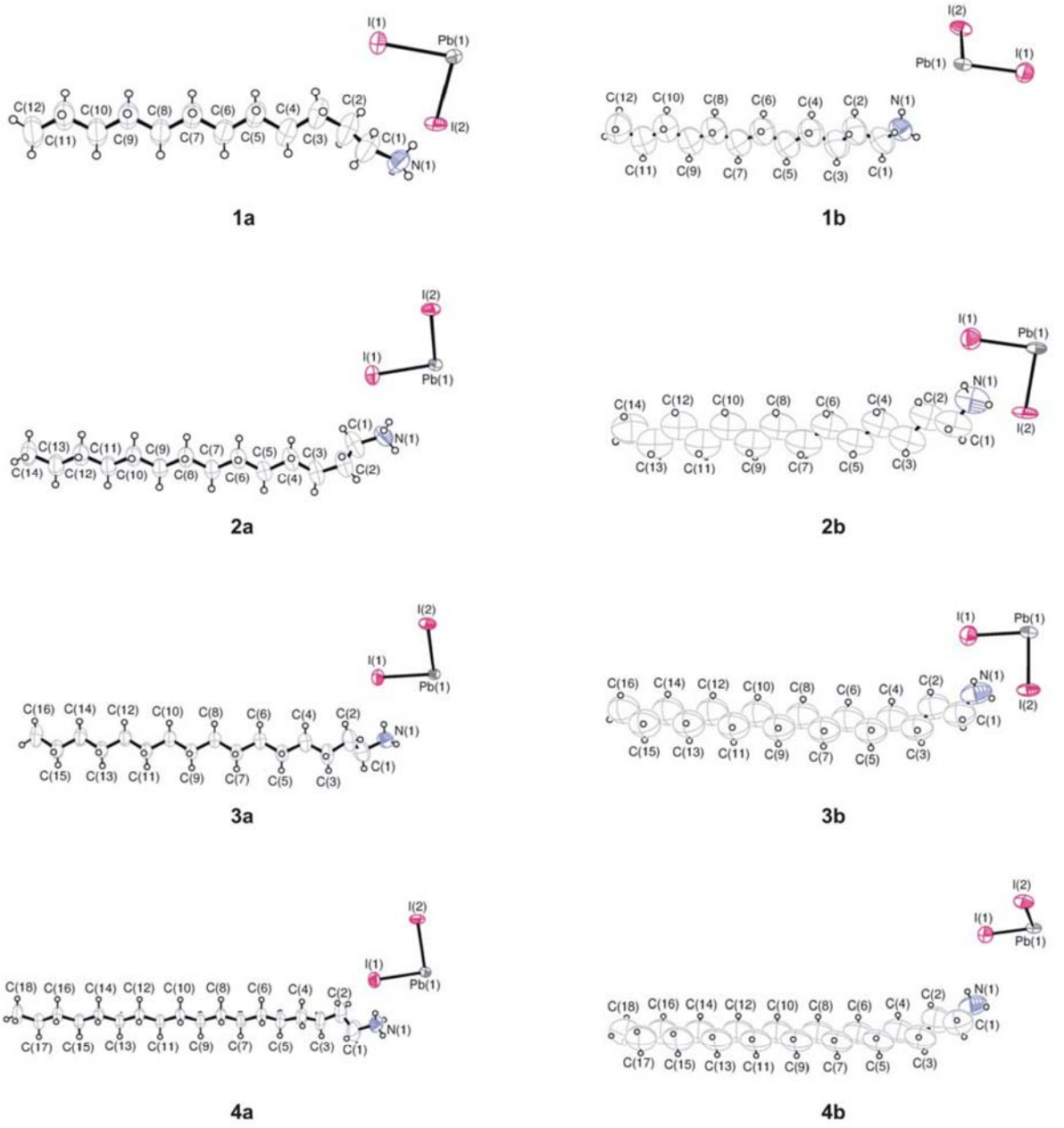


Fig. 1 The asymmetric unit and atomic numbering scheme of the four compounds **1-4**. The structures of phases **III** are shown in the left column and are labelled **1a-4a**, and their corresponding phase **II** structures are shown on the right, labelled **1b-4b**. The anisotropic displacement parameters are shown at the 50% probability level.

This journal © Royal Society of Chemistry

CREATED USING THE RSC ARTICLE TEMPLATE (VER. 2.0) - SEE WWW.RSC.ORG/ELECTRONICFILES FOR DETAILS

[JOURNAL NAME HERE] | www.rsc.org/[JOURNAL] Article

Introduction

Two-dimensional hybrids, $[(C_nH_{2n+1}NH_3)_2MX_4]$ (C_nMX for short), where M is a divalent metal and X is a halogen, have been the subject of many investigations since they show a variety of structural transitions with temperature. The general structure of these inorganic-organic hybrids consists of layers of corner-sharing MX_6 octahedra alternating with layers of n-$C_nH_{2n+1}NH_3$ cations. The NH_3 ammonium groups are linked to the inorganic layers by three weak N-H...X hydrogen bonds.[1] Van der Waals forces between the alkyl chains hold the overall inorganic-organic structure together. The hydrocarbon chains can be either interdigitated or non-interdigitated and be tilted at various angles and directions to the inorganic layers. The packing of the chains is often metal dependant, as in $C_{10}CdCl$, where the non-interdigitated chains on opposite sides of the $[CdCl_4]^{2-}$ layers are tilted at +40° and -40° relative to the inorganic layers in the compounds lowest temperature phase.[2] This type of packing is not seen in the analogues compounds $C_{10}MnCl$[3] and $C_{10}CuCl$,[4] where the chains are all parallel in one direction, tilted at approximately +40°. Interdigitated chains are seen in the compounds that offer the largest separation between the metals in adjacent corner-shared octahedra and have long chain lengths, as in C_9PbI,[5] which has a separation of 8.708(1) Å and 9.034(1) Å. In $C_{10}MnCl$[3] for example, the separation is only 7.213(8) Å and 7.337(2) Å. These compounds undergo single or multiple phase transitions which depend on the length of the alkyl chain and its conformation and have been investigated using DSC and DTA techniques, especially in $[(C_nH_{2n+1}NH_3)_2MX_4]$ (n = 8-18, M = Mn, Hg and Cu; X = Br and Cl).[6]

The most comprehensive investigation via single crystal techniques was performed on the compound $[(C_{10}H_{21}NH_3)_2CdCl_4]$.[2] The compound undergoes two phase transitions. The first one, at 308 K, is a displasive phase transition, and the second one, at 312 K, is a complete melting of the alkyl chain. These two types of phase transitions are characteristic for other long chain layered perovskite-type hybrids. The displasive phase transition is a minor transition that comes about from conformational changes within the alkylammonium chains, where the torsion angles around the N-C or C-C bonds change from trans to gauche or vice versa as the temperature increases. The enthalpy for this phase transition is less than for the second phase transition, where the entire alkylammonium chains can show dynamical disorder along their longitudinal axis, leading ultimately up to a 'quasi-melting' of the hydrocarbon part. This transition is usually the major transition. The sequence of the two phase transitions depends on the identitiy of the metal and the length of the chain.

The hybrids $[(C_nH_{2n+1}NH_3)PbI_4]$ undergo two phase transitions: the first phase transition is in the range from 235 K to 275 K for n = 4, 8, 9, 10,[7] and the second transiton in the range from 313 to 340 K.[8] The compounds with n = 12, 16 and 18 show both phase transitions above room temperature, in the range 318 K to 373 K.[9] These phase transitions are first order and arise from changes in thermal motion of the alkylammonium chains situated between the layers. The alkyl chains at room temperature are non-interdigitated and tilted at 55° to the inorganic layers[10] and are in a planar, all-*trans* conformation (See Fig. 2).[11] The chains are more ordered below the transition and as they become more disordered, a resultant change in symmetry is observed. The interlayer spacing between the layers increases with temperature as the rotational disordering increases (See Fig. 2).[9] The phase transitions of these lead iodide layered perovskite-type hybrids have not been studied by single-crystal diffraction, but rather by powder diffraction, IR, NMR and Raman techniques. The objectives of this present study is determine the packing arrangement of the long chain perovskites with lead iodide at room temperature by single-crystal diffraction, to observe their phase behaviour using differential scanning calorimetry and to determine the single-crystal structures of the various phases.

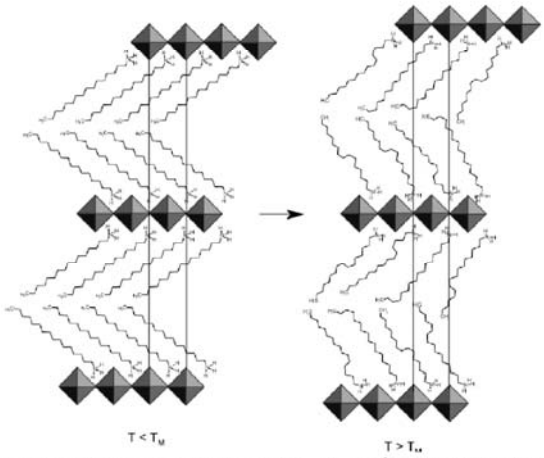


Fig. 2 The figure has been taken from Barman,[9] which schematically depicts the melting transition in the $[(C_nH_{2n+1}NH_3)_2PbI_4]$ hybrids studied. The structure on the left is the room temperature one in which the alkyl chains are tilted at a fixed angle and have an all-trans conformation. The chains are non-interdigitated and this feature is the major discrepancy between the structures reported in this study and by Barman.

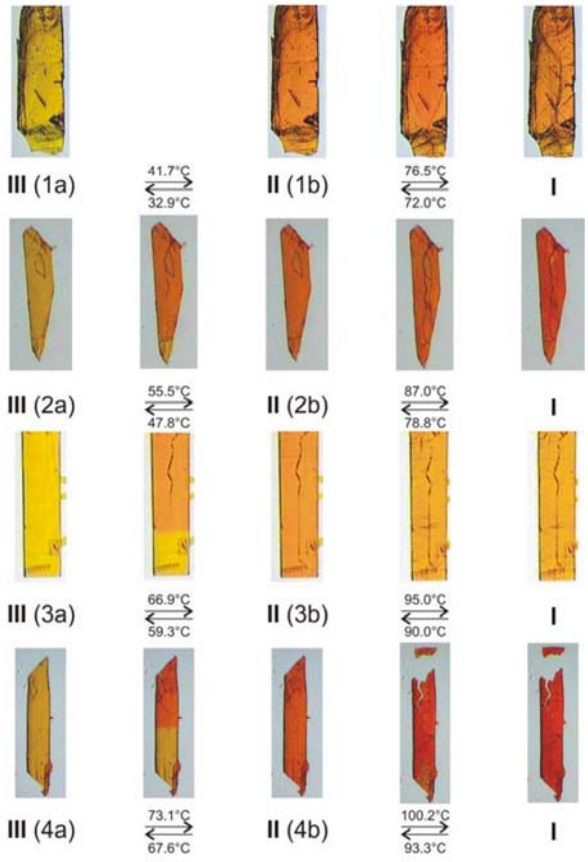


Fig. 3 Hot Stage Microscope pictures of crystals of the four hybrids. The crystals are yellow at room temperature, phase **III**, and then darken through orange to red in their high temperature phases, **II** and **I**.

Results and Discusion

Thermal studies of $[(C_nH_{2n+1}NH_3)_2PbI_4]$; n = 12, 14, 16, 18 by Differential Scanning Calorimetry and Hot Stage Microscopy

Differential scanning calorimetry (DSC) traces where done on all four compounds to determine the exact temperature and enthalpies for each transition (Table 1). The samples where first cooled to -50°C to confirm that all phase transitions occur above 0°C. This is further confirmed by the yellow colour of the crystals at room temperature as the first phase transitions always leads to a change in colour to orange or red (See Fig. 3). The samples where then heated to a temperature above the last transition to ensure completeness and then cooled back to 25°C to illustrate the reversibility of the phase transitions (See Fig. 4). On heating, there are two endotherms, a minor one preceding a major one, which shall be referered to as the premelting, T_1, and melting transitions, T_m, respectively, consistent with the designations of Barman.[9] Both the premelting and the melting transitions are observed as exotherms upon cooling, with signs of thermal hysterises as they occur at a low temperature than their corresponding endotherms. The reversibilty of both transitions for n = 12, 16, 18 compounds is not seen in the study by Barman,[9] which was the first indication that the structures of our compounds might be different to the proposed room temperature structure model by Venkataraman et al.[11] According to Barman, only the melting transition shows an exotherm on cooling and the premelting endotherm is only recovered after leaving the samples standing for a few days and repeating the scan then. Nonetheless, the trends observed by Barman are closely mimicked by our results as shown in Fig. 5. All the premelting and melting transitions have similar enthalpies, consistent with the single crystal data we observed that the structures undergo similiar geometric rearrangements at those temperatures. The melting transitions are much higher and increase with chain length. Every compound that was heated on the diffractometer to above the melting transition temperature showed a loss of crystallinity. Only a few low angle spots where observed and the spot shape was streaky.

Table 1 Differential Scanning Calorimetry

Chain length	T_1 (°C, K)	ΔH_1 (kJ mol^{-1})	T_m (°C, K)	ΔH_m (kJ mol^{-1})
n = 12				
heating	41.7 (314.9)	10.9	76.5 (349.7)	44.2
cooling	32.9 (306.1)	9.2	72.0 (345.1)	41.9
n = 14				
heating	55.5 (328.6)	10.6	87.0 (360.1)	54.6
cooling	47.8 (320.9)	9.6	78.8 (352.0)	51.7
n = 16				
heating	66.9 (340.0)	11.6	95.0 (369.1)	62.7
cooling	59.3 (332.4)	10.0	90.0 (363.2)	61.7
n = 18				
heating	73.1 (346.3)	13.4	100.2 (373.3)	79.5
cooling	67.6 (340.8)	12.1	93.3 (366.4)	75.9

a

CREATED USING THE RSC ARTICLE TEMPLATE (VER. 2.0) - SEE WWW.RSC.ORG/ELECTRONICFILES FOR DETAILS

[JOURNAL NAME HERE] | www.rsc.org/[JOURNAL] Article

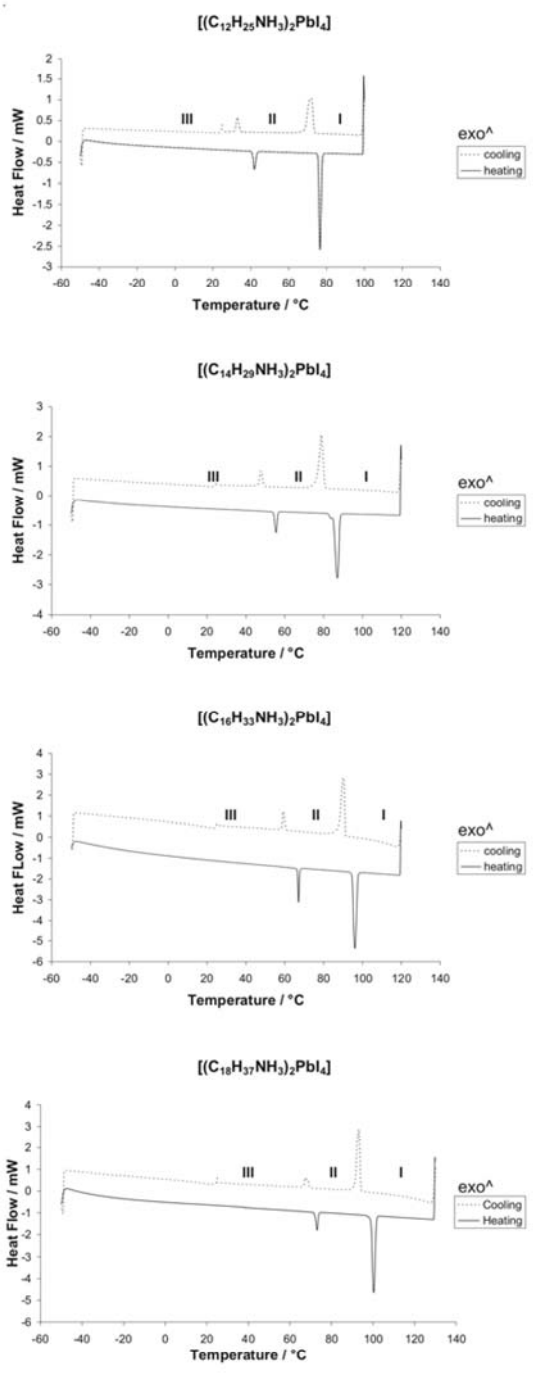


Fig. 4 Differential Scanning Calorimetric scans of the four layered perovskite-type hybrids. The vertical lines at either end of the scans are due to the change in the direction of the scan.

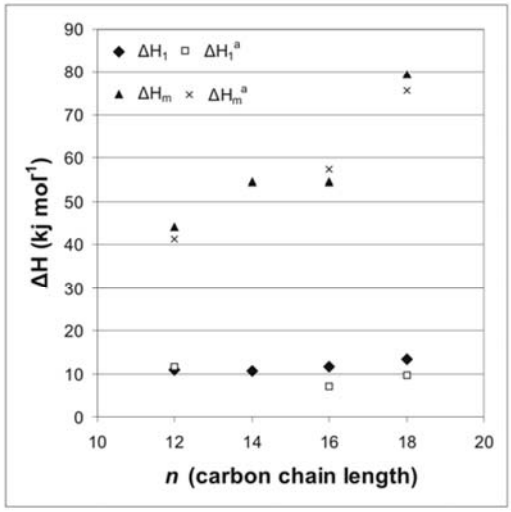


Fig. 5 Comparison of enthalpies determined in this report, shown as filled black triangles and diamonds, and those reported by Barman for $C_{12}PbI$, $C_{16}PbI$ and $C_{18}PbI$, shown as crosses and open squares. Barman did not report any values for $C_{14}PbI$.

The single crystal transformation of $[(C_{16}H_{33}NH_3)_2PbI_4]$ in detail

The compound $[(C_{16}H_{33}NH_3)_2PbI_4]$, abbreviated $C_{16}PbI$, was chosen to be discussed in detail as the features of its premelting phase transition, separated into the inorganic and organic halves, can be applied to $C_{12}PbI$ and $C_{18}PbI$ and to the inorganic component of $C_{14}PbI$ only. A further case in favour of $C_{16}PbI$ is that the phase transitions where observed using only one crystal, whereas two crystals each were used for $C_{12}PbI$ and $C_{18}PbI$. A dataset was collected of phase **III** at 20°C and a second one of phase **II** at 68°C. Fig. 3 clearly shows the colour change from yellow to orange that is associated with the premelting transition.

The most significant differences between the two phases for all compounds are the crystal system, unit cell dimensions and space group. Phase **III** has an orthorhombic unit cell (*Pbca*), designated the orthorhombic phase, that contains two half occupied inorganic layers at z = 0 and 1, and a fully occupied layer at z = 0.5., i.e. 2 complete inorganic layers per unit cell. Phase **II** has a monoclinic unit cell ($P2_1/c$), designated the monoclinic phase, that contains one complete inorganic layer per unit cell, a half each at x = 0 and 1. The unit cell has halved as a consequence. This behaviour is novel and not seen in the other long chain hybrid perovskites, such as $C_{10}CdCl$,[2] where the unit cell for the room temperature phase **III** is monoclinic and the spacegroup $P2_1/c$ (a = 7.354(1), b = 7.545(1), c = 51.520(3) Å, β = 91.74(1)°), which then transforms to an orthorhombic unit cell for phase **I**, space group *Amaa*, with no halving of the unit cell axis (a = 7.460(2), b = 7.546(2), c = 54.64(2) Å).

Doudin and Chapuis[12] introduced a geometric quantity for their discussion of the phase changes of $[(C_3H_7NH_3)_2CuCl_4]$. This was the tilt angle φ of the organic

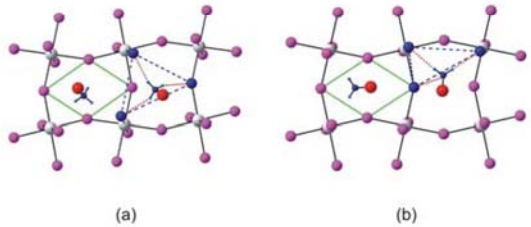
CREATED USING THE RSC ARTICLE TEMPLATE (VER. 2.0) - SEE WWW.RSC.ORG/ELECTRONICFILES FOR DETAILS

chains, "which defines the rotation angle of the N-C(3) axis". In this paper, we extend the definition of the tilt angle φ, abbreviated $\angle_\varphi$ to be the angle between a plane through the inorganic layers and a vector connecting the first and last atom of each chain, for example the nitrogen atom N(1) and the carbon atom C(12) in the case of $C_{12}PbI$. Two further quantities are required to track the motion of the alkylammonium chains before and after the phase transition. The tilt of the plane angle $\angle_\alpha$ of the chains, which defines the dihedral angle between a plane containing all the atoms of the alkylammonium chains and the lead atoms of the inorganic layers. The tilt angle $\angle_\beta$ of the ammonium group, which defines the angle between a vector connecting the atoms N(1) and C(1) and a plane through the lead atoms of the inorganic layers.

The position of the ammonium group by itself is affected by the phase changes and a procedure for describing its position is important as well as the effect on the hydrogen bridging configuration. The "box" within which the ammonium groups are positioned is defined by the four equatorial, or bridging iodides, and the four axial, or terminal iodides that protrude above the layer. In projection, the ammonium group is contained within a parallelogram defined by the four bridging iodides (See Fig. 2). By projection onto this parallelogram, the ammonium group is found in proximity to either an acute or an obtuse angle of the parallelogram.

In theory, the ammonium group can hydrogen bond to any of these eight iodides mentioned above but it is found that the three hydrogens either bond to two terminal iodides and one bridging iodide (terminal halogen configuration) or to two bridging iodides and one terminal iodide (bridging halogen configuration). This classification is mentioned in the review by Mitzi.[13] All the compounds, except $C_{14}PbI$, described here in their various phases adopt the terminal halogen configuration. However, there are two ways that the hydrogens can adopt the terminal or bridging halogen configuration: The three iodides to which the hydrogens bond can be at the vertices of either an equilateral triangle or a right-angled triangle (See Fig. 6). There is a correlation between the position of the ammonium group and the type of terminal halogen configuration: If the ammonium group is in the acute angled position, the ammonium group has the right-angled configuration of hydrogen bonds and the reverse case, if the ammonium group is in the obtuse angled position, the ammonium group has the equilateral configuration. The phase changes in $C_{12}PbI$, $C_{14}PbI$, $C_{16}PbI$ and $C_{18}PbI$ are as a result of the movement between these two geometries of their respective alkyl chains.

The corner-sharing PbI_6 octahedra that make up the 2-D layers are affected by these phase changes. For the layered perovskite-type hybrids, two out of a three possible tilts[14] are encountered: a tilt perpendicular to the inorganic sheets (θ tilt), so that adjacent corner-shared octahedra are rotated relative to each other. The angle of the θ tilt is mirrored in the bridging angle Pb-I-Pb, which deviates from 180°. The second kind of tilt is parallel to the layers (Ψ tilt), so that the layers are corrugated in one direction. The corrugation angle is measured by the angle between the normal to the inorganic layers and the vector connecting the Pb atom and the terminal I.



(a) (b)

Fig. 6 The parallelogram defined by the four bridging iodides is shown in green and the right-angled and equilateral triangles are shown as dashed blue lines. (a) The obtuse angled position and the right-angled configuration. (b) The acute angled position and the equilateral configuration.

The orthorhombic phase III of $C_{16}PbI$ (3a)

Crystal Packing

The crystal structure of the orthorhombic phase **III** of $C_{16}PbI$, **3a**, was collected at 20°C and crystallizes in the *Pbca* spacegroup. The atomic numbering scheme and anisotropic displacement parameters are shown in Fig 1. Fig. 7a clearly underlines a bidimensional arrangement in which two layers of interdigitated hexadecylammonium molecules are embedded between two consecutive inorganic $[PbI_6]$ sheets, forming an alternated inorganic-organic layered structure. The unit cell contains three inorganic layers. The lead atoms are offset from layer to layer, resulting in a staggered arrangement of adjacent layers. The packing diagram of $C_{16}PbI$ in phase **III** is closely related to the K_2NiF_4 structure type, which too has corner-sharing layers of NiF_6 octahedra, that are staggered.[14] In the direction perpendicular to the layers, the crystal cohesion is achieved by N-H...I hydrogen bonds, related to the NH_3 polar groups. There are van der Waals forces between two adjacent molecules (nearest neighbour distances is 4.162(1) Å).

The inorganic layer

The inorganic layer is built up from characteristic corner-sharing PbI_6 octahedra. The asymmetric unit consists of a lead atom on a special position and two iodide atoms, I(1) occupying the terminal position and I(2) occupying the bridging position in the layers. As shown in the projection perpendicular to the layers, along the *c*-axis, the PbI_6 octahedra are rotated by 149.53(3)° relative to each other (Fig. 8c). This rotation translates into a θ tilt = 30.47(3)°. Furthermore, the perovskite layers are corrugated in the *a*-direction by an angle of Ψ = 11.07(2)° with respect to the *ab*-plane. The coordination geometry around the Pb atom shows no axial compression of the octahedral geometry, with the bridging Pb(1)-I(2) distances shorter than the axial distances Pb(1)-I(1). The angle between *cis* related iodine atoms deviate from 90°, with all *trans* angles 180°

CREATED USING THE RSC ARTICLE TEMPLATE (VER. 2.0) - SEE WWW.RSC.ORG/ELECTRONICFILES FOR DETAILS

[JOURNAL NAME HERE] | www.rsc.org/[JOURNAL] Article

The organic part and the intermolecular arrangement

The hexadecylammonium molecule sits on a general position. The atomic numbering scheme is shown in Fig 1. The tilt of the chain relative to the inorganic layers is approximately $\angle_{\varphi}$ = 3.9(1)° (Fig. 8a). The chains are ordered within the inorganic layer and interdigitated up to the thirteenth carbon atom of the chain next to it. The plane of the chain is angled at $\angle_{\alpha}$ = 89.028° to the inorganic layer. The chain has a torsion angle of -103.6(2)° between C(1)-C(2)-C(3)-C(4), with the remainder of the bonds within the chain in an all-*trans* configuration (Fig. 9a).

The connection organic-inorganic

The hydrogen bonds between the organic and inorganic entities adopt the terminal configuration together with the equilateral configuration (See Table 3 and Fig. 9c)). The hydrogen acceptor distances to the terminal halides I(1) are 2.78 Å and 2.84 Å and to the bridging halide I(2(2.84 Å.

The monoclinic phase II of $C_{16}PbI$ (3b)

Crystal Packing

The crystal structure of the monoclinic phase **II** of $C_{16}PbI$, **3b**, was collected at 68°C and crystallizes in the $P2_1/c$ spacegroup. The atomic numbering scheme and anisotropic displacement parameters are shown in Fig. 1. Figure 7b clearly underlines a bidimensional arrangement in which two layers of interdigitated hexadecylammonium molecules are embedded between two consecutive inorganic [PbI_6] sheets, forming an alternated organic-inorganic layered structure. The unit cell contains one complete inorganic layer. The lead atoms are aligned from layer to layer, resulting in an eclipsed arrangement of adjacent layers, typical of monoclinic unit cells. The packing diagram of $C_{16}PbI$ in phase **II** is closely related to the $RbAlF_4$ structure type, which too has corner-sharing layers of AlF_6 octahedra, that are eclipsed.[15] In the direction perpendicular to the layers, the crystal cohesion is achieved on both ends of the organic molecules by N-H...I hydrogen bonds, related to the NH_3 polar groups. There are van der Waals forces between two adjacent molecules (nearest neighbour distances is 4.118(5) Å).

The inorganic motif

The inorganic layer is built up from characteristic corner-sharing PbI_6 octahedra. The asymmetric unit consists of a lead atom on a special position and two iodide atoms, I(1) occupying the terminal position and I(2) occupying the bridging position in the octahedra. The tilts of the PbI_6 octahedra are θ = 21.62(3)° around the *a*-axis and Ψ = 7.46(2)° along the *b*-axis. The coordination geometry around the Pb atom shows axial compression of the octahedral geometry, with the bridging Pb(1)-I(2) distances longer than the terminal distances Pb(1)-I(1). The angle between *cis* related iodine atoms deviate from 90°, with all *trans* angles 180°.

The organic part and the intermolecular arrangement

The hexadecylammonium molecule sits on a general position. The atomic numbering scheme is shown in Fig 1. The tilt of the chain relative to the inorganic layers is approximately $\angle_{\varphi}$ = 9.9(1)° (Fig. 8b). The chains are ordered within the inorganic layer and interdigitated up to the thirteenth carbon atom of the chain next to it. The plane of the chain is angled at $\angle_{\alpha}$ = 85.0(1)° to the inorganic layer. The carbon atoms in the chain are in an all-*trans* conformation (Fig. 9b).

The connection organic-inorganic

The hydrogen bonds between the organic and inorganic entities adopt the terminal configuration and the right-angled configuration (See Table 3 and Fig. 9d). The hydrogen acceptor distances to the terminal halides I(1) are 2.72 Å and 2.89 Å and to the bridging halide I(2) 3.03 Å.

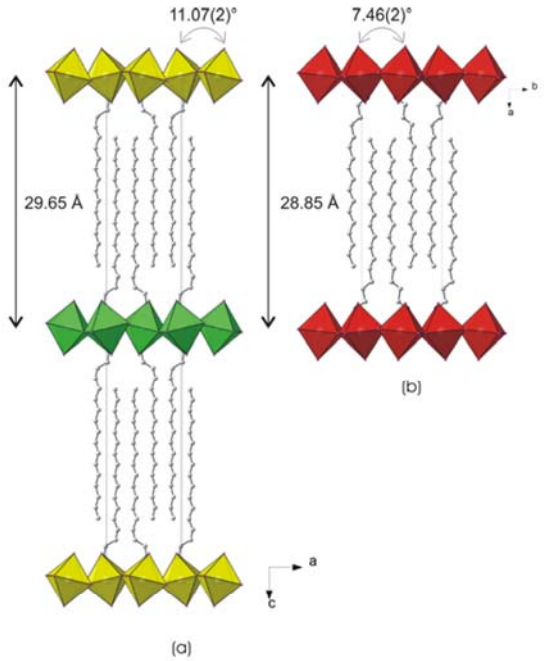


Fig. 7 The most striking feature of the phase transition is the change in crystal system from orthorhombic to monoclinic and the halving of the longest cell axis. (a) The orthorhombic phase **III** has successive inorganic layers staggered, shown in yellow and green. (b) The monoclinic phase **II** has eclipsed inorganic layers, shown in red.

The detail of the phase transition

The geometries before and after the transitions were determined. There are two main conformational changes that occur at 55.5°C. The alkyl chain looses its +anti-clinal torsion angle around the C(2)-C(3) bond so that phase **II** has a zig-zag arrangement of all the carbon atoms and the chain tilts so that it is no longer directly above the lead atoms. The second conformational change is a vertical shift of every middle

CREATED USING THE RSC ARTICLE TEMPLATE (VER. 2.0) - SEE WWW.RSC.ORG/ELECTRONICFILES FOR DETAILS

inorganic layer in phase **III** by half a unit cell in the direction of the corrugation resulting in all the lead atoms being exactly above each other in phase **II**. Two adjacent layers now eclipse each other and subsequently the unit cell axis perpendicular to the layers halves. These two changes go hand in hand and are accompanied by other small geometric changes.

The inorganic layer and octahedra

Phase **II** has the lead atoms offset from each other when viewed down the long *c*-axis and corrugated in opposite directions, i.e. every other layer is corrugated in the same direction. Every second layer has lead atoms with the same fractional x and y coordinates. To get the lead atoms aligned down each layer, one has to rotate the unit cell around the *a*-axis. Fig 8 shows the inorganic layers when viewed directly down the *c*-axis and when rotated until the layers eclipse approximately. The octahedra are now tilted the same in the *ab*-plane but are not corrugated in the same direction as they are in phase **II**. After the phase transition, the degree of corrugation decreases for all the layers from Ψ = 11.07(2)° to 7.46(2)°.

In both phases **III** and **II**, the octahedra have three unique bond distances. Iodides that are *trans* related have the same bond distances and are exactly 180° opposed to each other by virtue of the inversion centre of the lead atom. In the orthorhombic phase **III**, the average bond length is 3.1837(6)°. The bond to the terminal halide I1 is the same above and below the octahedra whereas the two bond lengths to the bridging halide I(2) are shorter by 0.0154 Å and 0.0238 Å. The maximum deviation from 90° for a *cis* angle is 3.453(6)°. The degree of puckering of the octahedra is measured by the Pb(1)-I(2)-Pb(1) bridging angle and is 149.53(3)°.

An increase in temperature leads to a more symmetrical geometry of the PbI_6 octahedra. The average bond length decreases slightly in the monoclinic phase **II** to 3.1826(6) Å but more significant is the decrease in the range of bond lengths to only 0.0058 Å. In the monoclinic phase, the longest bond length is no longer to the terminal halide but to the bridging halide (3.1862(9) Å) with the remaining two almost the same. The bond angles show the same pattern as the *cis* angles now deviate at most by 2.48° from 90° and the bridging angle has increased to 158.38(3)°.

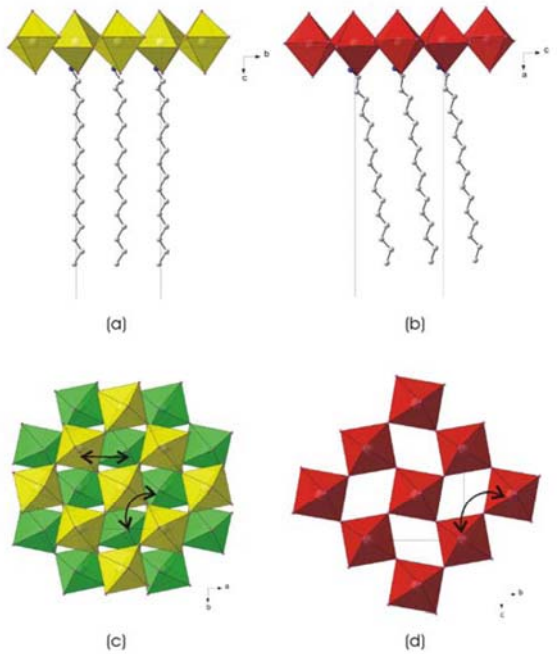


Fig. 8 The sixteen membered alkylchain has a tilt angle of 3.9(1)° in the orthorhombic phase **III** (a), which increases to 9.9(1) in the monoclinic phase **II** (b). (c) A topview of phase **III**, illustrating the staggered layers in this phase and the direction of the offset. (d) The same topview of phase **II**, where every inorganic layer is eclipsed. The θ tilt is shown by the curved double-headed arrows.

The alkyl chain and hydrogen bonding geometry

When the layers slide relative to each other, the alkyl chain is forced to change its orientation relative to the layers as the hydrogen bonds drag the chains with them. Since the ammonium headgroup is anchored to the iodide atoms and the chains are interdigitated, the chains can only accommodate the layer movement by: (i) rotating along the C(2)-C(3) bond (like a joint) and, (ii) tilting relative to the normal of the layers.

The rotation along the C(2)-C(3) bond is 59° which now gives the chain a zig-zag arrangement after the phase transition with all torsion angles ranging from 162(2)° to 179(2)°. As mentioned above, the layers shift in the direction of their corrugation and as a direct result, the chains increase their tilt angle from $\angle_{\varphi}$ = 3.9(1)° to 9.9(1)°. A consequence of the new arrangement of the chains between the layers is a reduction of the interlayer spacing by 0.8030 Å in going from the orthorhombic to the monoclinic phase.

In the orthorhombic phase **III**, the hexadecylammonium molecule lies along the short diagonal of the parallelogram. The ammonium group occupies the obtuse position and adopts the equilateral configuration. When the compound is heated and undergoes the phase transition, the hexadecylammonium molecule moves within the parallelogram away from the obtuse position to the acute position. The hydrogen bonding scheme is now right-angled. The rotation in the torsion angle and the change in position of the ammonium group relative to the inorganic layer is reflected in the increase of the tilt angle

 This journal © Royal Society of Chemistry

CREATED USING THE RSC ARTICLE TEMPLATE (VER. 2.0) - SEE WWW.RSC.ORG/ELECTRONICFILES FOR DETAILS

$\angle_\beta$ of the ammonium head group. This angle almost doubles from 28.8(7)° to 57.7(8)°.

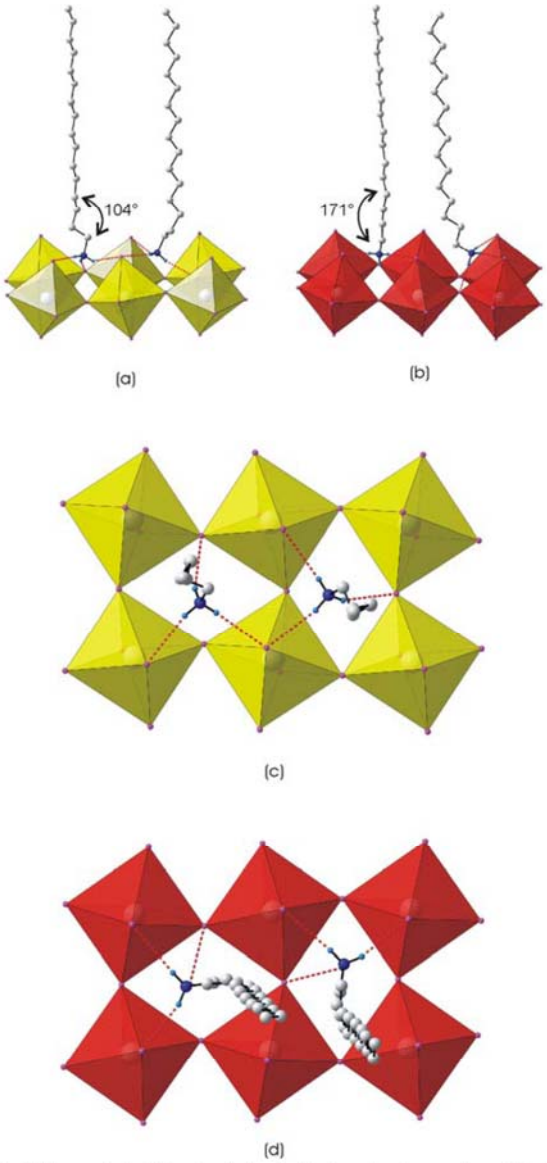


Fig. 9 The most significant variation in the hexadecylammonium chain is the change in the torsion angle around the C(2)-C(3) bond, (a) phase **III** and (b) phase **II**. As a consequence of the torsion angle change, the ammonium group changes its position relative to the inorganic layers from obtuse (c) to acute (d).

The transformations of C_{12}PbI and C_{18}PbI

The detailed analysis of the hybrid structure of C_{16}PbI before and after the phase transition can be applied to the structures of C_{12}PbI and C_{18}PbI before and after their respective first phase transition, at 41.7°C and 73.1°C respectively. Table 4 summarizes the main geometrical features that were discussed in the previous section as they apply to C_{16}PbI. The same trends are observed in C_{12}PbI and C_{18}PbI.

The special case of C_{14}PbI

The phase transition from the orthorhombic phase **III** of C_{14}PbI, **2a**, to the monoclinic phase **II**, **2b**, is via single-crystal-to-single crystal as in C_{16}PbI. The previous papers did not investigate this compound. The inorganic layer shifts as in the other three structures and the changes in the geometric parameters follow the same trends, shown in Table 4. However, when the phase transtion occurs, the torsion angle changes only from -94(3)° between C(1)-C(2)-C(3)-C(4) to 154(4)°. The ammonium group completes its movement from the obtuse position to the acute position as observed in the other three hybrids but the conformational change around the C(2)-C(3) bond is incomplete. This affects the hydrogen bonding scheme. Due to the net change in the torsion angle between the two phases being the smallest, 60°, the ammonium group does not adopt the terminal halogen cofiguration but the seldomly seen bridging halogen configuration. In the latter configuration, two hydrogens bond to iodides that are in the plane of the inorganic layer, the bridging iodides (Fig. 10b). The reason it is rare is that this orientation would cause the hydrogens on the second carbon atom in the chain to sterically interact with the terminal iodides. This steric interaction might be circumvented by the non-planar torsion angle and the position of the chain along the long diagonal of the parallelogram.

CREATED USING THE RSC ARTICLE TEMPLATE (VER. 2.0) - SEE WWW.RSC.ORG/ELECTRONICFILES FOR DETAILS

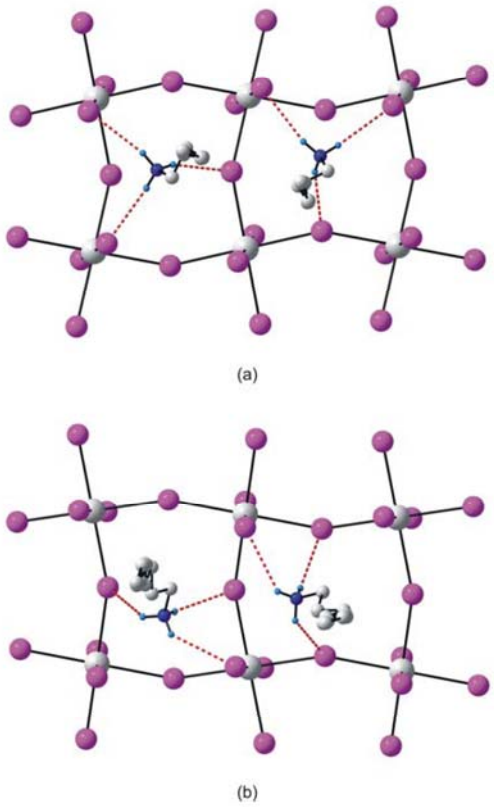


Fig. 10 (a) The orthorhombic phase **III** of $C_{14}PbI$, which is the same as the orthorhombic phases of all three other hybrids. (b) The monoclinic phase **II** of $C_{14}PbI$ is different from the other hybrids, as the ammonium group hydrogen bonds to two bridging iodides and one terminal iodide. This configuration is known as the bridging halogen configuration. The reason for this is the incomplete rotation around the C(2)-C(3) bond.

Conclusions

The compounds $[(C_nH_{2n+1}NH_3)_2PbI_4]$ (n = 12, 14, 16, 18), which belong to the family of inorganic-organic layered hybrids, have two phase transitions above room temperature. The first or premelting transition from phase **III** to phase **II** has a much lower enthalpy than the second, melting transition, and has been the subject of this report. Accurate single-crystal structures of the phases of the hybrids before and after the first transition shows that three major changes occur: (1) the packing of the inorganic layers changes from staggered to eclipsed, (2) the position of the ammonium group changes relative to the layers and, (c) the conformation of the hydrocarbon chains changes around the C(2)-C(3) bond. All these processes are concerted and consistent among the four hybrids. These findings are in disagrement with previous three major studies done on three of these compounds, n = 12, 16 and 18, by other techniques except Single-crystal XRD. Firstly, the packing of the chains was concluded to be non-interdigitated, and tilted by 55° relative to the inorganic layers. [10,11] The authors found no evidence of interdigitation in their study and classify interdigitated and non-interdigitated alkylammonium hybrids as separate polymorphic groups.[10] The mechanism they propose of the phase changes is as follows:[9] the chains are in an all-trans, static conformation at room temperature and after the premelting transition, there is an increase in gauche conformers in the chains. The NH_3^+ group becomes rotationally disordered within the cavity of the four terminal iodides. The interlayer spacing decreases slightly at the premlting transition. At the melting transition, there is an abrupt increase in the interlayer spacing attributed to a loss of the uniformity of the tilt angle across all the individual chains. There is also a marked increase in conformational disorder in the chains. The packing of the chains before and after the melting transition is shown schematically in Fig. 2. A question which remains unsolved is the correct structure model as it influences the phase behaviour.

Experimental

Materials

All reagents and solvents employed were commercially avalable and used as received without further purification. Differential Scanning Calorimetry (DSC) data were collected on a Mettler Toledo 822^e at a scan rate of 5 °C/min in sealed aluminium pans under air.

Synthesis

Preparation of $[(C_{12}H_{25}NH_3)_2PbI_4]$, 1. 0.048 g PbI_2 (0.104 mmol) was dissolved in 3 mL 47% HI in a sample vial. Thereafter, 0.030 g $C_{12}H_{25}NH_2$ (0.162 mmol) was added and the precipitate dissolved with a methanol (5mL) and ethylacetate (3mL) mixture. The crystals where grown by slow evaporation over a number of days. A yellow single crystal suitable for X-ray diffraction analysis was selected and studied. Elemental analysis (%). Found: C 24.97, H 4.81, N 2.66. Calc. for $C_{24}H_{56}I_4N_2Pb$: C 26.51, H 5.19, N 2.58.

Preparation of $[(C_{12}H_{25}NH_3)_2PbI_4]$, 2. 0.015 g PbI_2 (0.104 mmol) was dissolved in 1 mL 47% HI in a sample vial. Thereafter, 0.010 g $C_{14}H_{29}NH_2$ (0.047 mmol) was added and the precipitate dissolved with 5 mL ethylacetate. The crystals where grown by slow evaporation over a number of days. A yellow single crystal suitable for X-ray diffraction analysis was selected and studied. Elemental analysis (%). Found: C 30.16, H 5.74, N 2.46. Calc. for $C_{28}H_{64}I_4N_2Pb$: C 29.41, H 5.64, N 2.45.

Preparation of $[(C_{14}H_{29}NH_3)_2PbI_4]$, 3. 0.062 g PbI_2 (0.134 mmol) was dissolved in 1 mL 47% HI in a sample vial. Thereafter, 0.009 g $C_{16}H_{33}NH_2$ (0.037 mmol) was added and the precipitate dissolved with 8 mL ethylacetate. The crystals where grown by slow evaporation over a number of days. A yellow single crystal suitable for X-ray diffraction analysis was selected and studied. Elemental analysis (%). Found: C 32.38, H 5.91, N 2.40. Calc. for $C_{32}H_{72}I_4N_2Pb$: C 32.04, H 6.05, N 2.34.

This journal © Royal Society of Chemistry

CREATED USING THE RSC ARTICLE TEMPLATE (VER. 2.0) - SEE WWW.RSC.ORG/ELECTRONICFILES FOR DETAILS

Preparation of $[(C_{18}H_{37}NH_3)_2PbI_4]$, 4. 0.033 g PbI_2 (0.072 mmol) was dissolved in 1 mL 47% HI in a sample vial. Thereafter, 0.008 g $C_{18}H_{37}NH_2$ (0.030 mmol) was added and the precipitate dissolved with 15 mL ethylacetate. The crystals where grown by slow evaporation over a number of days. A yellow single crystal suitable for X-ray diffraction analysis were selected and studied. Elemental analysis (%). Found: C 34.71, H 6.11, N 2.24. Calc. for $C_{36}H_{80}I_4N_2Pb$: C 34.43, H 6.42, N 2.23.

X-Ray Crystallography

All diffraction data were collected on a Bruker Apex II CCD diffractometer[16] with graphite-monochromated Mo-Kα radiation (λ = 0.71073) at room temperature and at high temperature using a Oxford Cryostream 700. Data reduction and cell refinement where done using SAINT-NT[17] and space groups of these compounds were determined from systematic abscences by *XPREP*[17] and further justified by the refinement results. Face indexed absorption corrections where performed on all crystals using *XPREP*.[17] In all cases, the structures were solved in the *WinGx*[18] Suite by direct methods using *SHELXS97*[19] and refined using full-matrix least squares/difference Fourier techniques using *SHELXL97*.[19] All non-hydrogen atoms were refined with anisotropic displacement parameters. After that, all hydrogen atoms were placed at idealized positions and refined as riding atoms with the relative isotropic parameters of the heavy atoms to which the are attached. Diagrams and publication material were generated using *ORTEP*,[20] *PLATON*[21] and *DIAMOND*.[22] Experimental details of the X-Ray analyses are provided in Table 2.

References

1 A. Name, B. Name and C. Name, *Journal Title*, 2000, **35**, 3523; A. Name, B. Name and C. Name, *Journal Title*, 2000, **35**, 3523.

1 S. Kammoun, M. Kamoun, A. Daoud and F. Romain, *phys. stat. sol.* (a), 1996, **156**, 317.

2 R. Kind, S. Pleško, H. Arend, R. Blinc, B. Žekš, J. Seliger, B. Ložar, J. Slak, A. Levstik, C. Filipič, V. Žagar, G. Lahajnar, F. Milla and G. Chapuis, *J. Chem. Phys*., 1979, **71**, 2118.

3 M. R. Ciajolo, P. Corradini and V. Pavone, *Gazz. Chim. Ital.*, 1976, **106**, 807.

4 M. Koželj, V. Rutar, I. Zupančič, R. Blinc, H. Arend, R. Kind and G. Chapuis, *J. Chem. Phys*., 1981, **74**, 4123.

5 S. S. Nagapetyan, Yu. I. Dolzhenko, E. R. Arakelova, V. M. Koshkin, Yu. T. Struchkov and V. E. Shklover, *Russian Journal of Inorganic Chemistry*, 1988, **33**, 2806.

6 (a) K. W. Lee, C. H. Lee and C. E. Lee, *Phys. Rev. B*, 2003, **67**, 134424-1; (b) K. W. Lee and C. E. Lee, *Solid State Comm*., 2003, **126**, 343; (c) C. Carfagna, M. Vacatello and P. Corradini, *Gazz. Chim. Ital*., 1977, **107**, 131; (d) E. Landi, V. Salerno and M. Vacatello, *Gazz. Chim. Ital*., 1977, **107**, 27; (e) V. Busico, V. Salerno and M. Vacatello, *Gazz. Chim. Ital*., 1979, **109**, 581; (e) M. Vacatello and P. Corradini, *Gazz. Chim. Ital*., 1974, **104**, 773; (f) M. Vacatello and P. Corradini, *Gazz. Chim. Ital*., 1973, **103**, 1027; (g) M. Vacatello, M. De Girolamo and V. Busico, *J. Chem. Soc., Faraday Trans*., 1981, **77**, 2367; (h) C. Almirante, G. Minoni and G. Zerbi, *J. Phys. Chem*., 1986, **90**, 852; (i) G. F. Needham, R. D. Willett and H. F. Franzen, *J. Phys. Chem*., 1984, **88**, 674; (j) M. A. Arriandiaga, M. J. Tello, J. Fernandez, H. Arend and J. Roos, *phys. stat. sol*. (a), 1978, **48**, 53.

7 T. Ishihara, J. Takahashi and T. Goto, Phys. Rev. B, 1990, 42, 11099.

8 D. G. Billing and A. Lemmerer, 2006, unpublished result.

9 S. Barman, N.V. Venkataraman, S. Vasudevan and R. Seshadri, *J. Phys. Chem.* B, 2003, **107**, 1875.

10 N. V. Venkataraman, S. Bhagyalakshmi, S. Vasudevan and R. Seshadri, *Phys. Chem. Chem. Phys*., 2002, 4, 4533.

11 N. V. Venkataraman, S. Barman, S. Vasudevan, R. Seshadri, *Chem. Phys. Letters*, 2002, **358**, 139.

12 B. Doudin and G. Chapuis, *Acta Crystallogr. B*, 1990, **46**, 175.

13 D. B. Mitzi, *Progr. Inorg. Chem*., 1999, **48**, 1.

14 (a) D. M. Hatch, H. T. Stokes, K. S. Aleksandrov and S. V. Miguel, *Phys. Rev. B*, 1989, **39**, 9282; (b) D. M. Hatch and H. T. Stokes, *Phys. Rev. B*, 1987, **35**, 8509.

15 Wulf Depmeier, *Acta Crystallogr. B*, 1977, **33**, 3713-3718

16 Bruker 2005, *APEX2*. Version 1.0-27. Bruker AXS Inc., Madison, Wisconsin, USA.

17 Bruker 2004, *SAINT-PLUS*. Version 7.12 (including *XPREP*). Bruker AXS Inc., Madison, Wisconsin, USA.

18 L. J. Farrugia, *J. Appl. Crystallogr*., 1997, **30**, 565.

19 G. M. Sheldrick, SHELX, release 97-2 (includes SHELXS and SHELXL), University of Göttingen, 1997.

20 L. J. Farrugia, WinGX. *J. Appl., Cryst*., 1999, **32**, 837.

21 A. L. Spek, *J. Appl. Crystallogr*. 2003, **36**, 7.

22 K. Brandenburg, Diamond. Version 2.1e., Crystal Impact GbR, Bonn, Germany.

Table 2 Crystal Data for the compounds **1a**, **1b**, **2a**, **2b**

	1a, III	**1b, II**	**2a, III**	**2b, II**
Formula	$[(C_{12}H_{25}NH_3)_2PbI_4]$	$(C_{12}H_{25}NH_3)_2PbI_4]$	$(C_{14}H_{29}NH_3)_2[PbI_4]$	$(C_{14}H_{29}NH_3)_2[PbI_4]$
Mr	1087.50	1087.50	1143.60	1143.60
Temperature/K	293	319	293	335
Crystal size/mm	0.40 x 0.18 x 0.022	0.44 x 0.37 x 0.020	0.44 x 0.30 x 0.01	0.44 x 0.30 x 0.01
Crystal system	Orthorhombic	Monoclinic	Orthorhombic	Monoclinic
Space group	*Pbca* (61)	$P2_1/c$ (14)	*Pbca* (61)	$P2_1/c$
a/Å	8.8645(2)	23.8647(16)	8.8474(1)	26.412(6)
b/Å	8.5149(1)	9.0031(6)	8.5167(1)	9.0143(19)
c/Å	49.0253(9)	8.6882(6)	54.1561(7)	8.6774(16)
a/°	90	90	90	90
b/°	90	92.487(2)	90	92.492(13)
c/°	90	90	90	90
V/Å^3	3700.45(12)	1854.4(2)	4080.70(8)	2064.0(7)
Z	4	2	4	2
Dc/g cm^{-3}	1.952	1.937	1.861	1.840
μ(Mo-Ka)/mm^{-1}	7.909	7.849	7.177	7.095
Theta range/°	0.85 to 28.00	1.66 to 27.00	0.75 to 28.00	1.54 to 25.00
No. unique data	4034	2963	3437	2614
No. data with I ≥ 2s(I)	3081	4505	4924	3631
R1	0.0570	0.0398	0.0577	0.0525
wR2 (all data)	0.1404	0.1150	0.1732	0.1534

730

Table 2 cont. Crystal Data for the compounds **3a**, **3b**, **4a** and **4b**.

	3a, III	**3b, II**	**4a, III**	**4b, II**
Formula	$(C_{16}H_{33}NH_3)_2[PbI_4]$	$(C_{16}H_{33}NH_3)_2[PbI_4]$	$(C_{18}H_{37}NH_3)_2[PbI_4]$	$(C_{18}H_{37}NH_3)_2[PbI_4]$
Mr	1199.71	1199.71	1255.81	1255.81
Temperature/K	293	341	293	348
Crystal size/mm	0.36 x 0.17 x 0.03	0.36 x 0.17 x 0.03	0.48 x 0.27 x 0.01	0.41 x 0.12 x 0.01
Crystal system	Orthorhombic	Monoclinic	Orthorhombic	Monoclinic
Space group	*Pbca* (61)	$P2_1/c$ (14)	*Pbca* (61)	$P2_1/c$ (14)
a/Å	8.8167(1)	28.846(8)	8.7825(1)	31.424(4)
b/Å	8.5222(1)	9.012(3)	8.5401(1)	9.0456(10)
c/Å	59.2906(9)	8.673(2)	64.4472(11)	8.6917(9)
a/°	90	90	90	90
b/°	90	91.816(6)	90	91.586(8)
c/°	90	90	90	90
V/Å^3	4454.96(10)	2253.4(11)	4833.76(11)	2469.7(5)
Z	4	2	4	2
Dc/g cm^{-3}	1.789	1.768	1.726	1.689
μ(Mo-Ka)/mm^{-1}	6.579	6.503	6.068	5.938
Theta range/°	2.06 to 28.00	0.71 to 25.00	1.26 to 28.00	1.30 to 25.00
No. unique data	3716	2872	3895	2590
No. data with I ≥ 2s(I)	5367	3965	5827	4345
*R*1	0.0546	0.0421	0.0590	0.0407
*wR*2 (all data)	0.1399	0.1358	0.1688	0.1070

735

This journal © Royal Society of Chemistry

CREATED USING THE RSC ARTICLE TEMPLATE (VER. 2.0) - SEE WWW.RSC.ORG/ELECTRONICFILES FOR DETAILS

[JOURNAL NAME HERE] | www.rsc.org/[JOURNAL] Article

Table 3 Hydrogen bonding details of all compounds

D-H…A	D-H (Å)	H…A (Å)	D…A (Å)	<(D-H…A) (°)	Symmetry transformations
1a, III					
N(1)-H(1B)...I(1)	0.89	2.77	3.651(14)	171.2	-x+1/2,y-1/2,z
N(1)-H(1C)...I(1)	0.89	2.83	3.592(15)	144.5	x+1,y,z
N(1)-H(1A)...I(2)	0.89	2.88	3.700(14)	154.2	-x+1/2,y+1/2,z
1b, II					
N(1)-H(1B)...I(1)	0.89	2.74	3.609(9)	165.9	-x,y-1/2,-z+1/2
N(1)-H(1C)...I(1)	0.89	2.86	3.724(10)	165.7	-x,-y+2,-z
N(1)-H(1A)...I(2)	0.89	3.06	3.776(10)	139.4	-x,y-1/2,-z+1/2
2a, III					
N(1)-H(1A)...I(1)	0.89	2.78	3.652(13)	168.2	-x+1/2,y-1/2,z
N(1)-H(1B)...I(1)	0.89	2.84	3.603(15)	145.2	-
N(1)-H(1C)...I(2)	0.89	2.85	3.689(14)	157.9	-x+1/2,y+1/2,z
2b, II					
N(1)-H(1B)...I(1)	0.89	2.96	3.650(16)	135.9	x,-y-1/2,z+1/2
N(1)-H(1C)...I(2)	0.89	3.00	3.588(18)	125.3	-
N(1)-H(1A)...I(2)	0.89	3.05	3.86(2)	152.6	-x,-x,-z+1
3a, III					
N(1)-H(1B)...I(1)	0.89	2.78	3.655(11)	168.0	-
N(1)-H(1C)...I(1)	0.89	2.84	3.595(12)	144.1	-x+1,-y,-z+1
N(1)-H(1A)...I(2)	0.89	2.84	3.670(12)	156.7	x,y-1,z
3b, II					
N(1)-H(1A)...I(1)	0.89	2.72	3.583(15)	163.6	-
N(1)-H(1B)...I(1)	0.89	2.89	3.776(15	172.2	x,-y+3/2,z+1/2
N(1)-H(1C)...I(2)	0.89	3.03	3.621(14)	125.4	-x+2,-y+2,-z+2
4a, III					
N(1)-H(1B)...I(1)	0.89	2.76	3.645(12)	174.9	-
N(1)-H(1A)...I(1)	0.89	2.88	3.608(13)	139.6	-x+3/2,y-1/2,z
N(1)-H(1C)...I(2)	0.89	2.89	3.671(13)	147.9	x,y-1,z
4b, II					
N(1)-H(1A)...I(1)	0.89	2.71	3.585(12)	168.4	x,y,z+1
N(1)-H(1C)...I(1)	0.89	2.93	3.797(13)	164.8	x,-y+1/2,z+1/2
N(1)-H(1B)...I(2)	0.89	3.13	3.828(14)	136.3	-x,y−1/2,-z−3/2

Table 4 Geometric parameters for all compounds in their phases.

Geometric Parameter	**1a, III**	**1b, II**	**2a, III**	**2b, II**	**3a, III**	**3b, II**	**4a, III**	**4b, II**
Interlayer Spacing / Å	24.51(9)	23.8647(16)	27.0781(7)	26.412(6)	29.64845	28.846(8)	32.2236	31.424(4)
Bridging Angle Pb(1)-I(2)-Pb(1) / °	150.18(3)	157.41(2)	149.93(3)	158.43(4)	149.53(3)	158.38(3)	149.39(3)	158.84(2)
θ tilt / °	29.82(3)	22.59(2)	30.07(3)	21.57(4)	30.47(3)	21.62(3)	30.61(3)	21.16(2)
Corrugation or Ψ tilt / °	11.20(2)	6.85(2)	11.16(2)	7.33(3)	11.07(2)	7.46(2)	10.98(2)	7.70(1)
Tilt of Chains $\angle_{\varphi}$ / °	5.4(1)	12.1(1)	4.4(1)	10.7(1)	3.9(1)	9.9(1)	3.4(1)	8.9(1)
Tilt of plane $\angle_{\alpha}$ / °	89.1(1)	84.9(2)	88.9(1)	86.2(2)	88.9(1)	85.0(1)	89.1(1)	85.4(1)
Tilt of NH_3 group $\angle_{\beta}$ / °	29.9(9)	69.6(5)	27.3(7)	57.9(1)	28.8(7)	57.7(8)	30.2(6)	58.9(1)
Position of ammonium group	Obtuse	Acute	Obtuse	Acute	Obtuse	Acute	Obtuse	Acute
Hydrogen Bonding Configuration	Equilateral	Right-angled	Equilateral	Right-angled	Equilateral	Right-angled	Equilateral	Right-angled
Torsion angle C(1)-C(2)-C(3)-C(4)/ °	-100(2)	177.5(2)	-94(3)	154(4)	-103.6(2)	171(2)	108(2)	174(2)

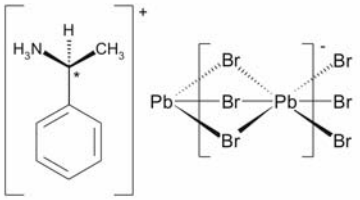
760

This journal © Royal Society of Chemistry

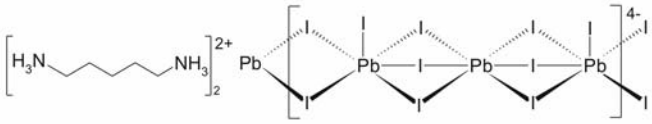
Chapter 6 Miscellaneous Structures and Motifs

6.1 Introduction

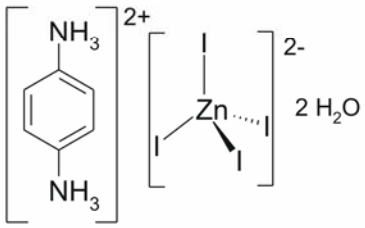
In this chapter I present the structures of 11 inorganic-organic hybrids that did not display any phase transitions. Chapter 4 consisted of the systematic studies of structural trends in the inorganic-organic hybrids. Those structures that did not fit together with the studies done in Chapter 4, except for those given in section 6.2 and 6.3 below, were published on their own in either Acta Crystallographica C or Acta Crystallographica E and these published articles are presented here.



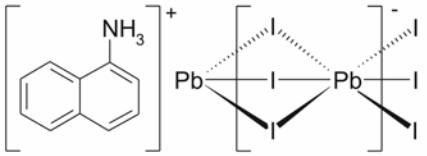
Section 6.2



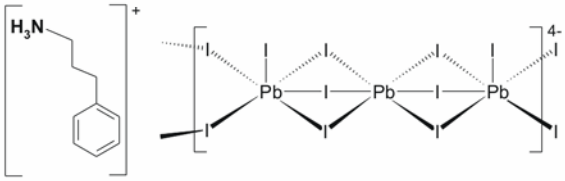
Section 6.3



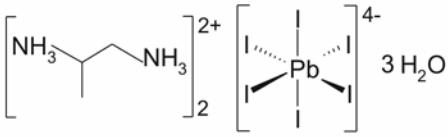
Section 6.4



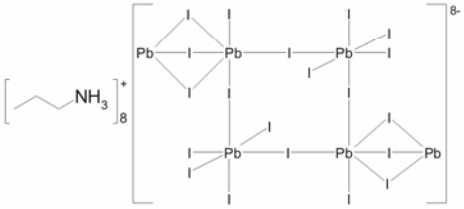
Section 6.5



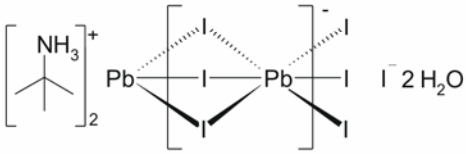
Section 6.6



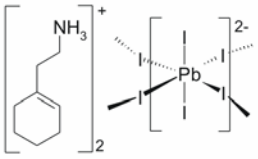
Section 6.7



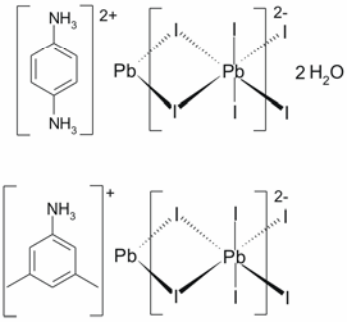
Section 6.8



Section 6.9



Section 6.10



Section 6.11

6.2 Bis[(S)-β-phenethylammonium] tribromoplumbate(II)

Journal: Acta Crystallographica Section E, Structure Reports Online

Date Submitted: 25 April 2003

Reference Code of Submitted Article: NA6231

Date Accepted: 19 May 2003

Final Reference: Billing, D.G., Lemmerer, A. (2003). *Acta Cryst*. E**59**, m381-m383.

Brief Synopsis

The inorganic-organic hybrid bis[(S)-β-phenethylammonium] tribromoplumbate(II) has 1-D chains of face-sharing $PbBr_6$ octahedra. This compound is part of the structural study reported in Section 4.2.

Acta Crystallographica Section E
Structure Reports Online
ISSN 1600-5368

Bis[(*S*)-β-phenethylammonium] tribromoplumbate(II)

David G. Billing* and Andreas Lemmerer

School of Chemistry, University of the Witwatersrand, Private Bag 3, PO Wits, 2050 South Africa

Correspondence e-mail: dave@aurum.wits.ac.za

Received 25 April 2003
Accepted 19 May 2003
Online 31 May 2003

Key indicators

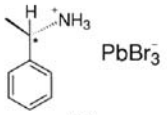
Single-crystal X-ray study
T = 293 K
Mean σ(C–C) = 0.010 Å
R factor = 0.033
wR factor = 0.065
Data-to-parameter ratio = 27.5

For details of how these key indicators were automatically derived from the article, see http://journals.iucr.org/e.

The title compound, $[(S)\text{-}C_6H_5C_2H_4NH_3][PbBr_3]$, crystallizes as an organic–inorganic hybrid. As such, the structure consists of extended chains of $[PbBr_3]^-$ units running along the a axis. Each Pb atom is octahedrally coordinated by six bromides, arranged as chains of face-sharing octahedra. These inorganic chains are separated by the isolated organic cations.

Comment

In recent years, a significant number of organic–inorganic hybrid materials, based on metal halide units, have been prepared and studied; for reviews, see Papavassiliou (1997) and Mitzi (2001). Haloplumbates, in particular, have demonstrated a propensity for forming a great variety of crystalline structures by self-assembling from suitable solution mixtures. It has been shown that their structures can vary considerably, ranging from systems based on isolated molecules to ones containing extended chains as in $[Me_4N][PbI_3]$ (Contreras *et al.*, 1983) and up to two- or three-dimensional networks (Mitzi, 1999). For systems containing extended chains, the extended chains may be formed by one, two or three bridging halides. Very few examples of the last kind, also described in terms of face-sharing octahedra, involving bromide are known, for example, $[Et_4N][PbBr_3]$ and $[Bu_4N][PbBr_3]$ (Vanek *et al.*, 1992). A search of the Cambridge Structural Database (Version 5.24, February 2003 release; Allen, 2002) for amine-containing compounds yielded only one similar case involving bromide, $[PhMe_3N]_4[Pb_3Br_{10}]$ (Wiest *et al.*, 1999), consisting of face-sharing trinuclear $[Pb_3Br_{10}]$ units connected by the sharing of a vertex.



(I)

Having previously reported the structure of organic–inorganic hybrid perovskite containing a racemic mixture of the cation 1-phenylethylammonium (Billing, 2002), we present here the room temperature structure of the title compound, $((S)\text{-}C_6H_5C_2H_4NH_3)[PbBr_3]$, (I). This is the first report of an inorganic–organic hybrid with only a single enantiomer of a chiral amine as the counterion.

Fig. 1 shows the asymmetric unit of the title compound, with its atomic numbering scheme. The bromide Br1 is axial and Br2 and Br3 are equatorial. The inorganic chains of distorted face-sharing octahedra orientated along the a axis, separated by isolated amides, are clearly visible in the packing diagrams

© 2003 International Union of Crystallography
Printed in Great Britain – all rights reserved

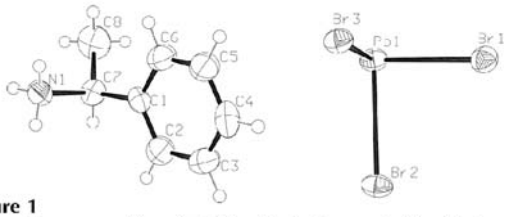


Figure 1
View of the asymmetric unit of (I), with displacement ellipsoids drawn at the 50% probability level.

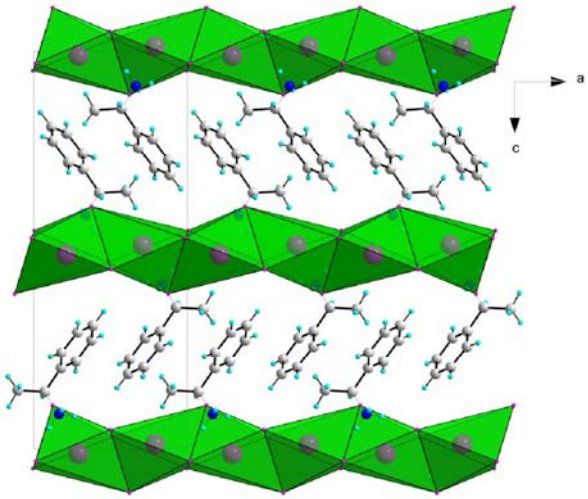


Figure 2
Packing diagram of (I), viewed along the *b* axis.

(Fig. 2 and Fig. 3). Within the chain, the shared face consists of two equatorial bromides and one axial bromide. The octahedra are severely distorted with all lead–bromide distances different, ranging from 2.8576 (11) Å to 3.3253 (17) Å (Table 1). The bond angles between *cis* ligands vary from 75.56 (4)° to 93.49 (5)° and *trans* angles from 154.83 (3)° to 167.54(2)°.

There is extensive hydrogen bonding, with the large ionic radius of bromine enabling contact with four different H atoms (Table 2). The hydrogen bonds are similar in length to the average lengths reported by Steiner (1998) for hydrogen bonds involving halide ions. The bifurcated Br2···H1*A*···Br3 distances are 2.76 Å and 2.88 Å, whereas the lengths in the simpler Br···H1*B* and Br···H1*C* are both 2.68 Å. Within the organic section, adjacent aromatic rings are separated by a centroid-to-centroid distance of 5.373 Å, which is probably too large to be considered as representing π-stacking interactions.

Experimental

Crystals of ((*S*)-$C_6H_5C_2H_4NH_3$)[$PbBr_3$] were grown at room temperature by first dissolving 0.204 g $PbBr_2$ (0.556 mmol) in 5 ml HBr and 5 ml of ethanol. 0.120 g (*S*)-$C_6H_5C_2H_4NH_2$(l) (0.990 mmol) was then added dropwise. The needle-shaped colourless crystals were harvested after seven days. Analysis calculated for $C_8H_{12}N_1PbBr_3$: C 16.89, H 2.13, N 2.46%; found: C 16.95, H 2.20, N 2.43%.

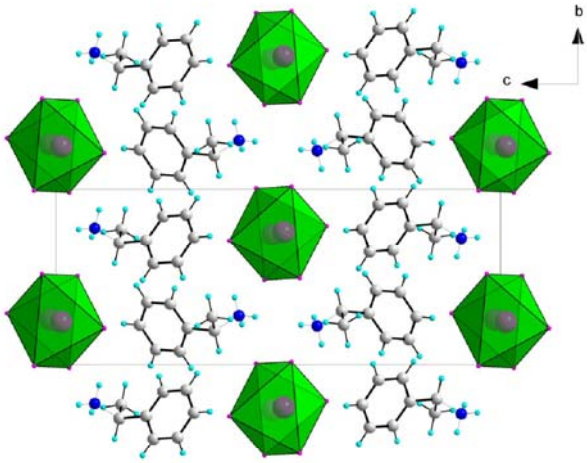


Figure 3
Packing diagram of (I), viewed along the *a* axis.

Crystal data

($C_8H_{12}N$)[$PbBr_3$]
M_r = 569.11
Orthorhombic, $P2_12_12_1$
a = 7.930 (5) Å
b = 8.147 (5) Å
c = 20.580 (5) Å
V = 1329.6 (12) Å^3
Z = 4
D_x = 2.843 Mg m^{-3}
Mo $K\alpha$ radiation
Cell parameters from 840 reflections
θ = 7.8–55.7°
μ = 21.67 mm^{-1}
T = 293 (2) K
Plate, colourless
0.22 × 0.16 × 0.03 mm

Data collection

Bruker CCD area-detector diffractometer
φ and ω scans
Absorption correction: by integration (*XPREP*; Bruker, 1999)
T_{min} = 0.056, T_{max} = 0.485
9328 measured reflections
3268 independent reflections
2587 reflections with $I > 2\sigma(I)$
R_{int} = 0.062
θ_{max} = 28.3°
$h = -10 \rightarrow 6$
$k = -10 \rightarrow 10$
$l = -27 \rightarrow 26$

Refinement

Refinement on F^2
$R[F^2 > 2\sigma(F^2)]$ = 0.033
$wR(F^2)$ = 0.065
S = 1.01
3268 reflections
119 parameters
H-atom parameters constrained
$w = 1/[\sigma^2(F_o^2) + (0.0222P)^2]$ where $P = (F_o^2 + 2F_c^2)/3$
$(\Delta/\sigma)_{max}$ = 0.001
$\Delta\rho_{max}$ = 1.21 e Å^{-3}
$\Delta\rho_{min}$ = −0.71 e Å^{-3}
Extinction correction: *SHELXL*97
Extinction coefficient: 0.0118 (3)
Absolute structure: Flack (1983)
Flack parameter = −0.032 (12)

Table 1
Selected geometric parameters (Å, °).

Pb1—Br1	2.8576 (11)	Pb1—Br2	3.0716 (16)
Pb1—Br3^{i}	2.8981 (14)	Pb1—Br3	3.2566 (16)
Pb1—Br2^{i}	2.9880 (15)	Pb1—Br1^{i}	3.3253 (17)
Br1—Pb1—Br3^{i}	88.80 (3)	Br3^{i}—Pb1—Br3	165.20 (2)
Br1—Pb1—Br2^{i}	84.84 (4)	Br2^{i}—Pb1—Br3	90.07 (5)
Br3^{i}—Pb1—Br2^{i}	93.49 (5)	Br2—Pb1—Br3	85.25 (5)
Br1—Pb1—Br2	82.86 (4)	Pb1^{ii}—Br2—Pb1	82.58 (5)
Br3^{i}—Pb1—Br2	88.28 (5)	Pb1^{ii}—Br3—Pb1	80.81 (5)
Br2^{i}—Pb1—Br2	167.54 (2)	Br1—Pb1—Br1^{i}	154.83 (3)
Br1—Pb1—Br3	77.21 (3)	Br3^{i}—Pb1—Br1^{i}	75.56 (4)

Symmetry codes: (i) $\frac{1}{2}+x, \frac{1}{2}-y, 2-z$; (ii) $x-\frac{1}{2}, \frac{1}{2}-y, 2-z$.

Table 2
Hydrogen-bonding geometry (Å, °).

D—H···A	D—H	H···A	D···A	D—H···A
N1—H1A···Br2^{i}	0.89	2.76	3.452 (7)	136
N1—H1A···Br3^{ii}	0.89	2.88	3.567 (7)	135
N1—H1B···Br1^{ii}	0.89	2.68	3.532 (7)	162
N1—H1C···Br3^{iii}	0.89	2.68	3.532 (7)	160

Symmetry codes: (i) $\frac{3}{2}-x,-y,z-\frac{1}{2}$; (ii) $\frac{3}{2}-x,1-y,z-\frac{1}{2}$; (iii) $1-x,y-\frac{1}{2},\frac{3}{2}-z$.

All H atoms were refined in idealized positions in the riding model approximation and with their isotropic displacement parameters fixed to 1.2 of the equivalent isotropic displacement parameter of the atom to which they are bonded. The highest residual peak is located 0.99 Å from Pb1.

Data collection: *SMART–NT* (Bruker, 1998); cell refinement: *SAINT-Plus* (Bruker, 1999); data reduction: *XPREP* (Bruker, 1999); program(s) used to solve structure: *SHELXS*97 (Sheldrick, 1997); program(s) used to refine structure: *SHELXL*97 (Sheldrick, 1997); molecular graphics: *ORTEP*-3 *for Windows* (Farrugia, 1997) and *DIAMOND* (Brandenburg, 1999); software used to prepare material for publication: *WinGX* (Farrugia, 1999) and *PLATON* (Spek, 2003).

The University of the Witwatersrand is thanked for the award of a research grant and for providing the infrastructure required to do this work.

References

Allen, F. H. (2002). *Acta Cryst.* B**58**, 380–388.
Billing, D. G. (2002), *Acta Cryst*, E**58**, m669–m671.
Brandenburg, K. (1999). *DIAMOND*. Version 2.1e. Crystal Impact GbR, Bonn, Germany.
Bruker (1998). *SMART–NT*. Version 5.050. Bruker AXS Inc., Madison, Wisconsin, USA.
Bruker (1999). *SAINT-Plus*. Version 6.02 (including XPREP). Bruker AXS Inc., Madison, Wisconsin, USA.
Contreras, J. G., Seguel, G V., Ungerer, B., Maier, W. F. & Hollander, F. J. (1983). *J. Mol. Struct.* **102**, 295–304.
Farrugia, L. J. (1997). *J. Appl. Cryst.* **30**, 565.
Farrugia, L. J. (1999). *J. Appl. Cryst.* **32**, 837–838.
Flack, H. D. (1983). *Acta Cryst.* A**39**, 876–881.
Mitzi, D. B. (1999). *Prog. Inorg. Chem.* **48**, 1–121.
Mitzi, D. B. (2001). *J. Chem. Soc. Dalton Trans.* pp. 1–12.
Papavassiliou, G. C. (1997). *Prog. Solid State Chem.* **25**, 125–270.
Sheldrick, G. M. (1997). *SHELXS*97 and *SHELXL*97. University of Göttingen, Germany.
Spek, A. L. (2003). *J. Appl. Cryst.* **36**, 7–13.
Steiner, T. (1998). *Acta Cryst.* B**54**, 456–463.
Vanek, P., Havráková, M. & Hybler, J. (1992). *Solid State Commun.* **82**, 509–512.
Wiest, Th., Blachnik, R. & Reuter, H. (1999). *Z. Naturforsch. Teil B*, **54**, 1099–1102.

6.3 Bis(pentane-1,5-diammonium) decaiodotriplumbate(II)

Journal: Acta Crystallographica Section C, Crystal Structure Communications

Date Submitted: 9 March 2004

Reference Code of Submitted Article: FG1746

Date Accepted: 30 March 2004

Final Reference: Billing, D.G., Lemmerer, A. (2004). *Acta Cryst*. C**60**, m224-m226.

Brief Synopsis

The inorganic-organic hybrid bis(pentane-1,5-diammonium) decaiodotriplumbate(II) has 1-D chains of edge- and face-sharing PbI_6 octahedra. This compound is part of the structural study reported in Section 4.7.

metal-organic compounds

Acta Crystallographica Section C
Crystal Structure Communications
ISSN 0108-2701

Bis(pentane-1,5-diammonium) decaiodotriplumbate(II)

David G. Billing* and Andreas Lemmerer

School of Chemistry, University of the Witwatersrand, Private Bag 3, PO Wits, 2050, South Africa
Correspondence e-mail: dave@aurum.wits.ac.za

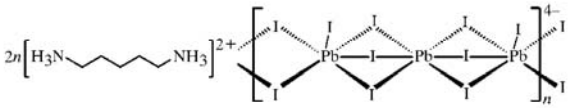
Received 9 March 2004
Accepted 30 March 2004
Online 30 April 2004

The title compound, $\{(NH_3C_5H_{10}NH_3)_2[Pb_3I_{10}]\}_n$, crystallizes as an organic–inorganic hybrid. As such, the structure consists of extended chains of $[Pb_3I_{10}]_n^{4n-}$ ions extending along [111]. The asymmetric unit contains two independent Pb atoms: one is in a general position and the other is on an inversion centre. Each Pb atom is octahedrally coordinated by six iodide ions and exhibits both face- and edge-sharing with adjacent atoms in the inorganic chain. The organic counter-ion, *viz*. pentane-1,5-diammonium, lies in channels formed by the chains and interacts with these chains *via* N—H···I hydrogen bonding.

Comment

In recent years, a significant number of organic–inorganic hybrid materials based on metal–halide units have been prepared and studied [for reviews, see Papavassiliou (1997) and Mitzi (1999)]. Haloplumbates, in particular, have demonstrated a propensity for forming a variety of crystalline structures by self-assembling from suitable solution mixtures. It has been shown that these structures can vary considerably, ranging from systems based on isolated molecules, to those containing infinite chains, as in $(Me_4N)[PbI_3]$ (Contreras *et al.*, 1983), right up to two- or three-dimensional networks (Mitzi, 1999). The lead iodide octahedra can be connected in one of three ways, *viz*. face-sharing between two equatorial halides and one axial halide, edge-sharing between two equatorial halides, and corner-sharing *via* a single halide. It is also possible to have combinations of the various types of sharing in one chain, as in $[Na(DMF)_3]_4[Pb_6I_{16}]$ (DMF is dimethylformamide) and $[PrN(C_2H_4)_3NPr][Pb_2I_6]$, in which the octahedra simultaneously share common faces, edges and vertices (Krautscheid *et al.*, 2001). The chains formed by the octahedra can be described by the shorthand notation $(f_me)_n$ for m adjacent face-sharing octahedra, f, connected by octahedra sharing an edge, denoted e. Structures with $m = 3$ have been synthesized for lead iodide (Krautscheid & Vielsack, 1997; Maxcy *et al.*, 2003) and tin iodide (Lode & Krautscheid, 2001) octahedra. The case with $m = 1$ contains PbI_6 octahedra that share a face with PbI_5 square pyramids, which in turn share an edge.

Pentadiamine has previously been incorporated into the layered perovskite structure type. For example, single-crystal structures of $(NH_3C_5H_{10}NH_3)CuX_4$ (X = Cl and Br; Garland *et al.*, 1990) have been determined. In general, the hybrid perovskite family displays structural phase transitions resulting from conformational changes within the amine groups between the layers, as well as the slipping of layers with respect to one another. The temperatures at which the phase changes occur are dependent on the length of the chain, as can be seen for $[NH_3(CH_2)_nNH_3]CdCl_4$ (n = 3, 4 and 5; Kind *et al.*, 1981).



(I)

We present here the crystal structure of the title compound, (I), an $m = 3$ case, which contains $[Pb_3I_{10}]_n^{4n-}$ chains extending approximately along [111], with the pentadiammonium ion as counter-cation (Fig. 1). The asymmetric unit contains two crystallographically independent Pb atoms, *viz*. atoms Pb1 and Pb2. Each face-sharing monomer unit consists of two Pb2 octahedra and one Pb1 octahedron, where the central Pb1 octahedron is connected to the Pb2 octahedra by shared faces. The Pb2 octahedra are linked *via* edge-sharing at both ends to adjacent monomers. The overall repeat pattern can be represented as $(f_2e)_3$ (Fig. 2).

Atom Pb1 is located on a centre of inversion, chosen for convenience as that at the centre of the unit cell, and is bonded to three unique halide atoms, *viz*. I1, I2 and I3, which then complete the full octahedron through the inversion centre. At the centre of a quadrilateral formed by atoms Pb2, I4, Pb2*A* and I4*A* [Pb2*A* and I4*A* are at the symmetry position $(-x, -y, -z)$; Fig. 1] is a second inversion centre, chosen for convenience as the cell origin. Atom Pb2 is bonded to four unique

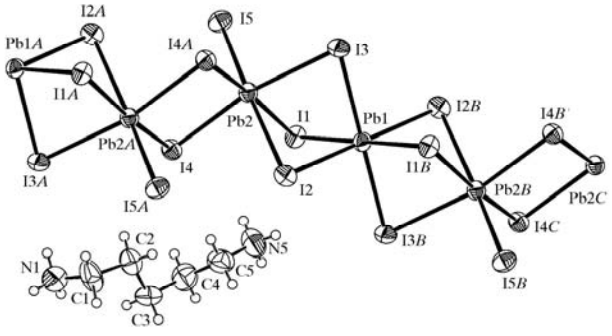


Figure 1
The asymmetric unit of (I) and some adjacent atoms, showing the atomic numbering scheme. Displacement ellipsoids are shown at the 50% probability level. Atoms labelled with the suffixes *A*, *B* and *C* are at the symmetry positions $(-x, -y, -z)$, $(1 - x, 1 - y, 1 - z)$ and $(1 + x, 1 + y, 1 + z)$, respectively.

 © 2004 International Union of Crystallography DOI: 10.1107/S0108270104007553

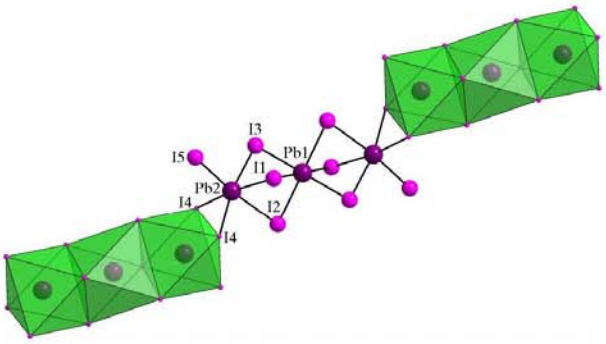


Figure 2
An illustration of the $(PB_3I_{10})_n^{4n-}$ chain.

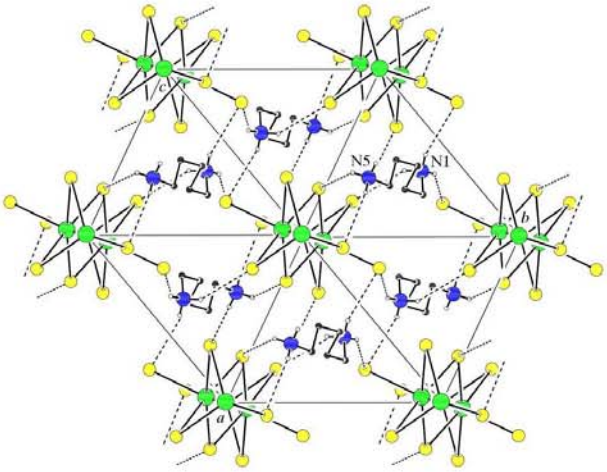


Figure 3
The crystal packing of (I), viewed along [111], showing the pseudo-hexagonal packing and the N—H···I hydrogen bonding (dashed lines).

halides, the extra halide, I4, being responsible for the edge-sharing between the Pb2 octahedra. This second inversion centre then generates the second I4 halide involved in edge-sharing. The metal–halide bond distances are very similar, possibly because of the lower strain imposed by the simpler sharing. Atoms I1, I2 and I3 participate in the face-sharing between the Pb1 and Pb2 octahedra. Axial atom I5 is the only halide not involved in any bonding to adjacent octahedra and has the shortest Pb—I distance [3.1221 (12) Å].

Atom Pb1 has a more regular coordination geometry, as it lies on an inversion centre, which ensures that all *trans* angles are exactly 180°; the Pb1 octahedron shares *trans* faces with the two adjacent Pb2 octahedra. Atom Pb2, in contrast, has a more distorted environment, with all *cis* and *trans* angles different (Table 1).

One unique inorganic chain runs through the unit cell along the body, diagonally from (0, 0, 0) to (1, 1, 1). The Pb1 octahedron is located at the centre of the unit cell, with the two Pb2 octahedra located along the body diagonal and related by the inversion centres at (0, 0, 0) and (1, 1, 1). In the crystal structure, the cations occupy channels that run parallel to the anion chains. Each diammonium cation is hydrogen bonded to three different chains in a pseudo-trigonal pattern. One anion chain lies along the body diagonal and the other two run through the corners of the unit cell in a pseudo-hexagonal pattern (Fig. 3).

Both ammonium groups on the cation form three hydrogen bonds to I atoms of the anion chains (details are given in Table 2). Ammonium atom N1 connects three chains, atom I5 being a bifurcated acceptor. The ammonium group containing atom N2 bonds to two chains. It connects *via* a short and a long hydrogen bond to atoms I2 and I4, respectively, and to a second chain *via* the N2—H2*B*···I1$(-x, 1-y, 1-z)$ interaction.

The pentadiammonium ion exhibits two types of conformational arrangement between the four possible torsion angles. There are antiperiplanar C1—C2—C3—C4 and C3—C4—C5—N5 angles of 174.0 (15) and −179.2 (14)°, and synclinal (*gauche*) C2—C3—C4—C5 and N1—C1—C2—C3 angles of 59 (2) and −71 (2)°.

Experimental

PbI_2 (0.125 g, 0.271 mmol) and $C_5H_{16}N_2$ (0.031 g, 0.507 mmol) were added to HI (3 ml) and the mixture was heated until all the components had dissolved. The solution was allowed to cool to room temperature, whereupon yellow plate-shaped crystals formed. A single crystal suitable for X-ray diffraction analysis was selected and studied. Analysis calculated for $C_{10}H_{32}I_{10}N_4Pb_3$: C 5.72, H 1.54, N 2.67%; found: C 5.74, H 1.63, N 2.73%.

Crystal data

$(C_5H_{16}N_2)_2[Pb_3I_{10}]$
M_r = 2098.97
Triclinic, $P\overline{1}$
a = 8.8543 (15) Å
b = 11.1457 (19) Å
c = 11.5725 (19) Å
α = 109.624 (3)°
β = 106.173 (3)°
γ = 107.339 (3)°
V = 931.4 (3) Å^3
Z = 1
D_x = 3.742 Mg m^{-3}
Mo $K\alpha$ radiation
Cell parameters from 849 reflections
θ = 2.6–25°
μ = 21.82 mm^{-1}
T = 293 (2) K
Plate, yellow
0.30 × 0.24 × 0.03 mm

Data collection

Bruker SMART CCD area-detector diffractometer
φ and ω scans
Absorption correction: by integration (*XPREP* in *SAINT-Plus*; Bruker, 1999)
T_{min} = 0.026, T_{max} = 0.643
5061 measured reflections
3257 independent reflections
2593 reflections with $I > 2\sigma(I)$
R_{int} = 0.052
θ_{max} = 25°
$h = -10 \rightarrow 7$
$k = -13 \rightarrow 13$
$l = -11 \rightarrow 13$

Refinement

Refinement on F^2
$R[F^2 > 2\sigma(F^2)]$ = 0.036
$wR(F^2)$ = 0.104
S = 1.10
3257 reflections
127 parameters
H-atom parameters constrained
$w = 1/[\sigma^2(F_o^2) + (0.0464P)^2 + 4.4173P]$
where $P = (F_o^2 + 2F_c^2)/3$
$(\Delta/\sigma)_{max} < 0.001$
$\Delta\rho_{max}$ = 1.25 e Å^{-3}
$\Delta\rho_{min}$ = −1.19 e Å^{-3}
Extinction correction: *SHELXL97*
Extinction coefficient: 0.00170 (19)

Table 1
Selected geometric parameters (Å, °).

Pb1—I2	3.1998 (11)	Pb2—I4^{i}	3.1718 (12)
Pb1—I3	3.2226 (10)	Pb2—I1	3.3102 (12)
Pb1—I1	3.2275 (10)	Pb2—I2	3.3187 (12)
Pb2—I5	3.1221 (12)	Pb2—I3	3.3222 (11)
Pb2—I4	3.1680 (10)		
I4^{i}—Pb2—I1	172.40 (3)	I4—Pb2—I3	169.37 (3)
I5—Pb2—I2	168.97 (3)		

Symmetry code: (i) $-x, -y, -z$.

Table 2
Hydrogen-bonding geometry (Å, °).

D—H···A	D—H	H···A	D···A	D—H···A
N1—H1A···I3^{i}	0.89	3.02	3.806 (15)	149
N1—H1B···I5^{ii}	0.89	2.93	3.669 (16)	142
N1—H1C···I5^{iii}	0.89	2.92	3.672 (15)	143
N5—H5A···I1^{iv}	0.89	2.79	3.668 (14)	169
N5—H5B···I2	0.89	2.87	3.531 (14)	132
N5—H5C···I4	0.89	3.31	4.001 (16)	136

Symmetry codes: (i) $-x, -y, -z$; (ii) $x-1, y, z-1$; (iii) $-1-x, -y, -z$; (iv) $-x, 1-y, 1-z$.

All H atoms were allowed for in idealized positions in the riding-model approximation [C—H = 0.97 Å, N—H = 0.89 Å and U_{iso}(H) = 1.2U_{eq}(C,N)].

Data collection: *SMART-NT* (Bruker, 1998); cell refinement: *SAINT-Plus* (Bruker, 1999); data reduction: *XPREP* in *SAINT-Plus* (Bruker, 1999); program(s) used to solve structure: *SHELXS*97 (Sheldrick, 1997); program(s) used to refine structure: *SHELXL*97 (Sheldrick, 1997); molecular graphics: *ORTEP*-3 *for Windows* (Farrugia, 1997) and *DIAMOND* (Brandenburg, 1999); software used to prepare material for publication: *WinGX* (Farrugia, 1999) and *PLATON* (Spek, 2003).

Supplementary data for this paper are available from the IUCr electronic archives (Reference: FG1746). Services for accessing these data are described at the back of the journal.

References

Brandenburg, K. (1999). *DIAMOND*. Version 2.1e. Crystal Impact GbR, Bonn, Germany.
Bruker (1998). *SMART-NT*. Version 5.050. Bruker AXS Inc., Madison, Wisconsin, USA.
Bruker (1999). *SAINT-Plus*. Version 6.02. Bruker AXS Inc., Madison, Wisconsin, USA.
Contreras, J. G., Seguel, G. V., Ungerer, B., Maier, W. F. & Hollander, F. J. (1983). *J. Mol. Struct.* **102**, 295–304.
Farrugia, L. J. (1997). *J. Appl. Cryst.* **30**, 565.
Farrugia, L. J. (1999). *J. Appl. Cryst.* **32**, 837–838.
Garland, J. K., Emerson, K. & Pressprich, M. R. (1990). *Acta Cryst.* C**46**, 1603–1609.
Kind, R., Plesko, S., Günter, P., Roos, J. & Fousek, J. (1981). *Phys. Rev. B Condens. Matter*, **23**, 343–350.
Krautscheid, H., Lode, C., Vielsack, F. & Vollmer, H. (2001). *J. Chem. Soc. Dalton Trans.* pp. 1099–1104.
Krautscheid, H. & Vielsack, F. (1997). *Z. Anorg. Allg. Chem.* **623**, 259–263.
Lode, C. & Krautscheid, H. (2001). *Z. Anorg. Allg. Chem.* **627**, 1454–1458.
Maxcy, K. R., Willett, R. D., Mitzi, D. B. & Afzali, A. (2003). *Acta Cryst.* E**59**, m364–m366.
Mitzi, D. B. (1999). *Prog. Inorg. Chem.* **48**, 1–121.
Papavassiliou, G. C. (1997). *Prog. Solid State Chem.* **25**, 125–270.
Sheldrick, G. M. (1997). *SHELXS*97 and *SHELXL*97. University of Göttingen, Germany.
Spek, A. L. (2003). *J. Appl. Cryst.* **36**, 7–13.

6.4 *p*-phenylenediammonium tetraiodozincate(II) dihydrate

Journal: Acta Crystallographica Section E, Structure Reports Online

Date Submitted: 9 March 2006

Reference Code of Submitted Article: BT2029

Date Accepted: 10 March 2006

Final Reference: Lemmerer, A., Billing, D.G. (2006). *Acta Cryst*. E**62**, m779-m781.

Brief Synopsis

The inorganic-organic hybrid *p*-phenylenediammonium tetraiodozincate(II) dihydrate has isolated ZnI_4 tetrahedra. This compound was part of preliminary work where as many different divalent metals with halide ligands where crystallized out with ammonium cations.

metal-organic papers

Acta Crystallographica Section E
Structure Reports Online
ISSN 1600-5368

p-Phenylenediammonium tetraiodozincate(II) dihydrate

Andreas Lemmerer* and David G. Billing

School of Chemistry, University of the Witwatersrand, Private Bag 3, PO Wits 2050, South Africa

Correspondence e-mail: andy@hobbes.gh.wits.ac.za

Key indicators

Single-crystal X-ray study
T = 293 K
Mean σ(C–C) = 0.008 Å
R factor = 0.027
wR factor = 0.071
Data-to-parameter ratio = 24.1

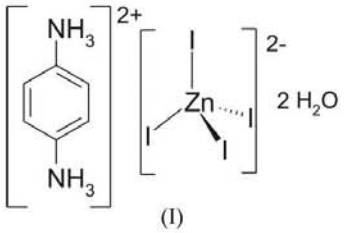
For details of how these key indicators were automatically derived from the article, see http://journals.iucr.org/e.

The title compound, $(C_6H_{10}N_2)[ZnI_4]\cdot 2H_2O$, crystallizes as an organic–inorganic hybrid. The ionic layer consists of isolated ZnI_4 tetrahedra. The hydrocarbon layer has two symmetry-independant centrosymmetric *p*-phenylenediammonium cations that link to the ionic layer *via* hydrogen bonding. Two water molecules of hydration lie between the anion and the two cations.

Received 9 March 2006
Accepted 10 March 2006

Comment

In recent years, a significant number of organic–inorganic hybrid materials based on metal halide units have been prepared and studied; for reviews, see Papavassiliou (1997) and Mitzi (1999). It has been shown that their structures can vary considerably, ranging from systems based on isolated molecules to ones containing extended chains as in $(Me_4N)[PbI_3]$(Contreras *et al.*, 1983) and up to two- or three-dimensional networks (Mitzi, 1999). Very few cases have been reported of the zero-dimensional form, in which the metal halide units exist isolated from each other and connect *via* hydrogen bonds to the organic counter-ion. Often, water molecules are able to coordinate to the two charged components, as in $(CH_3NH_3)_4[PbI_6]\cdot 2H_2O$ (Vincent *et al.*, 1986). $[ZnI_4]^{2-}$ usually consists of iodides tetrahedrally bonded to the zinc. The counter-ions contain tertiary or quaternary ammonium ions, which then hydrogen bond to the iodides, *e.g.* $(C_{11}H_{13}N_2)^+$ (Orioli & Lip, 1974), $[N(CH_3)_4]^+$ (Werk *et al.*, 1990) and $[N(C_2H_5)_4]^+$ (Harrison *et al.*, 2000). The structure of *p*-phenylenediammonium tetraiodozincate(II) dihydrate, (I), is the first reported case with primary ammonium cations as the counter-ion.



(I)

The unit cell of (I) contains two ZnI_4 tetrahedra, with one lying at $z \simeq \frac{1}{4}$ pointing along the negative *c* axis and the other at $z \simeq \frac{3}{4}$ towards the positive *c* axis (Fig. 2). The bond distances and angles are in similiar ranges to those of previously reported tetrahedra. Two short [2.6043 (16) and 2.6081 (12) Å] and two long [2.6236 (15) and 2.6274 (13) Å] distances cause a slight deviation of the ideal geometry. There are two unique *p*-phenylenediammmonium cations in the

© 2006 International Union of Crystallography
All rights reserved

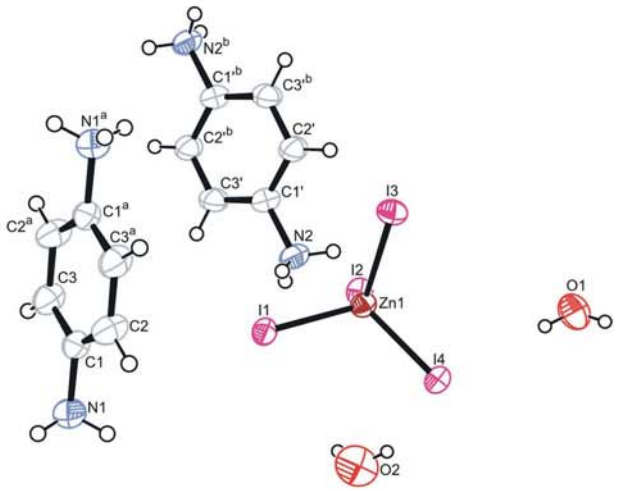


Figure 1
The asymmetric unit of (I) and some adjacent atoms, showing the atomic numbering scheme. Displacement ellipsoids are shown at the 50% probability level. Atoms labelled with the superscripts 'a' and 'b' are at the symmetry positions $(1-x, -y, 2-z)$ and $(-x, -y, 1-z)$, respectively.

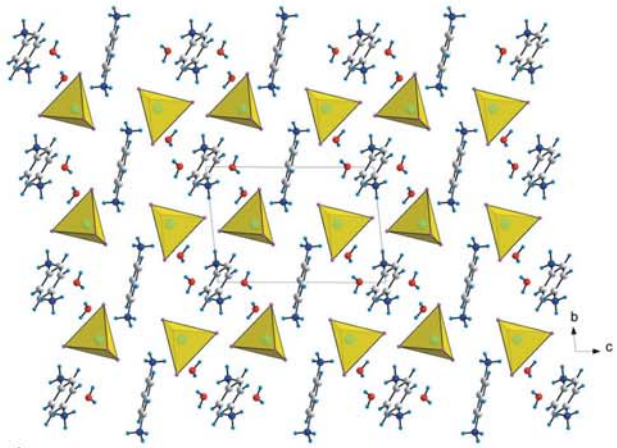


Figure 2
The arrangement of ions of (I), projected along the *a* axis.

asymmetric unit (Fig. 1). Cation 1 sits on the inversion centre at $(\frac{1}{2}, 0, 1)$ and cation 2 on another at $(0, 0, \frac{1}{2})$. There are also two water molecules of hydration. Atom O1 sits close to the *ac* plane and O2 is located completely in the unit cell.

Cation 1 has one simple hydrogen bond to I2 and two to O1. Cation 2 has a more complex pattern, with two long bifurcated bonds to I3 and $I3^{iii}$, a short simple one to I1 and a second bifurcated bond to two different acceptor toms $O2^{i}$ and $I4^{i}$ (Fig. 3) (symmetry codes as in Table 2). The N—H···O_w distances are in the range 2.05–2.19 Å, slightly longer than the maximum given by Steiner (2002) in his review of the hydrogen bond in the solid state. The O2 water molecule hydrogen bonds to the I atoms as well. The hydrogen-bond acceptor distances $O2_w$—H···I are longer than the average of 2.68 (1) Å quoted by Steiner (2002), but the $O2_w$···I distances comply with the average of 3.61 (1) Å (see Table 2). The

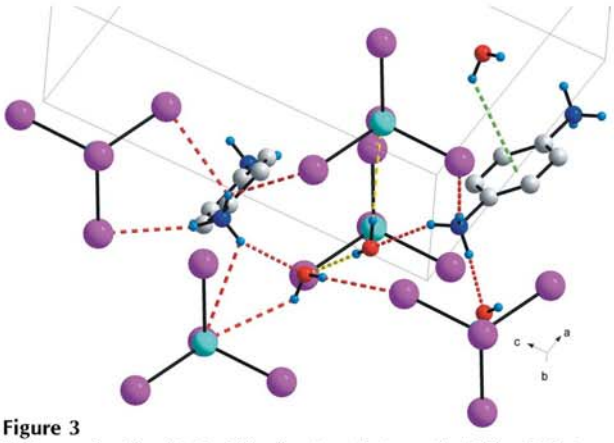


Figure 3
Hydrogen-bonding (dashed lines) pattern between the I, O and N atoms (red lines), weak interactions between water and iodide (yellow lines) and the O—H···π shown with a green line.

second water of hydration has $O1_w$···I distances of 3.923 (5) and 4.034 (6) Å, and can be considered weak interactions. An O—H···π interaction occurs between O2 and cation 1 with a distance of 3.22 Å from H22 to the ring centroid.

Experimental

Crystals of (I) were grown at room temperature by first dissolving ZnI_2 (0.225 g, 0.708 mmol) in ethanol (14 ml) and 57% HI (0.600 g). Then, $NH_3C_6H_4NH_3$ (0.080 g, 0.726 mmol) was added. The crystals, grown by slow evaporation, were harvested after 14 d. A colourless crystal suitable for X-ray diffraction studies was selected and studied. Analysis calculated for $C_6H_{14}I_4N_2O_2Zn$: C 10.02, H 1.96, N 3.90%; found: C 10.95, H 2.01, N 4.45%.

Crystal data

$(C_6H_{10}N_2)[ZnI_4]\cdot 2H_2O$	$Z = 2$
$M_r = 719.16$	$D_x = 2.787$ Mg m^{-3}
Triclinic, $P\overline{1}$	Mo $K\alpha$ radiation
$a = 8.398$ (5) Å	Cell parameters from 927 reflections
$b = 8.611$ (5) Å	$\theta = 2.6$–$28.2°$
$c = 12.540$ (5) Å	$\mu = 8.63$ mm^{-1}
$\alpha = 92.821$ (5)°	$T = 293$ (2) K
$\beta = 103.344$ (5)°	Plate, colourless
$\gamma = 102.407$ (5)°	0.35 × 0.20 × 0.08 mm
$V = 857.1$ (8) Å^3	

Data collection

Bruker SMART CCD area-detector diffractometer	3352 independent reflections
φ and ω scans	2967 reflections with $I > 2\sigma(I)$
Absorption correction: integration (*XPREP*; Bruker, 1999)	$R_{int} = 0.034$
$T_{min} = 0.152$, $T_{max} = 0.545$	$\theta_{max} = 26°$
5108 measured reflections	$h = -9 \rightarrow 10$
	$k = -10 \rightarrow 7$
	$l = -15 \rightarrow 15$

Refinement

Refinement on F^2	$w = 1/[\sigma^2(F_o^2) + (0.0333P)^2 + 1.4644P]$ where $P = (F_o^2 + 2F_c^2)/3$
$R[F^2 > 2\sigma(F^2)] = 0.028$	$(\Delta/\sigma)_{max} < 0.001$
$wR(F^2) = 0.071$	$\Delta\rho_{max} = 1.01$ e Å^{-3}
$S = 1.08$	$\Delta\rho_{min} = -0.65$ e Å^{-3}
3352 reflections	Extinction correction: *SHELXL97*
139 parameters	Extinction coefficient: 0.0036 (3)
H-atom parameters constrained	

Table 1
Selected geometric parameters (Å, °).

C1′—N2	1.468 (6)	Zn1—I1	2.6081 (12)
C1—N1	1.466 (7)	Zn1—I3	2.6236 (15)
Zn1—I4	2.6043 (16)	Zn1—I2	2.6274 (13)
I4—Zn1—I1	114.06 (4)	I4—Zn1—I2	106.87 (3)
I4—Zn1—I3	109.25 (3)	I1—Zn1—I2	107.10 (3)
I1—Zn1—I3	108.64 (4)	I3—Zn1—I2	110.91 (3)

Table 2
Hydrogen-bond geometry (Å, °).

D—H···A	D—H	H···A	D···A	D—H···A
N1—H1A···I2^{i}	0.89	2.76	3.620 (5)	162
N1—H1B···O1^{i}	0.89	2.16	2.995 (7)	157
N1—H1C···O1^{ii}	0.89	2.05	2.871 (7)	153
N2—H2A···I3^{iii}	0.89	3.14	3.809 (5)	133
N2—H2A···I3	0.89	3.19	3.701 (5)	119
N2—H2B···I1	0.89	2.81	3.681 (5)	166
N2—H2C···O2^{i}	0.89	2.19	2.966 (7)	145
N2—H2C···I4^{i}	0.89	3.21	3.703 (5)	117
O1—H12···I4	0.85	3.07	3.923 (5)	180
O1—H11···I3^{iv}	0.85	3.18	4.034 (6)	180
O2—H21···I2^{v}	0.85	2.77	3.554 (5)	156
O2—H22···I4	0.85	2.98	3.606 (6)	132

Symmetry codes: (i) $-x+1, -y+1, -z+1$; (ii) $x+1, y-1, z+1$; (iii) $-x, -y+1, -z+1$; (iv) $x, y+1, z$; (v) $-x+1, -y+1, -z$.

All H atoms were found in a difference map. For the H atoms bonded to O atoms, restraints were used to obtain reasonable details of O—H distances and H—O—H angles. Finally these H atoms were refined using a riding model, with U_{iso}(H) = 1.2U_{eq}(O). The remaining H atoms were refined in idealized positions in the riding-model approximation and with U_{iso}(H) = 1.2U_{eq}(aromatic C, N). The NH_3 groups were allowed to rotate but not to tip. The highest residual peak is located 0.78 Å from atom I2.

Data collection: *SMART-NT* (Bruker, 1998); cell refinement: *SAINT-Plus* (Bruker, 1999); data reduction: *XPREP* (Bruker, 1999); program(s) used to solve structure: *SHELXS97* (Sheldrick, 1997); program(s) used to refine structure: *SHELXL97* (Sheldrick, 1997); molecular graphics: *ORTEP-3 for Windows* (Farrugia, 1997) and *DIAMOND* (Brandenburg, 1999); software used to prepare material for publication: *WinGX* (Farrugia, 1999) and *PLATON* (Spek, 2003).

The University of the Witwatersrand is thanked for the award of a research grant and for providing the infrastructure required to do this work.

References

Brandenburg, K. (1999). *DIAMOND*. Version 2.1e. Crystal Impact GbR, Bonn, Germany.
Bruker (1998). *SMART-NT*. Version 5.050. Bruker AXS Inc., Madison, Wisconsin, USA.
Bruker (1999). *SAINT-Plus*. Version 6.02 (including *XPREP*). Bruker AXS Inc., Madison, Wisconsin, USA.
Contreras, J. G., Seguel, G V., Ungerer, B., Maier, W. F. & Hollander, F. J. (1983). *J. Mol. Struct.* **102**, 295–304.
Farrugia, L. J. (1997). *J. Appl. Cryst.* **30**, 565.
Farrugia, L. J. (1999). *J. Appl. Cryst.* **32**, 837–838.
Harrison, W. T. A., Howe, R. A., Skakle, J. & Wardell, J. L. (2000). *Acta Cryst.* C**56**, e124–e125.
Mitzi, D. B. (1999). *Progress Inorg. Chem.* **48**, 1–121.
Orioli, P. L. & Lip, H. C. (1974). *Cryst. Struct. Commun.* **3**, 477–480.
Papavassiliou, G. C. (1997). *Prog. Solid State Chem.* **25**, 125–270.
Sheldrick, G. M. (1997). *SHELXS97* and *SHELXL97*. University of Göttingen, Germany.
Spek, A. L. (2003). *J. Appl. Cryst.*. **36**, 7–13.
Steiner, T. (2002). *Angew. Chem. Int. Ed.* **41**, 48–76.
Vincent, B. R., Robertson, K. N., Cameron, T. S. & Knop, O. (1986). *Can. J. Chem.* **65**, 1042–1046.
Werk, M. L., Chapuis, G. & Zuniga, F. J. (1990). *Acta Cryst.* B**46**, 187–192.

6.5 1-Naphthylammonium triiodoplumbate(II)

Journal: Acta Crystallographica Section E, Structure Reports Online

Date Submitted: 24 March 2006

Reference Code of submitted article: BT2043

Date Accepted: 27 March 2006

Final Reference: Lemmerer, A., Billing, D.G. (2006). *Acta Cryst*. E**62**, m904-m906.

Brief Synopsis

The inorganic-organic hybrid (1-Naphthylammonium) triiodoplumbate(II) has 1-D chains of face-sharing PbI_6 octahedra.

metal-organic papers

Acta Crystallographica Section E
Structure Reports Online
ISSN 1600-5368

1-Naphthylammonium triiodoplumbate(II)

Andreas Lemmerer* and David G. Billing

School of Chemistry, University of the Witwatersrand, Private Bag 3, PO Wits, 2050, South Africa

Correspondence e-mail: andy@hobbes.gh.wits.ac.za

Key indicators

Single-crystal X-ray study
T = 293 K
Mean σ(C–C) = 0.019 Å
R factor = 0.036
wR factor = 0.079
Data-to-parameter ratio = 19.8

For details of how these key indicators were automatically derived from the article, see http://journals.iucr.org/e.

© 2006 International Union of Crystallography
All rights reserved

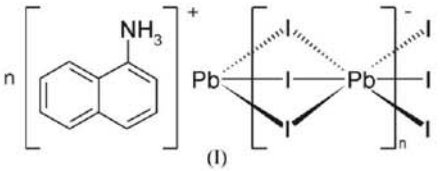
Received 24 March 2006
Accepted 27 March 2006

The title compound, $(C_{10}H_{10}N)[PbI_3]$, crystallizes as an organic–inorganic hybrid. As such, the structure contains extended chains of $[PbI_3]^-$ units running along the b axis. Each Pb atom is octahedrally coordinated by six iodides, arranged as chains of face-sharing octahedra. These inorganic chains are separated by the isolated organic cations.

Comment

In recent years a significant number of organic–inorganic hybrid materials based on metal halide units have been prepared and studied; for reviews see Papavassiliou (1997) and Mitzi (1999). Haloplumbates in particular have demonstrated a propensity for forming a great variety of crystalline structures by self-assembly from suitable solution mixtures. It has been shown that their structures can vary considerably, ranging from systems based on isolated molecules to ones containing extended chains as in $[Me_4N][PbI_3]$ (Contreras *et al.*, 1983) and right up to two- or three-dimensional networks (Mitzi, 1999). For systems containing extended chains, the extended chains may be formed by one, two or three bridging halides. A search of the Cambridge Structural Database (Version 5.27, November 2005 release; Allen 2002) revealed that the crystal structure of the unprotonated amine itself was reported only in 1945. Only the cell parameters and space group were determined, but no three-dimensional coordinates (Kitaigorodskii, 1945). A more recent structure incorporating the 1-naphthylamine system is seen in the ternary π–π^* charge-transfer salt pyridinium–1-naphthylamine–picrate (Bernstein *et al.*, 1980).

Having previously reported the structure of an organic–inorganic hybrid containing lead bromide face-sharing chains and the cation (*S*)-β-phenylethylammonium (Billing & Lemmerer, 2003), we present here the room temperature structure of the title compound, $(C_{10}H_7NH_3)[PbI_3]$ (**I**).



(I)

Fig. 2 clearly underlines the one-dimensional arrangement in which four chains of face-sharing PbI_6 octahedra extend through the unit cell, parallel to the b axis. The channels between the chains are occupied by 1-naphthylammonium cations. In the direction perpendicular to the chains, the crystal cohesion is achieved by N—H···I hydrogen bonds,

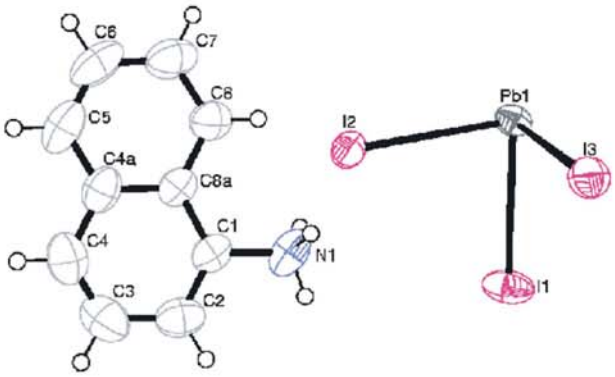


Figure 1
The asymmetric unit of (I), showing the atomic numbering scheme. Displacement ellipsoids are drawn at the 50% probability level.

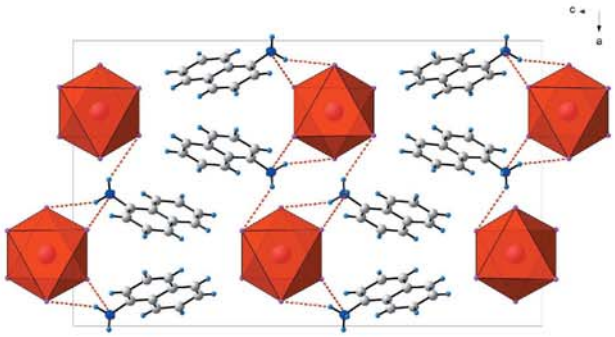


Figure 2
Packing of (I), viewed along the *b* axis. The hydrogen bonds between the ammonium ions and the iodine atoms are shown as dashed red lines.

related to the NH_3 polar groups, and by weak van der Waals forces between the ring systems as the nearest C···C distance is 3.891 (1) Å.

The inorganic motif is built up from characteristic face-sharing PbI_6 octahedra that form chains along the *b* axis. Two chains are at approximately *x* ~0.25 and the other two at *x* ~0.75. The octahedra are severely distorted, with all lead Pb—I distances different (Table 1). The bond angles between *cis* ligands vary from 74.98 (3)° to 95.13 (4)° and *trans* angles from 177.41 (2)° to 178.57 (3)°.

Within the organic component, adjacent naphthalene ring systems are separated by a centroid-to-centroid distance of 4.905 (7) Å, which is probably too large to be considered as representing π–π stacking interactions.

Experimental

0.038 g PbI_2 (0.082 mmol) was dissolved in 2 ml 47% HI in a sample vial. Thereafter, 0.016 g $C_{10}H_9N_1$ (0.112 mmol) was added and the precipitate dissolved by refluxing for 12 h at 373 K. The solution was slowly cooled at 2K/hour to room temperature. A yellow single crystal suitable for X-ray diffraction analysis was selected and studied. Analysis calculated for $C_{10}H_{10}I_3N_1Pb$: C 16.41, H 1.38 N 1.91%; found: C 16.50, H 1.64, N 2.04%

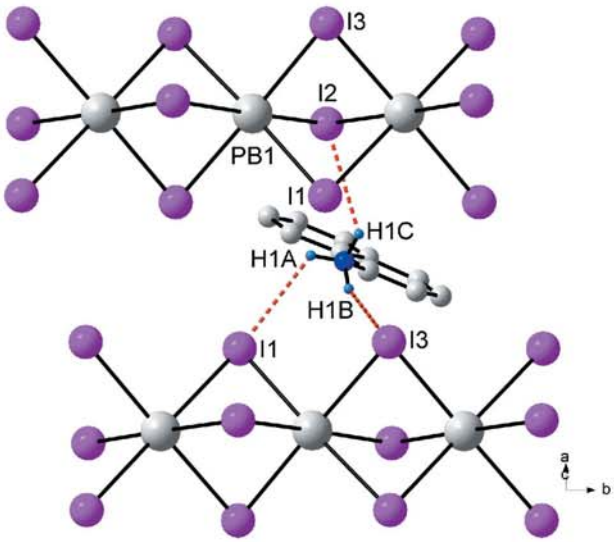


Figure 3
Magnified view of the face-sharing [Pb_6] octahedra and hydrogen-bonding (dashed lines) scheme.

Crystal data

$(C_{10}H_{10}N)[PbI_3]$	Mo $K\alpha$ radiation
M_r = 732.08	Cell parameters from 796 reflections
Orthorhombic, *Pbca*	θ = 3.5–28.1°
a = 15.546 (4) Å	μ = 16.66 mm^{-1}
b = 7.8944 (19) Å	*T* = 293 (2) K
c = 25.522 (7) Å	Rhomboid, yellow
V = 3132.2 (14) Å^3	0.18 × 0.14 × 0.04 mm
Z = 8	
D_x = 3.105 Mg m^{-3}	

Data collection

Bruker SMART CCD area-detector diffractometer	2729 independent reflections
φ and ω scans	1618 reflections with $I > 2\sigma(I)$
Absorption correction: integration (*XPREP*; Bruker, 1999)	R_{int} = 0.072
T_{min} = 0.067, T_{max} = 0.526	θ_{max} = 25°
9144 measured reflections	$h = -18 \rightarrow 15$
	$k = -9 \rightarrow 9$
	$l = -29 \rightarrow 25$

Refinement

Refinement on F^2	$w = 1/[\sigma^2(F_o^2) + (0.0299P)^2]$ where $P = (F_o^2 + 2F_c^2)/3$
$R[F^2 > 2\sigma(F^2)]$ = 0.036	$(\Delta/\sigma)_{max}$ = 0.001
$wR(F^2)$ = 0.079	$\Delta\rho_{max}$ = 0.88 e Å^{-3}
S = 0.96	$\Delta\rho_{min}$ = −0.97 e Å^{-3}
2729 reflections	Extinction correction: *SHELXL97*
138 parameters	Extinction coefficient: 0.00082 (3)
H-atom parameters constrained	

Table 1
Selected bond lengths (Å).

I3—Pb1	3.1443 (10)	I2—Pb1^i	3.2903 (10)
I3—Pb1^i	3.2347 (9)	I1—Pb1	3.2146 (10)
I2—Pb1	3.1938 (10)	I1—Pb1^i	3.2401 (10)

Symmetry code: (i) $-x+\frac{1}{2}, y-\frac{1}{2}, z$.

Table 2
Hydrogen-bond geometry (Å, °).

D—H···A	D—H	H···A	D···A	D—H···A
N1—H1A···I2^{ii}	0.89	2.7	3.554 (8)	161
N1—H1B···I1^{iii}	0.89	2.89	3.719 (10)	156
N1—H1C···I3	0.89	2.74	3.606 (9)	166

Symmetry codes: (ii) $-x+1, -y+2, -z+1$; (iii) $x+\frac{1}{2}, -y+\frac{3}{2}, -z+1$.

H atoms were refined in idealized positions in the riding-model approximation, with C—H = 0.93 Å and N—H = 0.89 Å and U_{iso}(H) = 1.2U_{eq}(C) or 1.5U_{eq}(N). The highest residual peak was 1.03 Å from Pb1.

Data collection: *SMART-NT* (Bruker, 1998); cell refinement: *SAINT-Plus* (Bruker, 1999); data reduction: *SAINT-Plus*; program(s) used to solve structure: *SHELXS97* (Sheldrick, 1990); program(s) used to refine structure: *SHELXL97* (Sheldrick, 1997); molecular graphics: *ORTEP-3 for Windows* (Farrugia, 1997) and *DIAMOND* (Brandenburg, 1999); software used to prepare material for publication: *WinGX* publication routines (Farrugia, 1999) and *PLATON* (Spek, 2003).

The University of the Witwatersrand and the National Research Fund are thanked for the award of a research grant and for providing the infrastructure required to do this work.

References

Allen, F. H. (2002). *Acta Cryst.* B**58**, 380–388.
Bernstein, J., Regev, H. & Herbstein, F. H. (1980). *Acta Cryst.* B**36**, 1170–1175.
Billing, D. G. & Lemmerer, A. (2003). *Acta Cryst.* E**59**, m381–m383.
Brandenburg, K. (1999). *DIAMOND*. Version 2.1e. Crystal Impact GbR, Bonn, Germany.
Bruker (1998). *SMART-NT*. Version 5.050. Bruker AXS Inc., Madison, Wisconsin, USA.
Bruker (1999). *SAINT*-Plus. Version 6.02 (including *XPREP*). Bruker AXS Inc., Madison, Wisconsin, USA.
Contreras, J. G., Seguel, G. V., Ungerer, B., Maier, W. F. & Hollander, F. J. (1983). *J. Mol. Struct.* **102**, 295–304.
Farrugia, L. J. (1997). *J. Appl. Cryst.* **30**, 565.
Farrugia, L. J. (1999). *J. Appl. Cryst.* **32**, 837–838.
Kitaigorodskii, A. I. (1945). *Proc. Natl Acad. Sci. USSR*, **50**, 315.
Mitzi, D. B. (1999). *Progress Inorg. Chem.* **48**, 1–121.
Papavassiliou, G. C. (1997). *Prog. Solid. State Chem.* **25**, 125–270.
Sheldrick, G. M. (1990). *Acta Cryst.* A**46**, 467–473.
Sheldrick, G. M. (1997). *SHELXL97*. University of Göttingen, Germany.
Spek, A. L. (2003). *J. Appl. Cryst.* **36**, 7–13.

6.6 *catena*-Poly[tetrakis(3-phenylpropylammonium) [iodoplumbate(II)-tri-μ-iodo-plumbate(II)-tri-μ-iodo-plumbate(II)-di-μ-iodo]]

Journal: Acta Crystallographica Section C, Crystal Structure Communications

Date Submitted: 7 March 2006

Reference Code of Submitted Article: FG3008

Date Accepted: 10 March 2006

Final Reference: Billing, D.G., Lemmerer, A. (2006). *Acta Cryst*. C**62**, m174-m176

Brief Synopsis

The inorganic-organic hybrid tetrakis(3-phenylpropylammonium) decaiodotriplumbate(II) has a 2-D net-type inorganic layer, built up from corner- and face-sharing PbI_6 octahedra.

metal-organic compounds

Acta Crystallographica Section C
Crystal Structure Communications
ISSN 0108-2701

catena-Poly[tetrakis(3-phenylpropylammonium) [iodoplumbate(II)-tri-μ-iodo-plumbate(II)-tri-μ-iodo-iodoplumbate(II)-di-μ-iodo]]

David G. Billing* and Andreas Lemmerer

School of Chemistry, University of the Witwatersrand, Private Bag 3, PO Wits 2050, South Africa
Correspondence e-mail: andy@hobbes.gh.wits.ac.za

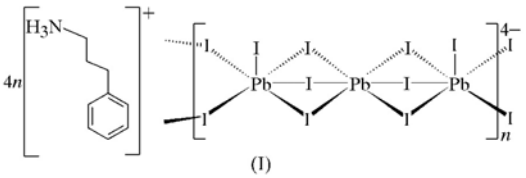
Received 7 March 2006
Accepted 10 March 2006
Online 13 April 2006

The title compound, $\{(C_9H_{14}N)_4[Pb_3I_{10}]\}_n$, crystallizes as an organic–inorganic hybrid. As such, the structure consists of a two-dimensional inorganic layer of $[Pb_3I_{10}]_n^{4n-}$ ions extending along [100]. The asymmetric unit contains two independent Pb atoms, *viz.* one in a general position and the other on an inversion centre. Each Pb atom is octahedrally coordinated by six iodide ions and exhibits both face- and corner-sharing with adjacent atoms in the inorganic layer. These anionic layers alternate with 3-phenylpropylammonium cations, which hydrogen bond to the iodides. Simple face-to-edge σ–π stacking interactions are observed between the aromatic rings that stabilize the overall three-dimensional structure. This net structure has only been observed five times previously.

Comment

In recent years, a significant number of organic–inorganic hybrid materials based on lead and tin halide units have been prepared and studied; for reviews, see Papavassiliou (1997) and Mitzi (1999). Haloplumbates in particular have demonstrated a propensity for forming a great variety of crystalline structures. This diversity is a result of the metal–halide octahedra engaging in different combinations of face-, edge- and corner-sharing. As a result, the MX_6 (X = Br and I, and M = Sn and Pb) octahedral building blocks become severely distorted. One of the possible structural motifs forms two-dimensional layers, where chains of two or three *trans* face-sharing octahedra are connected *via* four halides on both ends. This situation can be summarized by the formula $[M_nX_{3n+1}]^{(n+1)-}$. To our knowledge, only one structure with n = 2 has been reported; in this structure, isolated I^- anions lie between the lead iodide layers (Krautscheid *et al.*, 1998).

The case with n = 3 has been observed with both lead bromide in $(PhMe_3N)_4[Pb_3Br_{10}]$ (Wiest *et al.*, 1999) and tin iodide in $(PhMe_3N)_4[Sn_3I_{10}]$ (Lode & Krautscheid, 2001). We present here the synthesis and crystal structure of the title compound, (I), namely the n = 3 case that has $[Pb_3I_{10}]^{4-}$ two-dimensional layers separated by 3-phenylpropylammonium cations.



(I)

The atomic numbering scheme of (I) is shown in Fig. 1. The $[Pb_3I_{10}]^{4-}$ building block has two crystallographically independent Pb atoms, *viz.* Pb1 and Pb2. Atom Pb2 is the central Pb atom and sits on an inversion centre through which the third Pb atom, Pb1($-x+\frac{3}{2}$, $y+\frac{1}{2}$, z), is generated to complete the simplest repeat unit. The three Pb atoms are connected by sharing *trans* faces made up of μ_2-I bridges, with atoms I3, I4 and I5 and their inversion equivalents related through Pb2. The outer octahedra on either end connect to adjacent

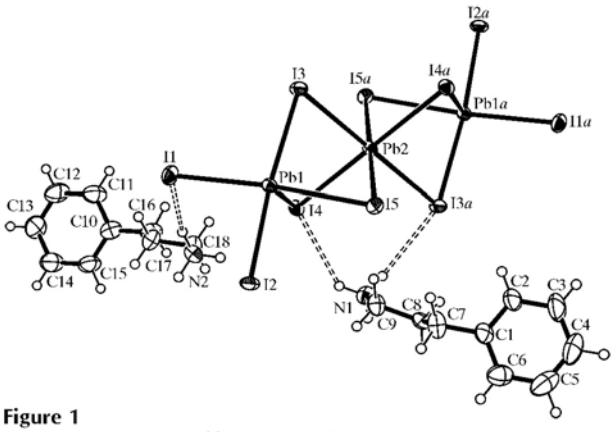


Figure 1
The asymmetric unit of (I) and some adjacent atoms, showing the atomic numbering scheme. Displacement ellipsoids are drawn at the 50% probability level. Atoms labelled with the suffix *a* are at the symmetry position $(-x, -y, -z)$.

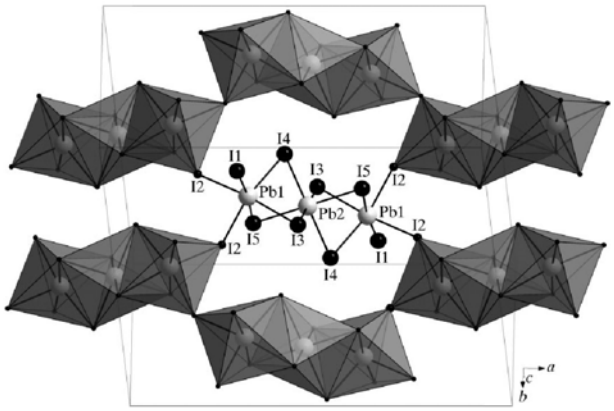


Figure 2
An illustration of the $[Pb_3I_{10}]_n^{4n-}$ two-dimensional net.

 © 2006 International Union of Crystallography DOI: 10.1107/S0108270106009127

$[Pb_3I_{10}]^{4-}$ units *via* μ_2-I2 bridges (see Fig. 2) that are far from linear [$Pb1^{i}$—I2—Pb1 = 142.51 (3)°], in contrast to the almost linear bridges found in $[Sn_3I_{10}]^{4-}$ [169.87 (3)°; Lode & Krautscheid, 2001]. The resulting inorganic layer sits in the *ab* plane and is corrugated as the trimeric units connect in an alternating *trans* fashion (see Fig. 3), as seen in $(C_6H_5NH_3)_4[Cd_3Br_{10}]$ (Ishihara *et al.*, 1994) and $[C_6H_5CH_2SC(NH_2)_2]_4[Pb_3I_{10}]$ (Raptopoulou *et al.*, 2002). In the other two n = 3 structures mentioned above, the individual building blocks are *cis* related.

The Pb atoms show different degrees of distortion. The central Pb2 atom has three almost equal bond lengths to the I atoms [3.2006 (7)–3.2090 (7) Å]. This uniformity is due to the identical face-sharing that occurs with the neighbouring Pb1 atoms. The outer Pb1 octahedra are more distorted, with long Pb—I bond lengths in the range 3.2288 (8)–3.3381 (9) Å when face-sharing occurs, and short bond lengths to the corner-sharing I2 and the terminal non-bridging I1 atoms (see Table 1).

Sandwiched between the inorganic nets are two unique organic aromatic amines, denoted cat1 and cat2. Fig. 3 clearly shows the two-dimensional arrangement of the cations. Both propylammonium groups have an all-*trans* conformation, and they deviate by 9.3 (11) and 14.2 (11)° from the normal to the aromatic rings, respectively. The two ammonium groups display the same hydrogen-bonding scheme, *viz.* one bifurcated and two normal hydrogen bonds. The bifurcated bond distances are similar for atoms N1 and N2 as they both bond to atoms I4 (2.95 and 2.94 Å) and I2 (3.11 and 3.07 Å). In addition, atom N1 forms a long hydrogen bond and a short normal hydrogen bond (2.95 and 2.66 Å), as it bonds to an equatorial (I3) and an axial (I5) I atom, respectively. Atom N2, however, has two similar hydrogen bonds (2.82 and 2.84 Å), as they both bond to the axial atom I1, which is not involved in any bridging (see Fig. 4).

Between the aromatic rings of cat1 and cat2, a face-to-edge σ–π interaction, C14—H14$\cdots$*Cg*1($1-x, 1-y, 1-z$), occurs with a distance of 2.92 Å and an angle of 143°. This interaction is between two cations that hydrogen bond to adjacent two-dimensional nets and so form a three-dimensional system (see Fig. 3).

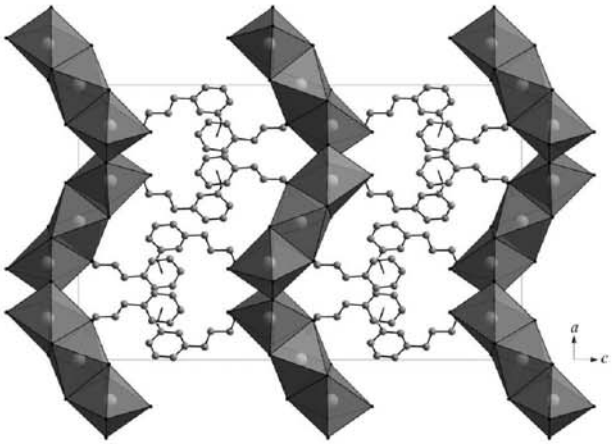


Figure 3
A packing diagram of (I), viewed along the *b* axis, showing the face-to-edge σ–π interaction between cat1 and cat2 which forms a three-dimensional system.

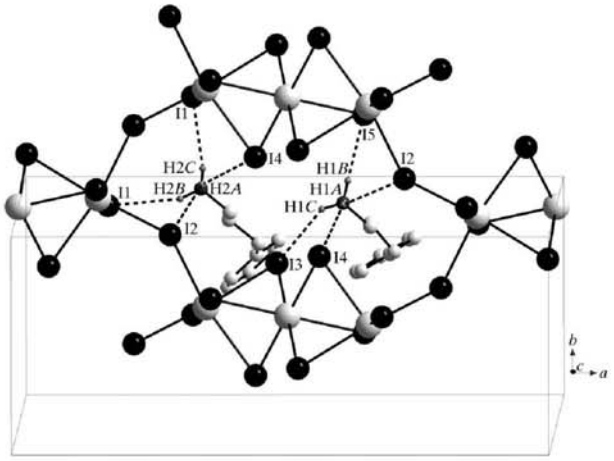


Figure 4
Hydrogen bridging interactions (dashed lines) between the ammonium heads and the halogen atoms of (I).

Experimental

PbO (0.184 g, 0.824 mmol) and 3-phenylpropylamine (0.167 g, 1.23 mmol) were dissolved in HI (3 ml) and then heated to form a clear solution. Upon slow cooling to room temperature, yellow crystals formed. A single crystal suitable for X-ray diffraction was selected and mounted on a glass fibre. Analysis calculated for $C_{36}H_{56}I_{10}N_4Pb_3$: C 17.75, H 2.32, N 2.30%; found: C 18.96, H 2.55, N 2.55%.

Crystal data

$(C_9H_{14}N)_4[Pb_3I_{10}]$	Mo $K\alpha$ radiation
M_r = 2435.42	Cell parameters from 903 reflections
Orthorhombic, *Pbca*	θ = 4.6–56.5°
a = 20.777 (3) Å	μ = 13.79 mm^{-1}
b = 8.4689 (11) Å	T = 173 (2) K
c = 33.550 (5) Å	Rectangular block, yellow
V = 5903.3 (14) Å^3	0.37 × 0.21 × 0.07 mm
Z = 4	
D_x = 2.74 Mg m^{-3}	

Data collection

Bruker SMART CCD area-detector diffractometer	7120 independent reflections
φ and ω scans	5479 reflections with $I > 2\sigma(I)$
Absorption correction: integration (*XPREP*; Bruker, 1999)	R_{int} = 0.075
T_{min} = 0.073, T_{max} = 0.393	θ_{max} = 28°
27663 measured reflections	$h = -27 \rightarrow 27$
	$k = -10 \rightarrow 11$
	$l = -44 \rightarrow 30$

Refinement

Refinement on F^2	$w = 1/[\sigma^2(F_o^2) + (0.0228P)^2 + 63.008P]$ where $P = (F_o^2 + 2F_c^2)/3$
$R[F^2 > 2\sigma(F^2)]$ = 0.049	$(\Delta/\sigma)_{max}$ = 0.001
$wR(F^2)$ = 0.094	$\Delta\rho_{max}$ = 1.49 e Å^{-3}
S = 1.14	$\Delta\rho_{min}$ = −2.10 e Å^{-3}
7120 reflections	
217 parameters	
H-atom parameters constrained	

Table 1
Selected bond lengths (Å).

C1—C7	1.490 (13)	I2—Pb1^{i}	3.1217 (8)
C7—C8	1.556 (15)	I2—Pb1	3.1492 (8)
C8—C9	1.508 (15)	I3—Pb2	3.2078 (7)
C9—N1	1.521 (14)	I3—Pb1	3.2288 (8)
C10—C16	1.513 (14)	I4—Pb2	3.2090 (7)
C16—C17	1.523 (18)	I4—Pb1	3.3077 (8)
C17—C18	1.483 (16)	I5—Pb2	3.2006 (7)
C18—N2	1.496 (16)	I5—Pb1	3.3381 (9)
I1—Pb1	3.1197 (9)		

Symmetry code: (i) $-x+\frac{3}{2}, y-\frac{1}{2}, z$.

Table 2
Hydrogen-bond geometry (Å, °).

D—H···A	D—H	H···A	D···A	D—H···A
N1—H1A···I4	0.91	2.95	3.655 (9)	136
N1—H1A···I2^{i}	0.91	3.11	3.676 (9)	122
N1—H1B···I5^{ii}	0.91	2.66	3.561 (9)	172
N1—H1C···I3^{iii}	0.91	2.95	3.750 (10)	148
N2—H2A···I4	0.91	2.94	3.641 (9)	135
N2—H2A···I2^{i}	0.91	3.07	3.629 (10)	122
N2—H2B···I1^{i}	0.91	2.82	3.677 (9)	159
N2—H2C···I1	0.91	2.84	3.680 (11)	155

Symmetry codes: (i) $-x+\frac{3}{2}, y-\frac{1}{2}, z$; (ii) $x, y-1, z$; (iii) $-x+1, -y, -z$.

All H atoms were allowed for in idealized positions in the riding-model approximation (C—H = 0.95 and 0.99 Å), with their U_{iso}(H) values fixed at $1.2U_{eq}$(C) or $1.5U_{eq}$(N).

Data collection: *SMART-NT* (Bruker, 1998); cell refinement: *SMART-NT*; data reduction: *SAINT-Plus* (Bruker, 1999) and *SHELXTL* (Bruker, 1999); program(s) used to solve structure: *SHELXTL*; program(s) used to refine structure: *SHELXL97* (Sheldrick, 1997); molecular graphics: *ORTEP-3* (Farrugia, 1997) and *DIAMOND* (Brandenburg, 1999); software used to prepare material for publication: *WinGX* (Farrugia, 1999) and *PLATON* (Spek, 2003).

The University of the Witwatersrand is thanked for the award of a research grant and for providing the infrastructure required to carry out this work.

Supplementary data for this paper are available from the IUCr electronic archives (Reference: FG3008). Services for accessing these data are described at the back of the journal.

References

Brandenburg, K. (1999). *DIAMOND* Version 2.1e. Crystal Impact GbR, Bonn, Germany.
Bruker (1998). *SMART-NT*. Version 5.050. Bruker AXS Inc., Madison, Wisconsin, USA.
Bruker (1999). *SHELXTL* (Version 5.1, including *XS*, *XL*, *XP* and *XSHELL*) and *SAINT-Plus* (Version 6.02, including *XPREP*). Bruker AXS Inc., Madison, Wisconsin, USA.
Farrugia, L. J. (1997). *J. Appl. Cryst.* **30**, 565.
Farrugia, L. J. (1999). *J. Appl. Cryst.* **32**, 837–838.
Ishihara, H., Krishnan, V. G., Dou, S., Paulus, H. & Weiss, A. (1994). *Z. Naturforsch. Teil A*, **49**, 213–222.
Krautscheid, H., Vielsack, F. & Klaassen, N. (1998). *Z. Anorg. Allg. Chem.* **624**, 807–812.
Lode, C. & Krautscheid, H. (2001). *Z. Anorg. Allg. Chem.* **627**, 1454–1458.
Mitzi, D. B. (1999). *Prog. Inorg. Chem.* **48**, 1–121.
Papavassiliou, G. C. (1997). *Prog. Solid State Chem.* **25**, 125–270.
Raptopoulou, C. P., Terzis, A., Mousdis, G. A. & Papavassiliou, G. C. (2002). *Z. Naturforsch. Teil B*, **57**, 645–650.
Sheldrick, G. M. (1997). *SHELXL97*. University of Göttingen, Germany.
Spek, A. L. (2003). *J. Appl. Cryst.* **36**, 7–13.
Wiest, Th., Blachnik, R. & Reuter, H. (1999). *Z. Naturforsch. Teil B*, **54**, 1099–1102.

6.7 Bis(propane-1,2-diammonium) hexaiodoplumbate(II) trihydrate

Journal: Acta Crystallographica Section E, Structure Reports Online

Date Submitted: 12 April 2006

Reference Code of Submitted Article: BT2054

Date Accepted: 18 April 2006

Final Reference: Billing, D.G., Lemmerer, A. (2006). *Acta Cryst.* E**62**, m1103-m1105.

Brief Synopsis

The inorganic-organic hybrid bis(propane-1,2-diammonium) hexaiodoplumbate(II) trihydrate has 0-D motif of isolated PbI_6 octahedra.

metal-organic papers

Acta Crystallographica Section E
Structure Reports Online
ISSN 1600-5368

Bis(propane-1,2-diammonium) hexaiodoplumbate(II) trihydrate

David G. Billing* and Andreas Lemmerer

School of Chemistry, University of the Witwatersrand, Private Bag 3, PO Wits 2050, South Africa

Correspondence e-mail: andy@hobbes.gh.wits.ac.za

Key indicators

Single-crystal X-ray study
T = 173 K
Mean σ(b–I) = 0.001 Å
Disorder in main residue
R factor = 0.030
wR factor = 0.059
Data-to-parameter ratio = 27.8

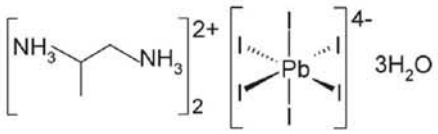
For details of how these key indicators were automatically derived from the article, see http://journals.iucr.org/e.

Received 12 April 2006
Accepted 18 April 2006

The title compound, $[NH_3CH_2CH(NH_3)CH_3]_2[PbI_6]\cdot 3H_2O$, crystallizes as an organic–inorganic hybrid, consisting of alternating inorganic and organic layers. The ionic layer consists of isolated $[PbI_6]^{4-}$ octahedra. The hydrocarbon layer has one propane-1,2-diammonium cation in the asymmetric unit which links to the ionic layer *via* hydrogen bonding. Two solvent water molecules lie between the anions and cations. The Pb atom lies on a centre of inversion.

Comment

In recent years, a significant number of organic–inorganic hybrid materials based on metal halide units have been prepared and studied; for reviews, see Papavassiliou (1997) and Mitzi (1999). It has been shown that their structures can vary considerably, ranging from systems based on isolated molecules to ones containing extended chains, as in $[Me_4N][PbI_3]$ (Contreras *et al.*, 1983), right up to two- or three-dimensional networks (Mitzi, 1999). Very few cases have been reported of the zero-dimensional form, where the metal halide units exist isolated from each other and connect *via* hydrogen bonds to the organic counter-ion. Often, water molecules are able to coordinate to the two charged components, as in $(CH_3NH_3)_4PbI_6\cdot 2H_20$ (Vincent *et al.*, 1986). We present here the crystal structure of the title compound, (I).



(I)

The unit cell of (I) contains four isolated $[PbI_6]$ octahedra and the hydrocarbon layer is comprised of propane-1,2-diammonium cations and isolated water molecules. Between the two layers, crystal cohesion is achieved by N—H···I, N—H···O, O—H···I and O—H···O hydrogen bonds.

The asymmetric unit of (I) consists of a Pb atom on a special position and three I^- ions occupying general positions. The full octahedral coordination is completed through the inversion centre at the Pb atom. The coordination geometry around the Pb atom is characterized by short and long Pb—I bonds. The Pb—I bond lengths for the I^- ions engaged in multiple hydrogen bonds are longest. Atom I1, which acts as an acceptor atom five times, has the longest bond [3.2361 (6) Å]. Atoms I2 and I3 act as acceptor atoms three times and twice, respectively, and have distances of 3.2071 (6) and 3.1935 (6) Å, respectively. The angles between *cis*-related I^-

© 2006 International Union of Crystallography
All rights reserved

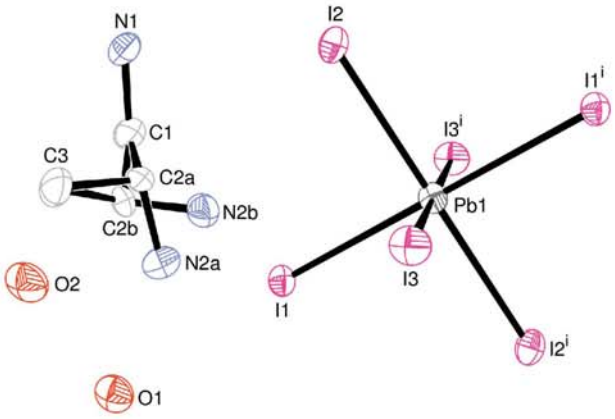


Figure 1
The asymmetric unit of (I), showing the atomic numbering scheme. Displacement ellipsoids are drawn at the 50% probability level and H atoms have been omitted. Both disorder components are shown **[Please check added text]** [Symmetry code: (i) $-x+\frac{1}{2}, -y+\frac{1}{2}, -z$.]

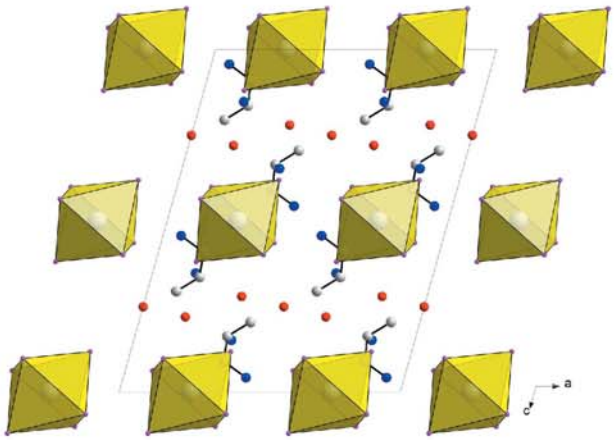


Figure 2
A packing diagram for (I).

ions deviate from 90° by 3.177 (17)° at most, whereas the *trans* angles are all 180°.

The propane-1,2-diammonium cations in the asymmetric unit occupy general positions and the atomic numbering scheme is shown in Fig. 1. The first and last C atoms of the propane chain are well ordered but the second C atom and its ammonium group are disordered.

The two ammonium groups on the propane chain display different hydrogen-bonding interactions with I^- ions and O atoms. Atom N1 is hydrogen bonded to three I^- ions *via* three normal hydrogen bonds. Atom N2, which is disordered over two positions, bridges to I^- ions and to atom O2 on one of the water molecules *via* five normal and one bifurcated hydrogen bond. Hydrogen-bonding acceptor distances range from 2.52 to 2.98 Å for the N—H···I pairs and from 1.83 to 2.49 Å for the N—H···O2 pairs. The two O atoms of the solvent water molecules form hydrogen bonds to I^- ions and O atoms. Atom O1 forms hydrogen bonds only to I1 and I3, with O1—H···I

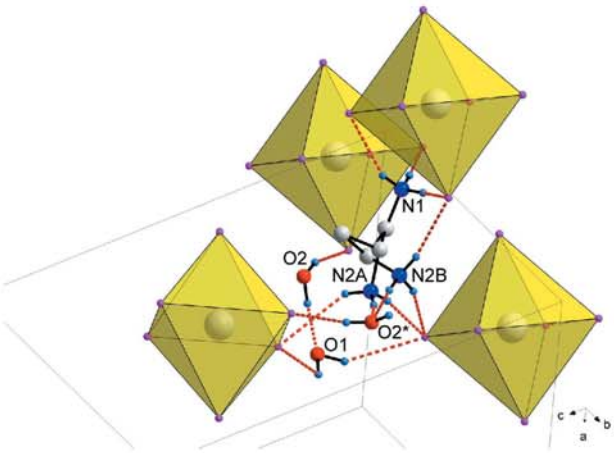


Figure 3
Hydrogen-bonding interactions (dashed lines) between the ammonium headgroups, I^- ions and O atoms. The O atom labelled with an asterisk (*) is at the symmetry position $(\frac{1}{2}-x, \frac{1}{2}+y, \frac{1}{2}-z)$.

distances of 2.93 (6) and 3.31 (9) Å, respectively. Atom O2 forms hydrogen bonds to the other water molecule (O2—H···O1 = 1.86 Å) and to I2 (2.61 Å).

Experimental

PbI_2 (0.220 g, 0.477 mmol) was dissolved in 47% HI (3 ml) in a round-bottomed flask. $NH_2CH_2CH(NH_2)CH_3$ (0.200 g, 2.70 mmol) was then added and the precipitate which formed was dissolved by refluxing for 12 h at 363 K. The solution was slowly cooled to room temperature at 2 K h^{-1}. A colourless crystal suitable for X-ray diffraction studies was selected and studied. Analysis calculated for $C_6H_{30}I_6N_4O_3Pb$: C 6.13, H 2.57, N 4.77%; found: C 6.22, H 2.56, N 4.73%.

Crystal data

$(C_3H_{12}N_2)_2[PbI_6]\cdot 3H_2O$
M_r = 1174.93
Monoclinic, $C2/c$
a = 15.093 (3) Å
b = 9.297 (2) Å
c = 19.142 (4) Å
β = 105.664 (4)°
V = 2586.3 (9) Å^3
Z = 4
D_x = 3.018 Mg m^{-3}
Mo $K\alpha$ radiation
μ = 13.69 mm^{-1}
T = 173 (2) K
Block, colourless
0.22 × 0.18 × 0.18 mm

Data collection

Bruker SMART CCD area-detector diffractometer
φ and ω scans
Absorption correction: integration (*XPREP*; Bruker, 1999)
T_{min} = 0.105, T_{max} = 0.216
8378 measured reflections
3119 independent reflections
2629 reflections with $I > 2\sigma(I)$
R_{int} = 0.050
θ_{max} = 28°

Refinement

Refinement on F^2
$R[F^2 > 2\sigma(F^2)]$ = 0.030
$wR(F^2)$ = 0.059
S = 1.05
3119 reflections
112 parameters
H-atom parameters constrained
$w = 1/[\sigma^2(F_o^2) + (0.0027P)^2 + 27.3459P]$ where $P = (F_o^2 + 2F_c^2)/3$
$(\Delta/\sigma)_{max}$ = 0.001
$\Delta\rho_{max}$ = 1.23 e Å^{-3}
$\Delta\rho_{min}$ = −1.63 e Å^{-3}

Table 1
Hydrogen-bond geometry (Å, °).

D—H···A	D—H	H···A	D···A	D—H···A
N1—H1A···I1^{i}	0.91	2.9	3.753 (5)	158
N1—H1B···I1^{ii}	0.91	2.74	3.629 (5)	167
N1—H1C···I2^{iii}	0.91	2.96	3.733 (6)	144
N2A—H2AA···O2^{iv}	0.91	1.98	2.859 (13)	164
N2A—H2AB···I1	0.91	2.52	3.416 (10)	170
N2A—H2AC···O2	0.91	2.49	3.241 (15)	140
N2A—H2AC···I3^{v}	0.91	2.98	3.681 (12)	135
N2B—H2BA···I1	0.91	2.96	3.805 (9)	155
N2B—H2BB···O2^{iv}	0.91	1.83	2.735 (10)	176
N2B—H2BC···I2^{iii}	0.91	2.84	3.718 (9)	162
O1—H11···I1^{vi}	0.95	2.93	3.755 (5)	147
O1—H11···I3^{v}	0.95	3.31	3.7684 (14)	112
O2—H21···O1	0.95	1.86	2.803 (7)	173
O2—H22···I2^{ii}	0.94	2.61	3.506 (5)	158

Symmetry codes: (i) $x-\frac{1}{2}, y-\frac{1}{2}, z$; (ii) $-x+\frac{1}{2}, -y+\frac{1}{2}, -z$; (iii) $-x, -y+1, -z$; (iv) $-x+\frac{1}{2}, y+\frac{1}{2}, -z+\frac{1}{2}$; (v) $-x+\frac{1}{2}, y-\frac{1}{2}, -z+\frac{1}{2}$; (vi) $-x+1, y, -z+\frac{1}{2}$.

All H atoms were found in a difference map. For H atoms bonded to O atoms, restraints were used to obtain reasonable values for O—H distances and H—O—H angles The 1,2-distances were restrained to 0.95 Å and the 1,3-distance to 1.5 Å using DFIX and DANG, respectively. Finally, these H atoms were refined using a riding model, with U_{iso}(H) = 1.2U_{iso}(O). H atoms bonded to C and N atoms were refined in idealized positions in the riding-model approximation, with C—H = 0.98 Å for methyl H, 0.99 Å for methylene H and 1.00 Å for methine H and N—H = 0.91 Å, and with U_{iso}(H) = 1.2U_{eq}(C) or 1.5U_{eq}(N). The conformational disorder around atoms C2 and N2 was resolved by finding alternative positions from the difference Fourier map for the respective atoms. These atoms were then refined anisotropically together with their site occupancy such that the sum of the occupancies for the two alternative atom positions equalled 1. H-atom positions were then calculated for the respective atoms using a riding model. The ratio of major to minor components is 0.580 (11):0.420 (11). The highest resudual peak is 0.70 Å from I3 and the deepest hole is 0.73 Å from I3.

Data collection: *SMART-NT* (Bruker, 1998); cell refinement: *SAINT-Plus* (Bruker, 1999); data reduction: *SAINT-Plus*; program(s) used to solve structure: *SHELXS97* (Sheldrick, 1997); program(s) used to refine structure: *SHELXL97* (Sheldrick, 1997); molecular graphics: *ORTEP-3 for Windows* (Farrugia, 1997) and *DIAMOND* (Brandenburg, 1999); software used to prepare material for publication: *WinGX* (Farrugia, 1999) and *PLATON* (Spek, 2003).

The University of the Witwatersrand is thanked for the award of a research grant and for providing the infrastructure required to do this work.

References

Brandenburg, K. (1999). *DIAMOND*. Version 2.1e. Crystal Impact GbR, Bonn, Germany.
Bruker (1998). *SMART-NT*. Version 5.050. Bruker AXS Inc., Madison, Wisconsin, USA.
Bruker (1999). *SAINT-Plus* (including *XPREP*). Version 6.02. Bruker AXS Inc., Madison, Wisconsin, USA.
Contreras, J. G., Seguel, G. V., Ungerer, B., Maier, W. F. & Hollander, F. J. (1983). *J. Mol. Struct.* **102**, 295–304.
Farrugia, L. J. (1997). *J. Appl. Cryst.* **30**, 565.
Farrugia, L. J. (1999). *J. Appl. Cryst.* **32**, 837–838.
Mitzi, D. B. (1999). *Prog. Inorg. Chem.* **48**, 1–121.
Papavassiliou, G. C. (1997). *Prog. Solid State Chem.* **25**, 125–270.
Sheldrick, G. M. (1997). *SHELXS97* and *SHELXL97*. University of Göttingen, Germany.
Spek, A. L. (2003). *J. Appl. Cryst.* **36**, 7–13.
Vincent, B. R., Robertson, K. N., Cameron, T. S. & Knop, O. (1986). *Can. J. Chem.* **65**, 1042–1046.

6.8 Octakis(3-propylammonium) octadecaiodopentaplumbate(II): a new layered structure based on layered perovskites

Journal: Acta Crystallographica Section C, Crystal Structure Communications

Date Submitted: 31 March 2006

Reference Code of Submitted Article: FG3016

Date Accepted: 20 April 2006

Final Reference: Billing, D.G., Lemmerer, A. (2006). *Acta Cryst*. C**62**, m238-m240.

Brief Synopsis

The inorganic-organic hybrid octakis(3-propylammonium) octadecaiodopentaplumbate(II) has a 2-D net-type inorganic layer motif that has not been observed before. The net-type layer is built up from corner- and face-sharing PbI_6 octahedra.

metal-organic compounds

Acta Crystallographica Section C
Crystal Structure Communications
ISSN 0108-2701

Octakis(3-propylammonium) octadecaiodopentaplumbate(II): a new layered stucture based on layered perovskites

David G. Billing* and Andreas Lemmerer

School of Chemistry, University of the Witwatersrand, Private Bag 3, PO Wits 2050, South Africa
Correspondence e-mail: andy@hobbes.gh.wits.ac.za

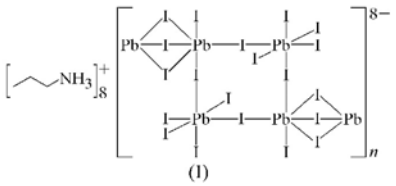
Received 31 March 2006
Accepted 20 April 2006
Online 16 May 2006

The title compound, $(C_3H_{10}N)_8[Pb_5I_{18}]$, crystallizes as an inorganic–organic hybrid. As such, the structure consists of two-dimensional sheets of corner- and face-sharing $[PbI_6]^{4-}$ octahedra, separated by layers of 3-propylammonium cations, which hydrogen bond to the I atoms. The asymmetric unit contains six independent Pb atoms; four are on general positions and the other two are on special positions, *viz*. a centre of inversion and a twofold axis. The inorganic sheets show a never before seen motif.

Comment

Compounds belonging to the hybrid system $(C_3H_7NH_3)_2[MCl_4]$ (M = Cu, Mn, Cd, Pd and Pb) have been extensively investigated for their phase behaviour (Mitzi, 1999; Depmeier, 1981; Doudin & Chapuis, 1990; Meresse & Daoud, 1989; Willett & Willett, 1977; Chapuis, 1978). The hybrid perovskites consist of inorganic semiconducting layers of $[MX_4]^{2-}$ perovskite sheets and organic ammonium cation $(RNH_3)^+$ bilayers. When trying to synthesize the compound $(C_3H_7NH_3)_2[PbI_4]$, a different inorganic motif was observed. A view of the asymmetric unit of the title compound, (I), is given in Fig. 1. Instead of the expected sheets of purely corner-sharing octahedra, the lead iodide layers can be built up from PbI_6 octahedra linked *via* corners into nominal zigzag chains that are *trans* to each other along the crystallographic *b* axis. Adjacent parallel chains are linked *via* face-shared octahedra to create infinite sheets parallel to the (201) plane through the unit cell.

Fig. 2 clearly displays the two-dimensional arrangement in which layers of 3-propylammonium molecules are embedded between two consecutive inorganic $[Pb_5I_{18}]$ sheets, forming an alternating organic–inorganic layered structure. In the direction perpendicular to the layers, the crystal cohesion is achieved by N—H···I hydrogen bridges, related to the NH_3 polar groups. There are no van der Waals forces between adjacent molecules. In the direction parallel to the layers, the cohesion is achieved by strong ionic bonds between axial and equatorial I and Pb atoms.



(I)

The inorganic layer is built up from corner- and face-sharing PbI_6 octahedra (see Fig. 3). The asymmetric unit consists of four Pb atoms on general positions that undergo corner-sharing of *cis*-related I atoms to form a square, similar to the corner-sharing hybrid perovskites. The sequence is Pb1—I5—Pb2—I9—Pb3—I14—Pb4—I18—Pb1, *i.e.* the Pb atoms are at the corners. Two of these corner-shared squares are connected to each other *via* atoms I1 and I13. This generates another square, where the sequence is now Pb1—I1—Pb2—I9—Pb3—I13—Pb4—I18—Pb1, which is at right angles to the former square because I1 is *cis* to I5 and I13 is *cis* to I14. The squares then form a zigzag sequence, running along the *b* axis. The two Pb atoms that are at opposite ends of the squares, *viz*. Pb1 and Pb3, connect adjacent zigzag squares *via* atoms Pb5 and Pb6, respectively, on special positions, by sharing faces. Atoms I2, I3 and I4 make up the face shared between atoms Pb1 and Pb5, and, similarly, atoms I10, I11 and I12 are shared by atoms Pb3 and Pb6. The Pb atoms show different degrees of distortion (Table 1). The central face-sharing atoms Pb5 and Pb6 each have three unique Pb—I bond lengths only by virtue of their special positions on a twofold axis and a centre of inversion, respectively. All six bond lengths are in a narrow

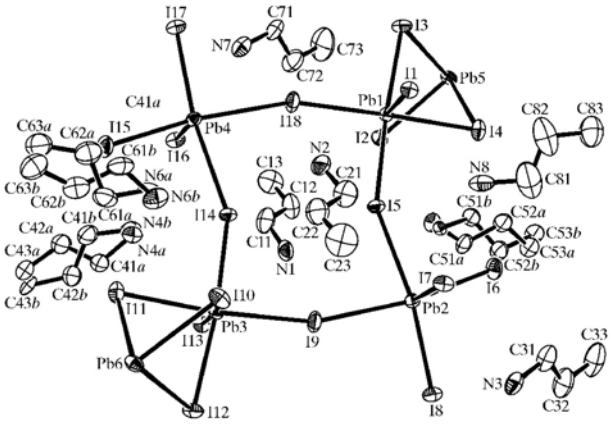


Figure 1
The asymmetric unit of (I), showing the atomic numbering scheme of the inorganic moieties and the eight organic cations. Displacement ellipsoids are shown at the 50% probability level and H atoms have been omitted for clarity.

 © 2006 International Union of Crystallography DOI: 10.1107/S0108270106014417

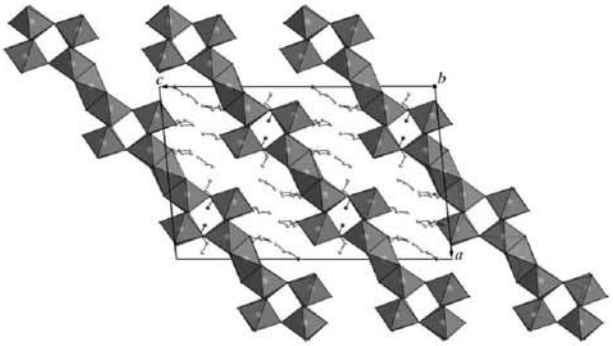


Figure 2
The packing of (I), viewed along the *b* axis.

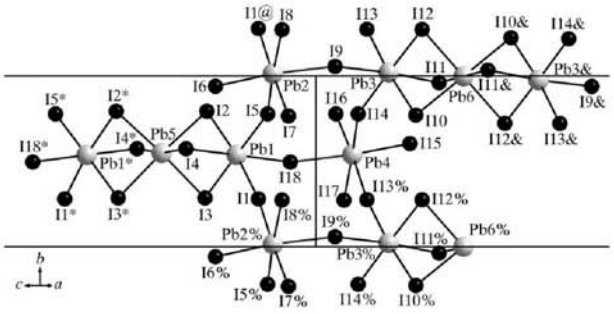


Figure 3
An illustration of the $[Pb_5I_{18}]_n^{8-}$ two-dimensional net. Atoms marked with an asterisk (*), ampersand (&), percentage sign (%) or 'at' sign (@) are at the symmetry positions $(-x, y, -z+\frac{1}{2})$, $(-x+1, -y+2, -z)$, $(x, y-1, z)$ and $(x, y+1, z)$, respectively.

range from 3.2154 (13) to 3.2486 (14) Å. The largest range of bond lengths is observed for atoms Pb2 and Pb4, which only undergo corner-sharing with three I atoms. The I atoms that are not involved in any sharing with adjacent octahedra, namely atoms I6, I7 and I8 for Pb2, and atoms I15, I16 and I17 for Pb4, have the shortest bond lengths [3.0341 (14)–3.0886 (15) Å]. In contrast, the bond lengths to the corner-shared I atoms are the longest in the structure [3.3462 (14)–3.4415 (14) Å]. The Pb1 and Pb3 octahedra, which have three I atoms involved in corner-sharing and three I atoms face-sharing, have a narrow range for all six Pb—I bonds [3.1546 (14)–3.2394 (14) Å], regardless of which type of sharing they are involved in.

There are eight crystallographically independent 3-propylammonium cations in the asymmetric unit (cat1 containing atom N1, *etc.*), which fill the gaps between the lead iodide systems; cat4, cat5 and cat6 are disordered. The cations are maximally extended with the moduli of the N—C—C—C torsion angles in the 160 (5)–179.3 (17)° range. The cations are held in place above the gaps by hydrogen-bonding interactions with the I atoms. Cat1, cat2, cat3, cat7 and cat8 have two simple N—H···I bonds and a bifurcated bond. The hydrogen bonds of the three disordered cations are also listed in Table 2. The hydrogen–acceptor distances range from 2.74 to 3.30 Å.

Experimental

PbI_2 (0.092 g, 0.200 mmol) was dissolved in 47% HI (2 ml) in a sample vial. Isopropylamine (0.026 g, 0.427 mmol) was added and the precipitate was dissolved by refluxing for 2 h at 363 K. The solution was cooled slowly at a rate of 2 K h^{-1} to room temperature. A yellow single crystal suitable for X-ray diffraction analysis was selected and studied. Analysis calculated for $C_{24}H_{80}I_{18}N_8Pb_5$: C 7.58, H 2.12, N 2.95%; found: C 7.63, H 2.27, N 3.04%

Crystal data

$(C_3H_{10}N)_8[Pb_5I_{18}]$
M_r = 3801.11
Monoclinic, $P2/c$
a = 23.988 (5) Å
b = 8.754 (5) Å
c = 37.986 (5) Å
β = 95.718 (5)°
V = 7937 (5) Å^3
Z = 4
D_x = 3.181 Mg m^{-3}
Mo $K\alpha$ radiation
μ = 17.60 mm^{-1}
T = 173 (2) K
Needle, yellow
0.44 × 0.06 × 0.06 mm

Data collection

Bruker SMART-NT CCD area-detector diffractometer
φ and ω scans
Absorption correction: integration (*XPREP*; Bruker, 1999)
T_{min} = 0.076, T_{max} = 0.392
52039 measured reflections
13878 independent reflections
9140 reflections with $I > 2\sigma(I)$
R_{int} = 0.090
θ_{max} = 25°

Refinement

Refinement on F^2
$R[F^2 > 2\sigma(F^2)]$ = 0.045
$wR(F^2)$ = 0.108
S = 1.00
13878 reflections
625 parameters
H-atom parameters constrained
$w = 1/[\sigma^2(F_o^2) + (0.0483P)^2]$ where $P = (F_o^2 + 2F_c^2)/3$
$(\Delta/\sigma)_{max}$ = 0.004
$\Delta\rho_{max}$ = 2.21 e Å^{-3}
$\Delta\rho_{min}$ = −1.85 e Å^{-3}

Table 1
Selected bond lengths (Å).

Pb1—I1	3.2345 (14)	Pb3—I12	3.1899 (14)
Pb1—I2	3.2106 (14)	Pb3—I13	3.2394 (14)
Pb1—I3	3.1546 (14)	Pb3—I14	3.2225 (14)
Pb1—I4	3.1943 (12)	Pb4—I13^{ii}	3.4333 (14)
Pb1—I5	3.2221 (14)	Pb4—I14	3.3796 (13)
Pb1—I18	3.2197 (13)	Pb4—I15	3.0699 (12)
Pb2—I1^{i}	3.4415 (14)	Pb4—I16	3.0351 (14)
Pb2—I5	3.3462 (14)	Pb4—I17	3.0788 (15)
Pb2—I6	3.0753 (12)	Pb4—I18	3.3779 (13)
Pb2—I7	3.0341 (14)	Pb5—I2	3.2154 (13)
Pb2—I8	3.0886 (15)	Pb5—I3	3.2359 (14)
Pb2—I9	3.3741 (13)	Pb5—I4	3.2486 (14)
Pb3—I9	3.1977 (13)	Pb6—I10	3.2234 (12)
Pb3—I10	3.1781 (14)	Pb6—I11	3.2397 (14)
Pb3—I11	3.2098 (13)	Pb6—I12	3.2335 (14)

Symmetry codes: (i) $x, y+1, z$; (ii) $x, y-1, z$.

H atoms bonded to C and N atoms were refined in idealized positions in the riding-model approximation, with C—H distances of 0.98 and 0.99 Å for methyl and methylene H atoms, respectively, N—H distances of 0.91 Å, and U_{iso}(H) values of $1.2U_{eq}$(C) (for CH_2 H atoms) or $1.5U_{eq}$(C,N) (for CH_3 and NH_3 H atoms). The conformational disorder around cations cat4, cat5 and cat6 was resolved by finding alternative positions from the difference Fourier map for all C

Table 2
Hydrogen-bond geometry (Å, °).

D—H···A	D—H	H···A	D···A	D—H···A
N1—H1A···I1^{i}	0.91	3.20	3.795 (13)	125
N1—H1B···I14	0.91	2.99	3.732 (13)	140
N1—H1B···I13	0.91	3.20	3.793 (13)	125
N1—H1C···I5	0.91	2.80	3.701 (13)	169
N2—H2A···I14	0.91	2.79	3.694 (15)	173
N2—H2B···I5	0.91	3.01	3.713 (14)	135
N2—H2B···I1	0.91	3.14	3.768 (15)	128
N2—H2C···I13^{ii}	0.91	3.08	3.765 (13)	133
N3—H3A···I8	0.91	2.74	3.631 (14)	166
N3—H3B···I7^{iii}	0.91	2.89	3.678 (12)	146
N3—H3B···I7	0.91	3.17	3.759 (14)	125
N3—H3C···I9^{iii}	0.91	2.76	3.623 (16)	160
N4A—H4AA···I15	0.91	2.78	3.68 (10)	174
N4A—H4AB···I17^{i}	0.91	2.97	3.70 (8)	138
N4A—H4AB···I16	0.91	3.16	3.80 (5)	130
N4A—H4AC···I13	0.91	3.02	3.77 (8)	141
N4A—H4AC···I14	0.91	3.23	3.88 (4)	130
N4B—H4BA···I17^{i}	0.91	2.67	3.56 (14)	168
N4B—H4BB···I13	0.91	3.24	3.94 (13)	136
N4B—H4BC···I15	0.91	2.93	3.66 (16)	138
N4B—H4BC···I16	0.91	3.01	3.61 (9)	125
N5A—H5AA···I1^{i}	0.91	3.04	3.83 (7)	146
N5A—H5AB···I3^{i}	0.91	2.94	3.69 (7)	142
N5A—H5AB···I2	0.91	2.93	3.52 (6)	123
N5A—H5AC···I4	0.91	3.05	3.96 (7)	179
N5B—H5BA···I1^{i}	0.91	3.16	3.79 (4)	128
N5B—H5BA···I3^{i}	0.91	3.22	3.95 (5)	139
N5B—H5BB···I2	0.91	3.10	3.85 (4)	142
N5B—H5BC···I6	0.91	2.70	3.60 (4)	168
N6A—H6AA···I12^{ii}	0.91	3.00	3.87 (7)	162
N6A—H6AB···I15	0.91	3.02	3.66 (6)	129
N6A—H6AB···I13^{ii}	0.91	3.12	3.73 (5)	126
N6A—H6AC···I11	0.91	3.03	3.77 (6)	140
N6A—H6AC···I14	0.91	3.30	3.92 (4)	127
N6B—H6BA···I11	0.91	2.93	3.71 (8)	146
N6B—H6BB···I10	0.91	2.95	3.64 (5)	134
N6B—H6BB···I12^{ii}	0.91	3.26	3.67 (8)	110
N6B—H6BC···I13^{ii}	0.91	3.08	3.88 (8)	147
N7—H7A···I17^{iv}	0.91	2.81	3.631 (15)	150
N7—H7B···I16^{iv}	0.91	2.90	3.669 (14)	144
N7—H7B···I17	0.91	3.14	3.754 (13)	127
N7—H7C···I18	0.91	2.74	3.645 (16)	171
N8—H8A···I1	0.91	2.91	3.751 (14)	154
N8—H8B···I8^{ii}	0.91	2.93	3.717 (15)	146
N8—H8B···I7	0.91	3.11	3.689 (14)	123
N8—H8C···I6	0.91	2.90	3.679 (12)	145

Symmetry codes: (i) $x, y+1, z$; (ii) $x, y-1, z$; (iii) $-x+1, y, -z+\frac{1}{2}$; (iv) $-x, -y+1, -z$.

and N atoms that make up the propylammonium chains. These atoms were then refined anisotropically together with their site occupancy such that the sum of the occupancies for the two chains summed to unity. H-atom positions were then calculated for the respective atoms using a riding model as above. For cat4 the major to minor ratio was 60:40%, for cat5 the major to minor ratio was 57:43%, and for cat6 the major to minor ratio was 54:46%.

Data collection: *SMART-NT* (Bruker, 1998); cell refinement: *SAINT-Plus* (Bruker, 1999); data reduction: *SAINT-Plus*; program(s) used to solve structure: *SHELXS97* (Sheldrick, 1997); program(s) used to refine structure: *SHELXL97* (Sheldrick, 1997); molecular graphics: *ORTEP-3 for Windows* (Farrugia, 1997) and *DIAMOND* (Brandenburg, 1999); software used to prepare material for publication: *WinGX* (Farrugia, 1999) and *PLATON* (Spek, 2002).

The authors thank the University of the Witwatersrand and the National Research Foundation of South Africa for financial support.

Supplementary data for this paper are available from the IUCr electronic archives (Reference: FG3016). Services for accessing these data are described at the back of the journal.

References

Brandenburg, K. (1999). *DIAMOND*. Version 2.1e. Crystal Impact GbR, Bonn, Germany.
Bruker (1998). *SMART-NT*. Version 5.050. Bruker AXS Inc., Madison, Wisconsin, USA.
Bruker (1999). *SAINT-Plus*. Version 6.02 (including *XPREP*). Bruker AXS Inc., Madison, Wisconsin, USA.
Chapuis, G. (1978). *Acta Cryst.* B**34**, 1506–1512.
Depmeier, W. (1981). *Acta Cryst.* B**37**, 330–339.
Doudin, B. & Chapuis, G. (1990). *Acta Cryst.* B**46**, 175–180.
Farrugia, L. J. (1997). *J. Appl. Cryst.* **30**, 565.
Farrugia, L. J. (1999). *J. Appl. Cryst.* **32**, 837–838.
Meresse, A. & Daoud, A. (1989). *Acta Cryst.* C**45**, 194–196.
Mitzi, D. B. (1999). *Prog. Inorg. Chem.* **48**, 1–121.
Sheldrick, G. M. (1997). *SHELXS97* and *SHELXL97*. University of Göttingen, Germany.
Spek, A. L. (2002). *PLATON*. Utrecht University, The Netherlands.
Willett, R. D. & Willett, J. J. (1977). *Acta Cryst.* B**33**, 1639–1641.

6.9 *catena*-Poly[bis(*tert*-butylammonium) [plumbate(II)-tri-μ-iodo] iodide dihydrate]

Journal: Acta Crystallographica Section C, Crystal Structure Communications

Date Submitted: 24 April 2006

Reference Code of Submitted Article: GD3019

Date Accepted: 2 May 2006

Final Reference: Billing, D.G., Lemmerer, A. (2006). *Acta Cryst.* C**62**, m264-m266.

Brief Synopsis

The inorganic-organic hybrid bis(tert-butylammonium) triiodoplumbate(II) iodide dihydrate has 1-D chains of face-sharing PbI_6 octahedra. This compound appeared on the cover of the June issue of Acta Crystallographica C.

ISSN 0108-2701

Volume 62

Part 6

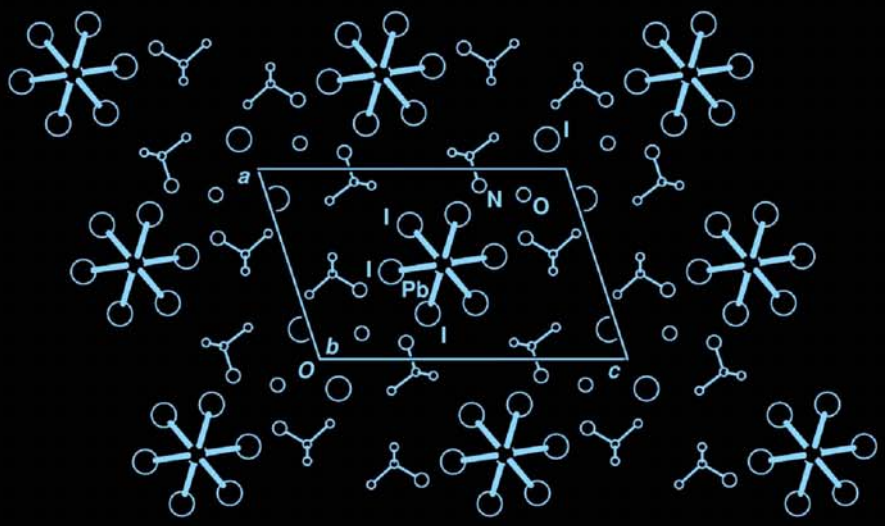
June 2006

Acta Crystallographica Section C

Crystal Structure Communications

Editor: George Ferguson

catena-Poly[bis(*tert*-butylammonium) [plumbate(II)-tri-μ-iodo] iodide dihydrate]: anionic $[PbI_3]^-$ chains and iodide ions in four-cation channels



Inorganic compounds

Metal-organic compounds

Organic compounds

journals.iucr.org
International Union of Crystallography
Blackwell Munksgaard

metal-organic compounds

Acta Crystallographica Section C
Crystal Structure Communications
ISSN 0108-2701

catena-Poly[bis(*tert*-butylammonium) [plumbate(II)-tri-μ-iodo] iodide dihydrate]

David G. Billing* and A. Lemmerer

School of Chemistry, University of the Witwatersrand, Private Bag 3, PO Wits 2050, South Africa
Correspondence e-mail: andy@hobbes.gh.wits.ac.za

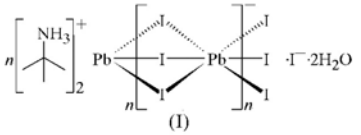
Received 24 April 2006
Accepted 2 May 2006
Online 24 May 2006

The title compound, $\{(C_4H_{12}N)_2[PbI_3]I{\cdot}2H_2O\}_n$, crystallizes as an organic–inorganic hybrid. The six-coordinate Pb atom lies on a centre of inversion and all the I atoms lie on mirror planes; the two independent cations both lie across mirror planes. The structure contains anionic chains along [100] of fused $[PbI_3]^-$ units forming face-sharing octahedra. Four cations enclose channels occupied by isolated iodide ions and water molecules of hydration.

Comment

In recent years, a significant number of organic–inorganic hybrid materials based on metal halide units have been prepared and studied; for reviews, see Papavassiliou (1997) and Mitzi (1999). Haloplumbates in particular have demonstrated a propensity for forming a great variety of crystalline structures by self-assembling from suitable solution mixtures. It has been shown that their structures can vary considerably, ranging from systems based on isolated molecules to systems containing extended chains, as in $(Me_4N)[PbI_3]$ (Contreras *et al.*, 1983), right up to two- or three-dimensional networks (Mitzi, 1999). For systems containing extended chains, these chains may be formed by one, two or three bridging halides. A search of the Cambridge Structural Database (Version 5.27, November 2005 release; Allen 2002) indicated that most crystal structures with tertiary butylammonium groups have isolated octahedra, as in $SnCl_6$ (Ghozlen *et al.*, 1991), $TeCl_6$ (Ishida & Kashino, 1992) and $TeBr_6$ (Baker *et al.*, 1995), or isolated $SnCl_4$ tetrahedra (Ishida & Kashino, 1993). To the best of our knowledge, only two structures have a one-dimensional system, *viz.* $(C_4H_{12}N)_2Sb_2Cl_8$, which has edge-sharing chains of square-pyramidal $SbCl_5$ (Belz *et al.*, 1992) units, and $[(t\text{-}C_4H_{12}N)CdBr_3]_2{\cdot}H_2O$, which has edge-sharing chains of trigonal-bipyramidal $CdBr_5$ units (Ishihara *et al.*, 1999).

The title compound, (I), has a one-dimensional arrangement in which chains of face-sharing PbI_6 octahedra run along the unit cell (see Fig. 1). The channels in between the chains are occupied by *tert*-butylammonium molecules, an isolated I atom on a mirror plane at $y = \frac{1}{4}$ (I4), and water molecules of hydration (Fig. 2). In the direction perpendicular to the chains, the crystal cohesion is achieved by N—H···I, N—H···O and O—H···I hydrogen bridges. In the direction parallel to the chains, the cohesion is achieved by strong ionic bonds between the I and Pb atoms.



(I)

The inorganic motif is built up from characteristic face-sharing PbI_6 octahedra, which form infinite chains along the *b* axis. One unique inorganic chain runs through the centre of the unit cell. The asymmetric unit consists of a Pb atom on a centre of inversion and three I atoms, all on special positions, with I1 and I3 lying on the mirror plane at $y = \frac{3}{4}$ and I2 on the

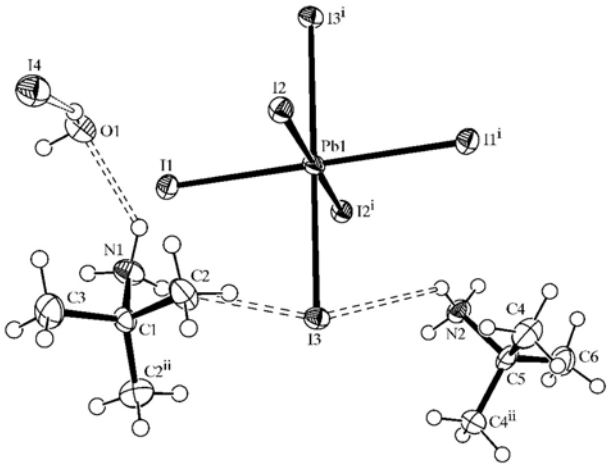


Figure 1
The asymmetric unit of (I), showing the atomic numbering scheme. Displacement ellipsoids are shown at the 50% probability level. The H atoms on N1 and N2 are disordered and only one set is shown at each site. [Symmetry codes: (i) $-x+1, -y+1, -z+1$; (ii) $x, -y+\frac{3}{2}, z$.]

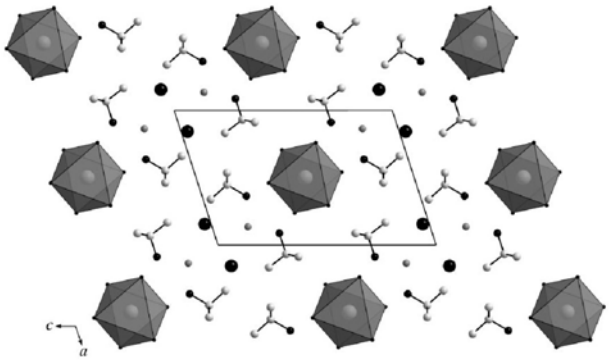


Figure 2
The packing of (I), viewed along the *b* axis.

 © 2006 International Union of Crystallography DOI: 10.1107/S0108270106016167

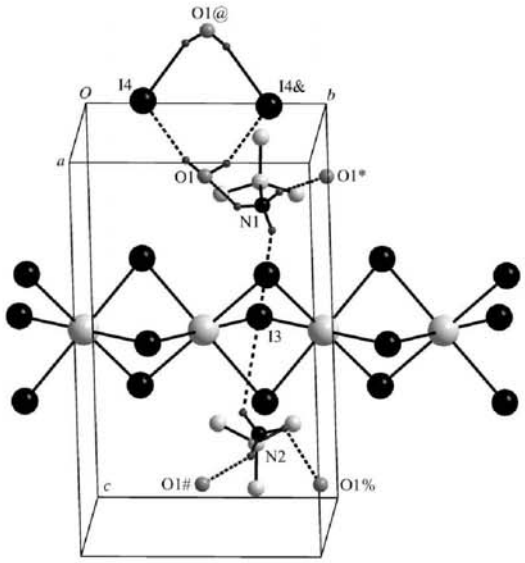


Figure 3
A magnified view of the face-sharing PbI_6 octahedra and hydrogen-bonding scheme. Atoms labelled with an ampersand (&), a percentage sign (%), a hash (#), an asterisk (*) and an 'at' sign (@) are at the symmetry positions $(-x, y+\frac{1}{2}, z)$, $(-x+1, y+\frac{1}{2}, -z+1)$, $(-x+1, -y+1, -z+1)$, $(x, -y+\frac{3}{2}, z)$ and $(-x, -y+1, -z)$, respectively.

mirror plane at $y = \frac{1}{4}$. Within the chains, the shared face consists of these three halides. The octahedra are somewhat distorted, with all three unique Pb—I distances different (Table 1), while the bond angles between *cis* ligands range from 83.346 (16) to 96.654 (16)°.

There are two unique *tert*-butylammonium cations in the asymmetric unit, labelled cat1 (containing atom N1) and cat2 (containing atom N2). In cat1, atoms N1, C1 and C3 lie on the mirror plane at $y = \frac{3}{4}$ and atom C2 occupies a general position. In cat2, atoms N2, C5 and C6 lie on the mirror plane at $y = \frac{1}{4}$, with atom C4 in a general position.

The two unique cations in the asymmetric unit interact with the inorganic chains *via* long N—H···I3 hydrogen bridges; the distances are 3.21 and 3.25 Å, respectively, for cat1 and cat2 (Table 2 and Fig. 3). The last two H atoms on the ammonium head groups bridge to the O atom of the water molecule of hydration. The N—H···O distances range from 2.05 to 2.48 Å. Lastly, the H atoms on the water molecule bridge towards the isolated I atom to form a symmetrical ring with graph-set notation $R_2^2(8)$, with donor–acceptor distances of 2.73 and 2.78 Å.

Experimental

PbI_2 (0.126 g, 0.273 mmol) was dissolved in 47% HI (2 ml) in a sample vial. Thereafter, $C(CH_3)_3NH_2$ (0.050 g, 0.684 mmol) was added and the precipitate was dissolved by refluxing for 12 h at 363 K. The solution was cooled slowly to room temperature at a rate of 2 K h^{-1}. A yellow single crystal suitable for X-ray diffraction analysis was selected and studied. Analysis calculated for $C_8H_{28}I_4N_2O_2Pb$: C 10.7, H 3.1, N 3.1%; found: C 10.8, H 3.3, N 3.2%.

Crystal data

$(C_4H_{12}N)_2[PbI_3]I\cdot 2H_2O$	$Z = 2$
$M_r = 899.11$	$D_x = 2.673$ Mg m^{-3}
Monoclinic, $P2_1/m$	Mo $K\alpha$ radiation
$a = 9.7917$ (10) Å	$\mu = 13.08$ mm^{-1}
$b = 7.9649$ (8) Å	$T = 173$ (2) K
$c = 15.0594$ (16) Å	Needle, yellow
$\beta = 107.985$ (3)°	0.28 × 0.1 × 0.09 mm
$V = 1117.1$ (2) $Å^3$	

Data collection

Bruker SMART CCD area-detector diffractometer	5842 measured reflections
φ and ω scans	2878 independent reflections
Absorption correction: integration (*XPREP*; Bruker, 1999)	2416 reflections with $I > 2\sigma(I)$
$T_{min} = 0.174$, $T_{max} = 0.388$	$R_{int} = 0.074$
	$\theta_{max} = 28°$

Refinement

Refinement on F^2	$w = 1/[\sigma^2(F_o^2) + (0.0497P)^2 + 0.2377P]$ where $P = (F_o^2 + 2F_c^2)/3$
$R[F^2 > 2\sigma(F^2)] = 0.039$	$(\Delta/\sigma)_{max} = 0.001$
$wR(F^2) = 0.101$	$\Delta\rho_{max} = 2.67$ e $Å^{-3}$
$S = 1.07$	$\Delta\rho_{min} = -2.32$ e $Å^{-3}$
2878 reflections	
96 parameters	
H-atom parameters constrained	

Table 1
Selected geometric parameters (Å, °).

Pb1—I3	3.1953 (5)	Pb1—I2	3.2355 (6)
Pb1—I1	3.2263 (6)		
I3—Pb1—I1^{i}	92.706 (16)	I3—Pb1—I2	93.491 (15)
I3—Pb1—I1	87.294 (16)	I1—Pb1—I2	96.654 (16)
I3—Pb1—I2^{i}	86.509 (15)	I1—Pb1—I2^{i}	83.346 (16)

Symmetry code: (i) $-x+1, -y+1, -z+1$.

Table 2
Hydrogen-bond geometry (Å, °).

D—H···A	D—H	H···A	D···A	D—H···A
N1—H1A···I3	0.91	3.21	4.016 (10)	148
N1—H1B···O1	0.91	2.21	2.936 (9)	136
N1—H1C···O1^{ii}	0.91	2.05	2.936 (9)	164
N2—H2A···O1^{i}	0.91	2.16	2.958 (9)	147
N2—H2B···I3	0.91	3.25	3.905 (10)	131
N2—H2C···O1^{iii}	0.91	2.48	2.958 (9)	113
O1—H2···I4	0.86	2.73	3.572 (6)	165
O1—H1···I4^{iv}	0.86	2.78	3.570 (6)	154

Symmetry codes: (i) $-x+1, -y+1, -z+1$; (ii) $x, -y+\frac{3}{2}, z$; (iii) $-x+1, y+\frac{1}{2}, -z+1$; (iv) $-x, -y+1, -z$.

All H were found in a difference map. For the H atoms bonded to O atoms, restraints were used to obtain reasonable O—H distances and H—O—H angles. Finally, these H atoms were refined using a riding model [U_{iso}(H) = 1.2U_{eq}(O)]. H atoms bonded to C and N atoms were refined in idealized positions using the riding-model approximation, with C—H distances of 0.98 Å, N—H distances of 0.91 Å and U_{iso}(H) values of 1.5U_{eq}(C,N). The highest residual peak is 0.83 Å from atom Pb1.

Data collection: *SMART-NT* (Bruker, 1998); cell refinement: *SAINT-Plus* (Bruker, 1999); data reduction: *SAINT-Plus*; program(s) used to solve structure: *SHELXS97* (Sheldrick, 1997); program(s) used to refine structure: *SHELXL97* (Sheldrick, 1997); molecular graphics: *ORTEP-3 for Windows* (Farrugia, 1997) and *DIAMOND* (Brandenburg, 1999); software used to prepare material for publication: *WinGX* (Farrugia, 1999) and *PLATON* (Spek, 2003).

The University of the Witwatersrand and the National Research Fund are thanked for the award of a research grant and for providing the infrastructure required to carry out this work.

Supplementary data for this paper are available from the IUCr electronic archives (Reference: GD3019). Services for accessing these data are described at the back of the journal.

References

Allen, F. H. (2002). *Acta Cryst.* B**58**, 380–388.
Baker, L.-J., Rickard, C. E. F. & Taylor, M. J. (1995). *Polyhedron*, **14**, 401–405.
Belz, J., Weber, R., Roloff, A. & Ross, B. (1992). *Z. Kristallogr.* **202**, 281–282.
Brandenburg, K. (1999). *DIAMOND*. Version 2.1e. Crystal Impact GbR, Bonn, Germany.
Bruker (1998). *SMART-NT*. Version 5.050. Bruker AXS Inc., Madison, Wisconsin, USA.
Bruker (1999). *SAINT-Plus*. Version 6.02 (including *XPREP*). Bruker AXS Inc., Madison, Wisconsin, USA.
Contreras, J. G., Seguel, G. V., Ungerer, B., Maier, W. F. & Hollander, F. J. (1983). *J. Mol. Struct.* **102**, 295–304.
Farrugia, L. J. (1997). *J. Appl. Cryst.* **30**, 565.
Farrugia, L. J. (1999). *J. Appl. Cryst.* **32**, 837–838.
Ghozlen, M. H. B., Daoud, A. & Pabst, I. (1991). *J. Solid State Chem.* **93**, 77–81.
Ishida, H. & Kashino, S. (1992). *Acta Cryst.* C**48**, 1673–1675.
Ishida, H. & Kashino, S. (1993). *Acta Cryst.* C**49**, 2117–2119.
Ishihara, H., Horiuchi, K., Dou, S., Gesing, T. M., Buhl, J.-C., Paulus, H., Svoboda, I. & Fuess, H. (1999). *Z. Naturforsch. Teil A*, **54**, 628–636.
Mitzi, D. B. (1999). *Prog. Inorg. Chem.* **48**, 1–121.
Papavassiliou, G. C. (1997). *Prog. Solid State Chem.* **25**, 125–270.
Sheldrick, G. M. (1997). *SHELXS97* and *SHELXL97*. University of Göttingen, Germany.
Spek, A. L. (2003). *J. Appl. Cryst.* **36**, 7–13.

6.10 Poly[bis[2-(1-cyclohexenyl)ethylammonium] di-μ-iodo-diodoplumbate(II)]

Journal: Acta Crystallographica Section C, Crystal Structure Communications

Date Submitted: 20 March 2006

Reference Code of submitted article: TR3004

Date Accepted: 18 April 2006

Final Reference: Billing, D.G., Lemmerer, A. (2006). *Acta Cryst.* C**62**, m269-m271.

Brief Synopsis

The inorganic-organic hybrid bis(2-(1-cyclohexenyl)ethylammonium) tetraiodoplumbate(II) has a layered perovskite-type motif.

Acta Crystallographica Section C
Crystal Structure Communications
ISSN 0108-2701

Poly[bis[2-(1-cyclohexenyl)ethylammonium] di-μ-iodo-diodoplumbate(II)]

David G. Billing* and Andreas Lemmerer

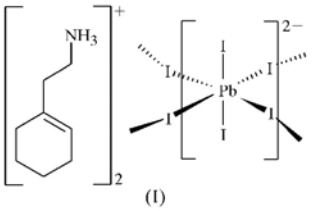
School of Chemistry, University of the Witwatersrand, Private Bag 3, PO Wits 2050, South Africa
Correspondence e-mail: andy@hobbes.gh.wits.ac.za

Received 20 March 2006
Accepted 18 April 2006
Online 15 June 2006

The title compound, $(C_8H_{16}N)_2[PbI_4]$, crystallizes as an inorganic–organic hybrid perovskite, adopting the unusual $2a_p \times 2a_p$ superstructure. As such, the structure consists of two-dimensional sheets of corner-sharing PbI_6 octahedra in the *ab* plane, separated by bilayers of 2-(1-cyclohexenyl)ethylammonium cations. The ethylammonium groups are not in the plane of the cyclohexenyl rings.

Comment

The hybrid perovskites $(C_6H_5C_2H_4NH_3)_2[PbX_4]$ (X = Cl, Br and I) have been investigated extensively for their photoluminescence, electroluminescence and non-linear optical properties (Mitzi, 1999*a*, and references therein). The hybrid perovskites are natural quantum-well structures as they consist of inorganic semiconducting layers of $[MX_4]^{2-}$ perovskite sheets and organic ammonium cation $(R{-}NH_3)^+$ bilayers. Highly efficient electroluminescence has been found in the related materials $(C_6H_5C_4H_8NH_3)_2[PbI_4]$ and $(C_6H_9C_2H_4NH_3)_2[PbI_4]$ (Hattori *et al.*, 1996). The latter and the title compound, (I), which contains a six-membered ring with a C=C bond, showed high luminescence, exceeding 4000 cd m^{-2}. The reason for the high electroluminescence observed is the nature of the organic carrier transport material, in this case the $C_6H_9C_2H_4NH_3^+$ cation (Hattori *et al.*, 1996). In this study, we present the detailed crystal structure of the hybrid perovskite (I) (Fig. 1).



(I)

Fig. 2 clearly underlines a bidimensional arrangement in which two layers of non-interdigitated 2-(1-cyclohexenyl)-ethylammonium ions are embedded between two consecutive inorganic PbI_6 sheets, forming an alternated inorganic–organic layered structure. The Pb atoms are aligned from layer to layer, resulting in an eclipsed arrangement of adjacent layers. In the direction perpendicular to the layers, the crystal cohesion is achieved at one end of the organic molecules by N—H···I hydrogen bridges, related to the NH_3 polar groups. There are van der Waals forces between molecules [the nearest neighbor distance is 3.792 (18) Å]. In the direction parallel to the layers, the cohesion is achieved by strong ionic bonds between equatorial I and Pb atoms, giving the classical perovskite structural arrangement. An interesting feature of this hybrid perovskite is that the triclinic unit-cell dimensions parallel to the perovskite layers are twice the simple cubic perovskite lattice parameter of $(CH_3NH_3)[PbI_3]$ [a_p = 6.3285 (4) Å; Mitzi, 1999*b*]. Most layered inorganic–organic hybrid perovskites show the $2^{1/2}a_p \times 2^{1/2}a_p$ superstructure not the unusual $2a_p \times 2a_p$ structure observed here (Mitzi, 1999*b*).

The inorganic layer is built up from characteristic corner-sharing PbI_6 octahedra. The asymmetric unit consists of Pb atoms, Pb1 and Pb2, on general positions and eight I atoms, *viz.* atoms I1–I4 occupying the axial positions and I5–I8

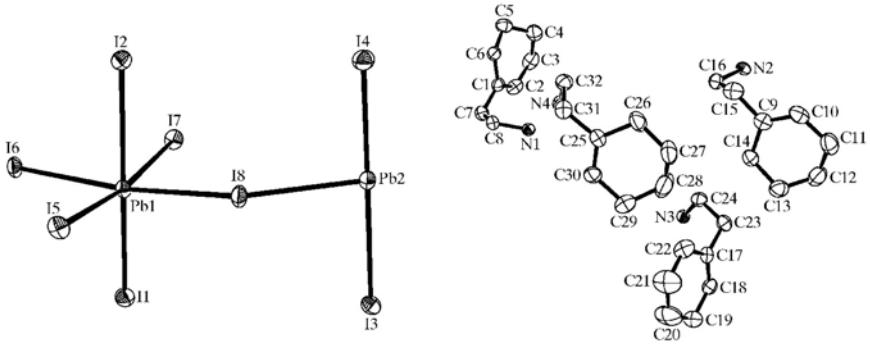


Figure 1
The asymmetric unit of (I), showing the atomic numbering schemes for the inorganic anion (left) and for the organic cations (right). Displacement ellipsoids are shown at the 50% probability level and H atoms have been omitted for clarity.

 DOI: 10.1107/S0108270106013953 © 2006 International Union of Crystallography

occupying the equatorial positions in the octahedra. The four equatorial I atoms are corner-shared by neighboring octahedra. As shown in the projection perpendicular to the layers, along the *c* axis, the PbI_6 octahedra are rotated relative to each other (Fig. 3). The degree of rotation ranges from 148.632 (15) to 150.948 (15)°, as there are four different bridging I atoms. Furthermore, the perovskite layers are corrugated. The tilt angle is 2.462° for Pb1 and 2.543° for Pb2. The coordination geometry around the Pb atoms shows axial compression of the octahedral geometry, with the bridging distances longer than the axial distances. The bridging lead–iodine bond distances are in a narrow range for both Pb1 and Pb2 [3.1626 (5)–3.1858 (5) Å; Table 1]. The longest bond distances are to the axial atoms I2 and I3 [3.3889 (6) and 3.3947 (6) Å, respectively], whereas the shortest distances are to the I atoms *trans* to them, *viz.* I1 [3.0626 (6) Å] and I4 [3.0622 (6) Å]. The size of the parallelograms that make up the voids depends on which bridging I atoms are used. There are four unique voids and the edge lengths range from 4.427 (12) to 4.556 (12) Å. The bond angles between *cis*- and *trans*-related I atoms within the octahedra all deviate from ideality. The *cis* angles range from 84.050 (13) to 96.074 (16)°. The *trans* angles between the bridging I atoms deviate more from 180° [171.223 (13)–172.639 (14)°] than those between the axial halides [179.490 (12) and 179.558 (12)°].

There are four unique 2-(1-cyclohexenyl)ethylammonium molecules in the asymmetric unit and their atomic numbering schemes are shown in Fig. 1. All four amine groups are well ordered between the layers; these groups are labeled cat1 (containing atom N1), cat2 (N2), cat3 (N3) and cat4 (N4). Three of the 1-cyclohexenyl rings are not planar. The r.m.s. deviation from the planes is 0.3041 (1) Å for cat1, 0.3095 (1) Å for cat2, 0.2591 (1) Å for cat3 and the least for cat4 [0.0586 (1) Å]. When viewing the cations perpendicular to the 1-cyclohexenyl rings, with the ethylammonium groups pointing towards you, they are bent towards the right for cat1, cat2 and cat4, and to the left for cat3. The direction is always to the side with the double bond. Futhermore, the terminal ethylammonium C and N atoms are not in the plane of the ring but in a J-shaped conformation, similar to the phenylethylammonium molecules in $(C_6H_5C_2H_4NH_3)_2[PbCl_4]$ (Mitzi, 1999*a*). Consequently, the 1-cyclohexenyl rings are slanted towards the layers (33.916, 35.053, 37.179 and 37.994°, respectively, for cat1–cat4).

The hydrogen bridges (Table 2) between the organic and inorganic entities adopt the terminal configuration for all four unique ammonium groups, *i.e.* two H atoms bond to axial I atoms and the third H atom to a bridging I atom (see Fig. 4). The H···*A* distances to the terminal halides range from 2.75 to 2.93 Å and to the bridging halides from 2.78 to 2.84 Å.

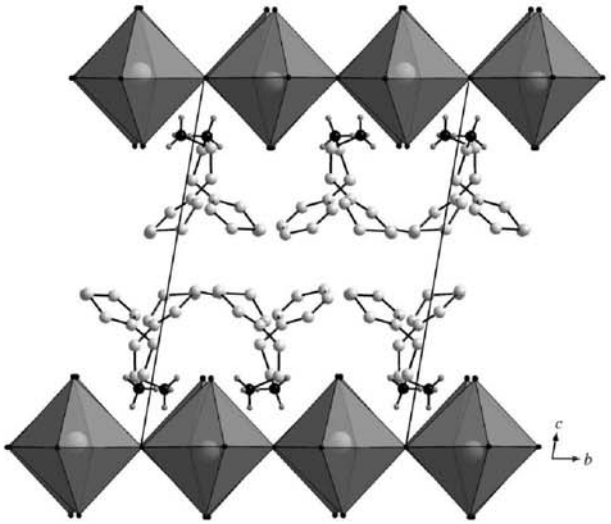


Figure 2
A packing diagram of (I), viewed along the *a* axis.

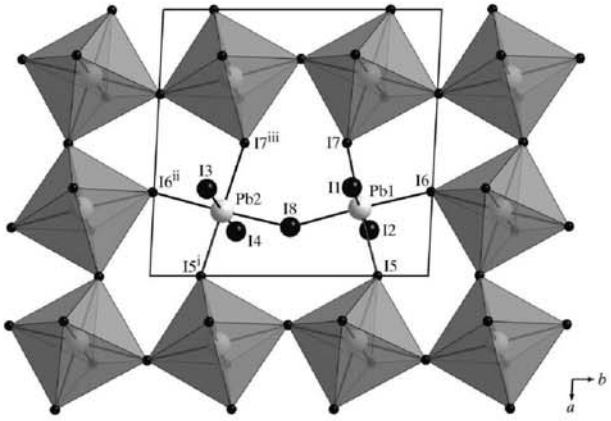


Figure 3
An illustration of the two-dimensional PbI_6 sheets, viewed down the *c* axis. The symmetry codes are as in Table 1.

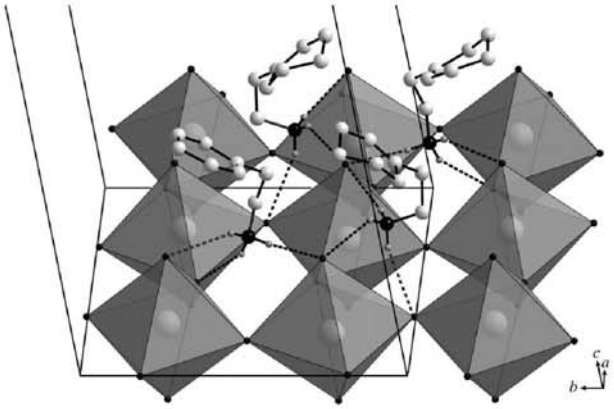


Figure 4
Hydrogen bridging interactions (dashed lines) between the ammonium heads and the halogen atoms of (I).

Experimental

PbI_2 (0.101 g, 0.219 mmol) was dissolved in 47% HI (4 ml) in a sample vial. 2-(1-Cyclohexenyl)ethylamine (0.055 g, 0.454 mmol) was added and the precipitate was dissolved with methanol (9 ml). Crystals where grown by slow evaporation over a period of a few days. An orange single crystal suitable for X-ray diffraction analysis was selected and studied. Analysis calculated for $C_{16}H_{32}I_4N_2Pb$: C 19.87, H 3.33, N 2.90%; found: C 19.81, H 3.19, N 3.00%.

Crystal data

$(C_8H_{16}N)_2[PbI_4]$
M_r = 967.23
Triclinic, $P\overline{1}$
a = 12.2053 (11) Å
b = 12.3053 (11) Å
c = 18.3182 (17) Å
α = 80.629 (6)°
β = 72.455 (6)°
γ = 89.961 (6)°
V = 2584.8 (4) Å^3
Z = 4
D_x = 2.485 Mg m^{-3}
Mo $K\alpha$ radiation
μ = 11.31 mm^{-1}
T = 173 (2) K
Plate, orange
0.48 × 0.44 × 0.04 mm

Data collection

Bruker SMART CCD area-detector diffractometer
φ and ω scans
Absorption correction: integration (*XPREP*; Bruker, 1999)
T_{min} = 0.03, T_{max} = 0.570
42465 measured reflections
12456 independent reflections
10208 reflections with $I > 2\sigma(I)$
R_{int} = 0.075
θ_{max} = 28°

Refinement

Refinement on F^2
$R[F^2 > 2\sigma(F^2)]$ = 0.035
$wR(F^2)$ = 0.093
S = 1.05
12456 reflections
415 parameters
H-atom parameters constrained
$w = 1/[\sigma^2(F_o^2) + (0.0373P)^2 + 9.0173P]$ where $P = (F_o^2 + 2F_c^2)/3$
$(\Delta/\sigma)_{max}$ = 0.002
$\Delta\rho_{max}$ = 1.26 e Å^{-3}
$\Delta\rho_{min}$ = −3.13 e Å^{-3}

Table 1
Selected interatomic distances (Å).

Pb1—I1	3.0626 (6)	Pb2—I4	3.0622 (6)
Pb1—I7	3.1636 (5)	Pb2—I5^{i}	3.1626 (5)
Pb1—I5	3.1772 (5)	Pb2—I7^{iii}	3.1750 (5)
Pb1—I6	3.1843 (5)	Pb2—I8	3.1848 (5)
Pb1—I8	3.1858 (5)	Pb2—I6^{ii}	3.1856 (5)
Pb1—I2	3.3889 (6)	Pb2—I3	3.3947 (6)

Symmetry codes: (i) $-x+2, -y+1, -z$; (ii) $x, y-1, z$; (iii) $-x+1, -y+1, -z$.

H atoms were refined in idealized positions in the riding-model approximation, with C—H = 0.95 (CH) and 0.99 Å (CH_2), and N—H = 0.91 Å [U_{iso}(H) = 1.2U_{eq}(C) and 1.5U_{eq}(N)]. The highest residual peak is 1.96 Å from atom H1*A*.

Table 2
Hydrogen-bond geometry (Å, °).

D—H···A	D—H	H···A	D···A	D—H···A
N1—H1*A*···I6	0.91	2.84	3.649 (5)	149
N1—H1*B*···I2	0.91	2.92	3.683 (5)	142
N1—H1*C*···I3^{iii}	0.91	2.78	3.656 (5)	161
N2—H2*A*···I8	0.91	2.83	3.644 (5)	150
N2—H2*B*···I3	0.91	2.93	3.685 (5)	142
N2—H2*C*···I2^{i}	0.91	2.79	3.659 (5)	160
N3—H3*A*···I7	0.91	2.78	3.628 (6)	155
N3—H3*B*···I4^{iii}	0.91	2.83	3.626 (5)	148
N3—H3*C*···I2^{iii}	0.91	2.76	3.644 (5)	166
N4—H4*A*···I5	0.91	2.78	3.623 (6)	154
N4—H4*B*···I3^{iv}	0.91	2.75	3.647 (6)	167
N4—H4*C*···I1	0.91	2.82	3.626 (5)	148

Symmetry codes: (i) $-x+2, -y+1, -z$; (iii) $-x+1, -y+1, -z$; (iv) $x, y+1, z$.

Data collection: *SMART-NT* (Bruker, 1998); cell refinement: *SMART-NT*; data reduction: *SAINT-Plus* (Bruker, 1999); program(s) used to solve structure: *SHELXS97* (Sheldrick, 1997); program(s) used to refine structure: *SHELXL97* (Sheldrick, 1997); molecular graphics: *ORTEP-3 for Windows* (Farrugia, 1997) and *DIAMOND* (Brandenburg, 1999); software used to prepare material for publication: *WinGX* (Farrugia, 1999) and *PLATON* (Spek, 2003).

The University of the Witwatersrand is thanked for the award of a research grant and for providing the infrastructure required to carry out this work.

Supplementary data for this paper are available from the IUCr electronic archives (Reference: TR3004). Services for accessing these data are described at the back of the journal.

References

Brandenburg, K. (1999). *DIAMOND*. Version 2.1e. Crystal Impact GbR, Bonn, Germany.
Bruker (1998). *SMART-NT*. Version 5.050. Bruker AXS Inc., Madison, Wisconsin, USA.
Bruker (1999). *SAINT-Plus*. Version 6.02 (including *XPREP*). Bruker AXS Inc., Madison, Wisconsin, USA.
Farrugia, L. J. (1997). *J. Appl. Cryst.* **30**, 565.
Farrugia, L. J. (1999). *J. Appl. Cryst.* **32**, 837–838.
Hattori, T., Taira, T., Era, M., Tsutsui, T. & Saito, S. (1996). *Chem. Phys. Lett.* **254**, 103–108.
Mitzi, D. B. (1999*a*). *J. Solid State Chem.* **145**, 694–704.
Mitzi, D. B. (1999*b*). *Prog. Inorg. Chem.* **48**, 1–121.
Sheldrick, G. M. (1997). *SHELXL97* and *SHELXS97*. University of Göttingen, Germany.
Spek, A. L. (2003). *J. Appl. Cryst.* **36**, 7–13.

6.11 Two packing motifs based upon chains of edge-sharing PbI_6 octahedra

Journal: Acta Crystallographica Section C, Crystal Structure Communications

Date Submitted: 18 August 2006

Reference Code of Submitted Article: AV3041

Date Accepted: 27 September 2006

Final Reference: Billing, D.G., Lemmerer, A. (2006). *Acta Cryst*. C**62**, m597-m601.

Brief Synopsis

The inorganic-organic hybrids bis(*p*-phenylenediammonium)tetraiodoplumbate(II) and bis(3,5-dimethylanilinium)tetraiodoplumbate(II) have 1-D chains of edge-sharing PbI_6 octahedra. These two compounds were the only inorganic-organic hybrids found in this work with that motif.

metal-organic compounds

Acta Crystallographica Section C
Crystal Structure Communications
ISSN 0108-2701

Two packing motifs based upon chains of edge-sharing PbI_6 octahedra

Andreas Lemmerer* and David G. Billing

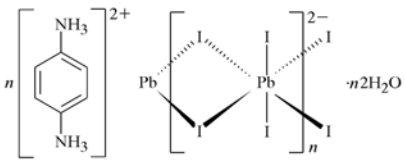
Molecular Sciences Institute, School of Chemistry, University of the Witwatersrand, Private Bag 3, PO Wits 2050, South Africa
Correspondence e-mail: andy@hobbes.gh.wits.ac.za

Received 18 August 2006
Accepted 27 September 2006
Online 22 November 2006

The compounds *catena*-poly[*p*-phenylenediammonium [[di-iodolead(II)]-di-μ-iodo] dihydrate], $\{(C_6H_{10}N_2)[PbI_4]\cdot 2H_2O\}_n$, (I), and *catena*-poly[bis(3,5-dimethylanilinium) [[di-iodolead(II)]-di-μ-iodo]], $\{(C_8H_{12}N)_2[PbI_4]\}_n$, (II), crystallize as organic–inorganic hybrids. As such, the structures consist of chains of $[PbI_2]^-$ units extending along the *c* axis in (I) and along the *b* axis in (II). The asymmetric unit in (I) contains one Pb atom on a site of 2/*m* symmetry, two I atoms and a water molecule on mirror planes, and a *p*-phenylenediammonium molecule that sits around a site of 2/*m* symmetry with the C and N atoms on a mirror plane. In (II), the Pb atom is on a twofold axis and the two I atoms are on general positions. Each Pb atom is octahedrally coordinated to six I atoms, arranged as chains of edge-sharing octahedra. Both compounds undergo hydrogen-bonding interactions between the ammonium groups and the I atoms. In addition, there are hydrogen bonds between the water molecules and the ammonium groups and halides in (I), and between the ammonium groups and the ring systems in (II).

Comment

In recent years, a significant number of organic–inorganic hybrid materials based on metal halide units have been prepared and studied. Haloplumbates in particular have demonstrated a propensity for forming a great variety of crystalline structures by self-assembly from suitable solution mixtures. It has been shown that their structures can vary considerably, ranging from systems based on isolated inorganic polyhedra (Billing & Lemmerer, 2006*a*) to ones containing extended chains, as in $(C_4H_{12})_2[PbI_3]I\cdot 2H_2O$ (Billing & Lemmerer, 2006*b*), right up to two- or three-dimensional networks (Billing & Lemmerer, 2006*c*). For systems containing extended chains, such chains may be formed by one, two or three bridging halides, referred to as corner-, edge- and face-sharing polyhedra, respectively. The most desired structure type, due to its suspected electroluminescence, photoluminescence and non-linear optical properties, is based on the K_2NiF_4 type system, which has two-dimensional layers of corner-sharing divalent metal halide octahedra, separated by organic compounds with primary ammonium cations, as in $(C_8H_{16}N)_2[PbI_4]$ (Billing & Lemmerer, 2006*d*). The organic cations can either consist of alkylammonium chains or systems containing aromatic groups, with either a monoammonium ($R-NH_3^+$) or a diammonium ($^+H_3N-R-NH_3^+$) group. One of the simplest aromatic systems with a primary amine is aniline, which has been incorporated into the two-dimensional type system with copper(II) chloride (Larsen, 1974). The diammonium version,



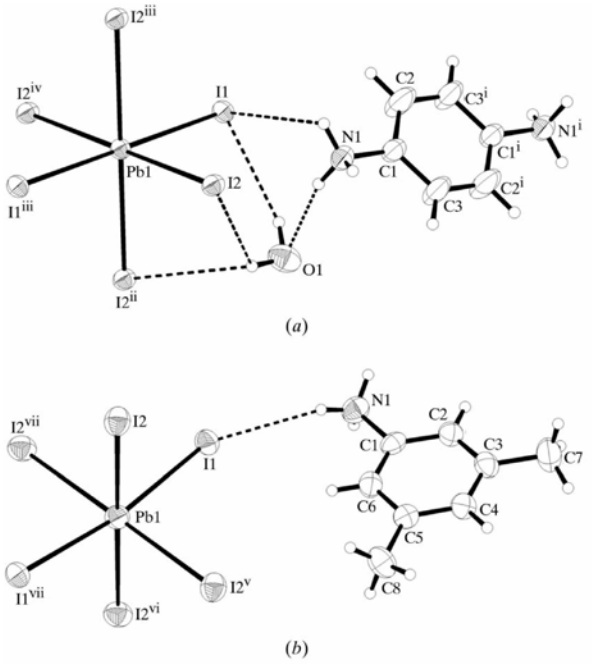


Figure 1
The asymmetric units of (*a*) (I) and (*b*) (II), showing the atomic numbering schemes. Displacement ellipsoids are drawn at the 50% probability level and H atoms are shown as small spheres of arbitrary radii. Only one position of the disordered NH_3^+ group is shown. [Symmetry codes: (i) $1-x, 1-y, z$; (ii) $x, y, -1+z$; (iii) $1-x, -y, z$; (iv) $1-x, 1-x, -y, -1+z$; (v) $x, -1+y, z$; (vi) $-x, -1+y, \frac{1}{2}-z$; (vii) $-x, y, \frac{1}{2}-z$.]

 DOI: 10.1107/S0108270106039746 © 2006 International Union of Crystallography

viz. *p*-phenylenediammonium, has also crystallized out in the K_2NiF_4-type system with a variety of metal halides, as in $(H_3NC_6H_4NH_3)[CdBr_4]$ (Ishihara *et al.*, 1996) and $(H_3N$-$C_6H_4NH_3)[CuCl_4]$ (Bourne & Mangombo, 2004). Continuing this work, we wished to investigate the packing of the hybrid compound with *p*-phenylenediamine and lead(II) iodide, and to study the influence of the methyl groups bonded to the aniline backbone in a second compound with lead(II) iodide.

The two compounds reported here, *viz*. $(H_3NC_6H_4NH_3)$-$[PbI_4]\cdot 2H_2O$, (I) (Fig. 1*a*), and $(C_8H_9NH_3)_2[PbI_4]$, (II) (Fig. 1*b*), adopt the same one-dimensional inorganic motif, albeit with different counter-ions to give unique packing arrangements. The inorganic chain consists of edge-shared PbI_6 octahedra, so these structures differ from the K_2NiF_4 archetype. Other one- and two-dimensional motifs that use the *p*-phenylene-diammonium cation and lead(II) halides that have been reported to date include the twin anionic chains of *cis* edge-sharing $\{[Pb_2I_6]^{2-}\}_\infty$ (Chakravarthy & Guloy, 1997) and the double-layer sheet of face-sharing square antiprisms of eight-coordinate lead(II) chloride (Bourne & Mangombo, 2004). To the best of our knowledge, there are only two previously reported cases of *trans* edge-sharing octahedral chains for lead(II) iodide, where square-pyramidal PbI_5 units are connected to form infinite one-dimensional chains. The reported counter-ions are tetrahedral $(Pr_4N)^+$ and octahedral $[Mg(dmf)_6]^{2+}$ (dmf is dimethylformamide; Krautscheid & Vielsack, 1998). The bridging Pb—I bond distances lie over a larger range with the former counter-ion [3.1017 (9)–3.4553 (9) Å] compared with the more symmetrical bond-length range [3.1836 (5)–3.2407 (6) Å] when the latter, bulkier, counter-ion is included in the hybrid structure (Krautscheid & Vielsack, 1998). *trans*-Edge-sharing has also been reported for mercury; a one-dimensional chain of alternating octahedral and tetrahedral mercury(II) chloride units is formed when the counter-ion is $(CH_3)_3NH^+$ (Salah *et al.*, 1983), while the lone H atom interacts with the Cl^- anions *via* hydrogen bonding.

The asymmetric part of the anionic layer of (I) contains a Pb atom on a site of 2/*m* symmetry and two I atoms on mirror planes. Within a given PbI_6 octahedron, the symmetry generates four equivalent positions for atom I2, in what is defined as the equatorial plane, and two equivalent positions for atom I1, deemed to be axial. Edge sharing between adjacent octahedra occurs through the equatorial I atoms only. The chains run parallel to the *c* axis, while the axial I atoms lie in the (001) plane, with an angle of 26.50 (1)° between the $I1\cdots I1^{iii}$ vector and the *b* axis [symmetry code: (iii) $1-x, -y, z$]. The coordination geometry around the Pb atom shows the typical axial compression of the octahedral geometry, with the bridging Pb1—I2 distances [3.2429 (6) Å] longer than the axial Pb1—I1 distances [3.1895 (8) Å]. The angle between all *cis*-related I atoms deviates by 0.457 (17)° from 90°, with all *trans* angles equal to 180° (Table 1).

The *p*-phenylenediammonium cation in (I) sits around a site of 2/*m* symmetry with the C and N atoms on a mirror plane (Fig. 1*a*). The cations all lie parallel to the (001) plane and are rotated by 16.57 (12)° away from the *b* axis, measured through the N1···N1 vector. Adjacent aromatic rings are separated by a centroid-to-centroid distance of 4.585 (1) Å, which is too

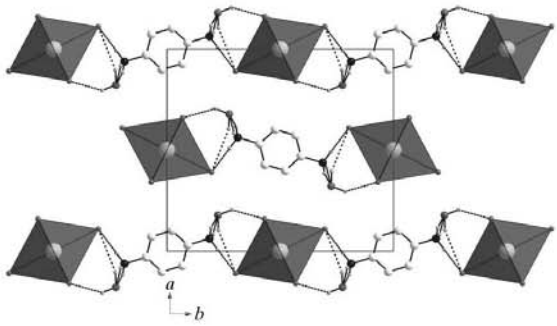


Figure 2
A packing diagram of (I), viewed along the *c* axis. Hydrogen bonds between the three components are shown as dashed lines.

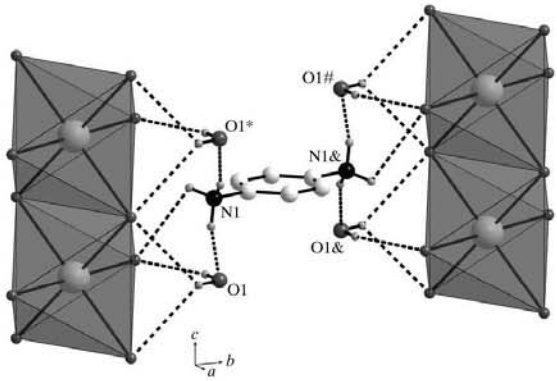


Figure 3
A magnified view of the edge-sharing PbI_6 octahedra in (I) and the hydrogen bonds (dashed lines). Atoms marked with an asterisk (*), a hash (#) or an ampersand (&) are at the symmetry positions $(x, y, 1+z)$, $(1-x, 1-y, 1+z)$ and $(1-x, 1-y, z)$, respectively.

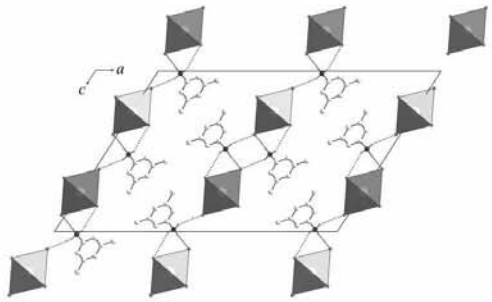


Figure 4
A packing diagram of (II), viewed along the *b* axis, showing the alternating organic–inorganic layers and the N—H···I hydrogen bonds (dashed lines).

large to be considered as representing π–π stacking interactions.

Fig. 2 clearly displays the one-dimensional inorganic motif adopted by (I), in which each *p*-phenylenediammonium molecule is surrounded by four one-dimensional chains of inorganic PbI_6 octahedra in a chessboard-like pattern. In other words, the cations occupy the channels created by the anionic edge-sharing chains. In the direction of the *b* axis, crystal cohesion is achieved by a single N—H···I hydrogen bond on either end of the organic molecule, related to the NH_3 polar groups. The water molecules, which lie on mirror planes, are embedded between the organic and inorganic moieties and held in place by O—H···I and N—H···O hydrogen bonds. Within the inorganic chains, cohesion is achieved by strong ionic bonds between equatorial I^- and Pb^{2+} ions.

There is only one hydrogen bond between the N-donor atom and the halide acceptor atom of (I), instead of three as found in the K_2NiF_4-type systems. Nevertheless, the chains of edge-sharing octahedra are connected by the cations along the *b* axis in the sequence Ar—N1—H1*C*···I1—Pb1—I1···H1*C*—N1—Ar (Fig. 2). The two remaining H atoms of the ammonium head group bond to the O atom of the water molecule. The two hydrogen bonds are related by a mirror plane on which the *p*-phenylenediammonium cation lies, and hence the O1···H1*B*—N1—H1*A*···O1 donor–acceptor distances are almost identical (1.93 and 1.94 Å) (Fig. 3). The H atoms on the water molecule themselves both bond to the equatorial and axial I atoms of the octahedra (Table 2).

In (II), the coordination geometry around the Pb atom (Table 3) and the edge-sharing PbI_6 chain geometry is essentially the same as in (I), except that the Pb atom sits on a twofold axis, while all other atoms are on general positions. The chains run parallel to the *b* axis and the vector through the axial I atoms makes an angle of 6.74 (12)° with the *c* axis. The angles between *cis*- and *trans*-related I atoms deviate significantly from 90 and 180°, respectively.

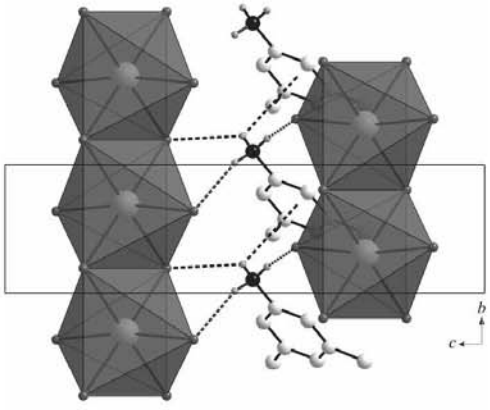


Figure 5
A magnified view of the edge-sharing PbI_6 octahedra in (II) and the N1—H1*C*···π hydrogen bond between the organic cations along the *b* axis.

Compound (II) has a different packing arrangement to (I). In this case, hydrocarbon layers of 3,5-dimethylanilinium molecules alternate with ionic layers of edge-sharing PbI_6 octahedra running along the *b* axis (Fig. 4). In the directions of the *a* and *c* axes, crystal cohesion between the inorganic and organic layers is achieved by three N—H···I hydrogen bonds, related to the NH_3 polar groups. There are N—H···π interactions between neighbouring ring systems perpendicular to the hydrogen bonds. In the direction parallel to the inorganic chains, cohesion is again achieved by strong ionic bonds between equatorial I and Pb atoms.

The three H atoms form hydrogen bonds between two neighbouring chains. Atom H1*C* forms a weak hydrogen bond to the equatorial atom I1, but a stronger bond to the ring system of an adjacent 3,5-dimethylanilinium molecule of 2.95 Å. The C—H···π angle is 110.35 (24)°. The remaining two H atoms form hydrogen bonds to two axial halides of adjacent chains, with shorter donor–acceptor distances of 2.57 and 2.84 Å (Fig. 5). The 3,5-xylidinium cation sits on a general position. The atomic numbering scheme is shown in Fig. 1(*b*). Within the organic layers, the molecules are stacked head-to-tail along the [101] direction at a dihedral angle of 87.3 (1)°, and head-to-head along the [001] direction.

Experimental

For the preparation of (I), PbI_2 (0.200 g, 0.434 mmol) was dissolved in 47% HI (7 ml) in a test tube. $NH_2C_6H_4NH_2$ (0.043 g, 0.398 mmol) was then added and the resulting precipitate dissolved by refluxing for 12 h at 393 K. The solution was then cooled slowly to room temperature at a rate of 2 K h^{-1}. A brown single crystal suitable for X-ray diffraction analysis was selected and studied. Analysis calculated for $C_6H_{14}I_4N_2Pb$: C 8.37, H 1.64, N 3.25%; found: C 8.23, H 1.79, N 3.13%. For the preparation of (II), PbI_2 (0.060 g, 0.130 mmol) was dissolved in 47% HI (2 ml) in a round-bottomed flask. $C_8H_9NH_2$ (0.040 g, 0.330 mmol) was then added and the resulting precipitate dissolved by refluxing for 12 h at 363 K. The solution was then cooled slowly to room temperature at a rate of 2 K h^{-1}. A yellow single crystal suitable for X-ray diffraction analysis was selected and studied. Analysis calculated for $C_{16}H_{24}I_4N_2Pb$: C 20.04, H 2.52, N 2.92%; found: C 19.96, H 2.48, N 2.89%.

Compound (I)

Crystal data

$(C_6H_{10}N_2)[PbI_4]\cdot 2H_2O$	$Z = 2$
$M_r = 860.98$	$D_x = 3.323$ Mg m^{-3}
Orthorhombic, *Pnnm*	Mo $K\alpha$ radiation
$a = 12.952$ (3) Å	$\mu = 16.97$ mm^{-1}
$b = 14.489$ (3) Å	$T = 173$ (2) K
$c = 4.5851$ (10) Å	Polyhedral, brown
$V = 860.4$ (3) $Å^3$	0.5 × 0.37 × 0.3 mm

Data collection

Bruker SMART CCD area-detector diffractometer	5460 measured reflections
φ and ω scans	1168 independent reflections
Absorption correction: integration (*XPREP* in *SAINT-Plus*; Bruker, 1999)	1095 reflections with $I > 2\sigma(I)$
$T_{min} = 0.012$, $T_{max} = 0.059$	$R_{int} = 0.056$
	$\theta_{max} = 28°$

metal-organic compounds

Refinement

Refinement on F^2	$w = 1/[\sigma^2(F_o^2) + (0.0479P)^2 + 2.0341P]$ where $P = (F_o^2 + 2F_c^2)/3$
$R[F^2 > 2\sigma(F^2)] = 0.032$	$(\Delta/\sigma)_{max} = 0.001$
$wR(F^2) = 0.081$	$\Delta\rho_{max} = 2.36$ e Å^{-3}
$S = 1.11$	$\Delta\rho_{min} = -1.02$ e Å^{-3}
1168 reflections	Extinction correction: *SHELXL97* (Sheldrick, 1997)
49 parameters	Extinction coefficient: 0.0204 (9)
H-atom parameters constrained	

Table 1
Selected geometric parameters (Å, °) for (I).

Pb1—I1	3.1895 (8)	Pb1—I2	3.2429 (6)
I1—Pb1—I2^{i}	89.543 (17)	I1^{i}—Pb1—I2^{i}	90.457 (17)

Symmetry code: (i) $-x+1, -y, -z$.

Table 2
Hydrogen-bond geometry (Å, °) for (I).

D—H···A	D—H	H···A	D···A	D—H···A
N1—H1C···I1	0.91	3.18	3.611 (6)	111
N1—H1A···O1^{ii}	0.91	1.94	2.794 (7)	156
N1—H1B···O1	0.91	1.93	2.794 (7)	158
O1—H6···I2^{iii}	0.95	3.16	3.771 (7)	124
O1—H7···I1	0.95	2.99	3.901 (8)	160

Symmetry codes: (ii) $x, y, z+1$; (iii) $x, y, z-1$.

Compound (II)

Crystal data

$(C_8H_{12}N)_2[PbI_4]$	$Z = 4$
$M_r = 959.16$	$D_x = 2.665$ Mg m^{-3}
Monoclinic, $C2/c$	Mo $K\alpha$ radiation
$a = 30.1215$ (19) Å	$\mu = 12.22$ mm^{-1}
$b = 4.6111$ (3) Å	$T = 293$ (2) K
$c = 20.4599$ (12) Å	Plate, yellow
$\beta = 122.725$ (3)°	0.2 × 0.13 × 0.02 mm
$V = 2390.7$ (3) Å^3	

Data collection

Bruker SMART CCD area-detector diffractometer	11071 measured reflections
φ and ω scans	2871 independent reflections
Absorption correction: integration (*XPREP* in *SAINT-Plus*; Bruker, 1999)	2337 reflections with $I > 2\sigma(I)$
	$R_{int} = 0.044$
$T_{min} = 0.174$, $T_{max} = 0.782$	$\theta_{max} = 28°$

Refinement

Refinement on F^2	H-atom parameters constrained
$R[F^2 > 2\sigma(F^2)] = 0.024$	$w = 1/[\sigma^2(F_o^2) + (0.0195P)^2]$ where $P = (F_o^2 + 2F_c^2)/3$
$wR(F^2) = 0.050$	$(\Delta/\sigma)_{max} = 0.005$
$S = 1.07$	$\Delta\rho_{max} = 0.59$ e Å^{-3}
2871 reflections	$\Delta\rho_{min} = -1.08$ e Å^{-3}
108 parameters	

Table 3
Selected geometric parameters (Å, °) for (II).

Pb1—I1	3.1984 (3)	Pb1—I2^{i}	3.2728 (4)
Pb1—I2	3.2426 (4)		
I1—Pb1—I1^{ii}	171.556 (13)	I1—Pb1—I2^{i}	92.250 (9)
I1—Pb1—I2	87.785 (9)	I1^{ii}—Pb1—I2^{i}	93.752 (9)
I1^{ii}—Pb1—I2	86.269 (9)		

Symmetry codes: (i) $-x, y-1, -z+\frac{1}{2}$; (ii) $-x, y, -z+\frac{1}{2}$.

Table 4
Hydrogen-bond geometry (Å, °) for (II).

D—H···A	D—H	H···A	D···A	D—H···A
N1—H1A···I1	0.89	2.84	3.663 (4)	155
N1—H1B···I1^{iii}	0.89	2.57	3.432 (4)	165
N1—H1C···I2^{iv}	0.89	3.15	3.789 (4)	131

Symmetry codes: (iii) $-x, -y+1, -z$; (iv) $x, -y+2, z-\frac{1}{2}$.

For compound (I), all H atoms were found in a difference map. For H atoms bonded to O atoms, restraints were used to obtain reasonable O—H distances and H—O—H angles. Finally, these H atoms were refined using a riding model, with U_{iso}(H) = 1.2U_{iso}(O). H atoms bonded to C and N atoms were refined in idealized positions in the riding-model approximation, with Ar—H = 0.95 Å and N—H = 0.91 Å, and with U_{iso}(H) = 1.2U_{eq}(C) or 1.5U_{eq}(N). There is a close contact between atom H7 of the water molecule and atoms H1*A* and H1*B* of the ammonium group (1.77 and 1.52 Å, respectively). The position of H7 is justified as it then forms a hydrogen bond to atom I1. The short intermolecular H···H contacts are due to the acute angle between the donor atom N1, atom O1 and the I1 acceptor atom. For compound (II), all H atoms were refined using a riding model, with Ar—H = 0.93 Å, C—H = 0.96 Å and N—H = 0.89 Å, and with U_{iso}(H) = 1.2U_{eq}(C) or 1.5U_{eq}(N). The NH_3 and CH_3 groups were allowed to rotate but not to tip in both compounds. The highest residual peaks are 0.82 Å from atom Pb1 in (I) and 0.87 Å from I2 in (II).

For both compounds, data collection: *SMART-NT* (Bruker, 1998); cell refinement: *SAINT-Plus* (Bruker, 1999); data reduction: *SAINT-Plus*; program(s) used to solve structure: *SHELXS97* (Sheldrick, 1997); program(s) used to refine structure: *SHELXL97* (Sheldrick, 1997); molecular graphics: *ORTEP-3 for Windows* (Farrugia, 1997) and *DIAMOND* (Brandenburg, 2001); software used to prepare material for publication: *WinGX* (Farrugia, 1999) and *PLATON* (Spek, 2003).

The University of the Witwatersrand and the National Research Fund (GUN 2069064) are thanked for the award of a research grant and for providing the infrastructure required to do this work. AL thanks Professor D. C. Levendis and Dr M. A. Fernandes for help with handling the disorder in compound (I).

Supplementary data for this paper are available from the IUCr electronic archives (Reference: AV3041). Services for accessing these data are described at the back of the journal.

References

Billing, D. G. & Lemmerer, A. (2006*a*). *Acta Cryst.* E**62**, m1103–m1105.
Billing, D. G. & Lemmerer, A. (2006*b*). *Acta Cryst.* C**62**, m264–m266.
Billing, D. G. & Lemmerer, A. (2006*c*). *Acta Cryst.* C**62**, m174–m176.
Billing, D. G. & Lemmerer, A. (2006*d*). *Acta Cryst.* C**62**, m269–m271.
Bourne, S. A. & Mangombo, Z. (2004). *CrystEngComm*, **6**, 437–442.
Brandenburg, K. (2001). *DIAMOND*. Release 2.1e. Crystal Impact GbR, Bonn, Germany.
Bruker (1998). *SMART-NT*. Version 5.050. Bruker AXS Inc., Madison, Wisconsin, USA.
Bruker (1999). *SAINT-Plus*. Version 6.02 (including *XPREP*). Bruker AXS Inc., Madison, Wisconsin, USA.
Chakravarthy, V. & Guloy, A. M. (1997). *J. Chem. Soc. Chem. Commun.* pp. 697–698.

Farrugia, L. J. (1997). *J. Appl. Cryst.* **30**, 565.
Farrugia, L. J. (1999). *J. Appl. Cryst.* **32**, 837–838.
Ishihara, H., Dou, S., Horiuchi, K., Krishnan, V. G., Paulus, H., Fuess, H. & Weiss, A. (1996). *Z. Naturforsch. Teil A*, **51**, 1216–1228.
Krautscheid, H. & Vielsack, K. (1998). *Z. Anorg. Allg. Chem.* **625**, 562–566.
Larsen, K. P. (1974). *Acta Chem. Scand. Ser. A*, **28**, 194–200.
Salah, A. B., Bats, J. W., Fuess, H. & Daoud, A. (1983). *Z. Kristallogr.* **164**, 259–272.
Sheldrick, G. M. (1997). *SHELXS97* and *SHELXL97*. University of Göttingen, Germany.
Spek, A. L. (2003). *J. Appl. Cryst.* **36**, 7–13.

Chapter 7 Conclusion

7.1 Concluding remarks

The synthesis and SC-XRD structures of 76 inorganic-organic lead(II) halide hybrids are described in this thesis. A diversity of inorganic motifs has been encountered, as listed in Table 8.1. Of the 76 hybrids, 47 hybrids have the layered perovskite-type motif with different organic ammonium countercations from alkyl chains to aromatics to various saturated hydrocarbons. All the layered perovskite-type hybrids with alkyl ammonium chains displayed reversible phase transitions as a function on temperature, as discussed in Chapter 5. The layered perovskite-type hybrids without alkyl chains displayed structural trends of the inorganic layers that depend on the size of the organic ammonium group and the identity of the halide atom, as discussed in Chapter 6. A simple way of describing the structural changes the inorganic layers and the ammonium cations undergo during the phase changes and the structural trends is using the acute and obtuse description of the position of the ammonium cations relative to the layers and the equilateral and right-angled description of the hydrogen bonding. These two descriptors are new and first reported in this thesis.

Table 7.1: Summary of the inorganic motifs of the 76 inorganic-organic hybrids that were made in this thesis.

	2-D		1-D					0-D
Section	layered perovskite-type	Other motif	face-sharing	edge-sharing	corner-sharing	Ribbon	edge + corner	
4.1	2		4		2			
4.2	4		2			2		
4.3	4		1		1			
4.4	8	1			1	2		
4.5	9				1			
4.6	7			1		1		1
5.1	3							
5.2	4							
5.3	4							
6.1-10	1	2	3	2			1	2

7.2 Future Work

All the work reported here focused on the metal lead. A logical extension would be to repeat the study using the metal tin. Preliminary work done on the compound $[(C_6H_{13}NH_3)_2SnI_4]$ shows a phase transition below room temperature, somewhere between -30 and -40°C. This phase transition is similar as the phase transition from phase **IV** to phase **III** reported for $[(C_6H_{13}NH_3)_2PbI_4]$ in this thesis. Figure 8.1 shows how the inorganic layers change from a staggered arrangement at -30°C to an eclipsed arrangement at -55°C. The hexylammonium cation does not change its position relative to the layers (acute).

For both lead and tin inorganic-organic hybrids, a study of their electronic and optical properties using various spectroscopic techniques, would be relevant

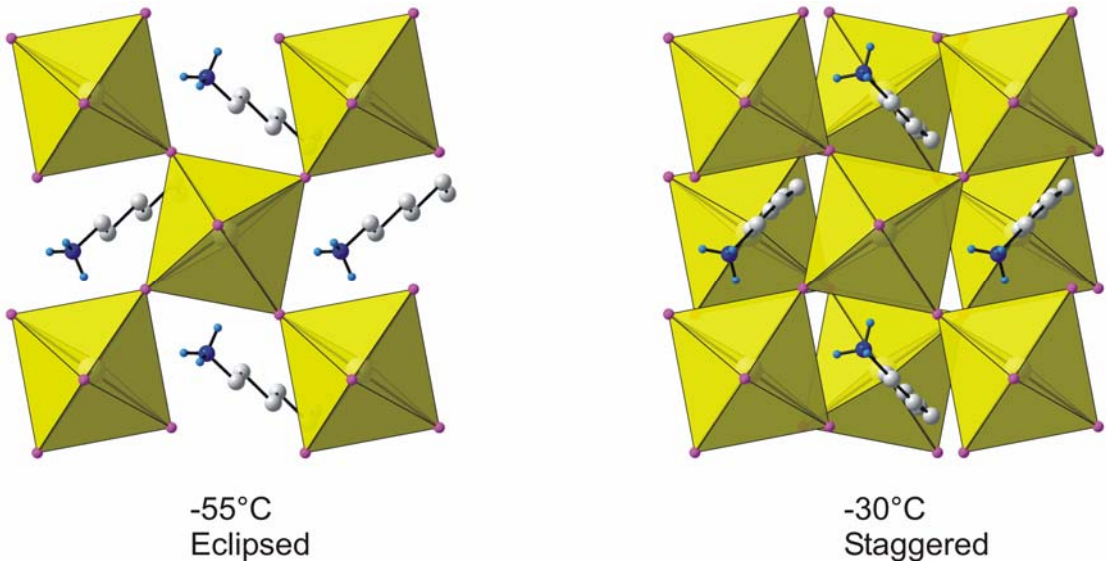


Figure 7.1: The hexylammonium cations and the arrangement of the inorganic layers in the two phases of $[(C_6H_{13}NH_3)_2SnI_4]$.

References

A

Allen, F. H. (2002). *Acta Cryst.* B**58**, 380-388.

Almirante, C., Minoni, G., Zerbi, G. (1986). *J. Phys. Chem.* **90**, 852-859.

Amami, M., Zouari, R., Salah, A.B., Burzlaff, H. (2002). *Acta Cryst.* E**58**, m357-m359.

Arend, H., Hofmann, Waldner, F. (1973). *Solid State Comm.* **13**, 1629-1632.

Arend, H., Gränicher, H. (1976). *Ferroelectrics* **12**, 537.

Arend, H., von Känel, H., Wachter, P. (1976a). *Phys. Status Solidi* (b) **74**, 151-157.

Arend, H., Tichý, K., Bàberschke, K., Rys, F. (1976b). *Solid State Comm.* **18**, 999-1003.

Arend, H., Huber, W., Mischgofsky, F. H., Richter-van Leeuwen, G.K. (1978). *J. Cryst. Growth* **43**, 213-223.

Atkins, P., Overton, T., Rourke, J., Weller, M., Armstrong, F. (2006). *Inorganic Chemistry*, 4th Ed., Oxford University Press, Oxford.

Azumi, R., Honda, K., Goto, M., Akimoto, J., Oosawa, Y., Tachibana, H., Nakamura, T., Tanaka, M., Matsumoto, M. (1995). *Acta Cryst. C***51**, 2534-2537.

Azumi, R., Honda, K., Goto, M., Akimoto, J., Oosawa, Y., Tachibana, H., Tanaka, M., Matsumoto, M. (1996). *Mol. Cryst. Liq. Cryst.* **276**, 237-243.

B

Baberschke, K., Rys, F., Arend, H. (1977). *Physica* **86-88**B, 685-686.

Barendregt, F., Schenk, H. (1970). *Physica* **49**, 465-468.

Barman, S., Venkataraman, N.V., Vasudevan, S., Seshadri, R. (2003). *J. Phys. Chem.* B **107**, 1875-1883.

Bellitto, C., Day, P. (1977). *J. Chem. Soc. Chem. Comm.*, 870-871.

Bellitto, C., Day, P. (1978). *J. Chem. Soc. Dalton Trans*., 1207-1212.

Bellitto, C., Day, P., Wood, T. E. (1986). *J. Chem. Soc. Dalton Trans*., 847-851.

Billing, D.G. (2002). *Acta Cryst*., E**58**, m669-m671.

Birrell, G.B., Zaslow, B. (1972). *J. Inorg. Nucl. Chem.* **34**, 1751.

Blinc, R., Burgar, M., Ložar, B., Seliger, J., Slak, J., Rutar, V., Arend, H., Kind, R. (1977). *J. Chem. Phys.* **66**, 278-287.

Blinc, R., Žekš, B., Kind, R. (1978). *Phys. Rev. B: Condens. Matter* **17**, 3409-3420.

Bloembergen, P. (1976). *Physica* **81**B, 205-229.

Bloembergen, P. (1977). *Physica* **85**B, 51-72.

Braun, M., Frey, W., (1999a). *Z. Kristallogr. - New Cryst. Struct* **214**, 331-332.

Braun, M., Frey, W., (1999b). *Z. Kristallogr. - New Cryst. Struct* **214**, 333-334.

Braun, M., Frey, W., (1999c). *Z. Kristallogr. - New Cryst. Struct* **214**, 335-336.

Braun, M., Tuffentsammer, W., Wachtel, H., Wolf, H.C. (1999a). *Chem. Phys. Lett.* **303**, 157-164.

Braun, M., Tuffentsammer, W., Wachtel, H., Wolf, H.C. (1999b). *Chem. Phys. Lett.* **307**, 373-378.

Breneman, G.L., Willett, R.D. (1981). *Acta Cryst*. B **37**, 1292-1294.

Brinkmann, D., Walther, U., Arend H. (1976). *Solid State Commun*. **18**, 1307-1309.

Bruker (2003). *XPREP2*, Version 6.14, Bruker AXS Inc., Madison, Wisconsin, USA.

Brunskill, I.H., Depmeier, W. (1982). *Acta Cryst*. A **38**, 132-137.

Busico, V., Salerno, V., Vacatello, M. (1979). *Gazz. Chim. Ital.* **109**, 581-584.

C

Calabrese, J., Jones, N.L., Harlow, R.L., Herron, N., Thorn, D.L., Wang, Y. (1991). *J. Am. Chem. Soc.* **113**, 2328-2330.

Carfagna, C., Vacatello, M., Corradini, P. (1977). *Gazz. Chim. Ital.* **107**, 131-133.

Chanh, N.B., Haget, Y., Hauw, C., Meresse, A., Ricard, L., Rey-Lafon, M. (1983). *J. Phys. Chem. Solids*. **44**, 589-594.

Chanh, N.B., Hauw, C., Meresse, A., Rey-Lafon, M., Ricard, L. (1985). *J. Phys. Chem. Solids* **46**, 1413-1420.

Chanh, N.B., Houstry, J.R., Meresse, A., Ricard, L., Rey-Lafon, M. (1989). *J. Phys. Chem. Solids* **50**, 829-838.

Chapuis, G. (1977). *Phys. Status Solidi* (a) **43**, 203-212.

Chapuis, G. (1978). *Acta Cryst*. B **34**, 1506-1512.

Chapuis, G., Arend, H., Kind, R. (1975). *Phys. Status Solidi* **31**, 449-454.

Chapuis, G., Kind, R., Arend, H. (1976). *Phys. Status Solidi* (a) **36**, 285-295.

Cheng, Z.Y., Wang, Z., Xing, R.B., Han, Y.C., Lin, J. (2003). *Chem. Phys. Lett.* **376**, 481-486.

Cheng, Z. Y., Wang, H. F., Quan, Z. W., Lin, C. K., Lin, J., Han, Y. C. (2005). *J. Cryst. Growth*, **285**, 352-357.

Chondroudis, K., Mitzi, D.B. (1999). *Chem. Mater.* **11**, 3028-3030.

Chondroudis, K., Mitzi, D.B., Brock, P. (2000). *Chem. Mater.* **12**, 169-175.

Ciajolo, M.R., Corradini, P., Pavone, V. (1976). *Gazz. Chim. Ital.* **106**, 807-816.

Contreras, J.G., Seguel, G.V., Ungerer, B., Maier, W.F., Hollander, F.J. (1983). *J. Mol. Struct*. **102**, 295-304.

Colpa, J.H.P. (1972). *Physica* **57**, 347-380.

Corradi, A.B., Ferrari, A.M., Pellacani, G.C., Saccani, A., Sandrolini, F., Sgarabotto, P. (1999). *Inorg. Chem.* **38**, 716-721.

Courseille, C., Chanh, N.B., Marias, Th., Daoud, A., Abid, Y., Laguerre, M. (1994). *Phys. Status Solidi* (a) **143**, 203-214.

Couzi, M., Daoud, A., Perret, R. (1977). *Phys. Status Solidi* (a) **41**, 271-282.

Crowley, J.C., Dodgen, H.W., Willett, R.D. (1982). *J. Phys. Chem.* **86**, 4046-4055.

D

Day, P. (1985). *Phil. Trans. R. Soc. Lond. A*, **314**, 145-158.

Depmeier, W. (1976). *Acta Cryst*. B32, 303-305.

Depmeier, W. (1977). *Acta Cryst*. B**33**, 3713-3718.

Depmeier, W. (1979). *J. Solid State Chem*. **29**, 15-26.

Depmeier, W. (1981). *Acta Cryst*. B**37**, 330-339.

Depmeier, W., Heger, G. (1978). *Acta Cryst*. B**34**, 1698-1700.

Depmeier, W., Mason, S.A. (1978). *Acta Cryst*. B**34**, 920-922.

Depmeier, W., Mason, S.A. (1982). *Solid State Comm.* **44**, 719-722.

Depmeier, W., Mason, S.A. (1983). *Solid State Comm.* **46**, 409-412.

Depmeier, W., Chapuis, G. (1979). *Acta Cryst*. B**35**, 1081-1084.

Depmeier, W. Felsche, J. Wildermuth, G. (1977). *J. Solid State Chem*. **21**, 57-65.

Desiraju, G. R. (2002). *Acc. Chem. Res*. 35, 565-573.

Devic, T., Canadell, E., Auban-Senzier, P., Batail, P. (2004). *J. Mater. Chem*. **14**, 135-137.

Doudin, B., Chapuis, G. (1988). *Acta Cryst*. B**44**, 495-502.

Doudin, B., Chapuis, G. (1990). *Acta Cryst*. B**46**, 175-180.

Drumheller, J. E., Dickey, D. H., Reklis, R. P., Zaspel. C. E., Glass, S. J. (1972). *Phys. Rev. B: Condens. Matter* **5**, 4631-4636.

Dupas, A., Le Dang, K., Renard, J.-P., Veillet, P., Daoud, A., Perret, R. (1976). *J. Chem. Phys.* **65**, 4099-4102.

Dupas, A., Khoi, L.D., Renard, J. P., Veillet, P. (1977). *Physica* **86-88**B, 687-688.

E

Era, M., Morimoto, S., Tsutsui, T., Saito, S. (1994). *Appl. Phys. Lett.* **65**, 676-678.

Era, M., Moromito, S., Tsutsui, T., Saito, S. (1995). *Synth. Metals*, **71**, 2013-2014.

Era, M., Hattori, T., Taira, T., Tsutsui, T. (1997). *Chem. Mater.* **9**, 8-10.

Era, M., Maeda, K., Tsutsui, T. (1998a). *Chem. Phys. Lett.* **296**, 417-420.

Era, M., Maede, K., Tsutsui, T. (1998b). *Thin Solid Films* **331**, 285-290.

Era, M., Kobayashi, T., Noto, M. (2005). *Current Appl. Phys*. **5**, 67-70.

Exarhos, G., Rien Jr., W., Baughman, R. (1976). *J. Am. Chem. Soc.* **98**, 481-487.

F

Ferguson, G.L., Zaslow, B. (1971). *Acta Cryst*. B**27**, 849-852.

Flandrois, S., Chanh, N.M., Duplessix, R., Maris, Th., Ne'grier, P. (1995). *Phys. Status Solidi* (a) **149**, 697-710.

Foster, J. J., Gill, N. S. (1968). *J. Chem. Soc*. A, 2625-2629.

Fujita, T., Sato, Y., Kuitani, T., Ishihara, T. (1998). *Phys. Rev. B: Condens. Matter* 57, 12428-12434.

Fujita, T., Nakashima, H., Hirasawa, M., Ishihara, T. (2000). *J. Lumin*. **87-89**, 847-849.

G

Garland, J.K., Emerson, K., Pressprich, M.R. (1990). *Acta Cryst*. C**46**, 1603-1609.

Gebauer, T., Schmid, G. (1999). *Z. Anorg. Allg. Chem.* **625**, 1124-1128.

Geselle, M., Fuess, H. (1995). *Acta Cryst*. C51, 242-244.

Geselle, M., Fuess, H. (1997). *Z. Kristallogr. - New Cryst. Struct* **213**, 239-240.

Goldschmidt, V.M. (1926). Naturwissenschaften **14**, 477-485.

Goldstein, M., Tok, G.C. (1975). *Spectrochim. Acta* A **31**, 1993-1994.

Goto, T., Ohshima, N., Mousdis, G.A., Papavassiliou, G.C. (2001). *Solid State Comm.* **117,** 13-16.

Greenhough, T. J., Ladd, M. F. C. (1977). *Acta Cryst.* B**33**, 1266-1269.

Groenendijk, H. A., van Duyneveldt, A. J., Willett, R. D. (1979). *Physica* **98**B, 53-59.

Groh, M., Spengler, R., Burzlaff, H., Zouari, F., Salah, A.B. (1997) *Acta Cryst*., C **53**, 1199-1201.

Guan, J., Tang, Z., Guloy, A.M. (1999). *Chem. Comm*., 1833-1834.

Guillaume, F., Sourisseau, C., Dianoux, A. J. (1989). *Physica* **156 -157**B, 359-362.

H

Hagen, H., Reimann, H., Schmocker, U., Waldner, F. (1977). *Physica* **86-88**B, 1287-1288.

Halepoto, D.M., Larkworthy, L.F., Povey, D.C., Ramdas, V. (1989) *Inorg. Chim. Acta* **162**, 71-74.

Halvorsen, K., Willett, R.D. (1988). *Acta Cryst*. C**44**, 2071-2076.

Harris, P., Larsen, F.K., Lebech, B., Achiwa, N. (1994). *Acta Cryst*. B**50**, 676-684.

Hatch, D. M., Stokes, H. T. (1987). *Phys. Rev. B: Condens. Matter* **35**, 8509-8516.

Hatch, D. M., Stokes, H. T., Aleksandrov, K. S., Misyul, S. V. (1989). *Phys. Rev. B: Condens. Matter* **39**, 9282-9288.

Hattori, T., Taira, T., Era, M., Tsutsui, T., Saito, S. (1996). *Chem. Phys. Lett.* **254**, 103-108.

Havorson, K.E., Patyel, B., Willett, R.D. (1995). *J. Chem. Cryst*. **25**, 537-542.

Heger, G., Henrich, E., Hanellakopulos, B. (1973). *Solid State Comm*. 12, 1157-1165.

Heger, G., Mullen, D., Knorr, K. (1975). *Phys. Status Solidi* (a) **31**, 455-462.

Heger, G., Mullen, D., Knorr, K. (1976). *Phys. Status Solidi* (a) **35**, 627-637.

Heygster, G., Kleeman, W. (1977). *Physica* **89**B, 165-176.

Hirasawa, M., Ishihara, T., Goto, T. (1993). *Solid State Comm.* **86**, 47-483.

Hirasawa, M., Ishihara, T., Goto, T., Uchida, K., Muira, N. (1994). *Physica* **201**B, 427-430.

Hong, X., Ishihara, T., Nurmikko, A.V. (1992a). *Solid State Comm.* **84**, 657-661.

Hong, X., Ishihara, T., Nurmikko, A.V. (1992b). *Phys. Rev. B: Condens. Matter* **45**, 6961-6964.

I

Ishihara, T. (1994). *J. Lumin.* **60-61**, 269-274.

Ishihara, T., Takahashi, J., Goto, T. (1989). *Solid State Comm* **69**, 933-936.

Ishihara, H., Krishnan, V.G., Dou, S., Paulus, H., Weiss, H. (1994). *Z. Naturforsch*. **49** a, 213-222.

Ishihara H., Dou, S., Horiuchi, K., Krishnan, V.G., Paulus, H., Fuess, H., Weiss A. (1996). *Z. Naturforsch*. **51** a, 1216-1228.

J

Jahn, I.R., Knorr, K., Ihringer, J. (1989). *J. Phys.: Condens. Matter* **1**, 6005-6017. 288

Jahn, I.R., Schwab, K., Knorr, K., Holocher, K. (1994). *J. Phys.: Condens. Matter* **6**, 10839-10853.

Janiak, C. (2000). *J. Chem. Soc., Dalton Trans*., 3885-3896.

Jaschinski, B., Blachnik, R., Reuter, H. (1999). *Z. Anorg. Allg. Chem.* **625**, 667-672.

Jeffrey, G. A. (1997). *An introduction to hydrogen bonding*, New York, Oxford University Press.

K

Kagan, C.R., Mitzi, D.B., Dimitrakopoulos, C.D. (1999). *Science* **286**, 945-947.

Kammoun, S., Daoud, A. (1997). *Phys. Status Solidi* (a) **162**, 575-586.

Kammoun, S., Kamoun, M., Daoud, A., Romain, F. (1996a). *Phys. Status Solidi* (a) **156**, 317-329.

Kammoun, S., Kamoun, M., Daoud, A., Lautie, A. (1996b). *J. Phys.: Condens. Matter* **8**, 8465-8475.

Kang, J.-K., Choy, J.-H., Rey-Lafon, M. (1993). *J. Phys. Chem. Solids* **54**, 1567-1577.

Kang, J.-K., Jeon, I. C. (1995). *Synth. Metals* **71**, 1879-1880.

Kataoka, T., Kondo, T., Ito, R., Sasaki, S., Uchida, K., Miura, N. (1993a). *Phys. Rev. B: Condens. Matter* **47**, 2010-2018.

Kataoka, T., Kondo, T., Ito, R., Sasaki, S., Uchida, K., Miura, N. (1993b). *Physica* B **184**, 132-136.

Kataoka, T., Kondo, T., Ito, R., Sasaki, S., Uchida, K., Miura, N. (1994). *Physica* B **201**, 423-426.

Kato, Y., Ichii, D., Ohashi, K., Kunugita, H., Ema, K., Tanaka, K., Takahashi, T., Kondo, T. (2003). *Solid State Comm.* **128**, 15-18.

Kempen, H. van, Mischgofsky, F.H., Wyder, P. (1977). Phys. Rev. B **15**, 4386-4391.

Kikuchi, K., Takeoka, Y., Rikukawa, M, Sanui, K. (2004). *Current Appl. Phys*. **4**, 599-602.

Kikuchi, K., Takeoka, Y., Rikukawa, M., Sanui, K. (2005). *Colloids and Surfaces A: Physiochem. Eng. Apects*, **257-258**, 199-202.

Kind, R. (1977). *Phys. Status Solidi* (a) **44**, 661-667.

Kind, R., Roos, J. (1976). *Phys. Rev. B: Condens. Matter* **13**, 45-54.

Kind, R., Plesko, S., Roos, J. (1978). *Phys. Status Solidi* (a) **47**, 233-240.

Kind, R., Pleško, S., Arend, H., Blinc, R., Žekš, B., Seliger, J., Ložar, B., Slak, J., Levstik, A., Filipič, C., Žagar, V., Lahajnar, G., Milla, F., Chapuis, G. (1979). *J. Chem. Phys.* **71**, 2118-2130.

Kind, R., Plesko, S., Gunter, P., Roos, J., Fousek, J. (1981). *Phys. Rev. B: Condens. Matter* **23**, 5301-5315.

Kitazawa, N. (1997). *Mater. Sci. Eng.,* B**49**, 233-238.

Kitazawa, N. (1998). *J. Mater. Sci*. **33**, 1441-1444.

Kitazawa, N., Enomoto, K., Aono, M., Watanabe, Y. (2004). *J. Mater. Sci*. **39**, 749-751.

Kitazawa, N., Ito, T., Sakasegawa, D., Watanabe, Y. (2006). *Thin Solid Films* **500**, 133-137.

Knorr, K., Jahn, I.R., Heger, G. (1974). *Solid State Comm.* **15**, 231-238.

Kondo, T., Iwamoto, S., Hayase, S., Tanaka, K., Ishi, J., Mizuno, M., Ema, K., Ito, R. (1998a). *Solid State Comm.* **105**, 503-506.

Kondo, T., Azuma, T., Yuasa, T., Ito, R. (1998b). *Solid State Comm.* **105**, 253-255. 165
Kosuge, H., Okada, S., Oikawa, H., Nakanishi, H. (2002a). *Mol. Cryst. Liq. Cryst.* **379**, 13-18.

Kosuge, H., Okada, S., Oikawa, H., Nakanishi, H. (2002b). *Mol. Cryst. Liq. Cryst.* **377,** 265-268.

Koželj, M., Rutar, V., Zupančič, I., Blinc, R., Arend, H., Kind, R., Chapuis, G. (1981). *J. Chem. Phys.* **74**, 4123-4129.

Koutselas, I.B., Ducasse, L., Papavassiliou, G.C. (1996). *J. Phys.: Condens. Matter* **8**, 1217-1227.

Krautscheid, H., Vielsack, F. (1995). *Angew. Chem. Int. Ed. Engl.* 34, 2035-2037.

Krautscheid, H., Vielsack, F. (1996). *Z. Anorg. Allg. Chem.* 623, 259-263.

Krautscheid, H., Vielsack, K. (1999). *Z. Anorg. Allg. Chem.* **625**, 562-566.

Krautscheid, H., Lekieffre, J.F., Besinger, J. (1996). *Z. Anorg. Allg. Chem.* **622**, 1781-1787.

Krautscheid, H., Vielsack, F., Klaassen, N. (1998). *Z. Anorg. Allg. Chem.* **624**, 807-812.

Krautscheid, H., Lode, C., Vielsack, F., Vollmer, H. (2001). *J. Chem. Soc., Dalton Trans.*, 1099-1104.

L

Landi, E., Salerno, V., Vacatello, M. (1977). *Gazz. Chim. Ital.* **107**, 27-30.

Larsen, K.P. (1974). Acta Chem. Scand. A **28**, 194-200.

Lartigue-Bourdeau, C., Chanh, N.B., Duplessix, R., Gallois, B. (1993). *J. Phys. Chem.* Sol. **54**, 349-356.

Lee, K.W., Lee, C.E. (2003). *Solid State Comm.* **126**, 343-346.

Lee, S.J., Kim, G.Y., Oh, E.-J., Kim, K.H., Yo, C.H. (2000). *Bull. Kor. Chem. Soc.* **21**, 317-320.

Lee, K.W., Lee, C.H., Lee, C.E. (2003). *Phys. Rev. B: Condens. Matter* **67**, 134424-1-5.

Lehner, N., Strobel, K., Geick, Heger, G. (1975). *J. Phys. C: Solid State Phys*. 8, 4096-4106.

Levstik, A., Filipič, C. Blinc, R., Arend, H., Kind, R. (1976). *Solid State Comm.* **20**, 127-130.

Liu, Z., Yu, W.-T., Tao, X.-T., Jiang, M.-H., Yang, M.-H., Yang, J.-X., Wang, L. (2004). *Z. Kristallogr. - New Cryst. Struct.* **219**, 457-458.

Lode, C., Krautscheid, H. (2001). *Z. Anorg. Allg. Chem.* **627**, 1454-1458.

Losee, D.B., Hatfield, W.E. (1974). *Phys. Rev. B: Condens. Matter* **10**, 212-218.

Löfving, I. (1976). *Acta Chem. Scand.* A **30**, 715-718.

M

Makino, H., Goto, T., Yao, T., Mousdis, G.A., Papavassiliou, G.C. (2005). *J. Lumin*. **112**, 54-57.

Matsui, T., Kawahara, M., Teshima, K., Rikukawa, M., Sanui, K. (2002). *Mol. Cryst. Liq. Cryst.* **376**, 89-94.

Matsuishi, K., Ishihara, T., Onari, S., Chang, Y.H., Park, C.H. (2004). *Phys. Status Solidi* (b) **241**, 3328-3333.

McGraw-Hill Encyclopedia of Science and Technology. (2005). The McGraw-Hill Companies, Inc., *Answers.com* 29 Nov. 2006. http://www.answers.com/topic/exciton

Mercier, N. (2005). *CrystEngComm* **7**, 429-432.

Mercier, N., Riou, A. (2004). *Chem. Comm*., 844-845.

Mercier, N., Poiroux, S., Riou, A., Batail, P. (2004). *Inorg. Chem.* **43**, 8361-8366.

Meresse, A., Daoud, A. (1989). *Acta Cryst*. C**45**, 194-196.

Mitzi, D. B. (1996). *Chem. Mater.* **8**, 791-800.

Mitzi, D. B. (1999a). Progr. *Inorg. Chem.* **48**, 1-121.

Mitzi, D. B. (1999b). *J. Solid State Chem*., **145**, 694-704.

Mitzi, D. B. (2001). *J. Chem. Soc., Dalton Trans*., 1-12.

Mitzi, D. B. (2004). *J. Mater*. Chem. **14**, 2355-2365.

Mitzi, D. B., Liang, K. (1997). *Chem. Mater.* **9**, 2990-2995.

Mitzi, D. B., Brock, P. (2001). *Inorg. Chem.* **40**, 2096-2104.

Mitzi, D. B., Feild, C.A., Harrison, W.T.A., Guloy, A.M. (1994). *Nature* **369**, 467-469.

Mitzi, D. B., Feild, C.A., Schlesinger, Z., Laibowitz, R.B. (1995). *J. Solid State Chem*. **114**, 159-163.

Mitzi, D. B., Liang, K., Wang, S. (1998). *Inorg. Chem.* **37**, 321-327.

Mitzi, D. B., Prikas, M.T., Chondroudis, K. (1999a). *Chem. Mater.* **11**, 542-544.

Mitzi, D. B., Chondroudis, K., Kagan, C.R. (1999b). *Inorg. Chem.* **38**, 6246-6256.

Mitzi, D. B., Chondroudis, K., Kagan, C.R. (2001a). *IBM J. Res. Dev.* **45**, 29-45.

Mitzi, D. B., Dimitrakopoulos, C.D., Kosbar, L.L. (2001b). *Chem. Mater.* **13**, 3728-3740.

Mitzi, D. B., Medeiros, D.R., Malenfant, P.R. (2002). *Inorg. Chem.* **41**, 2134-2145.

Maxcy, K. R., Willett, R.D., Mitzi, D.B., Afzali, A. (2003). *Acta Cryst*. E**59**, m364-m366.

Moral, B. A., Rodriguez, F. (1997). *J. Phys. Chem. Solids* **58**, 1487-1490.

Mostafa, M. F., Semary, M., Ahmed, M. A. (1977). *Physica* **86-88**B, 691-692.

Mousdis, G.A., Gionis, V., Papavassiliou, G.C., Raptopoulou, C.P., Terzis, A. (1998). *J. Mater. Chem*. **8**, 2259-2262.

Mousdis, G. A., Papavassiliou, G.C., Terzis, A., Raptopoulou, C.P. (1998a). *Z. Naturforsch*. **53** b, 927-931.

Mousdis, G. A., Papavassiliou, G.C., Raptopoulou, C.P., Terzis, A. (2000). *J. Mater. Chem*. **10**, 515-518.

Muljarov, E. A., Tikhodeev, S.G., Gippius, N.A. Ishihara, T. (1995). *Phys. Rev. B: Condens. Matter* **51**, 14370-14378.

N

Nagapetyan, S. S., Dolzhenko, Yu. I., Arakelova, E. R., Koshkin, V. M., Struchkov, Yu. T., Shklover, V. E. (1988). *Zh. Neorg. Khim*., **33**, 2806-2812 [*Russ. J. Inorg. Chem.* **33**, 2806-2812].

Needham, G. F., Willett, R.D, Franzen, H.F. (1984). *J. Phys. Chem.* **88**, 674-680.

Ning, G., Guangfu, Z., Shiquan, X. (1992a). *J. Phys. Chem. Solids* **53**, 437-441.

Ning, G., Guangfu, Z., Shiquan, X. (1992b). *J. Mol. Struct*. **275**, 85-94.

Ning, G. (1995). *J. Solid State Chem*. **117**, 97-102.

P

Pabst, I., Fuess., H., Bats, J.W. (1987). *Acta Cryst*. C**43**, 413-416.

Pabst, I., Karolyi, J., Fuess, H., Couzi, M. (1996). *Phys. Status Solidi* (a) **155**, 341-352.

Papavassiliou, G.C., Koutselas, I.B., Terzis, A., Whangbo, M.-H. (1994) *Solid State Comm.*, **91**, 695-698.

Papavassiliou, G.C., Mousdis, G.A., Koutselas, I.B. (1999a). *Adv. Mater. Opt. Electron*. **9**, 265-271.

Papavassiliou, G.C., Mousdis, G.A., Raptopoulou, C.P., Terzis, A. (1999b) *Z. Naturforsch*. **54** b, 1405-1409.

Papavassiliou, G.C., Mousdis, G.A., Raptopoulou, C.P., Terzis, A. (2000). *Z. Naturforsch*. **55** b, 536-540.

Peterson, E.R., Willett, R.D. (1972). *J. Chem. Phys.* **56**, 1879-1882.

Peyrard, M., Perret, R. (1979). *Phys. Status Solidi* (a) **52**, 521-528.

Phelps, D.W., Losee, D.B., Hatfield, W.E., Hodgson, D.J. (1976). *Inorg. Chem.* **15**, 3147-3152.

Philpott, M. F. (2002). *Conversion of a N/C/S Analyser for High Precision CHN Determination on Samples of 1 Milligram or Less*, Poster Presentation, Analytika 2002, Stellenbosch.

Poglitsch, A., Weber, D. (1987). *J. Chem. Phys.* **87**, 6373-6378.

Pohl, S., Saak, W., Mayer, P., Schmidpeter, A. (1986). *Angew. Chem. Int. Ed. Engl*. **25**, 825.

Pohl, S., Saak, W., Haase, D. (1987). *Z. Naturforsch.* **42** b, 1493-1499.

R

Rahman, A., Staveley, L.A.K., Bellito, C., Day, P. (1982). *J. Chem. Soc., Faraday Trans*. 2 **78**, 1895-1903.

Randall, C. A., Bhalla, A. S., Shrout, T. R., Cross, L. E. (1990). *J. Mater. Res*. 5, 829-834.

Raptopoulou, C.P., Terzis, A., Mousdis, G.A., Papavassiliou, G.C. (2002). *Z. Naturforsch*. **57** b, 645-650.

Ricard, L., Rey-Lafon, M., Biran, C. (1984). *J. Phys. Chem.* **88**, 5614-5620.

Ricard, L., Cavagnat, R., Rey-Lafon, M. (1985). *J. Phys. Chem.* **89**, 4887-4894.

Riedel, E. F., Willett, R. D. (1975). *Solid State Comm*. **16**, 413-416.

S

Salah, P.A.B., Daoud, A., Constant, G., Jaud, J., Galy, J. (1983a). *Acta Cryst*. C**39**, 63-66.

Salah, A.B., Bats, J.W., Fuess, H., Daoud, A. (1983b). *Z. Kristallogr*. **164**, 259-272.

Schenk, K.J., Chapuis, G. (1988). *J. Phys. Chem.* **92**, 7141-7147.

Schmidt, G.M.J. (1964). *J. Chem. Soc.*, 2014-2021.

Sekine, T., Okuno, T., Awaga, K. (1996a). *Chem. Phys. Lett.* **249**, 201-204.

Sekine, T., Okuno, T., Awaga, K. (1996b). *Mol. Cryst. Liq. Cryst. Section A* **279**, 65-72.

Sekine, T., Okuno, T., Awaga, K. (1996c). *Inorg. Chem.* **37**, 2129-2133.

Seliger, J., Blinc, R., Arend, H., Kind, R. (1976). *Z. Physik B* **25**, 189-195.

Shannon, R. D. (1976). *Acta Cryst. A **32***, 751-767.

Shibuya, K., Koshimizu, M., Takeoka, T., Asai, K. (2002), *Nucl. Instrum. Methods Phys. Res., Sect*. B **194**, 207-212.

Shikoh, E., Ando, Y., Era, M., Miyazaki, T. (2001). *J. Magn. Magn. Mater*. 226-230, 2021-2022.

Siemens (1996) *SADABS*: Area-Detector Absorption Correction; Siemens Industrial Automation, Inc., Madison, Wisconsin, USA.

Shimizu, M., Fujisawa, J. (2004). *J. Lumin*. **108**, 189-194.

Shimizu, M., Fujisawa, J.-I., Ishi-Hayase, J. (2005). *Phys. Rev. B: Condens. Matter* **71**, 205306-1-205306-9.

Skaarup, S., Berg, R.W. (1978). *Solid State Chem*. **26**, 59-67.

Snively, L.O., Tuthill, G.F., Drumheller, J.E. (1981). *Phys. Rev. B: Condens. Matter* **24**, 5349-5355.

Snively, L.O., Haines, D.N., Emerson, K., Drumheller, J.E. (1982). *Phys. Rev. B: Condens. Matter* **26**, 5245-5247.

Soos, Z.G., McGregor, K.T., Cheung, T.T.P., Silverstein, A.J. (1977). *Phys. Rev. B: Condens. Matter* **16**, 3036-3047.

Spengler, R., Zouari, R., Zimmerman, H., Salah, A.B., Burzlaff, H. (1998). *Acta Cryst*. C**54**, 1628-1631.

Stead, M. J., Day, P. (1982). *J. Chem. Soc. Dalton Trans*., 1081-1084.

Steadman, J.P., Willett, R.D. (1970). *Inorg. Chem.* Acta **4**, 367-371.

Steiner, T. (1998). *Acta Cryst*. B **54**, 456-463.

Steurer, W., Depmeier, W. (1989). *Acta Cryst*. B**45**, 555-562.

Stoelinga, J. H. M., Wyder, P. (1976). *J. Chem. Phys.* **64**, 4612-4615.

Stout, G.H., Jensen, L.H. (1989). *X-ray Structure Determination: A Practical Guide*. 2nd Ed., John Wiley and Sons, Inc.

T

Tabuchi, Y., Asai, K., Rikukawa, M., Sanui, K., Ishigure, K. (2000). *J. Phys. Chem. Solids* **61**. 837-845.

Takeoka, Y., Asai, K., Rikukawa, M., Sanui, K. (2001). *Chem. Comm*., 2592-2593.

Takeoka, Y., Asai, Keisuke, Rikukawa, M., Sanui, K. (2002). *Mol. Cryst. Liq. Cryst.* **379**, 383-388.

Tanaka, K., Sano, F., Takahashi, T., Kondo, T., Ito, R., Ema, K. (2002). *Solid State Comm.* **122**, 249-252.

Tanaka, K., Takahashi, T., Ban, T., Kondo, T., Uchida, K., Miura, N. (2003). *Solid State Comm.* **127**, 619-623.

Tanaka, K., Takahashi, T., Kondo, T., Umebayashi, T., Asai, K., Ema, K. (2005). *Phys. Rev. B: Condens. Matter* **71**, 045312-1-6.

Tang, Z., Guloy, A.M. (1999). *J. Am. Chem. Soc.* **121**, 452-453.

Tang, Z., Guan, J., Guloy, A.M. (2001). *J. Mater. Chem*. **11**, 479-482.

Tello, M.J., Arriandiaga, M.A. and Fernãndez, J. (1977). *Solid State Comm.* **24**, 299-302.

Tichý, K, Beneš, J., Hälg, Arend, H. (1978). *Acta Cryst*. B **34**, 2970-2981.

U

Ueda, T., Shimizu, K., Ohki, H., Okuda, T. (1998). *Z. Naturfosch*. **53** a, 983-988.

V

Vacatello, M., Corradini, P. (1973). *Gazz. Chim. Ital.* **103**, 1027-1036.

Vacatello, M., Corradini, P. (1974). *Gazz. Chim. Ital.* **104,** 773-780.

Vacatello, M., De Girolamo, M., Busico, V. (1981). *J. Chem. Soc., Faraday Trans. 1* **77**, 2367-2375.

Van Oort, M. J. M., White, M.A. (1985). *J. Chem. Soc., Faraday Trans*. 1 **81**, 3059-3065.

Van Amstel, W. D., de Jongh, L. J. (1972). *Solid State Comm*. **11**, 1423-1429.

Venkataraman, N.V., Bhagyalakshmi, S., Vasudevan S., Seshadri, R. (2002a). *Phys. Chem. Chem. Phys*. **4**, 4533-4538.

Venkataraman, N.V., Barman, S., Vasudevan, S., Seshadri, R. (2002). *Chem. Phys. Lett.* **358**, 139-143.

Vaněk, P., Havránková, M., Hybler, J. (1992). *Solid State Comm.* **82**, 509-512.

Vincent, B.R., Robertson, K.N., Cameton, T.S., Knop, O. (1987). *Can. J. Chem*. 65, 1042-1046.

W

Wang, W., Chen, X., Efrima, S. (1999). *Chem. Mater*. **11**, 1883-1889.

Whealy, R. D., Bier, D. H., McCormick, B. J. (1959). *J. Am. Chem. Soc*. 81, 5900-5901.

White, M.A. (1984). *J. Chem. Phys.* **81**, 6100-6105.

White, M.A., Staveley, L.A.K. (1982). *J. Phys. Chem. Solids* **43**, 1019-1020.

White, M.A., Granville, N.W., Davies, J., Staveley, L.A.K. (1981). *J. Phys. Chem. Solids* **42**, 953-965.

White, M.A., Granville, N.W., Staveley, L.A.K. (1982). *J. Phys. Chem. Solids* **43**, 341-349.

White, M.A., Davies, N.J., Staveley, L.A.K. (1983). *J. Chem. Soc., Faraday Trans*. 2 **79**, 1653-1661.

Willett, R.D. (1977). *Acta Cryst*. B**33**, 1641-1643.

Willett, R.D. (1990). *Acta Cryst*. C**46**, 565-568.

Willett, R. D., Extine, M. (1973a). *Chem. Phys. Lett.* **23**, 281-283.

Willett, R. D., Extine, M. (1973a). Phys. Lett. **44**A, 503-504.

Willett, R. D., Riedel, E. F. (1975). *Chem. Phys*. **8**, 112-122.

Willett, R.D., Liles, O.L., Michelson, C. (1967). *Inorg. Chem.* **6**, 1885-1889.

Willett, R.D., Jardine, F.H., Rouse, I., Wong, R.J., Landee, C.P., Numata, M. (1981). *Phys. Rev. B: Condens. Matter* **24**, 5372-5381.

Willett, R.D., Wong, R.J., Numata, M. (1983). *Inorg. Chem.* **22**, 3189-3194.

Willett, R. D., Place, H., Middleton, M. (1988). *J. Am. Chem. Soc*., **110**, 8639-8650.

Wortham, E., Zorko, A., Arcon, D., Lappas, A. (2002). *Physica* B **318**, 387-391.

Wang, S., Mitzi, D.B., Feild, C.A., Guloy, A. (1995). *J. Am. Chem. Soc.* **117,** 5297-5302.

Wiest, Th, Blachnik, R., Reuter, H. (1999). *Z. Naturforsch*. **54** b, 1099-1102.

X

Xiao, Z., Chen, H. Shi, M., Wu, G., Zhou, R., Yang, Z., Wang, M., Tang, B. (2005). *Mater. Sci. Eng.,* B **117**, 313-316.

Xu, C., Kodo, T., Sakakura, H., Kumata, K., Takahashi, Y., Ito, R. (1991a) *Solid State Comm.* **79**, 245-248.

Xu, C., Sakakura, H., Kondo, T., Takeyama, S., Miura, N., Takahashi, Y., Kumata, K., Ito, R. (1991b) *Solid State Comm.* **79**, 249-253.

Xu, C., Fukuta, S., Sakakura, H., Kondo, T., Ito, R., Takahashi, Y., Kumata, K. (1991c). *Solid State Comm.* **77**, 923-926.

Xu, Z., Mitzi, D.B. (2003). *Chem. Mater.* **15**, 3632-3637.

Xu, Z., Mitzi, D.B., Dimitrakopoulos, D., Maxcy, K.R. (2003a). *Inorg. Chem.* **42**, 2031-2039.

Xu, Z., Mitzi, D.B., Medeiros, D.R. (2003b). *Inorg. Chem.* **42**,1400-1402.

Y

Yin, R.-Z., Yo, C.H. (1998). *Bull. Kor. Chem. Soc*. **19**, 947-951.

Yamazaki, H. (1977). *Physica* B **86-88**, 649-650.

Ye, Q., Meng, Q., You, X., Huang, X. (1996). *Acta Cryst*. C**52**, 33-35.

Z

Zhu, X.-H.., Mercier, N., Riou, A, Blanchard, P., Frère, P. (2002). *Chem. Comm*., 2160-2161.

Zhu, X.-H., Mercier, N., Frère, P., Blanchard, P., Roncali, J., Allain, Pasquier, C., Riou, A. (2003). *Inorg. Chem.* **42**, 5330-5339.

Zhu, X., Mercier, N., Allain, M., Frère, P., Blanchard, P., Roncali, J., Riou, A. (2004). *J. Solid State Chem*. **177**, 1067-1071.

Zhou, P., Drumheller, J.E., Patyal, B., Willett, R.D. (1992a). *Phys. Rev. B: Condens. Matter* **45**, 12365-12376.

Zhou, P., Tuthill, G.F., Drumheller, J.E. (1992b). *Phys. Rev. B: Condens. Matter* **45**, 2541-2544.

Appendix

The quadrilateral ABCD consists of two triangles ABD and BCD. The triangles are congruent as the lengths are identical (AB = BC, AD = CD and BD is common). The area of a triangle is defined as

$$\text{Area} = 1/2 * \text{height} * \text{base}.$$

For example, in triangle ABD, the base is the diagonal BD and the height is AG. The formula for the area of triangle ABD is:

$$\text{Area (ABD)} = 1/2 * BD * AG.$$

Similarly, the area of triangle BCD is

$$\text{Area (BCD)} = 1/2 * BD * GC$$

Hence, the area of the polygon ABCD:

$$\text{Area (ABCD)} = \text{Area (ABD)} + \text{Area (BCD)}$$

$$\text{Area (ABCD)} = 1/2 * BD * AG + 1/2 * BD * GC$$

$$\text{Area (ABCD)} = 1/2 * BD * AC$$

